

NIST-114A (REV. 3-90)		U.S. DEPARTMENT OF COMMERCE NATIONAL INSTITUTE OF STANDARDS AND TECHNOLOGY		1. PB93-134104
<b>BIBLIOGRAPHIC DATA SHEET</b>				2. PERFORMING ORGANIZATION REPORT NUMBER
				3. PUBLICATION DATE
4. TITLE AND SUBTITLE Proceedings of the First U.S.-Japan Workshop on Seismic Retrofit of Bridges				
5. AUTHOR(S) Kazuhiko Kawashima and M.J. Nigel Priestley				
6. PERFORMING ORGANIZATION (IF JOINT OR OTHER THAN NIST, SEE INSTRUCTIONS) U.S. DEPARTMENT OF COMMERCE NATIONAL INSTITUTE OF STANDARDS AND TECHNOLOGY GAITHERSBURG, MD 20899			7. CONTRACT/GRANT NUMBER	
			8. TYPE OF REPORT AND PERIOD COVERED	
9. SPONSORING ORGANIZATION NAME AND COMPLETE ADDRESS (STREET, CITY, STATE, ZIP)  NIST Catalog No. NIST 140				
10. SUPPLEMENTARY NOTES  Also Available from <del>CPO # SN008-668</del> Not available from GPO				
11. ABSTRACT (A 200-WORD OR LESS FACTUAL SUMMARY OF MOST SIGNIFICANT INFORMATION. IF DOCUMENT INCLUDES A SIGNIFICANT BIBLIOGRAPHY OR LITERATURE SURVEY, MENTION IT HERE.)  The National Institute of Standards and Technology (NIST) and the Public Works Research Institute (PWRI), Japan sponsored their first workshop on seismic retrofit of bridges. The workshop was organized by the Task Committee on Wind and Earthquake Engineering for Transportation Systems of the Panel on Wind and Seismic Effects, U.S.-Japan Program in Natural Resources. Since 1971, Japanese and U.S. transportation officials have conducted extensive bridge inspections and strengthened their bridge superstructures. The workshop objective was to compare the U.S. and Japanese approaches to strengthening bridge structures. The workshop addressed a variety of topics including seismic design codes and inspection and strengthening methods for and research on reinforced concrete bridge piers. The workshop identified a fundamental difference in the U.S. and Japanese approach to strengthening bridge structures. The U.S. follows a systems approach; Japan follows a step-by-step approach based on performance of bridge structures during past earthquakes. The two day workshop was held in the Tsukuba Science City, Japan during 17 and 18 December 1993.				
12. KEY WORDS (6 TO 12 ENTRIES; ALPHABETICAL ORDER; CAPITALIZE ONLY PROPER NAMES; AND SEPARATE KEY WORDS BY SEMICOLONS) bridges; concrete; earthquakes; Loma Prieta Earthquake; retrofit; seismic design; strengthening; vulnerability				
13. AVAILABILITY <input type="checkbox"/> UNLIMITED <input type="checkbox"/> FOR OFFICIAL DISTRIBUTION. DO NOT RELEASE TO NATIONAL TECHNICAL INFORMATION SERVICE (NTIS). <input type="checkbox"/> ORDER FROM SUPERINTENDENT OF DOCUMENTS, U.S. GOVERNMENT PRINTING OFFICE, WASHINGTON, DC 20402. <input type="checkbox"/> ORDER FROM NATIONAL TECHNICAL INFORMATION SERVICE (NTIS), SPRINGFIELD, VA 22161.			14. NUMBER OF PRINTED PAGES	
			15. PRICE	

ELECTRONIC FORM

NIST-114A (REV. 3-90)		U.S. DEPARTMENT OF COMMERCE NATIONAL INSTITUTE OF STANDARDS AND TECHNOLOGY		1. PB93-134112	
<b>BIBLIOGRAPHIC DATA SHEET</b>				2. PERFORMING ORGANIZATION REPORT NUMBER	
				3. PUBLICATION DATE	
4. TITLE AND SUBTITLE An Overview of Damage to Highway Bridges During the Loma Prieta Earthquake					
5. AUTHOR(S) H.S. Lew					
6. PERFORMING ORGANIZATION (IF JOINT OR OTHER THAN NIST, SEE INSTRUCTIONS) U.S. DEPARTMENT OF COMMERCE NATIONAL INSTITUTE OF STANDARDS AND TECHNOLOGY GAITHERSBURG, MD 20899				7. CONTRACT/GRANT NUMBER	
				8. TYPE OF REPORT AND PERIOD COVERED	
9. SPONSORING ORGANIZATION NAME AND COMPLETE ADDRESS (STREET, CITY, STATE, ZIP)  NIST Category No. NIST- 140					
10. SUPPLEMENTARY NOTES Also Available from NIST available from GPO GPO as 5N008-0004					
11. ABSTRACT (A 200-WORD OR LESS FACTUAL SUMMARY OF MOST SIGNIFICANT INFORMATION. IF DOCUMENT INCLUDES A SIGNIFICANT BIBLIOGRAPHY OR LITERATURE SURVEY, MENTION IT HERE.) <p>At 5:04 p.m., Pacific Daylight Time, on October 17, 1989, an earthquake with a surface-wave magnitude of 7.1 occurred with its epicenter located about 10 miles (15 km) northeast of Santa Cruz and 60 miles (95 km) south-southeast of San Francisco, California. According to the U.S. Geological Survey, the earthquake ruptured a segment of the San Andreas fault below the Santa Cruz Mountains. The hypocenter was about 11 miles (18 km) beneath the Earth's surface, and the rupture propagated about 25 miles (40 km) both northwest and southeast within a 10-second period. The earthquake was felt over an area of 400,000 square miles (1,000,000 sq km), from Los Angeles to the south. Oregon to the north, and western Nevada to the east. This earthquake, named the Loma Prieta earthquake, was the largest on the San Andreas fault since the great San Francisco earthquake of 1906 (M = 8.3) when a 275-mile (440-km) stretch of the fault ruptured. This report presents an overview of damage to highway bridge structures during the earthquake.</p>					
12. KEY WORDS (6 TO 12 ENTRIES; ALPHABETICAL ORDER; CAPITALIZE ONLY PROPER NAMES; AND SEPARATE KEY WORDS BY SEMICOLONS) Bridges; damage; earthquake; highways; lifelines; seismic; structural engineering; viaducts					
13. AVAILABILITY <input type="checkbox"/> UNLIMITED <input type="checkbox"/> FOR OFFICIAL DISTRIBUTION. DO NOT RELEASE TO NATIONAL TECHNICAL INFORMATION SERVICE (NTIS). <input type="checkbox"/> ORDER FROM SUPERINTENDENT OF DOCUMENTS, U.S. GOVERNMENT PRINTING OFFICE, WASHINGTON, DC 20402. <input type="checkbox"/> ORDER FROM NATIONAL TECHNICAL INFORMATION SERVICE (NTIS), SPRINGFIELD, VA 22161.				14. NUMBER OF PRINTED PAGES	
				15. PRICE	

ELECTRONIC FORM

**PROCEEDINGS OF  
THE FIRST  
U.S.-JAPAN  
WORKSHOP ON  
SEISMIC RETROFIT  
OF BRIDGES**

**DECEMBER 17 AND 18, 1990  
PUBLIC WORKS RESEARCH INSTITUTE  
TSUKUBA SCIENCE CITY, JAPAN**

REPORT NO. 101  
U.S. DEPARTMENT OF COMMERCE  
NATIONAL TECHNICAL INFORMATION SERVICE  
SPRINGFIELD, VA 22161

## FORWARD

The appropriate maintenance and retrofit of older existing bridges to ensure they remain serviceable in the long term is becoming more and more important. In the light of lessons learned through past seismic damage, a number of highway bridges are considered to have low levels seismic safety from the view of current design practice. Therefore, it is of considerable importance to develop methods for the retrofit and strengthening of existing highway bridges which have high vulnerability for seismic damage.

The Japanese Ministry of Construction has made seismic inspections of highway bridges throughout the country several times from 1971, and has also conducted seismic strengthening projects following these inspections. As a result of such strengthening efforts, such as installing devices for preventing the superstructure from falling, the seismic safety of the highway bridges has been increased. Similar improvement of bridge behavior in California has resulted from an extensive program to install restrainers across superstructure movement joints. Further work is still in progress to bring the strength of bridges up to present design requirement and efforts are particularly being concentrated on developing appropriate strengthening methods for bridge substructures.

On the other hand, in the United States, the damage to bridges during Loma Prieta Earthquake of October 17, 1989 has made it necessary to urgently develop methods for increasing the seismic performance of existing bridge substructures. It is mutual benefit for both the U.S. and Japan to share the problems and the methods for solving them in order to promote methods for increasing the seismic performance of bridges.

Over the last 22 years, the Panel on Wind and Seismic Effects (Japan side Chairman : T. Iwasaki, Director-General of Public Works Research Institute, Ministry of Construction, and U.S. side Chairman : R. N. Wright, Director of Center for Building Technology, National Institute of Standards and Technology) under UJNR (U.S.-Japan Conference on Development and Utilization of Natural Resources) has promoted the sharing of information and technology for mitigating the effects of earthquakes on transportation systems. Separate workshops are also held to facilitate further exchange of information and ideas on specific areas of mutual interest.

The following proceedings document the results of the First U.S.-Japan Workshop on Seismic Retrofit of Bridges. This workshop was sponsored jointly by



the Public Works Research Institute (PWRI) of Japan and the National Institute for Standards and Technology (NIST) of the U.S.A.

The workshop was held at the PWRI facilities in Tsukuba Science City, Japan, between December 17 and 18, 1990, and was organized by Task Committee J "Wind and Earthquake Engineering for Transportation Systems, (Japan Side Chairman : Y. Shiota, Director of Bridge and Structure Department, PWRI, and U.S. Side Chairman : J. Cooper, Deputy Chief, Structures Division, Office of Engineering and Highway Operations Research and Development, Federal Highway Administration,)" Panel on Wind and Seismic Effects, UJNR.

The aims of this workshop were: (1) to bring together experts from both countries to exchange technical information on current research and practical efforts being made in the area of seismic inspection and strengthening of bridges, and (2) to identify future needs and opportunities between the two countries for cooperative research.

A broad range of special technical topics were presented at the workshop. These included:

- History of Seismic Damage and Preparation of Seismic Design Codes
- Damage to San Francisco Bridges in the Loma Prieta Earthquake
- Assessment and Prioritization of Vulnerable Bridges
- Inspection and Strengthening Methods for Reinforced Concrete Bridge Piers
- Research on Seismic Retrofitting and Strengthening of Reinforced Concrete Bridge Piers
- Research on Seismic Retrofitting and Strengthening

In total, nineteen papers were presented in the two days of plenary sessions; 12 papers from Japan and 7 papers from the United States.

The material in the proceedings are presented as follows: (1) all technical papers are given in the order in which they were presented during the workshop; (2) resolutions that were unanimously approved by the participants during the closing session of the workshop. The workshop program and list of participants are given in the Appendices of the proceedings.

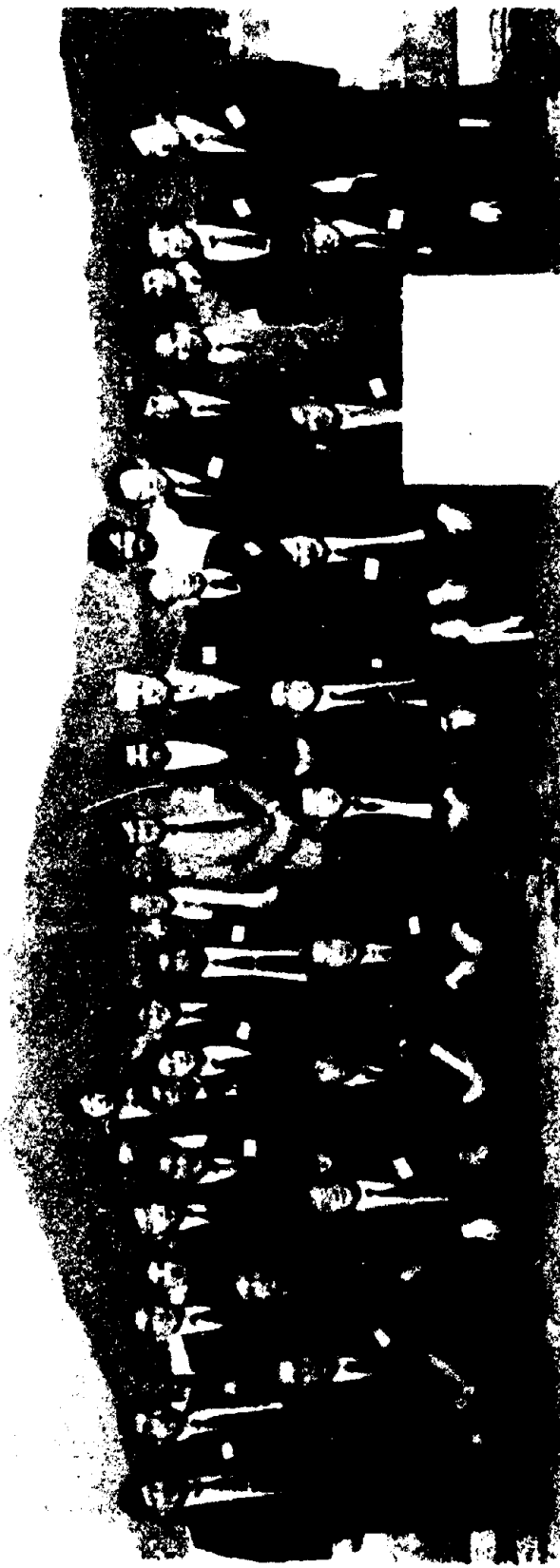
In concluding the forward, we wish to express our profound gratitude and sincere appreciation to all participants in the workshop for supporting the workshop by active discussion. We were able to close a very successful workshop in which participants from both sides came to understand the problems and

solution methods used by the other countries through the exchange of important technical information on the seismic retrofit of bridges.

Grateful thanks are extended to Japan Highway Public Corporation, Metropolitan Expressway Public Corporation, Hanshin Expressway Public Corporation, and Honshu-Shikoku Bridge Authority for the generous cooperation in the workshop and in particular during the study-tour of seismic strengthening efforts and construction projects in Japan. We also would like to thank Dr. G.A. MacRae of PWRI for translating English into Japanese and vice versa for Japanese participants, and the assisting staff, Messrs. K. Tamura, S. Unjoh, H. Nagashima, H. Hida, and H. Shimizu of PWRI for the smooth progress of the schedule.

Kazuhiko KAWASHIMA, and  
M. J. Nigel PRIESTLEY

December 18, 1990



## TABLE OF CONTENTS

### PAPERS

#### **Session 1 : History of Seismic Damage and Preparation of Seismic Design Codes**

- 1) Seismic Design, Seismic Strengthening and Repair of Highway Bridges ..... 3  
In Japan  
(K.Kawashima)
- 2) Bridge Substructures and Design Methods ..... 62  
(M.Okahara, S.Takagi and S.Nakatanl)
- 3) Design Details of Reinforced Concrete Bridges In Japan ..... 89  
(T.Akimoto)

#### **Session 2 : Damage to San Francisco Bridges In the Loma Prieta Earthquake**

- 1) An Overview of Highway Damage to Bridges During the Loma Prieta ..... 111  
Earthquake  
(H.S.Lew)
- 2) San Francisco Double Deckers - Observed Damage and a Possible Retrofit..... 140  
Solution  
(M.J.N.Priestley, F.Selbie)
- 3) Full-scale Tests on the Cypress Viaduct ..... 156  
(S.Mahin and J.Moehle)

#### **Session 3 : Assessment and Prioritization of Vulnerable Bridges**

- 1) Assessment and Retrofit Research for Multi-level, Multi-column Bents ..... 175  
(S.Mahin and J.Moehle)
- 2) Prioritizing Bridges for Seismic Retrofit ..... 187  
(J.Gates and B.Maroney)
- 3) Damage and Performance Assessment of Existing Concrete Bridges Under ..... 203  
Seismic Loads  
(F.Selbie and M.J.N.Priestley)
- 4) Large Earthquake Countermeasures for Bridge Substructures on Tomei ..... 223  
The Expressway  
(T.Tsubouchi, K.Ohashi and K.Arakawa)

#### **Session 4 : Inspection and Strengthening Methods for Reinforced Concrete Bridge Piers**

- 1) Seismic Inspection and Seismic Strengthening of Reinforced Concrete ..... 251  
Bridge Piers with Termination of Main Reinforcement at Mid-Height  
(K.Kawashima, S.Unjoh and H.Iida)

2) Seismic Strengthening of Reinforced Concrete Bridge Piers on Metropolitan Expressway (T.Akimoto, H.Nakajima and F.Kogure)	280
3) Seismic Strengthening Method for Reinforced Concrete Bridge Piers on Hanshin Expressway (Y.Matsuura, I.Nakamura and H.Sekimoto)	299

**Session 5 : Research on Seismic Retrofitting and Strengthening of Reinforced Concrete Bridge Piers**

1) Retrofit of Bridges Columns for Enhanced Seismic Performance (Y.H.Chai, M.J.N.Priestley and F.Selble)	321
2) Study on Ductility Estimation of Fiber Mixed RC Members (S.Kobayashi, H.Kawano, K.Morihama and H.Watanabe)	341
3) Effect of Carbon Fiber Reinforcement as a Strengthening Measure for Reinforced Concrete Bridge Piers (T.Matsuda, T.Sato, H.Fujiwara and N.Higashida)	356

**Session 6 : Research on Seismic Retrofitting and Strengthening**

1) Failure Criteria of Original and Repaired RC Members with Hybrid Experiments (H.Iemura, K.Izuno and Y.Yamada)	377
2) Formulation of Ductility of R/C Members and Influence of Ductility on Response of Behavior in R/C Frame Structures (H.Mutsuyoshi and A.Machida)	395
3) Repair and Retrofit of Steel Piers (G.A.Macrae, K.Kawashima and K.Hasegawa)	405

<b><u>R E S O L U T I O N S</u></b>	425
-------------------------------------	-----

**A P P E N D I C E S**

<b>WORKSHOP PROGRAM</b>	429
<b>ITINERARY OF STUDY-TOUR</b>	433
<b>PARTICIPANTS</b>	434

# **S e s s i o n 1**

## **H i s t o r y o f S e i s m i c D a m a g e a n d P r e p a r a t i o n o f S e i s m i c D e s i g n C o d e s**

- 1) Seismic Design, Seismic Strengthening and Repair of Highway Bridges  
in Japan  
(K.Kawashima)
- 2) Bridge Substructures and Design Methods  
(M.Okahara, S.Takagi and S.Nakatani)
- 3) Design Details of Reinforced Concrete Bridges in Japan  
(T.Akimoto)

## **SEISMIC DESIGN, SEISMIC STRENGTHENING AND REPAIR OF HIGHWAY BRIDGES IN JAPAN**

**Kazuhiko KAWASHIMA**

**Head, Earthquake Engineering Division, Public Works Research Institute,  
Ministry of Construction, Tsukuba Science City, Ibaraki-ken, Japan**

### **SUMMARY**

This paper presents earthquake hazard mitigation efforts for road transportation facilities in Japan. Emphasis is placed on seismic disaster prevention measures for highway bridges. Description is firstly given to seismic damage developed in the past earthquakes and the history of the development of the seismic design method. Current seismic practice is then presented based on the latest version of Seismic Design Specifications of Highway Bridges issued by the Ministry of Construction in 1990. Description is also given to new technical developments for passive and hybrid control of highway bridges, and for disaster information gathering and processing systems. Seismic inspection and strengthening methods based on the past experiences are presented. Finally, an assessment and repair method for seismically damaged highway bridges is presented.

### **INTRODUCTION**

Located along the Pacific Seismic Belt, Japan is one of the most seismically disastrous countries in the world and has often suffered significant damage from large earthquakes. Considerable efforts have been paid to earthquake hazard mitigation for transportation facilities. In particular, seismic safety of highway bridges has been a major concern because damage of highway bridges causes extensive interruption of road transportation and restoration often requires long time.

This paper presents pre-earthquake and post-earthquake measures for mitigating earthquake hazards on road transportation facilities in Japan, with emphasis on countermeasures for highway bridges. Development of new technology for reducing structural response by means of passive and hybrid control, and for disaster information gathering and processing systems is also presented.

### **DAMAGES OF HIGHWAY BRIDGES IN THE PAST EARTHQUAKES**

Highways in Japan consist of the Expressways (3,721 km), National Highways (46,661 km), Prefectural Roads (128,202 km), and Municipal Roads (925,138 km). Along the highways and roads, excluding the Municipal Roads, there are about 50,000 bridges with the length of 15 m or longer.

Table 1 shows the highway bridges which suffered damages in the past earthquakes since the Kanto Earthquake of 1923. It should be noted that although there were many bridges which suffered damages due to earthquakes, number of bridges which fell down is only 15.

Based on the survey of the damaged bridges, it is pointed out that there were three major factors which contributed to the damages of the bridges as follows :

- a) weakness of substructure,
- b) weakness of bearing supports, and
- c) weakness of surrounding subsolls.

From such factors, the following types of damages were most often developed in the past :

- a) substructure : tilting, settlement, sliding, cracks, and overturning
- b) superstructure : movement, buckling and cracks near the supports, and falling of girder
- c) bearing supports : failure of supports, and pull-out or rupture of anchor bolts

**Table 1 Damage of Highway Bridges in the Past since Kanto Earthquake of 1923**

DATE	EARTHQUAKE	MAGNITUDE	NUMBER OF BRIDGES DAMAGED	NUMBER OF BRIDGES WHICH FELL DOWN
1923. 9. 1	KANTO	7.9	1,785	6
1946.12.21	NANKAI	8.1	346	1
1948. 6.28	FUKUI	7.3	243	4
1949.12.26	IMAICHI	6.4	1	0
1952. 3. 4	TOKACHI-OKI	8.1	128	0
1962. 4.30	MIYAGI-KEN-HOKURU	6.5	187	0
1964. 6.16	NIIGATA	7.5	98	3
1968. 2.21	EBINO	6.1	10	0
1968. 5.16	TOKACHI-OKI	7.9	101	0
1978. 1.14	IZU-ONSHIMA	7.0	7	0
1978. 6.12	MIYAGI-KEN-OKI	7.4	95	1
1982. 3.21	URAKAWA-OKI	7.1	5	0
1983. 5.28	MINN-KAI-CHUBU	7.7	178	0
1984. 9.14	NAGANO-KEN-SEBU	6.8	14	0
TOTAL			3,191	15



Although these sorts of damage are the ones commonly observed in the past earthquakes, the damage types have been changing in accordance with the progress of the seismic design method and improvement of construction practice. Seismic damage since the 1923 Kanto Earthquake may be classified into three stages from their significance <sup>2)</sup> (refer to Table 2).

#### **Stage 1 - Damage due to Inadequate Strength of Foundations**

After experiencing the destructive damage of the 1923 Kanto Earthquake the first requirements for seismic design of highway bridges were included in the "Details of Road Structures (Draft)" issued by the Ministry of Internal Affairs in 1926. No seismic effects were considered for design of highway bridges prior to the Kanto Earthquake. Even after the first stipulations issued in 1926, seismic design was not adequate because the stipulations only described design force levels without providing a detailed design method or design details. Therefore, seismic safety of bridge substructures was inadequate until the 1950's when seismic design for foundations and substructures came to be widely adopted.

In those days, when seismic effects were either disregarded or inadequately considered, seismic damage was characterized by failure of foundations and substructures as shown in Photos 1 and 2. In most cases, foundations tilted, moved or even overturned due to inadequate strength of the foundations and the surrounding soils. This led to falling-off of the superstructures.



**Photo 1** Damage of Sakawa-gawa Bridge on National Highway No. 1 by the Kanto Earthquake of 1923

Table 2 Change of Damage Types

Year	Major Earthquakes	Change of Major Seismic Damage	Seismic Design Method	Seismic Inspection and Strengthening
1920	1923 Kanto Earthquake (M7.9)	Failure of Superstructure due to Tilting/Movement of Foundation	1926 Initiation of Seismic Design (Details of Road Structures)	
1930				
1940	1946 Nankai Earthquake (M8.1) 1948 Fukui Earthquake (M7.3)	Failure of Concrete around Fixed Bearing	1939 Introduction of Standard Seismic Coefficient (Design Specifications of Steel Highway Bridges)	
1950	1952 Tokachi-oki Earthquake (M8.1)	Damage due to Liquefaction		
1960	1964 Niigata Earthquake (M7.5)	Failure of RC Piers, and Bearing	1956 Seismic Coefficient depending on Zone and Ground Condition (Design Specifications of Steel Highway Bridges)	
1970	1978 Miyagi-ken-oki Earthquake (M7.4)		1971 • Seismic Coefficient depending on Zone, Ground Conditions, Importance and Structural Response • Introduction of Evaluation Method for Liquefaction (Specifications for Seismic Design)	1971 Seismic Inspection
1980	1982 Urakawa-oki Earthquake (M7.1) 1983 Nihon-kai-chubu Earthquake (M7.7)		1980 • Part V Seismic Design, Specifications for Design of Highway Bridges • Introduction of New Evaluation Method for Liquefactions	1976 Seismic Inspection 1979 Seismic Inspection
1990			1990 Part V Seismic Design, Specifications for Design of Highway Bridges	1986 Seismic Inspection

*Reproduced from  
best available copy*



Photo 2 Damage of Nakazuno Bridge by the Fukui Earthquake of 1948

#### Stage 2 Damage due to Soil Liquefaction

Although the damage due to inadequate strength of foundations became less frequent in accordance with the improvement of seismic design and construction methods, the next stage of damage encountered was soil failure during the 1964 Niigata Earthquake. Soil liquefaction, which took place extensively around sites, caused destructive damage to bridges. **Photos 3** and **4** shows the falling off of the decks of the Showa Bridge. Extensive soil movement associated liquefaction caused large lateral movements of bent pile foundations, which caused the dropping off of the deck.

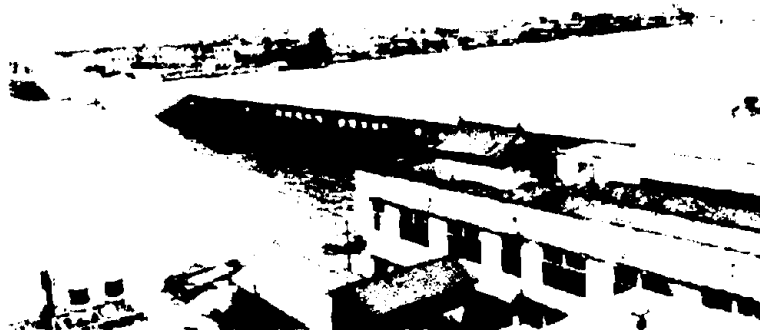
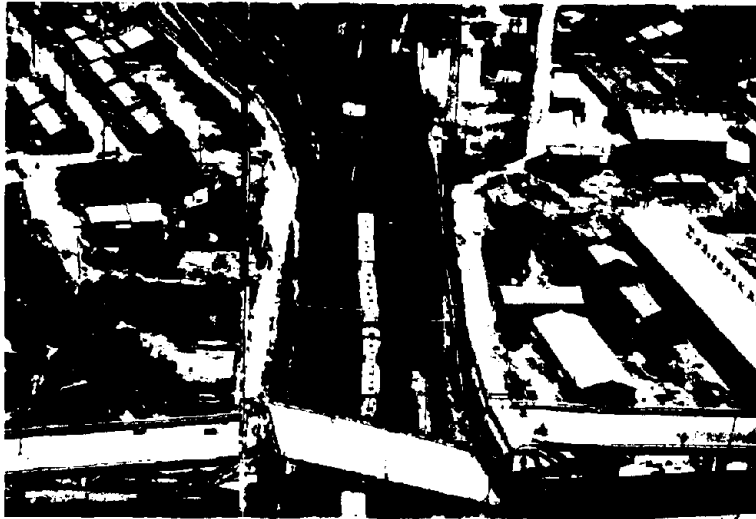


Photo 3 Damage of Showa Bridge by the Niigata Earthquake of 1964



**Photo 4 Damage of Higashi-Kosen Bridge by the Niigata Earthquake of 1964**

Through the damage, it was learned that it is important to take account of liquefaction in design of bridges, and various studies for assessing and evaluating the effects of liquefaction were initiated. Through such studies, the first stipulations for assessment of liquefaction were introduced in the "Seismic Design Specifications of Highway Bridges" in 1971.

One more important lesson gained from the Niigata Earthquake was that devices for preventing falling-off of superstructures from the crest of substructures are required. It was considered that even if large relative movements between the deck and substructures occurred due to either failure of substructures or failures of soils such as soil liquefaction, critical failure causing falling-off of deck could be prevented if such devices were provided. Various devices were then developed, and design recommendations were included in the Seismic Design Specifications of Highway Bridges issued in 1971.

### **Stage 3 - Damage to Piers and Bearing Supports**

In recent earthquakes including the Miyagi-ken-oki Earthquake (M7.4) of 1978 and the Nihon-kai-chubu Earthquake (M7.7) of 1983, substantial damage due to inadequate strength of foundations and effects of soil liquefaction was not developed in those bridges designed and constructed in accordance with the recent design specifications. However, damages to reinforced concrete piers and bearing supports were developed extensively as shown in Photos 5, 6 and 7. This is due to the fact that other modes of failures such as tilting or movement of the foundations, soil liquefaction, and falling-off of superstructures were prevented by the new design recommendations.

The new strengthening and earthquake resistant countermeasures brought damage at the next weak points such as the reinforced concrete piers and

**Reproduced from  
best available copy**



**Photo 5** Damage to Reinforced Concrete Piers of Sendai Bridge by the Miyagi ken-oki Earthquake of 1978



**Photo 6** Damage to Bearing Supports of Da-te Bridge by the Miyagi ken-oki Earthquake of 1978

the bearing supports. This obviously shows that engineering measures aiming only to minimize the damage observed in the 1978 earthquake do not necessarily contribute to avoid new types of damage by the future earthquakes. It is now required to take account of total seismic safety of highway bridges, and this was the main scope of the latest revision of the seismic design specifications in 1990.

It should be noted here that the damage shown in Photo 7 was developed



**Photo 7 Damage to Reinforced Concrete Piers of Shizunai Bridge by the Urakawa-oki Earthquake of 1982**

by shear at the mid-height of the reinforced concrete piers where main reinforcement was terminated. In the design specifications issued prior to 1980, the main reinforcement was terminated with the bond length of 12 times the diameter of the main reinforcement. Through the damage, such as that shown in **Photo 7**, the bond length was revised in the 1980 specifications to 12 times the diameter of the main reinforcement plus the effective width of the pier.

#### **HISTORY OF SEISMIC DESIGN OF HIGHWAY BRIDGES**

Seismic design was initiated for highway bridges in 1926 after the experience of the Kanto Earthquake in 1923. The importance of considering seismic effects in design of highway bridges was recognized from the extensive damage developed by the Kanto Earthquake. The first stipulations requiring seismic effects for highway bridges were included in "Details of Road Structures (Draft)" issued by the Ministry of Internal Affairs in 1926. It was stipulated in the draft details that the maximum lateral force expected to develop at the site shall be considered in seismic design. It was also recommended in the draft details that 30 % of gravity force shall be adopted for the reconstruction of the bridges damaged by the Kanto Earthquake at Tokyo and Yokohama.

After experiencing significant damage during strong earthquakes seismic regulations were reviewed and amended several times as shown in **Table 3**. "Design Specifications of Steel Highway Bridges (Draft)" were issued in 1939, and "Design Specifications of Steel Highway Bridges" and their revised version were issued in 1956 and 1964, respectively. A seismic lateral force of 20 % of the gravity force was stipulated in these specifications. The 20 %

**Table 3 History of Design Seismic Loads for Highway Bridges in Japan**

Year	Name of Regulations	Seismic Design Methods	Other Stipulations for Seismic Effects	Major Earthquakes
1886	Order No. 13, Ministry of Internal Affairs	Not Considered	Not Considered	1881 Nohbi (M8.4)
1926	Details of Road Structures (Draft), Road Law, MIA	Seismic Coefficient Method $k_h=0.15\sim0.4$ ( $k_h\geq 0.3$ advised in Tokyo and Yokohama)	Not Considered	1923 Kanto (M7.9)
1939	Design Specifications of Steel Highway Bridges (Draft), MIA	Seismic Coefficient Method ( $k_h=0.2$ , $k_v=0.1$ )	Not Considered	1946 Nankai (M8.1) 1948 Fukui (M7.3)
1956 (and 1964)	Design Specifications of Steel Highway Bridges, Ministry of Construction	Seismic Coefficient Method ( $k_h=0.1\sim0.35$ )	Not Considered	1952 Tokachi-oki (M8.2) 1964 Niigata (M7.5)
1971	Specifications for Seismic Design of Highway Bridges, MOC	<ul style="list-style-type: none"> <li>• Seismic Coefficient Method (<math>k_h=0.1\sim0.24</math>)</li> <li>• Modified Seismic Coefficient Method (<math>k_h=0.05\sim0.3</math>)</li> </ul>	<ul style="list-style-type: none"> <li>• Evaluation of Sandy Layers Vulnerable to Liquefaction</li> <li>• Device for Preventing Falling-off of Superstructure</li> </ul>	1978 Miyagi-ken-oki (M7.4)
1980	Part V Seismic Design of Design Specifications of Highway Bridges, MOC	<ul style="list-style-type: none"> <li>• Seismic Coefficient Method (<math>k_h=0.1\sim0.24</math>)</li> <li>• Modified Seismic Coefficient Method (<math>k_h=0.05\sim0.3</math>)</li> <li>• Check of Deformation Capability of RC Piers</li> <li>• Dynamic Response Analysis</li> </ul>	<ul style="list-style-type: none"> <li>• <math>F_L</math>-Method for Evaluation of Liquefaction</li> <li>• Device for Preventing Falling-off of Superstructure</li> </ul>	1982 Urakawa-oki (M7.1) 1983 Ninon-kai-chubu (M7.7)
1990	Part V Seismic Design of Design Specifications of Highway Bridges, MOC	<ul style="list-style-type: none"> <li>• Seismic Coefficient Method (<math>k_h=0.1\sim0.3</math>)</li> <li>• Check of Bearing Capacity of RC Piers for Lateral Force</li> <li>• Dynamic Response Analysis</li> </ul>	<ul style="list-style-type: none"> <li>• <math>F_L</math>-Method for Evaluation of Liquefaction</li> <li>• Device for Preventing Falling-off of Superstructure</li> </ul>	

gravity force was considered for long time as a basic design force for highway bridges.

The first comprehensive seismic design stipulations were issued by the Ministry of Construction in 1971 in a separate volume exclusively for seismic design as "Specifications for Seismic Design of Highway Bridges"<sup>23</sup>. It was described in the specifications that lateral force shall be determined depending on zone, importance and ground condition in the static lateral force method (seismic coefficient method) and structural response shall be further considered in the modified static lateral force method (modified seismic coefficient method). Evaluation of soil liquefaction was firstly incorporated in view of the damage caused in the 1964 Niigata Earthquake. Design details to increase the seismic safety such as devices for preventing falling-off of superstructure from substructures were newly introduced. Design methods for substructures were also issued between 1964 and 1971 in the form of "Design Specifications of Substructures". Therefore, it is considered that considerable increase of seismic safety was made for those

bridges designed and constructed in accordance with the 1971 Specifications.

The 1971 specifications were revised by the Ministry of Construction in the form of "Part V Seismic Design" of the "Design Specifications of Highway Bridges" in 1980. The Design Specifications of Highway Bridges consist of "Part I Common Part", "Part II Steel Bridges", "Part III Concrete Bridges", "Part IV Foundations", and "Part V Seismic Design". Although the Part V was essentially the same as the 1971 Specifications, a rational evaluation method for predicting soil liquefaction as well as practical design methods at the time when liquefaction is judged to occur<sup>7)</sup> was included in the Part V Seismic Design.

The latest specifications were issued by the Ministry of Construction in February 1990 in the form of "Part V Seismic Design" for the "Design Specifications of Highway Bridges"<sup>8)</sup>. Major revisions introduced in the 1990 Specifications were unification of static lateral force method (seismic coefficient method) and the modified static lateral force method (modified seismic coefficient method) including the revision of the seismic design force, a new method for computing inertia force for multi-span continuous bridges, a new ductility check for reinforced concrete piers, and detailed stipulations for dynamic response analysis. These revisions were incorporated based on the recent studies for predicting earthquake ground motions and strength of reinforced concrete piers<sup>9) ~ 12)</sup>.

## SEISMIC DESIGN OF HIGHWAY BRIDGES

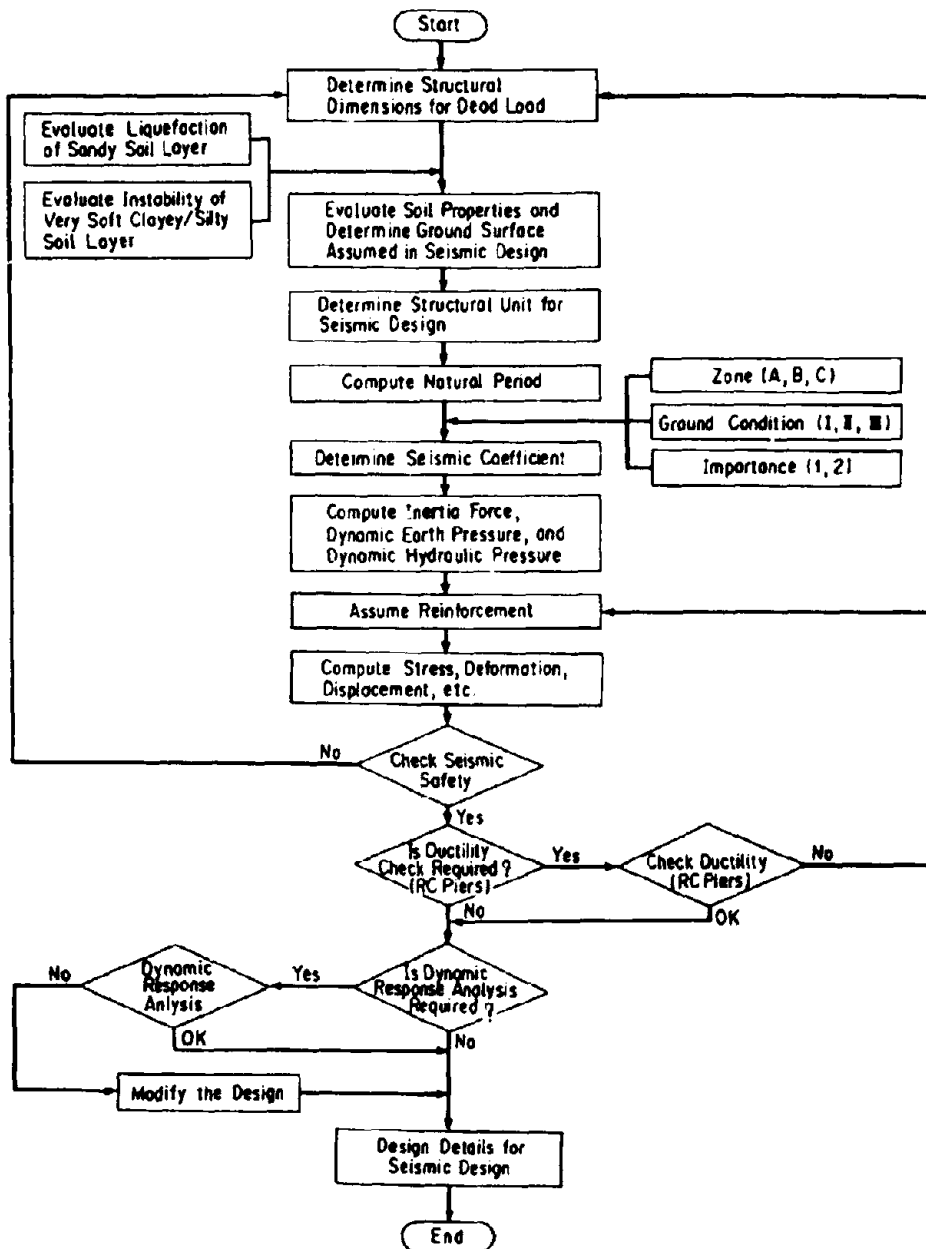
### Outline

Highway bridges are vital components of highways, and they have to be safe enough against earthquakes so that the function of highways be maintained. They have to be used without losing any structural functions against small to moderate earthquakes which have high to moderate possibility of occurring at the site. Critical failures causing total collapse of a bridge have to be avoided even during significant earthquakes such as the Kanto Earthquake of 1923.

The "Part V Seismic Design" of the "Design Specifications of Highway Bridges" is applied for the seismic design of highway bridges with span lengths not longer than 200 meters. The specifications stipulate the adoption of the static lateral force method (seismic coefficient method) based on the allowable stress design approach. A check of the ductility for reinforced concrete piers (Check of Bearing Capacity of Reinforced Concrete Piers for Lateral Force) and dynamic response analysis are recommended in accordance with flow chart presented in Fig. 1. Emphasis is placed on the need to install devices for preventing falling-off of the superstructures from the substructures.

The "Part V Seismic Design" of the "Design Specifications of Highway





**Fig.1 Flow of Seismic Design of Highway Bridge**

Bridges" have the contents as<sup>59</sup> :

**Chapter 1 General**

- 1.1 Scope and Application
- 1.2 Definition of Terms

**Chapter 2 Basic Principles of Seismic Design**

**Chapter 3 Loads and Design Conditions in Seismic Design**

- 3.1 Loads and Combinations for Seismic Design
- 3.2 Effects of Earthquakes
- 3.3 Inertia Force
  - 3.3.1 General
  - 3.3.2 Computation Method of Natural Period
  - 3.3.3 Computation Method of Inertia Force
- 3.4 Dynamic Earth Pressure
- 3.5 Hydrodynamic Pressure
- 3.6 Ground Conditions for Seismic Design
- 3.7 Soil Layers of Which Bearing Capacity Shall be Decreased in Seismic Design
  - 3.7.1 General
  - 3.7.2 Sandy Layers Vulnerable to Liquefaction
  - 3.7.3 Very Loose Clayey and Silty Soil Layers
  - 3.7.4 Soil Layers of Which Bearing Capacity Shall be Decreased and Treatment of the Layers
- 3.8 Ground Surface Assumed in Seismic Design

**Chapter 4 Seismic Coefficient**

- 4.1 General
- 4.2 Standard Horizontal Seismic Coefficient
- 4.3 Modification Factors for Standard Horizontal Seismic Coefficient

**Chapter 5 Check of Bearing Capacity of Reinforced Concrete Piers for Lateral Force**

- 5.1 General
- 5.2 Check of Safety
- 5.3 Horizontal Seismic Coefficient for Check of Bearing Capacity of Reinforced Concrete Piers for Lateral Force
  - 5.3.1 Equivalent Horizontal Seismic Coefficient for Check of Bearing Capacity of Reinforced Concrete Piers for Lateral Force
  - 5.3.2 Horizontal Seismic Coefficient for Check of Bearing Capacity of Reinforced Concrete Piers for Lateral Force
- 5.4 Bearing Capacity of Reinforced Concrete Piers for Lateral Force
  - 5.4.1 Bearing Capacity of Reinforced Concrete Piers for Lateral Force, Allowable Ductility Factor, and Equivalent Natural Period
  - 5.4.2 Bearing Capacity, Yielding Force, Ultimate Displacement and Yielding Displacement
  - 5.4.3 Bearing Capacity of Reinforced Concrete Piers for Shear

**Chapter 6 Dynamic Response Analysis**

- 6.1 General
- 6.2 Dynamic Response Analysis Method and Analytical Models
  - 6.2.1 Method of Dynamic Response Analysis

- 6.2.2 Analytical Models
- 6.3 Input Ground Motions for Dynamic Response Analysis
  - 6.3.1 Acceleration Response Spectra for Modal Response Spectral Analysis
  - 6.3.2 Accelerations for Time History Analysis
- 6.4 Check of Seismic Safety
- Chapter 7 Structural Details in Seismic Design
  - 7.1 General
  - 7.2 Device for Preventing Falling-off of Superstructure from Substructures
    - 7.2.1 General
    - 7.2.2 Devices for Preventing Falling-off of Superstructure
    - 7.2.3 Distance between Edge of Crest of Substructure and Edge of Deck
    - 7.2.4 Devices for Fall of Deck
  - 7.3 Design Details for Seismic Design at Bearing Supports
- Chapter 8 Devices for Reducing Lateral Force

(Appendix)

- I. References on Liquefaction
- II. Examples of Classification of Ground Condition
- III. References on Design Ground Motion
- IV. Example of Computation of Natural Period and Inertia Force
- V. Reference on Bearing Capacity of Reinforced Concrete Piers for Lateral Force
- VI. Practices of Design Details for Seismic Design

**Seismic Lateral Force for Static Lateral Force Method**

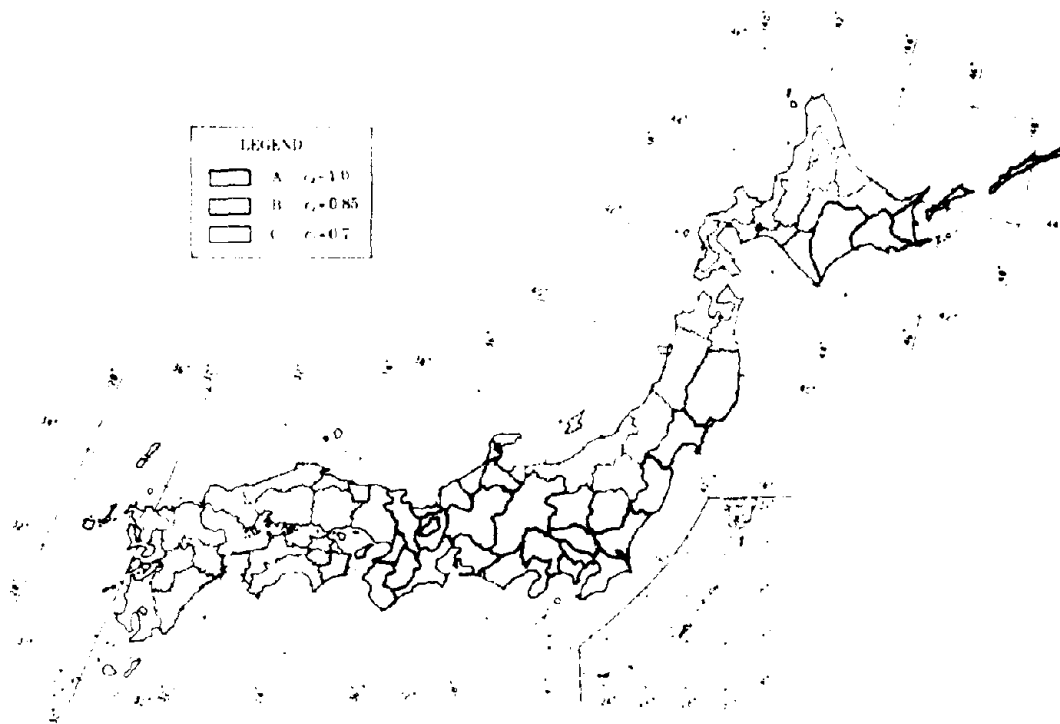
(1) In the static lateral force method (seismic coefficient method), the horizontal design seismic coefficient shall be determined by Eq.(1), but no less than 0.1.

$$k_h = c_z \cdot c_s \cdot c_i \cdot c_T \cdot k_{h0} \quad (1)$$

where

- $k_h$  : design horizontal seismic coefficient,
  - $k_{h0}$  : standard design horizontal seismic coefficient (=0.2),
  - $c_z$  : modification factor for zone (refer to Fig. 2),
  - $c_s$  : modification factor for ground condition (refer to Table 4),
  - $c_i$  : modification factor for importance (refer to Table 5), and
  - $c_T$  : modification factor for structural response (refer to Table 6).
- For computing inertia force associated with the weight of soils and dynamic earth pressure,  $c_T$  shall be 1.0.

Fig. 3 shows the horizontal seismic coefficient assuming  $c_z = c_i = 1.0$ .



**Fig.2 Seismic Zoning Map and Modification Coefficient  $c_z$**

**Table 4 Ground Condition Factor  $c_G$**

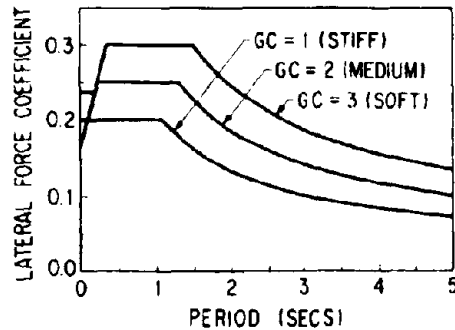
Ground Group	I	II	III
$c_G$	0.8	1.0	1.2

**Table 5 Importance Factor  $c_i$**

Group	$c_i$	Definition
1st class	1.0	Bridges on expressway (limited access highways), general national road and principal prefectural road. Important bridges on general prefectural road and municipal road.
2nd class	0.8	Other than the above

**Table 6 Structural Response Factor  $c_T$**

Ground Group	Structural Response Coefficient $c_T$		
Group I	$T < 0.1$	$0.1 \leq T \leq 1.1$	$1.1 < T$
	$c_T = 2.69T^{1/3} \geq 1.00$	$c_T = 1.25$	$c_T = 1.33T^{-2/3}$
Group II	$T < 0.2$	$0.2 \leq T \leq 1.3$	$1.3 < T$
	$c_T = 2.15T^{1/3} \geq 1.00$	$c_T = 1.25$	$c_T = 1.49T^{-2/3}$
Group III	$T < 0.34$	$0.34 \leq T \leq 1.5$	$1.5 < T$
	$c_T = 1.80T^{1/3} \geq 1.00$	$c_T = 1.25$	$c_T = 1.64T^{-2/3}$



**Fig.3 Horizontal Seismic Coefficient  $k_h$  for Static Lateral Force Method  
(  $c_z = c_1 = 1.0$  )**

(2) The vertical design seismic coefficient may be generally considered as zero, except for bearing supports.

(3) The seismic lateral force for structural members, soils and water below the "ground surface assumed in seismic design" shall be considered as zero. The ground surface assumed in seismic design depends on soil condition at the site, and is generally assumed as the base level of footing for pile foundations.

(4) Hydrodynamic pressure and earth pressure during earthquakes are stipulated in the specifications.

(5) Increase of allowable stresses of materials may be considered in seismic design. The magnitude of the increase for specific materials is specified in the respective parts. For seismic design of substructures, the allowable stress is increased 1.5 times for a load combination of primary load and seismic effects.

#### **Classification of Ground Condition**

Ground conditions are classified into three groups according to Table 7, in which characteristic value  $T_s$  shall be evaluated by Eq.(2).

**Table 7 Classification of Ground Condition**

GROUND CONDITION	DEFINITION	APPROXIMATE ESTIMATION
GROUP I	$T_s < 0.2 \text{ SEC}$	TERTIALY OR OLDER
GROUP II	$0.2 \leq T_s < 0.6 \text{ SEC}$	ALLUVIUM AND DILUVIUM
GROUP III	$0.6 \leq T_s$	SOFT ALLUVIUM

$$T_s = \sum_i \frac{4h_i}{V_{si}} \quad (2)$$

where

- $T_0$  : characteristic value (sec)
- $H_i$  : thickness of i-th subsoil layer (m)
- $V_{s,i}$  : shear wave velocity of i-th sublayer (m/sec)
- $i$  : sublayer's number counted from ground surface

**Evaluation Method of Inertia Force**

Inertia forces in the static lateral force method shall be applied to bridges in two ways depending on the seismic design structural unit. The seismic design structural unit shall be selected in accordance with **Table 8**.

Natural period and the inertia force shall be determined as:

- 1) Seismic design structural unit consisting of a substructure and the part of superstructure supported vertically by the substructure

Natural period and inertia force shall be determined by Eqs.(3) and (4)

$$F_{Di} = k_{Fi} R_i \tag{3}$$

$$T = 2.01 \sqrt{\delta} \tag{4}$$

where

- $F_{Di}$  : Inertia force associated with dead weight of superstructure for design of i-th substructure
- $k_{Fi}$  : seismic coefficient considered for i-th structural segment
- $R_i$  : reaction force developed at i-th substructure due to dead weight of the part of superstructure supported by the i-th substructure.
- $T$  : natural period, in second, of the seismic design structural unit
- $\delta$  : lateral displacement, in meter, of the substructure subjected to a lateral force equivalent with 80 % of the dead weight of a substructure above the ground surface assumed in seismic design and the dead weight of a part of the superstructure supported by the substructure.

- 2) Seismic design structural unit consisting of several substructures and the part of superstructure supported vertically by the substructures.

Inertia force shall be evaluated in accordance with **Fig. 4**, i.e.,

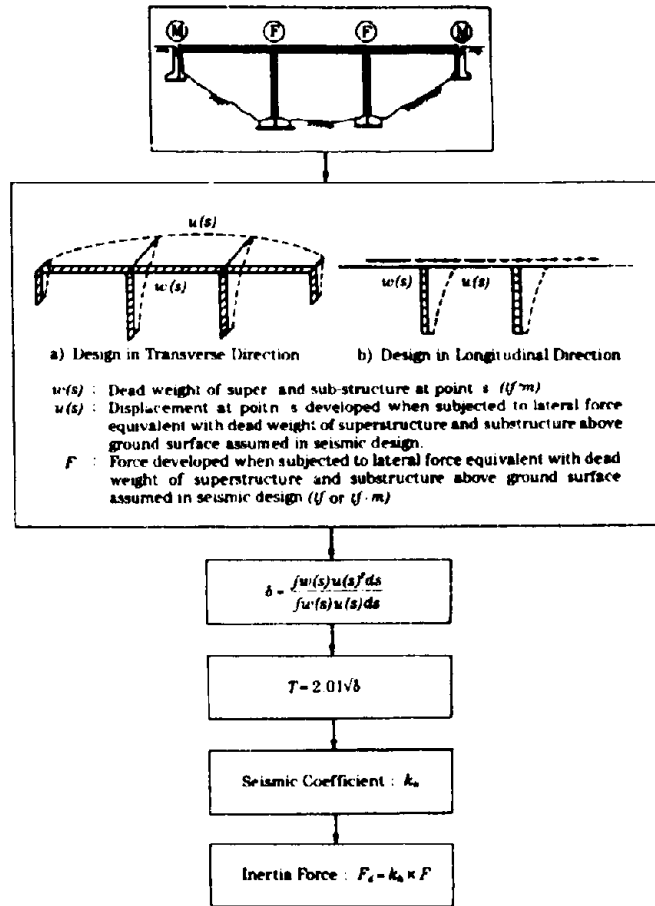
- i) Idealize the bridge by a linear elastic frame model
- ii) apply a lateral force equivalent with the dead weight of superstructure and substructures above the ground surface assumed in seismic design, and compute the natural period as

$$T = 2.01 \sqrt{\delta} \tag{5}$$

$$\delta = \frac{\int w(s)u(s)^2 ds}{\int w(s)u(s) ds}$$

**Table 8 Seismic Design Structural Unit**

	Longitudinal		Transverse		Seismic Design Unit	
Simple Girder					Regarded as A Unit Consisting of A Substructure and A Part of Superstructure Supported by the Substructure	
Continuous Girder	Support Condition in Longitudinal Direction	Fixed at One Support				
		Fixed at Multiple Supports				
	Difference of Natural Period between Piers		Small			Regarded as A Unit Consisting of Substructures and the Superstructure Supported by the Substructures
			Large			
Arch, Frame and Others						



**Fig.4 Determination of Inertia Force**

where

$w(s)$  : dead weight of the seismic design structural unit (superstructure and substructure above the ground surface assumed in seismic design) at point "s" (tf/m)

$u(s)$  : lateral displacement developed in the seismic design structural unit at point "s" (m) when subjected to  $w(s)$  in the direction considered in design.

iii) determine the seismic coefficient  $k_n$  depending on the natural period  $T$ .

iv) compute inertia force as

$$F_d = k_n \times F \quad (7)$$

where

$F_d$  : shear force (tf) or bending moment (tfm) due to inertia force

$k_n$  : seismic coefficient

$F$  : force developed in the seismic design structural unit when subjected to a lateral force equivalent to the dead weight of the



seismic design structural unit above the ground surface assumed in seismic design (tf/tfm)

For substructures supporting girder bridges, the shear force developed at the center of gravity of the superstructure shall be regarded as the lateral force for seismic design of substructures. However, when the inertia force computed by Eq.(7) is smaller than the inertia force computed by Eq.(3), the latter shall be adopted for design. This needs some explanation. The inertia force computed by Eq.(7) is approximately proportional to the stiffness of each substructure. This implies that the majority of the inertia force tends to be carried by the substructures with higher stiffness. Depending on the stiffness distribution of substructures, the inertia force carried by piers with lower stiffness takes even negative values. However, if failure of the structure, such as at a bearing support, occurs, the contribution of load carried by each substructure will be changed from the distribution computed by Eq.(7). Based on such considerations, a lower limit for the inertia force evaluated by Eq.(7) is included.

#### Strength of Sandy Soil Layer for Liquefaction

##### (1) Sandy Soil Layer Needed to be Checked for Liquefaction

Saturated alluvial sandy layers which have the water table within 10 m from the ground surface and have  $D_{50}$ -values on the grain size accumulation curve between 0.02 and 20. mm are vulnerable to liquefaction up to a depth of 20 m below the ground surface, and liquefaction potential of these layers shall be estimated according to item (2).

##### (2) Estimation of Liquefaction

For those soil layers which are judged to be vulnerable to liquefaction, liquefaction potential shall be checked based on the liquefaction resistance factor  $F_L$  defined as

$$F_L = R / L \quad (8)$$

where

$F_L$  : liquefaction resistance factor

$R$  : resistance of soil elements against dynamic load defined as

$$R = R_1 + R_2 + R_3$$

$$R_1 = 0.0882 \sqrt{\frac{N}{\sigma' + 0.7}}$$

$$R_2 = \begin{cases} 0.19 & (0.02 \text{ mm} \leq D_{50} \leq 0.05 \text{ mm}) \\ 0.225 \text{Log}_{10}(0.35/D_{50}) & (0.05 \text{ mm} < D_{50} \leq 0.6 \text{ mm}) \\ -0.05 & (0.6 \text{ mm} < D_{50} \leq 2.0 \text{ mm}) \end{cases}$$

$$R_3 = \begin{cases} 0.0 & (0 \% \leq F_c \leq 40 \%) \\ 0.004F_c - 0.16 & (40 \% < F_c \leq 100 \%) \end{cases}$$

$N$  : N-value of standard penetration test

$D_{50}$  : averaged grain size on grain size accumulation curve

$F_c$  : fine sand (grain size less than 74  $\mu\text{m}$ ) content

$L$  : dynamic load induced in soil elements during an earthquake

defined as

$$L = r_d \cdot k_s \frac{\sigma_v}{\sigma'_v}$$

$$r_d = 1.0 - 0.015x$$

$x$  : depth from the ground surface (m)

$k_s$  : seismic coefficient for evaluating liquefaction, and shall be determined as

$$k_s = c_z \cdot c_g \cdot c_i \cdot k_{SD}$$

$c_z$ ,  $c_g$  and  $c_i$  : modification factors for zone, ground condition, and importance (refer to Fig. 2, Table 4 and Table 5)

$k_{SD}$  : standard design horizontal seismic coefficient for check of liquefaction (= 0.15)

$\sigma_v$  : total overburden pressure (kgf/cm<sup>2</sup>), and

$$\sigma_v = \{ \gamma_{s1} h_w + \gamma_{s2} (x - h_w) \} / 10$$

$\sigma'_v$  : effective overburden pressure (kgf/cm<sup>2</sup>), and

$$\sigma'_v = \{ \gamma_{s1} h_w + \gamma'_{s2} (x - h_w) \} / 10$$

Soil layers having liquefaction resistance factors,  $F_L$ , smaller than 1.0 shall be judged to liquefy during earthquakes.

### (3) Treatment of Soil Layers Which Were Judged to Liquefy

For those soil layers which were judged to liquefy in the above estimation and which are within 20 m from the ground surface, the spring stiffness and other soil constants shall be either neglected or reduced in seismic design as shown in Fig. 5, by multiplying the original spring stiffness and other soil constants by the reduction factor  $D_E$  which is determined in accordance with  $F_L$ -value and tabulated in Table 9.

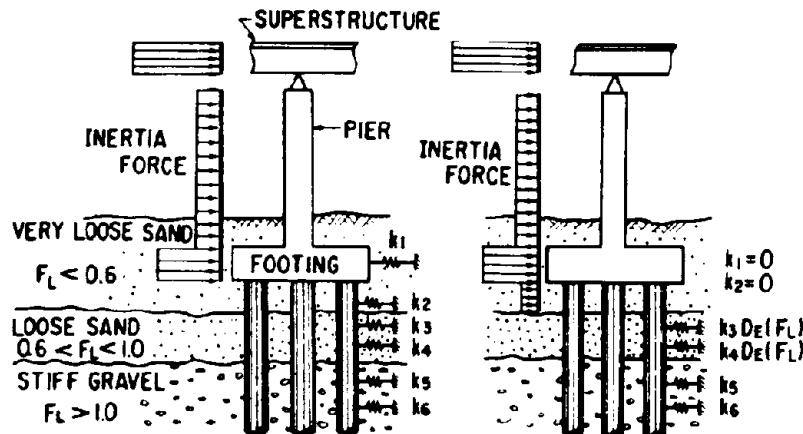


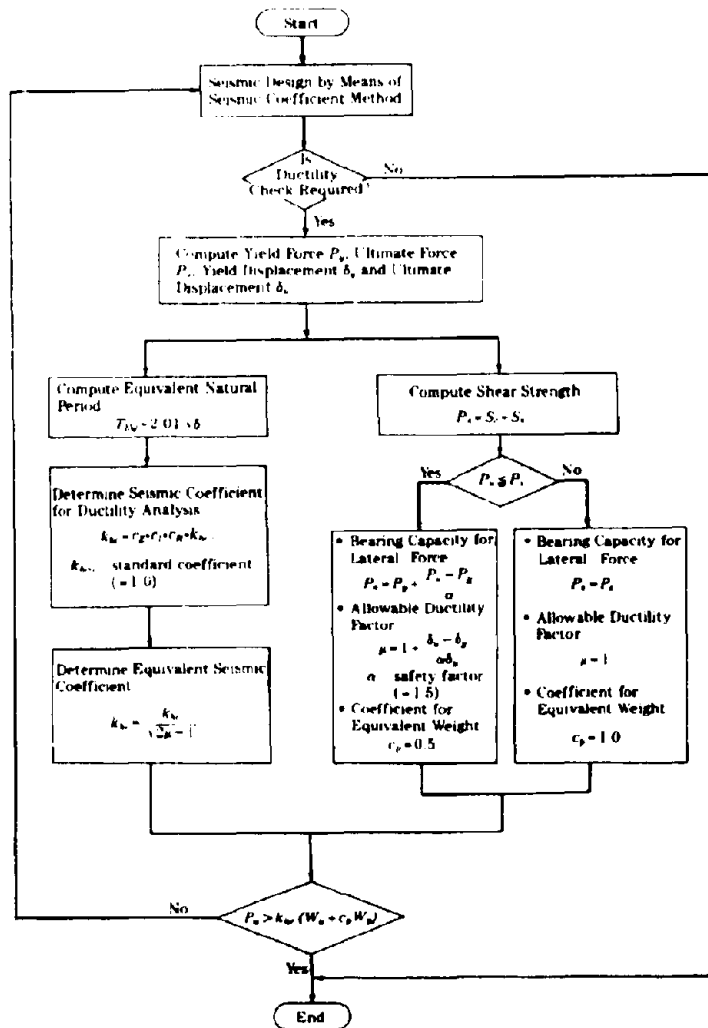
Fig.5 Treatment of Soil Layers Vulnerable to Liquefaction

### Check of Bearing Capacity of Reinforced Concrete Piers for Lateral Force

To prevent reinforced concrete piers from falling in a brittle manner, it is recommended that the bearing capacity of the reinforced concrete piers be checked in accordance with the flow-chart presented in Fig. 6.

**Table 9 Decreasing Rate  $D_E$  of Soil Constants Depending on  $F_L$  Value**

$F_L$ -VALUE	DEPTH FROM GROUND SURFACE	$D_E$
$F_L \leq 0.6$	$0m \leq x \leq 10m$	0
	$10m < x \leq 20m$	1/3
$0.6 < F_L \leq 0.8$	$0m \leq x \leq 10m$	1/3
	$10m < x \leq 20m$	2/3
$0.8 < F_L \leq 1.0$	$0m \leq x \leq 10m$	2/3
	$10m < x \leq 20m$	1



**Fig.6 Check of Bearing Capacity of Reinforced Concrete Pier For Lateral Force**

1) Judgement of bearing capacity of reinforced concrete piers for lateral force

Bearing capacity of reinforced concrete piers for lateral force shall be checked as

$$P_{\Delta} > k_{h\Delta} W \quad (9)$$

where

$P_{\Delta}$  : bearing capacity of the reinforced concrete piers for lateral force (tf)

$k_{h\Delta}$  : equivalent horizontal seismic coefficient for check of bearing capacity of the reinforced concrete piers for lateral load

$W$  : equivalent dead weight (tf), and shall be determined as

$$W = W_1 + C_P W_2 \quad (10)$$

$$C_P = \begin{cases} 0.5 & P_n \leq P_s \\ 1.0 & P_n > P_s \end{cases} \quad (11)$$

$W_1$  : dead weight of a part of superstructure supported by the reinforced concrete piers (tf)

$W_2$  : dead weight of the reinforced concrete piers (tf)

$P_n$  : bearing capacity of reinforced concrete piers for flexural failure (tf)

$P_s$  : bearing capacity of reinforced concrete piers for shear failure (tf)

2) Equivalent horizontal seismic coefficient for check of bearing capacity of reinforced concrete piers for lateral force

Equivalent horizontal seismic coefficient for check of bearing capacity of reinforced concrete piers for lateral force shall be determined according to the equal energy assumption as

$$k_{h\Delta} = \frac{k_{h\Delta 0}}{\sqrt{2\mu - 1}} \quad (12)$$

$$k_{h\Delta 0} = C_2 \cdot C_1 \cdot C_R \cdot k_{h\Delta 0 0} \quad (13)$$

where

$k_{h\Delta}$  : equivalent horizontal seismic coefficient for check of bearing capacity of reinforced concrete piers for lateral force

$k_{h\Delta 0}$  : horizontal seismic coefficient for check of bearing capacity of reinforced concrete piers for lateral force

$\mu$  : allowable ductility factor

$C_2$  : modification factor for zone (refer to Fig. 2)

$C_1$  : modification factor for importance (refer to Table 5)

$C_R$  : modification factor for structural response (refer to Table 10)

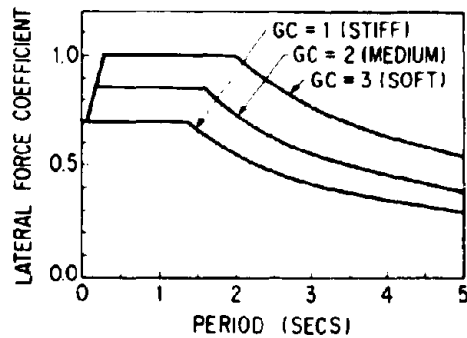
$k_{h\Delta 0 0}$  : standard horizontal seismic coefficient for check of bearing capacity of reinforced concrete piers for lateral force

The standard horizontal seismic coefficient  $k_{h\Delta 0 0}$  was determined to

**Table 10 Structural Response Factor  $c_R$**

Ground Group	Structural Response Coefficient $c_R$		
Group I	$T_{EQ} \leq 1.4$ $c_R = 0.7$		$1.4 < T_{EQ}$ $c_R = 0.876T_{EQ}^{-2/3}$
Group II	$T_{EQ} < 0.18$ $c_R = 1.51 T_{EQ}^{1/3} \geq 0.7$	$0.18 \leq T_{EQ} \leq 1.6$ $c_R = 0.85$	$1.6 < T_{EQ}$ $c_R = 1.16T_{EQ}^{-2/3}$
Group III	$T_{EQ} < 0.29$ $c_R = 1.51T_{EQ}^{1/3} \geq 0.7$	$0.29 \leq T_{EQ} \leq 2.0$ $c_R = 1.0$	$2.0 < T_{EQ}$ $c_R = 1.59T_{EQ}^{-2/3}$

represent a realistic ground motion developed during a significant earthquake with magnitude as large as 8. Fig.7 shows the horizontal seismic coefficient  $k_{hd}$  for the check of bearing capacity of reinforced concrete piers for lateral force when  $c_2 = c_1 = 1.0$ .



**Fig. 7 Horizontal Seismic Coefficient  $k_{hd}$  for Check of Bearing Capacity of Reinforced Concrete Piers for Lateral Force (  $C_z = c_1 = 1.0$  )**

**3) Bearing capacity of reinforced concrete piers for lateral force and allowable ductility factor**

Bearing capacity of reinforced concrete piers for lateral force  $P_d$  and the allowable ductility factor  $\mu$  shall be determined based on the failure mode as :

**a) Flexural failure**

$$P_d = P_v + \frac{P_u - P_v}{\alpha} \tag{14}$$

$$\mu = 1 + \frac{\delta_u - \delta_v}{\alpha \delta_v} \tag{15}$$

where

$P_u, \delta_u$  : bearing capacity (tf) and ultimate displacement (m) for

flexural failure  
 $P_y, \delta_y$  : yielding force (tf) and yielding displacement (m) for  
flexural failure  
 $\alpha$  : safety factor ( = 1.5)

b) Shear failure

$$P_s = P_s \quad (16)$$

$$\mu = 1 \quad (17)$$

where

$P_s$  : bearing capacity (tf) for shear failure

Photos 8 and 9 show dynamic loading tests and shaking table tests conducted to study inelastic behavior of reinforced concrete piers<sup>11,12)</sup>

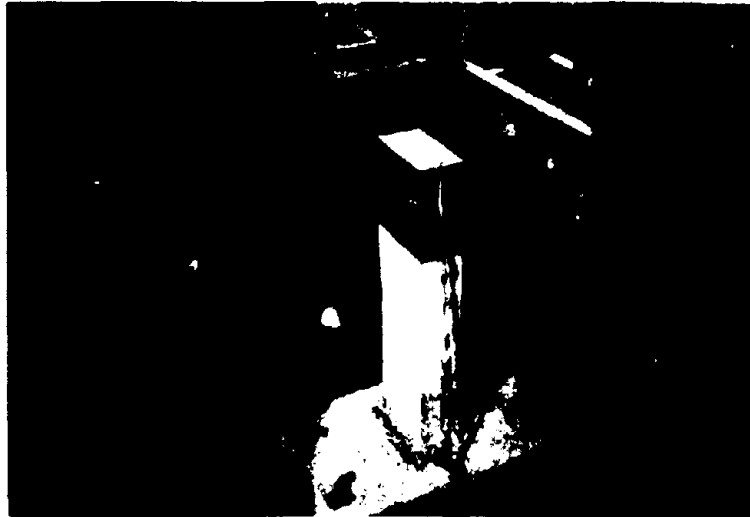


Photo 8 Dynamic Loading Tests of Reinforced Concrete Pier Models

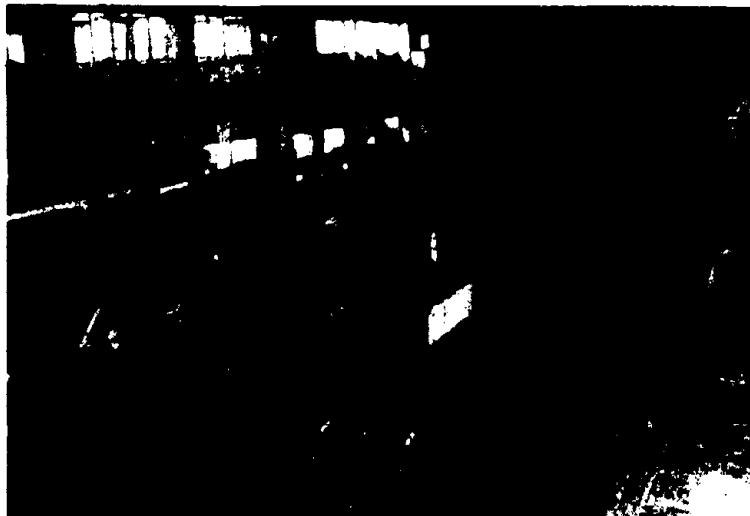


Photo 9 Shaking Table Tests of Reinforced Concrete Pier Supporting Two Span Simply Supported Girders ( Weight = 40 tf)

### Dynamic Response Analysis

For bridges with complicated dynamic response and for new types of bridges, dynamic response analysis is recommended to be made to check seismic safety of the design made by means of the static lateral force method.

In principle, dynamic response analysis shall be made by means of modal response spectral analysis with use of an analytical model which simulates dynamic characteristics of the bridge. Acceleration response spectrum for the modal response spectrum analysis shall be determined as

$$S = c_z \cdot c_i \cdot c_D \cdot S_0 \quad (18)$$

where

$S$  : response spectrum for modal response spectrum analysis (gal (=cm/sec<sup>2</sup>))

$c_z$  : modification factor for zone (refer to Fig. 2)

$c_i$  : modification factor for importance (refer to Table 5)

$c_D$  : modification factor for damping, and shall be determined based on modal damping ratio  $h_i$  as

$$c_D = \frac{1.5}{40h_i + 1} \quad (19)$$

$S_0$  : standard response spectrum for modal response analysis method (gal) (refer to Table 11)

Table 11 Standard Response Spectral Value  $S_0$  for Modal Dynamic Response Analysis

Ground Condition	$S_0$ (gal)		
Group I	$T_i < 0.1$ $S_0 = 431T_i^{1/3} \geq 160$	$0.1 \leq T_i \leq 1.1$ $S_0 = 200$	$1.1 < T_i$ $S_0 = 220/T$
Group II	$T_i < 0.2$ $S_0 = 427T_i^{1/3} \geq 200$	$0.2 \leq T_i \leq 1.3$ $S_0 = 250$	$1.3 < T_i$ $S_0 = 325/T_i$
Group III	$T_i < 0.34$ $S_0 = 430T_i^{1/3} \geq 240$	$0.34 \leq T_i \leq 1.5$ $S_0 = 300$	$1.5 < T_i$ $S_0 = 450/T_i$

Fig. 8 shows the design response spectra assuming  $c_z = c_i = 1.0$  and  $c_D = 1.0$  ( $h_i = 5\%$ ). Fig. 9 shows the modification factor  $c_D$ .

When a time history analysis is required, strong motion records which have the similar characteristics with  $S$  by Eq.(18) shall be used with the consideration on site condition and structural response of the bridge. Three

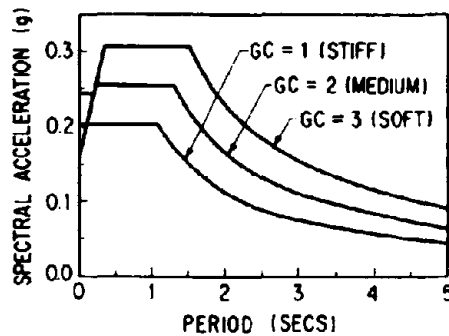


Fig. 8 Design Acceleration Response Spectra  $S_D$  for Dynamic Response Analysis (  $c_z = c_t = 1.0$  and  $c_D = 1.0$  (  $h_t = 0.05$  ) )

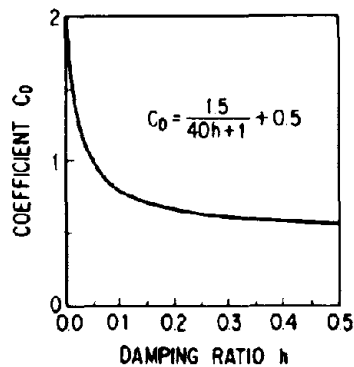


Fig. 9 Modification Factor  $C_0$

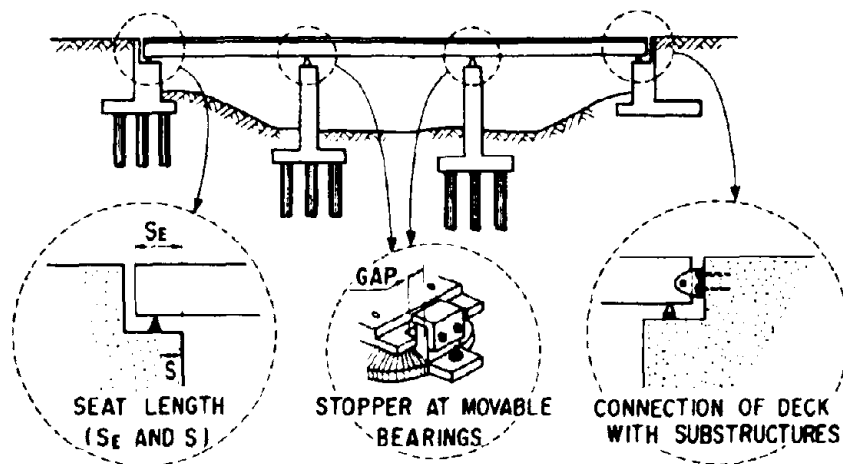
ground acceleration records which were modified in frequency domain so that their response characteristics match with  $S_D$  in Eq.(18) are provided in the Specifications.

#### Device for Preventing Superstructure from Falling

Because connections between superstructure and substructure or between two adjacent superstructures are quite susceptible to earthquake damage, special structural considerations are required to prevent falling-off of the superstructure from the substructures due to damage of those sections. For such a purpose, the following measures are applied as shown in Fig. 10 :

- (1) At movable bearings, devices to prevent dislodgement of upper-bearings from the lower-bearings (stopper) are provided
- (2) At the both ends of superstructure, either of the following measures are used to prevent the superstructure from dislodging from the crest of the substructures :
  - a) The distance from the edge of superstructure to the edge of sub-





**Fig. 10 Devices for Preventing Superstructure from Falling**

structure (Seat Length)  $S_E$  shall be longer than the value as

$$S_E = \begin{cases} 70 + 0.5 \times l & l \leq 100 \text{ m} \\ 80 + 0.4 \times l & l > 100 \text{ m} \end{cases} \quad (20)$$

In which  $S_E$  and  $l$  represent the seat length in cm and the span length in m, respectively.

b) Installation of devices for preventing falling-off of superstructure from substructures

(3) In addition to the Items (1) and (2), the distance from the edge of the bearing supports to the edge of substructure (Bearing Seat Length)  $S$  shall be longer than the value as

$$S = \begin{cases} 20 + 0.5 \times l \\ 30 + 0.4 \times l \end{cases} \quad (21)$$

in which  $S$  and  $l$  represent the bearing seat length in cm and the span length in m, respectively

#### **DEVELOPMENT OF PASSIVE AND HYBRID CONTROL OF HIGHWAY BRIDGES**

##### **Development of Guidelines for Design of Base-Isolated Highway Bridges**

For studying the application of base isolation technology to seismic design of highway bridges, a committee chaired by Professor Tsuneo Katayama, University of Tokyo, was formulated through 1986 to 1989 at the Technology Research Center for National Land Development. Three programs were studied in the committee, i.e., 1) a survey of isolators and energy dissipators which can be used for highway bridges, 2) a study on the key points of the design of base-isolated highway bridges, and 3) design of base-isolated highway bridges. As the final accomplishment of the study,

"Guidelines for Design of Base-Isolated Highway Bridges (draft) " was published in 1989<sup>14)</sup>.

The draft guidelines includes the following contents:

**Chapter 1 General**

- 1.1 Related Regulations
- 1.2 Definition of Terms

**Chapter 2 Fundamental Strategy of Base Isolation Design**

**Chapter 3 Design of Isolators and Energy Dissipators**

- 3.1 General
- 3.2 Design Displacement of Base Isolation Device
- 3.3 Equivalent Natural Frequency and Damping Ratio of Base Isolator
- 3.4 Dynamic Characteristics of Base Isolation Device
- 3.5 Static Characteristics of Base Isolation Device

**Chapter 4 Design of Base-Isolated Highway Bridge**

- 4.1 General
- 4.2 Static Lateral Force Method
  - 4.2.1 General
  - 4.2.2 Horizontal Design Seismic Coefficient
  - 4.2.3 Evaluation of Natural Period of Base-Isolated Bridge
  - 4.2.4 Evaluation of Sectional Force and Displacement due to Inertia Force
- 4.3 Check of Bearing Capacity for Lateral Force
  - 4.3.1 General
  - 4.3.2 Seismic Coefficient used to Check Bearing Capacity for Lateral Force
  - 4.3.3 Evaluation of Natural Period
  - 4.3.4 Evaluation of Damping Ratio
  - 4.3.5 Evaluation of Sectional Force and Displacement due to Inertia Force
  - 4.3.6 Equivalent Seismic Coefficient Used to Check Bearing Capacity for Lateral Force
  - 4.3.7 Bearing Capacity for Lateral Force

**Chapter 5 Dynamic Response Analysis**

- 5.1 Method of Dynamic Response Analysis
- 5.2 Modelling of Base-Isolated Bridges by Dynamic Response Analysis
- 5.3 Input Motion for Dynamic Response Analysis
  - 5.3.1 Input Motion to Check Design by Means of Static Lateral Force Method
  - 5.3.2 Input Motion to Check Bearing Capacity for Lateral Force
- 5.4 Investigation of Safety

**Chapter 6 General Provisions for Design of Structural Details**

- 6.1 General
- 6.2 Distance between Structures
- 6.3 Design Gap of Expansion Joint
- 6.4 Devices for Preventing Falling-off of Superstructure from Sub structure
- 6.5 General Provisions for Design Details of Base Isolation Devices

## Appendix

- I Design of Base-Isolated Highway Bridges
- II Design Method of Base Isolation Devices
- III Example of Design Calculation of a Base-Isolated Highway Bridge  
Constructed on Group I Ground Condition Site
- IV Example of Design Calculation of a Base-Isolated Highway Bridge  
Constructed on Group II Ground Condition Site
- V Example of Structural Details
- VI Example of Various Base-Isolation Devices

### **Joint Research between PWRI and 28 Private Firms for Developing Base Isolation Systems for Highway Bridges**

Based on the study presented above, a joint research program between PWRI and 28 private firms on "Development of Base-isolation Systems for Highway Bridges" was initiated in 1989 for aiming to develop further practical design methods for base-isolated highway bridges which are both safe and cost efficient. The research is scheduled to be completed in 1992.

Scopes of the joint research contain the following research and development programs :

- 1) Development of isolators and energy dissipators suitable for highway bridges by using new materials and technology
- 2) Development of expansion joints and falling-off prevention devices suitable for base-isolated bridges
- 3) Development of design methods for base-isolated bridges
- 4) Application of base-isolation for highway bridges

In the project 1), it is aimed to develop less expensive isolators and energy dissipators which have better characteristics and are superior for long-term use. In the project 4), application of the base isolation for super-long multiple-continuous highway bridges with a total length over 1 km and for the seismic retrofitting of vulnerable existing highway bridges are being investigated.

The 28 private firms consist of material makers such as rubber and automobile tire makers, bearing supports fabricators, consulting engineering firms, steel superstructure fabricating companies, and general constructors.

Table-12 shows the research subjects and contributions. Photos 10 and 11 show dynamic loading tests of isolators and shaking table tests of a base-isolated highway bridges model conducted at the Public Works Research Institute for studying effectiveness of the base isolation.

Table 12 Research Theme and Organizations of Joint Research between the Public Works Research Institute and 28 Private Firms for Developing Base Isolation Systems of Highway Bridges

Research Theme	P	Ka	Si	Ob	Ku	Tn	H	Ni	Su	M	G	Dr	Ti	I	Nk	Ko	Ns	Ol	Y	To	Bs	Bb	Se	Sh	Pc	J	N	Chief	Sub-Chief
1. Development of Device for Isolation																													
1.1 High Energy Absorbing Rubber Bearing								○											○	○	○			○					
1.2 Friction Damper													○									○	○						
1.3 Steel Damper								○							○														
1.4 Link Bearing Develop of																		○											
1.5 Viscous Damper																		○	○	○	○	○	○						
1.6 Test Method	○							○										○	○	○	○	○	○						
2. Development of Expansion Joint and Falling-off Prevention Device for Isolated Bridge																													
2.1 Expansion Joint				○									○																
2.2 Falling-off Prevention Device	○												○					○											
3. Development of Design Method for Isolated Bridge																													
3.1 Design Philosophy	○	○	○	○		○						○	⊙					○							○	○	○		
3.2 Dynamic Responce Analysis Method	○		○		○	⊙		○			○			○															
3.3 Design Method of Device for Isolation	○						○	○				⊙	○				○	○	○	○	○	○	○						
3.4 Simplified Design Method	○	○	⊙		○	○					○	○																	
3.5 Design Method of Expansion Joint and Falling-off Prevention Device	○			○			○																		⊙				
4. Application of Base Isolation to Bridge																													
4.1 Application to Prestressed Concrete Bridge	○	⊙							○	○			○														○		
4.2 Application to Steel Bridge	○												○	○	○											○	○	○	
4.3 Application to Multiple Super-long Bridge	○			⊙					○				○												○	○	○		
4.4 Application to Seismic Retrofit	○									○				○											○	○	○		

P: Public Works Research Institute, Ka: Kajima, Si: Shimizu, Ob: Ohbayashi, Ku: Kumagai, Tn: Takenaka Doboku + Takenaka, H: Hazama, Ni: Nishimatsu, Su: Sumitomo, M: Mitsui, G: Goyoh, Ok: Okumura, Ti: Taisei + Tokyo Fabric + Nippon Chuzo, I: Ishikawajima Harima, Nk: NKK + Nippon Chuzo, Ko: Kobe Steel, Ns: Nippon Seiko, Oe: Oiles, Y: Yokohama Rubber, To: Toyo Rubber, Bs: Bridgestone, Bb: BBM, Se: Seibu Polymer, Sh: Showa Densen, Pc: Pacific Consultants, J: Japan Engineering Consultant, N: New Structural Engineering Consultants.

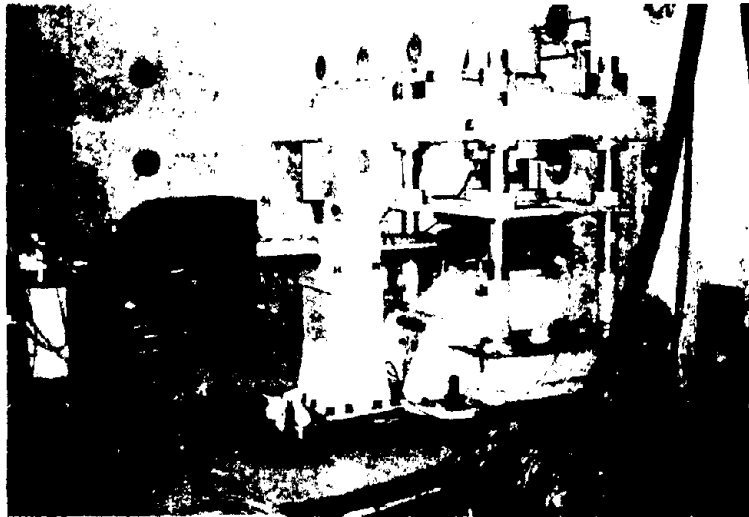


Photo 10 Dynamic Loading Tests of Isolators and Energy Dissipators

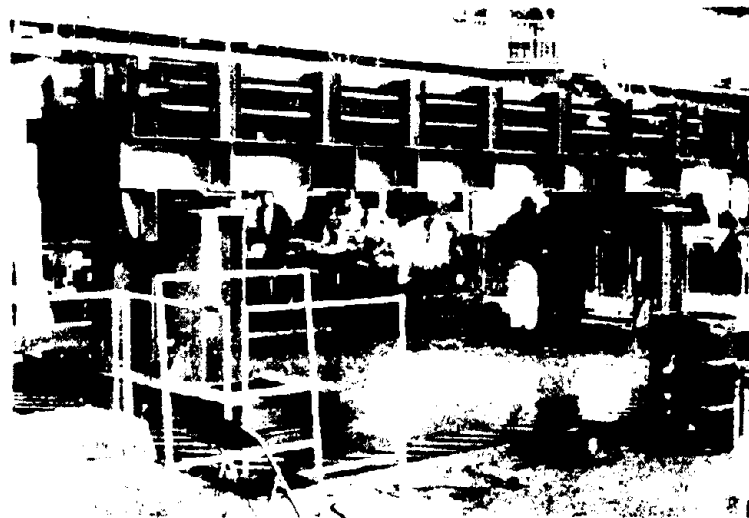


Photo 11 Shaking Table Tests of a Base Isolated Bridge Model

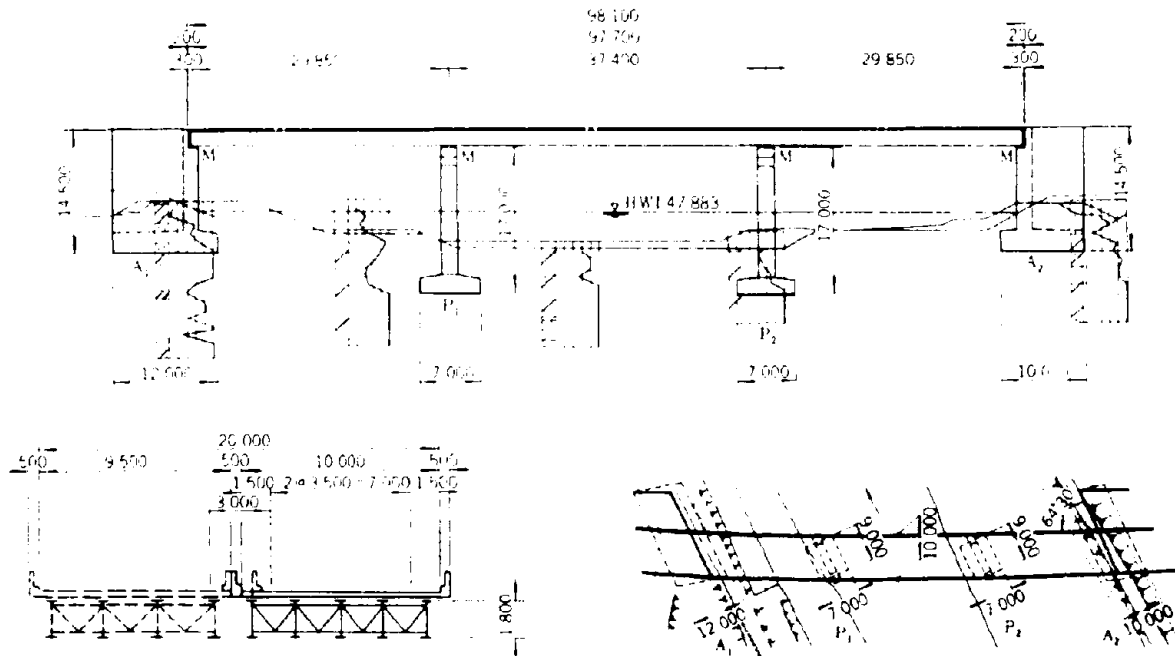
#### Construction of Base-Isolated Highway Bridges

Seven base-isolated highway bridges as shown in Table-13 are currently being constructed by or with the support of the Ministry of Construction for the purpose of incorporating base isolation in practical use. After completion of the construction, a series of experiments including push-pull tests, forced excitation tests with use of eccentric-mass shakers and strong motion observations are scheduled for studying the dynamic characteristics of the bridges.

Fig.11 shows the Nagaki-gawa Bridge<sup>16)</sup> which is now under construction by the Ministry of Construction.

**Table 13 Construction Project of Base-Isolated Highway Bridges**

Owner	Bridge Name	Type of Super-structure	Length (m)
Hokkaido Developing Bureau	Onnetoh Bridge	Steel Girder	456
Tohoku-Regional Bureau, MOC	Nagaki-gawa Bridge	"	97
Kantoh-Regional Bureau, MOC	Not Yet Selected	Not Yet Decided	Not yet Determined
Chubu-Regional Bureau, MOC	"	"	"
Iwate-ken	Manuki Bridge	Prestressed Concrete	92
Tochigi-ken	Karasuyama Bridge	"	250
Shizuoka-ken	Miyagawa Bridge	Steel Girder	110



**Fig. 11 General View of Nagaki-gawa Bridge**

**Hybrid Control of Structural Response**

A combination of active and passive control, which is designated here as hybrid control, seems attractive for reducing energy supply for active control. Decrease of structural response by means of passive control will make the energy supply requirement for active control small enough to achieve the control of structural response within a satisfactory level during significant earthquakes. Increase of lateral displacement of decks induced by the passive control may be improved by the active control.

A 5-year research program on hybrid control of seismic response was initiated in 1990 at the Public Works Research Institute<sup>17)</sup>. The objectives of this research program are to study applications of hybrid control for

bridge structures such as

- 1) Control of super long-span continuous bridges
- 2) Control of bridges on relatively soft ground
- 3) Improvement of seismic performance of bridges on the important urban routes

As part of this research, the following items are considered for study :

- 1) Development of passive control elements suitable for hybrid control systems
  - Development of variable dampers
  - Development of damper with fail-safe functions
- 2) Development of active control systems suitable for hybrid control
- 3) Development of optimal hybrid control systems by combining 1) and 2)

Among these developments, the variable damper is quite a unique device in which the viscous coefficient is varied depending on structural response displacement and velocity so that the best energy dissipation can be made. The viscous coefficient is also controlled to increase smoothly after the structural response displacement becomes excessively large so that the variable damper acts as a stopper.

This research program is to be executed as a U.S.-Japan cooperative research program through the Panel on Wind and Seismic Effects of UJNR.

## **SEISMIC INSPECTION AND SEISMIC STRENGTHENING**

### **Outline**

The nationwide seismic inspection and seismic strengthening of highway bridges were made in 1971, 1976, 1979, 1986 by the Ministry of Construction. The first and second seismic inspection of 1971 and 1976 were to inspect deteriorated highway bridges susceptible to falling-off of superstructure during earthquakes. The third and fourth seismic inspection of 1979 and 1986 was to classify structural resistance of highway bridges against falling-off of superstructures during destructive earthquakes. For those bridges which were judged vulnerable to severe damages during earthquakes, seismic strengthening works have been made. In the 1986 inspection, about 40,000 bridges were inspected and 11,700 bridges were found to require seismic strengthening. Most of them require installation of the device for preventing superstructure falling-off from the substructures.

### **Seismic Inspection of Vulnerability of Highway Bridges**

Seismic inspection methods to detect highway bridges vulnerable to earthquakes have been developed and amended several times to reflect progress of bridge earthquake engineering and lessons gained from the past seismic damage. The most important requirement for the inspection method was

to be able to assess the vulnerability of a number of highway bridges at the site without complex calculations. The latest seismic inspection method<sup>1,2)</sup> which was referenced in the 1986 seismic inspection was formulated on the statistical analyses of 105 bridges damaged in the past earthquakes<sup>20)</sup>.

In the statistical analyses, factors which are likely to affect the seismic vulnerability of highway bridges were firstly studied with use of the Type II quantification analysis. The rank of damage degree was classified into high vulnerability (Rank A), moderate vulnerability (Rank B) and low vulnerability (Rank C) as shown in Table 14. From the analysis of the past seismic damage, 15 items, as shown in Table 15, were selected as the factors likely to affect seismic vulnerability. The 15 items consists of four principal factors, i.e., intensity of earthquake ground motions, properties of superstructure and substructures, devices for preventing falling-off of superstructure from substructures, and ground condition. Each item was further divided into several categories.

**Table 14 Definition of Seismic Vulnerability**

Rank	Vulnerability of Seismic Damage	Rank of Damage Degree in Table 1
Rank A - High Vulnerability	Possibility for suffering damage or damage degree is high	5: Falling off of Superstructure or 4: Extensive Damage
Rank B - Moderate Vulnerability	Possibility for suffering damage or damage degree is moderate	3: Moderate Damage
Rank C - Low Vulnerability	Possibility for suffering damage or damage degree is low	2: Slight Damage or 1: Minor Damage or 0: No Damage

Predicted damage rank  $y_i$  was assumed to have a form of

$$y_i = \sum_j \sum_k \delta_{ijk} \cdot x_{jk} \quad (22)$$

In which  $x_{jk}$  represents a weighting factor for the k-th category of the j-th item, and  $\delta_{ijk}$  represents a variable corresponding to the category k in the item j of the i-th bridge. The variable  $\delta_{ijk}$  was so defined that it takes a value of 1 if the characteristics of the i-th bridge correspond to the category k in the item j, and is 0 otherwise. The weighting factor  $x_{jk}$  was determined so as to minimize the sum of square of the difference between the predicted damage rank and the actual damage rank.

From the weighting factors presented in Table 15, the effects of each item were found as shown in Table 16. The following considerations were subsequently included in the statistical analysis to formulate an inspection method.

a) Because the objectives of the inspection method are to assess the seismic vulnerability of highway bridges subjected to ground shaking of JMA Intensity V or larger ( peak ground acceleration larger than 0.25 g), the Intensity of Peak Ground Acceleration  $a_{m,ex}$  is dropped from the evaluation item assuming that  $a_{m,ex}$  is larger than 0.25 g.



Reproduced from  
best available copy

Table 15 Items and Categories Which Affect Seismic Vulnerability of Highway Bridges

Item	Category	Seismic Damage Rank					Results of Statistical Analysis			
		0 No Damage	1 Minor Damage	2 Slight Damage	3 Moderate Damage	4 Extensive Damage	5 Falling off of Superstructure	Normalized Score	Range	Partial Correlation Coefficient
1 Intensity of Peak Ground Acceleration Area (cm/sec <sup>2</sup> )	Less than 200	1 ( 5%)			1 ( 5%)			0.169		
	200 g area < 300	13 ( 68%)	5 ( 42%)	36 ( 65%)	8 ( 40%)	1 ( 13%)		-0.283		
	300 g area < 400	5 ( 26%)	5 ( 42%)	18 ( 33%)	10 ( 50%)	6 ( 25%)	4 ( 40%)	0.176	1.219	0.343
	400 g area < 500		2 ( 17%)	7 ( 2%)	1 ( 5%)	1 ( 13%)	2 ( 20%)	0.936		
	500 g area						4 ( 40%)	0.616		
2 Design Specifications	1926 or 1939	1 ( 5%)		6 ( 11%)	6 ( 30%)	5 ( 63%)	7 ( 70%)	0.517		
	1956 or 1964	17 ( 89%)	8 ( 50%)	41 ( 75%)	11 ( 55%)	3 ( 18%)	3 ( 30%)	0.223	0.740	0.319
	1971 or 1980	1 ( 5%)	6 ( 50%)	8 ( 15%)	3 ( 15%)			0.284		
	Girder or Simply Supported Girders (2 or More Spans)	12 ( 63%)	7 ( 68%)	40 ( 73%)	17 ( 85%)	8 ( 100%)	10 ( 100%)	0.381		
	One span Simply Supported Girders or Continuous Girders with 2 spans or More	5 ( 26%)	4 ( 28%)	11 ( 20%)	2 ( 10%)			-0.232	0.390	0.161
3 Type of Superstructure	Arch Frame One span Two span Continuous Girders Cable Stayed Bridge Suspension Bridge	2 ( 11%)	2 ( 17%)	4 ( 7%)	1 ( 5%)			0.318		
	Skewed or Curved	3 ( 16%)	1 ( 8%)	4 ( 7%)				0.396		
4 Shape of Superstructure	Straight	16 ( 84%)	11 ( 91%)	51 ( 93%)	20 ( 100%)	8 ( 100%)	10 ( 100%)	0.027	0.474	0.122
	RC or PC	2 ( 32%)	3 ( 42%)	22 ( 40%)	7 ( 35%)	1 ( 13%)	6 ( 60%)	-0.141	0.233	0.131
5 Materials of Superstructure	Steel	12 ( 63%)	7 ( 58%)	31 ( 60%)	13 ( 65%)	7 ( 68%)	4 ( 40%)	0.092		
	6% or Steeper			1 ( 2%)		1 ( 13%)	1 ( 10%)	0.919		
6 Slope in Bridge Axis	Less than 6%	14 ( 100%)	12 ( 100%)	54 ( 98%)	10 ( 100%)	7 ( 68%)	9 ( 90%)	-0.013	0.941	0.161
	None	1 ( 5%)	1 ( 8%)	20 ( 36%)	8 ( 40%)	6 ( 25%)	10 ( 100%)	0.459		
7 Device to Prevent Falling off of Superstructure	One Device	16 ( 83%)	6 ( 50%)	26 ( 51%)	11 ( 55%)	2 ( 25%)		-0.181	1.106	0.358
	Two Devices or More	2 ( 11%)	5 ( 42%)	7 ( 13%)	1 ( 5%)			-0.647		
	Single wire Bent Pile	1 ( 5%)		5 ( 9%)	2 ( 10%)		3 ( 30%)	0.292		
	Reinforced Concrete Frame	1 ( 5%)	1 ( 8%)	9 ( 16%)	8 ( 40%)	4 ( 50%)	4 ( 40%)	0.259	0.411	0.178
8 Type of Substructure	Others	12 ( 89%)	11 ( 92%)	41 ( 75%)	10 ( 50%)	4 ( 50%)	3 ( 30%)	-0.114		
	10m < H	4 ( 21%)	5 ( 42%)	12 ( 22%)	8 ( 40%)	2 ( 25%)	3 ( 30%)	0.172		
9 Height of Pier H	5m < H < 10m	7 ( 37%)	3 ( 25%)	29 ( 53%)	7 ( 35%)	6 ( 25%)	5 ( 50%)	-0.038	0.284	0.125
	H < 5m	8 ( 42%)	4 ( 33%)	14 ( 25%)	5 ( 25%)		2 ( 20%)	-0.112		
	Extremely Soft in Group 4	1 ( 5%)			1 ( 5%)	2 ( 25%)		0.523		
10 Ground Condition	Group 4	5 ( 26%)		2 ( 4%)	11 ( 35%)	4 ( 50%)	7 ( 70%)	0.224		
	Group 3	3 ( 16%)	8 ( 61%)	33 ( 60%)	6 ( 30%)	1 ( 13%)	3 ( 30%)	0.040	0.983	0.273
	Group 2	1 ( 5%)	1 ( 8%)	8 ( 15%)	1 ( 5%)			0.112		
	Group 1	9 ( 47%)	3 ( 23%)	12 ( 22%)	1 ( 5%)	1 ( 13%)		-0.461		
11 Irregularity of Supporting Ground	Irregular		1 ( 8%)	1 ( 2%)	4 ( 20%)	1 ( 13%)		0.307	0.420	0.104
	Almost Uniform	19 ( 100%)	11 ( 92%)	54 ( 98%)	16 ( 80%)	7 ( 88%)	10 ( 100%)	-0.024		
12 Effect of Soil Liquefaction	Liquefiable			4 ( 7%)	2 ( 10%)	2 ( 25%)	6 ( 60%)	0.724		
	Non liquefiable	10 ( 100%)	12 ( 100%)	51 ( 93%)	18 ( 90%)	6 ( 25%)	4 ( 40%)	-0.092	0.816	0.255
13 Effect of Scouring	Recognized				1 ( 5%)			0.312		
	None	19 ( 100%)	12 ( 100%)	55 ( 100%)	19 ( 95%)	8 ( 100%)	10 ( 100%)	-0.003	0.315	0.033
14 Materials of Substructure	Plane Concrete in Accordance with 1926 Specs or 1939 specs				1 ( 5%)		2 ( 20%)	0.995		
	RC PC Steel or Unreinforced Concrete in Accordance with Specs. in 1956 or Later	19 ( 100%)	12 ( 100%)	55 ( 100%)	19 ( 95%)	8 ( 100%)	8 ( 80%)	-0.025	1.020	0.167
15 Type of Substructure	Timber Brick Masonry Other Old Unknown Materials		1 ( 8%)	1 ( 2%)	1 ( 5%)	1 ( 13%)	4 ( 40%)	0.383		
	RC Piles Pedestal Piles or Pier Supported by Two Independent Carsons	2 ( 11%)	1 ( 8%)	9 ( 16%)	4 ( 20%)	2 ( 25%)	2 ( 20%)	-0.314	0.697	0.171
	Foundations Designed by Specs in 1971 or Later	17 ( 89%)	10 ( 83%)	45 ( 82%)	15 ( 75%)	5 ( 63%)	4 ( 40%)	0.034		

**Table 16 Factors Which Affect Seismic Vulnerability of Highway Bridges**

Items	Seismic Vulnerability
① Design Specifications	Those designed in accordance with 1926 or 1939 Specifications have higher vulnerability
② Type of Superstructure	<ul style="list-style-type: none"> <li>• Gerber or simply supported girders with 2 or more spans have higher vulnerability</li> <li>• Arch, frame, continuous girders, cable-stayed bridges or suspension bridges have lower vulnerability</li> </ul>
③ Shape of Superstructure	Skewed or curved bridges do not necessarily have higher vulnerability than straight bridges
④ Materials of Superstructure	Reinforced concrete bridges or prestressed concrete bridges have lower vulnerability than steel bridges although the difference is small
⑤ Slope in Bridge Axis	Bridges with slope in bridge axis have higher vulnerability
⑥ Device for Preventing Falling-off of Superstructure	Bridges with devices for preventing falling-off of superstructure have lower vulnerability
⑦ Type of Substructure	Bridges supported by single-line bent piles or by reinforced concrete frame placed on two separate caisson foundations have higher vulnerability
⑧ Height of Piers	Bridges supported by higher piers have higher vulnerability
⑨ Ground Condition	Bridges constructed on soft soil have higher vulnerability
⑩ Effect of Soil Liquefaction	Bridges constructed on sandy soil layers susceptible to liquefaction have higher vulnerability
⑪ Irregularity of Supporting Soil Condition	Bridges constructed on soils with irregularity of supporting conditions have higher vulnerability
⑫ Effect of Scouring	Bridges where the surface soils are scoured have higher vulnerability
⑬ Materials of Substructures	Bridges supported by plane-concrete substructures designed in accordance with 1926 or 1939 specifications have higher vulnerability
⑭ Type of Foundation	Bridges supported by timber, brick, masonry or other old unknown type substructures have higher vulnerability
⑮ Intensity of Ground Motion	Bridges subjected to higher intensity of ground acceleration have higher vulnerability. In particular, vulnerability becomes quite high when the bridges are subjected to peak ground acceleration larger than 400 gal (0.4g)

b) Evaluation of the strength of reinforced concrete piers at the mid-height where main reinforcement is terminated was introduced.

c) Because collapse, such as falling-off of superstructure, generally occurred because of excessive relative movements between the superstructure and the substructures, and failure of substructures due to inadequate strength, the evaluation of the seismic vulnerability for both the relative movement and for the strength of substructures should be made.

d) Even if there are some unsatisfactory conditions in the evaluation, final evaluation may not consider them to be critical if the remaining factors are in good evaluation. Consequently, it was decided that those bridges with at least one "critical" or "safe" condition are to be considered

to have either high or low seismic vulnerability. Below are some examples of evaluation of such specific types of structure :

- Those designed in accordance with the 1980 Specifications shall be classified into Rank C (safe) unless appreciable deterioration is detected
- Those constructed by timber, brick, masonry, or old unknown materials shall be classified into Rank A (vulnerable).
- Those supported by single-line bent piles foundation which are constructed on loose alluvial sandy layer vulnerable to liquefaction or very loose clayey deposits shall be classified into Rank A (vulnerable).
- Single-span simply supported girder bridges with the span length less than 15 m shall be classified into Rank C (safe).

The procedure of seismic inspection and an inspection sheet are shown in Fig. 12 and Table 17, respectively. The evaluation of the seismic vulnerability is made in accordance with the points which reflect the vulnerability to excessive relative movement between superstructure and substructures (point X), and the strength of substructures (point Y) as shown in Table 18.

**Table 18 Evaluation of Seismic Vulnerability**

Rank of Seismic Vulnerability	Evaluation Points		
	X	Y	P
A - Vulnerable	$X \geq 60$	$Y \geq 10$	$P \geq 10$
B - Moderate	$20 \leq X < 60$	$5 \leq Y < 10$	$50 \leq Y < 100$
C - Safe	$X < 20$	$Y < 5$	$Y < 50$

Note: Out of two ranks obtained from X point and Y point, higher rank (A is the highest) should be taken as the final ranking of the bridge inspected. For obtaining evaluation points X and Y, refer to Table 2

### Seismic Strengthening of Highway Bridges Vulnerable to Earthquakes

Table 19 shows the feasibility of seismic strengthening against the 16 factors which would affect the seismic vulnerability of highway bridges (refer to Table 16). Among the 16 factors, ⑥ Devices for Preventing Falling-off of the Superstructure, ⑦ Type of Substructure, ⑩ Effect of Soil Liquefaction, ⑪ Effect of Scouring, ⑬ Materials of Substructures, ⑭ Types of Foundation, and ⑮ Effect of Termination of Main Reinforcement at Mid-height are the factors for which countermeasures for strengthening the bridge are feasible. Countermeasures against for the remaining 9 factors can not be made unless the whole bridge be replaced.

Fig. 13 shows how the countermeasures can be made for the above described 7 factors. Installation of devices for preventing falling-off of superstructure, strengthening of foundations, and strengthening of piers and abutments are the main measures of seismic strengthening.

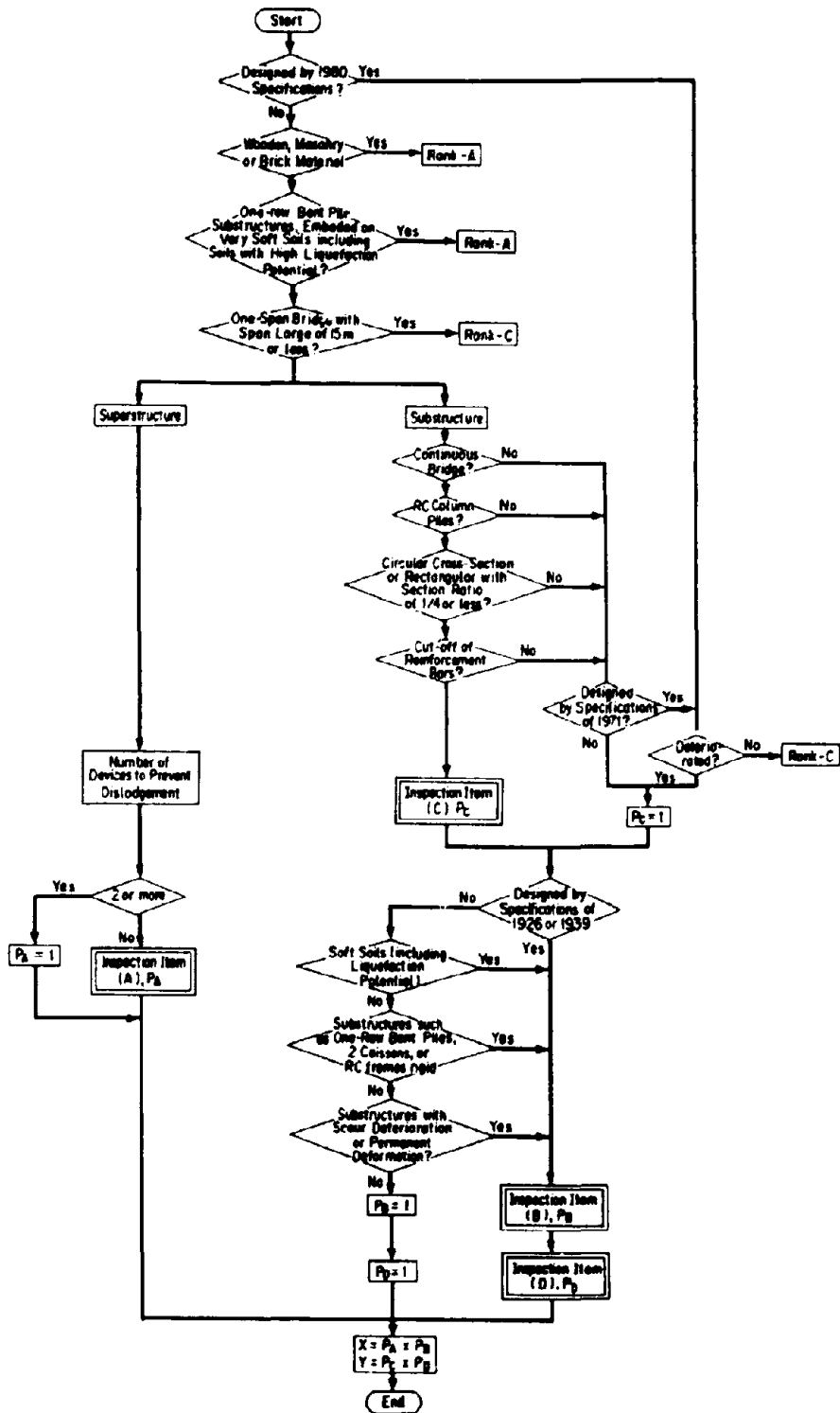


Fig. 12 Procedure of Seismic Inspection for Highway Bridges

Reproduced from  
best available copy

Table 17 Inspection Sheet for Seismic Vulnerability of Highway Bridges

Point of Inspection	Factors of Inspection	Evaluation		
Inspection for Vulnerability to Develop Excessive Deterioration	1. Design Specifications	4.0 1926 Specs or 1939 Specs	2.0 1956 Specs or 1964 Specs	1.0 1971 Specs or 1980 Specs
	2. Superstructure Type	3.0 Gerber Girder or Simply supported Girders with Two Spans or More	1.5 Simply supported Girder or Continuous Girders Consisting of Two Spans or More	1.0 Arch, Flare, Continuous Girder (One Span), Cable-stayed Bridge, Suspension Bridge
	3. Shape of Superstructure	1.2 Skewen or Curved Bridge	1.0 Straight Bridge	
	4. Materials of Superstructure	1.2 RC or PC	1.0 Steel	
	5. Gradient	1.2 6% or Steeper	1.0 Less Than 6%	
	6. Falling off Prevention Device	2.0 None	1.0 One Device	
	$P_a = 1 + 2 + 3 + 4 + 5 + 6$	$P_a =$		
	7. Type of Substructure	2.0 Single pile Bent, Pier Foundation	1.0 Others	
	8. Height of Pier, H	2.0 $H > 10m$	1.5 $5 < H < 10m$	1.0 $H < 5m$
	9. Ground Condition	5.0 Extremely Soft in Group 4	2.5 Group 4	2.0 Group 3 1.0 Group 2 1.0 Group 1
Inspection for Deterioration of Substructure	1. Effects of Liquefaction	2.0 Liquefiable	1.0 Non liquefiable	
	2. Supporting Ground Condition	1.2 Irregular	1.0 Almost Uniform	
	3. Scouring	1.5 Recognized	1.0 None	
	$P_b = 1 + 2 + 3 + 4 + 5 + 6 + 7 + 8 + 9$	$P_b =$		
	4. Linear Spacing Ratio, $h/d$	2.0 $1 < h/d < 4$	1.0 $h/d \geq 4$	0.5 $h/d \geq 1$
Inspection for Strength of RC Pier at Termination of Reinforcement	1. Tension Cracks at Flexure at Terminated Point of Main Reinforcement	2.0 Cracks Will Occur	1.0 Cracks Will Possibly Occur	0.3 Cracks will Not Occur
	2. Safety Factor for Tensile Strength at Terminated Section of Main Reinforcement	3.0 $S_1 < 1.1$ 3.0 $S_2 < 1.1$	2.0 $1.1 < S_1 < 1.5$ 2.0 $1.1 < S_2 < 1.3$	0.5 $S_1 \geq 1.5$ 1.0 $1.3 < S_2 < 1.5$ 0.5 $S_2 \geq 1.5$
Inspection for Vulnerability to Develop Failure Due to Inadequate Strength of Substructure	3. Shear stress $\sigma < 45$	3.0 $\sigma < 45$	2.0 $30 \leq \sigma < 45$	1.0 $15 \leq \sigma < 30$ 0.5 $\sigma < 15$
	$P_c = 1 + 2 + 3 + 4 + 5 + 6 + 7 + 8 + 9 + 10 + 11 + 12$	$P_c =$		
	7. Failure of Fixed Supports and Proximity	5.0 Extensive Failure	2.0 Small Failure	1.0 None
	8. Extraordinary Damage of Pier	5.0 Extensive Damage	2.0 Small Damage	1.0 None
	9. Materials of Substructure	2.0 Plane Concrete Older Than 1926 Excluding Gravity type Abutment	1.0 Others	
Inspection for Strength of Substructure	10. Construction method of Foundation	2.0 Timber Pile, Masonry Brick, Other Old Construction Methods	1.5 RC Piers, Pedestal Piers, Pier Supported by Two Independent Caissons	1.0 Foundation Designed by 1971 Specs. and Other Later Specs
	11. Foundation Type	1.5 RC Flare Supported by Two Independent Caisson Foundations	1.0 Others	
	12. Extraordinary Failure of Foundation	2.0 Recognized	1.0 None	
$P_d = 11 + 12 + 13 + 14 + 15 + 16 + 17 + 18$		$P_d =$		
Evaluation of Deformation and Strength		$X = P_a + P_b =$	and	$Y = P_c + P_d =$

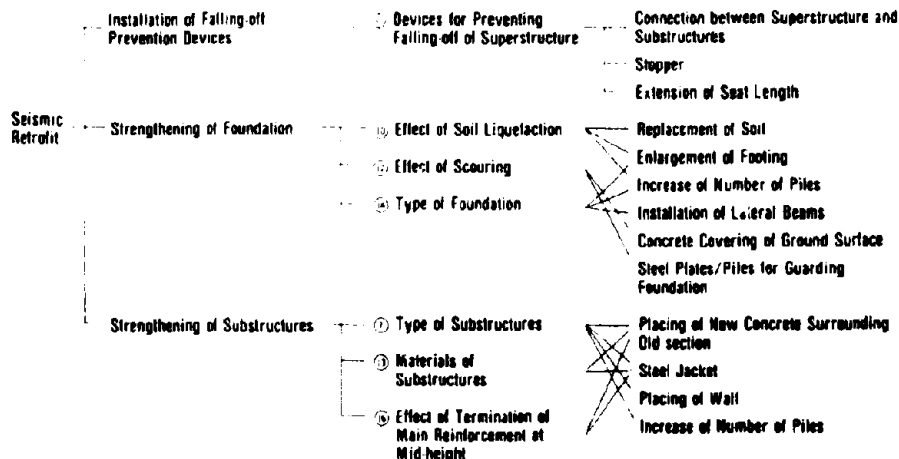


Fig. 13 Selection of Seismic Strengthening Measures for Highway Bridges

**Table 19 Feasibility of Seismic Strengthening for 16 Factors Which Affect Seismic Vulnerability of Highway Bridges**

Items	Feasibility of Seismic Strengthening	Principles of Countermeasures
① Design Specifications	×	—————
② Type of Superstructure	×	—————
③ Shape of Superstructure	×	—————
④ Materials of Superstructure	×	—————
⑤ Slope in Bridge Axis	×	—————
⑥ Device for Preventing Falling-off of Superstructure	○	Installation of Devices
⑦ Type of Substructure	○	Strengthening of Substructures
⑧ Height of Piers	×	—————
⑨ Ground Condition	×	—————
⑩ Effect of Soil Liquefaction	○	Strengthening of Foundations or Strengthening of Surrounding Soils
⑪ Irregularity of Supporting Soil Condition	×	—————
⑫ Effect of Scouring	○	Treatment for Prevention of Scouring, or Strengthening of Foundations
⑬ Materials of Substructures	○	Strengthening of Substructures
⑭ Type of Foundation	○	Strengthening of Foundations
⑮ Intensity of Ground Motion	×	—————
⑯ Effect of Termination of Main Reinforcement at Mid-height	○	Strengthening of Substructures

Note ○ Items for which seismic strengthening is feasible  
 × Items for which seismic strengthening is not feasible

Figs. 14, 15 and 16 show the methods for selecting the installation of the stoppers at movable supports, falling-off prevention devices, and elongation of seat length  $S_E$  and bearing seat length  $S$  as measures of seismic strengthening for existing bridges. The methods are based on a number of practices in the past<sup>12), 20)</sup>.

Figs. 17 and 18 show measures for strengthening foundations and strengthening substructures for existing bridges, respectively.

Photos 12 and 13 show dynamic loading tests of reinforced concrete piers which have the termination of main reinforcement at mid-height. Effectiveness of steel jacket is studied.

The seismic inspection and strengthening methods of transportation facilities including highway bridges were compiled and published from the Japan Road Association in the form of the "Guide Specifications for Earthquake Hazard Mitigation for Transportation Facilities - Pre-Earthquake Countermeasures -" in 1987<sup>21)</sup>.

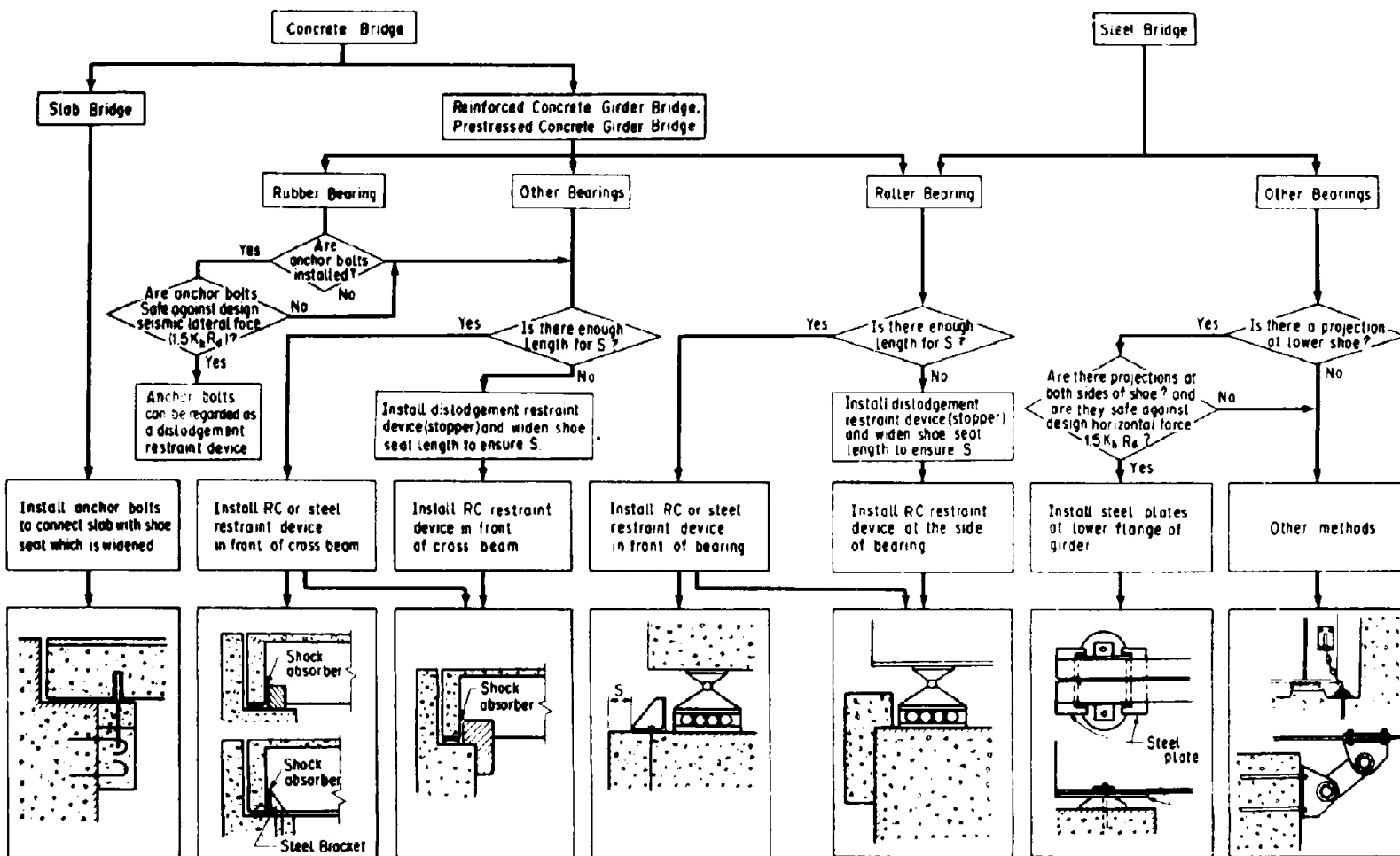


Fig. 14 Installation of Stopper at Movable Bearings for Existing Bridges

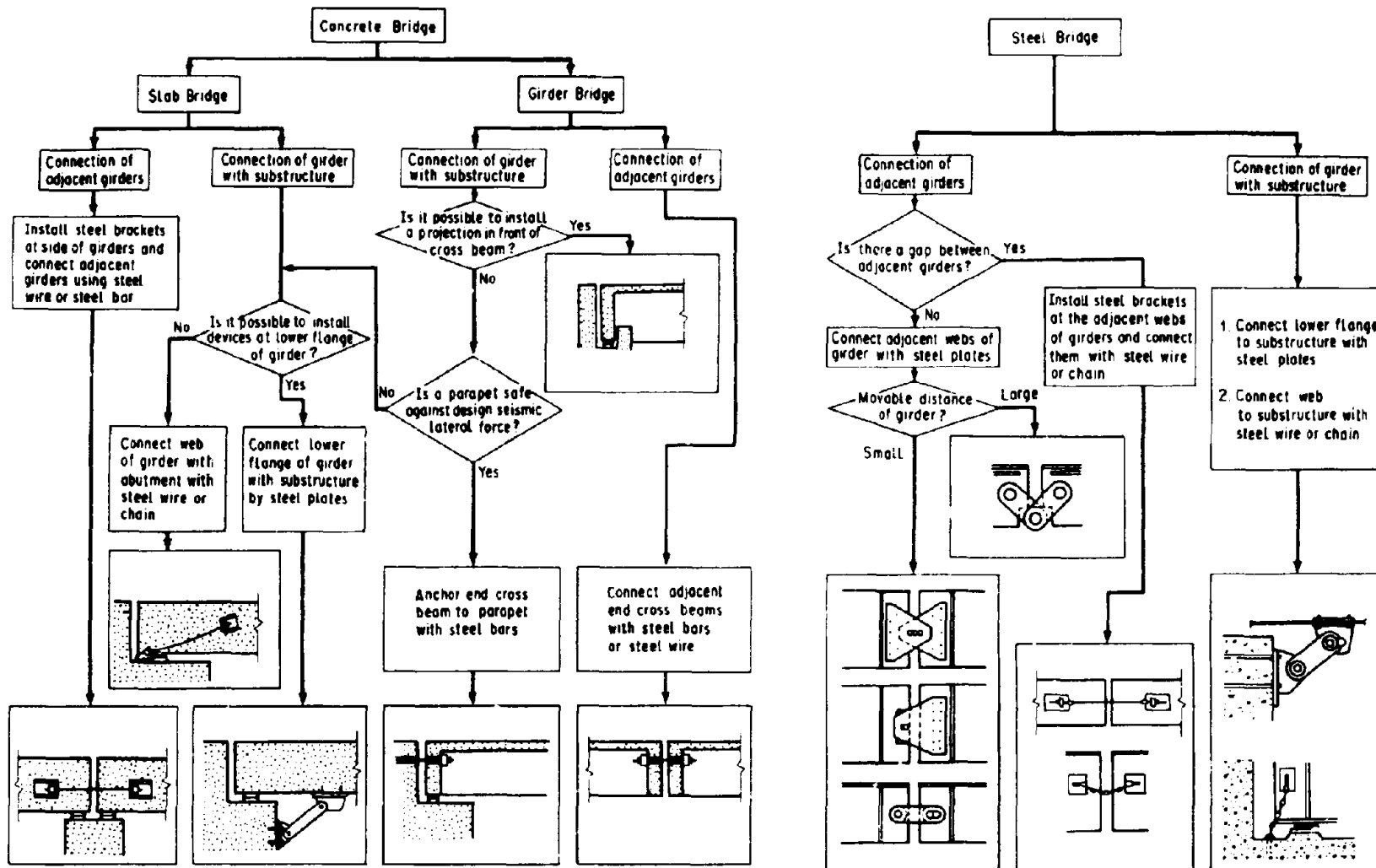
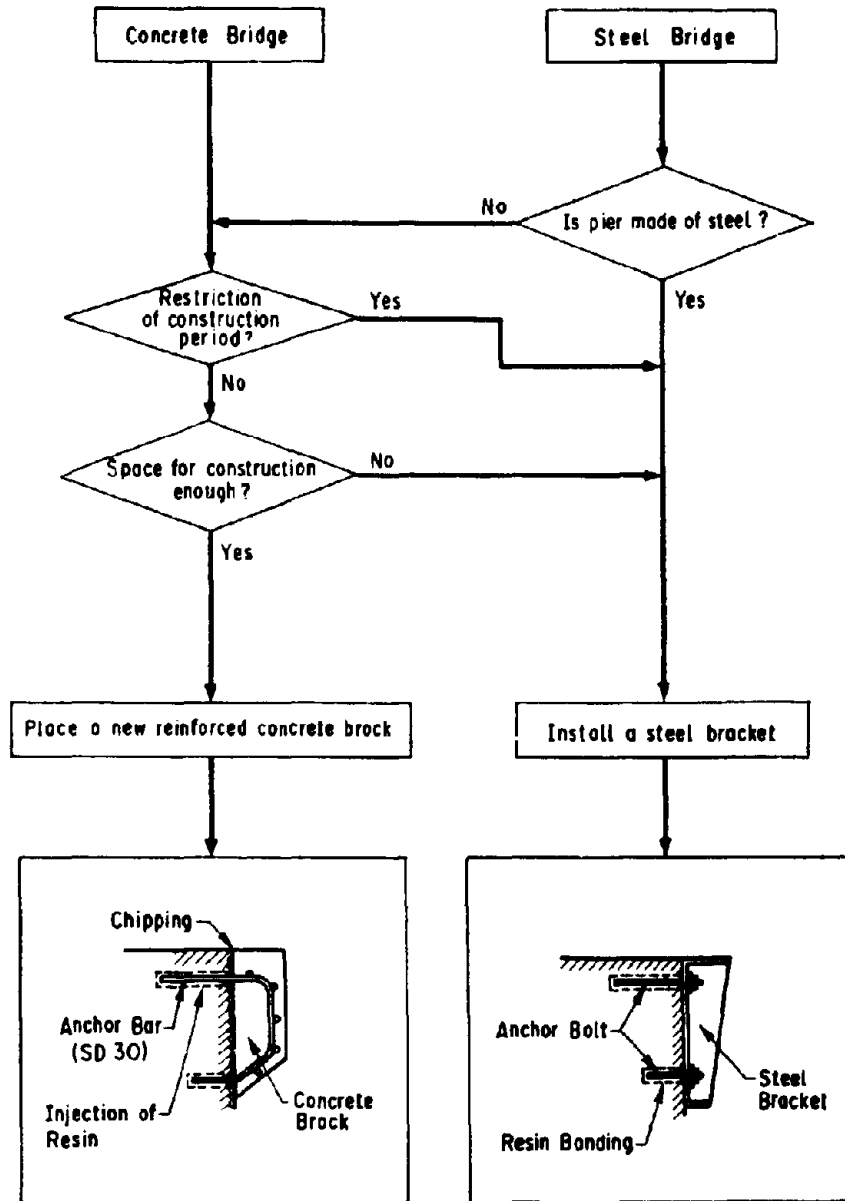
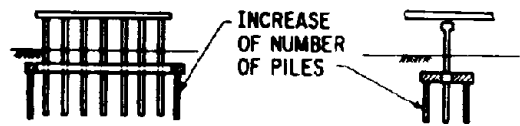


Fig. 15 Installation of Devices Connecting Deck and Substructure, and Device Connecting Two Adjacent Decks for Existing Highway Bridges

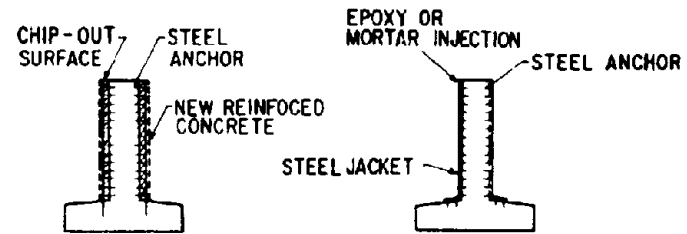




**Fig. 16 Elongation of Seat Length  $S_e$  and Bearing Seat Length  $S$  for Existing Highway Bridges**



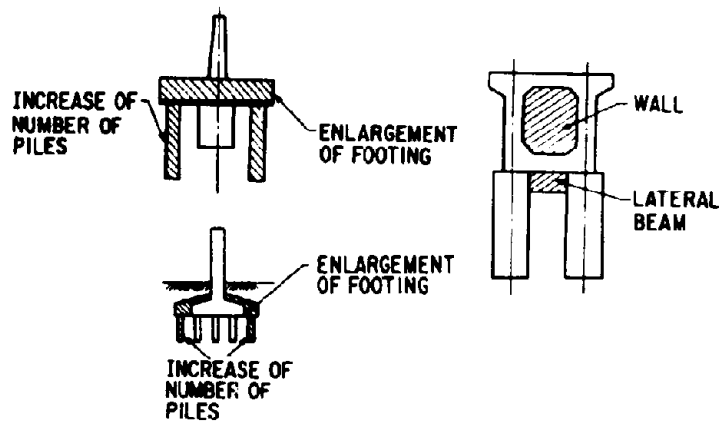
(1) STRENGTHENING OF BENT PILE



(A) NEW RC SECTION

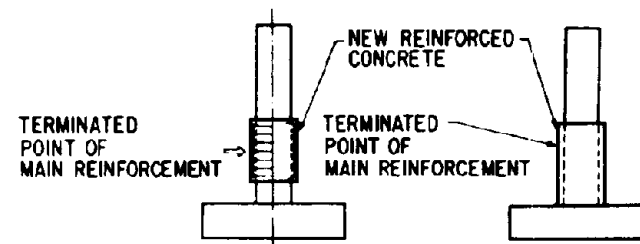
(B) STEEL JACKET

(1) STRENGTHENING OF WEAK PIERS

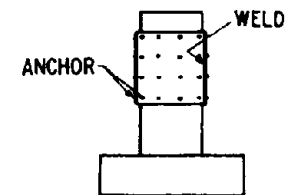


(2) STRENGTHENING OF FOUNDATION WITH INADEQUATE BEARING CAPACITY

(3) STRENGTHENING OF RC FRAME ON TWO INDEPENDENT CAISSON FOUNDATIONS



(A) NEW RC SECTION



(B) STEEL JACKET

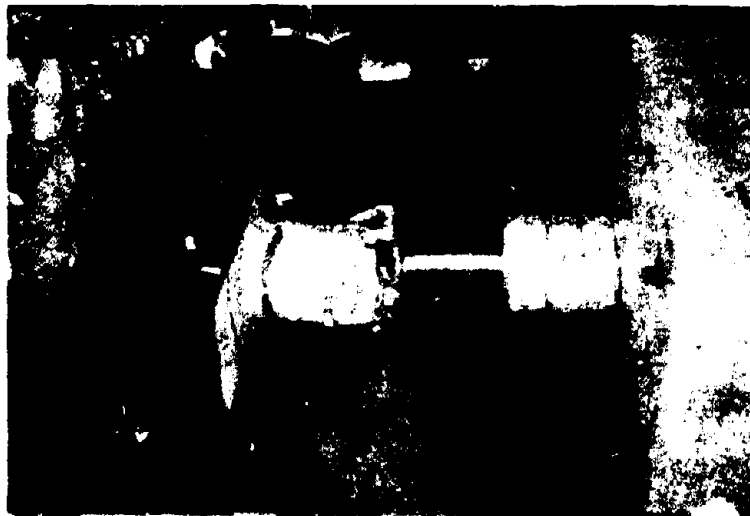
(2) STRENGTHENING OF RC PIERS WITH TERMINATION OF MAIN REINFORCEMENT AT MID-HEIGHT

Fig. 17 Strengthening of Foundations

Fig. 18 Strengthening of Piers



**Photo 12 Loading Tests of Reinforced Concrete Pier with Termination of Main Reinforcement at Mid-height ( Square Section )**



**Photo 13 Loading Tests of Reinforced Concrete Pier with Termination of Main Reinforcement at Mid-height ( Circular Section )**

#### **REPAIR OF TRANSPORTATION FACILITIES DAMAGED BY EARTHQUAKES**

##### **Outline**

The recent advancement in earthquake engineering has enabled transportation facilities and structures to be safely designed and constructed. Catastrophic disasters due to the entire collapse of structures have decreased, and accordingly the number of human fatalities has become appreciably smaller during recent large earthquakes. It is

considered, however, that partial failures may still take place in future large earthquakes, as observed in recent ones. In view of such facts, post-earthquake measures are still of significant concern.

A comprehensive 5 year research project entitled "Development of Repair Methods for Structures Damaged by Earthquakes," was made by the Ministry of Construction between 1981 and 1986. The project is to develop post earthquake measures by providing procedures of inspection, assessment of damage extent, repair methods, and overall evaluation for repairing seismically damaged structures. In executing the project, the Technological Research Center for National Land Development established the Committee for Development of Repair Methods for Civil Engineering Structures Damaged by Earthquakes, which was chaired by Dr. Shunzo Okamoto, Professor Emeritus of the University of Tokyo. Final accomplishment of the project was compiled in 1986 in the form of "Manual for Repair Methods for Civil Engineering Structures Damaged by Earthquakes"<sup>23)</sup>. The essence of the Manual in the area of the repair and restoration method for transportation facilities was later reorganized and published from the Japan Road Association in the form of "Guide Specifications for Earthquake Hazard Mitigation for Transportation Facilities - Pre-Earthquake Countermeasures -"<sup>24)</sup>.

This chapter outlines the Manual for the assessment of damage extent and repair method of seismically damaged transportation facilities with placing emphasis on highway bridges from the Manual.

### **Flow of Repair and Restoration**

Repair and restoration of seismically damaged transportation facilities must be correctly and immediately conducted because it significantly affects restoration activities of the public and stabilization of national life. Repair and restoration is made in accordance with the disaster countermeasures plans by correctly understanding the whole damage, and by consulting and exchanging information with related organizations and authorities. Procedure of repair and restoration after the occurrence of an earthquake can be classified into three stages as shown in Fig. 19. The fundamental aims of the three stages are the following :

#### **(1) First Stage of Repair and Restoration**

To inspect an outline of damage with emphasis on damage of critical and important facilities as early as possible, and to decide the strategy for repair and restoration. When large secondary disasters are likely to happen, it is necessary to conduct appropriate urgent treatments.

#### **(2) Second Stage of Repair and Restoration**

To inspect the damage of all facilities and structures, and to judge the necessity of temporary repair and restoration with consideration of possible large secondary disasters, urgency for restoration, types and importance of the facilities, and the time required for initiation of permanent restoration. When temporary repair and restoration are required, it is necessary to promptly repair, by considering priority and restoration level.

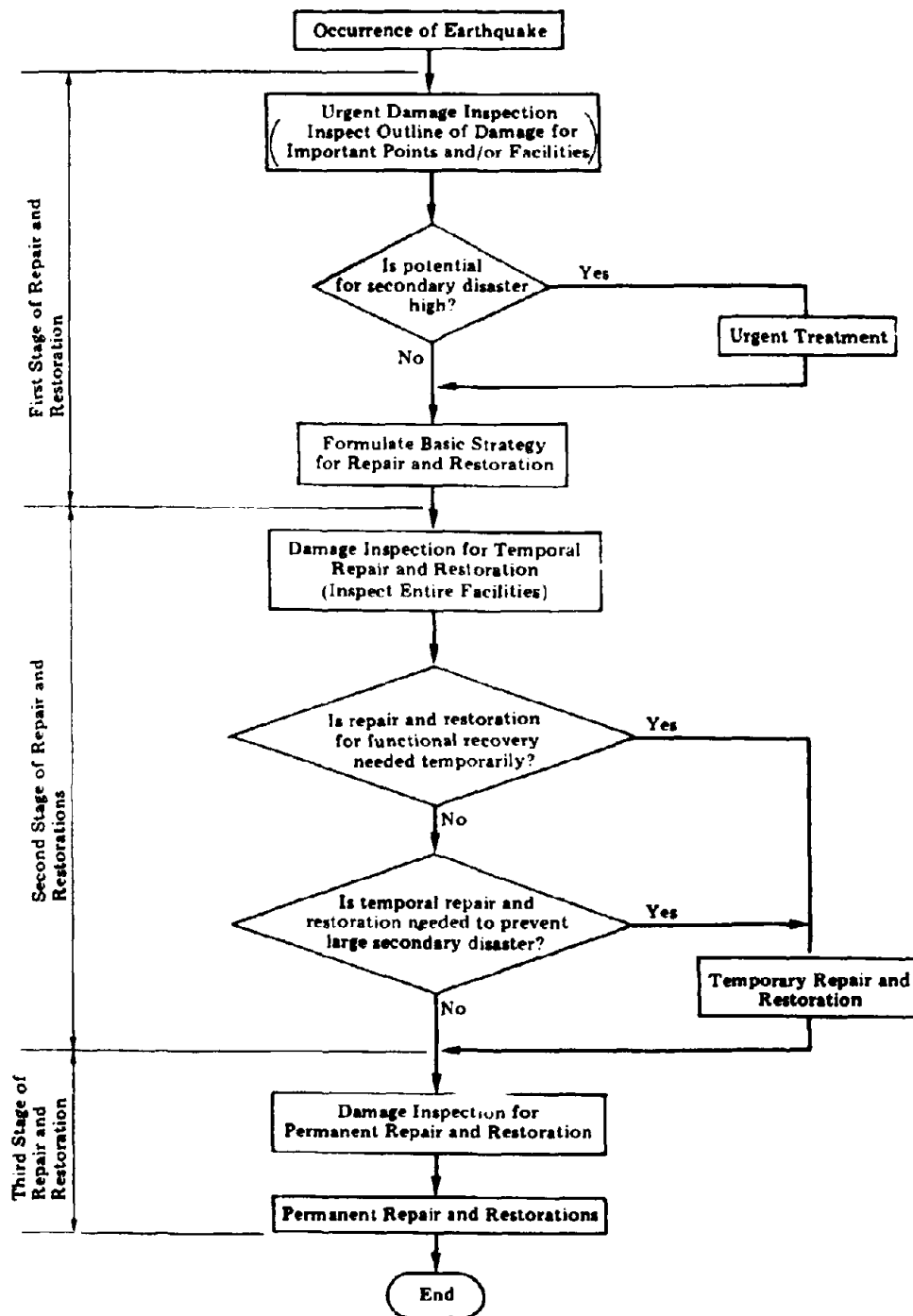


Fig. 19 Procedure of Repair and Restoration of Seismically Damaged Facilities

### (3) Third Stage of Repair and Restoration

To determine the level required for permanent repair and restoration based on the considerations of importance, location of the damage, damage degree, difficulties of repair and restoration, and future construction plans, and to conduct permanent repair and restoration by taking future development plans and restoration plans into account.

### Urgent Inspection and Urgent Treatment of Highway Bridges (1st Stage)

Fig. 20 shows a procedure of the urgent inspection and urgent treatment for transportation facilities. It should be noted that main purpose of the urgent inspection is to survey whether the road is passable. Detailed inspection and repair could not be made at this stage because it would require considerable time. Such a detailed inspection would also

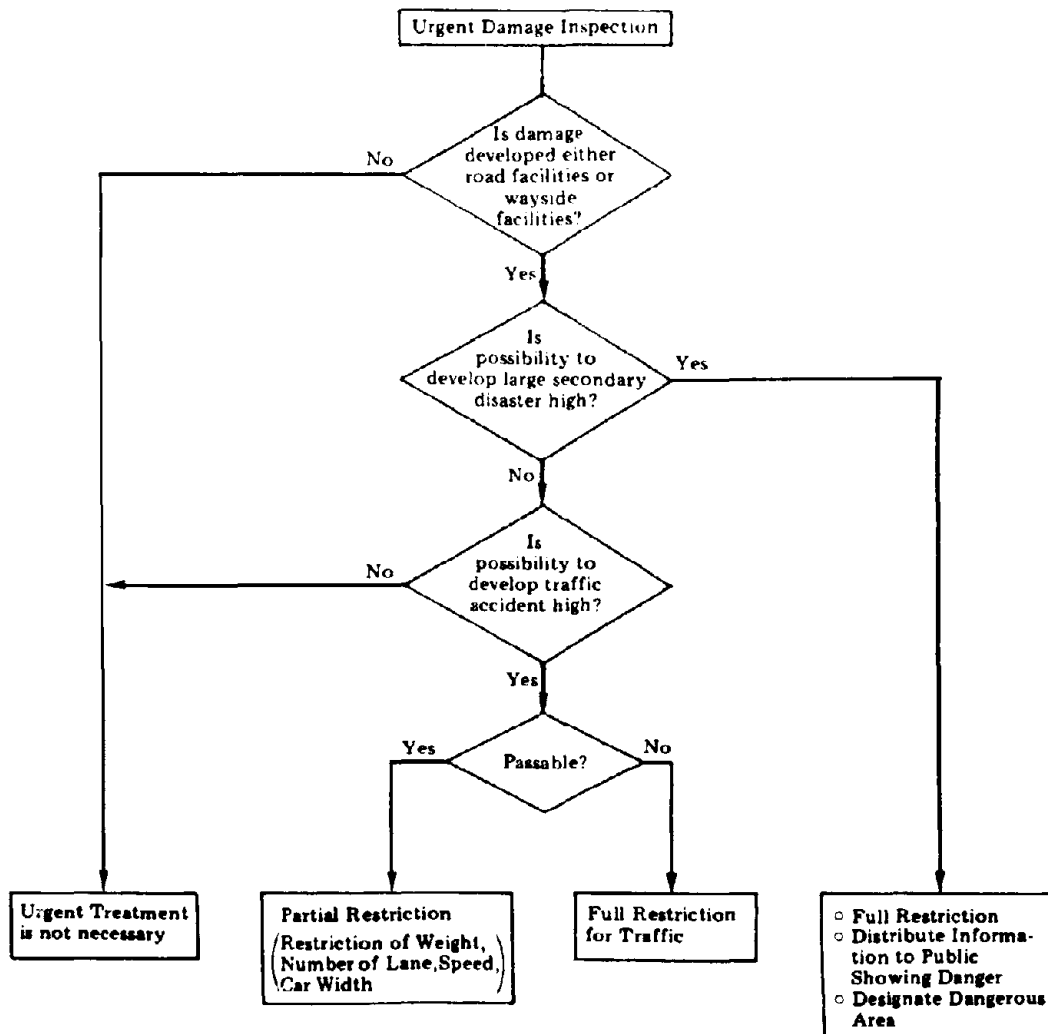


Fig. 20 Procedure of Urgent Inspection and Urgent Treatment

prevent the formulation of a repair plan at the head-quarters. Table 20 shows main check points for the urgent damage inspection.

### **Damage Inspection for Temporary Repair, and Temporary Repair Method for Highway Bridges (2nd Stage)**

Table 21 shows types of damage developed in highway bridges. Among the various types of damage, failure of piers, failure of seat concrete (concrete supporting bearings) and rupture of main structural members of superstructure are regarded as critical damages which are liable to cause falling off of superstructure. Therefore, damage inspection at the urgent inspection stage is to be made for these three types of damage first.

The degree of damage at the 2nd stage is required to be decided based on bearing capacity (load capacity) of the bridge structure and road surface condition. Because suspension of traffic on highway bridges would critically affects essential post-earthquake transportation. It is required to judge whether damaged bridges can be used even for short period for emergency transportation.

- I) Damage degree depending on bearing capacity
  - A : No Damage - No special damage is detected
  - B : Slight Damage - Damaged, but not considerable for short term service
  - C : Medium Damage - Considerable damage, but may be used for short-term service unless progress of damage due to aftershocks and live load is not developed.
  - D : Critical Damage - Possible falling-off of superstructure has to be taken in mind
  - E : Falling-off - Falling-off of superstructure

Fig. 21 shows examples of how the damage degree is judged for reinforced concrete piers suffering cracks, spalling-off of concrete and rupture of main reinforcement in a form of flexure failure at the base. Fig. 22 shows the same example for the degree of damage at the bearing supports. It is suggested that inspectors should judge the damage degree by comparing the actual damage with Figs. 21 and 22. Similar tables are prepared for various types of damage including shear failure of reinforced concrete piers and for the failure of superstructures.

- II) Damage degree depending on road surface condition
  - a : No Damage - No special damage is detected
  - b : Passable with Care - Damaged, but can be opened for short term traffic if sufficient care is paid
  - c : Unpassable - Badly damaged, and has to be closed

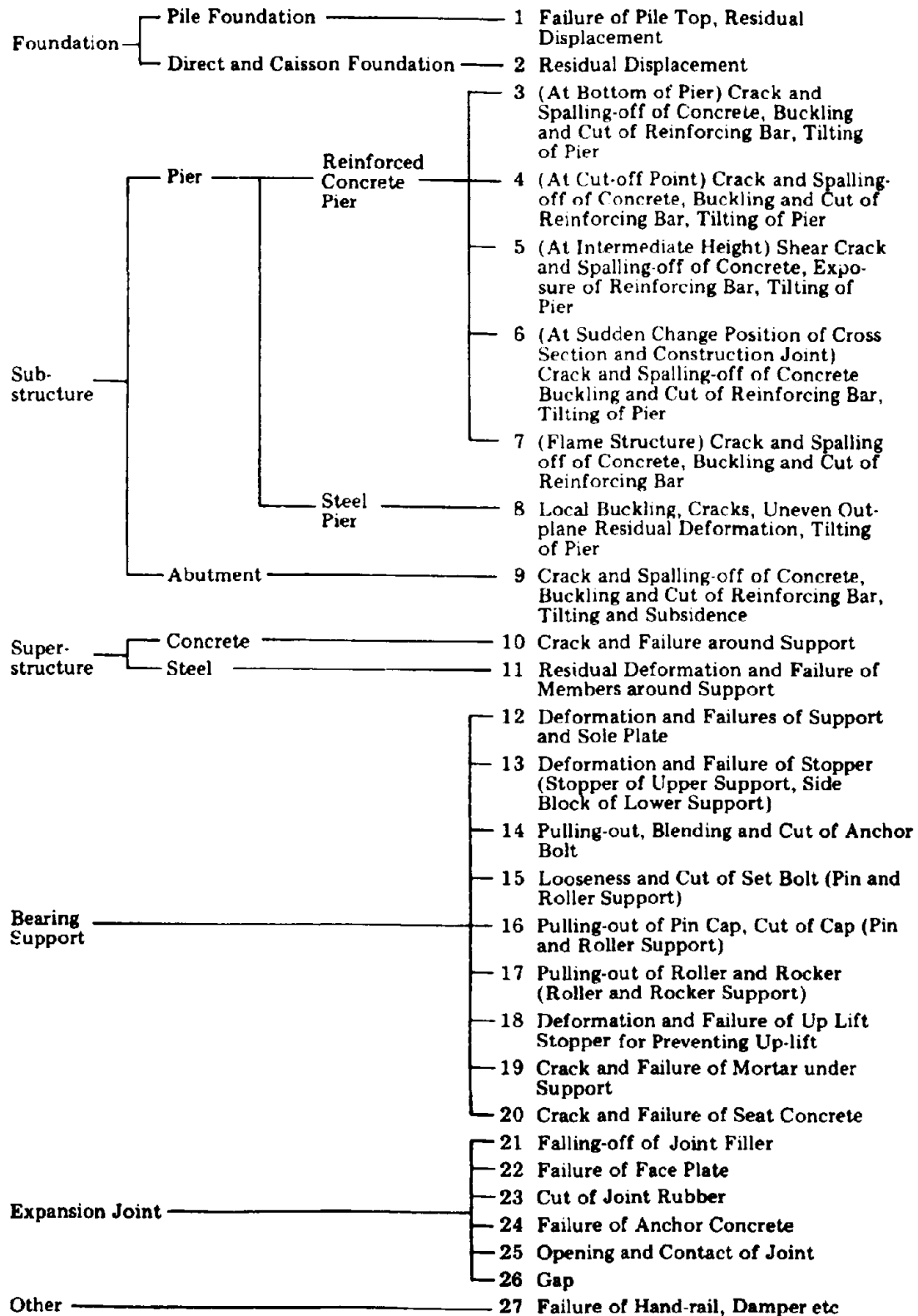
Fig. 23 represents a procedure for deciding whether highway bridges be closed or opened with care.

**Table 20 Check Points for Urgent Inspection**

Facilities		Check Point	
Road Itself	Road	Flat Road	Large Subsidence of Road Surface
		Low ~ High Embankment	Large Subsidence of Road Surface, Large Subsidence and Failure of Embankment
		Natural and Cut Slope	Huge Failure of Slope, Large Fallen Stone on Road, Large Failure of Road
	Bridge	General	Fall-off of Bridge
		From the Surface	Slipping off and Gap of Hand Rail
			Sudden Change of Leveling Large Opening, Upheaval and Gap at Expansion Joint
	Side View	Superstructure	Sudden Change of Deformation and Leveling
		Substructure	Large Subsidence, Tilting, Large Cracks and Spalling-off of Concrete
	Tunnel		Large Slope Failure near Tunnel, Large Spalling-off of Covering Concrete
	Common Duct		Uplift to Ground Surface, Critical Damage of Storing Facilities
Culvert and Underground Pedestrian Pass		Large Subsidence on Road Surface	
Pedestrian Bridge		Falling-off, Critical Failure of Pier	
Other	Way-side Facilities		Collapse of Building on Road Secondary Disaster caused by Damage of Road Facilities
	Exclusive Use Facilities		Influence of Damage of Exclusive Use Facilities on Road
	Others		Critical Innaduation, Tsunami, Fire, etc.



**Table 21 Damage Types of Bridges**



Observed Damage		1 Only Small Cracks	2 Diagonal Cracks (Not Penetrated)	3 Diagonal Cracks (Penetrated)	4 Spalling-off of Cover Concrete	5 Out-Plane Deformation of Reinforcing Bar	6 Cut of Reinforcing Bar and Tilting of Pier
Out-view of Damage	Side View						
	Front View						
	Side View						
	Front View						
Damage-Degree		B: Slight Damage	B: Slight Damage	B: Slight Damage	C: Medium Damage	C: Medium Damage	D: Critical Damage
Residual Strength		$\frac{P_u}{(1.1 P_y \sim 1.3 P_y)}$	$\frac{P_u}{(1.1 P_y \sim 1.3 P_y)}$	$1.1 P_y$	$1.0 P_y$	less than $P_y$	less than $P_y$
Residual Deformability		70%	50%	30%	10%	0%	0%

Fig. 21 Damage Degree of Reinforced Concrete Piers Subjected to Flexural Failure at Base

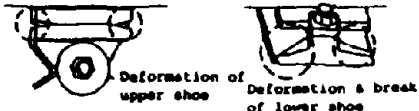









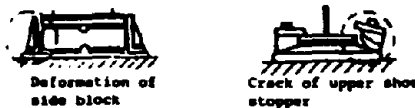





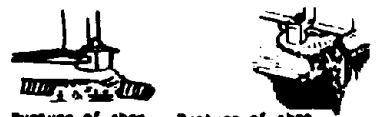

	B : Small damage	C : Medium damage	D : Extensive damage
Cast section of upper & lower shoe	 <p>Deformation of upper shoe Deformation &amp; break of lower shoe</p>		
Set bolt	 <p>Looseness of set bolt</p>	 <p>Break of set bolt</p>	 <p>Break of set bolt and damage of sole plate &amp; hub</p>
Roller	 <p>Falling off of roller</p>	 <p>Falling off of roller</p>	
Pin and pin cap	 <p>Falling off of pin cap</p>	 <p>Shearing of pin</p>	
Upper shoe stopper	 <p>Crack of upper shoe stopper</p>	 <p>Break of upper shoe stopper</p>	
Side block	 <p>Deformation of side block Crack of upper shoe stopper</p>	 <p>Break of side block stopper bolt Break of upper shoe stopper</p>	
Anchor bolt	 <p>Falling off of anchor bolt (&lt; 1cm)</p>	 <p>Falling off anchor bolt (&gt; 1cm)</p>	 <p>Break of anchor bolt</p>
Shoe pedestal mortar and concrete	 <p>Crack of shoe pedestal mortar Crack of shoe pedestal concrete</p>	 <p>Rupture of shoe pedestal mortar Rupture of shoe pedestal concrete</p>	 <p>Rupture of shoe pedestal concrete</p>

Fig. 22 Damage Degree of Bearing Supports

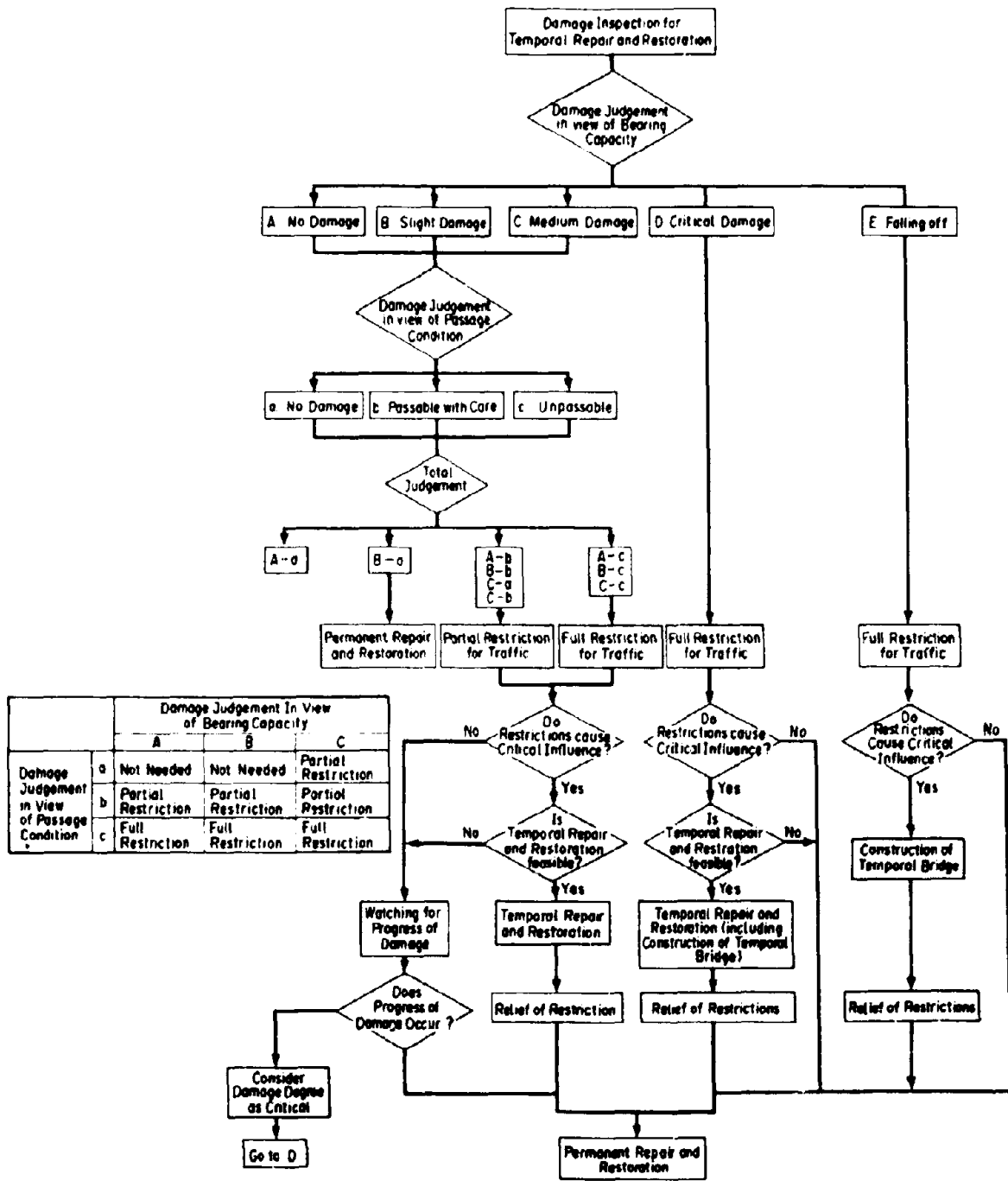


Fig. 23 Procedure of Judgement for Temporary Repair of Bridges

### **Damage Inspection for Permanent Repair, and Permanent Repair Method of Highway Bridges (3rd Stage)**

For permanent repair, the degree of damage has to be decided from a different inspection than that used by the temporary repair. Inspection of repair needs is required for long term use in the 3rd stage. Upgrading may be required for those bridges which suffered critical damage. The damaged degree is determined as

- |                     |   |
|---------------------|---|
| A : No Damage       | - No damage or minor damage which does not affect function for long-term service. |
| B : Slight Damage   | - Damage which does not affect the bearing capacity                               |
| C : Medium Damage   | - Damage which affects the bearing capacity                                       |
| D : Critical Damage | - Damage which significantly affects the bearing capacity                         |

Time required, cost, workability, availability of construction materials and visual appearance of repairing works have to be considered. Table 22 represents one of examples of a permanent repair method for reinforced concrete piers which suffered flexure failure at the base.

### **DEVELOPMENT OF INFORMATION GATHERING AND PROCESSING SYSTEMS FOR SEISMIC DAMAGE MITIGATION**

After a destructive earthquake, it is of significant importance to immediately gather correct information on the extent of damage in the area affected by the earthquake. Road transportation is expected to be interrupted in a very large earthquake, particularly in urban areas such as Tokyo, as a result of damage of not only transportation facilities but of falling-off of building attachments along the road. Confusion of people and automobiles left on road would also cause considerable disruption to the transportation. It is required therefore to develop new information gathering and processing systems which will enable the extent of damage to be recognized immediately after the earthquake for formulating a repair and restoration strategy.

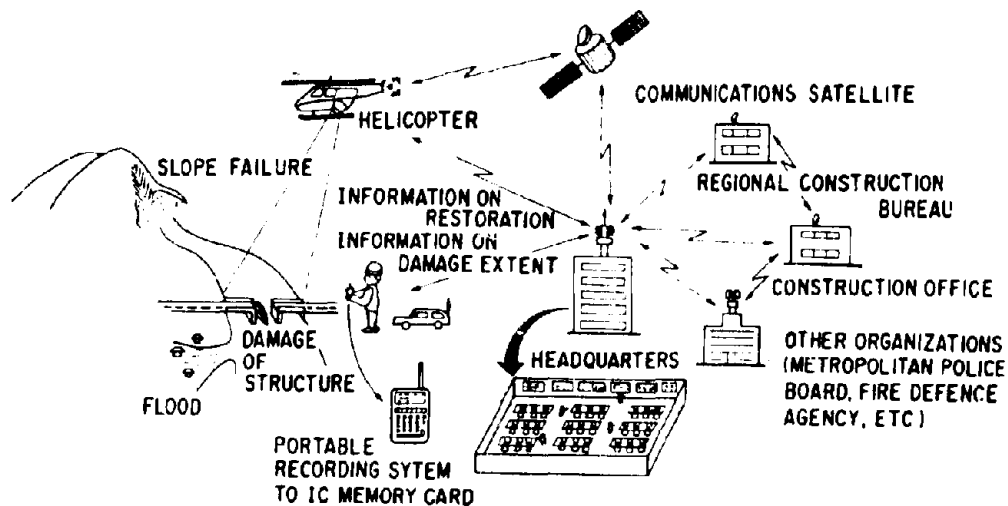
A comprehensive 5 year research program entitled " Development of Information Gathering and Processing Systems for Disaster Mitigation" was initiated in 1988 by the Ministry of Construction. The objectives of this research project were to develop new information correction and processing systems, using advanced new technology, for various disasters such as earthquakes, floods and debris flows. Key items of the research development are (refer to Fig. 24) :

- a) Bird's eye information correction systems from helicopters,
- b) On-line information processing systems, and
- c) Real-time digital mapping systems.

**Table 22 Permanent Repair of Reinforced Concrete Bridge Piers with Flexural Failure at Bottom**

Level of Damage	Damage Patter Presented in Fig. 4-2	Repair and Restoration Method	Design for Normal Load	Design by Ductility Analysis	
				Yield Stage	Ultimate Stage
Before Yield of Reinforcing Bar	Before Stage 1	Injection of Epoxy Regin	Normal	Normal	Normal
		Covering by Reinforced Concrete	Hybrid	Hybrid	Hybrid
		Covering by Steel Plate	Hybrid	Hybrid	Hybrid
After Yield but Before Ultimate	Stage 2 and 3	Injection of Epoxy Regin	2/3 Es for Reinforcing Bar	2/3 Es for Reinforcing Bar	Normal
		Covering by Reinforced Concrete	Ignore Original Section	1/3 Es for Original Reinforcing Bar	Hybrid
		Covering by Steel Plate	Ignore Original Section	1/3 Es for Original Reinforcing Bar	Hybrid
After Ultimate	Stage 4, 5 and 6	Covering by Reinforced Concrete	Ignore Original Section	Ignore Original Section	Hybrid

**Note** 1) Normal: Usual design procedure in accordance with Design Specifications of Highway Bridge.  
 2) Hybrid: Original damaged section can be treated to work for load with new section.



**Fig. 24 Information Gathering and Processing Systems**

For this purpose, measuring technology of the degree of seismic damage of structures, using helicopter picture information and new media high-grade disaster prediction methods as well as planning systems for repair and restoration in the damaged area are under development. To avoid distortion of information during transferring information from the regional office to headquarters, it is aimed to develop visual motion picture systems.

In executing the project, the Technological Research Center for National Land Development established the Committee for the Development of Disaster Information Systems, which is chaired by Dr. H. Umemura, Professor Emeritus of the University of Tokyo. Final accomplishments of the project are to be compiled in 1992 in the form of guidelines.

#### **CONCLUDING REMARKS**

The preceding pages presented the present earthquake engineering efforts to mitigate earthquake hazards of road transportation facilities in Japan. Japan has been experiencing many destructive earthquakes in the past and it is critically important that the functions for rescue, evacuation, repair and restoration be able to be carried out. Replacement and strengthening of existing highway bridges is extremely difficult in urban areas. Transportation facilities, in particular important ones such as highway bridges, have to be provided with a very high level of seismic safety.

The level of seismic safety required for transportation facilities has been increasing in recent years as a result of past experiences where confusion caused by the interruption was considerable in urban area. Indirect damage caused by the interruption of urban transportation was much larger than the direct damage. It is therefore required to develop new seismic design and countermeasure concepts which enable structures with higher and with various levels of seismic safety to be constructed.

## ACKNOWLEDGEMENTS

The author would like to express his sincere thanks to Mr. Kanoh, T. and Iida, H., staff members of the Earthquake Engineering Division of the Public Works Research Institute, for their assistance in making the manuscript. Special thanks are extended to Dr. Gregory MacRae, visiting research engineer at the Public Works Research Institute from New Zealand, for his suggestions and corrections to the manuscript.

## REFERENCES

- 1) Iwasaki, T., Penzien, J. and Clough, R.W.: Literature Survey - Seismic Effects on Highway Bridges, Report No. EERC 71-11, Earthquake Engineering Research Center, University of California, Berkeley, 1972
- 2) Kawashima, K. : Seismic Design and Seismic Damage Mitigation of Highway Bridges, Journal of Road, 1990
- 3) Japan Road Association : Seismic Design Specifications for Highway Bridges, 1978
- 4) Iwasaki, T., Tatsuoka, F., Tokida, K., and Yasuda, S. : A Practical Method for Assessing Soil Liquefaction Potential Based on Case Studies at Various Sites in Japan, Proc. 6th Japan Earthquake Engineering Symposium, 1978, Tokyo
- 5) Japan Road Association : "Part V Seismic Design" of the "Design Specifications for Highway Bridges", 1990
- 6) Iwasaki, T., Kawashima, K. and Hasegawa, K. : New Seismic Design Specifications of Highway Bridges in Japan, 22nd Joint Meeting, U.S.-Japan Panel on Wind and Seismic Effects, UJNR, Gaithersburg, U.S.A., May 1990
- 7) Kawashima, K., Aizawa, K. and Takahashi, K. : Attenuation of Peak Ground Motions and Absolute Acceleration Response Spectra, Report of the PWRI, Vol. 166, Public Works Research Institute, 1985
- 8) Katayama, T., Iwasaki, T. and Saeki, M. : Statistical Analysis of Earthquake Acceleration Response Spectra, Proc. Japan Society of Civil Engineers, Vol. 275, 1978
- 9) Kawashima, K. and Hasegawa, K. : New Seismic Design Method of Multi-span Continuous Bridges, Bridges and Foundations, Vol. 90-10, 1990
- 10) Ohta, M.: A Study on Earthquake Resistant Design for Reinforced Concrete Bridge Piers of Single-Column Type, Report of the Public Works Research Institute, Vol. 153, 1980
- 11) Kawashima, K. and Koyama, T. : Effects of Cyclic Loading Hysteresis on Dynamic Behavior of Reinforced Concrete Bridge Piers, Structural Eng./Earthquake Eng., Vol. 5, No.2, Proc. of Japan Society of Civil Engineers, 1988, and Kawashima, K. and Koyama, T. : Effects of Number of Loading Cycles on Dynamic Characteristics of Reinforced Concrete Bridge Piers, Structural Eng./Earthquake Eng., Vol.5, No.1, Proc. of the Japan Society of Civil Engineers, 1988
- 12) Kawashima, K. and Hasegawa, K. : Hysteretic Behavior of Reinforced Concrete Bridge Piers by Dynamic Loading Tests and Shaking Table Tests, 9th World Conference on Earthquake Engineering, Tokyo/Kyoto, Japan,



1988

- 13) Hamada, M., Yasuda, S., Isoyama, R. and Emoto, K. : Observation of Permanent Ground Displacements Induced by Soil Liquefaction, Proc. of Japan Society of Civil Engineers, Vol. 376, III-6, 1986, and, Hamada, M., Yasuda, S., Isoyama, R. and Emoto, K. : Study on Liquefaction-Induced Permanent Ground Displacements and Earthquake Damage, Proc. of Japan Society of Civil Engineers, Vol. 376, III-6, 1986
- 14) Guidelines for Design of Base-Isolated Highway Bridges, Final Report of A Committee for Study of Application of Base Isolation to Seismic Design of Highway Bridges (Chairman : Professor T. Katayama), Technology Research Center for National Land Development, March 1989
- 15) Kawashima, K. : Development and Future Scope of Seismic Isolation of Structures - A Review -, Proc. of Japan Society of Civil Engineering, Structural Eng./Earthquake Eng., Vol.398/I-10, Proc. of JSCE, 1988
- 16) New Zealand- Japan Workshop on Base Isolation of Highway Bridges, Head Office of Ministry of Works and Development, Wellington, New Zealand, 1987
- 17) Taguchi, J., Iwasaki, T., Adachi, Y. and Kawashima, K. : U.S.-Japan Cooperative Research Program on Hybrid Control of Seismic Response of Bridge Structures, 22nd Joint Meeting, U.S.-Japan Panel on Wind and Seismic Effects, UJNR, Gaithersburg, Maryland, U.S.A., 1990
- 18) Kakizaki, H. and Itoh, T.: Design of the Nagaki-gawa Bridge - A Based Isolated Bridge, Bridge and Foundation, Vol. 24, No.9, 1990
- 19) Japan Road Association: Countermeasures for Roads against Earthquakes, 1986
- 20) Kawashima, K. and Unjoh, S.: An Inspection Method of Seismically Vulnerable Existing Highway Bridges, Structural Eng./Earthquake Eng., Vol.7, No.1, Proc. Japan Society of Civil Engineers, April 1990
- 21) Japan Road Association : Guide Specifications for Earthquake Hazard Mitigation for Transportation Facilities - Pre-Earthquake Countermeasures -, 1987
- 22) Kawashima, K. Unjho, S. and Azuta, Y.: Examples of Seismic Strengthening of Highway Bridges, Technical Note of PWRI, No.2674, Public Works Research Institute, 1988
- 23) Public Works Research Institute : Manual for Repair Methods for Civil Engineering Structures Damaged by Earthquakes, Technical Note of the Public Works Research Institute, Vol.45, December 1986 (in Japanese). Translated version is published from the National Center for Earthquake Engineering Research, University of New York, Buffalo, U.S.A.
- 24) Japan Road Association : Guide Specifications for Earthquake Hazard Mitigation for Transportation Facilities - Post-Earthquake Countermeasures-, 1987 (In Japanese)

## Bridge Substructures and Design Methods

Michio Okahara(I)  
Shoji Takagi(II)  
Shoichi Nakatani(III)  
Presenting Author; Michio Okahara

### SUMMARY

This paper presents general status of adopted bridge substructures, maintenance and reinforcement of damaged bridges and design concept of substructures based on the latest standard. Technical standards which have been used in Japan and their history are also introduced for the design and construction of newly-established bridge and maintenance for existing bridges.

### INTRODUCTION

The highways in Japan have been steadily improved under the Five-Year Road Improvement Programs, enacted by the ministry of construction, which have reached the tenth. The stock of highway bridges with bridge length of over 15 m have piled up to more than 110 thousand. In order to maintain quantity and function of these substructures and make them last as long as possible, several inspection's methods, maintenance and reinforcement measures have been adopted by technical standards. And then to design and construct many new bridges under the above 5-year plan, several technical standards have been revised.

Study results on over all status of bridge substructures, recently developed measures for maintenance and reinforcement of damaged substructures and design fundamentals based on the latest specifications are mainly said in this paper.

### TRANSITION OF BRIDGE SUBSTRUCTURE

#### 1 Transition of the forms, construction method and present situation of maintenance of bridge substructures

##### 1-1 Transition of the forms and construction methods of bridge substructures

Foundations, which are parts of bridge substructures, constructed in fiscal 1966, 1976 and 1985 were mainly investigated concerning their scale, type, construction method, etc. throughout the country in each fiscal year. The transition of the forms and construction methods of foundations are

- 
- (I) Head, Foundation Engineering Division, P.W.R.I., M.O.C.
  - (II) Senior Research Engineer, ditto
  - (III) Senior Officer for Technical Standards and Cost Estimation, Engineering Affairs Management Section, Minister's Secretariat, M.O.C.  
(former Research Engineer, Foundation Engineering Division, P.W.R.I.)

presented here using there data.

Fig. 1.1 shows the transition for actual usage of each foundation type from the number of foundations constructed in each fiscal year. Though caisson foundation accounted for about one fourth of the whole in fiscal 1966, it decreased to few percent after fiscal 1976. On the contrary, pile foundation usage gradually increased, and it accounted for about a half of the whole in fiscal 1985. Spread foundation also has high actual usage and is typical foundation type in Japan together with pile foundation.

Figs. 1.2 and 1.3 show the investigation results concerning the actual usage of pile construction methods. With regard to environmental problems from pile setting, the cast in place pile or auger pile (with low vibration and low noise) is used increasingly, while use of the driving pile is decreasing. Because of increasing road bridge construction in mountainous areas where it is difficult to carry machines and other instruments, the necessity for the cast in place pile construction method with man power digging also seems likely to increase in the future.

As there are steel pipe piles, PC piles, PHC piles and RC piles among the types of existing piles used for the driving or auger pile construction method, the percentage of steel pipe piles amounts to about 80 % of existing piles after fiscal 1977 and, on the contrary, the usage of the RC pile is almost zero.

The number of bridges of each foundation type is indicated in Table 1.1, where all the established bridge in Japan are classified paying attention to the foundation type which supports the maximum part of the effective span. The direct foundation and the pile foundation account for about 70 % and 25 % of all the bridges, respectively, and they amount to over 90 % of the whole.

## 1-2 Present situation of bridge substructure maintenance

The maintenance of road bridge is conducted by each road administrator for each road category (national expressways, national highways, prefectural road and municipal roads). So the maintenance of bridge substructures is also conducted in accordance with the various maintenance levels applicable to each road administrator.

Here the present situation of maintenance is mentioned from the point of view of inspection and repair and reinforcement methods for bridge substructures. The following data is the result of questionnaire investigation by the Public Works Research Institute, objective road bridge are cases in which abutments, piers of foundations were repaired or reinforced within five years during 1983 to 1987 (most of them are the responsibility of prefectures and cities by government ordinance). Responses to the questionnaire brought data on 605 bridges (the number of substructures is 2054).

### 1-2-1 Acknowledgment of abnormality or damage to bridge substructures and types of inspection

The types of inspection after acknowledgment of abnormality of damage are listed in order in Fig. 1.4 among 605 bridges of which substructures were repaired or reinforced. The number of measured bridges due to seismic

Inspection is overwhelmingly high and accounts for 65 % of the total when the number of measured bridges due to disaster prevention inspection is added to it. This fact shows maintenance is steadily conducted under seismic or disaster prevention inspection.

On the other hand, the number of measured bridges under other inspections of road bridges accounts for 35 % of the total; the importance of daily inspection activities, such as road patrol, is pointed out by the fact that the percentage of ordinary inspections is high. The number of bridges measured by inspection during abnormal states is also the same level as those by periodic inspection; this indicates the necessity for rapid inspection during abnormal states.

### 1-2-2 Damage of abutments and piers and repair and reinforcement methods

#### 1) Damage of abutments and piers.

The shoe bed is the most common part for conducting repair and reinforcement (Fig. 1.5). The shoe bed is used as the generic name of repair or reinforcement for the purpose of preventing bridge fall by seismic inspections, including the widening of the shoe bed and the establishment of devices for preventing the superstructure from falling. Column (or wall) follows it, accounting for 20 %, and next is the cross-beam of the column head. There are many cases of repair or reinforcement resulting from cracks.

#### 2) Repair and reinforcement methods of abutments and piers

Though it is difficult to clearly classify the methods of repair and reinforcement of abutments and piers (concrete materials in all investigated cases), they are classified according to the following points:

- a) a case where repair has the purpose of repairing damage of established substructures and recovering their original function,
- b) a case where reinforcement is used in an attempt to improve the original function by damage repair or to positively improve the function of the established substructure without damage.

The following shows a sum result according to the above mentioned classification.

#### (I) Repair methods

In many cases the surface coating method or injection method is used as the repair method when damage caused by a crack is relatively slight (Fig. 1.6). Repair by flexible waterproof materials is the most common as the surface coating method, and that by epoxy resin accounts for about 70 % in the injection method.

#### (II) Reinforcement methods

Instances of the section increasing method are the most common as the reinforcement methods, followed by the steel plate affixing method and the addition of structural members (Fig. 1.7).

### 1-2-3 Damage of foundations and repair and reinforcement methods

#### 1) Damage of foundations

The most frequent cause of damage of foundations is scouring, accounting for about 50 % of the total. Displacement, inclination and movement follow it. Fig. 1.8 also shows instances for the purpose of increasing bridge functions such as for lane widening, sidewalk attachment, etc. The spread

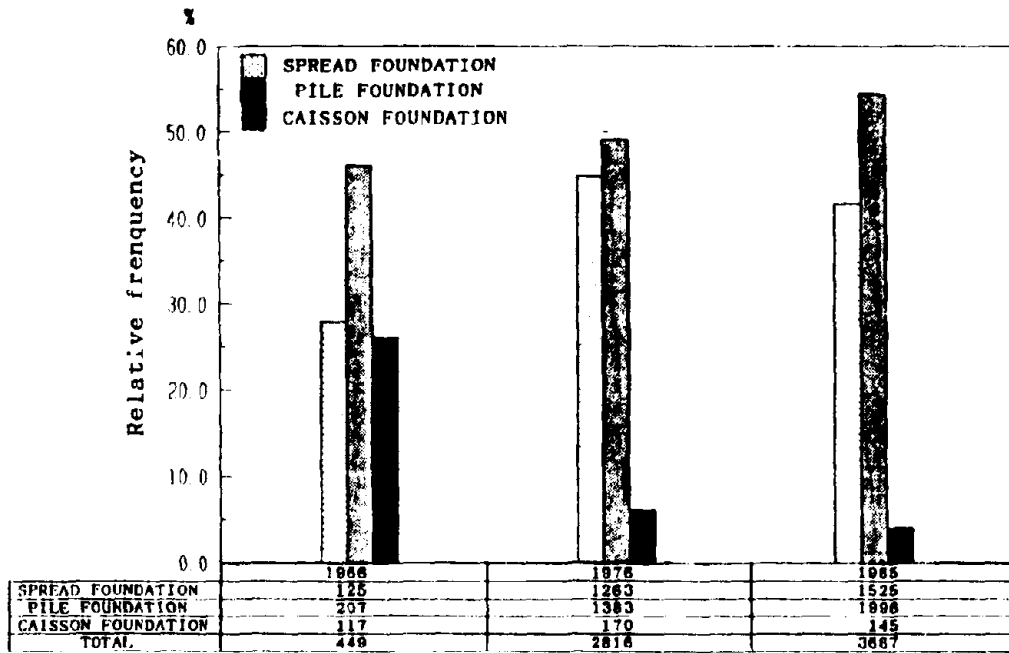


Fig. 1.1 Transition of actual usage of foundation types.

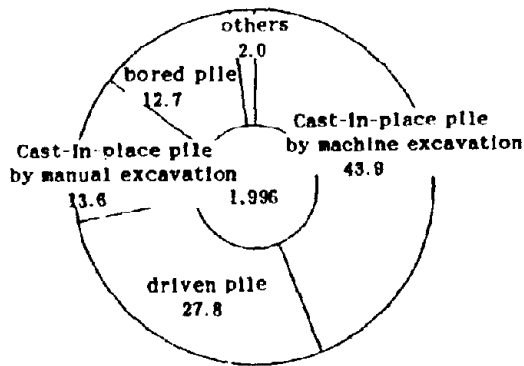


Fig. 1.2 Actual usage of pile construction methods in fiscal 1977.

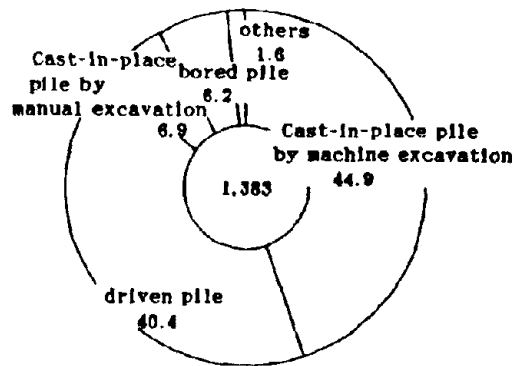


Fig. 1.3 Actual usage of pile construction methods in fiscal 1985.

Table 1.1 Number of bridges by foundation and road types.

road type / foundation types	national expressway	national highway	(outside designated)	principal local-load	prefectural load	municipal road (primary) (secondary)		(others)	total
spread foundation	1787	3518	5377	8089	10318	10733	8993	28738	78861
open caisson	106	593	313	466	611	299	125	267	2739
pneumatic caisson	63	118	58	85	93	67	23	72	577
cast in place pile	1292	851	491	440	613	315	196	568	4668
ready-made steel pipe pile	414	1385	581	1072	1453	1470	810	2180	9345
ready-made RC pipe pile	273	858	275	548	743	844	713	2841	6696
ready-made PC pipe pile	64	441	281	476	655	1198	869	2748	6633
wooden pile	0	305	111	229	264	267	332	1072	2460
others	5	320	270	404	498	497	300	1873	4228
total	4014	8036	8757	11809	18099	18781	12261	40039	125796

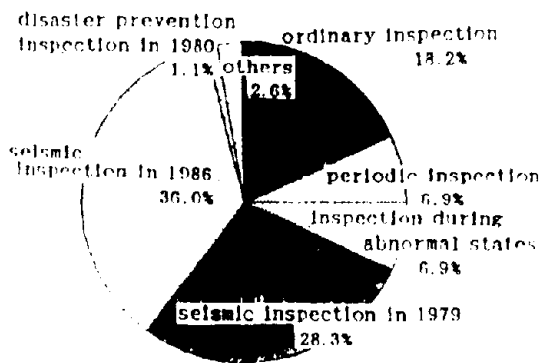


Fig. 1.4 Percentage of measured bridges (605 cases).

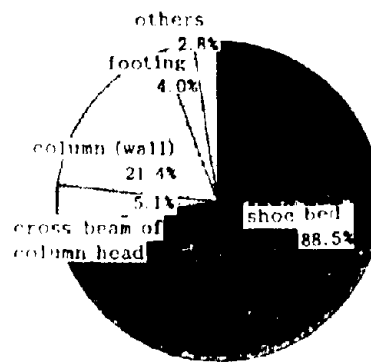


Fig. 1.5 Percentage of body parts on which repair or reinforcement was conducted (670 cases).

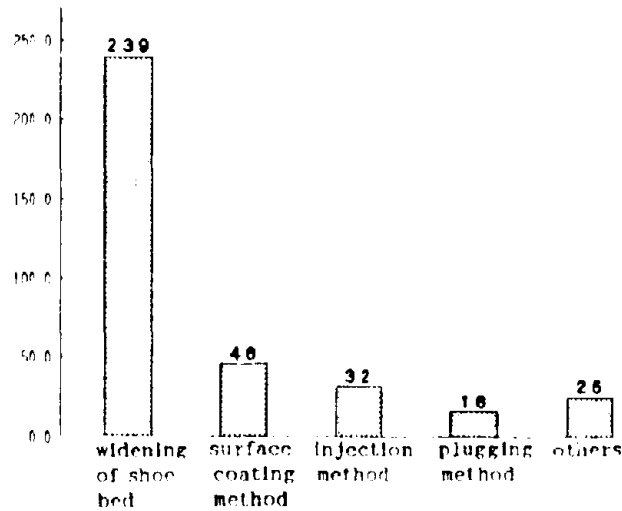


Fig. 1.6 Repair methods for abutment or piers.

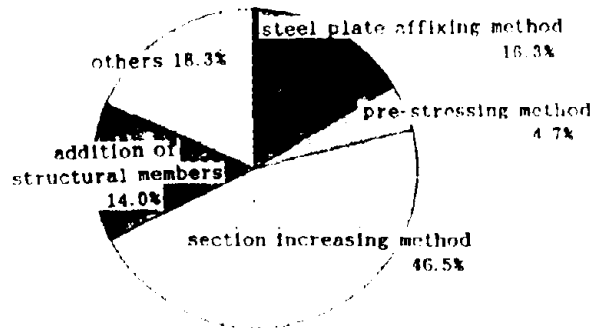


Fig. 1.7 Reinforcement methods for abutments or piers.

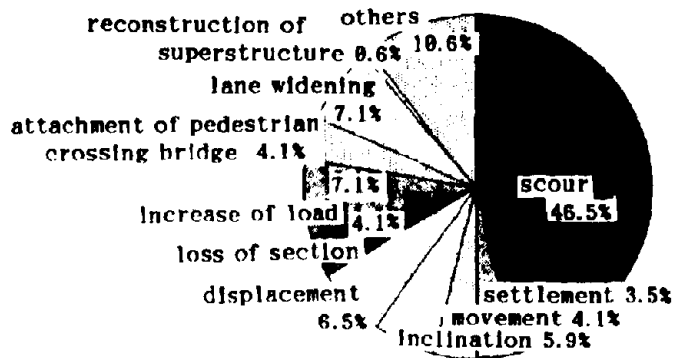


Fig. 1.8 Causes of repair and reinforcement of foundations

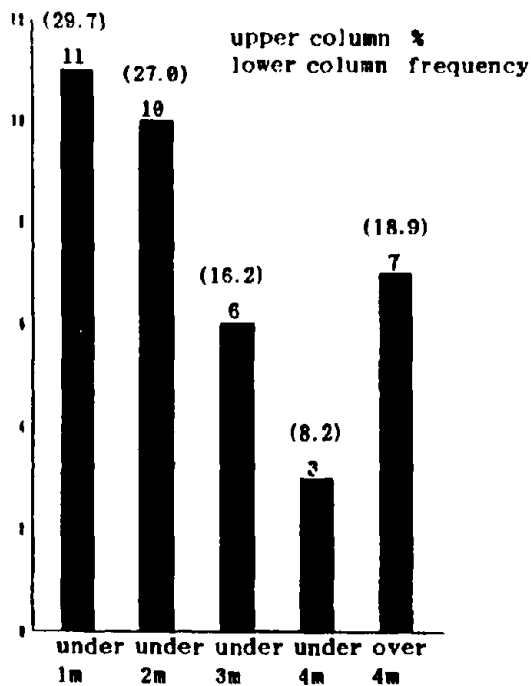


Fig. 1.9 Maximum depth of scour.

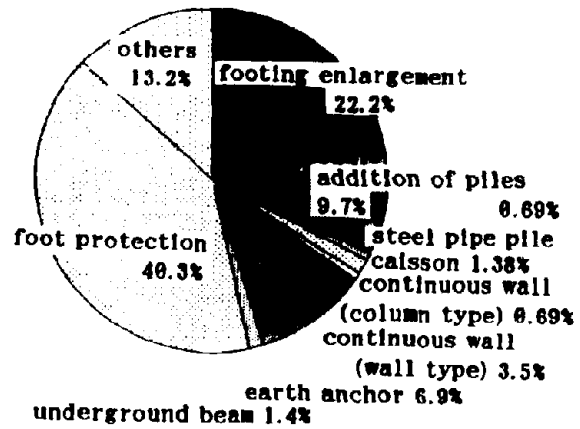


Fig. 1.10 Repair and reinforcement methods of foundations

foundation is the most common foundation requiring countermeasures against scour and caisson foundation follows it.

The result of investigation concerning the maximum depth of scour (37 scours) is shown in Fig. 1.9. The depth of scour is measured from the upper side of footing in the case of foundation with footing and from the upper side of the top slab in the case of caisson foundation. Most scours over 2m in depth are in cases of the caisson foundation; some scours over 4m in depth are included and may be in fairly dangerous situation. The scour so rapidly progresses with flooding that it is necessary to fully examine inspection methods or systems against scours.

## 2) Repaired and reinforcement methods for foundations

There are many instances where the foot protection method has been adopted using as repair and reinforcement methods. It can also be well understood by citing many instances where damage is caused by scours. Footing enlargement, addition of piles, measures by earth anchor and the underground continuous wall method follow it (Fig. 1.10).

## 2 Technical standards for bridge substructures

### 2-1 Provision of technical standards for bridge substructures

In the technical standards used up to now, there are standards for the design and construction of newly-established bridges and those for the maintenance of established bridges. Moreover, in standards for the design and construction of newly-established bridges, besides those for stability checks and design of cross section, there are some standards especially for the maintenance of substructures, such as countermeasures against salt damage and alkali-aggregate reaction or matters in need of consideration from the point of view of river administration.

Fig. 2.1 shows the transition of technical standards required for bridge substructures. Guidelines for Design of Substructure of Highway Bridges had begun to be made for foundation types from the 1960s. The Guidelines were completed in the late 1970s and were included in the system of Specifications for Highway Bridge as Part IV Specifications for Substructures in 1980. Since then, as the scale of the foundations has increased in size and their forms have become more variable with advance in construction techniques, the arrangement of design guidelines for new foundation types, such as assembled steel pipe sheet pile foundation and underground continuous wall foundation, have also been advanced. Hence, new provisions for the design and construction of assembled steel pipe sheet pile foundation were included in the Specifications for Highway Bridges in 1990. The basic design concept shown in Part IV Specifications for Substructures is concerned with the behavior of foundations and structural members against the design external forces, such as earthquake inertia force, etc., are held in elastic range. The design is not considered to suffer damage requiring immediate repair or reinforcement against an estimated external force. In Japan, quite few bridge foundations are constructed on soft cohesive soil, thus a design to deal with long term changes of the ground should be required for abutments. Fig. 2.2 shows a typical movement of an abutment with lateral flow of the ground. In some cases, the potential of such a movement is judged and



measures may be taken beforehand, such as improvement of the ground, reduction of the weight of the embankment, etc. As the bridge substructure is a large section, in many cases with a low reinforcing steel bar, and is easily influenced by temperature changes or drying contraction, a detailed arrangement of the bars is also shown for preventing cracks caused by them.

Moreover, consideration must be taken to prevent scouring caused by floods near piers or abutments and not to have negative influence upon river administration facilities like the bank, etc. Requirements for the river control points, like the establishment of river-protection works near an abutment, etc. are regulated in Cabinet Order concerning Structural Standards for River Administration Facilities, etc.

In the 1980s, the Guideline for Countermeasures against Salt Damage to Road Bridges (draft) were made for the purpose of improving durability of concrete materials. It gives guidelines for the covering of reinforcing steel bars of road bridges constructed in coastal areas, the water cement ratio, etc., and separately gives notice of regulations for the total amount of chloride in concrete. In addition to them, because it has begun to be noticed that the concrete material is damaged by alkali-aggregate reaction mainly on substructures, guidelines also show some measures for using low-alkali cement or blended cement with neutralizing effect against alkali-aggregate reaction, etc.

Concerning the maintenance of established bridges, the Outline for Road Maintenance and Repair and the Handbook of Road Bridge Repairs have been produced to introduce construction methods and examples of repair.

## 2-2 Provision of technical standards for earthquake-resistant design of bridges and earthquake disaster countermeasures

### 2-2-1 Technical standards for earthquake-resistant design of bridges

In Japan, the Kanto Earthquake of 1923 and enormous damages by it gave an opportunity to take the influence of earthquakes into concrete consideration for the design of bridges. Thus, in 1924 the Public Works Bureau, the Ministry of Home Affairs, introduced, "Earthquake Resistant Method for Abutments and Piers", noticing that the horizontal earthquake forces had to be considered in the design. Changes in earthquake-resistant standards and seismic forces up to the present are shown in Table 2.1. In June, 1926, the regulation to deal with the seismic force as one of the design loads was included for the first time in the "Specifications for Design of Roads (draft)" issued by the Public Works Bureau, the Ministry of Home Affairs; the expected earthquake load for the bridges was subject to regulations to deal with the maximum stress on every member of the bridge by "the maximum seismic force at each location". Replacing these specifications, was "Specifications for Design of Steel Road Bridges (draft)" issued in 1936. The horizontal acceleration of 0.2 g and the vertical acceleration of 0.1 g were regulated as the standard values of seismic design coefficients and to increase or decrease the values considering the condition of the location. In the revised "Specifications for Design of Steel Road Bridges" (1956 and 1964), the horizontal seismic coefficient was regulated to vary from 0.10 to 0.30 according to the area and ground condition, and the vertical seismic

coefficient was regulated to be 0.1 as a standard.

The provision of detailed standards for earthquake-resistant design was in "Specifications for Earthquake-Resistant Design of Road Bridges" enacted in March, 1971, taking the lessons learned from the damage caused by the Niigata Earthquake of 1964. In the specifications, the seismic design coefficient was systematically regulated according to seismic zoning, ground condition and importance of the bridge. The modified seismic coefficient method was also adopted for bridges which vibrate easily, such as those with high piers. In addition to the rules regarding the seismic design coefficient, the effects of earthquakes including the deformation of ground caused by earthquakes were comprehensively estimated. Also introduced was a safety consideration to treat the bridge as a total structure system by giving the structural detail to prevent superstructures from falling due to relative displacement between the super- and substructures. In May, 1980, Design Specifications for Road Bridges Part V: Earthquake Resistant Design were issued, in which the evaluation method of liquefaction of the ground was prescribed. Moreover, new ideas to consider the expected effects of liquefaction were applied into the design of foundations. And the regulations concerning ductility calculation of RC piers and earthquake input motions for the earthquake response analysis were newly added.

After that, in February, 1990, Specifications Part V for Earthquake-Resistant Design of Road Bridges were revised. The purpose of the current earthquake-resistant design method is to ensure that the bridge structures will not be damaged by small to middle scale earthquakes which occur with relatively considerable frequency and that bridge collapse will not occur during large-scale earthquakes like the Kanto Earthquake of 1923. Fig. 2.3 shows the flow chart of earthquake-resistant design for road bridges.

#### 2-2-2 Technical standards for earthquake disaster measures

In February, 1988, the "Manual for Earthquake Disaster Prevention Measures (Measures before Earthquake and Post-Earthquake Repair Method)" was published for the purpose of reducing damage to road facilities during large earthquakes and ensuring road traffic after an earthquake.

With regard to measures before earthquakes, while there are some hard measures to provide earthquake-resistant design methods for road structures, so as to have the necessary earthquake resistance and to strengthen road structures with relatively low earthquake-resistance by adding necessary seismic strengthening. There are also some soft measures to provide alternative road structures or routes for minimizing damage effects on road traffic and various measures for rapid repair of damaged structures and restoration of necessary functions after an earthquake. This manual summarizes the methods for evaluating vulnerable structures and seismic strengthening method for the road structures, such as embankments, bridges, tunnels, slopes, etc., and various matters which it is desirable to examine before an earthquake.

For post earthquake measures, roads are indispensable and important facilities for evacuation, transport of emergency goods and reconstruction of various facilities. When roads themselves suffer damage, it is necessary rapidly and precisely to judge the damage situation, to take proper action

Fig. 2.1 Progress of arrangement of technical standards for bridge substructures.

fiscal year	1965	1970	1980	1990	2000
standards for design and construction method of bridge substructures	Guidelines for Design of Substructures of Highway Bridges		Specifications of Highway Bridges, Part IV Specifications for Substructures	Revision of Specifications of Highway Bridges, Part IV Specifications for Substructures	
	Survey and Design in General				
	Design of Abutments and Piers				
	Design of Spread Foundation				
	Design of Caisson Foundation				
	Construction of Caisson Foundation				
	Design of Pile Foundation				
	Construction of Pile Foundation				
	Design and Construction of Cast in Place Piles				
	Guidelines for Design of Steel Pipe Sheet Pile Foundation				
other related standards	Guidelines for Design and Construction of Underground Continuous Wall Foundation		Handbook for Design of Pile Foundation Handbook for Construction of Pile Foundation Handbook for Design for Steel Pipe Sheet Pile Foundation		
	Handbook for Design of Pile Foundation				
	Handbook for Construction of Pile Foundation				
	Handbook for Design for Steel Pipe Sheet Pile Foundation				
	Guideline for Countermeasures against Salt Damage to Road Bridges (draft)				
	Standard for Limitation of the Total Salt Content in Concrete				
	Temporary Measures for Alkali-Aggregate Reaction				
	Cabinet Order concerning Structural Standards for River Administration Facilities, etc.				
	Outline of Road Maintenance and Repair				
	Handbook of Road Bridge Repair				

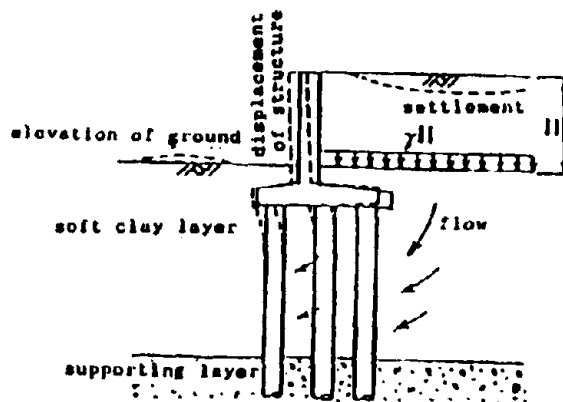


Fig. 2.2 Lateral moving of abutment.

Table 2.1 History of Design Loads for Highway Bridges in Japan

Year	Name of Regulations	Design Live Loads			Impact Loads	Seismic Loads k: Horizontal Seismic Coefficient	Major Earthquake
		Class	Truck Roller Loads Streetcar	Uniform Loads			
1) 1886	Order No. 13 Ministry of Home Affairs (MHA)			U-454 kg/m		not considered	
2)	Order MHA		R-13.6 t S-12.7	U-400 600 kg/m (carriage way) U-270 400 kg/m (footway)		not considered	
3) 1919	Road Laws MHA		R-13.6 t T-11.2 t S-30 t	Same as 2)		not considered	
4) 1926	Specifications for Design for Roads, Road Laws, MHA	1st 2nd 3rd	T-12 t T-8 T T-6 t	U-600 kg/m U-500 kg/m U-500 kg/m		considered Seismic Coefficient Method k=0.15-0.4 depending on location and ground condition (k=0.3 advised in Toyo, Yokohama)	
5) 1939	Specifications for Design for steel Road Bridges, MHA	1st 2nd	T-13 t T-8 T	U-500 kg/m U-400 kg/m		considered Seismic Coefficient Method k=0.2, k=0.1	1946 Nankai (M-8.1)
6) 1956 (and 1964)	Revision of Specifications for Design of Steel Road Bridges, JRA	1st 2nd	T-20 t T-14 t		L-20 (5m) L-14 (3.5m)	considered Seismic Coefficient Method k=0.1-0.35 depending on location and ground conditions	1948, Fukui (M-7.3) 1952 Tochigi-oki (M-8.2)
7) 1964 to 1971	Specifications for Design of Substructure of Road Bridges, JRA		Same as 6)			Same k as (6) Detailed calculation methods	1964 Niigata (M-7.3)
8) 1971	Specifications for Earthquake-Resistant Design of Highway Bridges, JRA		Same as 6)			Seismic Coef. method k=0.1-0.24 (Rigid) Modified SOM k=0.05-0.3 (Flexible)	
9) 1980 Modified SOM	Part V Seismic Design Specifications for Highway Bridges, JRA		Same as 6)			Seismic Coef. Method k=0.1-0.24 (Rigid)  k=0.05-0.3 (Flexible) Earthquake Response Analysis (Very Flexible Bridges)	1978 Miyagi-oki (M-7.4)
10) 1980	Same as 9)		Same as 6)			Seismic Coefficient Method k=0.1-0.3 Bearing Capacity of RC Piers for Lateral Load Dynamic Response	1982 Urakawa-oki (M-7.1)  1982 Nihon-Ichi-chubu (M-7.7)

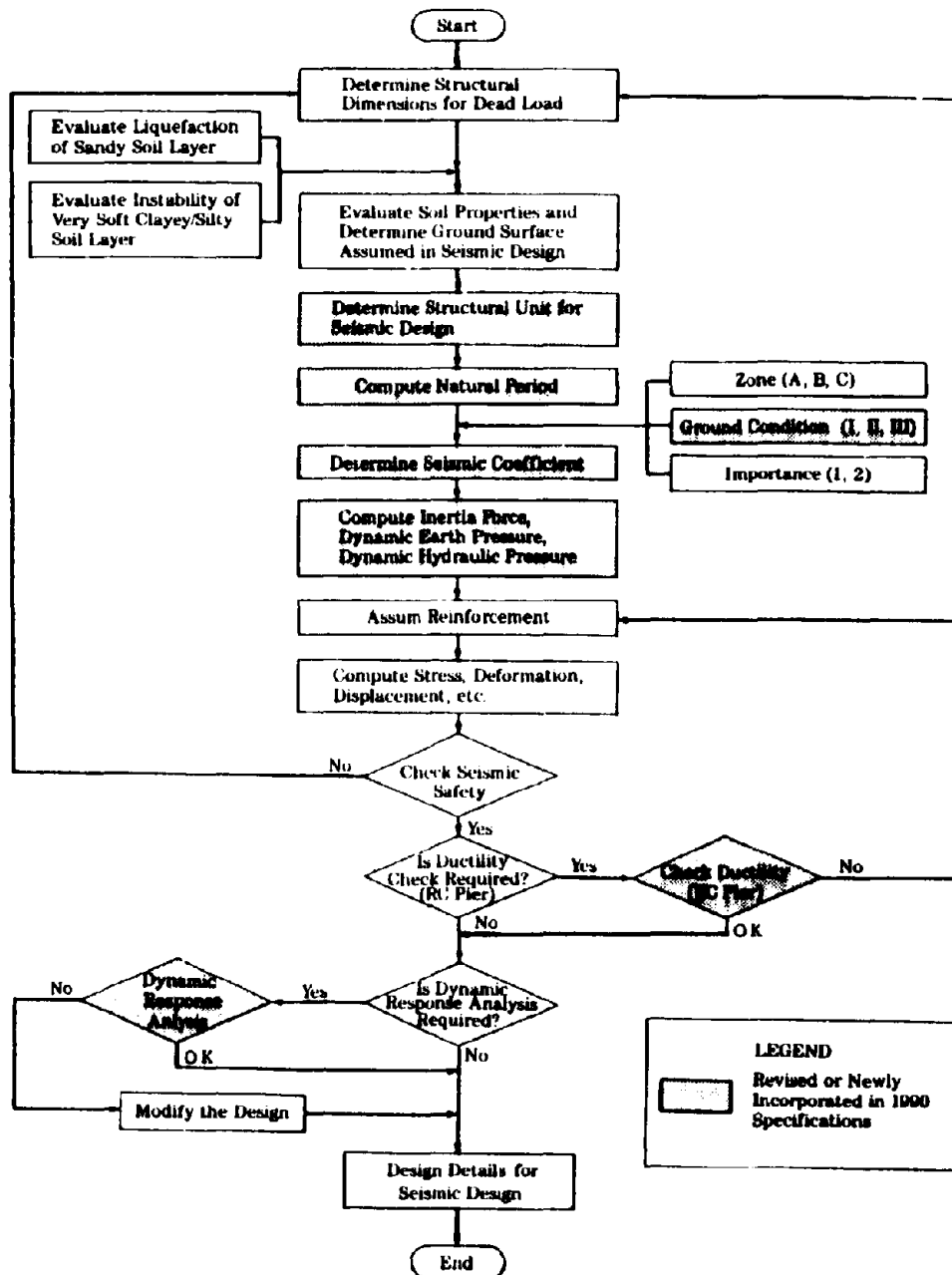


Fig. 2.3 Flow of Seismic Design of Road Bridge

and to precisely carry out temporary and permanent repairs. This manual shows technical methods for damage investigation, judgment of the damage degree and repair methods for various structures, such as embankments, bridges, tunnels, slopes, etc. At the same time, it shows ways to carry out the rapid restoration work, such as strategy for repair of damaged structures, the rehabilitation system, information connection, information to the public, conference between related agencies, etc.

### 3. Design Methods for Substructures

#### 3-1 Distinction of foundation forms by design

Foundations can be classified into shallow and deep ones. Both direct foundations and caisson foundations can be regarded as rigid structures. The difference between them lies in the penetration depth. Generally, they are distinguished by the ratio of penetration depth to foundation width.

Deep foundations can be classified into pile foundations, caisson foundations, assembled steel pile sheet pile foundations, etc. The design method is determined by whether they are regarded as rigid or elastic structures. Generally, the value of  $\beta l$  is used as the criterion of rigidity.

In specifications for Highway Bridges, direct foundations, caisson foundations, pile foundations and steel pipe sheet pile foundations are distinguished as shown in Fig. 3.1 and Fig. 3.2.

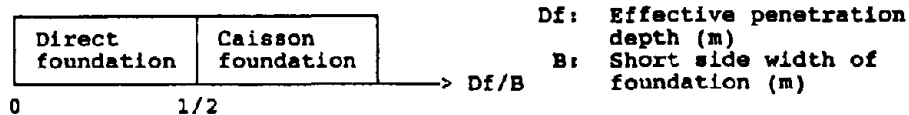


Fig. 3.1 Distinction between Direct Foundation and Caisson Foundation

Foundation form		Rigidity evaluation of foundation	Guideline of $\beta l$ indicating application range of designing method			
Direct foundation		Rigid structure	1	2	3	4
Caisson foundation		Rigid structure (Elastic structure)	←————→			
Steel pipe sheet pile		Elastic structure	←————→			
Pile foundation	Limited length pile	Elastic structure	←————→			
	Semi-unlimited length pile		←————→			

1: Effective penetration depth of foundation (cm)

$\beta$ : Characteristic value of foundation ( $\text{cm}^{-1}$ ),  $\beta = 4 \sqrt{\frac{KH}{4EL}}$

Fig. 3.2 Foundation Forms and Range of  $\beta l$

### 3-2 Concept of Stability Calculation of Foundations

The foundation transmits the loads applied to the superstructure and the substructure to the supporting ground. Therefore, it must be dynamically stable, and must not give rise to harmful displacements. A foundation's mechanism for resisting loads depends on the construction method and the depth of the foundation, as well as the relative rigidity of the foundation and the ground. Therefore, resisting mechanisms must be considered carefully enough to make a design model and to select check items for stability calculation.

Table 3.1 shows stability check items which are used for various types of foundations. Here, horizontal displacement is the horizontal displacement which is restricted by the substructure.

1) A foundation must be stable against bearing, overturning and sliding. Examination relating to overturning is necessary for shallow foundations, such as direct foundations, but is generally unnecessary for deep foundations.

Table 3.1 Check Items for Stability Calculation

Check item		Bearing power		Over- turn	Slid- ing	Horizontal displace- ment
		Verti- cal	Horizon- tal			
Direct foundation		o	(o)	o	o	-
Caisson foundation	$\beta \leq 1$	o	o	-	o	-
	$1 < \beta < 2$	o	o	-	o	o
Steel pipe sheet pile foundation		o	-	-	-	o
Pile	Limited length pile	o	-	-	-	o
	Semi-unlimited length pile	o	-	-	-	o

( o ) means that the item must be checked when the penetrated part partly bears the load.

2) As amounts of displacement allowable for foundations, the following must be considered:

① Allowable displacement determined from the superstructure: This value limits the displacement of a foundation in order to protect the superstructure from harmful influences. It is applicable to a statically indeterminate structure and a statically determinate structure to which displacement is given at the crown of the pier or at the bearing position.

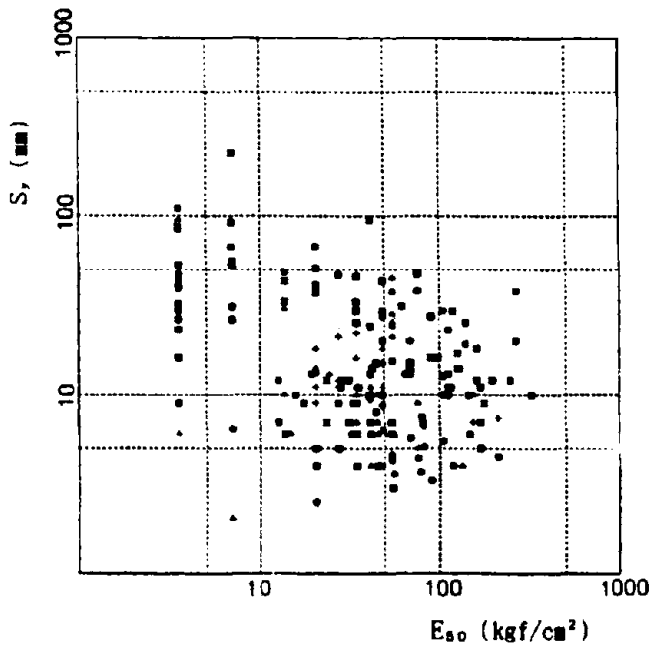


Fig. 3.3 Relationship between Yielding displacement  $S_y$ , and Deformation Modulus of Ground  $E_{50}$

	No. of Data	Symbols
Steel pipe pile	120	□
Cast-in-place pile	29	○
PC pile	31	△
PHC pile	24	+
Total	204	

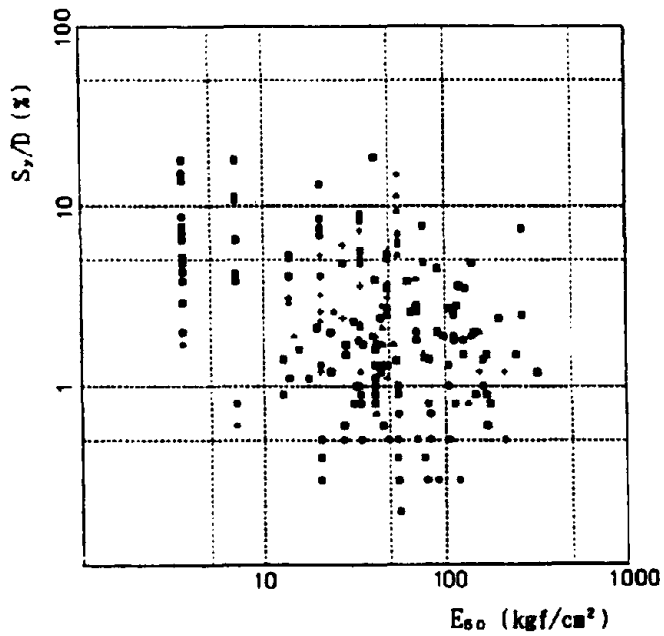


Fig. 3.4 Relationship between  $S_y/D$  and  $E_{50}$



② Allowable displacement determined from the substructure: Excessive horizontal displacement of an elastic foundation is a cause of harmful residual displacement. Therefore, the horizontal displacement of a foundation generally must be within the elastic displacement for assuring its design stability. In other words, the allowable displacement has been determined with the meaning of keeping the horizontal displacement of a foundation within its elastic displacement. Allowable displacement has been set at 1% of the foundation width from many loading tests(Fig. 3.4 and 3.5). In case of a large elastic foundation of more than 5 m in width, 5.0 cm has been set as the limit because only a small amount of loading test data are available and the yield displacement region of a foundation cannot be determined easily. In the case of a pile foundation, 1.5 cm has been set as the minimum value because previous records prove its safety. In case of a rigid foundation, horizontal stability is checked by passive earth pressure because of its large rigidity. Therefore, there is no special restriction as to allowable displacement in the sense of keeping the horizontal displacement within the elastic displacement.

### 3-3 Selection of Bearing Layer and Penetration Depth

A good bearing layer cannot be uniformly defined because it depends on the importance of a structure and the load applied to a foundation. Generally, the following items may be used as criteria.

- 1) A viscous soil layer requires careful study when used as a bearing layer because its bearing power is smaller and its settlement is larger compared to a sand layer. However, it may be considered to be a good bearing layer if its N value is roughly over 20(its unconfined compression strength  $q_u$  is over 4 kgf/cm<sup>2</sup>.)
- 2) A sand layer or a gravel layer may be regarded as a good bearing layer if its N value is over 30. However, the decision must be made carefully because the N value obtained with a gravel layer sometimes appears larger than it really is.

### 3-4 Design Fundamentals

Design methods for spread foundations, caisson foundations, pile foundations and assembled steel pipe pile foundations have been prescribed in the Japanese Specifications. The design guideline for the underground diaphragm wall foundation is under study but at the final stage.

#### 3-4-1 Basics of design of spread foundation

- 1) The vertical ground reaction at the bottom of a spread foundation should not exceed the allowable vertical bearing power of the bottom foundation.
- 2) The position of the resultant loads operation on the spread foundation should be within 1/6 of the bottom width from the center at normal times and 1/3 during earthquakes.
- 3) The shearing resistance at the bottom of the spread foundation should not exceed the allowable shearing resistance of the bottom foundation.

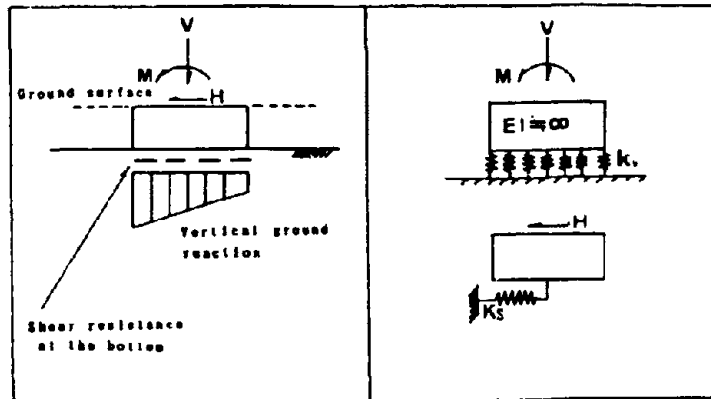


Fig. 3.5 Spread foundation

- 4) The horizontal reaction operating on the embedded depth of the spread foundation should not exceed the allowable horizontal bearing power of the foundation.
- 5) The displacement of the spread foundation should not exceed the allowable amount.

#### 3-4-2 Basics of design of caisson foundation

- 1) Vertical load is to be supported only by the bottom of caisson as a rule. Maximum unit subgrade reaction at the bottom of caisson is not to exceed the allowable unit bearing capacity of the ground at the same location.
- 2) Horizontal load is to be supported by the vertical subgrade reaction at the bottom of caisson, horizontal subgrade reaction of the periphery and shearing resistance at the bottom as a rule.
- 3) Maximum unit subgrade reaction at the front of caisson is not to exceed the allowable unit bearing capacity of the ground, and also the allowable shear resisting force acting between the bottom of caisson and ground.
- 4) Displacement at the top of caisson is to be reviewed by taking account of the allowable displacement determined from the relation with the superstructure.
- 5) Unit stress at each part of caisson is not to exceed the allowable unit stress during and after the work.

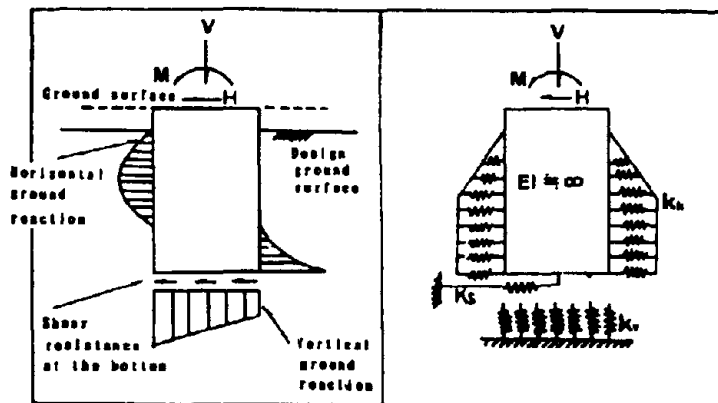


Fig. 3.6 Caisson foundation

### 3-4-3 Basics of design of the pile foundation

- 1) Pile foundation is to be so designed that the reaction at the head of each pile will be lower than the allowable bearing capacity of the pile.
- 2) If the displacement is restricted by the relationship to the superstructure or by the required rigidity of pile foundation, it is required to examine the displacement.
- 3) Depth of embedment of pile is to be determined by comprehensively taking account of the type and functions of superstructure, bearing mechanism of pile and workability.
- 4) When using piles for the ground which may cause the consolidation settlement after work, it is required to examine the influence of ground settlement upon the foundation.
- 5) Vertical load is to be supported only by piles as a rule.
- 6) It is better to support also the horizontal load only by piles as a rule. When supporting the load together with piles and embedded portion of footing, it is desired to calculate the proportion of the load to be supported by each of them by taking account of the displacement.
- 7) It is desired to arrange piles in such a manner that long-sustained load will be supported by all piles as uniformly as possible. Also, the piles are to be arranged by taking account of the rigidity of footing and shares of load.
- 8) Standard minimum interval of piles is to be 2.5 times the diameter of pile.

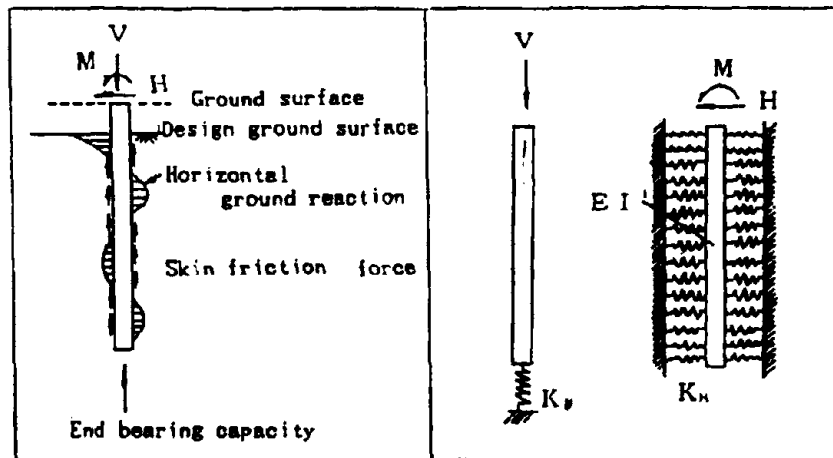


Fig. 3.7 Pile foundation

### 3-4-4 Basics of design of assembled steel pipe foundation

- 1) Vertical load is to be supported by the bottom ground reaction and skin frictional force.
- 2) The vertical ground reaction at the bottom of steel pipe pile should not exceed the allowable vertical bearing power at the bottom of foundation.
- 3) Horizontal load is to be supported by the vertical subgrade reaction, sharing resistance at the bottom of foundation and the horizontal subgrade reaction of the periphery.
- 4) The displacement of steel pipe pile foundation should not exceed the allowable amount determined from the relation with superstructure.

- 5) Unit stress at each part of foundation is not exceed the allowable unit stress during and after the work.

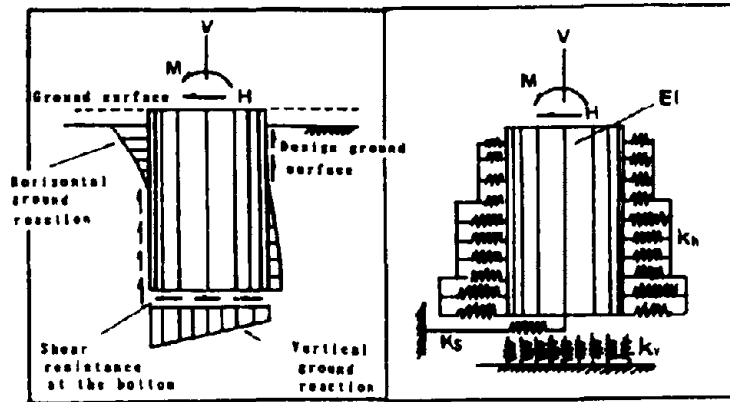


Fig. 3.8 Assembled steel pipe pile foundation

#### 3-4-5 Basics of design of underground diaphragm wall foundation

- 1) Vertical load is to be supported by the bottom ground reaction and skin frictional force.
- 2) The vertical ground reaction at the bottom of foundation should not exceed the allowable vertical bearing power at the bottom of foundation.
- 3) Horizontal load is to be supported by the vertical subgrade reaction and shearing resistance at the bottom of foundation, the horizontal subgrade reaction of the front of foundation, shearing resistance of the both sides of foundation.
- 4) The displacement of diaphragm wall foundation should not exceed the allowable amount determined from the relation with superstructure.
- 5) Unit stress at each part of foundation is not exceed the allowable unit stress during and after the work.

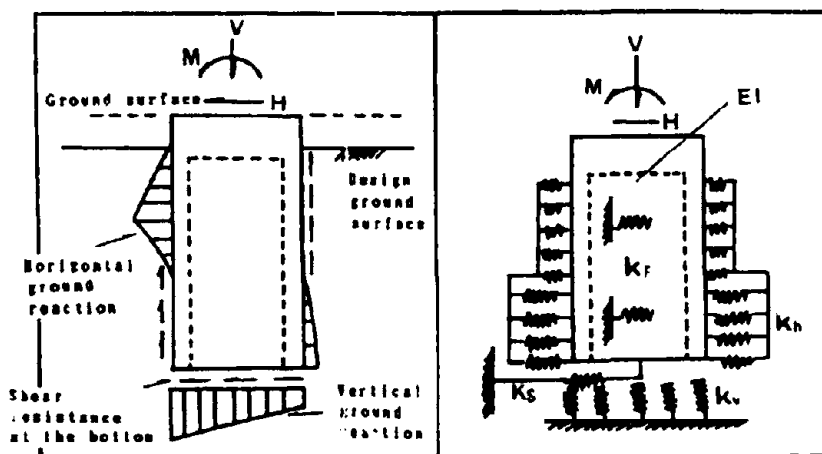


Fig. 3.9 Underground diaphragm wall foundation

### 3-5 Design Procedure of Pile Foundation

#### 3-5-1 The design procedure of pile foundation

The design procedure of pile foundation is shown in Fig.3.10.

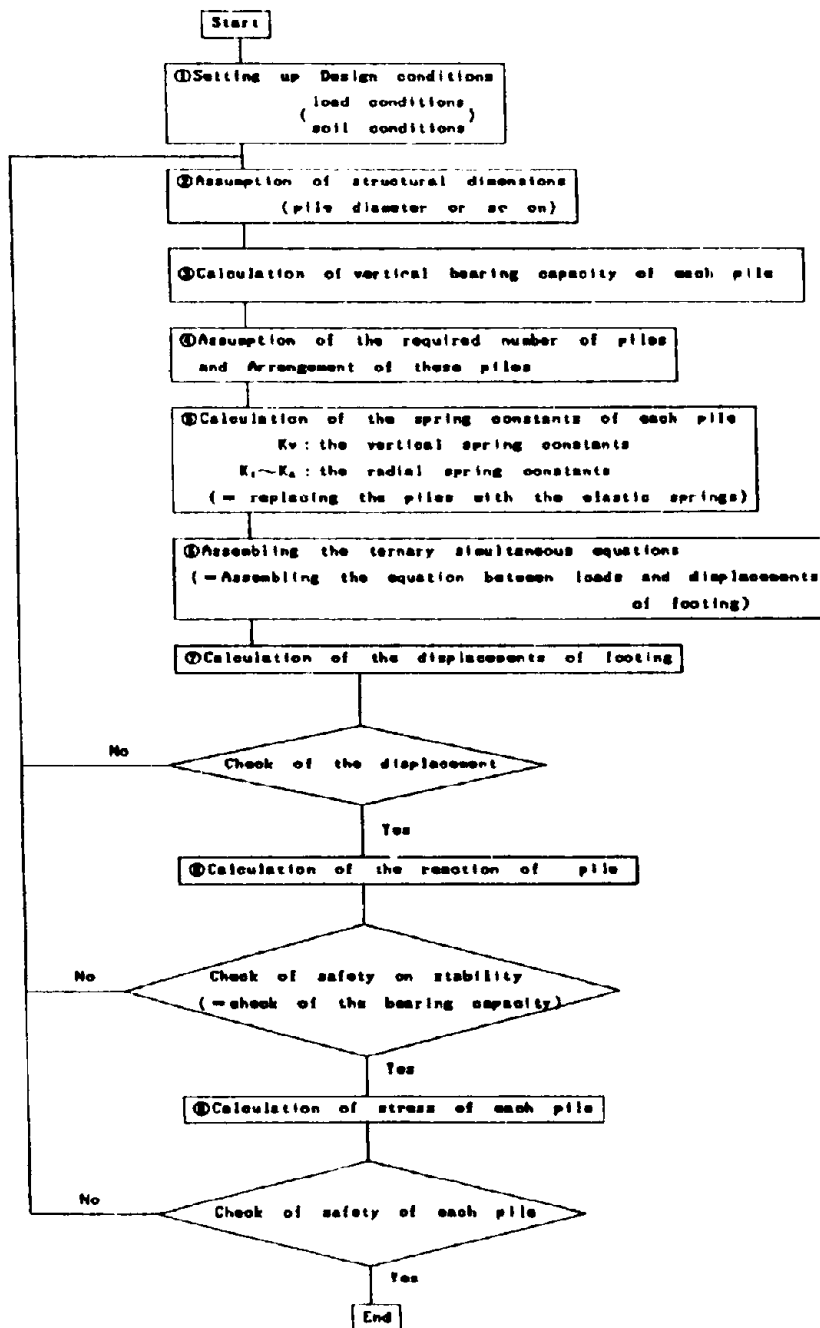


Fig. 3.10 Design Procedure of Pile Foundation

### 3-5-2 Vertical bearing capacity

Formula of bearing capacity of a pile is given below.

$$R_a = \frac{\gamma}{n} (R_u - W_s) + W_s - W$$

In which  $R_a$ : Allowable push bearing capacity in the axial direction at the pile head (tf)

$n$  : Safety factor shown in Table 3.2

$\gamma$  : Safety factor correction coefficient according to differences in the ultimate bearing capacity estimating method.

$R_u$ : Ultimate bearing capacity of pile determined from the ground (tf)

$W_s$ : Effective weight of the earth to be replaced by the pile (tf)

$W$  : Effective weight of the pile and earth in the pile (tf).

Table 3.2 Safety Factors

Pile type Loading type	Bearing pile	Friction pile*
	During normal times	3
During earthquakes	2	3

If the friction pile under the following conditions is used, the safety factors for bearing piles are applied to friction piles which have the same degree of safety as bearing piles.

- ① Heavy ground settlement is neither in progress at present, nor anticipated in the future.
- ② The pile length is at least 25 times as large as the pile diameter (Fig. 3.11). (The length must be at least 25m for piles with a diameter larger than 1m.)
- ③ If the ground is cohesive, at least 1/3 of the overall pile length is penetrated into over consolidated ground.

For a friction pile, the bearing capacity of the end is not considered in principle. Since inner digging piles of the friction pile type have not been used and their bearing capacity characteristics are unknown, they should not be adopted in principle.

Safety relating to the bearing capacity of a pile is to be guaranteed by the safety factor correction coefficient which is determined with consideration given to the accuracy of the ultimate bearing capacity estimating method (Table 3.3).

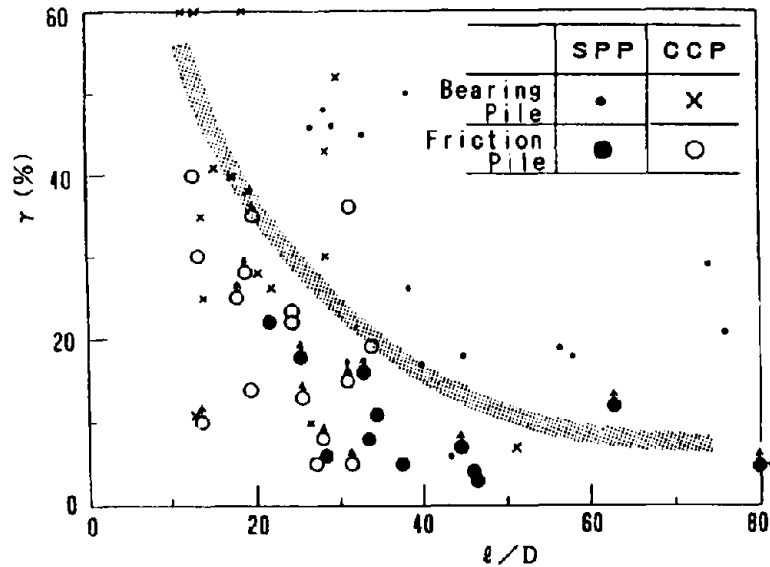


Fig. 3.11 Percentage of transmitted load to the end bearing ground  $\gamma$  and penetration ratio  $\ell/D$

Table 3.3 Safety Factor Correction Coefficient  $\gamma$  according to Ultimate Bearing Capacity Estimating Method (Fig. 3.12)

Ultimate bearing capacity estimating method	Safety factor correction coefficient
Bearing capacity formula	1.00
Vertical loading test	1.20

$R_u$  is the ultimate bearing capacity of a pile which is determined from the ground. It is determined by the following equation from the end bearing capacity and the skin friction bearing capacity.

$$R_u = q_d \cdot A + U \sum \Delta z_i \cdot f_i$$

In which  $q_d$ : Ultimate bearing capacity per unit area at pile end ( $\text{tf}/\text{m}^2$ )

$A$ : Pile end area ( $\text{m}^2$ )

$U$ : Circumferential length of pile (m)

$\Delta z_i$ : thickness of layer requiring consideration of skin frictional force (m)

$f_i$ : Maximum skin frictional force of layer requiring consideration of skin frictional force ( $\text{tf}/\text{m}^2$ )

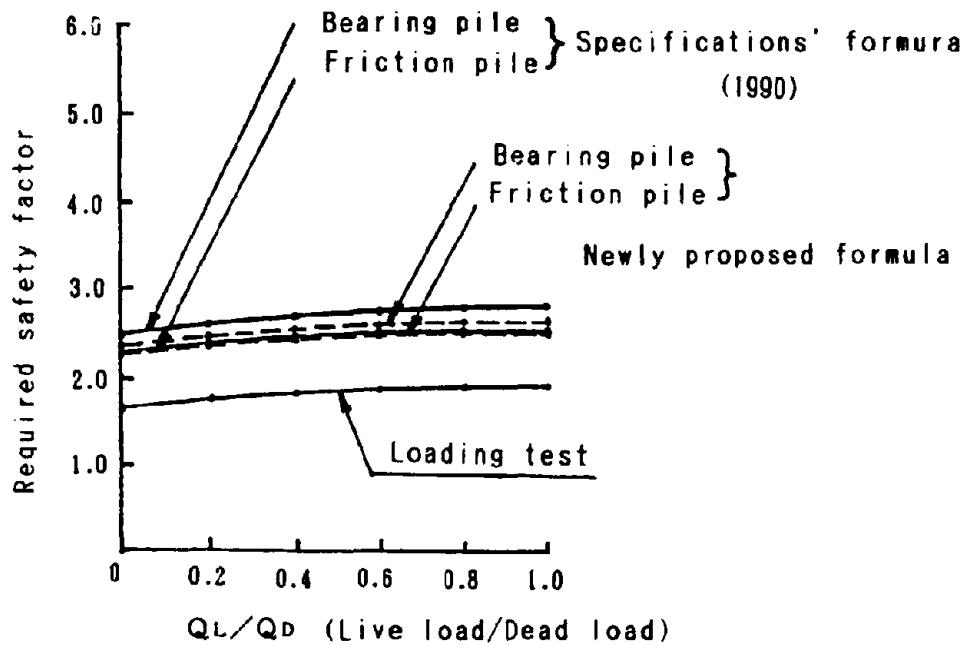


Fig. 3.12 Comparison of required safety factor for prediction methods of bearing capacity (in case of cast in place pile)

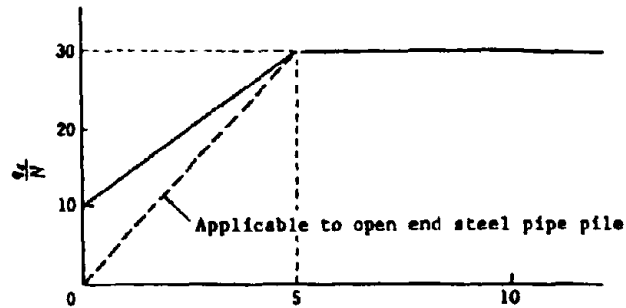
1) Estimation of end bearing capacity  $q_d$

① Estimation of ultimate bearing capacity of pile end  $q_d$ .

In case of driving pile, the ultimate bearing capacity of the pile end is estimated from Fig. 3.13.



In Fig. 3.13,  $\bar{N}$  (N value of pile end ground used for design) is obtained with the following equation:



$$\left( \frac{\text{Converted penetration depth to bearing layer}}{\text{Pile diameter}} \right)$$

Fig. 3.13 Ultimate Bearing Capacity  $q_d$  of Pile End Ground

$$\bar{N} = \frac{N_1 + \bar{N}_2}{2} \quad (\bar{N} \leq 40)$$

In which  $N_1$ : N value at pile end position

$\bar{N}_2$ : Average N value in a range of 4 x the pile diameter in an upward direction from the pile end

② In case of cast in place pile,  $q_d$  is given by Table 3.4.

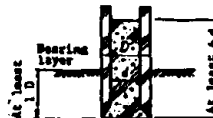
Table 3.4 Estimated  $q_d$  of Cast-in-place Piles (tf/m<sup>2</sup>)

Ground type	Ultimate bearing capacity of end
Gravel layer or sand layer ( $N \geq 30$ )	300
Hard cohesive earth layer	$3q_u$

Note that  $q_u$  is the unconfined compression strength (tf/m<sup>2</sup>)

③ For inner digging piles,  $q_d$  is taken from Table 3.5, according to the end treatment method.

Table 3.5 Ultimate Bearing Capacity of End of Inner Digging Piles

End treatment method	Calculation method of end bearing capacity
(a) Final impact	The method used for a driving pile is applied.
(b) Cement milk eruption and agitation	Bearing capacity of end ( $tf/m^2$ ) $q_d = \begin{cases} 15N (\leq 750) & \text{Sand layer} \\ 20N (\leq 1,000) & \text{Gravel layer} \end{cases}$ in which N: N value of pile end ground
(c) Concrete placing 	The end bearing capacity of a cast-in-place pile is applied.

2) Estimation of maximum frictional force of pile skin  $f_s$

The maximum frictional force of pile skin is estimated from Table 3.6, according to the pile construction method and the ground type.

Table 3.6 Skin Frictional Force ( $tf/m^2$ )

Ground type	Driving pile method	Cast-in-place pile method	Inner digging pile method
Sandy ground	$0.2N (\leq 10)$	$0.5N (\leq 20)$	$0.1N (\leq 5)$
Cohesive ground	$C \text{ or } N (\leq 15)$	$C \text{ or } N (\leq 15)$	$0.5C \text{ or } 0.5N (\leq 10)$

Note: Skin frictional resistance should not be considered in the case of a soft layer of  $N \leq 2$ .

### 3-5-3 Coefficient of ground reaction in the horizontal direction

The coefficient of ground reaction in the horizontal direction is obtained by the following equation.

$$k_H = k_{H0} \cdot \left( \frac{B_H}{30} \right)^{-3.4}$$

In which

$k_H$  : Coefficient of ground reaction in the horizontal direction (kgf/cm<sup>3</sup>).

$k_{H0}$ : Coefficient of ground reaction in the horizontal direction (kgf/cm<sup>3</sup>) which is equivalent to the value of a plate loading test using a rigid disc of 30 cm (diameter). It is obtained by the following equation when it is estimated from the modulus of deformation obtained from various soil tests and investigations.

$$k_{H0} = \frac{1}{30} \alpha \cdot E_0$$

$B_H$  : Converted loading width (cm) of the foundation perpendicular to the loading direction. In case of ground related to the horizontal resistance of an elastic foundation, a range from the design ground level to about  $1/\beta$  should be considered.

$E_0$  : Modulus of ground deformation of the position usually obtained by N-values(kgf/cm<sup>2</sup>).

$\alpha$  : Modulus used for estimating the coefficient of ground reaction.

$A_H$  : Loading area of the foundation (cm<sup>2</sup>) perpendicular to the loading direction.

$D$  : Loading width of the foundation (cm) Perpendicular to the loading direction.

$1/\beta$  : Depth of ground related to the horizontal resistance (cm). It should not be less than foundation length.

$\beta$  : Characteristic value of the foundation

$$\sqrt[4]{\frac{k_H \cdot D}{4EI}} \quad (\text{cm}^{-1})$$

$EI$  : Bending rigidity of the foundation (kgf·cm<sup>2</sup>)

Fig. 3.14 shows comparison of observed and calculated k-values.

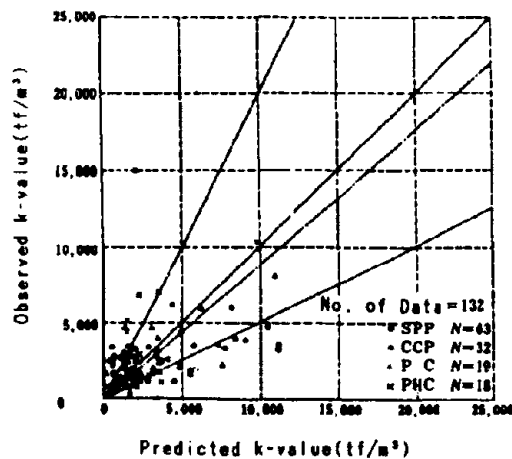


Fig. 3.14 Comparison of k-values

### 3-5-4 Coefficient of pile head reaction in the vertical direction

The coefficient of pile head reaction in the vertical direction  $k_v$  (vertical spring constant of a pile) is defined by the following eq.

$$k_v = a \frac{A_p E_p}{l}$$

Where,

a: Coefficients (Table 3.7)

$A_p$ : Sectional area of a pile

$E_p$ : Yang's modulus of a pile

$l$ : Pile length

In case of steel pipe piles, Fig. 3.15 shows prediction errors of  $k_v$ -values compared with observed values.

Table 3.7 Prediction formula of a constants

Construction methods	$a = \alpha (l/D) + \beta$
S P P	$0.014(l/D) + 0.78$
P C · P H C	$0.013(l/D) + 0.61$
C C P	$0.031(l/D) - 0.15$
Embedded S P P	$0.009(l/D) + 0.39$
Embedded P C	$0.011(l/D) + 0.36$
P B P	$0.009(l/D) + 0.81$

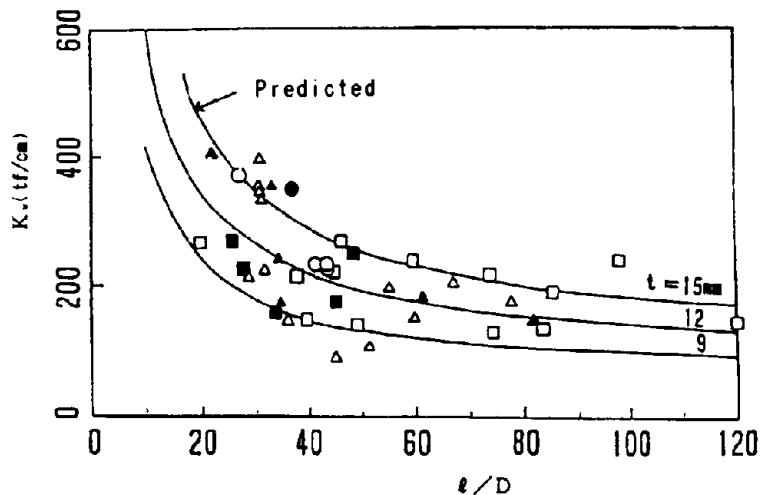


Fig. 3.15 Comparison of predicted and observed  $k_v$  values (in case of SPP)

## DESIGN DETAILS OF REINFORCED CONCRETE BRIDGES IN JAPAN

Taisuke Akimoto (I)

### HISTORY OF SPECIFICATIONS OF CONCRETE BRIDGES

"Standard Specifications for Concrete" (Japan Society of Civil Engineers (JSCE)) had been revised again and again since its establishment in 1931, and in 1949 it became almost the same format as is today. The revision was repeated in 1956, 1967, and 1974. Finally, after design method for shear forces was changed in 1980, basic design concept was changed from "Allowable Stress Design" to "Limit Design" in 1986.

In designing reinforced concrete highway bridges, loads and allowable stresses were decided based on "Road Law". On the other hand, design calculation and structural details were determined using "Standard Specifications for Concrete" (JSCE). In addition, "Specifications for Reinforced Concrete Highway Bridges" was established in 1964 as the first specifications for concrete highway bridges. While loads and structural details were specified in "Specifications for Reinforced Concrete Highway Bridges", design calculation was made based on "Standard Specifications for Concrete" of 1956 (JSCE).

In 1978, "Specifications for Highway Bridges, Part III: Concrete Bridges" was established, combining "Specifications for Reinforced Concrete Highway Bridges" and "Specifications for Prestressed Concrete Highway Bridges (1968)". Before that, in 1971, "Seismic Specifications for Highway Bridges" was established, contributing successfully to the seismic design of Japan. Furthermore, in 1975, "Guide for Reinforced Concrete Structures Using D51 Reinforcing Bars (Tentative)" (JSCE) was established, in which a design idea of the anchorage of longitudinal reinforcement at mid-height of a reinforced concrete bridge pier was clearly presented. At the same time, "Limit Design" was energetically discussed outside Japan. Consequently, the revision of 1978 became drastic. The major changes are as follows:

- (1) In addition to conventional stress checks based on "Allowable Stress Design", "Limit Design" under ultimate loads was obliged.
- (2) Design method for shear forces and allowable stresses were changed, while design method for torsion, structural details (minimum amount of reinforcement, anchorage in a tensile zone, and etc.), and construction were added.

Other parts of "Specifications for Highway Bridges" (Part I: Common Specifications (Loads, Materials, and etc.), Part II: Steel Bridges, Part IV: Substructures, and Part V: Seismic Design) were revised in 1980, and the design of bridge piers and foundations could be made based on "Part IV". Before the revision, "Specifications for Reinforced Concrete Highway Bridges" and "Standard Specifications for Concrete" (JSCE) were used for stress calculation and structural details.

---

(I) Head, Design and Research Division, Engineering Department  
Metropolitan Expressway Public Corporation, Tokyo 100, Japan

Since there is a possibility that the difference in the degree of safety might be induced between the old and new design of concrete bridge piers and etc. due to the "Specifications for Highway Bridges" revision of 1978 to 1980, the necessity of preventive maintenance has been studied.

In 1990, "Specifications for Highway Bridges (Part I - V) were revised. While there is no big change in Part III (Concrete Bridges), drastic change is made in Part V that check for horizontal ultimate strength of reinforced concrete bridge piers at the time of earthquake is specified. Consequently, the design for ductility of reinforced concrete bridge piers became clear. As the change might also cause the difference in the degree of safety between existing and future bridge piers, the necessity of preventive maintenance is examined.

The specifications of JSCE employed "Limit Design" in 1986. As for highway bridges, research is being carried out to revise the specifications based on "Limit Design" in 2001.

#### MAJOR CHANGES IN SPECIFICATIONS FOR REINFORCE CONCRETE HIGHWAY BRIDGES

In this section, major changes concerning seismic design in "Specifications for Reinforced Concrete Highway Bridges" are discussed except for loads and materials.

##### Design Methods

The 1978 revision of general rule for design calculation in "Specifications for Highway Bridges Part III: Concrete Bridges" was that check for safety factor based on "Limit Design" was specified in addition to conventional check for stresses based on "Allowable Stress Design". In other words, this "Specifications" is considered to be at a transition stage to the future specifications based on "Limit Design". The revision made design a little complicated. But, at the same time, the "Specifications" clarifies the way the future design specifications should be since it shows the dilemma of both design concepts.

The "Limit Design" has not been established yet in the "Specifications" since only the following loads are specified.

- o 1. 0 or 1. 3\* (Dead Load) + 2. 5\* (Live Load + Impact)
- o 1. 7\* (Dead Load + Live Load + Impact)
- o 1. 0 or 1. 3\* (Dead Load) + 1. 3\* (Earthquake Force)

The yield strength of members is supposed to check for sectional forces due to the above-mentioned loads. In general, the design of main girder with shorter span, slab, and substructure tends to be determined by "Limit Design".

In the design of many reinforced concrete piers, the check based on "Limit Design" will be unnecessary when finishing check for horizontal ultimate strength at the time of earthquake based the "Specifications, Part V" of 1990. Consequently, the design method will be established based on future research.

##### Design of Members Subject to Shear Forces

Before the 1978 revision of "Specifications for Highway Bridges, Part

III: Concrete Bridges", the design of members for shear forces was made as follows:

o  $\tau = S/(b \cdot j \cdot d) \leq \tau_{a1}$  ..... (1) (Minimum shear reinforcement shall be arranged since concrete resists shear forces.)

o  $\tau_{a1} \leq \tau \leq \tau_{a2}$  ..... (2) (Required shear reinforcement shall be arranged using the following equation.)

$$A_w = (S \cdot a) / [\sigma_{as} \cdot j \cdot d (\sin \theta + \cos \theta)] \dots \dots \dots (3)$$

o  $\tau > \tau_{a2}$  ..... (4) (Larger concrete cross section shall be used.)

where, S: Shear force at the section of a member

b: Web thickness or width of a member

j · d: Distance from the action point of the resultant of compressive stresses to the centroid of the tension steel

a: Pitch of diagonal tension reinforcements in the axial direction of the member

θ: Angle between the diagonal tension reinforcement and the axial direction of the member

σ<sub>su</sub>: Allowable stress of reinforcement BSD30 .. 1800 kg/cm<sup>2</sup>)

τ<sub>a1</sub>: Allowable shear stress of concrete (Table 2)

τ<sub>a2</sub>: Maximum allowable shear stress of concrete (Table 2)

Table 2 Allowable shear stress of concrete (kg/cm<sup>2</sup>)

Specified compressive strength of concrete	210	240	270	300
τ <sub>a1</sub>	6	7	8	9
τ <sub>a2</sub>	18	20	22	24

In the 1978 revision, the design of members for shear forces was changed as follows:

o  $\tau_m = S/(b \cdot d) \leq \tau_a$  ..... (5) (Minimum shear reinforcement shall be arranged since concrete resists shear forces.)

o  $\tau_a \leq \tau_m \leq 2\tau_a$  OR  $\tau_a \leq \tau_m$ ,  $\tau_m = S_u/(b \cdot d) \leq \tau_{max}$  .. (6) (Required shear reinforcement shall be arranged using the following equation.)

$$A_w = 1.15 [(S - 0.5 \cdot S_c) \cdot a] / [\sigma_{as} \cdot d (\sin \theta + \cos \theta)] \quad (7)$$

$$\text{or, } A_w = 1.15 [(S_u - S_c) \cdot a / \sigma_{sy} \cdot d (\sin \theta + \cos \theta)] \quad (8)$$

o  $\tau_m \leq \tau_{a2}$  OR  $\tau_m \leq \tau_{max}$  ..... (9) (Larger concrete cross section shall be used.)

where,  $d$ : Effective depth of the section of a member, the distance from the extreme compressive fiber of the member to the centroid of the tension reinforcements

$S_u$ : Shear force due to the ultimate loads at the section of a member

$S_c$ : Shear force carried by concrete

$$S_c = \tau_a \cdot b \cdot d \quad \dots\dots\dots (10)$$

$\sigma_{sy}$ : Specified yield strength of diagonal tension reinforcements

$\tau_a$ : Allowable shear stress of concrete (Table 3)

$\tau_{max}$ : Upper limits of shear stress of concrete (Table 3)

Table 2 Allowable and Upper Limits of Shear Stress of Concrete (kg/cm<sup>2</sup>)

Specified compressive strength of concrete	210	240	270	300
$\tau_a$	3.6	3.9	4.2	4.5
$\tau_{max}$	28	32	36	40

Figure 1 shows the relationship between shear stress and stress supported by stirrup concerning the above-mentioned revision.

Furthermore, the 1990 revision specifies the check for horizontal ultimate strength of reinforced concrete bridge piers at the time of earthquake to design ductile bridge piers, which are expected to show bending failure prior to shear failure during earthquake.

Minimum Reinforcement

Before the 1978 revision, structural details were designed based on "Standard Specifications for Concrete" (JSCE).

Minimum amount of reinforcement was specified as follows:

- o Tension or compression reinforcement of beam  $A_{st} \dots A_{st}/(b \cdot d) \leq 15/\sigma_{sy} = 0.5\%$  (SD30;  $\sigma_{sy} = 3000 \text{ kg/cm}^2$ )
- o In beams, stirrups ( $D \leq 6 \text{ mm}$ ) shall be arranged. The spacing of stirrups 1 shall be (1) In case  $\tau_{a1} \leq \tau \leq \tau_{a2}$ ,  $1 \leq 2/d$  and  $b$ , and (2) In case  $1 \leq d$ . When compression reinforcement is provided,  $1 \leq 15 \times (\text{Diameter of Compression Reinforcement})$  and  $48 \times (\text{Diameter of Stirrup})$ .
- o As for the longitudinal reinforcement of columns, (Diameter)  $\leq 12 \text{ mm}$ , (number)  $\leq 4$ , and  $0.8\% \times (\text{Concrete Cross Sectional Area}) \leq (\text{Area}) \leq 6\% \times (\text{Concrete Cross Sectional Area})$ .
- o As for ties of column, (Diameter)  $\leq 6 \text{ mm}$ , (Spacing)  $\leq (\text{Minimum Horizontal Dimension of Column})$ ,  $12 \times (\text{Diameter of Longitudinal Reinforcement})$ , and  $48 \times (\text{Diameter of Tie})$ . Enough ties shall be provided at column joints of beams and etc.



The following changes were made in the 1978 revision. No other changes were made, then.

- o At any section, bonded steel ( $\leq D13$ ; Deformed bar, diameter 13 mm) of 0.15% or more of the area of the member shall generally be arranged.
- o Girder - Area of axial tension main reinforcements  $A_{st} \leq 0.005b \cdot d$   
 - However, the above needs not be applied for a girder having arranged reinforcements not less than 4/3 of the required value by calculation.  
 - Area of diagonal tension reinforcements  $A_w \leq 0.002b \cdot a \cdot \sin \theta$   
 -  $a \leq d/2$  and 30 cm ( $\tau_{a1} \leq \tau_{a2}$ ),  $a \leq 3d/4$  and 40 cm ( $\tau \leq \tau_{a1}$ )
- o Column - Area of axial main reinforcements  $A_s \leq 0.008 A$   
 (A; Sectional area of the column)  
 - Area of diagonal tension reinforcements  $A_w \leq 0.0015b \cdot a \cdot \sin \theta$   
 -  $a \leq b_{min}/2$  and 30 cm ( $b_{min}$ ; Minimum size of member section)  
 - Arrangement of reinforcements at an intermediate joint of rigid frame members ..... Fig. 2

The following changes are made in the 1990 revision.

- o Column: In Part IV, appropriate amount of tie is specified for longitudinal reinforcement.

Table 3 Appropriate Tie

$p_t$ (%)	$0 < p_t \leq 0.5$	$0.5 < p_t \leq 1.0$	$1.0 < p_t$
$p_w$ (%)	0.15	0.20	0.25

(Note) Where  $p_t$ : Longitudinal tensile reinforcement ratio  
 $p_w$ : Tie ratio  
 In case  $D \leq 35$  mm, stirrups ( $D \leq 16$ ) shall be arranged.

Tie arrangement at column joints of beams or footing is changed as shown in Fig. 3.

Since 1967 "Standard Drawings for Reinforced Concrete Structures" of the Metropolitan expressway Public Corporation has been specifying that D16-22 ties shall be used for longitudinal reinforcement with a diameter of more than D29.

Anchorage of Main Reinforcement in Tensile Zone of a Member

As for development of reinforcement, no drastic change has been made since the establishment of "Standard Specifications for Concrete" of 1956 (JSCE). (Fig. 4)

In general, the anchorage of reinforcement shall be made in compression zone of a member. But in some cases such as anchorage at mid-height of reinforced concrete bridge pier, it is unavoidable to anchor bars in tensile zone of a member. In such cases, as specified in "Standard Specifications for Concrete" of 1967 (JSCE), reinforcement shall be extended beyond a point of concrete where design calculation shows reinforcement does not need to support bending moment. Although the article

specifies the anchorage length shall be determined to avoid harmful cracking of concrete near the end of anchored bar as well as to have enough development length, no specific values are given. At this point, "Guide for Reinforced Concrete Structure Using D51 Reinforcing Bars (Tentative)" of 1975 (JSCE) specifies clearly that the reinforcing bars at the second layer may be cut at the point where reinforcing bars are extended by the same length as the effective depth of the beam from the cross section where design calculation shows no reinforcement is necessary, bent at an appropriate angle, and extended 20 from the bending point. In this case, enough consideration shall be given to avoid affecting concrete cracking and ultimate shear strength. In addition, "Commentary" indicates that in case anchored bars occupy more than 20% of whole tensile reinforcement arranged at the cross section, design shall be made to meet the following two articles for shear stress near the bending point of reinforcing bars: (a)  $\tau \leq 0.6 \tau_{a2}$ . (b) Even if  $\tau \leq \tau_{a1}$ , all the shear forces shall be supported by ties.

In response to the above, "Specification for Highway Bridges, Part III: Concrete Bridges" of 1978 indicates the following in "Commentary".

When it is inevitable to anchor the main reinforcements in the tensile portion of a member, either of the following measures must be taken.

- (1) The reinforcements to be anchored shall be extended from the section where the reinforcements are calculated to be not necessary by a length equal to the effective depth, and at the position, be bent at a proper angle so as to take a large cover. Then, they shall be extended from there by a length of not less than 20 times the diameter of reinforcements and be stopped. However, in this case, the shear stress under the ultimate loads between the position of no necessity for reinforcements and the point of the stop shall be 1/3 or less of the value  $\tau_{max}$ .
- (2) Reinforcements to be anchored shall be extended and stopped at the position where the tensile stress of continuous reinforcements becomes 1/2 or less of the allowable stress  $\sigma_{sa}$ . However, in this case, the shear stress under the service loads between the position of no necessity for reinforcements and the point of the stop shall be 2/3 or less of the value  $\tau_{a1}$ , and the length between the two positions shall not be less than the required anchorage length.

In the 1990 revision, the condition for shear stress is  $\tau \leq 2/3 \tau_{a2}$  to be applicable to check for design loads.

Additionally, since 1967 "Standard Drawings for Reinforced Concrete Structures" of the Metropolitan Expressway Public Corporation has been specifying that at least one half of whole main reinforcement of column shall be extended to the top, and that the rest shall be divided into at least two parts and anchored at mid-height.

#### Splices of Reinforcement

Although there is no big changes from the previous one, articles for design and execution of gas welding splices were specified in 1978. Generally, reinforcing bars with a diameter of more than D29 are welded with gas. In 1982, "Guide for Splices of Reinforcement" (JSCE) was established and quality criteria for mechanical splices were specified. Various types of splices are now used which meet the criteria.

### Other Details

Other structural details are as follows:

- o Traditionally, haunches are generally made at column joints of beams, and haunch reinforcement is provided as shown in Fig. 6.
- o Bending Radiuses of reinforcing bars, which are traditionally used, are shown in Fig. 7.
- o Reinforcement arrangement for torsion, which was specified in the 1978 revision, is shown in Fig. 8.
- o Ties for large cross section, which was specified in the 1978 revision, is shown in Fig. 9.
- o Reinforcement arrangement for joints of rigid frame, which was specified in 1978 revision, is shown Fig. 10.
- o Reinforcement arrangement for footing, which was specified in 1980 revision, is shown in Fig. 11.
- o Reinforcement arrangement for pile, which was specified in 1980 revision, is shown in Fig. 12.
- o Traditionally, specified compressive strength of concrete  $\sigma_{ck}$  is 210 kg/cm<sup>2</sup>. As for reinforcing bars, SD30 ( $\sigma_{sy}$ =3000 - 4000 kg/cm<sup>2</sup>,  $\sigma_{su}$  4500 kg/cm<sup>2</sup>, and elongation 16% was generally used. But since then 1978 revision, SD35 ( $\sigma_{sy}$ =3500 - 4500 kg/cm<sup>2</sup>,  $\sigma_{su}$ =5000 kg/cm<sup>2</sup>, and elongation 18%) has been used.

### EXAMPLES OF REINFORCEMENT ARRANGEMENT FOR CONCRETE SUBSTRUCTURES

- (1) Reinforcement arrangement for rigid frame bridge pier is shown in Fig. 13 (1) and (3).
- (2) Reinforcement arrangement for footing is shown in Fig. 14.
- (3) Reinforcement arrangement for cast-in-place concrete pile is shown in Fig. 15.
- (4) Reinforcement arrangement for two storey rigid frame bridge pier is shown in Fig. 16.

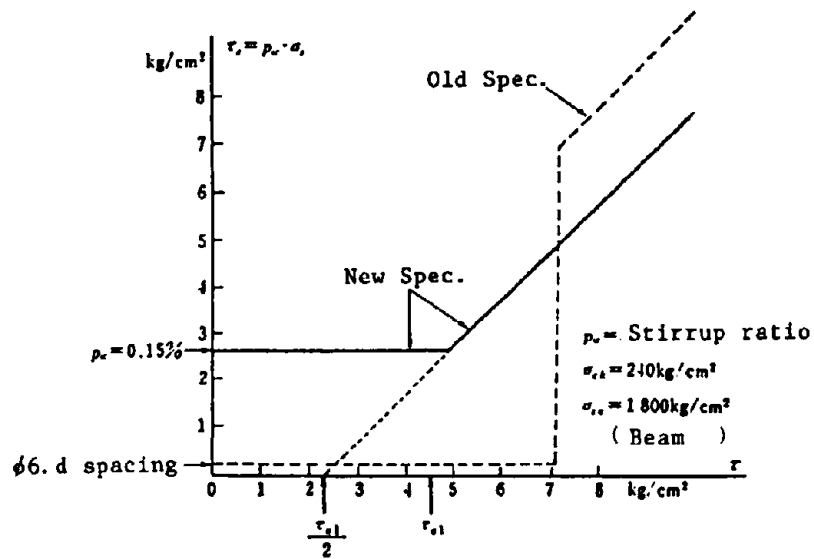


Fig. 1 Relationship between Applying Shear Stress and Shear Stress Supported by Stirrup

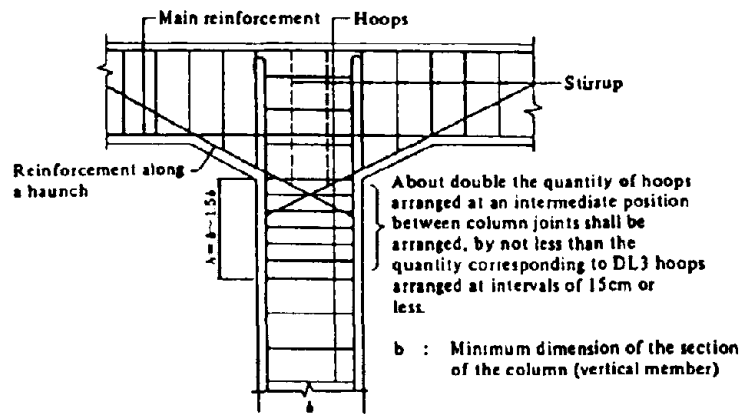
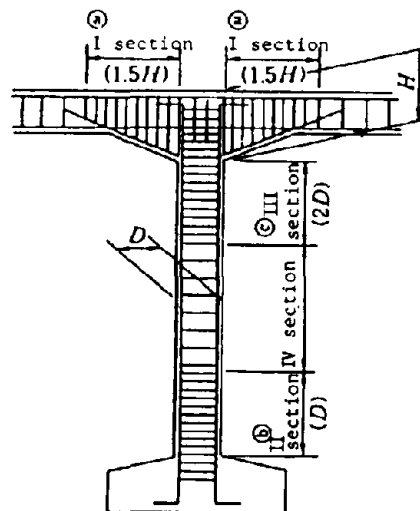


Fig. 2 Arrangement Reinforcements at an Intermediate Joint of Rigid Frame Members

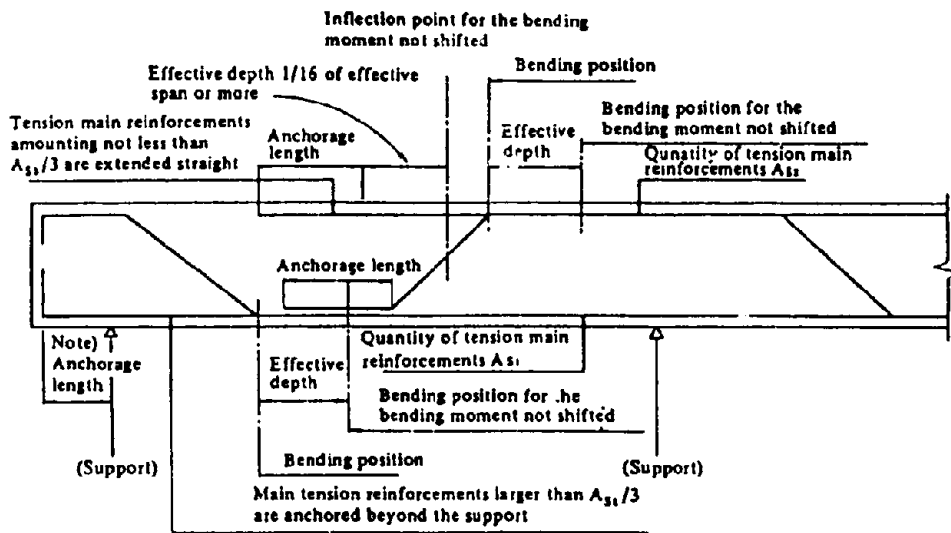


The following amount of stirrup should be arranged.

- I section: More than  $0.002b \cdot a$  and more than  $1.2x$ (required amount at the time of earthquake).
- II section: More than  $0.002b \cdot a$ .
- III section: More than  $0.0025b \cdot a$ .
- IV section: More than  $0.0015b \cdot a$ .

where  $b$ : Beam width (cm)  
 $a$ : Stirrup or tie spacing (cm)

Fig. 3 Reinforcement Arrangement at an Intermediate Joint of Rigid Frame and Bridge Pier



Note: The anchorage length shall be the determined  $l_a$  [anchorage length by equation (4.2.1)]. However, when the ends are hooked, it is enough that the anchorage length be not less than twice the cover of tension steel or 20 cm or more from the support.

Fig. 4 Anchorage of Longitudinal Main Tension Reinforcements

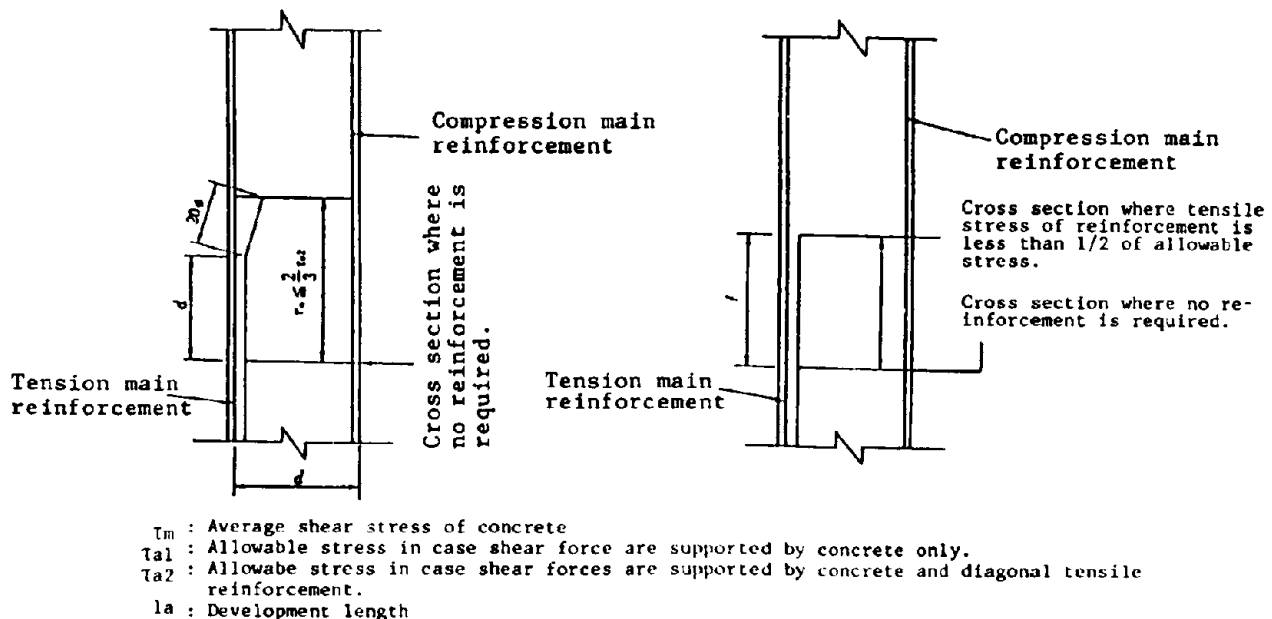


Fig. 5 Main Reinforcement Anchorage in Tensile Zone of a Member

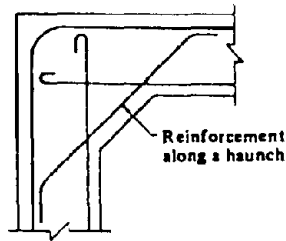
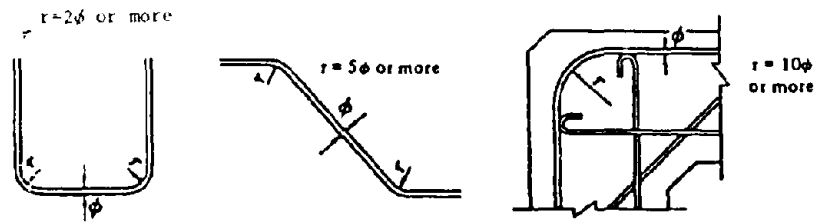


Fig. 6 Reinforcement Along a Haunch



(a) Stirrup and tie (b) Bent reinforcement (c) Reinforcement along the outside of an end joint of a rigid-frame structure

$\phi$  : Diameter of reinforcement (cm)  
 $r$  : Bend radius of reinforcement (cm)

Fig. 7 Bend Radius of Reinforcement

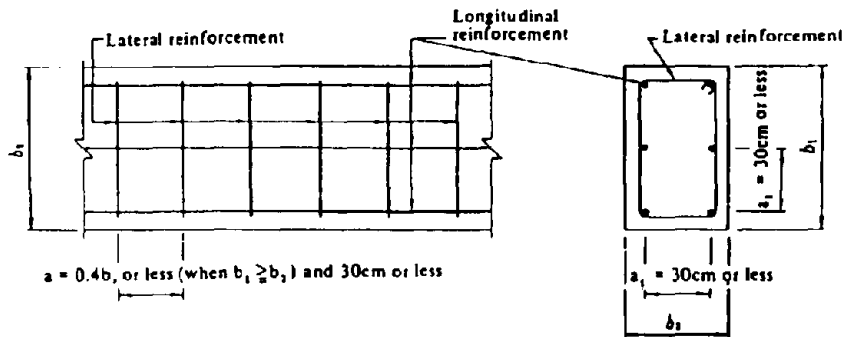
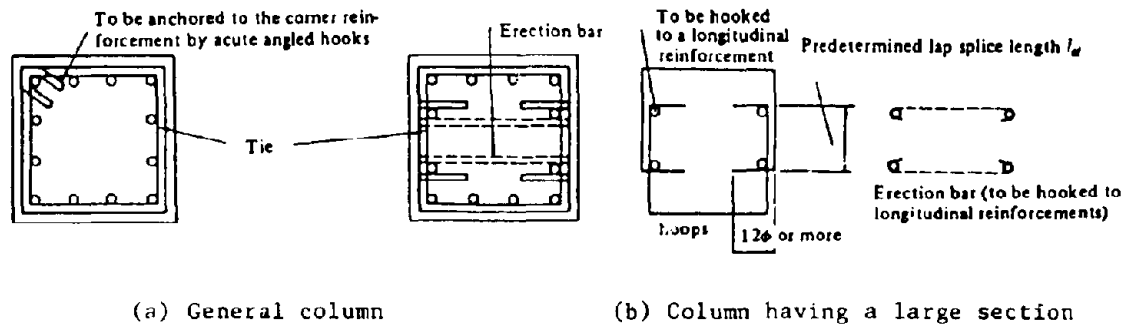
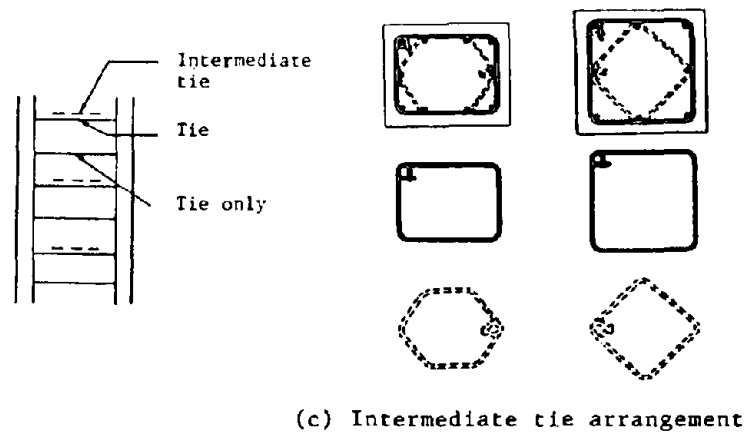


Fig. 8 Arrangement of Reinforcement Against Torsional Moment



(a) General column

(b) Column having a large section



(c) Intermediate tie arrangement

Fig. 9 Arrangement of Ties

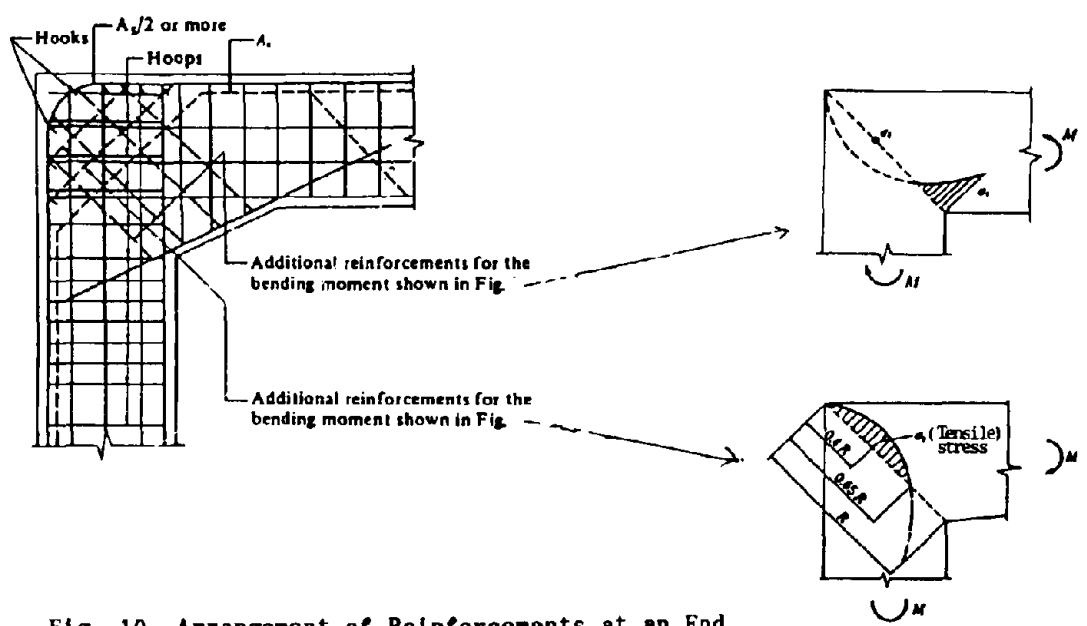
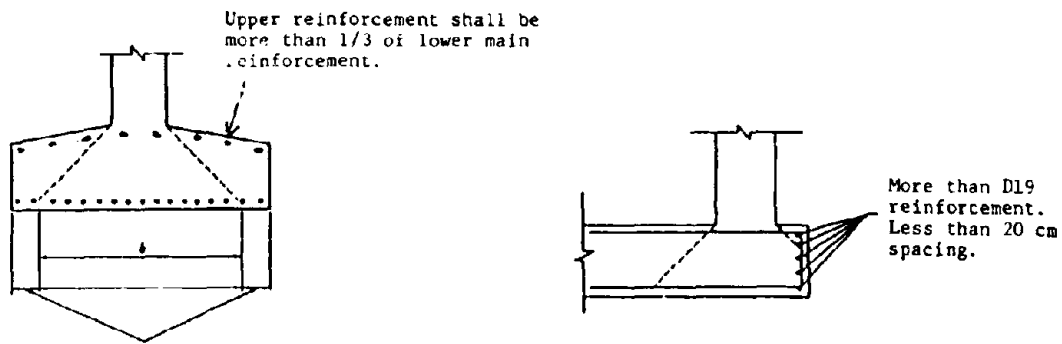


Fig. 10 Arrangement of Reinforcements at an End Joint of Rigid Frame Members





(a) Reinforcement arrangement  
(Lower main reinforcement)

(b) Reinforcement at a  
footing end

Fig. 11 Reinforcement Arrangement of a Footing

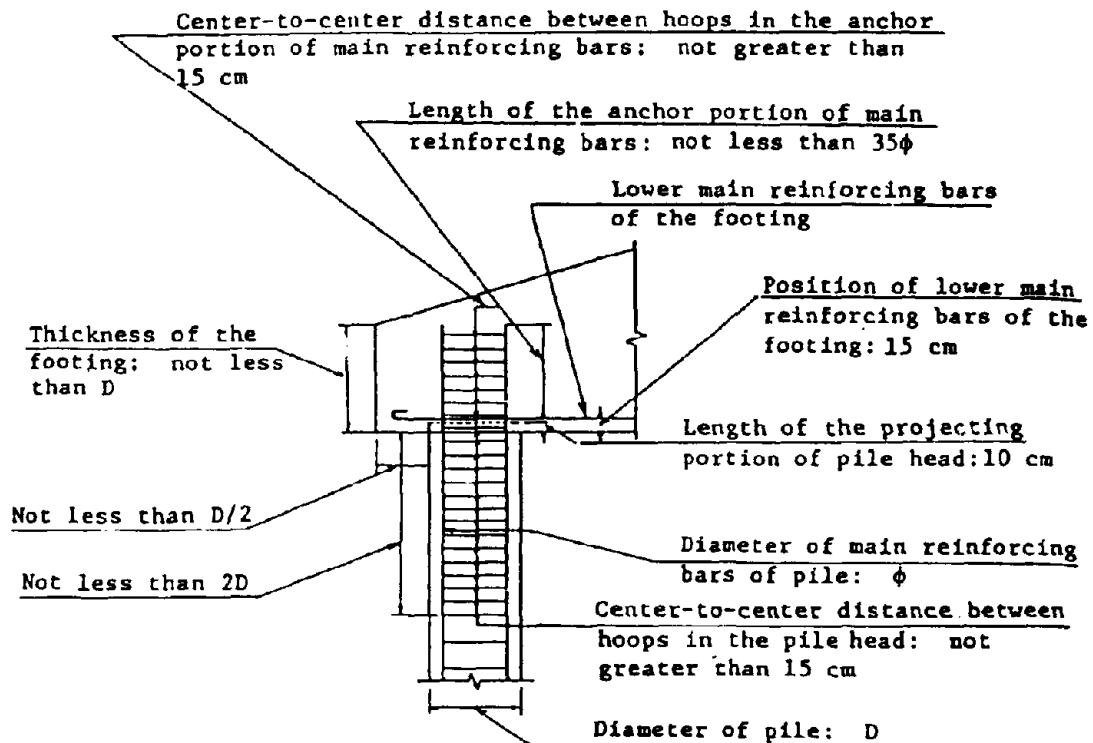
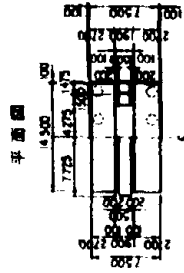
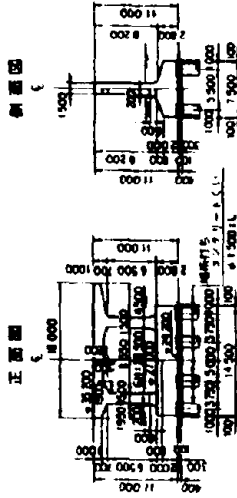
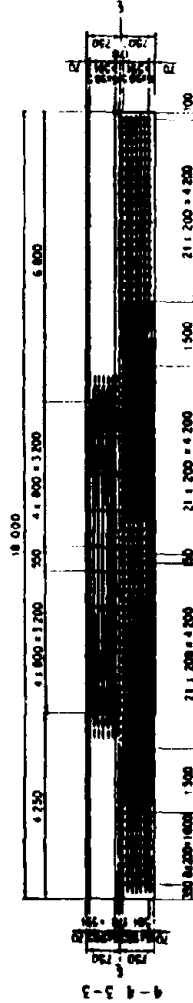
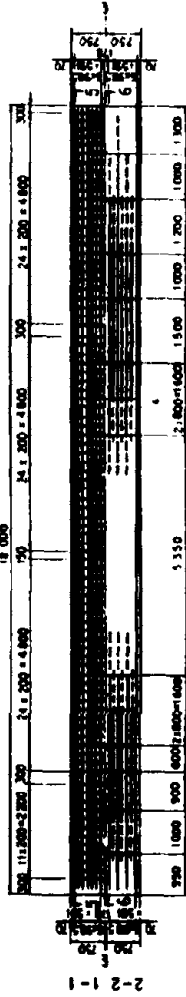


Fig. 12 Reinforcement Arrangement of a Pile (Insert)

構造一般図



平面図



正面図

5-5

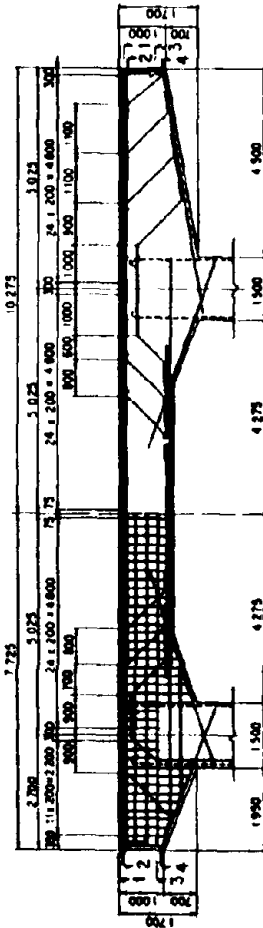
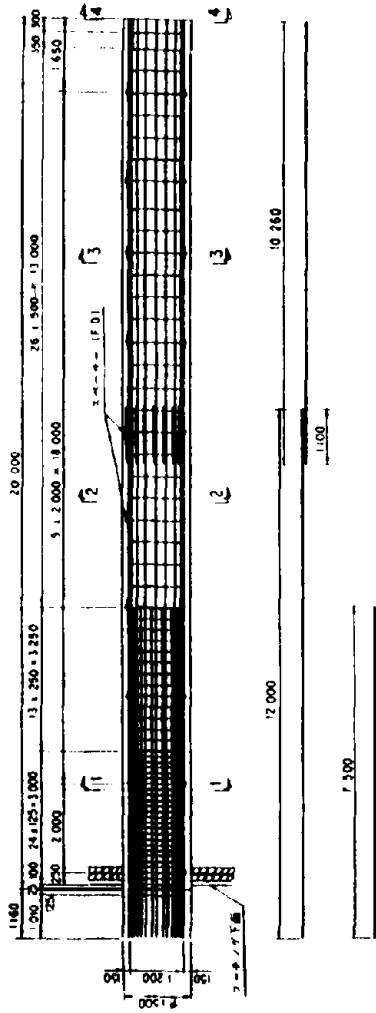


Fig.-13 Rigid-frame pier(1)

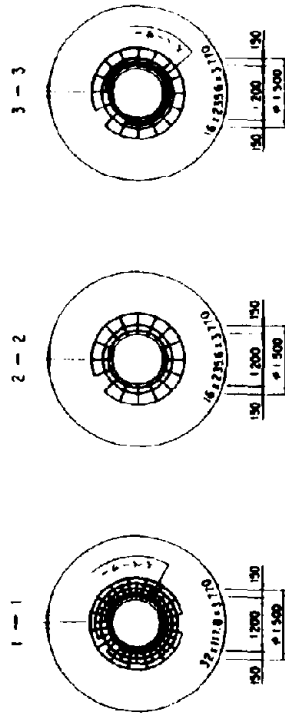




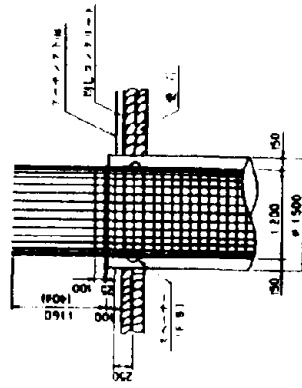
場所打ちコンクリートぐい棒構造図



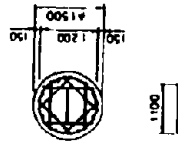
断面図



ぐい棒構造図



4-4



かぶり構造図



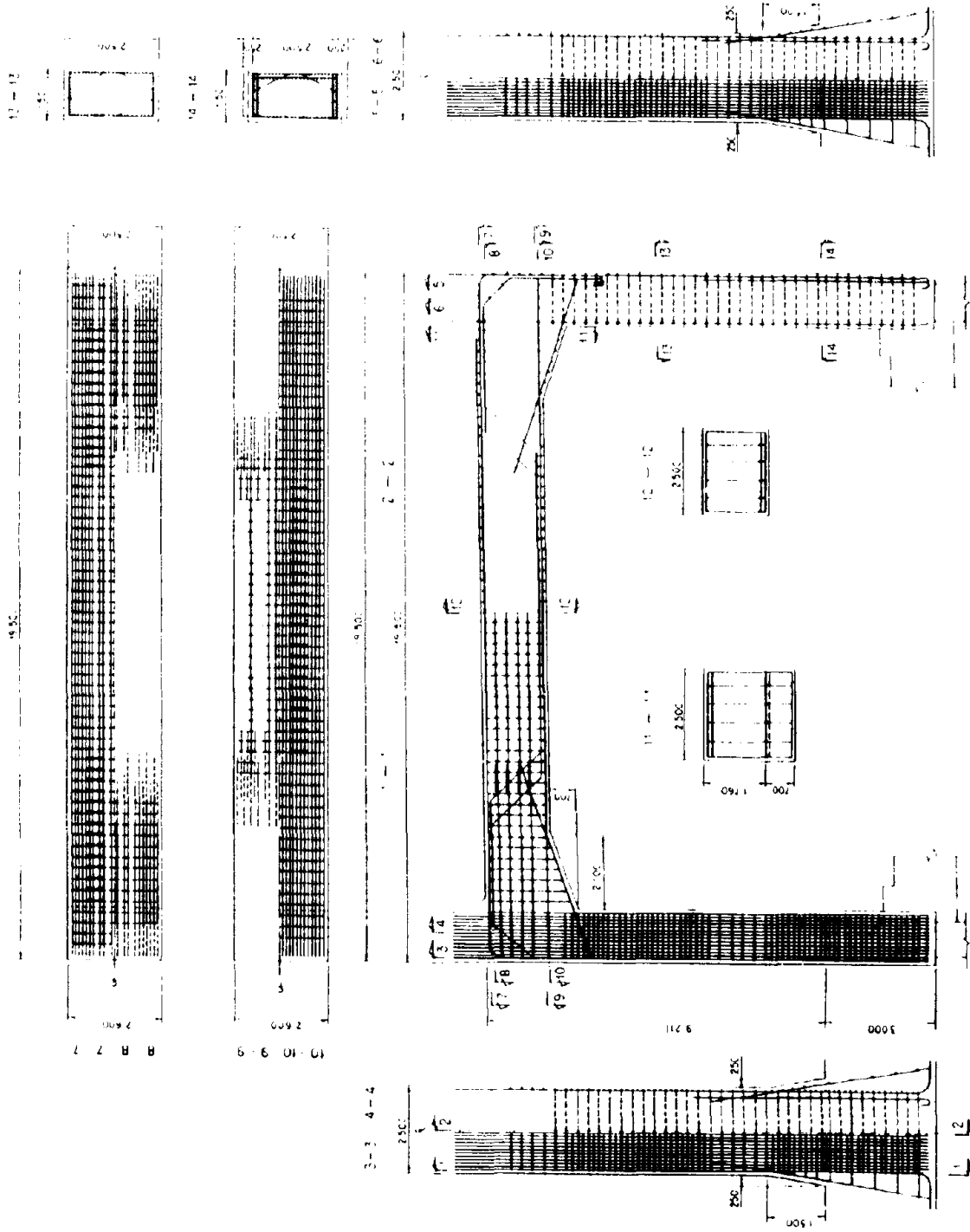
スベーク



Fig.-15 Cast-in-place pile



樓面配筋圖



3.14 Fig.-16 Two storey Rigid-frame pier(2) 6.5

## **S e s s i o n 2**

### **D a m a g e t o S a n F r a n c i s c o B r i d g e s i n t h e L o m a P r i e t a E a r t h q u a k e**

- 1) An Overview of Damage to Highway Bridges During the Loma Prieta Earthquake of October 1989  
(H.S.Lew)
- 2) San Francisco Double Deckers - Observed Damage and a Possible Retrofit Solution  
(M.J.N.Priestley, F.Selble)
- 3) Full-scale Tests on the Cypress Viaduct  
(S.Mahin and J.Moehle)



**AN OVERVIEW OF DAMAGE TO HIGHWAY BRIDGES  
DURING THE LOMA PRIETA EARTHQUAKE**

by H. S. Lew  
Building and Fire Research Laboratory  
National Institute of Standards and Technology

→ At 5:04 p.m., Pacific Daylight Time, on October 17, 1989, an earthquake with a surface-wave magnitude of 7.1 occurred with its epicenter located about 10 miles (15 km) northeast of Santa Cruz and 60 miles (95 km) south-southeast of San Francisco, California. According to the U.S. Geological Survey, the earthquake ruptured a segment of the San Andreas fault below the Santa Cruz Mountains. The hypocenter was about 11 miles (18 km) beneath the Earth's surface, and the rupture propagated about 25 miles (40 km) both northwest and southeast within a 10-second period. The earthquake was felt over an area of 400,000 square miles (1,000,000 sq km), from Los Angeles to the south, Oregon to the north, and western Nevada to the east. This earthquake, named the Loma Prieta earthquake, was the largest on the San Andreas fault since the great San Francisco earthquake of 1906 (M = 8.3) when a 275-mile (440-km) stretch of the fault ruptured. This report presents an overview of damage to highway bridge structures during the earthquake. ←

### Introduction

The main highway network in the San Francisco Bay region sustained serious damage at several locations. The most notable is the damage to and collapse of the long, double decked viaduct sections of freeway in the San Francisco and Oakland areas. Except for the collapse of a single link span of the double-deck section of the San Francisco-Oakland Bay Bridge, most bridges in the area of the San Francisco Bay survived the earthquake with relatively minor damage. Most bridges and viaducts had been strengthened in the California Department of Transportation (Caltrans) Phase I seismic retrofit program which included identification of structures that are vulnerable to excessive displacements in the longitudinal direction and have the potential to have spans collapse. Typically, these structures have narrow hinge seats or discontinuities in the superstructure across piers or abutments and were constructed prior to 1971. Cables or bars were placed across these joints, tying the elements of the superstructure together.

Following the Loma Prieta earthquake Caltrans engineers conducted preliminary inspections of more than 1500 bridge structures in the area affected by the earthquake and determined that some 73 bridges had suffered minor damage of varying degrees, that five major viaducts and five other bridges suffered significant structural damage, and that major or partial collapses occurred at three sites. Figure 1 depicts the locations of the five damaged viaducts and the collapsed span of the Bay Bridge, indicated by shaded circles, and the I-880 collapse by the shaded oval.

## The I-880 Collapse

Interstate 880, also known as the Nimitz Freeway, is a primary north-south oriented 8-lane highway connecting San Jose with Interstates 580 and 80, adjacent to the east end of the San Francisco-Oakland Bay Bridge. Generally, I-880 is a ground level freeway with the exception of a 2 mile (3 km) elevated segment which is oriented approximately north-south and is bounded by 7th Street on the south and 34th Street on the north in Oakland (see fig. 2). The configuration of the elevated portion, known as the Cypress Structure, consisted of a bi-level system with four lanes of north-bound traffic on the first level, approximately 25 feet (8 m) above ground level, and four lanes of south-bound traffic on the upper level, approximately 50 feet (15 m) above ground level. Surface level traffic paralleled the Cypress Structure on both sides with underpasses at the major cross streets. Design work for this section was begun in 1951 and construction was completed in 1957. It is to be noted that the AASHTO design specifications for highway structures for this period (AASHTO, 1953) make no reference to design requirements for resisting lateral loads. However, the Caltrans Bridge Department design supplement for earthquake loads (Caltrans, 1949) did require bridge structures to resist earthquake loads of 0.06 times the weight of the structure for bridges on pile foundations as used for the elevated portion of I-880.

The structural configuration of the Cypress Structure consists of a series of 124 reinforced concrete transverse bents which support longitudinal cellular box girders that carry the road deck. The box girders vary from 71 to 90 feet (22 to 27 m) in length by 55 feet (17 m) wide and are integrally cast flush with the tops of the bent girders as shown in figure 3. The road deck has a relatively uniform weight of approximately 8 tons per foot (230 kN/m) along the longitudinal direction, which can be used to determine vertical and inertially induced loads to the various bents.

There were 11 distinctively different bent configurations used on the Cypress Structure, but only three primary types were present in the majority of the collapsed section, which extended from the first expansion joint north of Bent 63 at 18th Street to just short of Bent 113 at 34th Street. The total length of the collapsed section was 3970 feet (1210 m), contrary to the 1.5 mile (2.4 km) figure commonly quoted in the media following the quake. The three predominant bent configurations are shown in figures 3 through 5 and are labelled as Type 1, 2, and 3 bents. A fourth type, which was similar to the Type 3 bent but with an additional support column for the first level and prestressing for the upper bent girder, is shown in figure 6. A fifth variant, similar to a Type 2 bent, but with a cantilevered detail for the lower level girder, is shown in figure 7.

There are several characteristics common to most bents for the Cypress Structure. In all cases the lower portion of each bent, comprising two vertical support columns and a horizontal (some were superelevated) connecting girder, was designed to achieve a moment resisting connection between the columns and girder. The columns generally measured 72 inches (1.83 m) deep by 48 inches (1.22 m) wide and were heavily reinforced with 44-#18 Grade 40 longitudinal reinforcing bars. Contrasting this massive axial reinforcement, #4 bar rectangular ties with 90-degree hooked ends were provided on 12 inch (310 mm) centers as lateral

confinement. The columns were supported by a 36 to 54 inch (0.91 to 1.52 m) thick reinforced pile caps which in turn were cast on top of driven pile foundations.

Type 1 bents, which comprised more than half of those in the collapsed section, were designed similarly to the lower bents, that is, moment resisting connections between the columns and cross girder, and pinned connections at the base of both columns. The upper columns were tapered from 48 inches in width at the top, to accommodate girder reinforcement, to 36 inches (910 mm) at the bottom with a constant 48 inch section depth.

Figure 8 shows a ground-level view looking northward from Bent 86 on the west side of the expressway. All of the bents visible in this photo were Type 1 which invariably exhibited a symmetrical failure with both upper columns shearing free at their base and being splayed outward as the upper deck fell. The timber posts visible beneath the lower deck were installed by Caltrans under each bent to insure that there was no subsequent settling of the structure during rescue operations. Further evidence that the upper deck fell nearly squarely on the lower deck with no significant sidesway is shown in figure 9 which is looking northward from atop Bent 80.

Figure 10 shows a closeup of a Type 2 bent failure in which the eastern half of a series of three-hinged prestressed bents collapsed, due to shearing failure at the base of the east column, leading to a rigid body rotation of the upper deck about the western, two-hinged columns. As can be seen, the western column shear keys did perform as hinges even under rotations sufficient to cause compressive spalling on the interior face of the columns (fig. 11).

#### Interstate 280

Aside from the damage to I-880, structural damage at four other locations are shown in figure 12.

Interstate 280 (I-280) traverses the southern part of San Francisco from west to east and proceeds in a northern direction along the eastern shoreline. The highway was named the Southern Freeway when it was designed. The portion south of Army Street was designed according to the 1961 AASHO Specifications (AASHO, 1961), and the portion near Sixth Street was designed according to the 1965 AASHO Specifications (AASHO, 1965). Damage was observed at two locations: several blocks south of Army Street and at the Sixth Street ramp (see fig.12).

Figure 13 is an aerial view, looking south, of I-280 south of Army Street. At this location a two-level elevated highway (to the south) transforms into to a single level divided highway (to the north). In addition, there is an exit ramp for the lower level northbound section. Damage was observed at Bent numbers 48, 51, and 52.

Figure 14 is a schematic elevation view (looking north) of Bent 48. The top girder is post-tensioned and supports at the columns are designed as pinned connections, with details similar to those used on I-880. The column reinforcement includes #18 longitudinal bars and #4 ties at 12 in. (0.30 m) spacing. The damage occurred at the top of the west-side column. Figure 15 shows the nature of the damage, which appears to be a combination of diagonal

tension failure and splitting parallel to the longitudinal column steel. Note that the girder is permanently displaced toward the east.

Figure 16 is a schematic elevation view of Bent 52. The configuration of Bent 51 is similar. The upper, post-tensioned girder is monolithic with the column on the west side and is supported as a pinned connection on the east side. Figure 17 is view (looking south) as seen from the lower northbound lanes; the upper girder of Bent 52 is in clear view. Damage occurred to the east-side columns of Bents 51 and 52 at approximately the elevation of the roadway. Figure 18 shows the damage in Bent 52 as it appeared on the northern column face. The damage in Bent 51 was similar.

Some minor damage occurred due to pounding. It is seen in figure 13 that where the roadways become side-by-side, the columns supporting the upper roadway are close to the lower roadway of these columns which support the upper roadway was damaged due to pounding with the lower roadway, as can be seen in figure 19.

The complex geometry of this portion of I-280 is likely to be a factor in explaining the causes of the damage. Figure 20 is a schematic to illustrate the changing structural configuration as the highway changes from a two-level elevated structure to a single-level divided structure. In part (c) of the figure, a tall structure is connected to a short structure. The natural period of vibration of the short structure is shorter than the natural period of the tall structure. Hence it is likely that at some time during the shaking, the roadways were moving in opposite directions. This would lead to high lateral forces at the junction of the two structures, which is consistent with the location of the observed damage. Where the two roadways are completely separated, as in figure 20(d), motion in opposite directions would lead to pounding as was observed.

The other damage to I-280 was observed at the Sixth Street ramp, where the highway crosses China Basin. Figure 21 is an aerial view of the site showing the elevated exit ramp crossing over the main highway. Figure 22 is a ground-level view (looking west) showing the exit ramp above the northbound lane of I-280 exit. The photograph was taken several weeks after the earthquake, and wooden cribbing was being positioned to provide temporary support. The exit ramp is typically supported by a single pier except at this location, where it is supported by a bent (number N-35). The supporting structure for the high-level ramp is attached to the lower highway in a manner similar to that shown in figure 20(c), i.e., one column is part of the bent for the main roadway, and the other column is free-standing. Damage occurred in the girder supporting the ramp. Figures 23(a) and 23(b) show the nature of the damage on the east side and west side of the bent, respectively. On the east-side, diagonal cracks developed in the girder with a major crack running diagonally across the corner. On the west side, many cracks developed toward the corner.

#### **Embarcadero Freeway (I-480)**

The Embarcadero Freeway (I-480) is a two-level elevated highway which provides the Financial District with access to the San Francisco-Oakland Bay Bridge. According to the as-built drawings supplied by Caltrans, the freeway was designed according to the 1953 AASHO Specifications (AASHO, 1953). Figure 24 is an aerial

view of the portion of I-480 north of Mission Street. The historic Ferry Building is east of the freeway.

Figure 25 is a ground-level view looking north along the west side of the freeway; Bent 76 is in the foreground. The vertical metal covers which can be seen at the top girder-column joints protect restraining tendons which were added during the earthquake upgrading in 1972. The observed damage occurred at the lower girder-column joints in bents located north and south of Mission Street.

Figure 26 shows the configurations of the bents to the north and south of Mission Street. As can be seen at the bottom of the aerial photograph in figure 24, the Embarcadero Freeway undergoes a transition in width south of Mission Street, and this is the reason for the different bent configurations. For the wide portion of the freeway, the upper girder is post-tensioned and supported on pinned joints. A detail similar to that used in the design of I-880 was used for the pinned joints. Likewise, for bents with post-tensioned girders, column segments were pinned at both ends on one of side of the bent. The predominant damage was in the form diagonal cracking within the lower girder-column joint, as indicated by the heavy lines in figure 26. This indicates that the weakness of the Embarcadero Freeway is similar to that of the collapsed portion of I-880. In no cases were the cracks as severe as those observed in the columns of I-280.

Figure 27(a) is a close-up view of the damaged joint on the west side of Bent 78. Cracking was observed in the joints at both sides of the bent. Diagonal cracks in the joint were in the opposite direction to those at other joints on the west side of the bents. On the south face of the column in figure 27(a), the cracking was more severe and some of the concrete cover had spalled. Figure 27(b) is a close-up view of the joint of Bent 79 on the east side. This was the most severe damage observed on the east side of the freeway.

#### U.S. Highway 101

The northernmost portion of U.S. 101 (originally named as the Central Viaduct) was designed according to the 1953 AASHO Specifications (AASHO, 1953). This was the last section of the highway to be built and extends from South Van Ness Avenue to Turk Street. At the southern end, U.S 101 is a divided, elevated highway. It undergoes a transition to a two-level elevated highway as its direction changes from east-west to north-south. At the southern end near Van Ness Avenue, the concrete roadway is supported by a steel frame. From north of Mission street, the roadway is supported by concrete structures.

One block south of Hayes Street, the highway becomes two lanes in each direction. At Bent 40, the roadway widens to accommodate additional lanes in the future. Damage was observed in the widened, elevated section at Bents 42 and 43, which are located north of Hayes Street. These are shown in figure 28, a view of the east side of the highway. Figure 29 is a schematic of the configuration of Bent 43 where serious damage was observed. The configuration of Bent 42 is similar to Bent 43 except that the bent is skewed to the direction of the roadway. The design was similar to the other elevated highways built in the mid 50's. The post-tensioned girders are supported on columns with pinned connections.

Figure 30(a) is close-up view of the east-side column of Bent 42. A series of diagonal cracks occurred at the middle of the column, and finer cracks developed at the top of the column inclined in the opposite direction. The more serious damage was observed at Bent 43. As shown in figure 30(b), extensive diagonal cracking developed just above the roadway.

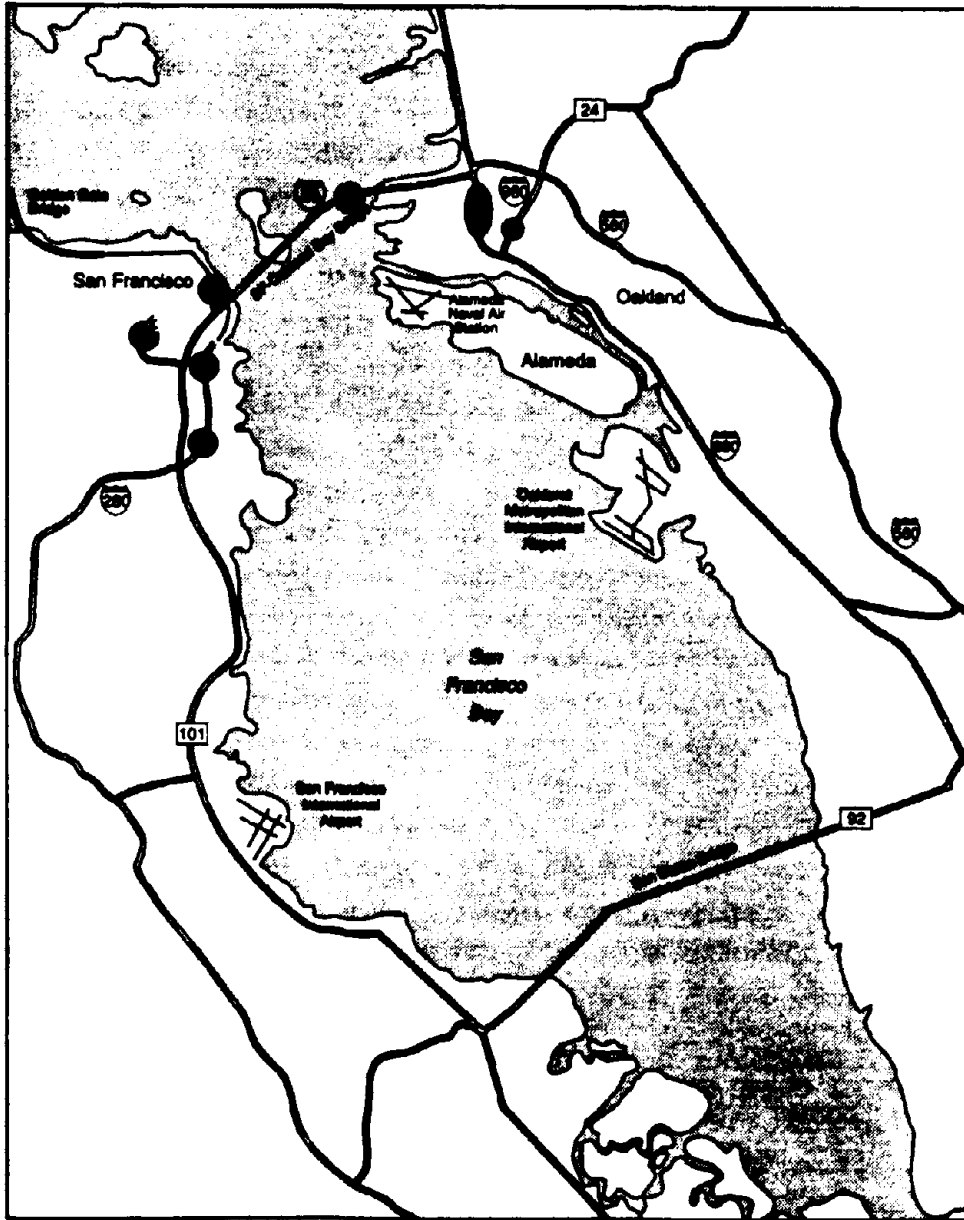


Figure 1 General location of bridge and viaduct in the San Francisco bay area

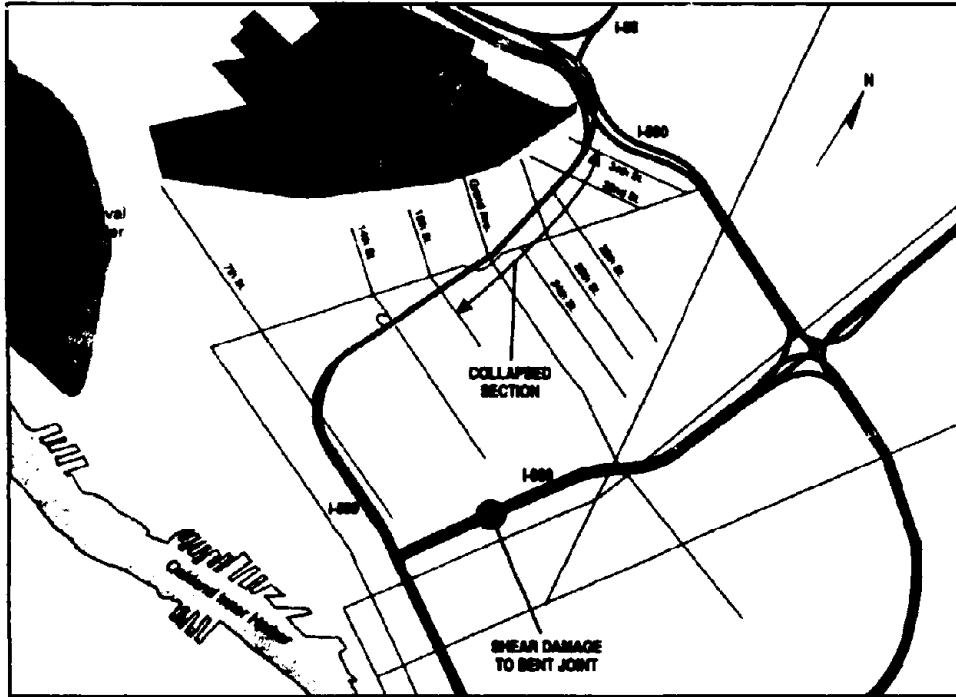


Figure 2 Map depicting the location of the collapse of I-880



### TYPE 1 BENT: I-880

[Bents 64-69; 82-94; 100-106]

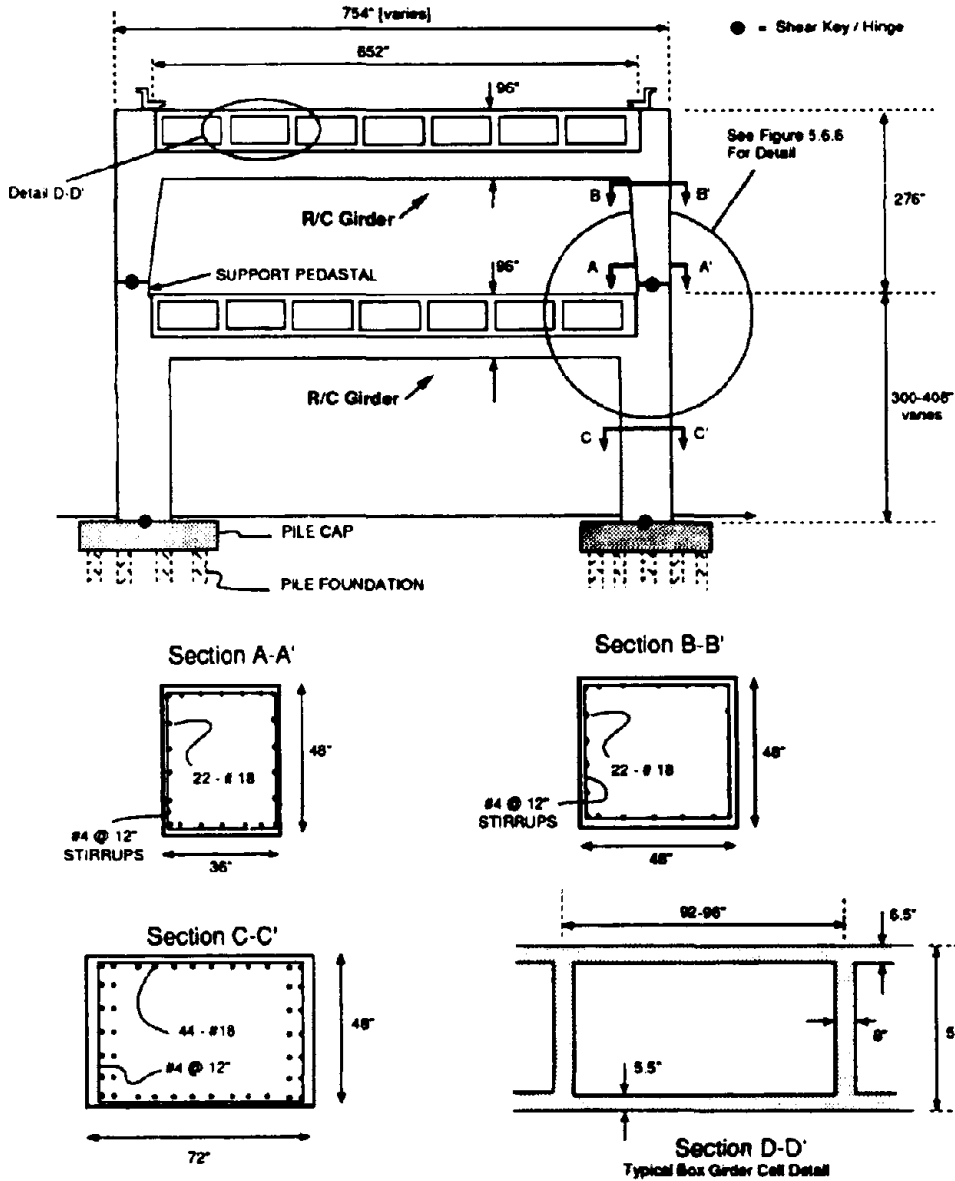
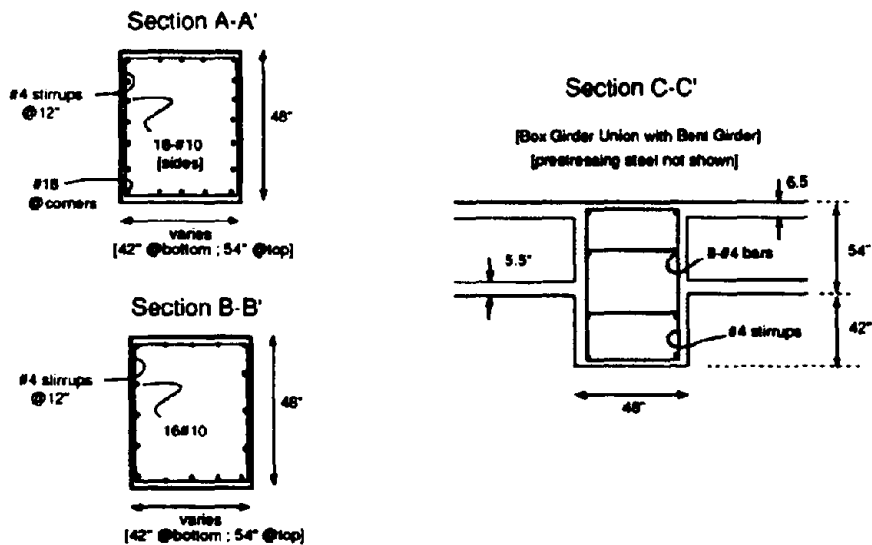
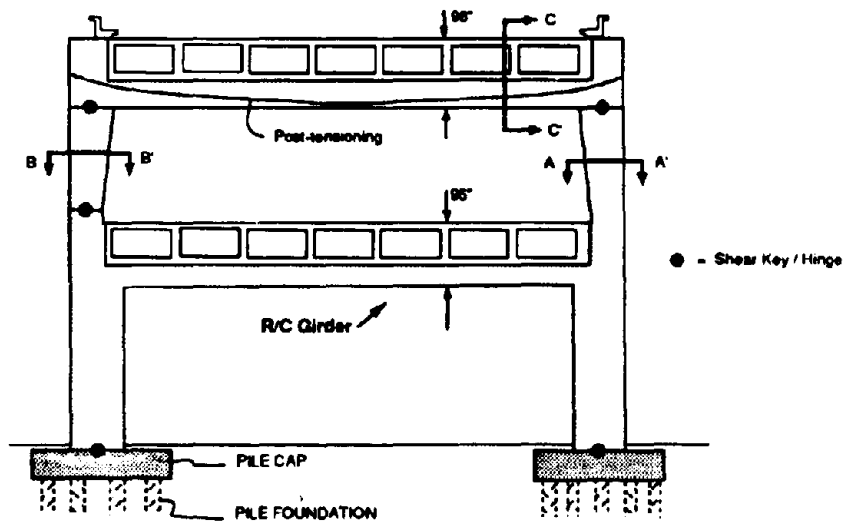


Figure 3 Structural configuration of Type 1 bents

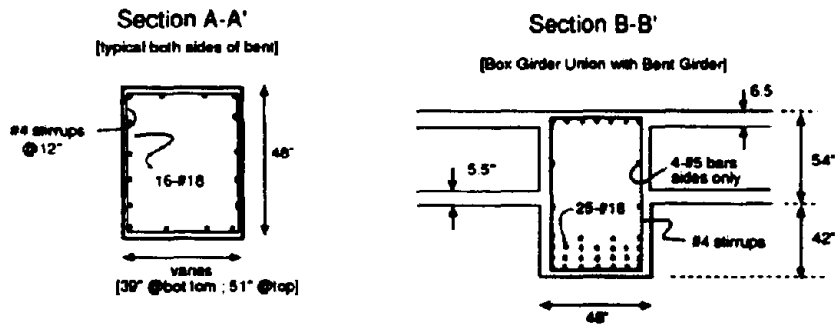
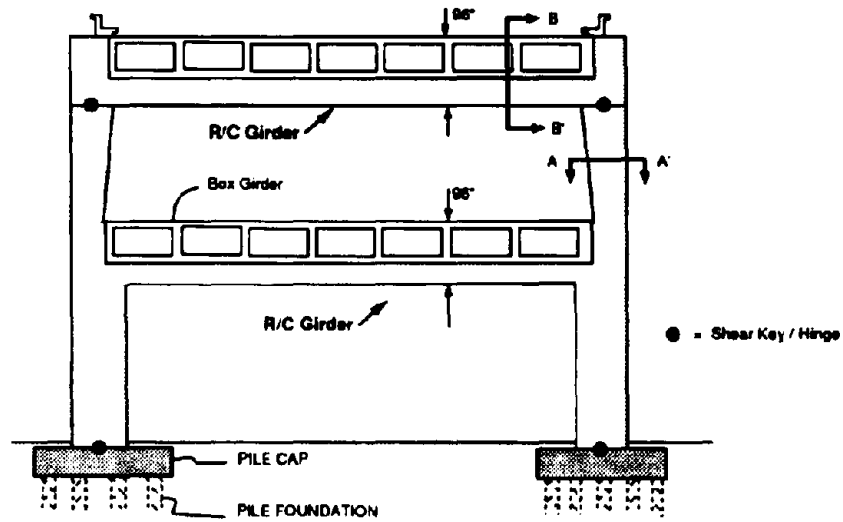
**TYPE 2 BENT: I-880**

[Bent 71, 72, 75-80]



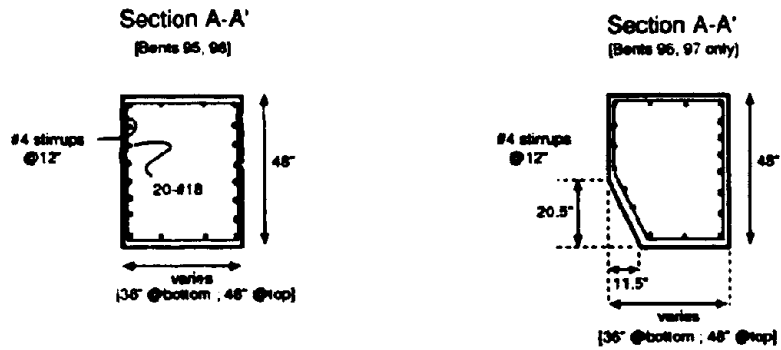
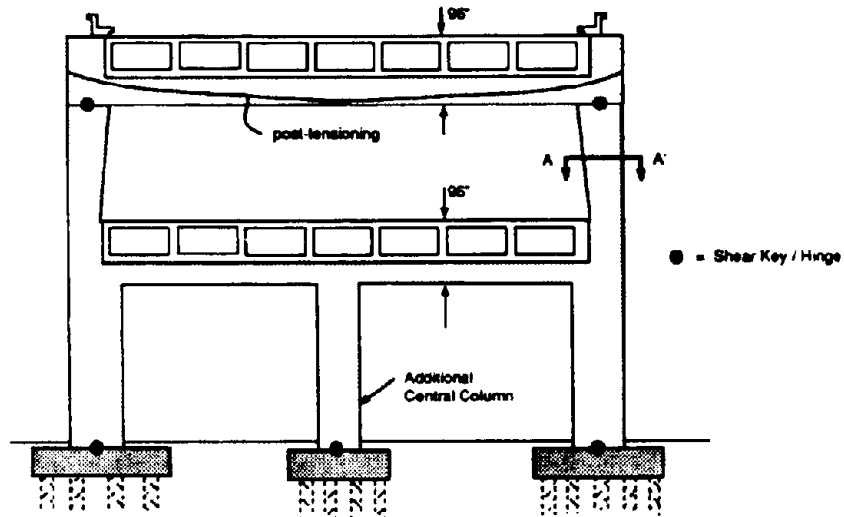
**Figure 4** Structural configuration of Type 2 bents

**TYPE 3 BENT: I-880**  
[Bent 70]



**Figure 5** Structural configuration of Type 3 bents

**TYPE 4 BENT: I-880**  
[BENT 95-98]



**Figure 6** Structural configuration of Type 4 bents

# TYPE 5 BENT: I-880

[Bent 73, 74]

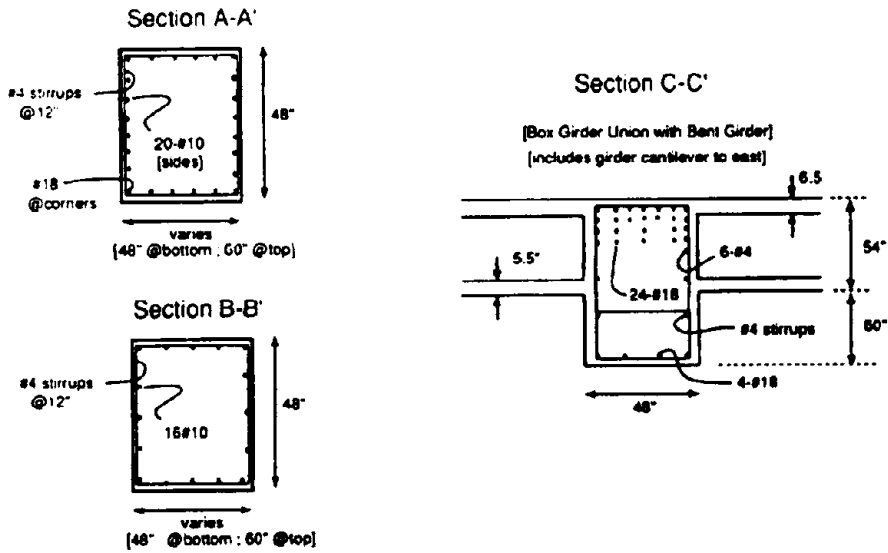
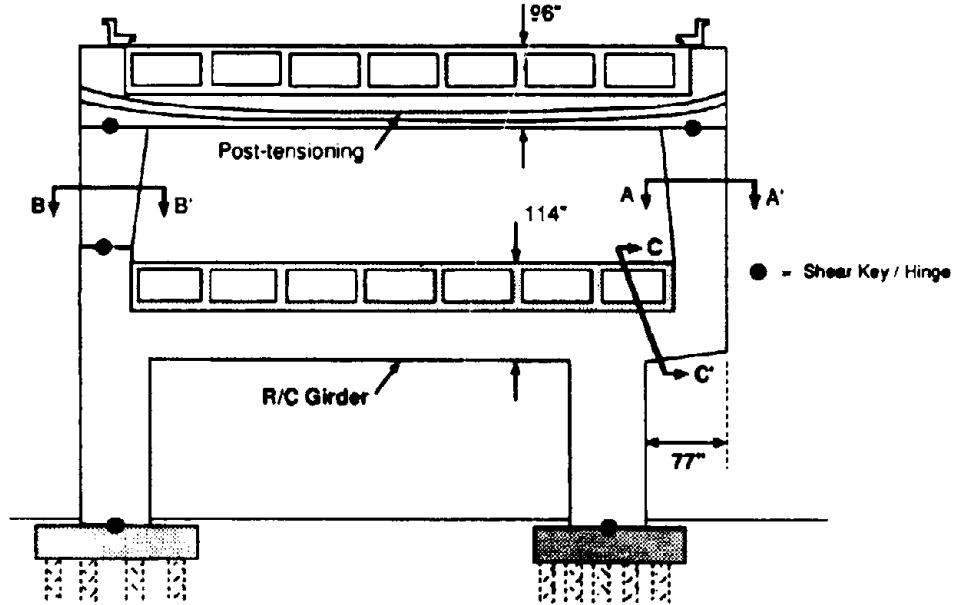


Figure 7 Structural configuration of Type 5 bents

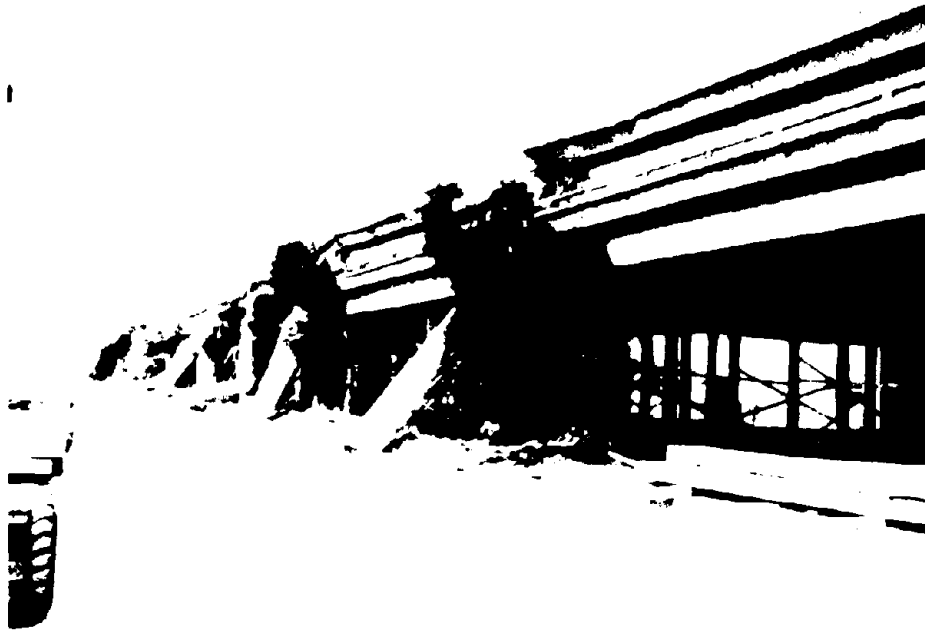


Figure 8 Collapse of Type 1 bents

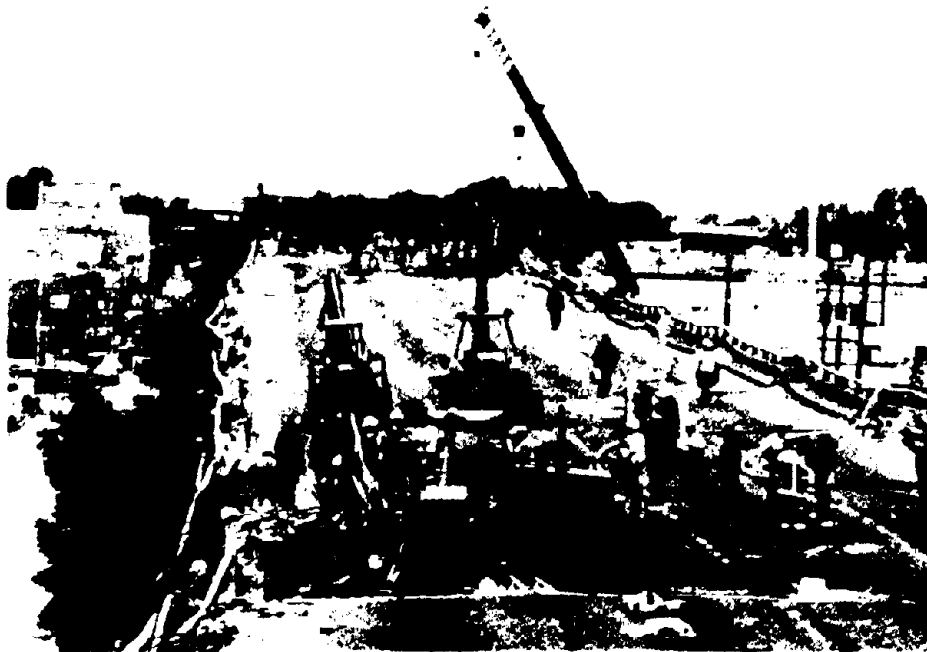


Figure 9 View of the upper deck of Cypress Structure.



Figure 10 Failure of Type 2 bents



Figure 11 A close-up view of failure of Type 2 bents





Figure 12 Location of damage to elevated highway structures in San Francisco



Figure 13 Aerial view of I-280 south of Army Street

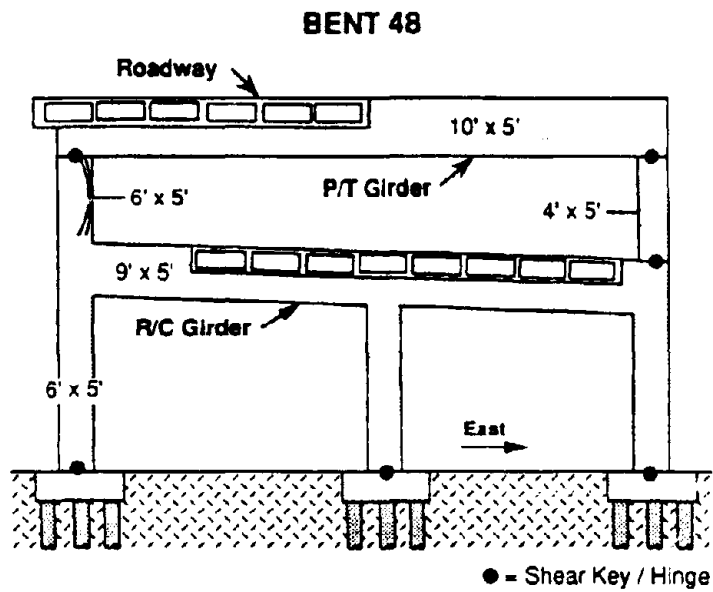


Figure 14 Schematic elevation view of Bent 48 of I-280

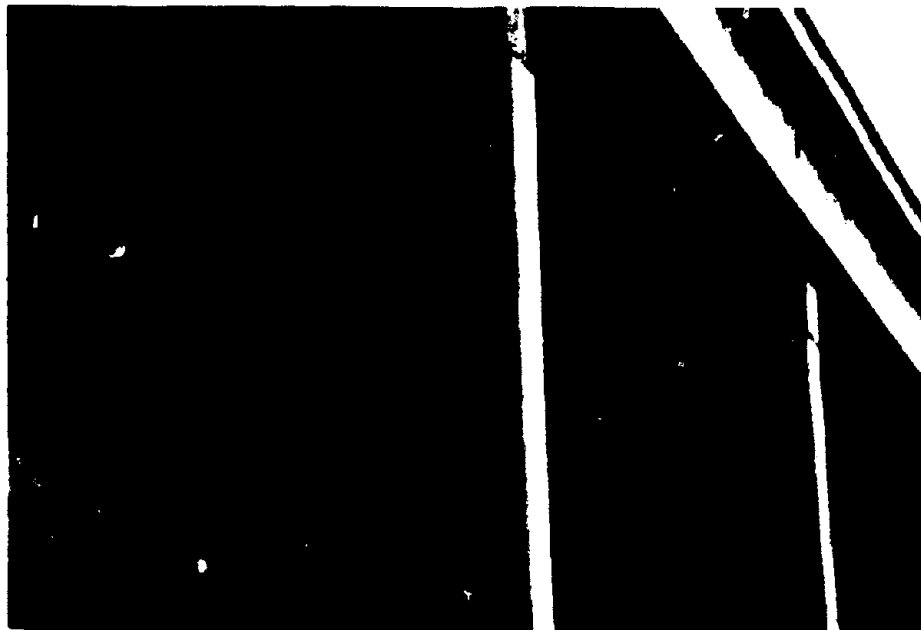


Figure 15 Damage to west-side column of Bent 48

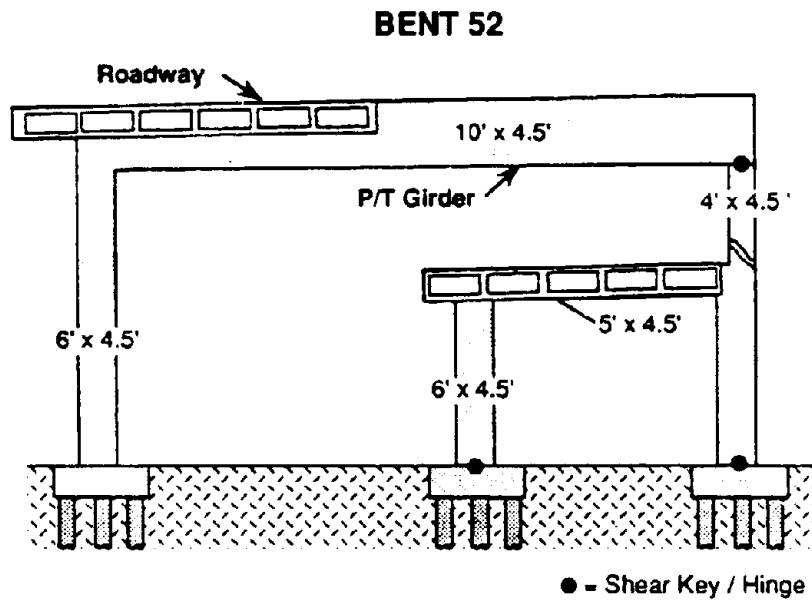


Figure 16 Schematic elevation view of Bent 52 of I-280



Figure 17 View looking south on I-280 showing the upper girder of Bent 52

*Reproduced from  
best available copy*

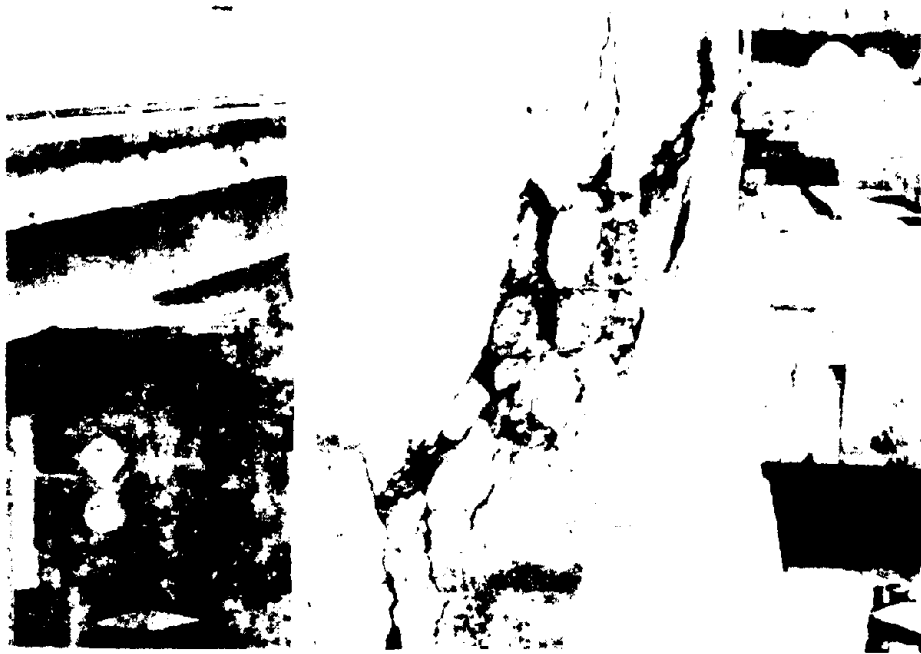


Figure 18 Pounding damage at 1-280 south of Army Street



Figure 19 Pounding damage at 1-280 south of Army Street

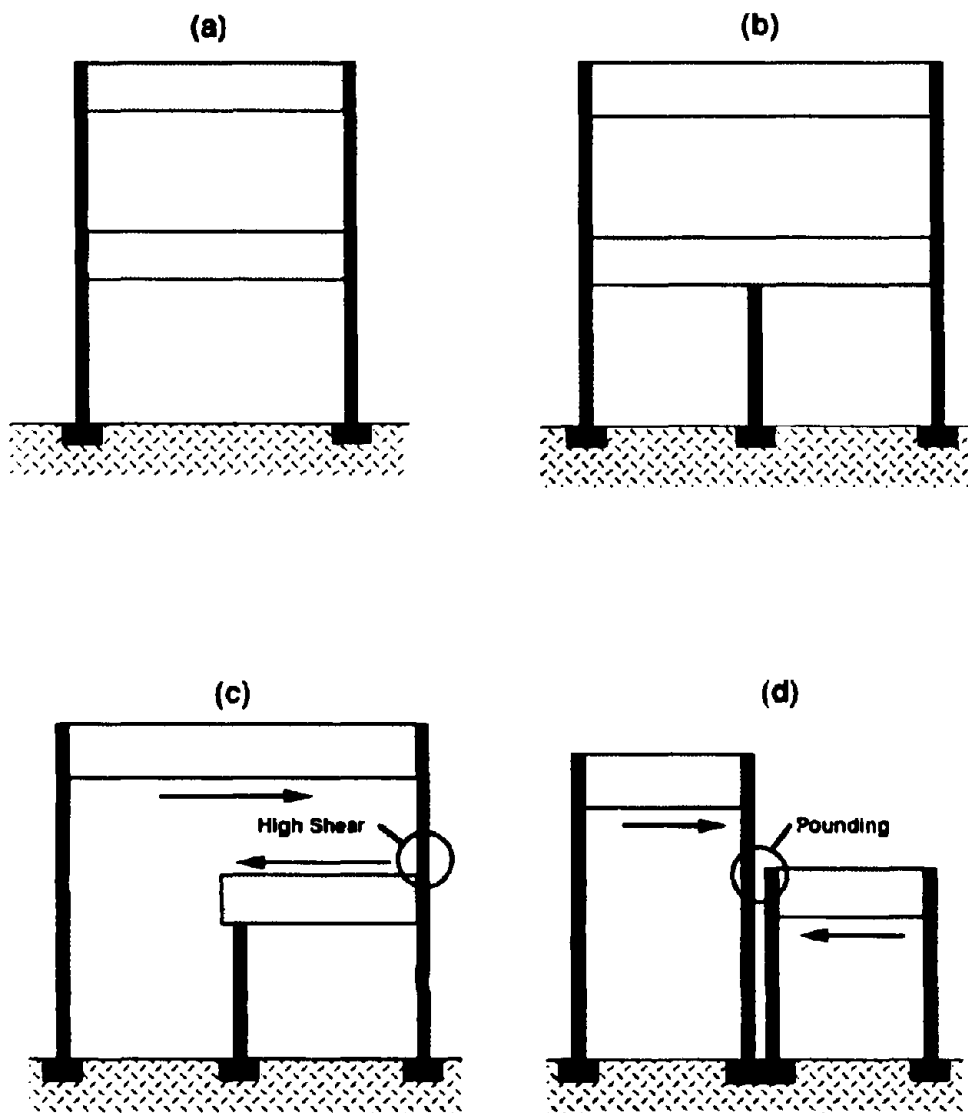


Figure 20 Schematic illustration of the various structural configurations of I-280.



Figure 21. Aerial view of the Six Street exit ramp



Figure 22. The Six Street exit ramp over I-280



(a)



(b)

Figure 23 Damage to girder supporting exit ramp:  
(a) eastern portion and (b) western portion





Figure 24 Aerial view of the Embarcadero Freeway



Figure 25 West side of Embarcadero Freeway

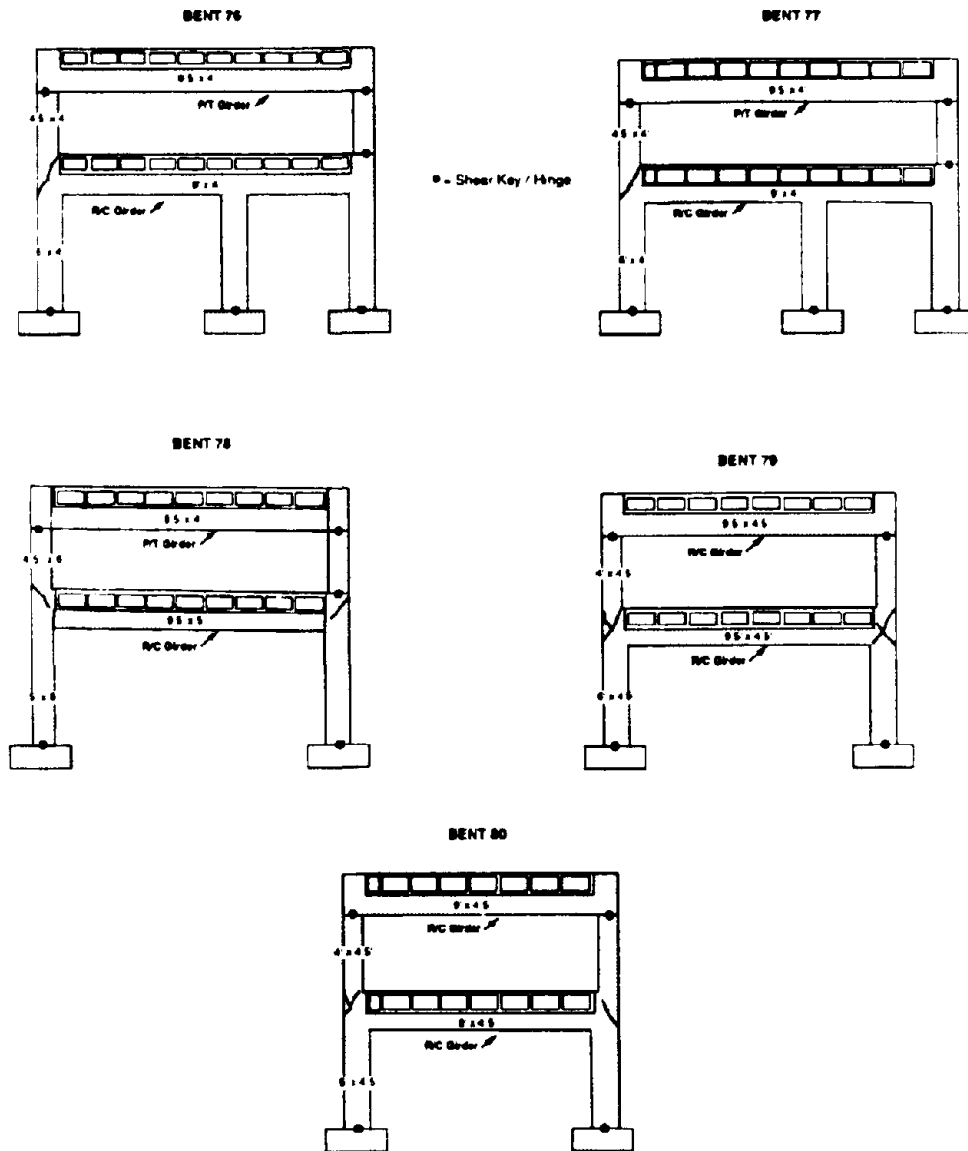
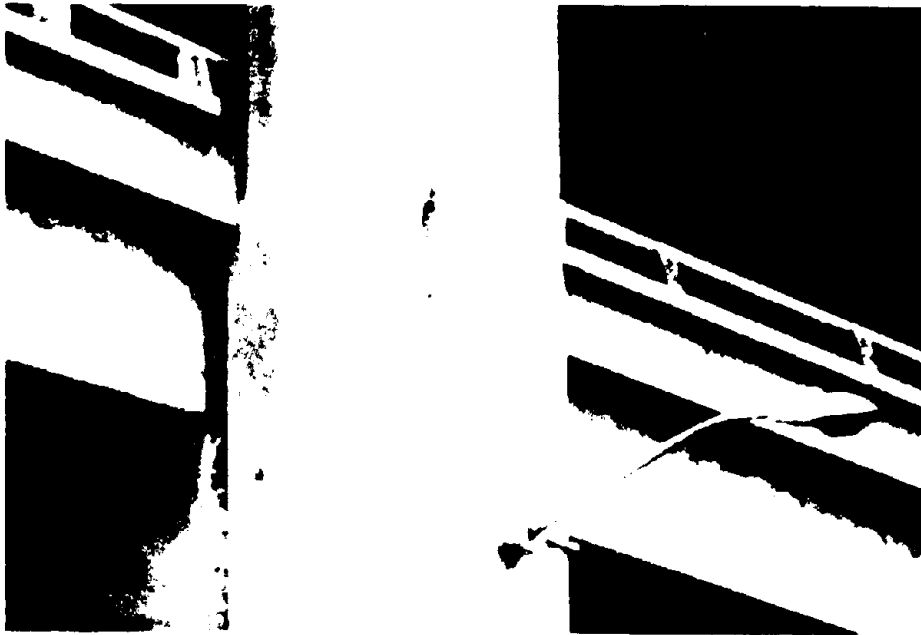
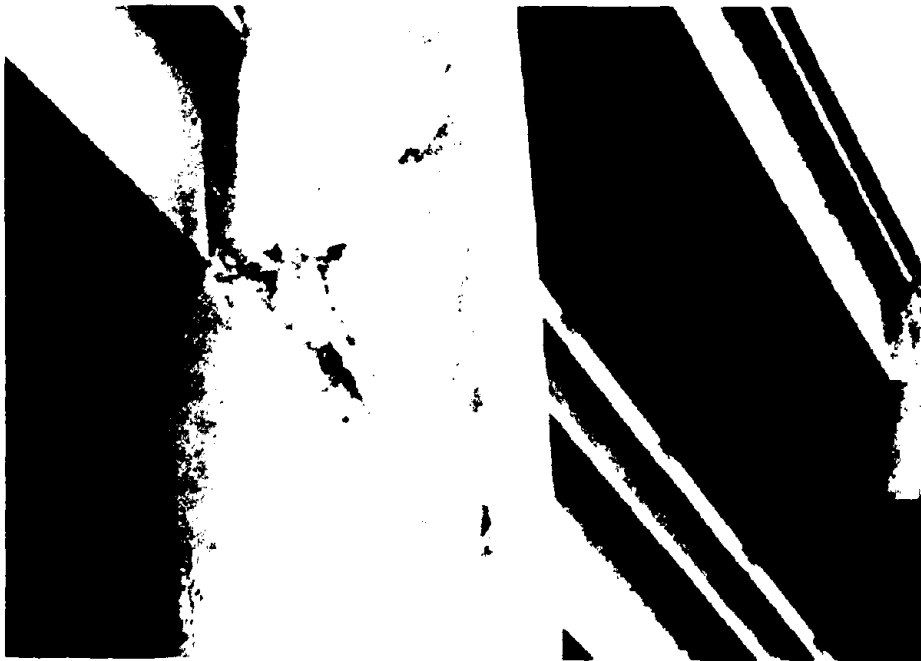


Figure 26 Schematics of bent configurations and damage at lower girder-column joints

Reproduced from  
best available copy



(a)



(b)

Figure 27 (a) Close-up view of west side of Bent 78  
(b) Close-up view of east side of Bent 79



Figure 28 View of east side U.S. 101

BENT 43

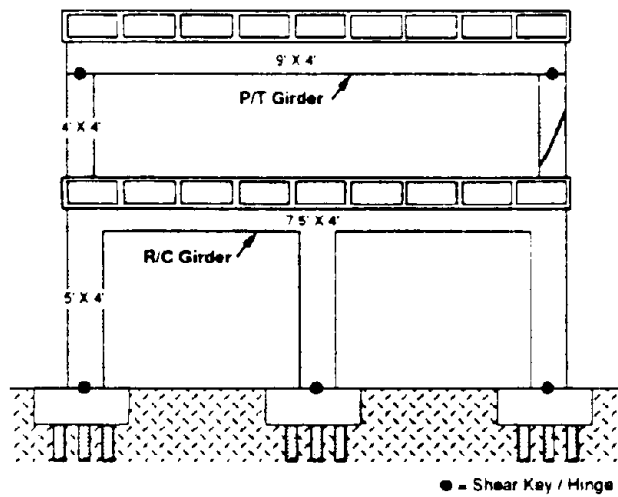
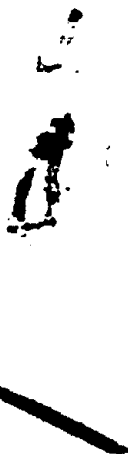


Figure 29 Schematic of Bent 43



(a)



(b)

Figure 30 Close-up views of east side column of  
(a) Bent 42 and (b) Bent 43

## SAN FRANCISCO DOUBLE-DECKERS – OBSERVED DAMAGE AND A POSSIBLE RETROFIT SOLUTION

M.J. Nigel Priestley (I)  
Frieder Seible (I)  
Presenting Author: M.J.N. Priestley

### INTRODUCTION

San Francisco is unique in the seismically active regions of the U.S.A. in its extensive use of double-decker freeway viaducts. As well as the I-880 Cypress Viaduct on the Oakland side of San Francisco Bay, where collapse has been well documented, there are several double-deckers of considerable length on the San Francisco side of the bay. These include the Embarcadero Viaduct (I-480), China Basin/Southern Freeway Viaduct (I-280), Terminal Separation (I-80/480), Central Viaduct (Highway 101), and the Alemany Interchange (I-280/Hwy.101). Typically the structures are long (up to 50 spans) with complex geometry including many on and off ramps, changes from single-deck to double-deck, and in cases triple-deck, significant horizontal curvature, and variable foundation conditions. Superstructures are generally supported by cap beams and rectangular columns. In many cases the columns are outside the width of the superstructures, and on occasions geometry associated with ramps or separations results in cap beam outriggers of considerable length and flexibility.

Ramps are often supported on single-column bents formed of rectangular section, with transverse section dimension substantially greater than longitudinal dimension. The column base detail features a connection to the footing intended to act as a hinge longitudinally, but to be moment resisting transversely.

Rather than attempt a 'broad-brush' overview of observed damage and possible repair and retrofit strategies, this paper will concentrate on the characteristics of typical double-decker portions of the viaduct, which represent some 75% of the structures. This should not be taken to indicate that major problems are not apparent elsewhere. One area of particular concern is the strength and ductility of knee joints resulting from connections between columns and long outriggers. Some aspects of the transverse response of these regions have been considered in a companion paper to this workshop [Ref.1]. Joint shear strength is generally inadequate, and flexural and shear capacity of the cap beam are also suspect. A prime reason for this is the allocation of flexural strength on the basis of a low estimate of lateral seismic force inherent in the elastic design philosophy current in the 1950's and 1960's, with the result that longitudinal reinforcement is often prematurely terminated causing unexpected sections to become critical under seismic response.

A further concern with these outriggers is the torsional capacity under longitudinal response. Typically the torsional strength is considerably lower than that required to develop the moment capacity at the top of the column. Torsional hinging of the cap beam can thus be expected with great loss of stiffness, and perhaps with a loss of capacity to support gravity loads.

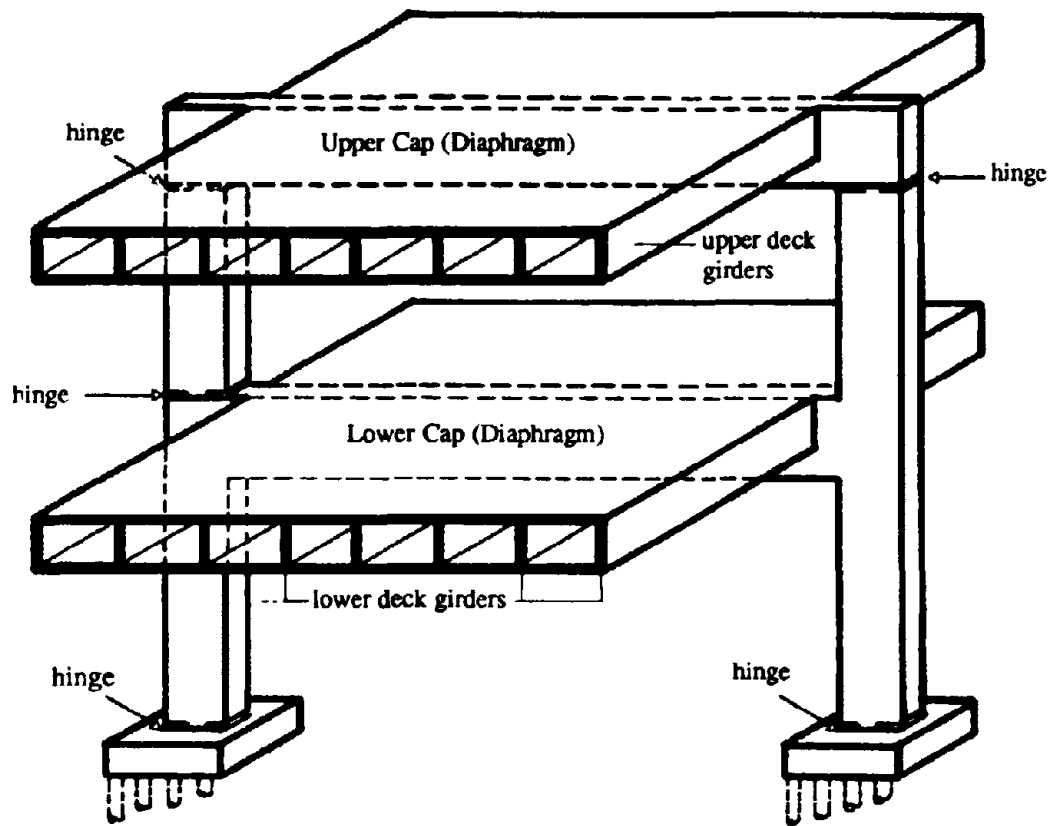
### OBSERVED DEFICIENCIES IN THE REGULAR DOUBLE-DECKERS

#### Structural Description

Figure 1 describes the typical structure considered in this paper. The double-deck superstructure is comprised of a multi-cell reinforced concrete box girder, typically about 4'-6" to 5'-6" deep. Bents support the superstructure at spans that vary, but are typically in the 70-100 ft span range. Superstructure width also varies, typically within the range of 40-70 ft.

---

(I) Professor of Structural Engineering, University of California, San Diego, USA



**Fig.1 Double-Deck Viaduct Overview**

The superstructure frames into a cap beam which is deeper than the superstructure, with section dimensions about 4 ft wide by 8 to 9 ft deep. The lower cap beam has a moment-resisting connection to the outer columns, which may be partly under the superstructure, or wholly outside it. For wide superstructures, there may be a third (central) column supporting the lower deck, where local geometric constraints permit. The lower cap beam is reinforced with mild steel reinforcement. The upper cap beam has to span the entire superstructure width, and for this reason is prestressed when superstructure width is high.

Columns are of rectangular section, typically about 6 ft × 4 ft in section for the lower column, often reducing to about 4 ft × 4 ft for the section between the lower and upper decks. Longitudinal reinforcement is generally #18 bars with reinforcement ratios that are frequently 4-5%, and on occasions as high as 8%. Transverse reinforcement is inevitably #4 peripheral ties at 12 in. centers, though occasionally one central cross link is provided at the center of the long side.

The columns are pinned to foundation pads supported by piles. The intent of this detail is to reduce the moments required to be supported by the foundation structure. The pin detail is achieved by reducing the effective section at the base by a ring of flexible material and termination of the longitudinal column reinforcement at the base. Shear transfer at the base is assisted by a small number (typically four #10 bars) of centrally located reinforcing bar dowels. As noted earlier, the lower cap beam is designed with a moment-resisting connection to the lower column. As subsequently noted, this connection is generally inadequate. No special joint shear-reinforcement is provided.

Where the columns frame into the upper cap beam, again a pinned connection, similar to that at the column base, is often adopted. This is always the case where the upper cap beam is prestressed, in an attempt to minimize column moments induced by creep and shrinkage. For the same reason, a hinge is placed in one of the two upper columns adjacent to the lower cap beam, as indicated in Fig. 1. Shorter cap beams are generally conventionally reinforced, with moment-resisting connections at the top of the columns. Complete reinforcement details are provided in [Ref.1].

### Transverse Response

Transverse response requires a load path from superstructure inertia force into the cap beam by essentially diaphragm action. Bending moments and shear forces are then induced in the cap beam and column. The expected level of base shear necessary to assure elastic response under the design level of excitation is approximately 1.0 g to 1.25 g. No parts of the transverse load path are strong enough to support that level of response, and it remains to determine which are the most critical elements.

#### (i) Columns

It is natural to look first at the columns. Flexural strength may correspond to force-reduction factors, related to the elastic response level, of  $R = 2$  to  $5$ . Expected ductility demand may be higher than this because of the potential for developing a soft-story sway mode. Although these levels of ductility can be sustained by well detailed columns, the very low transverse reinforcement ratio (typically  $\rho_s \leq 0.0015$ ) means that no effective confinement can be achieved, and ductility will be limited to that of an unconfined section. A conservative limit of  $\mu = 1.5$  has been used in assessing the ductility capacity of these columns, though test results indicate that  $\mu \geq 2$  should be achievable.

Shear capacity of the columns is even more suspect. We may assume the shear capacity of the columns to be comprised of additive concrete and steel truss components given by

$$V_i = V_c + V_s = v_c b d + \frac{A_v f_y d}{s} \quad (1)$$

where  $v_c$  is the nominal shear strength of the concrete shear resisting mechanisms,  $b$  and  $d$  are the column width and effective depth, and  $A_v$  is the area of shear reinforcement, of yield strength  $f_y$  at vertical spacing  $s$ .



Recent tests described in a companion paper [Ref.2] indicate that  $v_c$  may be conservatively taken as  $3.0\sqrt{f'_c}$  (psi). Using this figure, and assuming  $f'_c = 5000$  psi, the shear strength of a 6 ft  $\times$  4 ft column reinforced with two #4 legs at 12 in. centers could be  $V_i = V_c + V_s = 600 + 80 = 680$  kips. This is generally less than the shear corresponding to development of flexural strength, indicating that shear failure may be expected. It should also be noted that if the shear strength as calculated above exceeds flexural strength, shear failure may still develop, since the value of  $V_c$  will decrease as the ductility increases.

The prevalence of shear failures, or incipient shear failure in many columns during the Loma Prieta earthquake support these calculations.

Where one upper column is pinned to the lower cap beam, as shown in Fig. 1, for example, all lateral resistance may be provided by the moment capacity at the base of the opposite column. Typically, ductility capacities of 6 to 9 would be required under the design level earthquake, and no redundancies exist in the load-path from upper deck inertial response down to the lower level columns.

#### (ii) Cap beams

When cap beams are fixed to columns above and below, moment equilibrium at the joint requires the cap beam to support higher moment than the columns, as shown in Fig. 2. However, inspection of the reinforcement details in the cap beam at the column face invariably indicate that the flexural reinforcement, again typically #18 bars, provided in the cap beam will result in a moment capacity much lower than for the lower column. As shown in [Ref.1], top reinforcement may be adequately anchored by a 90° bend toward the outer edge of the joint region, but bottom reinforcement is only anchored by a short (3-5 ft) straight extension into the joint. The bottom reinforcement is particularly inadequate in both reinforcement area, and anchorage length, and the position moment capacity may correspond to elastic force reduction factors as high as  $R = 12$  or more. Top reinforcement provides a negative moment capacity that corresponds to  $R$  values in the range 6-10. Since the cap beams are not detailed for flexural capacity, it is clear that their capacity will be suspect. Bond failure of the bottom reinforcement, with a possible reduction of shear capacity at the critical column face, is expected at an early stage of response. Again this is supported by observed damage in several of the San Francisco viaducts.

#### (iii) Column-cap beam joints

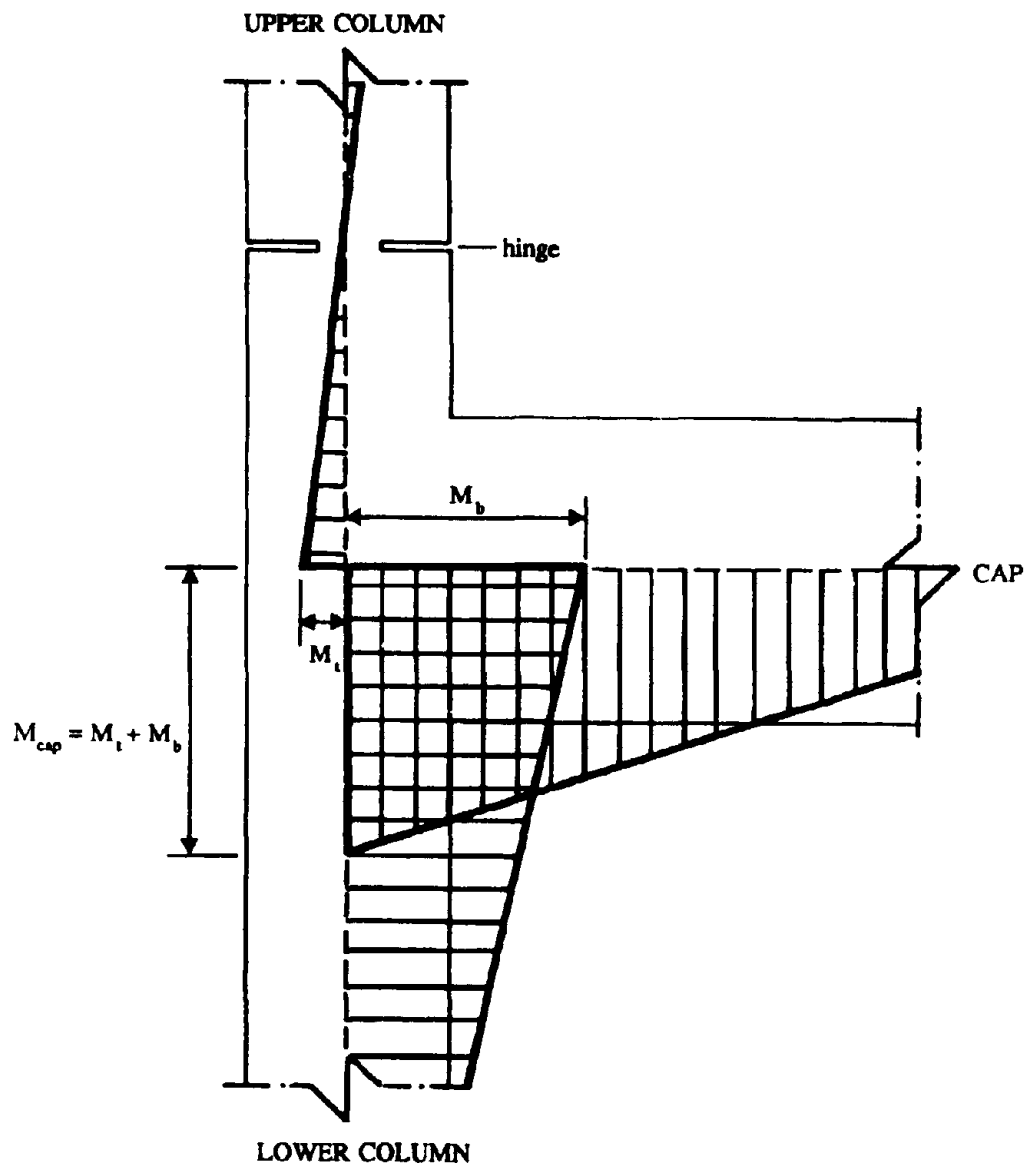
It is now well established that joint shear strength inadequacies contributed to failure of the Cypress Viaduct. High vertical and horizontal shear forces are induced in the joint region if adjoining members have sufficient integrity to develop their flexural strength. Because of a lack of understanding of joint-shear mechanisms when the viaducts were designed, they have virtually no shear reinforcement to assist in supporting these joint shears.

Thus it is seen that all elements of the transverse load-resisting mechanism are substandard. In addition, shear connection at the top or bottom column pin joints are suspect under uplift seismic reactions, and in some cases the lateral capacity of the piles supporting the fastings may be inadequate to support the column shear forces.

#### Longitudinal Response

The longitudinal response of a multi-bent section of double-decker freeway is somewhat more complex than the transverse response. The mechanism for transfer of superstructure inertia force to the ground involves longitudinal bending of the superstructure deck girders, torsional bending of the cap beam, and flexural and shear action in the column.

Again the column capacity, though too low for elastic response, is generally higher than that of other elements and mechanisms on the load path. The superstructure longitudinal moment capacity is typically less than the columns, particularly on the positive-moment side of the cap beam, where only



**Fig. 2 Lower Joint Seismic Moment Demands**

nominal reinforcement is carried from the soffit slab into the cap beam. Consequently, extensive positive-moment cracking can be expected soon after the dead-load negative moment has been equilibrated by the seismic moment.

It will be appreciated that, with the longitudinal deck girders developing moments of opposite sign on opposite sides of the cap beam, the rotational flexibility of the cap beam may be such that only comparatively small moments can develop in the girders, particularly those most distant from the columns. If the superstructure girders are capable of developing adequate moments, and the cap beam is stiff enough torsionally to resist them, then the weak link on the load path would appear to be the torsional capacity of the cap beam, which does not contain reinforcement specifically designed for torsion.

Weaknesses in the cap-beam/column joint region, and the column itself, are similar to those pertaining for transverse response.

It is generally considered unacceptable to allow plastic hinges to form in superstructure girders. In order to investigate the propensity for superstructure hinging, and the ability of the cap beam to transmit superstructure forces by torsion, a series of analyses of a superstructure/cap beam/column superassembly, as illustrated in Fig. 3, were carried out.

Two models were used, each representing a typical cap beam, and that portion of superstructure for one half span on either side of the cap beam. The first model, based on a grillage analogy, is shown in Fig. 3a. Each deck girder, including tributary deck and soffit slab areas, was modeled longitudinally by grillage members, representing flexural and torsional stiffness of the deck. Transverse linking members represented transverse stiffness characteristics of the superstructure. A single member running transversely represented the cap beam. A more sophisticated three-dimensional finite element simulation [Ref.3], shown in Fig. 3b, was used to verify the simpler grillage analogy, which was used for the majority of analyses.

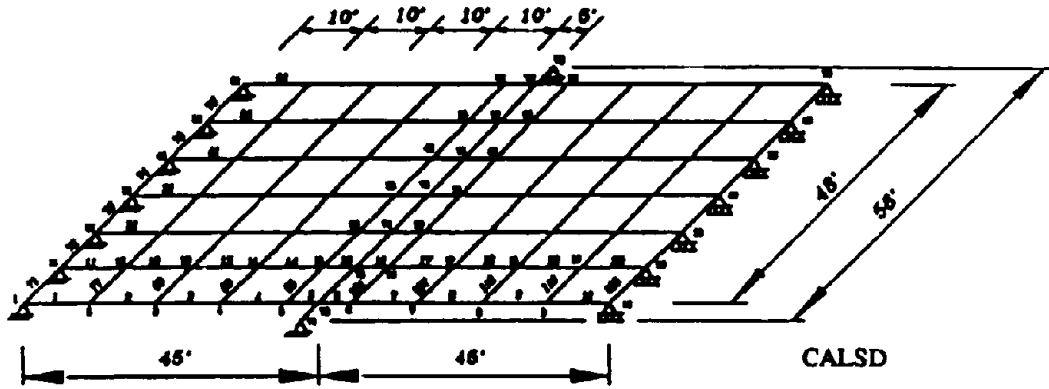
Each model was supported vertically at each girder locations at the midspan, as shown in Fig. 3, and the cap beam was supported at each end. Loading was provided by a torque of arbitrary value 10,000 kip ft applied at each end of the cap beam, simulating moments induced by longitudinal bending of the columns, which were not directly modeled in the analysis. The purpose of the analyses was to investigate the distribution of cap beam torque and longitudinal girder moments that would exist in conjunction with the cap beam end torques.

The two models gave essentially identical results, for a test case, verifying the validity of the grillage analogy. Figure 4 shows results for the transverse distribution of girder moments and cap beam torques resulting from the two analyses (grillage = CALSD; 3DFE = NOBOX) based on uncracked gross-section stiffnesses, and also for a second case where the cap beam torsional stiffness was reduced to 20% of gross stiffness to model the effect of expected torsional cracking of the cap beam.

Figure 4 confirms the similarity of results between the 3DFGE and grillage analogy. The girder moments (Fig. 4a) are shown in bar-chart form, with each bar representing the moment in a longitudinal girder on one side of the cap beam. The girder on the same line on the other side of the cap beam has an identical seismic moment. It will be seen that the outer girder moments are a maximum, with the central girders resisting very little moment, because of the torsional flexibility of the cap beam. This is particularly apparent for the case where the cap beam is cracked, where the outer girders G-1 and G-7 each have longitudinal moments of 3800 kip ft, indicating that 76% of the end cap beam torque is induced by bending of the outer girders. Figure 4b, showing cap beam torque with distance from the cap beam (diaphragm) center line, presents the same information in different form.

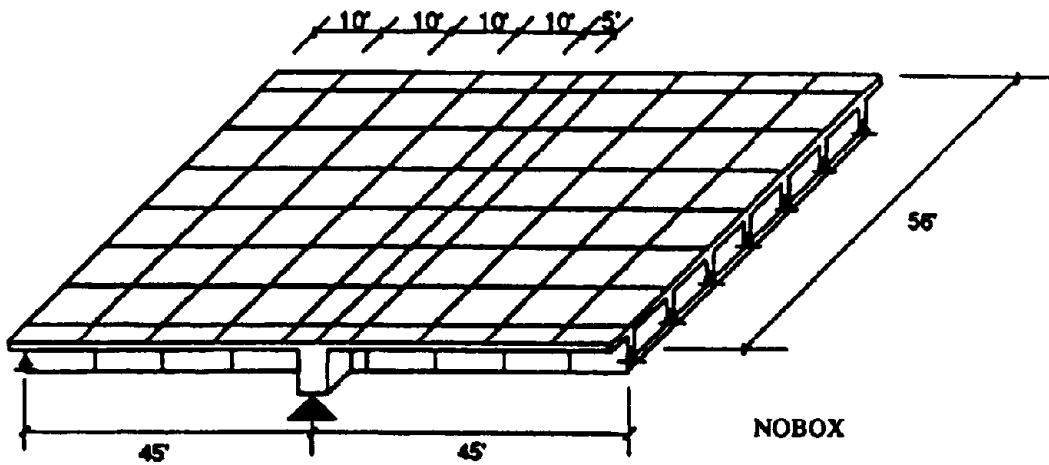
As a consequence of cap-beam flexibility, damage to outer superstructure girders can be expected at an early stage of longitudinal response. If these girders are capable of ductile plastic hinging, adjacent girders would start to develop higher moments, involving higher cap beam torques.

I-280 TORSIONAL BRIDGE DECK ANALYSIS  
Typical Bent No. 34



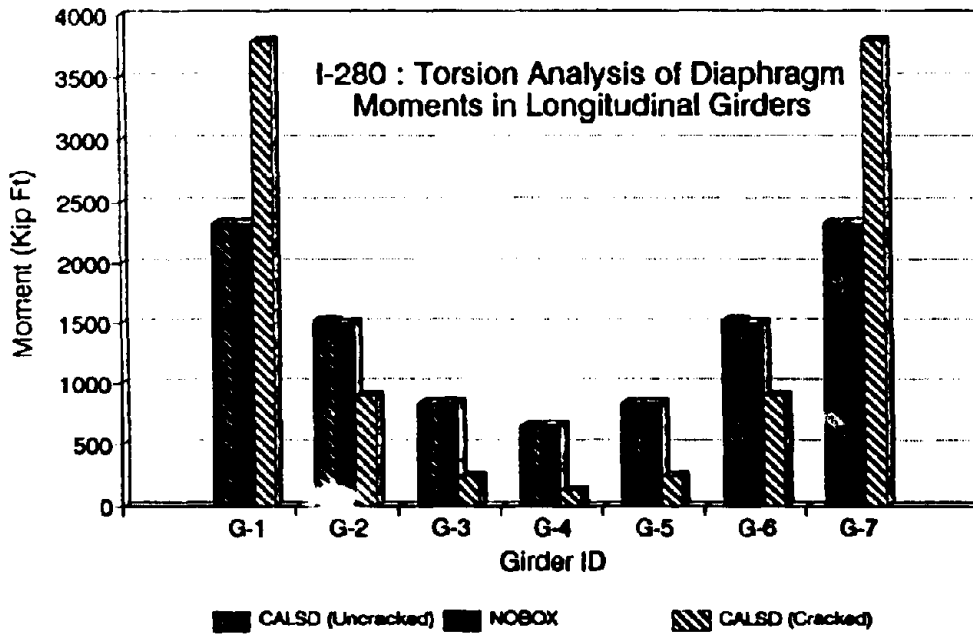
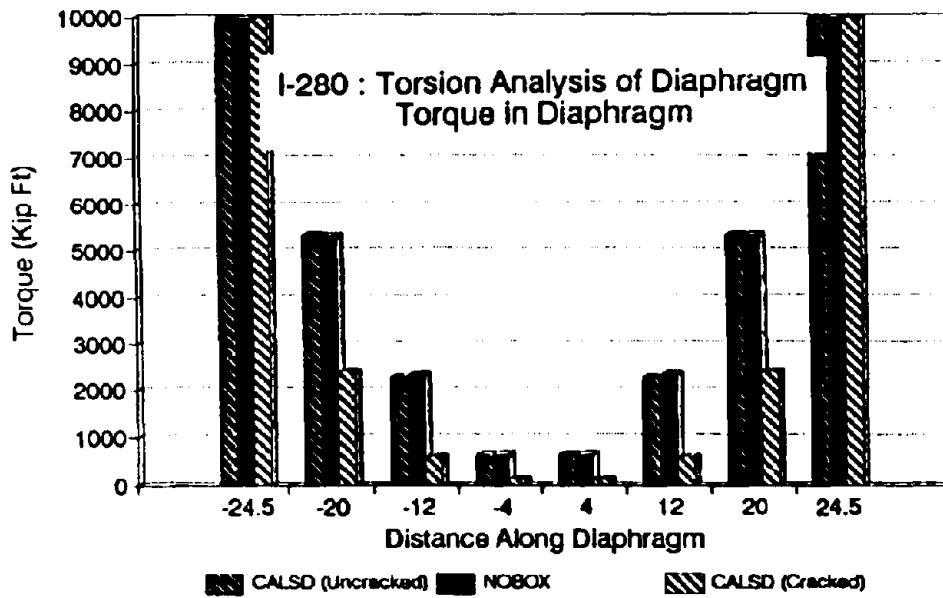
(a) 2-D Grillage Model

GRID SIMULATION FOR TORSIONAL ANALYSIS



(b) 3-D Box Girder Model

Fig. 3 Longitudinal Response Models



**Fig. 4** Transverse Distribution of Longitudinal Action

However, cap beam torsional capacity is typically less than 20% of that corresponding to a system ductility of about  $\mu = 4$ . Further, torsional hinging is not an acceptable means of dissipating seismic energy, since after torsional cracks develop, the available strength provided by existing reinforcement is less than the cracking torque, and the shape of torsional hysteresis loops is extremely poor.

## A RETROFIT STRATEGY

The arguments presented above indicate widespread areas for potentially unsatisfactory performance during seismic attack. Initial attempts to find retrofit solutions concentrated around increasing the ductility capacity and shear strength of columns under transverse response, typically by a variety of different methods of steel jacketing. As well as the oval-jacket retrofit, which has proved to be very effective in tests and is discussed in a companion paper [Ref.2], retrofits using various methods of stiffened rectangular jackets were proposed. Tests at the University of California, San Diego found these to be largely ineffective.

It was soon realized that these early retrofit solutions did not address most of the critical areas, such as inadequacy of cap beam flexural strength and column/cap beam shear strength under transverse response, and inadequacy of cap beam torsional strength, longitudinal girder flexural strength, and joint capacity under longitudinal response.

Current retrofit solutions for the regular double-decker portions of the viaducts are based on variations of the scheme summarized in Figs. 5 and 6.

### Transverse Retrofit

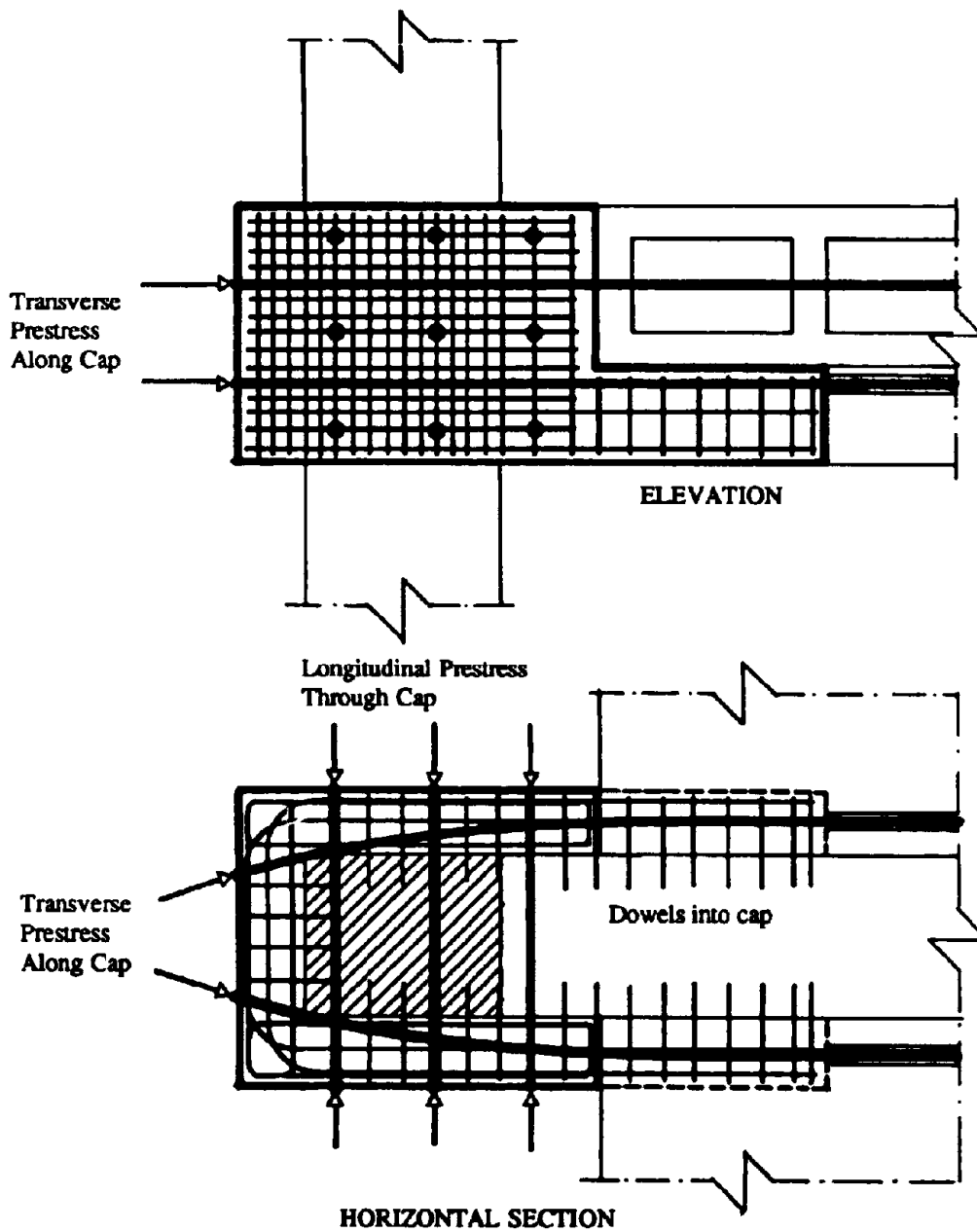
To improve transverse response, the existing columns and joint connections to the lower cap beam will be removed and replaced by ductile circular columns or rectangular columns with intersecting spirals for confinement designed for high ductility capacity. The end region of the cap beam will be strengthened by adding additional width to the lower region, with significant amounts of longitudinal reinforcement to bring the positive moment capacity up to the existing negative moment capacity. Additional moment capacity is provided by cap beam prestressing anchored beyond the column. This increases the moment capacity to the level where either cap beam ductility requirements are reduced to an acceptably low level (about  $\mu = 3$ ), or, preferably, hinging is forced into the ductile columns. It was found to be necessary to remove the existing columns and joints because of difficulties in assuring satisfactory joint shear performance with existing details. No convincing retrofit strategy could be developed for the joints without total replacement. This was partly the result of uncertainties associated with methods of splicing lower and upper column longitudinal reinforcement within the joint.

The longitudinal prestressing in the cap beam provides a secondary function of helping to resist cap beam vertical shear force at the column interface, in the event that high ductilities are required of the cap beam.

A variation of this transverse retrofit strategy would use an all-mild steel solution rather than the partially prestressed method described above. In this case, the cap beam must be widened and strengthened over the whole width. With the partial prestress solution, strengthening of the cap beam is typically only required over the end 10 ft. Over the rest of the span, the cap beam prestressing is external to the beam, running in a grouted galvanized duct for corrosion protection, and thus enhancing the strength as with an unbonded internal tendon.

### Longitudinal Retrofit

In the longitudinal direction, the main concern is to reduce the level of cap beam torsion and longitudinal deck girder moment. To this end, new 'supergirders' will be placed between existing columns in the longitudinal direction, as shown in Fig. 6. These may be precast and lifted into position, or constructed in situ. The design requirement for the supergirders is that their flexural



**Fig. 5 Transverse Retrofit Details**

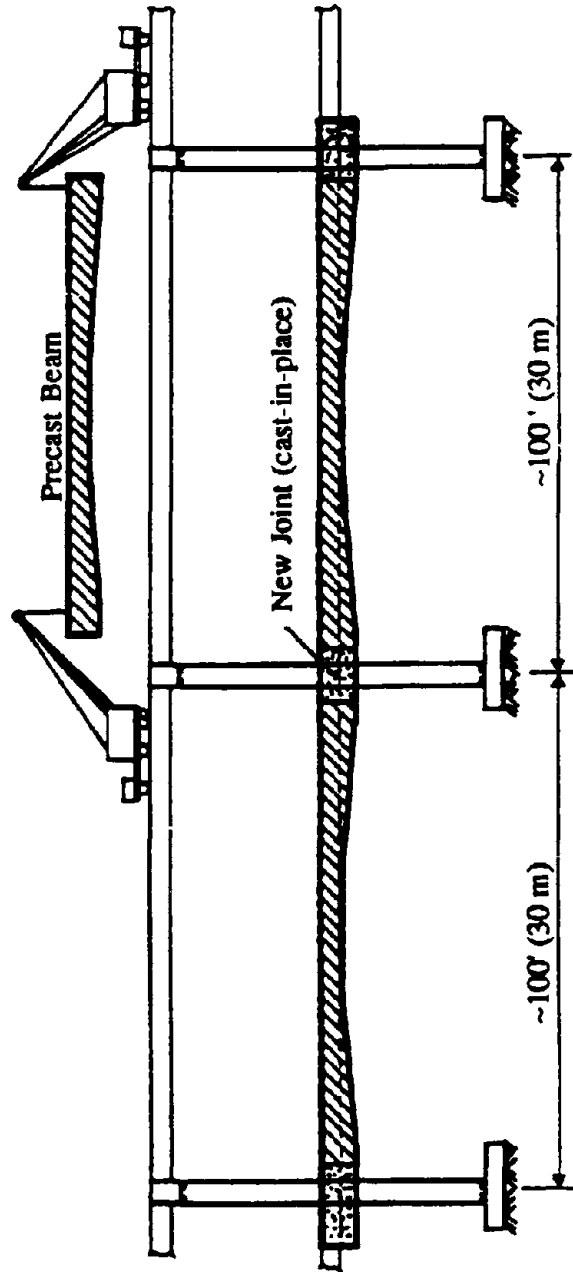


Fig. 6 Longitudinal Retrofit Scheme



strength exceed that of the new columns by a sufficient margin to ensure that plastic hinges will form in the columns. As a consequence, the torsional rotations required of the cap beam will be small, since all inelastic rotation occurs above or below the cap beam.

Although the supergirders have lower stiffness than the existing superstructure girders, their location in the same longitudinal plane as the columns makes them effectively stiffer than the existing deck girders which are connected to the columns through the torsionally flexible cap beam.

To confirm this assumption, additional grillage analyses were carried out using the model described in Fig. 3, with the addition of longitudinal supergirders outside deck girders G-1 and G-7. Results are shown in Figs. 7 and 8 for the analyses based on uncracked and cracked cap-beam torsional stiffness, respectively. In Figs 7a and 8a, R-1 and R-2 refer to the supergirders. It will be seen that the deck girder moments and cap beam torques are substantially reduced by the inclusion of the supergirders. In the worst cast, based on uncracked cap beam properties (Fig. 7), the supergirders take 72% of the column moment, with the edge deck girder moment reducing to about 7% of column moment. Cap beam torque is reduced to 28% of the value without the supergirders.

Figure 8, based on cap-beam cracked-section properties, shows even more dramatic improvement, with the supergirders supporting 88% of the column moment, the edge deck girders moment dropping to 5% of column moment, and cap beam torque reducing to 12% of the value without the supergirders. Actual response is likely to be intermediate between these figures, since the levels of torque predicted in Fig. 7 are still sufficient to induce torsional cracking.

It should be noted that with the adopted philosophy of weak column/strong supergirder for longitudinal response, the torsional moment induced in the cap beam depends on the true cap beam stiffness, but the torsional rotation is almost independent of the cap beam stiffness, since the joint rotation is effectively dictated by the supergirders. As a consequence, any uncertainty about the strength and stiffness of superstructure and cap-beam become largely irrelevant to the longitudinal seismic performance.

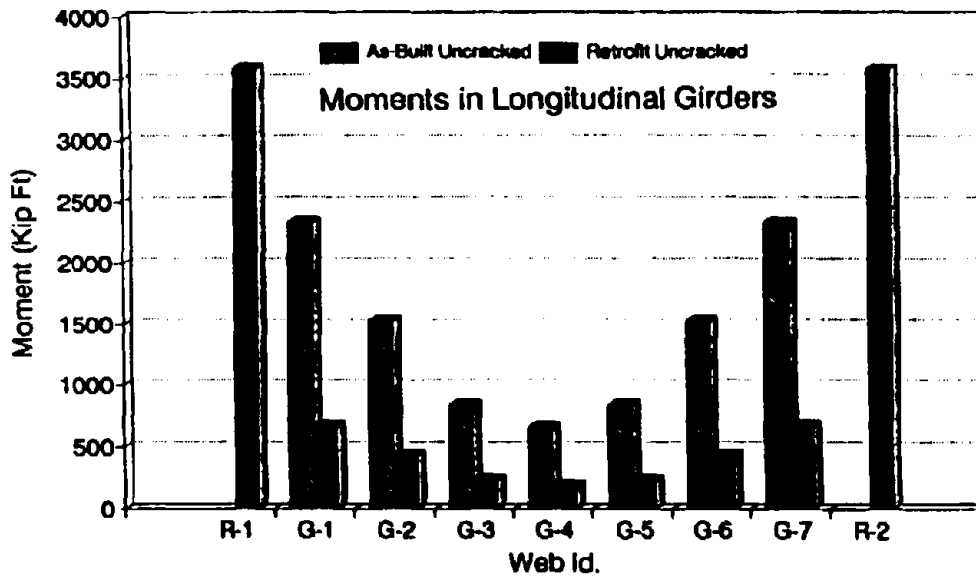
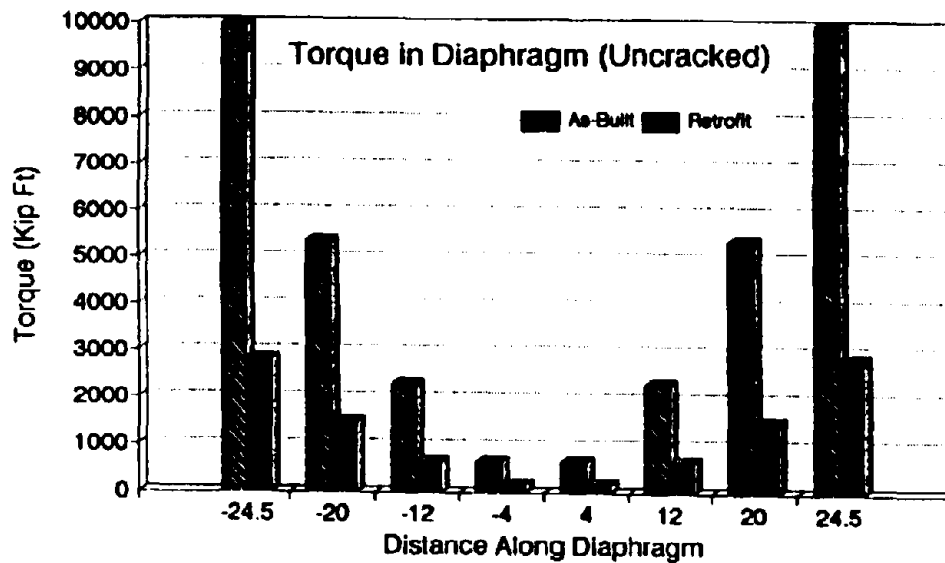
Again, variations in the supergirder concept are being considered for different viaducts. In situ versus precast concepts are being considered, and the relative merits of completely isolating the supergirder from the deck girder, or joining by a deck slab extension are still under discussion.

#### Proof Testing of Retrofit Schemes

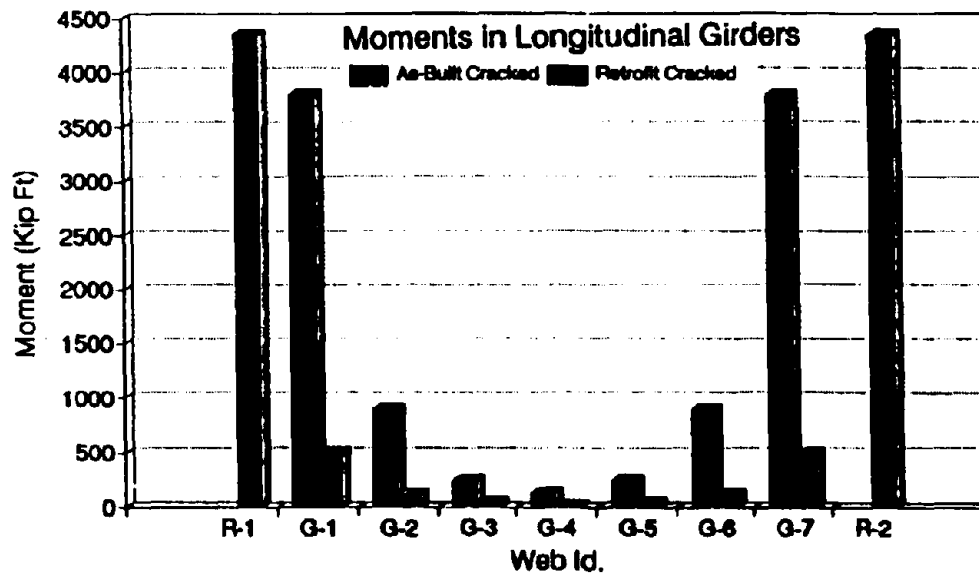
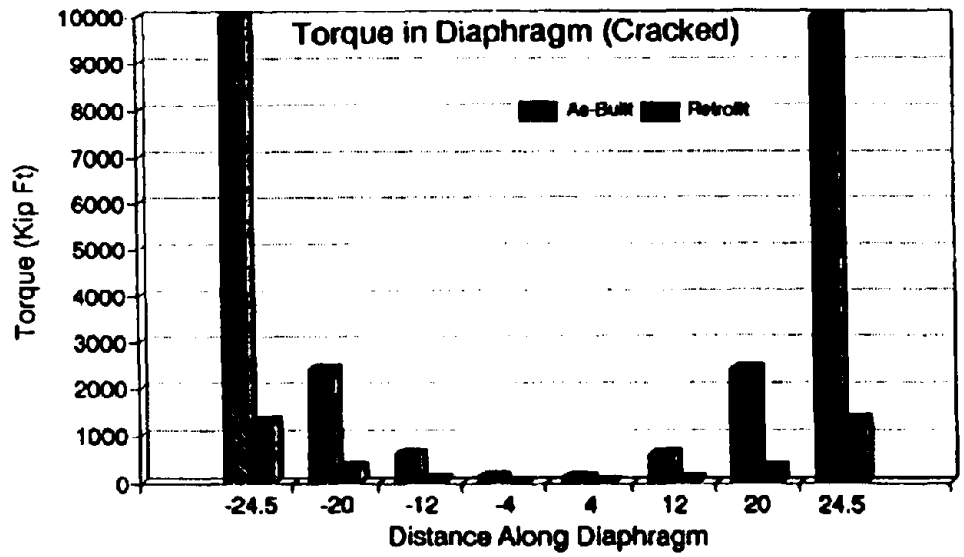
In order to verify the concepts described above for bringing the potential seismic performance of the San Francisco double-deckers up to that expected for new bridges, plans are being finalized for testing two large-scale models; one at U.C. San Diego and one at U.C. Berkeley. The structures, built to approximately half scale, will represent a two-level column and lower cap beam and half a span of lower deck superstructure on either side of the cap beam. Only that portion of superstructure from the column to the center of the cap beam will be modeled. Figure 9 shows a schematic of one of the models with the intended loading system which will ensure accurate representation of both longitudinal and transverse response. It is intended that the models will be tested under longitudinal, transverse, and simultaneous longitudinal and transverse response.

Two different schemes will be investigated. One will have a partial prestress design for the cap beam retrofit; the other will have an in situ supergirder connected to the existing superstructure. One will represent an end connection between a supergirder and column; the other will represent an interior connection, with supergirders on either side of the column.

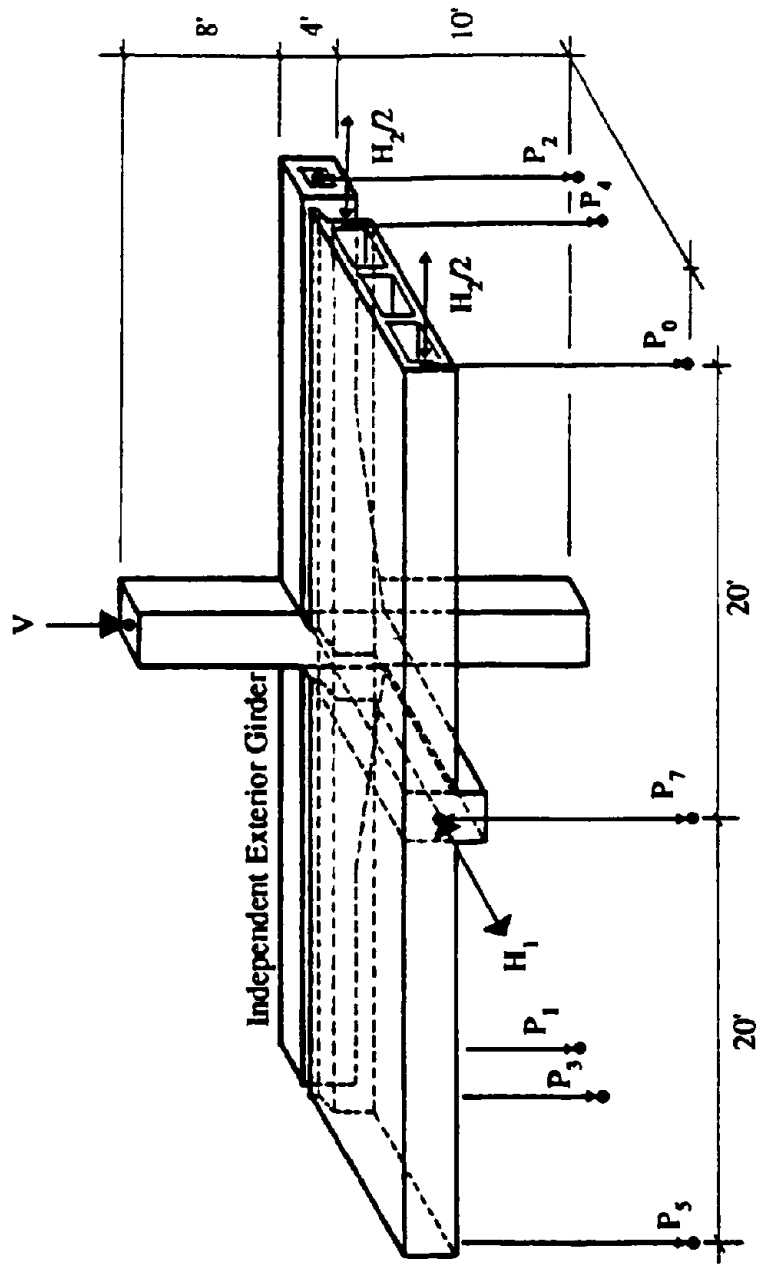
Construction of the models is expected to start early in 1991, with completion planned for July 1991.



**Fig. 7 Transverse Distribution of Longitudinal Action - Retrofit and Uncracked Diaphragm**



**Fig. 8** Transverse Distribution of Longitudinal Action - Retrofit and Cracked Diaphragm



**Fig. 2 Proposed Proof Test Setup**

## DISCUSSION AND CONCLUSIONS

Design of the retrofit strategies for the San Francisco double-decker viaducts has proved to be a complex task involving many iterations before acceptable solutions have been developed.

Although the need for improving strength and ductility under transverse response is obvious, and the solutions adopted are comparatively straightforward, it is the longitudinal response that has proven to be most difficult to improve. Despite the conclusions from calculations which indicate that the viaducts are much weaker longitudinally than transversely, there was no evidence of damage resulting from longitudinal response of the viaducts to the Loma Prieta earthquake, except for minor pounding damage at movement joints.

It appears possible that this lack of damage is the result of the length of the viaducts, and the difficulty in developing longitudinal resonant response. During an earthquake, structures of the length of these viaducts (up to 2 km in length) will be subject to non-cohesive excitation at the individual foundations. The presence of movement joints and superstructure flexibility will allow segments of the viaducts to move relative to each other and still develop resonant response. The longitudinal stiffness of the superstructure will prevent this occurring in the longitudinal direction.

Full longitudinal resonant response could only develop with a perfectly straight bridge on perfectly uniform ground conditions subjected to a perfect shear wave excitation traveling exactly perpendicular to the axis of the bridge. This is of course impossible, and sections of the ground at one part of the viaduct will be moving out of phase with other parts. Since the seismic wave length is expected to be of the order of 5 to 10 spans, this out of phase response could develop over comparatively short distances along the bridge. The resultant attempt of different sections of the bridge to respond in different directions can be expected to cause an interaction reducing seismic response in the longitudinal direction. If such a hypothesis is valid, it could be argued that longitudinal strength is unimportant, and it would be sufficient to retrofit the bridges longitudinally to sustain the relative out-of-phase motion of adjacent segments, or frames of superstructure separated by movement joints. In such a retrofit strategy, increased importance is placed on the restrainers connecting adjacent frames across movement joints.

Because of uncertainties and lack of relevant research on this phenomenon of non-cohesive response, it has not been adopted for the retrofit solution to the San Francisco double-deckers, and the more conventional solution described in detail above has been adopted.

## ACKNOWLEDGEMENTS

The retrofit solutions described above have resulted from the interactions between the consultants involved in the retrofit designs, and the independent review panel set up by Caltrans and chaired by Nicholas Forell of Forell/Elsesser Engineers, San Francisco. The authors wish to acknowledge the input of all members of the review panel and their advisors in developing these strategies.

## REFERENCES

- [1] SEIBLE F. and PRIESTLEY, M.J.N., Damage and Performance Assessment of Existing Concrete Bridges under Seismic Loads. Proceedings of Workshop on U.S. and Japanese Experience in Seismic Retrofit of Bridges, Tsukuba, Japan, December 17-18, 1990.
- [2] CHAI, Y.H., PRIESTLEY, M.J.N. and SEIBLE, F., Retrofit of Bridge Columns for Enhanced Seismic Performance. Proceedings of Workshop on U.S. and Japanese Experience in Seismic Retrofit of Bridges, Tsukuba, Japan, December 17-18, 1990.
- [3] SEIBLE F. and SCORDELIS A.C., Nonlinear Analysis of Multi-cell Reinforced Concrete Box Girder Bridges. Eng. Struct., Vol. 5, 1983, pp. 45-57.

## FULL-SCALE TESTS ON THE CYPRESS VIADUCT

Stephen A. Mahin (I)  
Jack P. Moehle (I)  
Presenting Author: Stephen A. Mahin

### SUMMARY

The Loma Prieta earthquake of October 17, 1990 damaged several reinforced concrete double deck freeway structures in the San Francisco Bay Area. The most severe damage occurred in Oakland, where a 3/4 mile long portion of the Cypress Street viaduct on Interstate Route 880 collapsed. Following the earthquake, a series of field experiments were carried out on an undamaged portion of this viaduct. Results of low amplitude forced vibration tests and of destructive, static lateral load tests are reported in this paper. Tests were performed on the test structure in its original configuration as well as after the installation of one of three different retrofits. Implications of these tests to the evaluation and retrofit of other freeway structures is discussed.

### INTRODUCTION

The Cypress Street viaduct was a double deck portion of Interstate 880 located in the western part of Oakland, California. During the October 17, 1989 Loma Prieta earthquake the upper deck of the viaduct suddenly collapsed onto the lower deck (Fig. 1) over about half of the viaduct's 1.5 mile length, resulting in 41 fatalities and scores of injuries. The urgent need to repair and reopen six other damaged double deck structures in the Bay Area led to the development of a field study on the capabilities of various retrofit techniques. A 170- ft. long segment of the Cypress Street viaduct, virtually undamaged by the earthquake, served as the platform for these studies. The objectives of the field test program were to identify the primary structural deficiencies that led to the viaduct's collapse and to evaluate the efficacy of several retrofit techniques being considered for application to the other damaged viaducts. The results of these tests and of subsequent analyses are summarized in this paper. Additional information may be found in Refs. 1 and 2.

### DESCRIPTION OF TEST STRUCTURE

The Cypress Street viaduct was designed in accordance with 1953 AASHTO specifications, and construction was completed in 1957. The roadway structure consisted of multi-cell reinforced concrete box girders supported on either reinforced concrete or combined reinforced/prestressed concrete bents. Figure 2 illustrates the most common box girder cross section and supporting bent elevation. The typical box girder had a width of 52 feet and a span of approximately 70 feet. Deck expansion joints (previously retrofit with cable restrainers) were provided typically every third span.

The typical bent shown in Fig. 2 consisted of reinforced concrete bent caps framing rigidly into reinforced concrete columns. The upper columns were connected at their base to the lower bent cap through 27 in. tall pedestals. Hinged joints were provided between the pedestals and upper level columns. The columns in the lower level were also connected through hinged joints to reinforced concrete pile caps and piles. Bents of different configuration also were used along the length of the viaduct, primarily at locations where

---

(I) Profs. of Civil Engineering, University of California, Berkeley.

ramps entered and exited the freeway, and where the upper and lower decks merged and diverged at either end of the viaduct length. A complete description of the viaduct geometry is presented elsewhere [3].

Concrete in the structure was specified to be normal weight with a design working stress of 1250 psi. Mild reinforcement was specified to be Grade 40. Tests of materials indicated an average concrete compressive strength of 6275 psi and a reinforcement yield strength of 43 ksi.

During the earthquake a 3/4-mile length of the upper deck of the Cypress Street viaduct collapsed onto the lower deck. The collapse extended from the northern end of the viaduct to 26th Street, at which location two bents and one deck span remained standing, and from there south to 18th Street. South of 18th Street, the viaduct sustained visible damage ranging from none (no apparent cracking) to severe (joint cracking indicative of incipient joint failure and possible collapse). Based on damage observations, it appears that the collapse was triggered by failure of the reinforced concrete section that includes the lower beam-column joint and the upper column pedestal just above the joint.

A portion of the undamaged viaduct between 13th Street and 14th Street (i.e. Bents 45 through 47) was selected for testing. All of the bents within the test structure had the same geometry and detailing as illustrated in Fig. 2. The test structure included the three bents plus the upper and lower decks spanning between and cantilevering beyond the bents (Fig. 3).

#### TEST PROGRAM

The test structure was subjected to a series of tests. These included forced vibration tests and static lateral load tests. Because of the nature of the observed failures and because longitudinal bracing was initially planned to be part of the retrofit scheme, tests focused on the transverse response of the bents. For the dynamic tests, two vibration generators were fixed to the upper deck. The maximum dynamic force developed in the structure by the generators during the dynamic tests was approximately 150 kips.

For the static tests, steel reaction frames were positioned along both sides of each bent (Fig. 4). The A-shaped frames were clamped to the lower columns near the pile cap, extended up through openings made in the lower deck, and supported pairs of hydraulic actuators that applied load to steel blocks attached to the underside of the upper deck. The loading system was capable of applying in excess of 4 million pounds to upper level of the structure. The total weight of the structure was about 5,700 kips.

Dynamic and static tests were performed on the test structure in its original configuration and after retrofits had been installed. Preparation for testing began in mid-November and the site was vacated by the end of December 1989.

#### Retrofit Systems

Given time constraints, it was necessary to select simple retrofit devices and systems. These were intended to represent the concept, rather than the detail, of systems that might be adopted for field implementation. Only "semi-permanent" type retrofits were considered. Furthermore, the time available for testing precluded consideration of schemes utilizing reinforced concrete. A different retrofit scheme was selected for each bent. It was not possible in the time available to completely evaluate the structure and engineer all of the details for the selected systems, so standard practices were often followed and emphasis was placed on the region near the base of the pedestals.

Details of the retrofits are shown in Figs. 5-7. Several common features were incorporated. For example, each bent cap was externally post-tensioned to help confine and strengthen the joints and to improve continuity of the bent cap longitudinal reinforcement. The joints were essentially devoid of transverse reinforcement and the anchorage length provided for the bottom cap reinforcement was about 18 bar diameters. The nominal prestress added to the bent caps was about 130 psi. In addition, external shear reinforcement was added to all of the columns. On Bent 46, the post-tensioning rods used for this reinforcement were left initially loose so that the shear capacity of the columns could be determined. Once shear cracks developed, the rods were tightened and testing continued. Specific details of the retrofits for each bent follow:

**Bent 45.** -- Bent 45 was retrofit with four steel wide flange sections clamped to the outer and inner faces of the columns (Fig. 5). On the east side of the structure, the outer wide flange sections were continuous over their full height. On the west side, the outer wide flange sections extended over the full height of the structure, but they were discontinuous at the elevation of the bottom of the upper bent cap. The wide flange sections on the inside faces of the east and west side columns were discontinuous at the bottoms of the bent caps and at the top of the pedestal in the upper level (i.e., at the column hinge). The inside face of the column pedestal was reinforced using a 1-1/4 in. thick steel plate. The wide flange sections and steel plates were held in place using steel rectangular tubes and post-tensioning rods. It was impracticable to use sufficient post-tension rods to ensure fully composite action; a smaller number was selected on the basis of ultimate load transfer.

**Bent 46.** -- Four 1-3/8 inch threaded post-tensioning rods were grouted in 2-inch diameter holes cored through the joint (Fig. 6). The holes extended from the outer face of the pedestal (just above its base) toward the bent cap, at a downward angle of 30 degrees. The rods were installed unstressed.

**Bent 47.** -- A steel collar was clamped around the pedestal and lower portion of the upper level column (Figs. 2.16 and 2.19). The collar was fabricated from 2-1/2 inch thick steel plates. Two steel flanges, 1 in. thick, extended downward from the collar onto the sides of the lower joint. These side plates were clamped to the joint using longitudinally-oriented, post-tensioning rods. In addition, one-half inch thick steel plates extended over the full height of the inner and outer faces of the columns in much the same way as did the wide flange sections on Bent 45. The plates were held in place using steel rectangular tubes and external post-tensioning rods.

#### Instrumentation

Instrumentation for the forced vibration tests consisted of accelerometers and seismometers. For the static tests, more than 110 channels of instrumentation were installed. These included load cells to measure applied loads and forces in selected post-tensioning rods. Displacement transducers were employed to measure global and local deformations. Strain gages were attached to some reinforcement in the existing structure as well as to the steel retrofits. A microcomputer based data acquisition system was used to record the dynamic and static test results.

## ORIGINAL STRUCTURE

#### Dynamic Tests

The forced vibration tests of the original structure indicated first and second mode translational periods (frequencies) of 0.42 sec. (2.4 Hz) and 0.14 sec. (7.0 Hz), respectively, for the transverse direction. Damping was estimated in the first mode to be 2.3 percent of critical. A linear elastic finite element computer model was developed. This model represented the structure as being fixed based, and gross section properties were



considered in modeling of the bent caps and columns. The decks were represented by shell elements. The computed periods (frequencies) were 0.38 sec. (2.6 Hz) and 0.14 sec. (7.0 Hz) for the first two transverse modes, indicating that the actual structure was not quite as stiff as the analytical model. This would be expected as minor amounts of cracking would likely exist in the actual structure. However, the predicted mode shapes differ significantly from measured values. This discrepancy appears to be consistent with movements of the foundations during the forced vibration tests. Since the analytical model resembles the actual boundary conditions for the static tests, this aspect of the response was not investigated further.

### Static Test Results

Three cycles of loading were applied towards the west (Fig. 8). The first cycle was used to check the loading apparatus and instrumentation, and to measure the lateral stiffness. As seen from Fig. 8, the predicted lateral stiffness, based on a fixed base, gross section model, was about 9 % higher than measured. This is consistent with anticipated effects of pre-existing cracks in the structure.

During the second cycle cracks were observed to form near the base of the pedestal on the west side of the structure. The crack pattern was similar to that observed in the damaged portions of the viaduct following the Loma Prieta earthquake. The cracks extended from the inside face of the pedestal near its base and ran downward towards the outside of the column roughly following the projection to the surface of the hooks anchoring the top reinforcement in the lower bent cap (Fig. 1.5). These cracks formed at a total load of about 1400 kips and at a displacement of 0.79 inches at the top deck (less than 0.14 % drift). The pedestals and joints were then clamped to prevent failure and loading was increased to about 1800 kips without additional damage in the structure.

It should be noted that the orientation of the cracks in the lower joint was inconsistent with joint shear, but rather parallels the direction associated with column shear. The computed shear capacities for the upper columns and especially for the pedestals are only marginally larger than needed to develop a plastic mechanism in the upper level. The capacity of the pedestal would likely be reduced due to the splitting action of the dowels transferring shear across the pin. However, a more likely explanation is found in Fig. 2 where it can be noticed that the upper part of the joint, unlike the pedestal and column, had no transverse reinforcement with which to resist shear. Thus, shear cracks in the pedestal would naturally tend to extend down into the joint. Simple design oriented, elastic (lower bound) estimates of the load needed to initiate inclined cracking in the joint come within 5% of the measured value. A limit analysis representing the bent following the formation of a shear failure plane (inclined downward at a 45 degree slope) indicates that the base of the pedestal would slide downward and outward under the influence of gravity loads alone.

Tests of Bent 46 during the retrofit test phase provide an indication of the actual shear capacity of the columns. During these tests, the column shear reinforcement was in place, but not attached. Column shear cracking occurred at a load on the bent estimated to be 900 kips. It is estimated that the nominal shear stress in the column at the time of failure was at least 220 psi, or  $3.3 \sqrt{f'_c}$ . Using current ACI recommendations for axially loaded elements, one would conservatively predict a capacity of  $2.8 \sqrt{f'_c}$ . These shears are almost 100% higher than needed to form a shear crack at the base of the pedestal.

The load needed to initiate a shear crack in the pedestal was about 1400 kips. Since the upper level weighs around 3300 kips, the shear coefficient for the upper level is about  $1400/3300 = 0.42$ . If lateral loads during dynamic response are assumed to be distributed in a 2:1 (upper:lower deck) ratio, the effective base shear coefficient associated

with the shear failure would be about 0.32. While this value is low compared to today's criteria, it is much larger than might be expected considering the original design employed a working stress base shear coefficient of 0.06.

#### Expected Response During the Loma Prieta Earthquake

Precise determination of the response of the viaduct during the Loma Prieta earthquake requires consideration of many factors outside the scope of this investigation. Factors such as traveling waves in the soil and the structure, the variability of the soil under the structure, alignment variations, access ramps, expansion joints and so on would have to be considered. However, a general idea of the structural vulnerability of the viaduct can be obtained from a simple elastic dynamic analysis of the test structure in the transverse direction. For these analyses the input motion considered was obtained during the Loma Prieta earthquake at the Oakland Wharf, about a mile west of the viaduct. Soil conditions at this site are similar to those underlying the portion of the viaduct that collapsed.

Calculated upper level displacement and acceleration, base shear and input acceleration are plotted in Fig. 9. The waveforms indicate that significant response lasted about 14 seconds. The maximum displacement achieved was 1.29 inches (0.24% of the total height), maximum base shear was 3690 kips (56% of the total weight) and the maximum shear in the upper level was about 2240 kips. These values exceed by about 60% those needed to initiate a shear failure in the lower joint. While elastic analyses are not valid once the shear failure occurs, the dynamic response predicts at least 9 excursions beyond this level. Thus, the formation of these shear cracks would be very likely during the Loma Prieta earthquake, and as demonstrated previously, formation of these cracks is sufficient to cause brittle collapse of the viaduct.

### RETROFIT STRUCTURE

#### Dynamic Tests

After the retrofits were installed the dynamic characteristics of the test structure were measured again. The forced vibration tests indicate a stiffer structure with first and second mode translational periods (frequencies) of 0.38 sec. (2.6 Hz) and 0.13 sec. (7.6 Hz), respectively, for the transverse direction. Damping was increased to about 4.4 % of critical in the first mode. The measured mode shape for the first mode is nearly triangular.

#### Static Tests Results

Static tests of the retrofitted structure followed the schematic load and displacement pattern shown in Fig. 10. The atypical load history involving several cycles in one direction followed by several in the reversed direction was selected to facilitate completion of testing within the allotted time.

The retrofits permitted the structure to sustain loads and deformations far in excess of those developed by the original structure. The maximum displacement reached by the test structure was nearly 10 inches (1.8 % overall drift) which was 12.5 times greater than could be sustained by the original structure. It corresponds to an overall displacement ductility of about 6. However, loading was stopped at this point because of the extensive damage and it is unlikely that the structure could have undergone additional cycling at this point.

The load-displacement relations developed by the structure were essentially linear until a load of 3,000 kips was reached. The results indicate that the retrofits increased the stiffness of the structure about 30 %. Because the change in measured periods would correspond to about a 20% increase in period, and the deformed shapes measured by

static and dynamic means do not match, it is believed that foundation-structure interaction may have had a significant effect on the response. In addition, it is noted that the displacements gradually concentrated in the upper level, so that by the end of the test, more than 90% of the applied lateral displacement developed in the upper level, resulting in a drift index for the upper level of 3.3%.

The maximum load achieved was slightly in excess of 4000 kips (70% of the weight of the structure). Assuming, as before, a 2 to 1 distribution of dynamic forces between the upper and lower levels, the force sustained by the retrofit structure were equivalent to a base shear coefficient of 0.9. This is more than 2.8 times the capacity of the original structure.

Lower Joints. -- Significant local damage developed throughout the structure. In spite of the retrofits, the lower joints all developed inclined cracks similar to those observed in the damaged portions of the viaduct during the Loma Prieta earthquake. These cracks initiated early in the tests: at a total load of about 1800 kips (Cycle 2) for Bent 45 and 47. They formed in Bent 45 during the static and dynamic testing of the original structure. These cracks became more extensive and distinct as testing progressed, generally following the contour of the hook at the end of the #18 top bars used to reinforce the lower cap. With the exception of Bent 46, the inclined cracks in the lower joint only occurred with this orientation.

The relatively flexible unbonded post-tensioning bars and wide flange sections clamped to the columns in Bent 45 were unable to prevent these cracks from opening wide. Because of the relative stiffnesses of the concrete skeleton and the steel retrofit, little load was carried by the external joint reinforcement until the inclined cracks formed. At that point, the crack opening was controlled by the elastic elongation of the strong, but flexible (long) post-tensioning rods. Under cycling, damage accumulated in this joint, resulting in substantial spalling and disintegration of the joint by the end of the test.

In contrast, the bonded post-tensioning rods grouted in Bent 46, while not preventing the formation of the inclined cracks, limited adjacent crack widths to less than 0.1 inches. By the end of the test evidence of secondary distress was seen relative to spalling of the concrete, loss of longitudinal bar anchorage at the base of the pedestal, and joint shear. These aspects of the behavior were not considered in the retrofit and practical problems also exist related to coring holes in the heavily congested joints.

The steel collar placed around the critical region in Bent 47 prevented direct visual observation of concrete cracking during the test. This retrofit emitted loud popping noises starting in Cycle 2. Based on the computed behavior of this joint, it is believed that the joint cracked in Cycle 2 and the flanges clamped to the sides of the lower joint began to slip at the same time. By the end of the test the collar rotated significantly with respect to the lower joint. The concrete in the joint and pedestal was observed during demolition and found to be highly cracked or pulverized.

Upper Joints. -- The upper joints were also observed to develop diagonal shear cracks at an early stage ( Bents 45 and 46: 2700 kips and a upper level drift of 0.47%, and Bent 47 : 1800 kips and a drift of 0.23%). Shear cracking in the joints occurred in an orthogonal direction during load reversals, resulting in a distinct x-shaped cracking pattern. The upper joints all eventually began to disintegrate, with cracks as wide as 0.5 inches forming, and the concrete bulging and spalling from the exposed faces of the joints. The upper west joint in Bent 46 was instrumented to assess joint rotation. Figure 12 shows the force- rotation relation. It can be noticed that the joint deformations are relatively small until a load of 3350 kips is reached. It can be noted from Fig. 11 that this also corresponds to the load at which large inelastic deformations begin to develop in the structure as a whole. It appears that a substantial portion of the apparent ductility of the structure is associated with shearing

deformations in the upper joints rather than with ductile yielding of the retrofitted portions of the structure.

The maximum shear stress in the upper joint can be conservatively estimated from the maximum tensile force that can be developed by the upper bent cap top reinforcement. During the final stages of testing this steel yielded. Stain gage readings indicate that it probably did not enter the strain hardening range. Thus, the total joint shear force is estimated to be about 670 kips. This results in a nominal maximum joint shear stress equal to 291 psi or  $3.7\sqrt{f'_c}$ .

Early in the tests the incremental loads in the cap post-tensioning rods varied consistent with beam-bending theory (i.e. tension forces developed on one side while compression increments developed on the other). However, as the joints began to severely crack and disintegrate all of the rods were observed to carry significantly increased tension forces. In some cases, computed rod forces exceeded their nominal yield capacities. For example, Fig. 13 shows that the force in the top post-tension rod on the west side of Bent 46 initially develops tensile forces as the bent moves toward the west and compressive forces as it moves toward the east. However, during later cycles, the incremental forces are tensile for both directions of movement. Clearly, insufficient confinement and shear reinforcement has been provided in the upper joint.

Bent Caps -- Bent caps developed flexural cracks at their ends. At the top the cracks were located in the narrow interface between the edge of the deck and the column. The deck proved sufficient to suppress any significant extension of the plastic hinge into the deck. At the bottom the cracks divided and some inclined away from the column, consistent with the shear present in the cap. Both top and bottom bars were observed to yield. In some cases, strains of as much as 2% were recorded. Evidence, however, exists that during later stages of testing the bond broke down between the concrete and some of the bottom cap bars. The development length provided for these bars was only 18 bar diameters.

Columns -- Flexural cracking and yielding were noted in upper level columns just below the upper bent caps. This yielding initiated during Cycle 9 for all bents. The column bars exhibited strains in excess of 1.8% in tension and compression during the later test cycles.

The columns in Bent 45 were not able to develop composite action. To develop the full composite action along the column in the upper level would require development of a longitudinal frictional force between the concrete column and the steel wide flange sections equal to about twice the tensile strength of the steel sections, 2370 kips. Assuming a friction coefficient of 0.5 and a prestressing force of 95 kips per rod, a total of 25 levels of prestressing rods would have been required to develop full composite action. This is more than four times the amount actually provided. As a result of this, strain gages attached to the wide flange sections exhibit highly nonlinear relations starting very early in the response, even though the maximum strain reached are far less than the yield strains (Fig. 15). Another aspect of this design is that there is an incompatibility between the ideal deformed shape of bent and of the steel wide flange sections. The transverse post-tensioning rods were not able to provide sufficient clamping force to keep the steel and concrete in contact (Fig. 16). Again, these rods had sufficient strength but not sufficient prestress or stiffness to control the opening of gaps. Gaps as large as 1/2 inch were observed during the testing. This resulted in a significant loss of confinement for both the upper and lower joints on Bent 45.

Built-in Pins -- The built-in column hinges at the top of the upper level pedestals were observed to rotate and slip, and splitting cracks started to develop at the tops of the pedestals. Instrumentation on the pin indicated that the vertical opening was as much as 0.65 inches. This was most severe for Bent 45 in spite of the wide flange sections clamped to the adjacent pedestal and column. Horizontal slip nearly reached a half an inch.

## OBSERVATIONS

Tests on the Cypress Street viaduct have provided a considerable amount of information on the behavior of existing and retrofit structures. Based on a review of the experimental data, the following observations are offered.

1. Failure of the structure on October 17, 1989 can be explained in terms of simple lateral response of the structure and the limited shear capacity of the short pedestal supporting the upper column. Conventional engineering design calculations can be used to identify the failure mode and to estimate the failure load to within 5%.
2. A gross-section computer idealization of the structure overestimates the stiffness and frequency of the structure. It appears from discrepancies between results based on forced vibration tests (which include foundation motion) and static tests (which restrict base movement) that foundation flexibility may also have a significant influence on dynamic properties.
3. Observed reinforcement anchorage strengths and column shear capacities initially exceeded values commonly used in design. Whether this is a function of the design details employed or simply associated with the wide scatter of the results typically associated with these phenomenon remains the subject of future research.
4. External shear reinforcement is effective in enhancing shear capacity.
5. Unbonded reinforcement may be ineffective as a retrofitting tool in certain circumstances. The difficulty in developing sufficient prestress to maintain contact or prevent relative sliding between existing concrete and new steel cladding was evidenced several times in these tests. Once contact is lost, long unbonded lengths result in large cracks, gaps or slips. Issues of deformability should be considered along with strength in order to control and limit damage.
6. Joints in existing multilevel and outrigger bents need to be carefully considered. Ideally, they should be strengthened to avoid inelastic action within the joints. Failure to do this may lead to rapid deterioration of structural integrity.
7. Evaluation and retrofit of existing bridge structures should look at the structure as a system. Rather than simply fixing a weak link, the hierarchy of possible inelastic actions should be identified. Otherwise, one weak link may imply replace another.

## ACKNOWLEDGMENT

The research reported herein was supported generously by the California Department of Transportation. In particular, the efforts of James Roberts of Caltrans were instrumental in arranging for the tests. The research was carried out by engineers from Caltrans as well as from the University of California at Berkeley. The unstinting work by Robert Jones and Irving Schroeder of Caltrans and Roy Stephen, X. Qi, Martin Bollo of the University of California at Berkeley made the research possible.

## REFERENCES

1. Mahin, S. A. et al, "Observations and Implications of Tests on the Cypress Street Viaduct Test Structure," Earthquake Engineering Research Center (EERC) Report, Univ. of Calif., Berkeley, Dec. 1990.

2. George Housner, Chairman, "Competing Against Time," Report to Governor George Deukmejian from the Governors Board of Inquiry, Department of General Services, State of California, May 1990.
3. Nims, D. "Collapse of the Cypress Street Viaduct as a Result of the Loma Prieta Earthquake," EERC Report, Univ. of Calif., Berkeley, Nov. 1989.

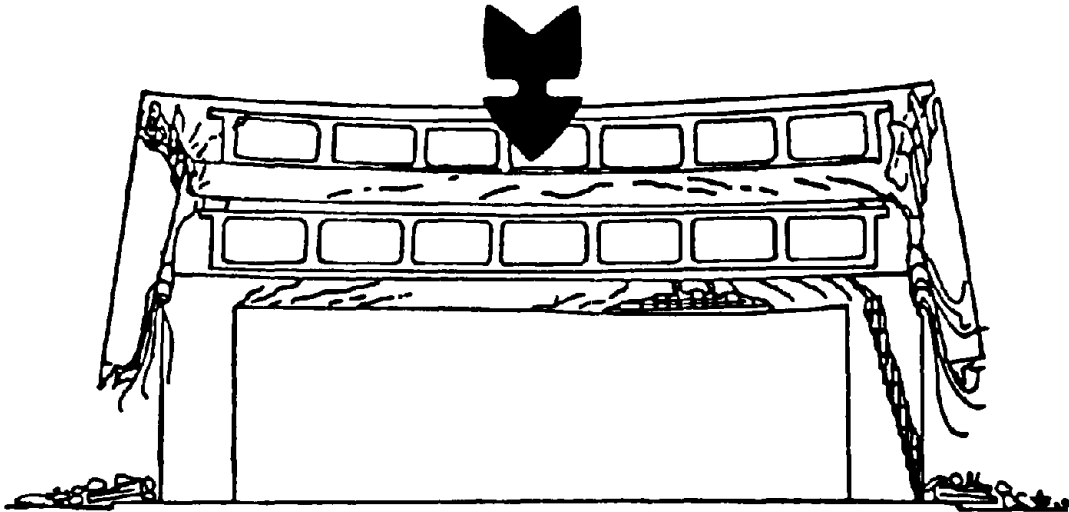


Fig. 1 Typical Collapse Mode (after J. Rogers)

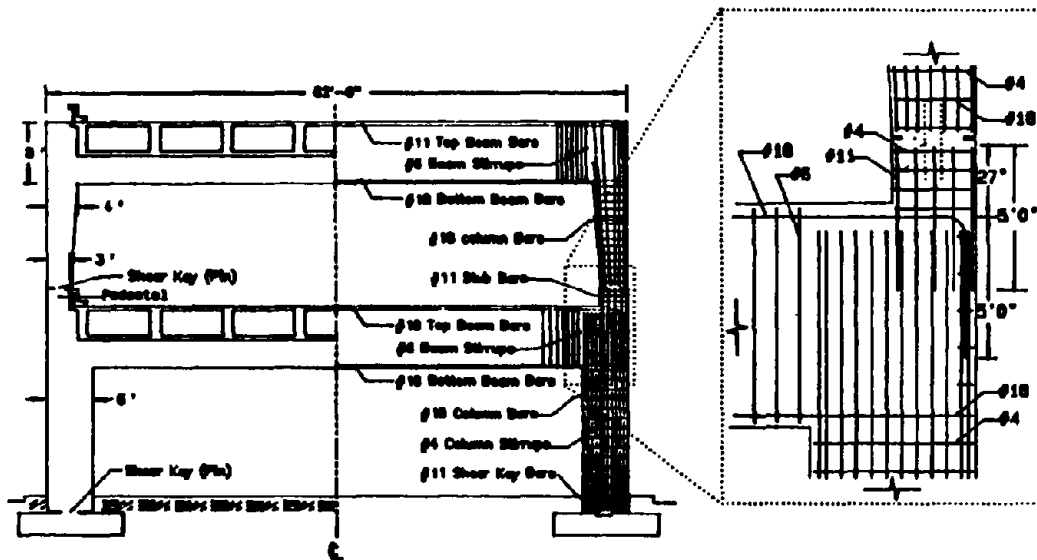


Fig. 2 Typical Bent Details

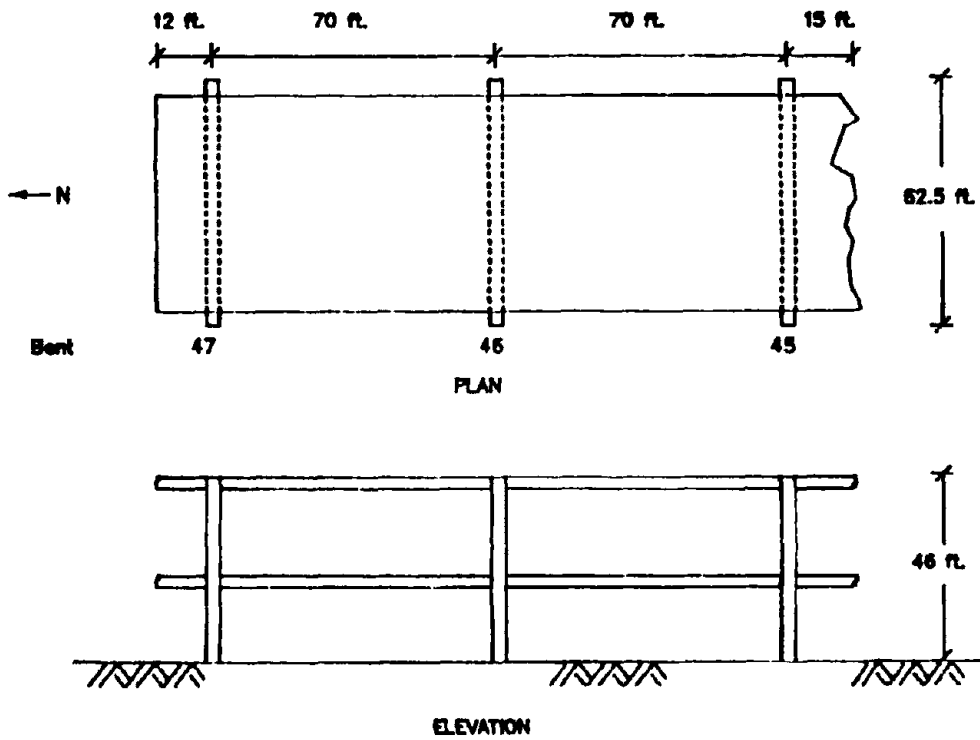


Fig. 3 Test Structure and Longitudinal Elevation

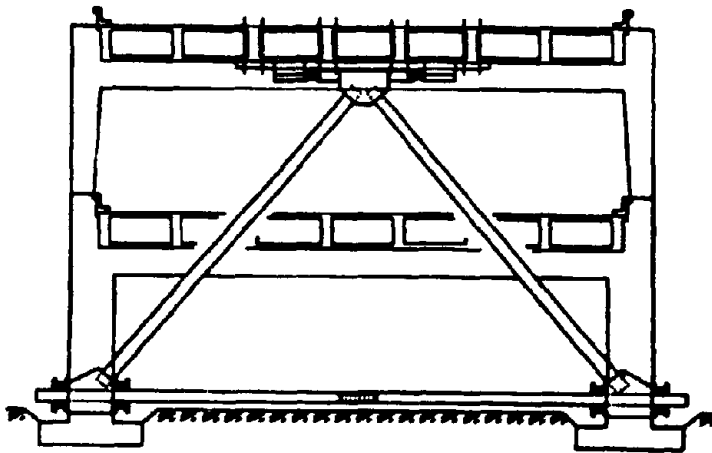


Fig. 4 Loading Frame for Static Tests





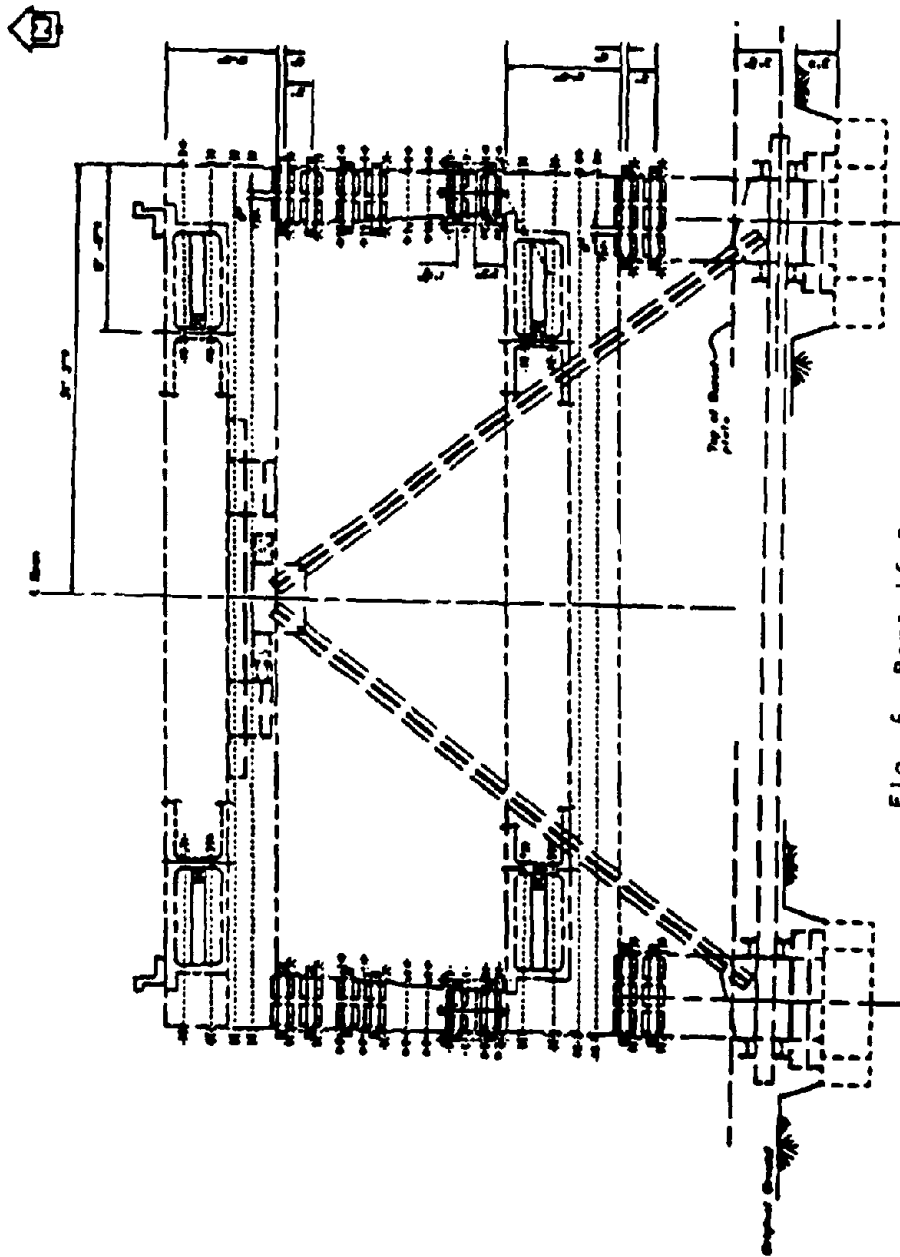


Fig. 6 Bent 46 Retrofit

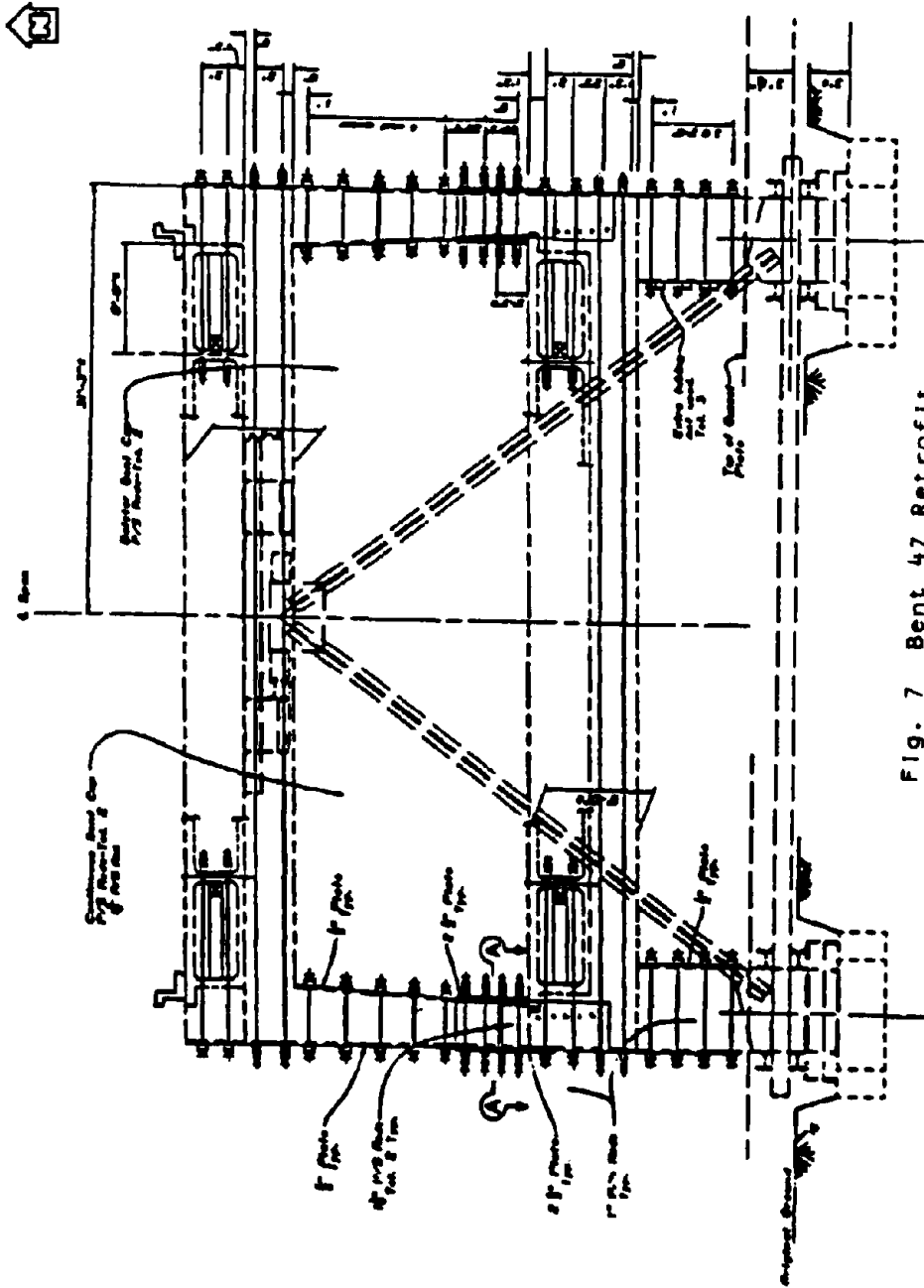


Fig. 7 Bent 47 Retrofit

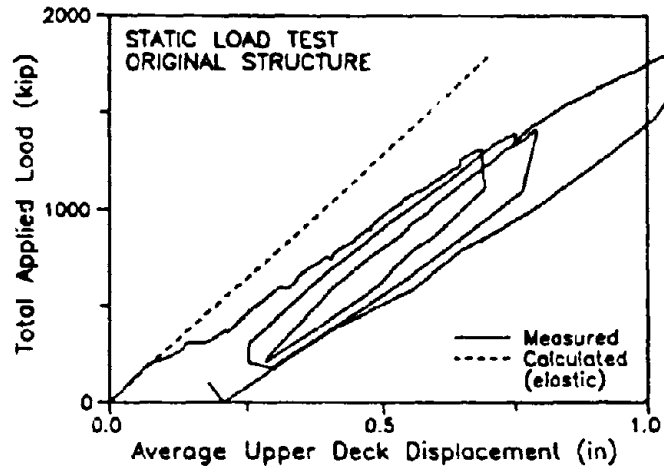


Fig. 8 Load-Displacement Relation Before Retrofit

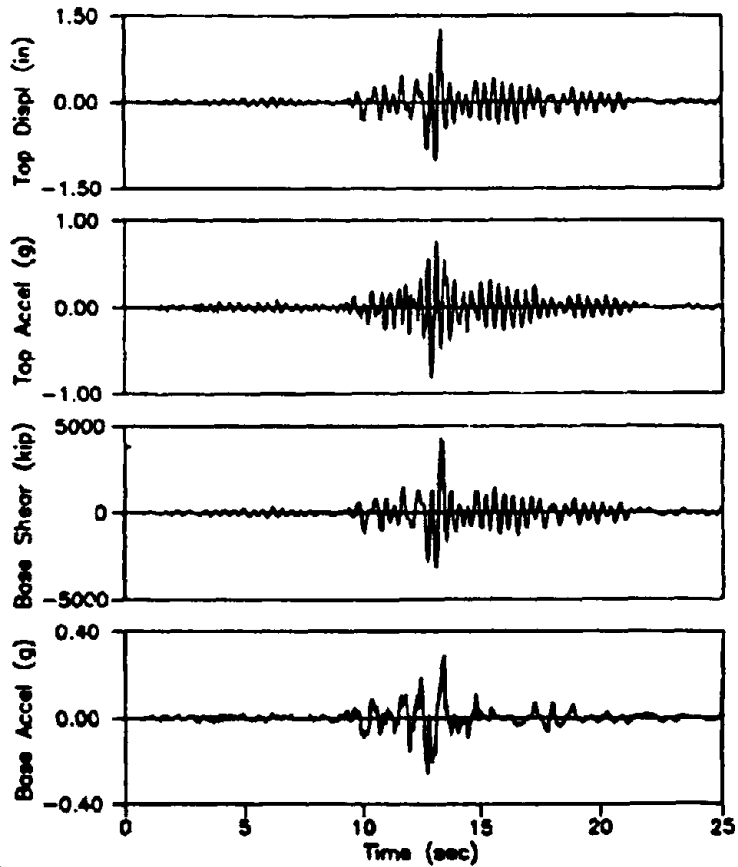


Fig. 9 Calculated Dynamic Response to Oakland Outer Wharf Record of Test Structure prior to Retrofit

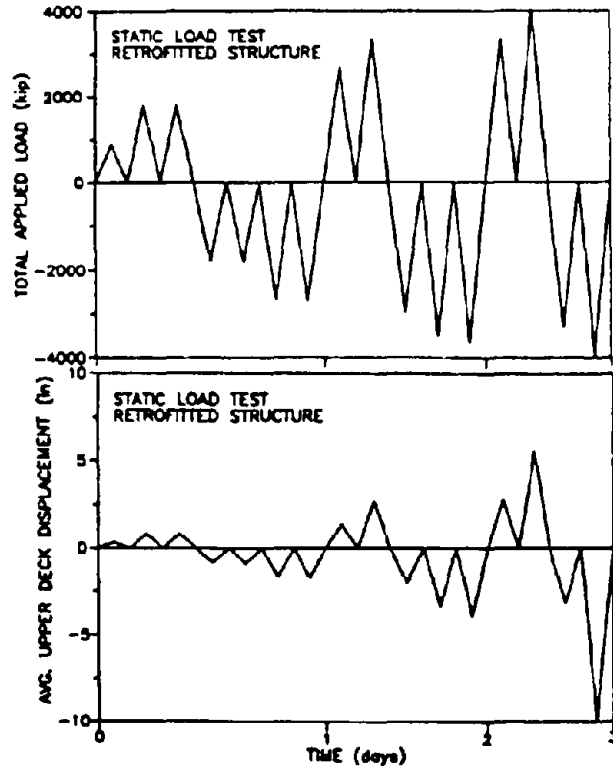


Fig. 10 Load and Displacement History after Retrofit

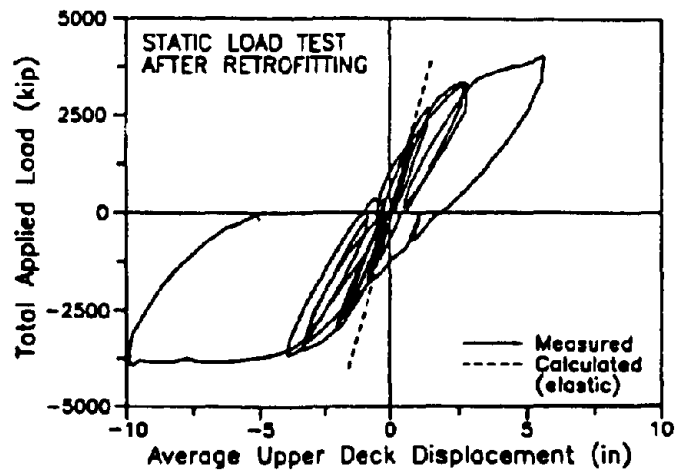


Fig. 11 Load-Displacement Relation after Retrofit

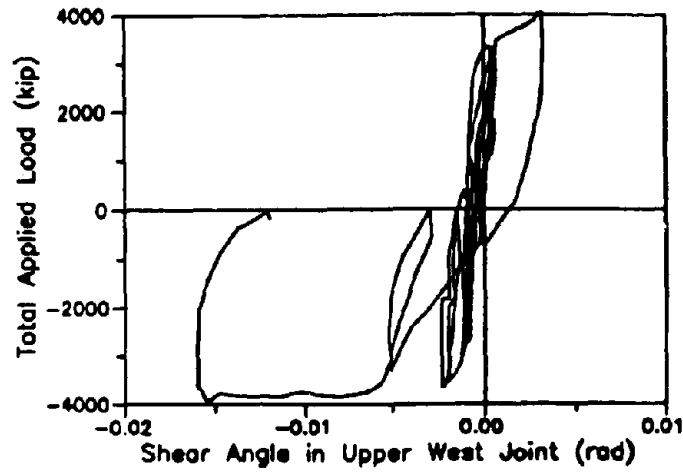


Fig. 12 Joint Shear Strain Relations -- Upper Level Bent 46

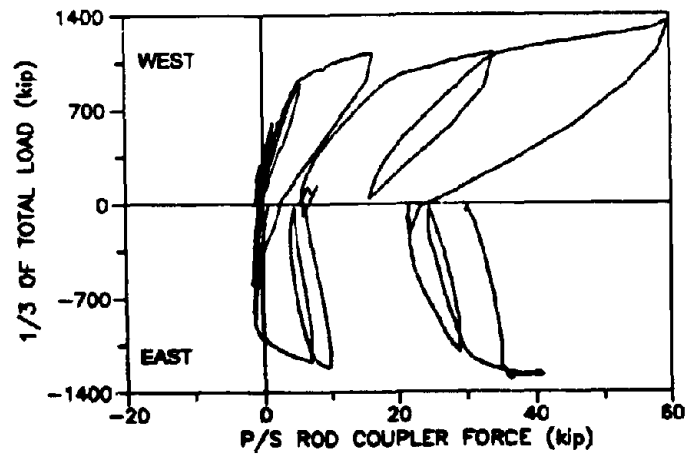


Fig. 13 Incremental Load in Post-Tensioning Rod at Top of Bent 46

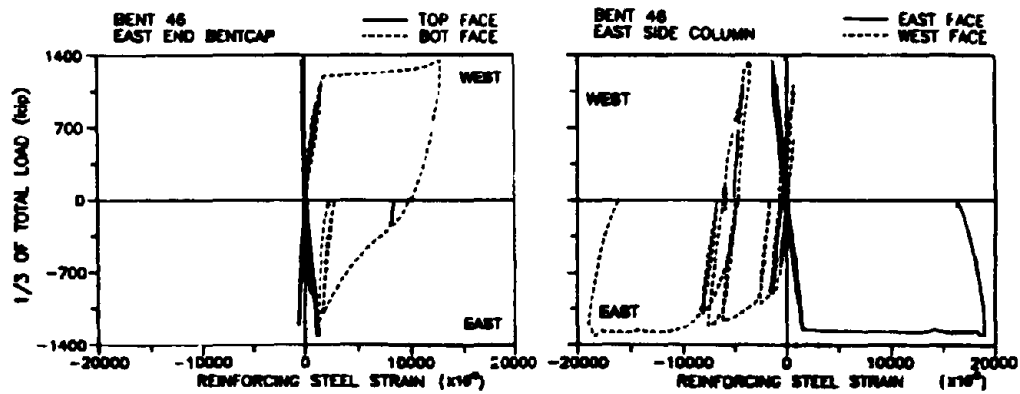


Fig. 14 Typical Bent Cap and Column Rebar Strain Histories

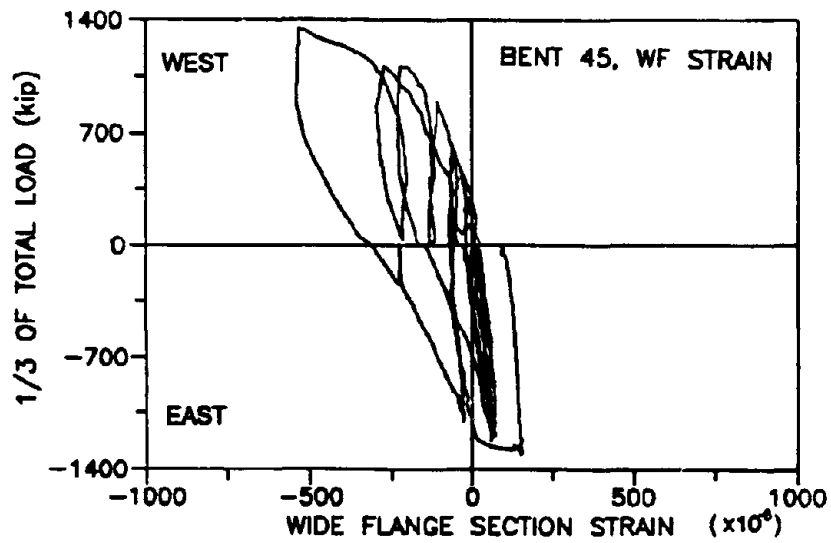


Fig. 15 Nonlinear Strain Histories In Wide Flange Retrofits In Bent 45

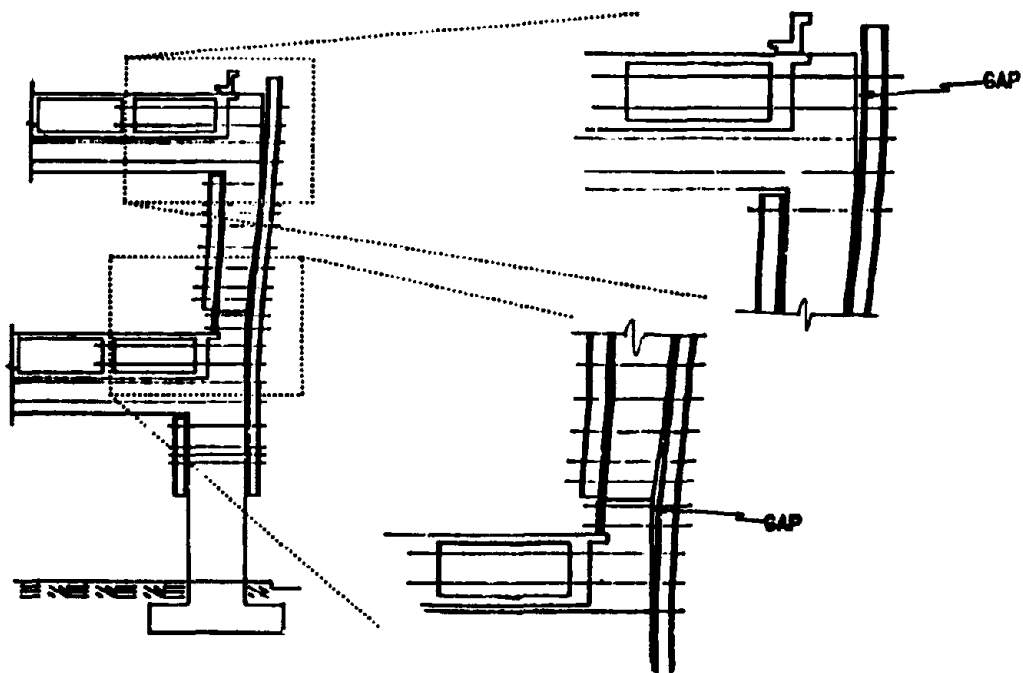


Fig. 16 Separation of Wide Flange Retrofits From Columns

# **S e s s i o n 3**

## **A s s e s s m e n t a n d P r i o r i t i z a t i o n o f V u l n e r a b l e B r i d g e s**

- 1) **Assessment and Retrofit Research for Multi-level, Multi-column Bents**  
(S.Mahin and J.Moehle)
- 2) **Prioritizing Bridges for Seismic Retrofit**  
(J.Gates and B.Maroney)
- 3) **Damage and Performance Assessment of Existing Concrete Bridges**  
**Under Seismic Loads**  
(F.Selble and M.J.N.Priestley)
- 4) **Large Earthquake Countermeasures for Bridge Substructures on**  
**The Tomei Expressway**  
(T.Tsubouchi, K.Ohashi and K.Arakawa)

ASSESSMENT AND RETROFIT RESEARCH FOR  
MULTI-LEVEL, MULTI-COLUMN BENTS

Stephen A. Mahin (I)  
Jack P. Moehle (I)  
Presenting Author: Stephen A. Mahin

SUMMARY

In this paper a number of the factors that should be considered in the evaluation and retrofit of multicolumn reinforced concrete bridge bents are reviewed and illustrated with specific examples. Issues range from predicting seismic demand at the global and local levels, to assessing the strength and deformation capacities of the members and joints, and to establishing details capable of achieving the designers objectives. At the end of the paper the scope of a research program related evaluation and retrofit of multi-level, multi-column bents is presented.

INTRODUCTION

Assessment of the seismic vulnerability of reinforced concrete bridge structures is a problem that has not until recently been considered by many designers. The assessment process is different in many fundamental ways from that used in the design of new structures. Generally, current codes, such as those promulgated by AASHTO or JSCE, achieve ductile seismic behavior in new structures by specifying minimum design forces for determination of flexural capacities, establishing auxiliary procedures for estimating maximum shears and axial forces in a member or joint corresponding to development of a desired flexural yield state, limiting reinforcement ratios, bar spacings and member sizes, and requiring sufficient confinement in potential critical regions to provide a large reserve for energy dissipation. While a sound understanding of the fundamentals of structural engineering and structural dynamics are needed to accomplish an effective and economical design, the freedom permitted in the design process makes satisfaction of the various criteria relatively easy. On the other hand, it becomes more difficult for a designer to assess the likely performance of a structure if some of the criteria are not met. While some cases are easy to assess (e.g., too little shear capacity to develop a plastic hinge at the ends), others are not (e.g., insufficient anchorage length, bar spacing violations, and so on).

Thus, the designer must have good insight into the desired performance of the structure, the likely behavior of the various inadequate details discovered, the capabilities and limitations of various analytical models and the techniques for

---

(I) Prof. of Civil Engineering, Univ. of Calif., Berkeley, USA.



upgrading the behavior of joints and members. While experimental research is the keystone to developing this understanding, it is important that the designer understand the various factors influencing seismic performance. It is unlikely that the evaluation and retrofit of major bridge structures can be reduced to the level of a menu of items simple tasks.

In this paper a few items, mainly related to analytical and design issues, are raised and explored with examples. The topic is, however, much broader than discussed here. Some areas of on-going research are identified at the end of the paper.

#### ACCURACY OF MODAL SUMMATION METHODS

In the U.S. it is common to develop an elastic model of a structure and analyze that model considering a site dependent response spectrum. If the analytical model is large or has a complex geometry, numerous modes, often with closely spaced natural frequencies, will result. To achieve realistic response estimates, many modes must be included in the analysis. For example, in the analysis of a model of the Interstate 101 Central Freeway in San Francisco, a double deck structure being evaluated by consultants for retrofit purposes, nearly 200 modes needed to be considered. Since each of the individual modes in such cases have little physical significance related to the structure's response to a global seismic load condition, it often becomes difficult to interpret numerical results.

This is in part true because of limitations regarding the output capabilities of many computer program. For example, many programs incorporate features to model rigid cap-column joints of finite size, but do not provide output of the forces acting within the joint. Modal summation rules, such as the "square root of the sum of the squares" (SSRS) technique, provide information only on the amplitude of internal forces, but not their signs. Thus, it is (virtually) impossible to infer joint shear from static considerations knowing the maximum shears and moments applied to the edges of a joint. Joint shears and other such quantities also have to be summed on a modal basis and not using the summed maxima. In simple structures, governed by a single, intuitively natural, mode of response, appropriate estimates may be made. However, if many modes are involved, this is no longer possible.

Nonetheless, there remains a more fundamental problem of how to numerically combine the individual modal response values when modes are closely spaced. It has been shown in such cases that sum of absolute values or SSRS techniques can lead to grossly spurious results, both conservative and unconservative [1]. The Complete Quadratic Combination (CQC) and other procedures have been developed to remedy these deficiencies. Because of the relatively new development of such techniques,

methods like the SRSS method continue to be used. To provide some light on the nature of this problem, a simple analysis of a double deck viaduct segment has been performed using time history, SRSS and CQC methods.

The structural model is shown in Fig. 1. The geometry is typical of San Francisco double deck structures. In many of these structures pin connections are provided at the top of the upper level columns and at the base of the lower level columns. In order to produce more closely spaced and coupled modes, the pins along one side of the top of the structure are assumed to have been retrofit to a fixed condition. The model was analyzed using the record and response spectrum for the north-south component of the 1940 El Centro earthquake. This record was applied to the model independently in the transverse (EW) and longitudinal (NS) directions and simultaneously in both directions (EW + 0.3NS). Viscous damping was considered to be 5% of critical. In order to have 95% of the mass of the structure contribute to the base shear, 10 modes were considered in the analysis.

Because of mass and stiffness eccentricities, mode shapes are complex and not oriented along the principal axes of the structure (Fig. 1). This results in forces and deformations orthogonal to the direction of an applied excitation. However, it is not possible, given the kinematics of structural response, for response maxima for these coupled modes to occur at the same time in orthogonal directions. Thus, summation rules that combine the absolute or squared values of modal responses in all directions are bound to be erroneous. Only by retaining the relative signs of the responses in orthogonal directions for a particular mode can reasonable estimates be made. The CQC method does this [1].

The effect of this on the example structure can be seen in Table 1. In this case, a relatively small base shear is developed in the NS direction when the input is in the EW direction. The SRSS method predicts values nearly the same in both directions. The largest errors for the SRSS method appear to be in the direction perpendicular to the direction of loading. The CQC method predicts response values in much better agreement with the time history, though still with some error.

It is interesting to note that the SRSS method appears to provide more reasonable results when bidirectional input is considered. This is a result of compensating errors. The SRSS method underestimates the response in the direction of loading and overestimates it in the orthogonal direction. Thus, when loads are applied in two directions, the errors compensate. However, the degree of error may still be quite large depending on the nature of the structure and loading.

Table 1 Comparison of Modal Combination Rules  
(Percentage Errors given in parentheses)

Combination Method	Input Orientation		
	EW	NS	(EW + 0.3NS)
EW Base Shear (kips):			
Time History	2684	784	2919
SRSS	2148 (-20)	1717(+119)	2363 ( -9)
CQC	2768 ( +3)	1028 (+31)	3076 ( +5)
EW Moment in Elm. 36 (k-in):			
Time History	40340	16290	45227
SRSS	37641 ( -7)	21708 (+33)	44154 ( -2)
CQC	38699 ( -4)	18524 (+14)	44256 ( -2)

#### PREDICTION OF DUCTILITY DEMANDS USING ELASTIC ANALYSIS

Typically elastic analyses are used to assess the potential seismic behavior of structures. While this may have some theoretical justification for the case of single column structures, its applicability to multicolumn and multilevel systems is questionable. Past research has demonstrated the problems of estimating the internal distribution of damage for structures with stiffness, strength and mass irregularities. It has also been shown that structures having soft stories (as would multilevel viaducts with yielding concentrated in the columns) are likely to have much different response than can be predicted by elastic analysis. In addition, ductility demands are generally unconservatively predicted for structures with periods shorter than the characteristic period of the ground.

To assess this situation an example analysis has been undertaken on a representative bent from the Terminal Separator interchange in San Francisco. The example bent (Fig. 2) has a single bay, but three levels. Roadway decks, however, are provided only at the top and bottom levels. The intermediate level is provided to enhance lateral stiffness and increase stability.

A series of analyses were performed on this structure. Gravity effects due to dead loads were considered in all analyses. Flexural capacities of the members were estimated from the structural drawings and specified material strengths. Shear failures and deformations in the members and the joints were disregarded. Analyses were performed with a general purpose nonlinear finite element program capable of static and dynamic response analysis.

Results of the static elastic analysis are shown in Fig. 3 and Table 2. Lateral loading was distributed with height

assuming a mode shape in the form of an inverted triangle. Results were scaled to produce a maximum ratio of moment to plastic moment (here defined as  $1^3M_n$ ) in the lower bent cap equal to 4. At this stage the top of the structure displaces laterally about 3.4 inches. The figure indicates that many elements are overstressed at this stage, particularly the second level cap. However, the results indicate the formation of statically inadmissible joint mechanisms, at the upper right hand joint and at both joints at the lowest level. Without the aid of limit analysis, a designer would have difficulty interpreting these results.

A static nonlinear analysis of the same structure was performed. The base shear-top deflection relation is shown in Fig. 4. This shows that a plastic mechanism forms at a displacement of about 2.5 inches. However, the first plastic hinge forms (at the middle level) at a displacement of 0.31 inches and significant nonlinearity is noted at a top deflection of 1.7 inches. For a displacement of 3.4 inches, corresponding to the lateral displacement imposed for the elastic analysis, the locations of the plastic hinges are shown in Fig. 5 and some of the rotation ductility demands are listed in Table 2. These demands are defined for simplicity as the maximum plastic hinge rotation computed divided by  $M_n L / 6EI$ , plus one. There are fewer plastic regions noted by this analysis, and the magnitude and distribution of inelastic demands differ from that indicated by the elastic analysis.

Table 2 - Comparison of Elastic Overstress and Plastic Hinge Rotation Ductility For Bent Caps on Left Side of Three Level Example Structure.

Model	Middle Cap Max.	Cum.	Bottom Cap Max.	Cum.
<u>Static Elastic</u>				
All gross section	3.99		4.00	
Ig/4 for columns	1.90		1.46	
<u>Static Nonlinear</u>				
	2.92		5.91	
<u>Dynamic Nonlinear</u>				
18%g	2.38	12.1	2.49	2.49
25%g	2.47	14.7	3.77	3.77
50%g	5.49	26.8	15.5	15.5

For the case of the nonlinear dynamic analyses, the Taft earthquake record was considered scaled to three different levels as indicated in Table 2. Locations of plastic hinges are shown in Fig. 5. The displacement time histories at the top level are shown in Fig. 6. It can be noted from these data that

the ductilities in the caps are smaller than predicted by the elastic analysis considering gross section properties, but that analysis better predicts the ratio of demands between the two levels than does the modified elastic analysis. As the intensity of the input increases, the magnitude of the plastic rotations and lateral displacements increases. However, the distribution of damage, as reflected in the ratio of plastic rotation demands for the two levels presented in Table 2, changes dramatically. A linear elastic analysis is not able to detect such changes.

In addition, the maximum plastic rotation demands do not indicate the complete picture regarding inelastic demands. For example, a criteria based on energy dissipation or cumulative inelastic deformation may be more meaningful in terms of retrofitting a structure to sustain repeated damage. Table 2 contains cumulative plastic rotation ductility demands. These are generally larger than the maximum values since the elements may yield more than one time. For the example structure, the middle level cap is weak and sustains many plastic excursions. On the other hand, the lower level only undergoes a single inelastic excursion. Again, elastic analysis cannot provide this type of information.

It is clear that elastic analysis methods are powerful tools that can provide considerable information for the evaluation and retrofit of bridges. However, their results should not be used blindly, or with undue belief in their accuracy. Analytical models that can be used for predicting the nonlinear response of existing bridge structures are still relatively primitive and thus may not provide accurate results. In addition, there is no general agreement on the best method for characterizing damage in the structure. An important implication of this is that differing definitions at different stages of analysis and design can result in misinterpretations and ineffective design solutions.

#### SOME COMMENTS ON CONSISTENCY

One of the perennial problems in earthquake engineering has been the difficulty in defining a single parameter representative of structural damage. Ductility, defined as the maximum displacement divided by the yield displacement, has often been used as a quantitative term in this regard. As indicated previously, there are difficulties with this definition if one wants to consider situations with cyclic loading. In addition, for complex systems definition of maximum and yield displacement may not be straight-forward. Similarly, it is well recognized that values of ductility evaluated on the basis of displacement will differ from those based on rotation, curvature or strain.

Because of these various definitions, it is important to maintain a consistency of definition from test data to analysis to design. As an example of this problem consider the design of

columns. Test results on the cyclic inelastic behavior of such members are relatively sparse considering the wide variety of conditions that can be encountered. The data available shows that ductility improves with increased nominal axial stress. Based on this observation, a designer wishing to improve the behavior of a structure would use as small of cross section, and as high of longitudinal steel percentage, as possible to improve ductility.

This may not lead to anticipated results. For example, in a study of more than 150 column tests and column failures in bridges during previous earthquakes it was noted that while ductility increases with axial stress, deformability decreases. Thus, if one wishes to have a structure or member that is able to dependably achieve a certain displacement amplitude, a smaller axial stress should be used. The difference relates to the fact that the yield displacement of columns significantly increases with axial load, thereby decreasing yield displacement and increasing the ductility. However, in analysis and design such refinements are not usually taken into account (gross stiffness properties are often used independent of axial load). Thus, consistency and simplicity is needed in using terms such as ductility in analysis and design.

#### FUTURE RESEARCH

A research program has just been initiated at the University of California at Berkeley related to multicolumn bents. This research has three emphases. First, to develop consistent criteria for the evaluation and retrofit of reinforced concrete multicolumn bridge structures. Currently, methods for evaluating columns and assessing inelastic demands on bents are being studied.

The second area relates to improved global and local finite element modeling of multicolumn viaduct structures. Factors such as traveling wave effects, variations in soil properties along the length of the viaduct and expansion joint effects are to be studied. In addition, the work examines refined methods for predicting local nonlinear behavior of joints and other complex critical regions.

The third and main part of the research focuses on experimental investigations of some of the special features of multicolumn bents. Six research areas are planned as shown in Fig. 7. In many of these structures the decks are separated from the columns. The resulting outrigger is subjected to a complex state of stress. In addition, older caps generally are not designed to carry significant torsion. Thus, one of the first sets of specimens to be investigated will be outriggers. Both as-built and retrofit specimens will be tested. Emphasis will be placed on the torsional behavior of the outrigger, but longitudinal, transverse and vertical motion of the bent will be simulated in the tests.

Another critical problem relates to the behavior of cap-column connections. These joints in older bridges in the U.S. typically have little or no shear reinforcement. Techniques for assessing the strength and deformability of these joints is needed. Similarly, specimens will be tested to assess the efficacy of strengthening techniques.

In many older bridges relatively short anchorage lengths have been provided for large diameter bars. A fundamental study of single and multiple bars similar to existing and new construction will be performed.

The behavior of columns is critical to multicolumn bents. As such a series of tests will be performed on short columns subjected to bidirectional excitations.

The move towards retrofit of the double deck freeway structures in San Francisco by removal and replacement of columns raises a number of other questions that will be examined in the research project. In particular, the ability of the proposed retrofits to achieve the stated objectives, and the need for special shear reinforcement in the beam column joints will be investigated.

#### ACKNOWLEDGMENTS

The research work being initiated at Berkeley is sponsored by the California Department of Transportation. The comments in this paper are not the policy of that organization. The authors are joined by several colleagues at Berkeley in this effort. These faculty members are V. Bertero, G. Fenves, F. Filippou, and C. Thewalt.

#### REFERENCES

1. Wilson, E., Der Kiureghian, A., and Bayo, E., "A Replacement for the SRSS Method in Seismic Analysis," *Earthquake Engineering and Structural Dynamics*, Vol. 9, 1981.

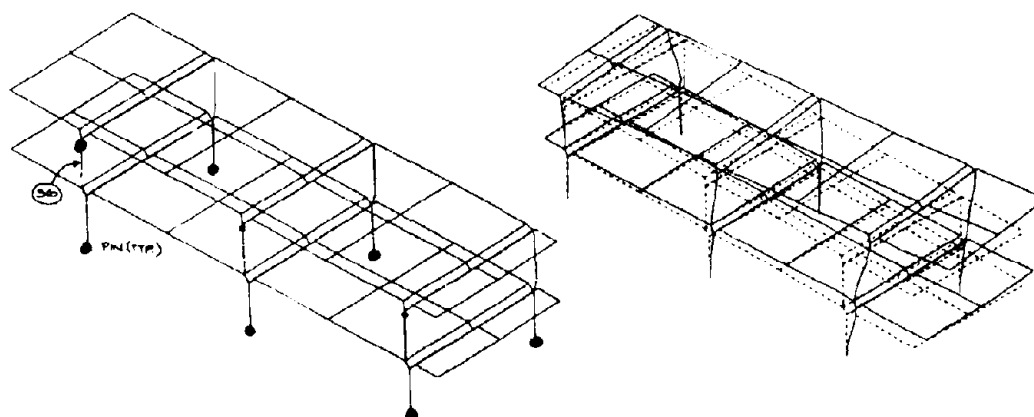


Fig. 1 Example Structure and Typical Mode Shape

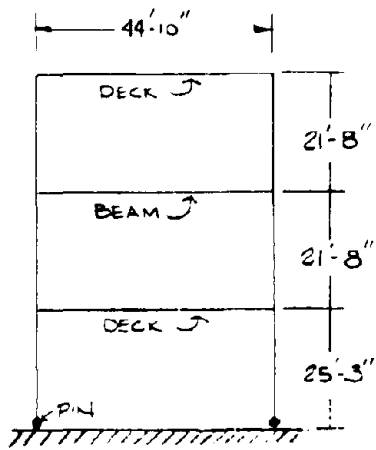
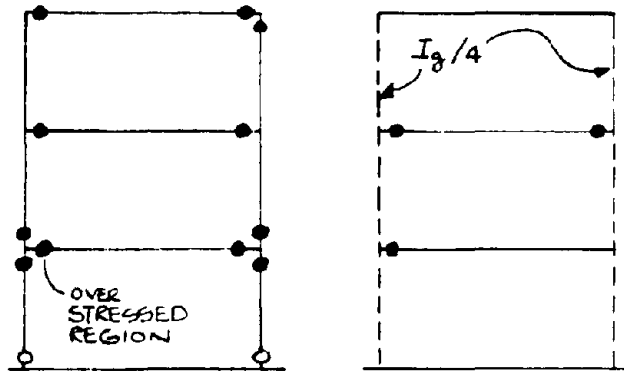


Fig. 2 Three Tier Example Structure



GROSS SECTION MODEL +MODIFIED MODEL

Fig. 3 Overstress Ratios for Different Elastic Models

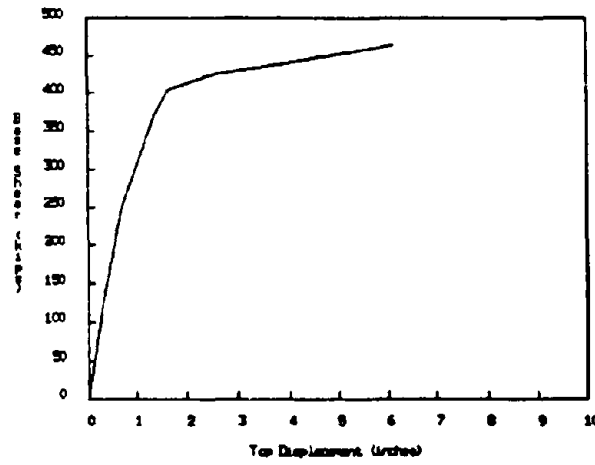


Fig. 4 Inelastic Static Response of Three Tier Example Structure



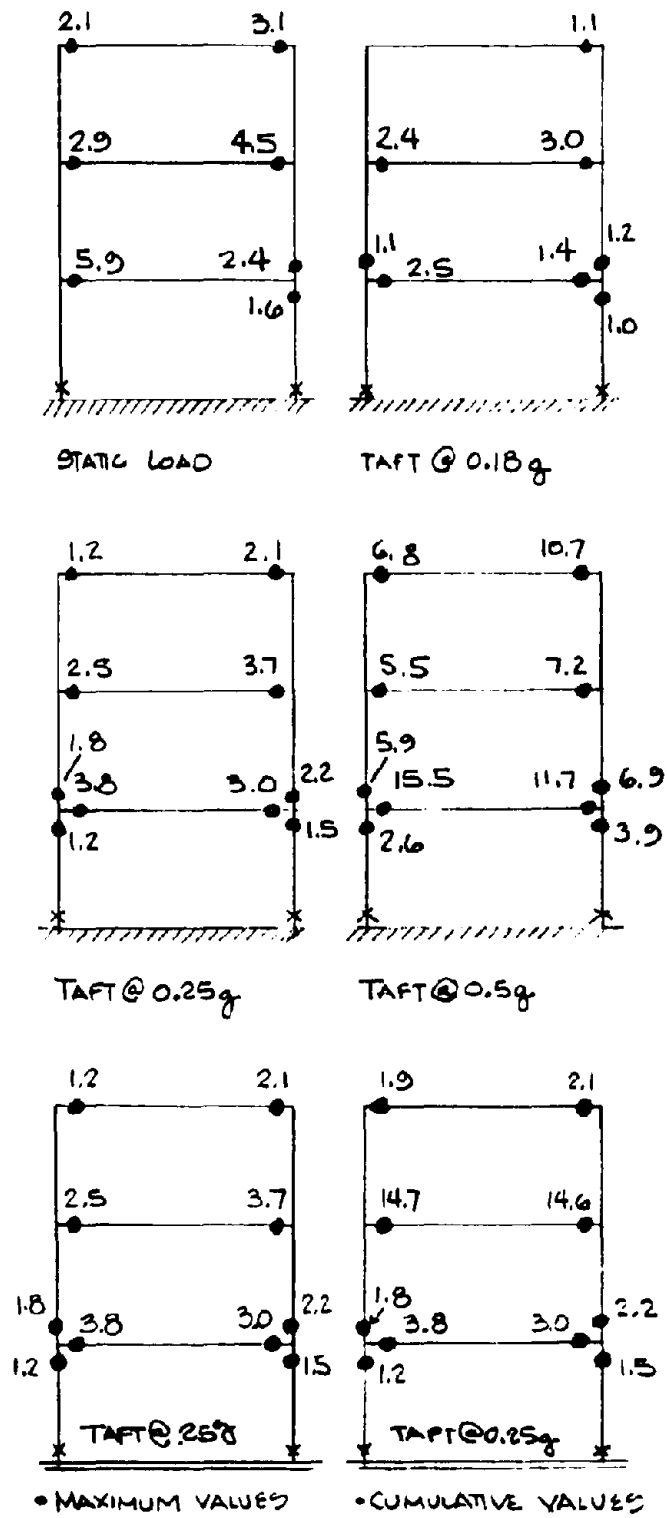


Fig. 5 Plastic Rotation Ductilities For Static and Dynamic Loading

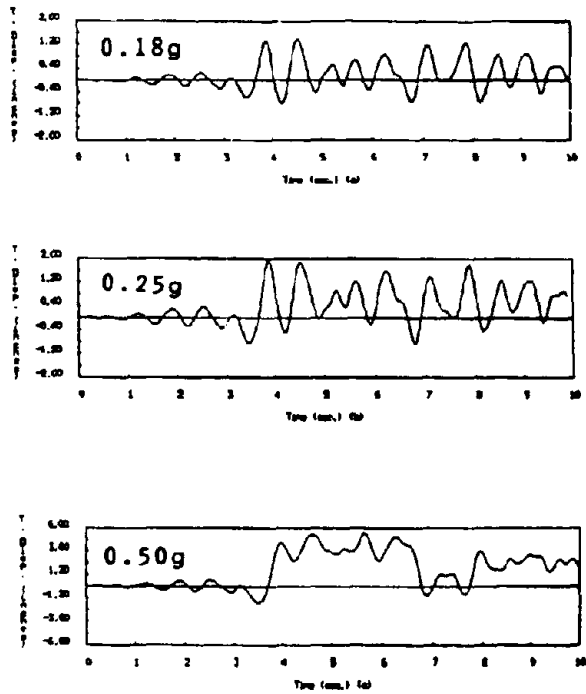


Fig. 6 Top Level Displacement Histories

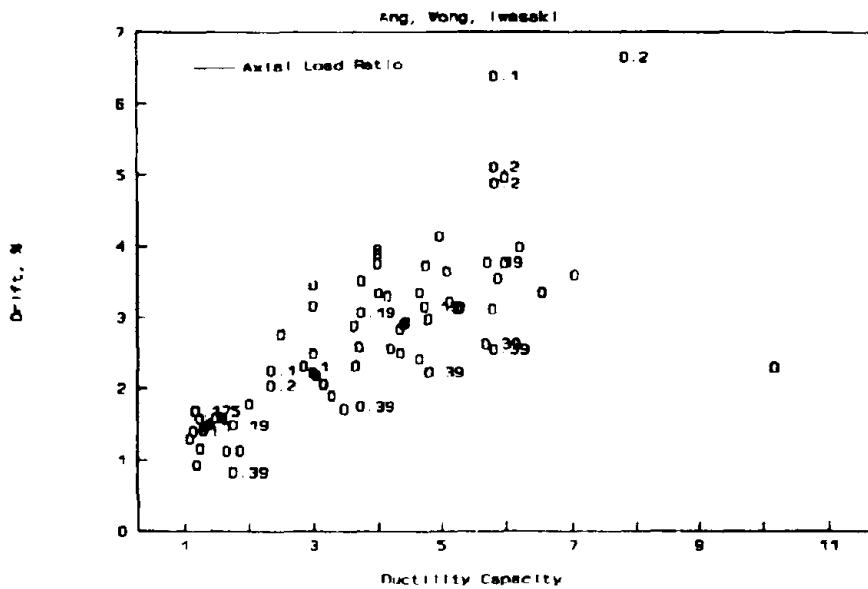
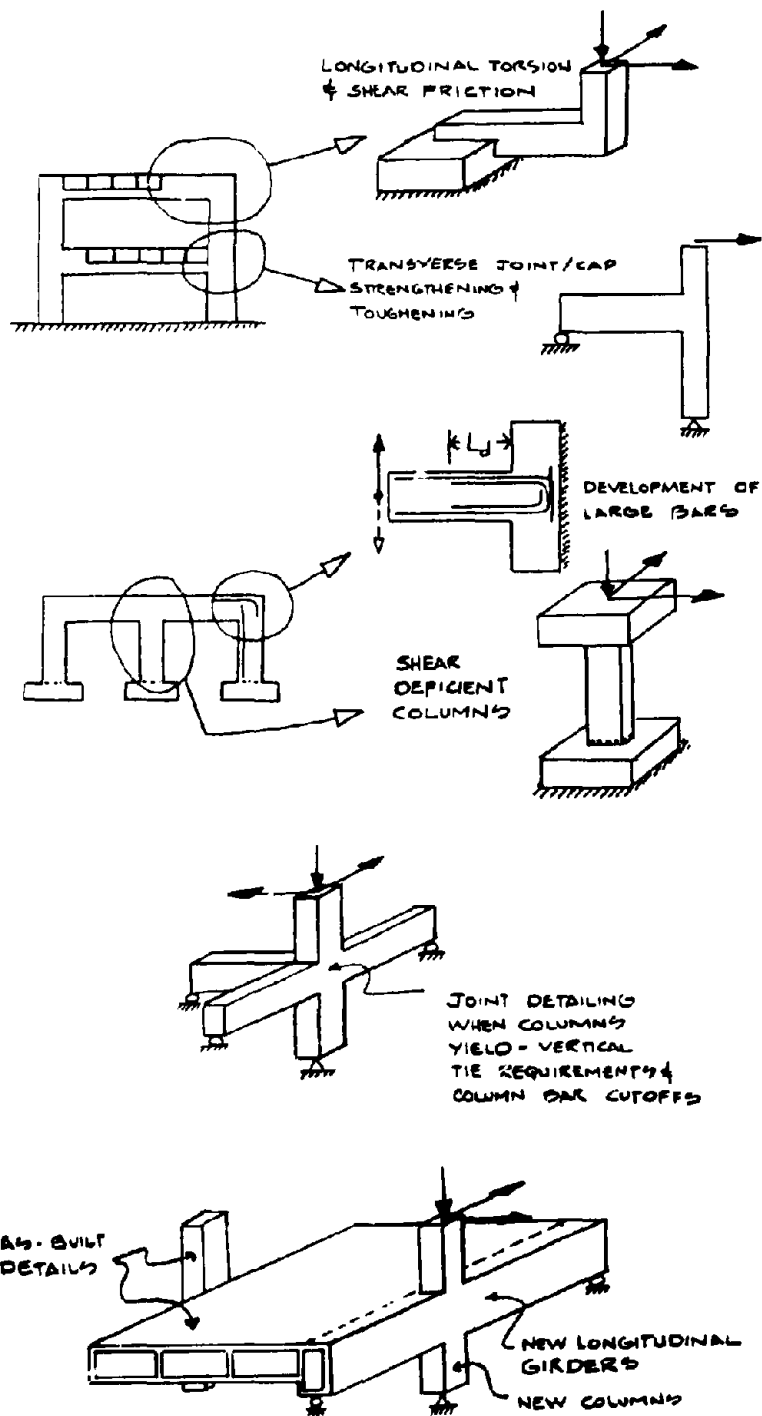


Fig. 7 Effect of Axial Load on Drift and Ductility Capacities



**PROOF TEST - LONGITUDINAL GIRDER**

**Fig. 8 Schematic Illustration of Planned Test Specimens**

## PRIORITIZING BRIDGES FOR SEISMIC RETROFIT

J. H. Gates (I)

B. H. Maroney (II)

Presenting Author: J. H. Gates

### SUMMARY

The procedure used by the California Department of Transportation's Seismic Retrofit Program to identify and prioritize the most vulnerable bridges to earthquake damage is presented. A risk analysis is developed in which expert judgements are used to replace a typically large statistical database. The result is a risk analysis based on expert knowledge gained from past earthquakes and bridge characteristics which can be quickly applied to the decision making process.

### INTRODUCTION

The 1971 San Fernando earthquake revealed a number of inadequacies in existing bridge design details and specifications. New bridge designs were immediately modified to correct these inadequacies and a seismic retrofit program was also started to address the various deficiencies in existing structures. The initial objective of the seismic retrofit program was to insure continuity at all of the bridge superstructure joints to prevent drop-type failures. Approximately 1,300 bridges were retrofitted at a cost of \$55 million between 1971 and 1989. Typical methods used were to add restraining cables or rods at joints and shear keys at abutments and bearings. In 1987, shortly after the Whittier earthquake, \$64 million was made available for additional retrofitting. These funds were to be directed toward the retrofit of structures with single column bents in high seismic zones as they were perceived to be less redundant and therefore at higher risk. This effort was underway when the San Francisco Bay Area was rocked by the Loma Prieta earthquake on October 17, 1989.

Caltrans has subsequently received specific direction in response to the Loma Prieta earthquake. Following the Loma Prieta earthquake Senate Bill No. 36X (Ref. 1) was passed which appropriated \$80 million immediately, and potentially a significantly greater amount for future seismic retrofit projects. This bill identified Caltrans as the lead agency for inspection and retrofit if necessary for all publicly (i.e., local and state) owned bridges throughout the State, except for those bridges not on the State highway system in Los Angeles and Santa Clara counties. The local agencies in these two counties have been designated as the lead agencies for the retrofit of their own bridges. The Governor's Board of Inquiry on the 1989 Loma Prieta Earthquake (Ref. 2) stated in a list of recommended actions, "... specific goals of this policy shall be that all transportation structures be seismically safe and that important transportation structures maintain their function after earthquakes." With this direction and funding, Caltrans has been charged with the task of providing safety to the traveling public through necessary retrofit modifications to all transportation structures which may not be adequate during a large earthquake.

---

(I) Supervising Bridge Engineer, CALTRANS, Sacramento, California

(II) Senior Bridge Engineer, CALTRANS, Sacramento, California

Caltrans' is currently responding to these directions. Figure 1 illustrates the strategy adopted within the Division of Structures to identify and prioritize, group into projects, and submit to Structures Design personnel the bridges requiring retrofit.

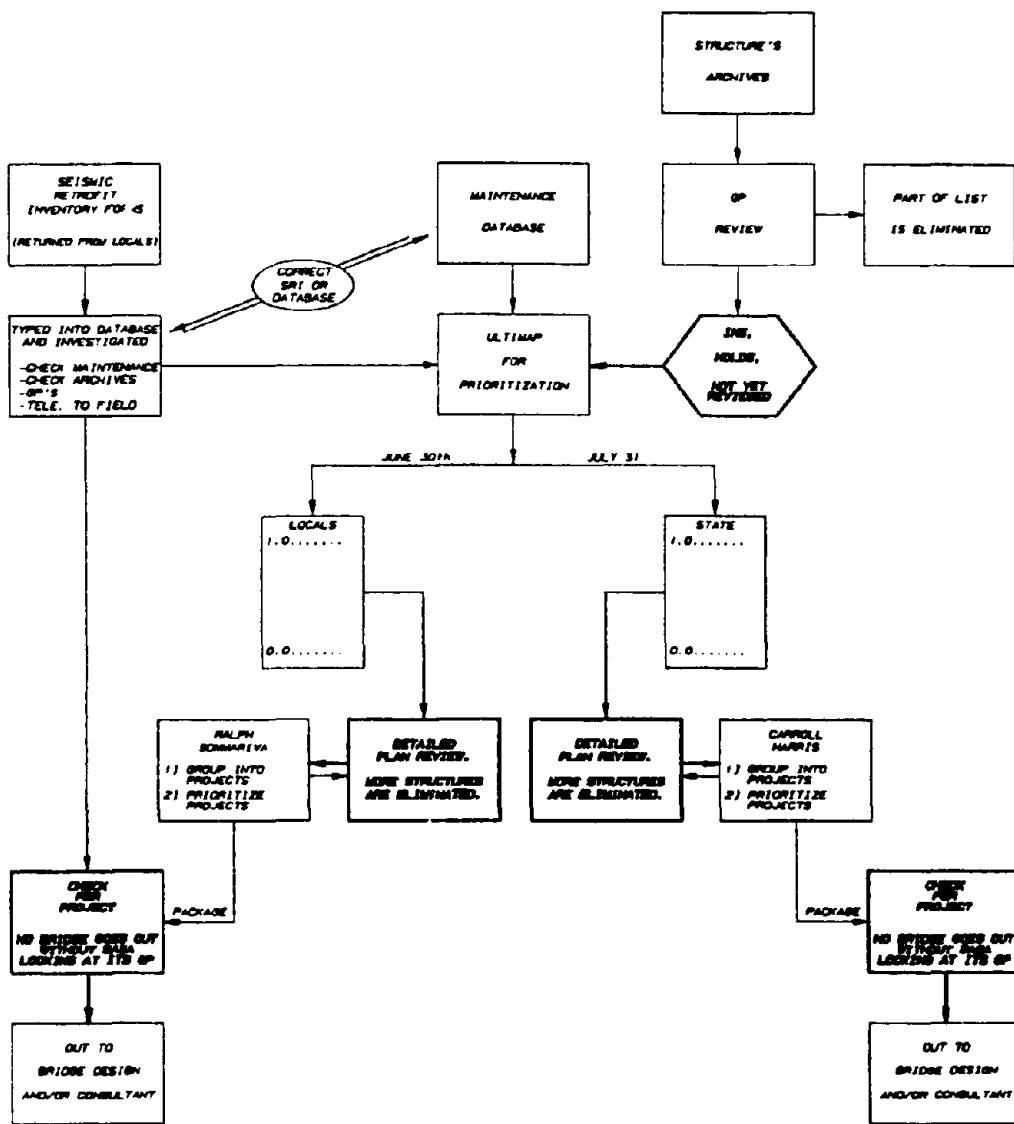


Figure 1. SEISMIC RETROFIT PROJECT FLOWCHART

There are some 24,000 (approximately 12,000 state and 12,000 city or county) bridges in the state of California (see Figure 2).

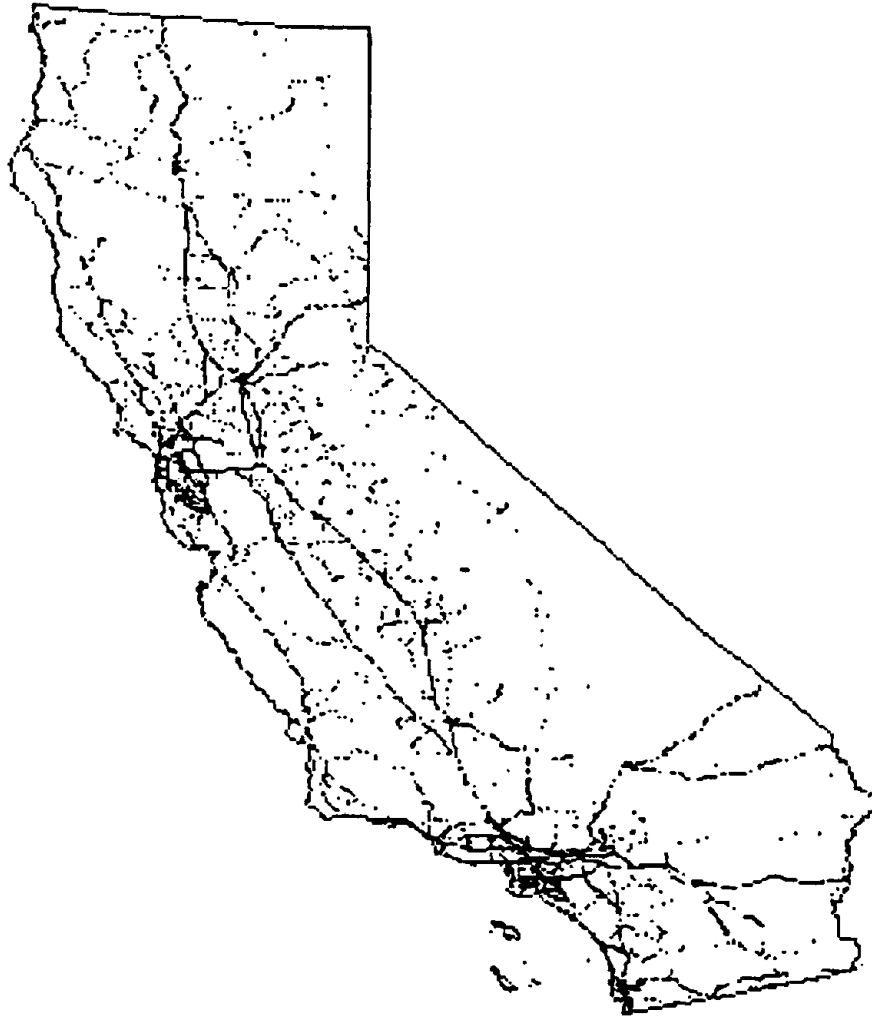


Figure 2. CALIFORNIA BRIDGES

There are more than 200 faults (see Figure 3), which threaten California bridges.



Figure 3. CALIFORNIA SEISMIC FAULTS

Considering the large number of bridges that Caltrans is responsible for in some capacity, it was and still is economically unrealistic to require that every structure be immediately retrofitted to withstand large magnitude earthquakes without some damage. A retrofit philosophy was adopted at the start of the seismic retrofit program which offers reasonable direction.

It is Caltrans philosophy to first retrofit those structures which are at greatest risk and are the most vital. The ultimate goal is to see that all of the bridges in the state are capable of surviving large earthquakes. Some damage is inevitable but collapse is believed to be preventable with proper retrofitting. The exception to this is in the case of important lifeline structures. If undue stress or hardship will be placed on a community due to a structure being temporarily out of service, every attempt will be made to strengthen the structure to increase the chances of surviving a maximum level event with nominal damage.

#### IDENTIFICATION & PRIORITIZATION

Identification of bridges likely to sustain damage during an earthquake is an essential first step in a retrofit program. What can be classified as a level one risk analysis was employed as the framework of the process which led eventually to a consensus list of prioritized bridges.

A conventional risk analysis determines a probability of failure or survival. This probability is derived from a relationship between the load and resistance sides of a design equation. Not only is an approximate value for the absolute risk determined, but relative risks can be obtained by comparing determined risks of a number of structures. Such analyses generally require vast collections of data to define statistical distributions for all or at least the most important elements of some form of analysis, design, and/or decision equations. The acquisition of this information can be extremely costly if obtainable at all. Basically, what is typically done is to execute an analysis, evaluate both sides of the relevant design equation, and define and evaluate a failure or survival function. All of the calculations are carried out taking into account the statistical distribution of every equation throughout the entire procedure.

To avoid such a large questionable investment in resources and to obtain results which could be applied quickly as part of the seismic retrofit program, an alternative was recognized and developed. What can be called a level one risk analysis procedure was used. A similar risk evaluation to identify and prioritize bridges for retrofitting was used in the single column retrofit program (Ref. 3). The difference between a conventional and level one risk analysis is that in a level one risk analysis expert judgements take the place of data supported statistical distributions.

The level one risk analysis procedure employed can be summarized in the following steps:

1. Survey the available expert database to identify and weight high risk structural and transportation characteristics,
2. Define preweight scoring schemes,
3. Calculate bedrock accelerations at all bridge sites,
4. Identify high risk soil sites which possess the capacity to substantially amplify bedrock acceleration, and
5. Prioritize bridges by summing weighted bridge structural and transportation characteristics.



Step 1 was performed by surveying experts in the fields of bridge design, maintenance, and construction and geotechnical and geological sciences. Typically, bridge structural and transportation characteristics with high correlations to past earthquake bridge damage would be used to identify variable components of a risk evaluation. Due to the absence of a substantial database of maximum credible California earthquakes and their effects on California bridge structures an alternative database was identified and tapped. Expert judgements by professionals in the field of bridge engineering were used to derive and calibrate a risk algorithm. The survey was used to determine which characteristics would have high correlations to bridge damage or cost to public transportation and what their relative correlations would be. This panel of experts represented hundreds of years of bridge experience. The result of this step is illustrated in Figure 4.

## RISK ALGORITHM

$$R = \sum [(wt) \cdot (pre-wt)]$$

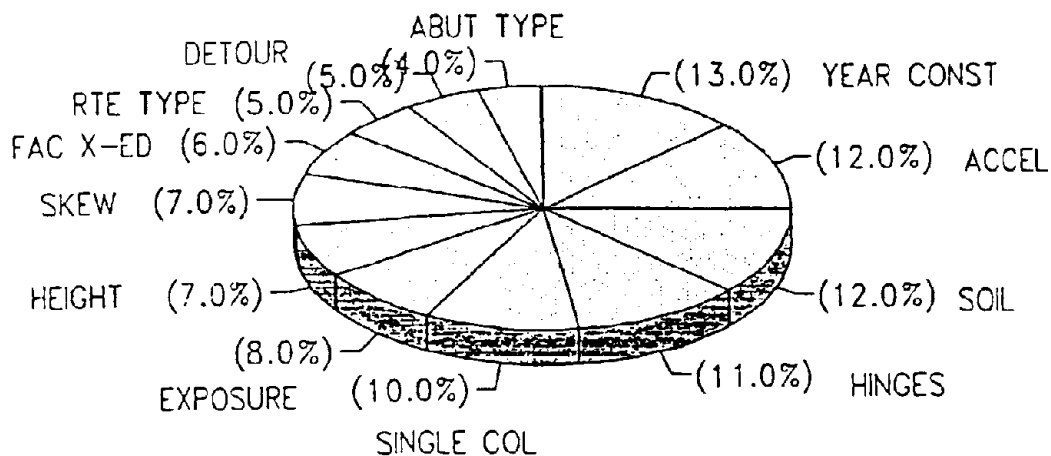


Figure 4. PRIORITIZATION WEIGHTS

Prewrite scoring schemes were developed in step 2. These were developed using engineering judgement considering available data, their forms, and engineering/mechanical relationships between the particular characteristics and typical structural or transportation system responses. Each preweight score is a number between 0.0 and 1.0. A number close to 0.0 reflects a relatively low risk and a number close to 1.0 reflects a relatively high risk.

Typical preweight scoring schemes are presented in Figure 5.

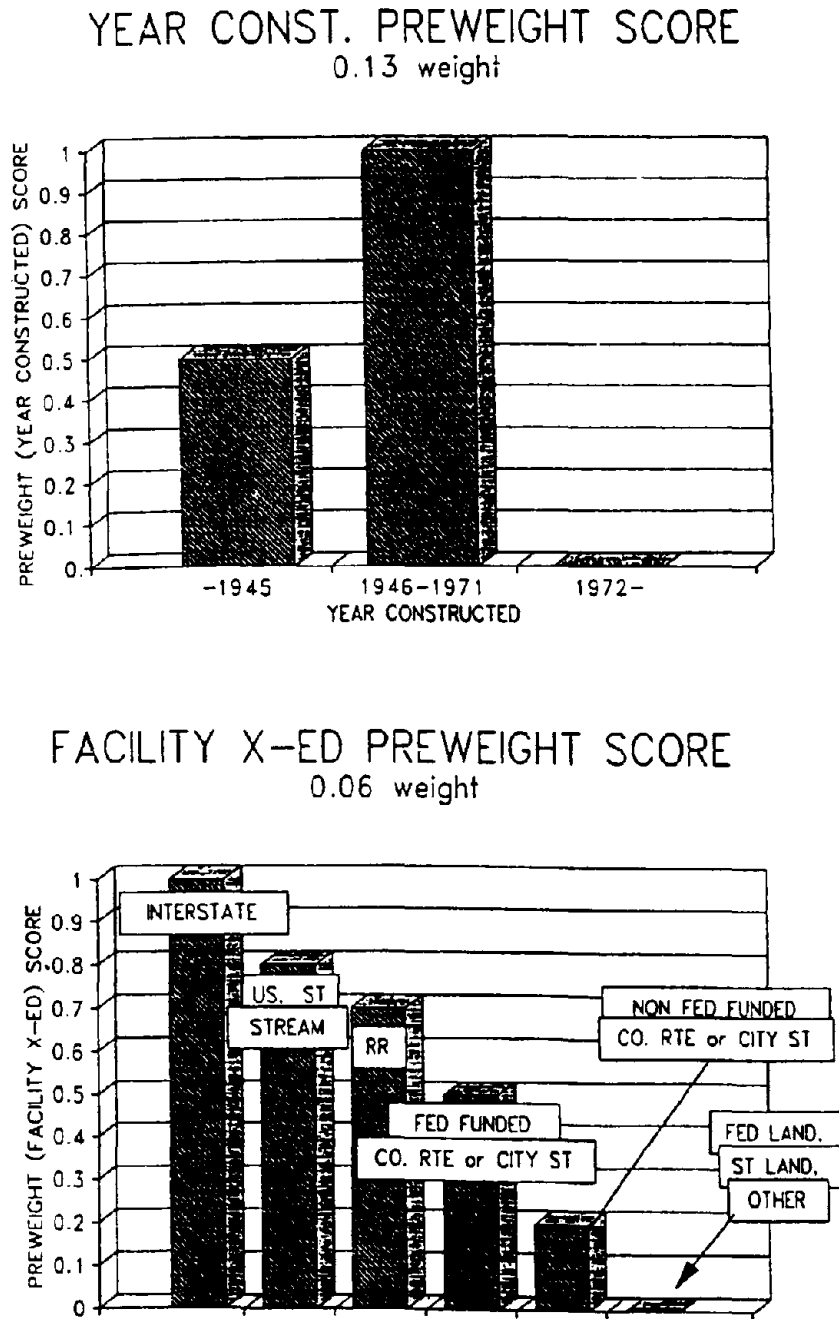


Figure 5. TYPICAL PREWEIGHT SCORING SCHEMES

The final risk algorithm details including preweight ranges is shown in Figure 6.

<b>YEAR CONSTRUCTED</b>	<b>0.13 *</b> (0.0 → yr >71; 0.5 → yr ≤45; 1.0 → 45 < yr ≤ 71)
<b>PEAK ROCK ACC.</b>	<b>0.12 *</b> (MCE acc, normalized to 0.7g)
<b>SOIL AT SITE</b>	<b>0.12 *</b> (0.0 → low risk site; 1.0 → high risk site)
<b># OF HINGES</b>	<b>0.11 *</b> (0.0 → 0; 0.5 → 1; 1.0 → 2 or more)
<b>COLUMNS PER BENT</b>	<b>0.10 *</b> (0.5 → multi-col; 1 → single col)
<b>TRAFFIC EXPOSURE</b> (length & ADT on deck)	<b>0.08 *</b> (neg. parabola, normalized to $2 \cdot 10^8$ ADT · LENGTH)
<b>HEIGHT (length)</b>	<b>0.07 *</b> ((LOCAL) neg. cubic, normalized to 30) ((STATE) 0.0 → 0-300; 0.5 → 300-600; 1.0 → >600)
<b>SKEW</b>	<b>0.07 *</b> (pos. parabola, normalized to 90)
<b>FACILITY CROSSED</b>	<b>0.06 *</b> (same as RTE TYPE, STREAM = 0.8)
<b>ROUTE TYPE</b> (on structure)	<b>0.05 *</b> (INTERSTATE → 1.0; U.S. ROUTE → 0.8; STATE ROUTE → 0.8; RAILROAD → 0.7; FED. FUNDED CO. ROUTE OR CITY ST. → 0.5; NON-FED. FUNDED CO. ROUTE OR CITY ST. → 0.2; FED LAND, STATE LAND, & UNDEFINED → 0.0)
<b>LENGTH OF DETOUR</b>	<b>0.05 *</b> (linear, normalized to 100)
<b>ABUT. TYPE</b>	<b>0.04 *</b> (0.0 → monolithic; 1.0 → nonmonolithic)

---

**THE SUM OF THESE WILL BE BETWEEN 0.0 AND 1.0**

**Figure 6. RISK ALGORITHM**

Step 3 was carried out by consulting the California Division of Mines and Geology. A team of seismologists and engineers identified seismic faults believed to be the sources of future significant events. Selection criteria included location, geologic age, time of last displacement (late quaternary and younger), and length of fault (10 km minimum). Each fault was evaluated for style, length, dip, and area of rupture surface in order to estimate potential earthquake magnitude. Fault locations were digitized for computer use. An appropriate attenuation model was developed by Mualchin of the California Division of Mines and Geology to be used throughout the state. It is a weighted average of several published models.

These two efforts combined to produce a method for determining the maximum credible peak bedrock acceleration at the site of each bridge in California. This is achieved by attenuating maximum credible ground accelerations from the closest fault segment to the bridge site. This was greatly simplified by use of the map produced by Mualchin of the California Division of Mines and Geology (Ref. 4). This map presents the maximum credible peak bedrock accelerations throughout the state of California.

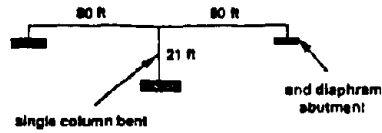
Caltrans engineering geologists from throughout California collaborated to complete step 4. A knowledge base constructed by years of studying and working with the geologic strata of California was thus made available to the Division of Structures. The team of engineering geologists, working with 26 geologic maps, conservatively identified high risk soil sites which possess the potential to substantially amplify bedrock accelerations. The identified high risk soil sites were then digitized for computer use.

Step 5 is the process of combining the previous efforts via a logical, dependable, and repeatable algorithm which can be computerized. This was performed with a graphical interface system by ULTIMAP at Caltrans. A final single risk number for each structure was calculated by summing the products of risk algorithm weights and each structure's preweight scores, producing a numerical measure of relative risk between 0.0 and 1.0. An example calculation is shown in Figure 7. An indepth description of each component and each preweight scoring scheme is presented in another paper by Maroney (Ref. 5).

#### DATA COLLECTION

Acquisition of the bridge structural and transportation data was a formidable task. The Caltrans Structures Maintenance database was relied upon heavily. This database is a federally mandated library of records which describe a variety of structural, transportation, and economic bridge data. However, any single source of information cannot be relied upon alone. Parallel information seeking efforts were initiated to gather the best available information on all state and locally owned bridges. These additional efforts include a solicited Seismic Retrofit Inventory (SRI) survey of locally owned bridges (Figure 8), and a state wide General Plan (GP) review (Figure 9), of all bridges, and a collection of special knowledge on selected structures which engineers statewide are independently identifying as threatened.

GIVEN :



- YEAR DESIGNED	1955
- PEAK BEDROCK ACCELERATION	0.45g
- HIGH RISK SOIL SITE	not in a high risk soil zone
- # OF HINGES	0
- COLUMNS / BENT	1
- ADT ON BRIDGE	20,000 $\frac{\text{veh}}{\text{day}}$
- HEIGHT	21 ft (SRI form calls out 20 - 30 ft)
- LENGTH	160 ft
- SKEW	15 degrees
- FACILITY CROSSED	U.S. route
- ROUTE TYPE	county route
- DETOUR LENGTH	10 miles
- ABUTMENT TYPE	end-diaphragm

- YEAR DESIGNED	0.13 * (1.0)	0.13
- PEAK BEDROCK ACCEL.	0.12 * ( $\frac{.45g}{.7g}$ )	0.077
- HIGH RISK SOIL SITE	0.12 * (0)	0.0
- # OF HINGES	0.11 * (0)	0.0
- COLUMN/BENT	0.10 * (1.0)	0.1
- TRAFFIC EXPOSURE	0.08 * (20000 $\frac{\text{veh}}{\text{day}}$ * 160 ft = $3.2 * 10^6$ ==> 0.0317)	0.0025
	see TRAFFIC EXPOSURE PREWEIGHT CURVE	
- HEIGHT	0.07 * (0.995)	0.07
	If height available use HEIGHT PREWEIGHT CURVE if height not available use length to estimate height in this case SRI form is the best available data, and an average for the 20-30 ft range is used.	
- SKEW	0.07 * (0.025)	0.0018
	see SKEW PREWEIGHT CURVE	
- FACILITIES X-ED	0.06 * (0.8)	0.048
	U.S. route crossed	
- ROUTE TYPE	0.05 * (0.5)	0.025
	county route on bridge	
- DETOUR LENGTH	0.05 * (0.1)	0.005
	see DETOUR PREWEIGHT CURVE	
- ABUTMENT TYPE	0.04 * (0)	0.0
	monolithic	

RISK RATING ==>  $\sum = 0.46$

Figure 7. EXAMPLE RISK ALGORITHM CALCULATION

The SRI requested local agencies to survey their structures and return to Caltrans data which would assist in evaluating their potential need for retrofitting. An SRI form is shown in Figure 8. All fifty-eight counties and nearly 300 cities have completed over 11,000 SRI forms. Approximately 570 forms are outstanding and 640 forms have been received that do not match any existing records (11/90). Caltrans processed, corrected if necessary, and entered the returned form's information into a database. This information is serving as a vital element in the retrofit program.

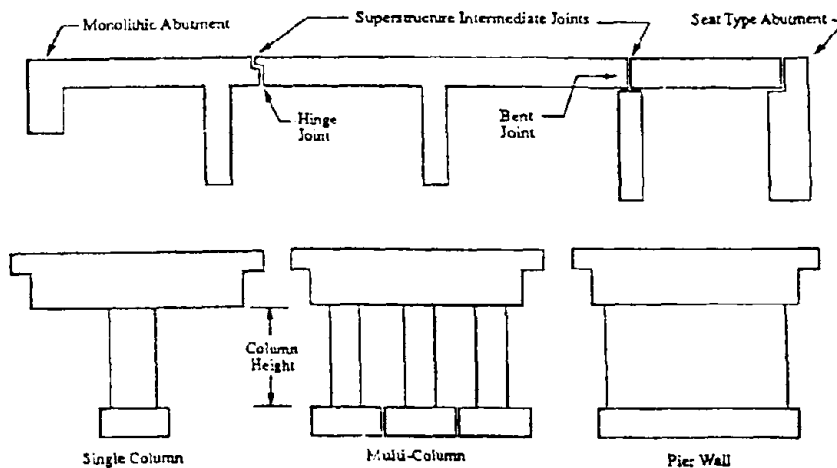
BRIDGE NO.   BRIDGE NAME

NUMBER OF INTERMEDIATE SUPERSTRUCTURE JOINTS (HINGE)   
 (BENT)

SUBSTRUCTURE: (CHECK APPROPRIATE BOXES)

<u>COLUMNS:</u>	Y	N	PLANS AVAILABLE?:	Y	N
SINGLE COLUMN:	<input type="checkbox"/>	<input type="checkbox"/>		<input type="checkbox"/>	<input type="checkbox"/>
MULTI-COLUMN:	<input type="checkbox"/>	<input type="checkbox"/>	ESTIMATED ADT:	<input type="text"/>	
PIER WALL:	<input type="checkbox"/>	<input type="checkbox"/>	MAXIMUM COLUMN / PIER HEIGHT: (CHECK ONE)	0 TO 20':	<input type="checkbox"/>
PILE BENT:	<input type="checkbox"/>	<input type="checkbox"/>		20 TO 30':	<input type="checkbox"/>
OTHER (DESCRIBE):	<input type="text"/>			OVER 30':	<input type="checkbox"/>
<u>ABUTMENTS:</u>					
SEAT ABUTMENT:	<input type="checkbox"/>	<input type="checkbox"/>			
MONOLITHIC ABUTMENT:	<input type="checkbox"/>	<input type="checkbox"/>			

DEFINITIONS:



PREPARED BY: \_\_\_\_\_ CONTACT: \_\_\_\_\_  
 DATE: \_\_\_\_\_ OWNER/AGENCY: \_\_\_\_\_  
 ADDRESS: \_\_\_\_\_  
 COMMENTS ON BACK (SKETCHES, ETC.) PHONE: \_\_\_\_\_

Figure 8. SEISMIC RETROFIT INVENTORY (SRI) FORM

The GP and detailed review utilized engineers examining at least one plan sheet for every structure Caltrans has in its archives. The goals of this effort were twofold. The first was to remove all structural types from the retrofit program which have proven to be not susceptible to catastrophic failure due to earthquakes. These kinds of structures include: modern bridges designed since 1980 without outrigger knee joints, flat slab, timber, single-span monolithic, typical two-span monolithic, and well-seated single-span bridges. This effort reduced the number of bridges which required a more detailed review or analysis. The second reason for the GP review was to serve as a check for bridge identification and data-base quality. This proved valuable in cases in which bridge structures had been replaced, renamed, or renumbered. A copy of the GP Seismic Review data sheet is shown in Figure 9, and the Detailed Seismic Review data sheet in Figure 10. It should be noted that the data sheets were modified as new conditions were encountered which suggested modification. Approximately 9000 state and 4000 locally owned bridge GPs have been reviewed and over 3000 detailed seismic reviews have been performed (11/90).

Special knowledge pertaining to bridge structures throughout the state has proven valuable. The Division of Structures maintains an open door policy for engineers and other professionals to contribute to the effort in identifying high risk structures through special knowledge of structures or site characteristics which they have gained through professional experience with a bridge or site in the state of California.

In order to respect previously committed time schedules, the bridge plan review effort has two levels of review. They are the GP Review discussed earlier and a Detailed Seismic Review which is providing an opportunity to remove more bridges from the retrofit program by investigating the structural plans in detail. Such details include support widths, column reinforcement, footing reinforcement, bearing type, etc.... The detailed review also allows reviewers to take advantage of additional knowledge gained from recent retrofit structural analyses. This review is taking place before and following the assignment of the risk values.

It is recognized that certain structures on the state transportation system can be identified as having unusually high levels of risk associated with them. Examples include: structures with rigid outrigger bents, structures with leased space below, structures spanning faults, and structures on routes which can be categorized as lifeline arteries. These structures are being identified by numerous methods and will be appropriately analyzed and if necessary retrofitted.

# G. P. SEISMIC REVIEW

BRIDGE # \_\_\_\_\_

DEPARTMENT OF TRANSPORTATION  
Division of Structures  
Special Projects Branch  
Seismic Retrofit Program

year designed? \_\_\_\_\_

- 0) special class reason:  
in, out, or hold, for reason(s) not listed below  
Comments are required on the back of this page.
- out 1) structures with all of the following:  
modern structure and details (1980+); ductile elements; no outriggers
- out 2) single-span structures with monolithic abutments
- out 3) timber bridges
- out 4) multi-span structures with all of the following:  
monolithic; multi-column or pier wall bents; end-diaphragm or well seated  
seat-type abutments; fairly balanced spans of less than 130 ft; total length  
less than 300 ft; (deck area)/(no. of columns) less than 5000;  
less than 25 ft of height; small to moderate skews; standard-like design
- hold 5) structures with all of the following:  
good superstructure details; reasonably good spiral spacing, but lapped at ends;  
footings lack the capacity to hold plastic moment; (i.e., no top mat of steel and/or  
no shear reinforcement)  
This would be a typical mid 70s vintage structure.
- hold 6) structures with all of the following:  
monolithic; multi-column; end-diaphragm or well seated seat-type abutments;  
fairly balanced spans between 130 ft and 175 ft; less than 50 ft of height;  
(deck area)/(no. of columns) less than 7000; small to moderate skews;  
standard like design
- in 7) multi-span structures with simple beam construction  
(typically precast or steel I-girders)
- in 8) any structure with outriggers, C-bents, or shared columns
- in 9) any structure with rented airspace or public facilities below
- in 11) structures with any of the following:  
nonductile structural elements (except for cases 2, 3, or 4); multiple frames;  
seat or support widths which are small or unknown; unrestrained hinge seats;  
steel or precast sections simply supported on seats or piers; single column frames.

STATUS: \_\_\_\_\_

REASON(B): \_\_\_\_\_

REVIEWED

NAME: \_\_\_\_\_ DATE: \_\_\_\_\_

CHECKED

NAME: \_\_\_\_\_ DATE: \_\_\_\_\_

(Rev 6-09-90)

Figure 9. G P REVIEW FORM



# DETAILED SEISMIC REVIEW DATA SHEET

BRIDGE # \_\_\_\_\_

DEPARTMENT OF TRANSPORTATION  
Division of Structures  
Special Projects Branch  
Seismic Retrofit Program

year designed? \_\_\_\_\_

**SUPERSTRUCTURE DETAILS:**

outriggers:  YES  NO  
 C-bents?  YES  NO  
 any rocker bearings?  YES  NO  
 shared columns?  YES  NO  
 super/sub conn. type?  Monolithic joints  Simple span supports  
 material type?  P.S. concrete  C.R. concrete  Steel  Timber  
 section type?  I-girder  Box-girder  Slab  Arch  T-girder  Truss  Suspension  
 number of spans? \_\_\_\_\_  
 maximum span length? \_\_\_\_\_ minimum span length? \_\_\_\_\_ average span length? \_\_\_\_\_  
 maximum span width? \_\_\_\_\_ minimum span width? \_\_\_\_\_ average span width? \_\_\_\_\_  
 maximum skew? \_\_\_\_\_ minimum skew? \_\_\_\_\_ average skew? \_\_\_\_\_  
 overall length measured in feet? \_\_\_\_\_  
 curvature:  
 smallest radius in feet? \_\_\_\_\_ arc angle in degrees? \_\_\_\_\_

**HINGE DETAILS:**

number of hinges? \_\_\_\_\_ hinge seat width in inches? \_\_\_\_\_  
 restrainers?  YES  NO  
 seat extenders?  YES  NO

**ABUTMENT DETAILS:**

abut. type?  Seal-type  End-diaphragm  Other (tied down)  Other (not tied down)  
 abut. seat width in inches? \_\_\_\_\_  
 shear keys?  YES  NO  YES, but very small  
 retrofit?  YES  NO

**COLUMN DETAILS:**

Is column confined in regions of possible yielding (can it behave in a ductile manner)?  
 YES  YES  NO  NO  
 material type?  P.S. concrete  C.R. concrete  Steel  Timber  
 number of columns per bent? \_\_\_\_\_ minimum per bent \_\_\_\_\_ maximum per bent \_\_\_\_\_  
 number of single-column bents? \_\_\_\_\_ number of multi-column bents? \_\_\_\_\_  
 maximum column height? \_\_\_\_\_ minimum column height? \_\_\_\_\_ average column height? \_\_\_\_\_  
 transverse reinforcement:  spirals # \_\_\_\_\_ bars @ \_\_\_\_\_ inches  
 ties # \_\_\_\_\_ bars @ \_\_\_\_\_ inches  
 trans. reinf. well into footing & superstructure?  YES  NO  
 longitudinal reinforcement:  
 (to what degree are the columns reinforced?) ---> percent of longitudinal steel in column \_\_\_\_\_  
 lap splices in regions of possible yielding?  YES  NO

**FOOTING DETAILS:**

top mat of steel?  YES  NO  
 pedestal?  YES  NO  
 shear reinforcement?  YES  NO  construction only  
 column/footing connection?  pinned  fixed  
 piles or spread footings?  pile  spread  shaft  
 if piles, can they carry tension?  YES  NO  too difficult to judge

**SOIL DATA:**

log of test borings?  YES  NO date? \_\_\_\_\_  
 soil type?  sand  clay  silt  too difficult to judge  
 blow count greater than 20 at a depth of 15 feet below the surface?  YES  NO  
 depth to rock-like material in feet? \_\_\_\_\_  too difficult to judge  
 depth to water-line in feet? \_\_\_\_\_ date? \_\_\_\_\_  too difficult to judge  
 if geology contacted, ARS curve? \_\_\_\_\_  
 liquefaction potential?  High  Low  None

STATUS: \_\_\_\_\_ REASON(S): \_\_\_\_\_

REVIEWED NAME: \_\_\_\_\_ DATE: \_\_\_\_\_

CHECKED NAME: \_\_\_\_\_ DATE: \_\_\_\_\_

DATA COLLECTOR & DATE NAME: \_\_\_\_\_ DATE: \_\_\_\_\_

Reviewers and checkers: List suggested retrofit strategies on the back of this sheet.

(Rev 6-22-90)

Figure 10. DETAILED REVIEW FORM

## PROJECT CLASSIFICATION

Identified bridges are being grouped into projects. The total inventory of bridges is separated first into three groups respecting the three lead agencies jurisdictions and then further by the results of the GP review effort. Respective lists were provided to the state, and Santa Clara and Los Angeles counties with seismic risk factors associated with all bridges. Methods employed to oversee the retrofitting bridge structures at the project level in the counties is the responsibility of the respective lead agencies. Each of the bridge structures which fall under Caltrans jurisdiction not eliminated by the GP review will be assigned a seismic risk factor. The risk factors will be used to prioritize the bridges.

Project grouping will consider ownership, number of bridges, estimated costs, and geographic locations. All bridges in any single project shall be owned by the same city or county. The maximum number of bridges in any one project will be 20. (It is estimated that 50% of these will usually be eliminated in a detailed final screening. Maximum estimated costs per project will not exceed \$4 million. Reasonable geographic limitations will be used to group bridge sites into projects.

Each project will be prioritized. Projects will be assigned a Seismic Project Priority Number (SPPN). The SPPN will be the average of each bridge's risk factor in a project weighted by each respective bridge's estimated retrofit construction cost. It is estimated that project prioritization will be completed in late 1990.

## CONCLUSIONS

Past earthquakes have exposed potentially threatening deficiencies in California bridges. Caltrans recognized this situation as early as 1971 and immediately initiated a retrofit program, however modest state funding of the program limited it's scope to high potential areas. The Loma Prieta Earthquake brought attention to the program and with legislation and government recommendations from the governor's board of inquiry, Caltrans is being directed to accelerate the seismic retrofit program. Important initial steps to the strengthened program are to identify and prioritize bridge structures which possess a high probability of severe damage in a maximum credible earthquake. This is currently underway at Caltrans using what can be termed a level one risk analysis. The risk analysis employs an expert knowledgebase and good engineering judgement to produce a prioritized list of bridges which will be grouped into projects and released for design and construction.

#### REFERENCES

1. Copp, Q., Senate Bill No. 36x, California State Senate, November 4, 1989.
2. Governor's Board of Inquiry, George W. Housner, Chairman, Competing Against Time, Report to Governor George Deukmejian from The Governor's Board of Inquiry on the 1989 Loma Prieta Earthquake, May 31, 1990.
3. Maroney, B., Prioritization In The Phase II Retrofit Program, Presented at the 5th Joint U.S.-Japan Workshop on Bridge Engineering Performance, Strengthening, and Innovation, San Diego, California, U.S.A., May, 1988.
4. Mualchin, L. & Jones, L., Peak Acceleration from Maximum Credible Earthquakes in California, Department of Conservation, California Division of Mines and Geology, Open File Report, 124pp and a Plate, 1990.
5. Maroney, B., Caltrans Seismic Risk Algorithm For Bridge Structures, A paper documenting the risk algorithm, June 1990.

## DAMAGE AND PERFORMANCE ASSESSMENT OF EXISTING CONCRETE BRIDGES UNDER SEISMIC LOADS

Frieder Seible (1)  
M.J. Nigel Priestley (1)  
Presenting Author: F. Seible

### SUMMARY

Based on encountered damage in elevated concrete freeway structures during the October 17, 1989 Loma Prieta (San Francisco) Earthquake, a preliminary damage and performance assessment procedure was developed to evaluate the seismic performance characteristics of existing concrete bridge structures. The assessment of cap-column joint behavior is discussed in this paper within the framework of this general preliminary damage and performance assessment procedure, and extended all the way to detailed joint behavior studies using nonlinear analytical finite element procedures. Finally, considerations for repair and retrofit solutions for knee joints in outrigger bents are presented.

### INTRODUCTION

The Loma Prieta (San Francisco) earthquake of October 17, 1989 reemphasized the vulnerability of structural concrete systems to cyclic displacements resulting from seismic attack. The dramatic collapse of a one-mile section of the Cypress Viaduct in Oakland can be traced to inadequate performance of the cap-column joint region in the supporting bents of the double-deck bridge structure. Investigation of the joint reinforcement showed inadequate structural detailing of the joint region for the encountered seismic force levels. While the Cypress collapse was well publicized in the press and technical literature, only limited information can be found on similar structural joint damage to other elevated roadways in the San Francisco-Oakland Bay Area which led to the temporary or permanent closure of several major freeway arteries including the Embarcadero Viaduct (I-480), the China Basin/Southern Freeway Viaduct (I-280) and the Central Viaduct (Highway 101) in San Francisco, as well as the Southbound Connector (I-980) in Oakland [Ref.1].

While most of these bridge sections were designed and built in the 1950's and 1960's, some of them were completed as late as 1985. This raises questions concerning not only past but current detailing practice for structural concrete joints. Design rules for beam and column members of structural concrete frame systems seem to be widely accepted and standardized in similar form around the world. However, as soon as aspect ratios of structural members approach unity, design guidelines and supporting design models show a wide range of different approaches. Limited detailed design models for these regions exist when full three-dimensional force transfer of axial, flexural and torsional structural action is required simultaneously. Also, most design models focus on single monotonic structural loading and do not address fully reversed cyclic loading patterns. Thus, the question arises whether a unified approach for design and analysis models in support of structural concrete detailing exists or if the state-of-the-art in structural concrete detailing still relies primarily on experience to design and detail complex members for realistic loading conditions.

Both analytical models to study the in-depth mechanism of structural concrete behavior through various limit states and design models developed to unify the structural detailing and design approach have seen comprehensive recent developments. In a direct extension of early structural concrete design principles by Ritter (1899) and Mörsch (1909), Schlaich et al. have developed a comprehensive design approach toward structural concrete detailing which ensures internal force transfer through discrete compression and tension (strut and tie) members, satisfying equilibrium by simple truss mechanisms [Ref.2]. This approach has become a powerful design tool since it allows a variety of detailing solutions as long as basic anchorage and stress limit states are observed, but most importantly it allows and forces the design engineer to develop a consistent design model resulting in

---

(1) Professor of Structural Engineering, University of California, San Diego, USA

an engineered solution rather than in a design resulting from a recipe application. Problems and limitations arise when design solutions based on inappropriate truss mechanisms are attempted and when the discrete member forces are of magnitudes which cause stress limit and anchorage problems and thus require a distributed or smeared approach. Parallel to the consistent strut and tie model development, Collins, et al. developed the juxtaposed position of a smeared or distributed behavior model [Ref.3], which is based on homogeneous behavior of structural concrete even in its cracked state and resulting orthogonal principal compression and/or tension fields of the internal forces. Based on mechanical principles of an orthotropic homogeneous material, the orientation of the resulting stress fields is derived from compatibility and equilibrium conditions. The resulting stress fields are subsequently discretized in concrete and reinforcement action which forms the basis for a rational structural concrete design approach. Similar to the discrete strut and tie model, additional considerations for anchorage and local concentrated force transfer are required and limitations exist where either reinforcement is heavily concentrated rather than distributed, and where structural action results in a few large cracks rather than in the ideal distributed (smeared) crack pattern. Thus, while both design models are different in the approach, they are rather complementary in the overall design process, especially when in addition to the force transfer in the joint or member, deformation limit states also need to be considered.

Both of the above models provide comprehensive design approaches to structural concrete detailing but are fully applicable only when simple monotonic loading conditions exist up to design levels with sufficient margin to the ultimate limit state. Where deteriorating bond phenomena along the reinforcement, opening and closing of cracks under reversed cyclic loading, deterioration of concrete contribution in developing local failure mechanisms, and the development of ductile hinges (which incorporate all of the above aspects) are present, the above models may not be adequate and additional considerations to both design approaches are needed as outlined by Paulay et al. for structural concrete joints under seismic action [Ref.6]. It will be shown in the following that, with these additional considerations, the above design models can also be directly applied toward the design of retrofit measures of existing critical structural concrete regions as found in the San Francisco double-deck freeways. Further, it will be shown that complete failure sequences and limit states of these structural systems can be traced using advanced nonlinear analytical structural concrete models.

The critical role of structural concrete joints in beam-column systems and their behavior under seismic loading is evaluated in this paper on the example of joint performance in elevated bridge structures during the Loma Prieta earthquake and the applicability of various design and analysis models to the structural concrete joint problem is demonstrated, both for the assessment of joint performance during the earthquake and subsequent repair and retrofit strategies.

## SEISMIC PERFORMANCE ASSESSMENT

### General Assessment Approach

To assess the expected seismic performance of structural concrete beam column joints, it is important that the joint under consideration is evaluated in direct relationship to the actual adjacent member capacities. This requires a state or capacity determination of adjacent beams and columns with consideration of (1) actual material properties at the time of evaluation, i.e., probable concrete strength, not the design strength  $f_c$ , actual stress strain behavior for the reinforcement not nominal specified design yield levels, (2) proper consideration of axial load effects, (3) proper consideration of possible confinement effects from transverse reinforcement, (4) reduced concrete shear contribution in areas of large fully reversed cyclic deformation, and (5) realistic bond and anchorage estimates particularly for large diameter reinforcing bars. A preliminary performance assessment of joints comprises the following general steps: Step I: Realistic member capacities based on the above considerations are derived for both flexure and shear, and the critical failure mechanism is determined by direct comparison of the shear capacity with the plastic flexural limit state shear  $V_p$  derived from the appropriate flexural plastic hinge failure model of the member. If  $V_p$  is larger than the calculated shear capacity, a potentially brittle shear failure can be expected without the formation of ductile

flexural plastic hinge mechanisms. Step II: Based on the possible member failure mechanisms, the expected global collapse mechanism for the complete structural system is derived by comparing combined dead load and lateral seismic force action with the derived capacities. Step III: From the identified systems collapse mechanism, critical joint forces can now be determined at the collapse state and a direct comparison with most probable joint capacities will indicate if joint distress degrades the capacity of the collapse mechanism or if the joint behaves as ideally assumed within or close to the elastic range. Finally, equivalent seismic base shear forces are estimated corresponding to the lateral force level which causes collapse based on the above failure mechanism. Excessive joint distress can lead to a reduction of this base shear coefficient, particularly when a large number of cyclic load reversals and the associated joint degradation is considered. A complete summary of the proposed preliminary damage and assessment procedure for existing concrete bridges under seismic loads is compiled in Appendix A, addressing not only the joint problem but rather the complete assembly of individual components, bents and frames.

Application of the above preliminary seismic assessment procedure to the San Francisco double-deck bridge bents has shown that particularly the joints did not meet design criteria for earthquake resistant ductile structures summarized by Paulay et al. [Ref.5] as:

- (1) joint strength should exceed the maximum strength of the weakest connecting member,
- (2) structure capacity should not be jeopardized by strength degradation in the joint,
- (3) joint response should be elastic during moderate seismic disturbances.

The preliminary joint behavior assessment outlined above can be supplemented and refined by more detailed analysis and design models as demonstrated in the following for specific case studies performed following the 1989 Loma Prieta earthquake.

#### Cypress Viaduct Overview

The collapse of the Cypress Viaduct in Oakland was caused by inadequate structural detailing of the lower cap-column joint region. A typical failed bent of the Cypress Viaduct is shown in Fig. 1a, while probably more instructively, Figs. 1b,c and d depict the joint distress pattern of the cap-column joints in portions of the Cypress Viaduct which did not collapse during the Loma Prieta earthquake. Both vertical and horizontal joint reinforcement detailing, see Fig. 2, is insufficient to transmit the required joint shear forces and both a capacity design check with joint equilibrium model and a compression field based nonlinear finite element model [Ref.1] yielded joint shear forces of less than 1.8 MN [400 kip], sufficient to fail the pedestal in the joint region. While the simple equilibrium check on the joint provides a quick assessment of the joint shear capacity, the nonlinear finite element investigation of the joint also provides the sequential crack and yield development patterns and associated deformation limit states which allow estimates of the ultimate failure mode, see Fig. 3.

As shown by the failure mode postulated in Fig. 3 and the distress patterns in Fig. 1, the failure most likely initiated in the lower part of the upper column or the column pedestal which featured insufficient transverse reinforcement  $D = 13 \text{ mm @ } 30 \text{ cm}$  (#4 @ 12 in.) to confine the column/pedestal concrete and to provide the required shear resistance.

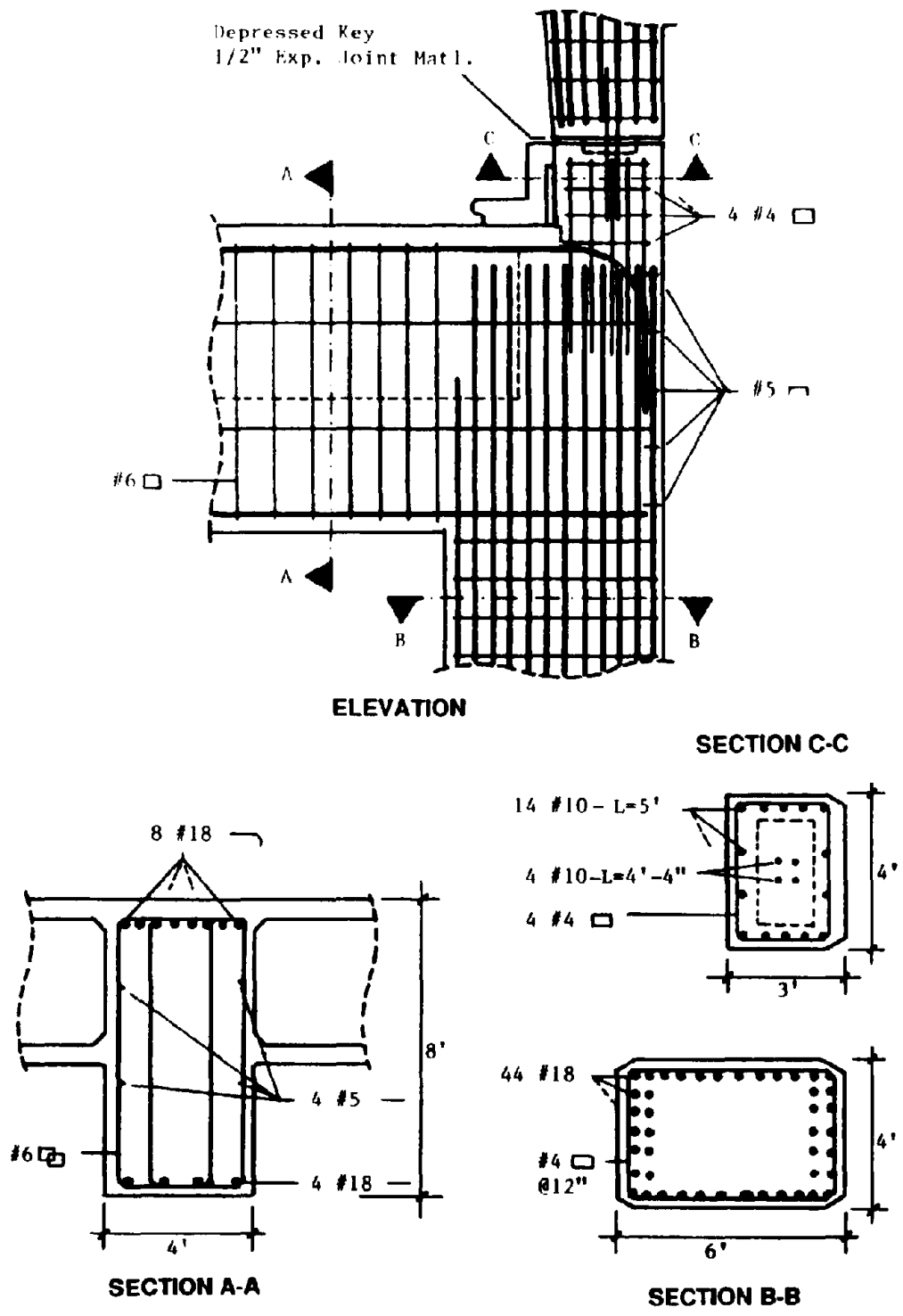
While the Cypress failure originated in the column pedestal or extended joint region, distress patterns encountered in other elevated roadways such as the China Basin Viaduct (I-280) and the Oakland Southbound Connector (I-980) clearly show extensive joint distress, particularly in the knee joints of outrigger bents as shown in Fig. 4. These outrigger bent damage patterns will be evaluated in the following.

#### The China Basin Viaduct, I-280 Bent N1-35

An overview of the China Basin Viaduct bent N1-35 is given in Figs. 5 and 6. The upper roadway (N1-line) is supported by a large outrigger bent which sustained both joint shear and cap

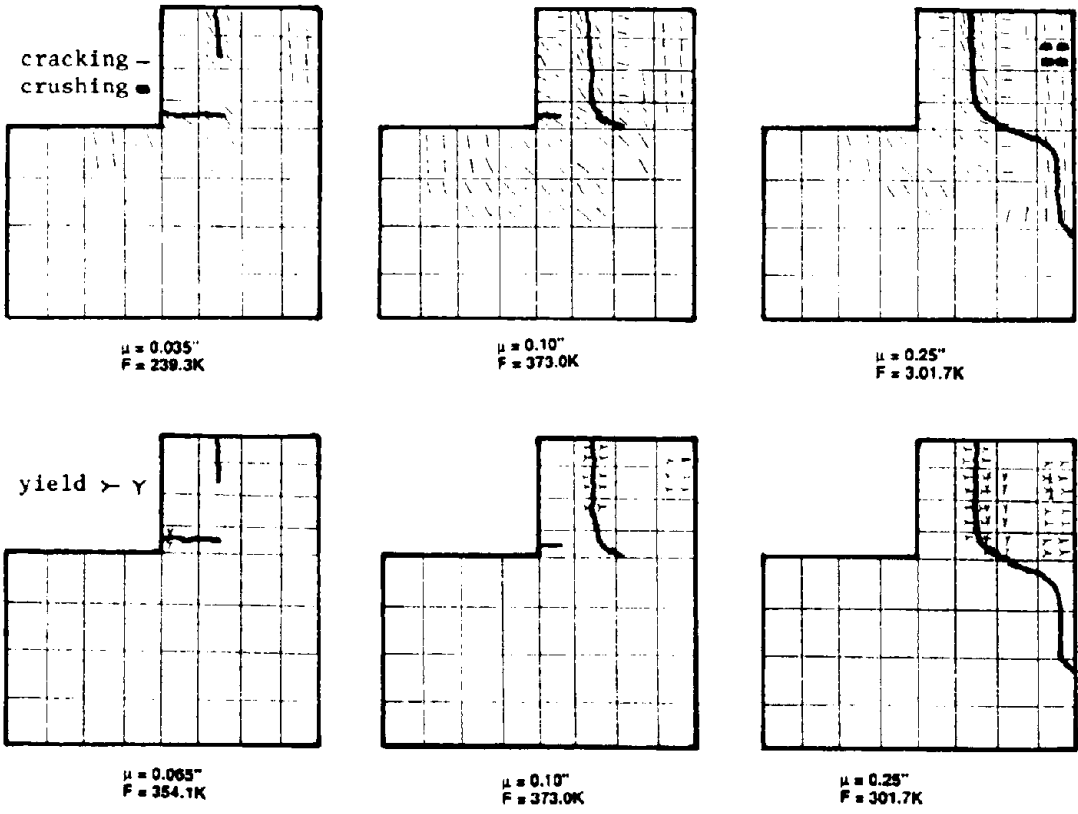
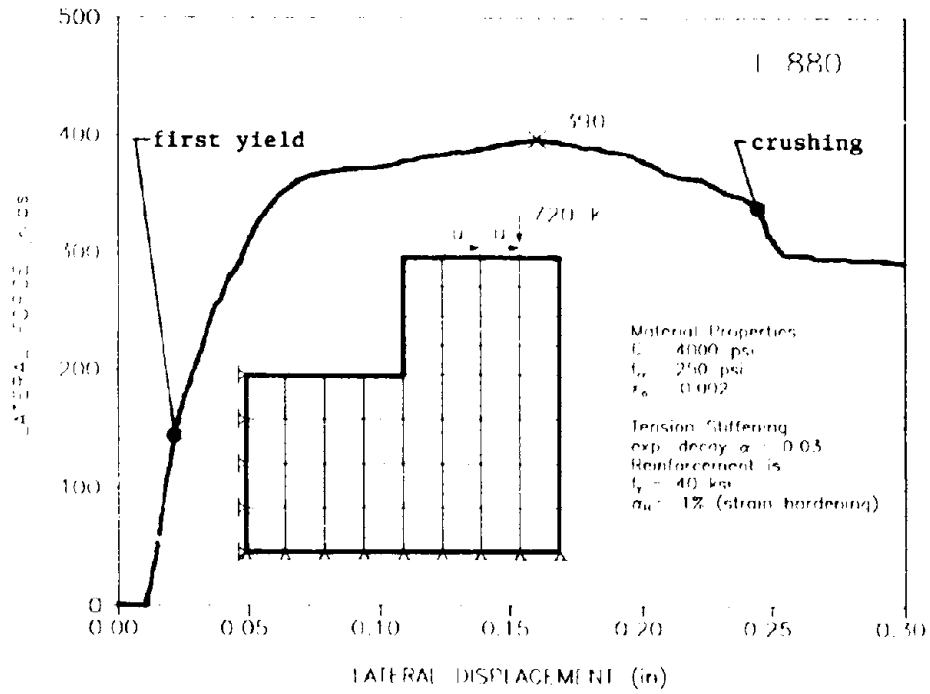


Fig 1 Cypress Viaduct collapse and distress patterns



**Fig.2 Cypress Viaduct joint reinforcement detail**

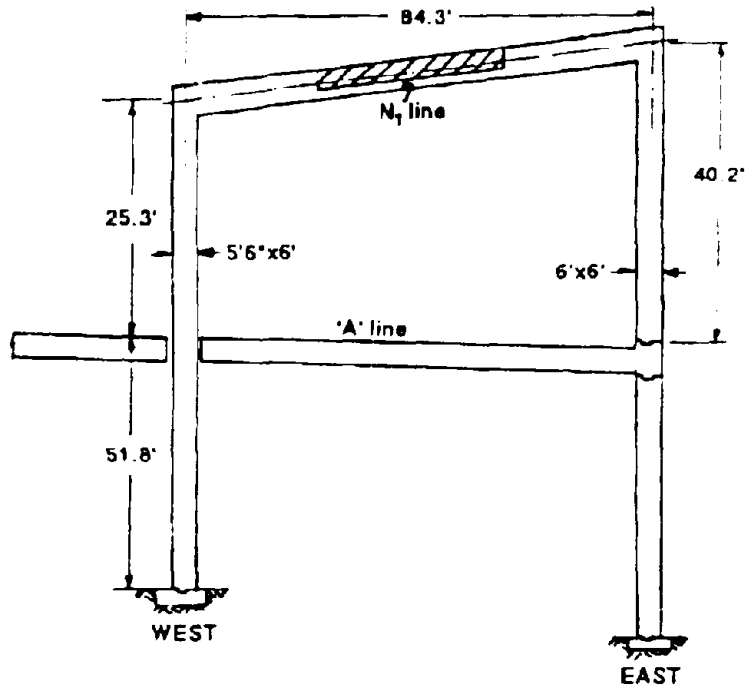




**Fig. 3 Load-deformation history and distress pattern development in lower cap-column joint of the Cypress Viaduct**



**Fig. 4** Outrigger bent joint damage



**Fig. 5** Elevation, bent N<sub>1</sub>-35, China Basin Viaduct  
[1 ft = 0.305 m]



**Fig. 6** China Basin Viaduct, bent N<sub>1</sub>-35

flexure/shear damage as outlined in Fig. 6b. To assess the expected seismic performance of bent N<sub>1</sub>-35, a dead load estimate and a capacity estimate [Ref.1] of the upper cap beam and columns was performed, as outlined above and summarized for the cap beam in Fig. 8, based on the as-built dimensions and reinforcement details depicted in Fig. 8. For bent N<sub>1</sub>-35, the flexural capacities of the cap beam were well below the column capacities and were thus critical for the overall seismic performance assessment. A unit lateral (seismic) force was subsequently applied to the bridge bent, superimposed separately for two support assumptions (I, II) and the two loading directions with the dead load estimates and scaled until the combined action exceeded the flexural cap beam capacity envelope, see Fig. 7.

Lateral response force levels of  $\vec{E} = 0.63 \text{ g}$  and  $\overleftarrow{E} = 0.69 \text{ g}$  in the two directions, respectively, were found to be sufficient to cause local hinge mechanisms to develop. Particularly under loading to the right, see Figs. 6 and 7, the termination of negative or top reinforcement at a distance of 6.1 m (20 ft) from the column center line is cause for the onset of a negative moment crack which propagates toward the column in shear aided by the lack of cap beam shear reinforcement in this region, see Fig. 8. A wide flexural-shear crack was observed in this region, as predicted, see Fig. 6b.

Joint shear cracking was calculated for both joints at lateral force levels less than that corresponding to the first hinge formation. Approximate values corresponding to a joint shear stress of  $0.33\sqrt{f_c}$  MPa ( $4\sqrt{f_c}$  psi) are  $\vec{E} = 0.45 \text{ g}$ ;  $\overleftarrow{E} = 0.40 \text{ g}$ . Thus, significant joint distress as seen in Fig. 6b can be expected. Although the level of cracking visible in the positive knee joint moment regions of the bent cap beam indicates that the bent probably did not reach first hinge formation, the shear stresses in the joints were high enough to cause joint failure. Hence the response accelerations appear to have exceeded 0.4 g in each direction.

However, since both cap beam and joint mechanisms form at very similar lateral load levels and the distress pattern in the cap beam also indicates reinforcement inadequacies, no repair or retrofit measure but rather complete replacement of the entire bent was recommended [Ref.1].

#### The Oakland Southbound Connector, I-980, Bent 38

A single-deck outrigger bent (bent #38) with only a 0.92 m (3 ft) outrigger cap beam extension past the superstructure on I-980 featured heavy joint damage as shown in Figs. 4 and 9. Built in 1985, the column was well confined with an interlocking spiral, see Fig. 10, however, this spiral did not continue into the joint region where it was replaced by a 5 gauge wire spiral with  $D = 5 \text{ mm}$  at 10 cm ( $\phi 0.2 \text{ in. @ } 4 \text{ in.}$ ). Also, the cap beam reinforcement aside from the top and bottom bars, see Fig. 10, did not extend into the joint region.

A capacity check on the cap beam and column capacities showed that the cap beam capacity is critical for positive moment due to the insufficient anchorage length of 1.8 m (72 in.) for the  $D = 57 \text{ mm}$  (#18) bars which, based on ACI 318-89, require a basic development length of 3.0 m (117 in.) which is likely to be on the conservative side. In the other loading direction (negative moment in the joint), the column capacity is critical. Joint shear force levels derived from simple stress models, Fig. 11, show joint shear stress levels of  $0.37\sqrt{f_c}$  MPa ( $4.3\sqrt{f_c}$  psi) and  $0.5\sqrt{f_c}$  MPa ( $6.0\sqrt{f_c}$  psi), under positive and negative moment loading, respectively, which are both above an assumed level of  $0.33\sqrt{f_c}$  MPa ( $4.0\sqrt{f_c}$  psi), where diagonal tension cracking in the joint can be expected. Since the shear capacity of the 5 gauge wire spirals does not add significant joint shear capacity, the formation of any flexural hinge mechanism in adjacent members was inhibited. This explains the encountered diagonal joint crack patterns during the Loma Prieta earthquake, see Fig. 4.

In addition to the diagonal crack patterns, large areas of cover concrete spalling along the outer cap corner as well as a ruptured  $D = 57 \text{ mm}$  (#18) reinforcement bar which was bent on a 45 cm (1'-6") radius were observed, see Fig. 9.

The first phenomenon of cover concrete spalling can be explained with the fully reversed cyclic loading. Under negative moment, flexural cracks open on the cap surface as shown in Fig. 11 and under subsequent positive moment loading, the entire compression force has to be transferred through

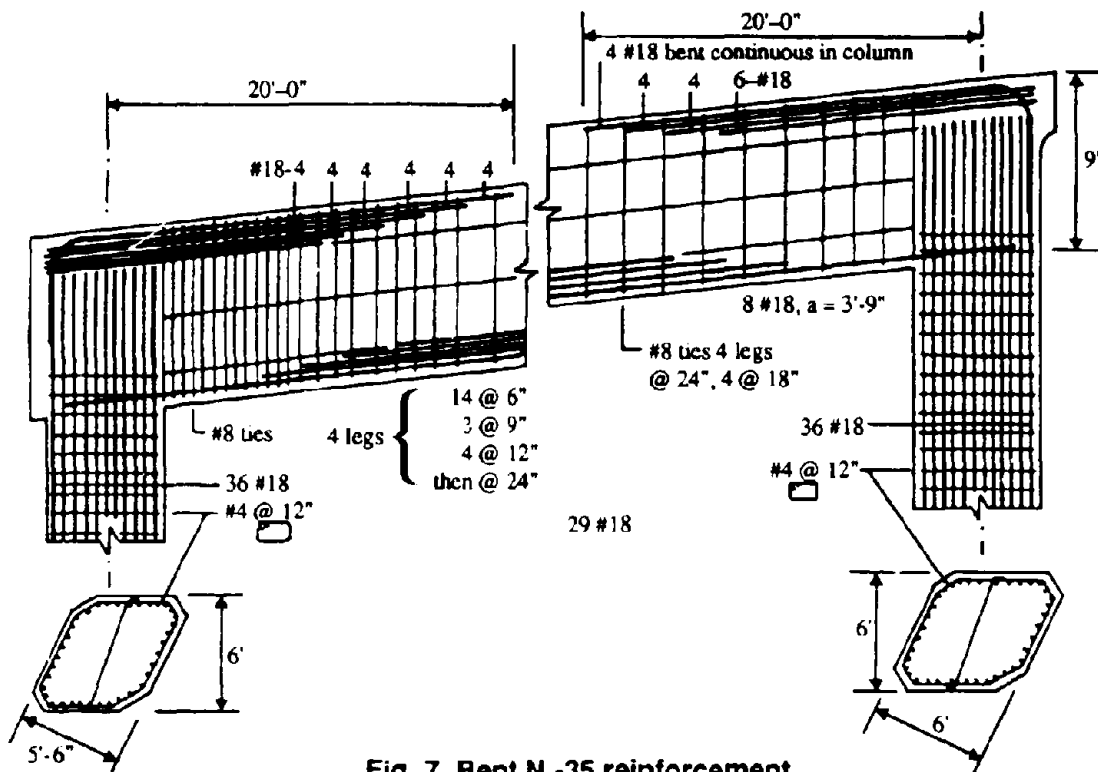


Fig. 7 Bent N<sub>1</sub>-35 reinforcement

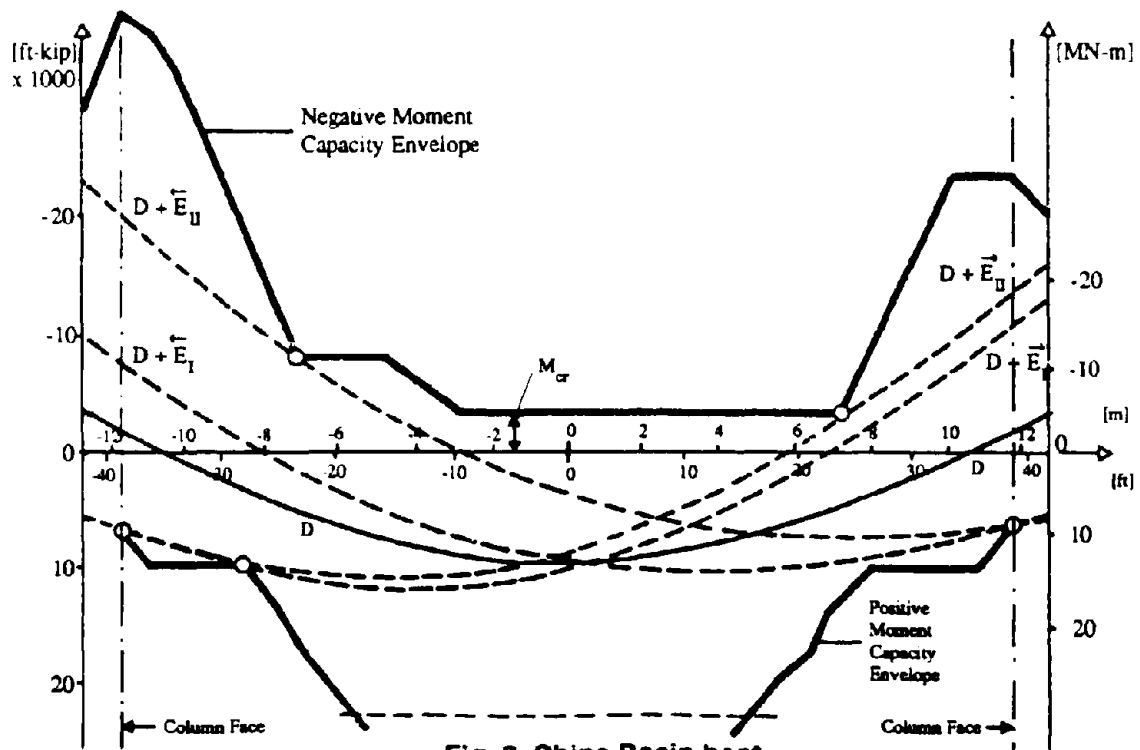


Fig. 8 China Basin bent

the negative moment reinforcement until the cracks can close. These high compression forces in the negative moment reinforcement transferred to the concrete by bond, have a tendency to spall off the concrete cover between flexural cracks developed in the previous tensile excursions.

The second phenomenon, the ruptured reinforcing bar, points to a potentially critical problem which needs further investigation. Common ultimate strain levels in  $D = 57 \text{ mm}$  (#18)  $f_y = 414 \text{ MPa}$  (Grade 60) bars are in a range from 7 to 15%. Introducing a  $R = 45 \text{ cm}$  (18 in.) radius bent into a  $D = 57 \text{ mm}$  (#18 or  $\phi = 2.25 \text{ in.}$ ) bar causes strain levels of  $D/(2R) = 225/(2 \times 18) = 6.25\%$ , which is close to the ultimate strain range. The very low strain reserves and possible strain aging effects which raise the notch ductile temperature at which steel will fail in a brittle mode can cause sudden failure in these bent bars at very low additional strain levels.

In addition to the simple stress models of the knee bent joint, detailed nonlinear finite element simulations based on extended compression field principles were performed to determine analytically failure modes and joint deformation contributions to the overall bent deformations. Reinforcement development of straight bars was modeled by assuming a reduced yield level in the anchor zone decreasing linearly from the full yield at the ACI 318-89 basic development location to zero at the bar end. Subsequently derived yield patterns in bar anchorage regions therefore are indicative of bond failure or slip. Superimposed to the dead load case, the half bent, Fig. 12, was subjected to lateral force and force-deformation envelopes with major event indicators were obtained. Associated crack, slip/yield and first crushing patterns, see Fig. 13, indicate the failure mechanisms in the joint region. The heavy yield in the joint center, both horizontally and vertically, indicates the deficiency of both vertical and horizontal joint shear reinforcement, particularly under loading to the left or negative moment on the joint. Also, the crushing of the concrete in the outer joint region under the bent negative moment reinforcement under loading to the left or negative moment indicates the high compressive stress state and associated transverse prying forces in this region and the need for sufficient transverse confinement reinforcement, as outlined by Schlaich et al. [Ref.6], for strut and tie models for negative moment knee joints.

For repair and retrofit considerations, the emphasized diagonal nature of the joint yield and joint crack patterns strongly suggest the addition of both horizontal and vertical joint shear reinforcement. Also, the prying forces in the negative moment reinforcement generated under fully reversed cyclic positive moment need to be anchored back to the compression zone on the inside of the joint through a diagonal tie back.

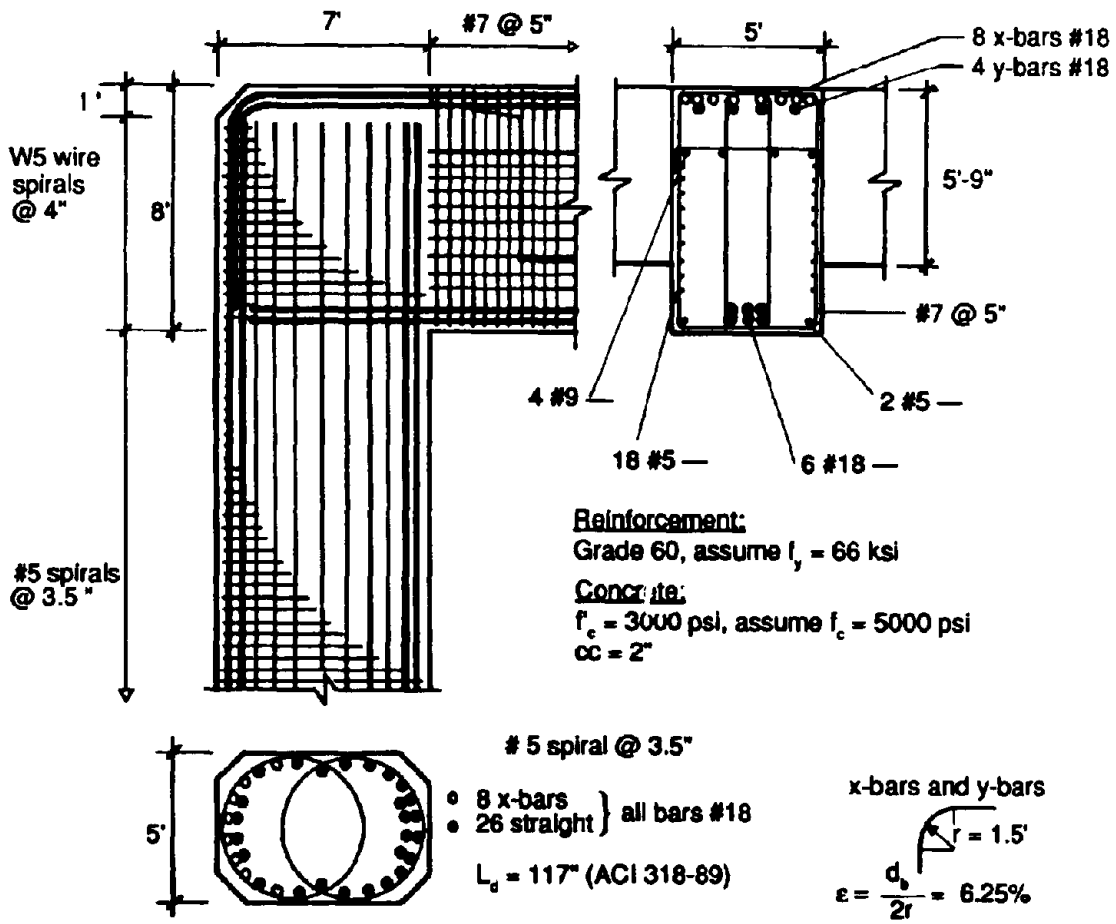
A comparison of the force-deformation envelope in the two loading directions, see Fig. 12, shows that loading to the left or negative moment loading results in a sudden failure with crushing in both joint corners, Fig. 13, while loading to the right or positive moment loading deteriorates due to the slip in the positive moment reinforcement of the cap beam and the column. However, under fully reversed cyclic loading, this bond slip will deteriorate even further causing a drop in positive flexural capacity (not shown in Fig. 12).

Since joints should be detailed based on capacity considerations such that the major inelastic action occurs in the cap or column, and since they should remain effectively elastic for small seismic disturbances (Paulay et al. [Ref.5]), the nonlinear finite element analysis was repeated with a linear elastic joint for a direct comparison of deformation limit states. As can be seen from Fig. 12, while joint deformations did not contribute significantly to the initial overall structural deformations, the failure mode in the positive moment direction (loading to the right) shows improved ductile behavior when the failure mechanism is shifted from joint distress to flexural cap beam hinging. It should be noted that the cap beam capacity still may be artificially low due to the reduced yield strength in

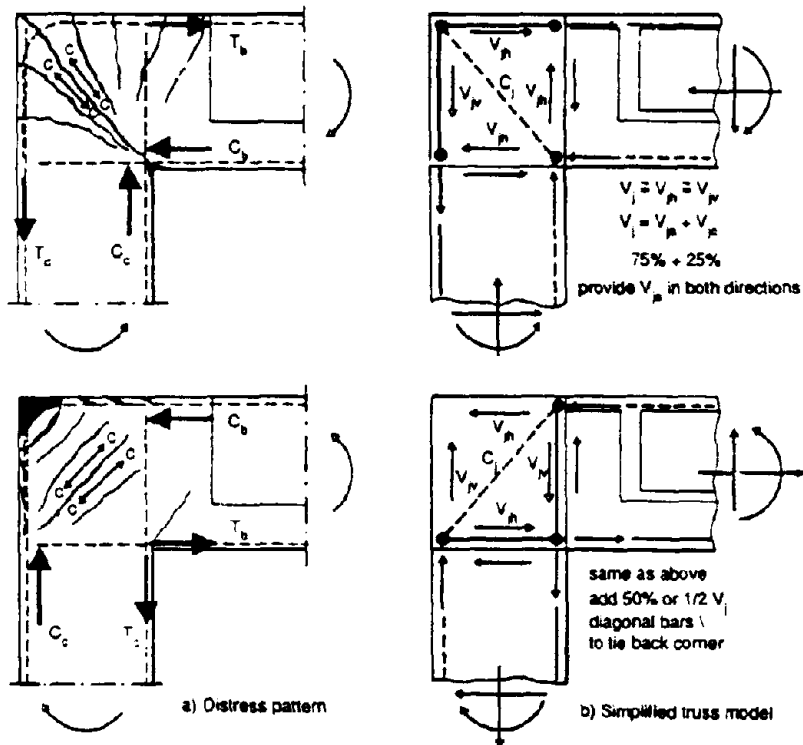
the bottom  $D = 57 \text{ mm}$  (#18) reinforcing bars based on a reduced development length according to ACI 318-89. Negative moment loading behavior is also improved by forcing the yield mechanism clearly into the column. Since the bent joint failure is the critical link in the overall behavior, repair/retrofit of these joints is a logical next step.



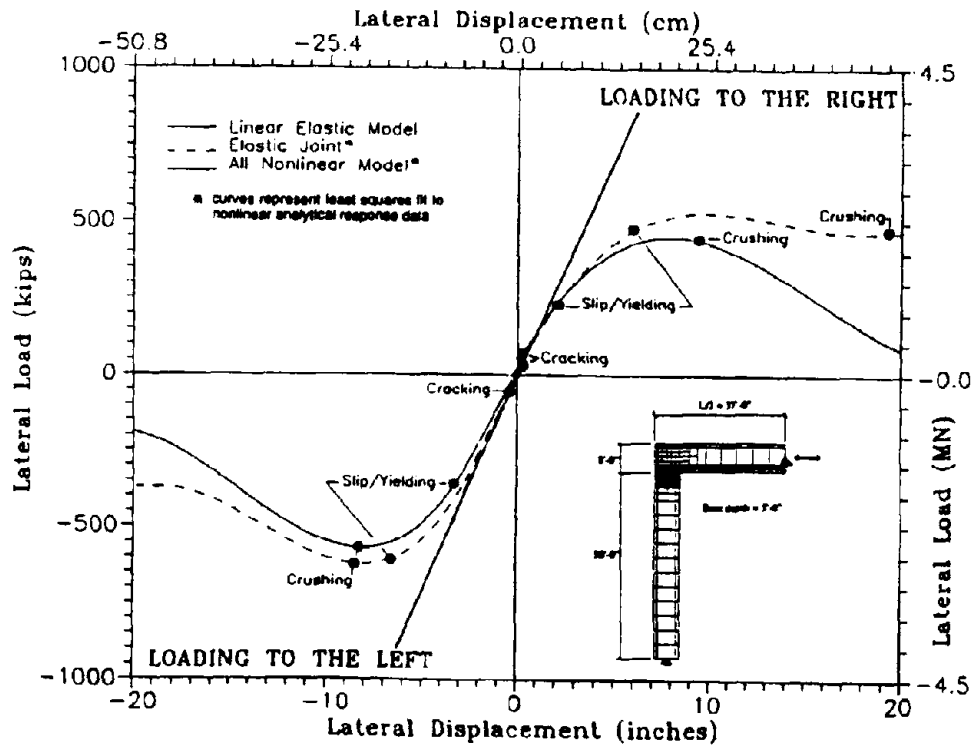
**Fig. 9** Joint damage in I-980 outrigger bent #38



**Fig. 10** I-980, bent #38 reinforcement details

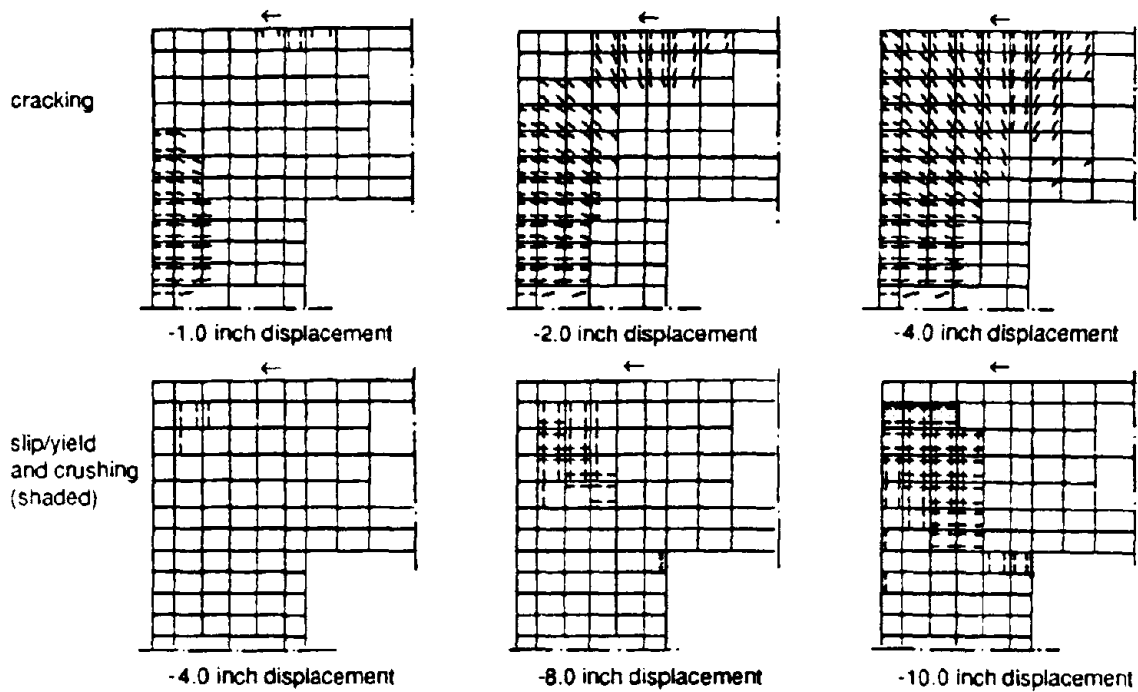


**Fig. 11 Joint behavior models**

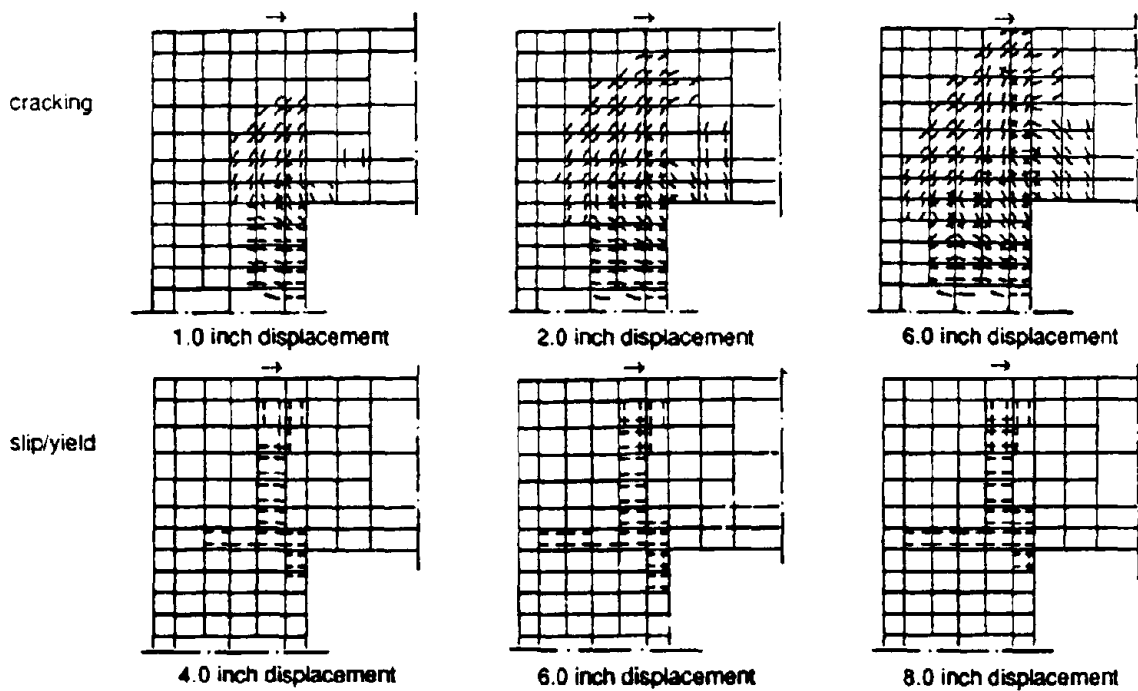


**Fig. 12 Bent #38, I-980, load-deformation behavior**





a) Loading to the left



b) Loading to the right

**Fig. 13** Development of cracks, slipping/yielding of reinforcement, and crushing of concrete in the joint region, bent #38, I-980

## REPAIR AND RETROFIT

Cap/column joints in elevated roadways are probably the most difficult members in a bridge bent to successfully repair and/or retrofit for seismic loading. Both horizontal and vertical heavy reinforcement patterns from cap beams and columns provide for complex geometric and congested reinforcement patterns in the joint. Also, the critical aspects of bar anchorage within the joint as well as plastic hinge development directly adjacent to the joint complicate the retrofit design.

Criteria for seismic retrofit design of cap/column joints have to follow the philosophy of providing a reliable ductile structural system. Since ductility within the joints is very hard to achieve, the joint retrofitting is geared toward the formation of clearly defined and well behaved ductile plastic hinges in either the cap beam or the column. In many bridge decks, the cap beam is an integral component of the superstructure which would make post-earthquake repair in this member difficult. Thus, frequently in bridge design, the ductile framing system is provided by reliable column hinges.

For the retrofit design, again a capacity design approach should be employed which ensures in the case of the joint retrofit predominantly elastic behavior of the joint region. This can be achieved by joint design which is based on factored nominal column design moments, e.g.,  $1.5 \times M_n$ , where the factor accounts for reinforcement overstrength, including strain hardening, confinement effects and concrete strength increase with time. In detailing of the joint repair retrofit, the congested reinforcement layout within the joint as well as high nominal joint shear stress levels typically require an increase in size of the joint region.

Detailing for repair or retrofit of the damaged knee joint on I-980 bent #38 can be derived using either strut and tie models as outlined in Fig. 11 with additional considerations as outlined in [Ref.6] for transverse splitting under negative moment and tie back for fully reversed cyclic loading, or directly from the force states derived from the compression field analysis, see Fig. 13. A possible repair measure consists of providing an additional 23 cm (9 in.) concrete jacket around the existing joint with horizontal and vertical distributed joint reinforcement and a diagonal corner tie back based on force and reinforcement quantities derived in Fig. 11. The damaged joint concrete can either be removed and the joint rebuilt completely or the damaged joint can be epoxy injected subsequent to removal of loose concrete, roughening of the interface, and adequate doweling bonding of the added structural concrete jacket.

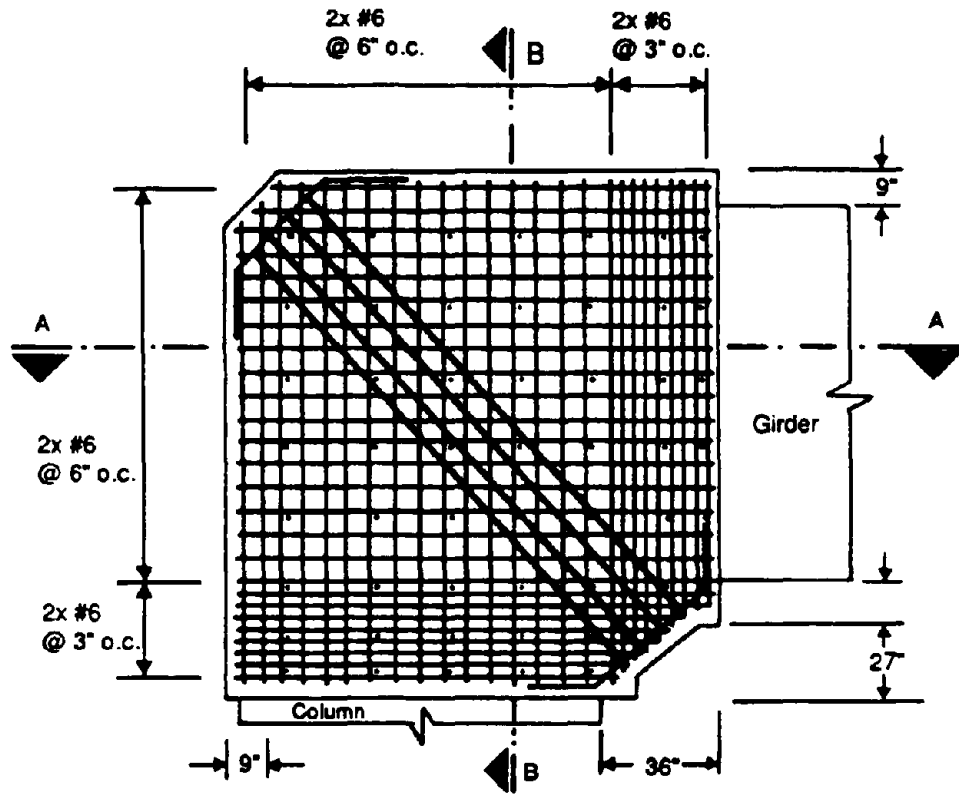
A schematic overview of the repair measure suggested for I-980, bent #38, is depicted in Fig. 14, for an added concrete jacket without prior removal of the joint concrete core. Subsequent to the joint repair work, lateral load deformation characteristics exceeding those depicted in Fig. 12 for the elastic joint case can be expected.

## CONCLUSIONS

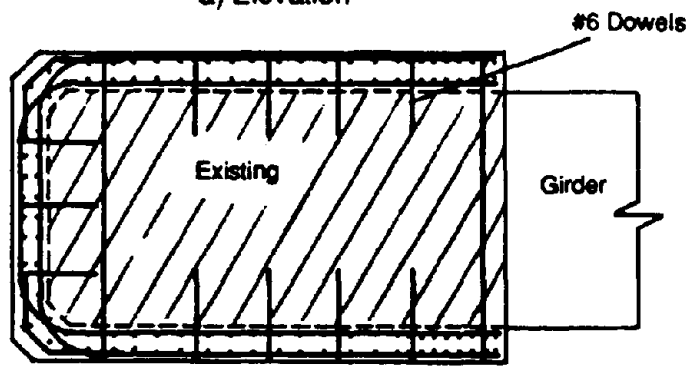
Damage in cap-column joints of elevated roadways during the October 17, 1989 Loma Prieta earthquake was used to demonstrate both preliminary seismic performance assessment procedures for existing concrete bridges as well as detailed analytical models for performance evaluation throughout all critical limit states. A complete summary of the proposed preliminary performance assessment procedure is presented to stimulate discussions on a unified evaluation, design and analysis approach in assessing and retrofitting existing concrete bridge structures for seismic loads. The presented models range from discrete strut and tie analogies to complex nonlinear finite element analyses to demonstrate the various analytical support levels for seismic performance assessment and retrofit.

## REFERENCES

- [1] PRIESTLEY M.J.N. and SEIBLE F., Assessment of Bridge Damage During the Loma Prieta Earthquake. Structural Systems Research Project, Report No. SSRP-90/01, March 1990.
- [2] SCHLAICH J., SCHÄFER K. and MATTIAS J., Toward a Consistent Structural Concrete Designs. PCI Journal, May-June 1987, pp. 74-150.



a) Elevation



b) Section A-A  
(diagonal bars not shown)

**Fig. 14** Retrofit/repair for bent #38, I-980

- [3] COLLINS M.P., Towards a Rational Theory for RC Members in Shear. ASCE Journal of the Structural Division, Vol 104, April 1978, pp. 649-666.
- [4] COLLINS M.P. and MITCHELL D., A Rational Approach to Shear Design – The 1984 Canadian Code Provisions. ACI Journal, November-December 1980, pp. 925-933.
- [5] PAULAY T., PARK R. and PRIESTLEY M.J.N., Reinforced Concrete Beam-Column Joints under Seismic Actions. ACI Journal, Vol. 75, No. 11, November 1978, pp. 585-593.
- [6] SCHLAICH J. and SCHÄFER K., Konstruieren im Stahlbetonbau. Betonkalender 1989, Verlag Ernst & Sohn, pp. 563-715.

## APPENDIX - A\*

### Preliminary Performance Assessment Procedure for Existing Concrete Bridge Structures Under Seismic Loading

<u>Procedure</u>	<u>Commentary</u>
<p><b>I. Standalone Bent Evaluation</b></p> <p>1. Dead load evaluation of bent.</p> <p>2. Lateral load analysis due to unit seismic load E.</p> <p>3. Determine member capacities based on probable material properties.</p> <p>3.1 Flexural capacities including confinement effects, development length effects and gravity on axial load effects.</p>	<p><b>I. Standalone Bent Evaluation</b></p> <p>1. Estimate contributory dead load from superstructures to bent, self weight of bent components and establish dead load bending moment diagram for the bent.</p> <p>2. Apply inverse triangular unit seismic lateral load pattern at superstructure levels to the bent, e.g.</p> <div style="text-align: center;"> </div> <p>in both directions.</p> <p>3. Determine most probable material data at the time of evaluation based on tests or assume a 50% strength increase from the nominal concrete design strength <math>f_c</math> and a 12.5% overstrength in the yield capacity of the reinforcement; e.g. concrete <math>f_c = 4000</math> psi <math>\rightarrow f'_c = 6000</math> psi, reinforcement grade 40 <math>\rightarrow f_y = 44</math> psi.</p> <p>3.1 Development length of flexural reinforcement should be taken from ACI 318-89 until new guidelines are available. For shorter development length, the effective yield stress should be reduced proportionally. For lapped starter bars with 20 <math>d_b</math> lap splice, assume a 75% effectiveness in flexure.</p> <p style="margin-left: 40px;">Confinement of the concrete by ties or spirals should be accounted for by means of an increase in ultimate compressive strain <math>\epsilon_{cu}</math> as</p> $\epsilon_{cu} = \frac{1.4 \rho_s f_{yh} \epsilon_{sm}}{f_{cc}}$ <p style="margin-left: 40px;">with <math>\rho_s</math> = effective volumetric ratio of hoop or confining steel, <math>f_{yh}</math> = hoop yield stress, <math>\epsilon_{sm}</math> = strain at peak strain of hoop steel <math>\cong 0.12</math>, <math>f_{cc}</math> = confined strength of concrete <math>\leq 1.5 f_c</math> or alternatively as <math>\epsilon_{cu} = 0.005</math>.</p> <p style="margin-left: 40px;">Axial effects due to gravity and overturning should be considered. Correct iteratively for overturning effects.</p>
<p>*Proposed procedure open for discussion</p>	

Procedure

I. Standalone Bent Evaluation (cont)

- 3.2 Shear capacities including axial load and longitudinal reinforcement ratio effects and deteriorating concrete contributions for hinge regions.

- 3.3 Determine member failure mode and member mechanism location.

4. Determine moment capacity envelope for bent and determine lateral load levels which cause local mechanisms based on dead load and factored E loads.
5. Determine the equivalent base shear coefficient corresponding to the collapse mechanism as  $C_b = E/W$ .
6. Check of joint regions for joint shear. If joint degradation is likely, reduce associated base shear coefficient.
7. Check footing capacities for critical mechanism.

Commentary

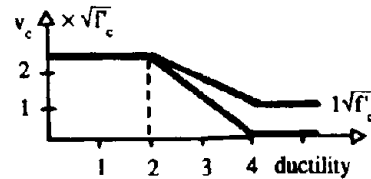
I. Standalone Bent Evaluation (cont)

- 3.2 Determine member shear based on joint ACI/ASCE Committee 426 recommendation as

$$V_n = v_c b d \left[ 1 + \frac{3P_u}{f'_c A_g} \right] + \frac{A_v f_{yd}}{s} \text{ with}$$

$$v_c = (0.85 + 120 \rho_w) \sqrt{f'_c} \leq 2.4 \times \sqrt{f'_c}$$

In hinging regions the concrete contribution should be reduced based on the ductility demand



- 3.3 Check if flexural plastic hinge state can develop in member or if shear mechanisms dominates. Assume that  $V_p$  is the shear corresponding to the flexural plastic hinge failure mode of the member

$$V_p = \frac{M_p \cdot l - M_p \cdot r}{L}$$

If  $V_p > V_n$ , a potentially brittle shear failure mechanism in the member can be expected.

4. For the determination of the overall collapse mechanism, assume initially that the joints will perform elastically.
5. E represents the total applied scaled lateral load, see Section 1, and w represents the weight and tributary dead load to the bent under consideration.
6. Joint shear capacity can be taken as  $v_c = 3.5 \sqrt{f'_c}$  plus  $v_s$ . If the joint shear demand from the critical overall collapse mechanism is equal to or less than  $v_c + v_s$ , joint deterioration is likely, the concrete shear contribution should be reduced based on the ductility demand following the column concrete shear reduction in Section 3.2, and the associated bent base shear coefficient should be reduced accordingly.
7. Check analysis assumptions for footing connection based on critical collapse mechanism forces, e.g. uplift, lateral capacities, etc. and iterate if necessary.

### Procedure

#### II. Frame Evaluation

1. Based on individual bent capacities, determine total frame capacity and compare with elastic demands from spectral analysis to obtain characteristic frame force reduction factor.

2. Determine the nominal base shear capacity for frame.

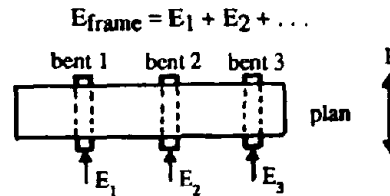
#### III. Global Structural Considerations

1. Repeat spectral analysis for a multi-frame assembly with limiting critical boundary conditions to check global validity of force reduction values and need for retrofit. If failure response mode is in flexure, force reduction factors of 2 or less are acceptable without retrofit. If force reduction demand > 2 retrofit required. If failure response mode includes shear mechanisms or joint failure, a force reduction demand > 1 requires retrofit.
2. Check longitudinal structural response, particularly tension in caps and outrigger bents.
3. Define desirable ultimate response mode to outline and design retrofit strategy.

### Commentary

#### II. Frame Evaluation

1. Determine lateral frame capacity as

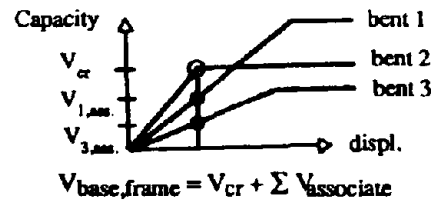


Neglecting torsional effects, compare with linear elastic spectral analysis values to obtain the required force reduction factor as

$$R_w = \frac{E_{\text{demand}}}{E_{\text{frame}}}$$

This force reduction factor is a measure for the ductility demand assuming that force redistribution between bents in a frame is possible. Use cracked sections for spectral analysis, i.e. beams  $I = 0.3 I_g$ , columns  $\rho_s = 2.5\%$ ,  $I = 0.5 I_g$ , and  $\rho_s = 75\%$ ,  $I = 0.7 I_g$ .

2. Define frame base shear capacity for the formation of the first bent collapse mechanism as



#### III. Global Structural Considerations

1. Spectral analysis based on linear elastic cracked section properties should be performed for a multi-frame assembly to capture possible torsional effects, and dynamic response characteristics of geometrically complex regions such as end frames, on/off ramps, curvature effects, etc.  
  
For force reduction factors > 2, a detailed analysis of actual ductility capacities based on advanced section analysis models can show that no retrofit is required.
2. The longitudinal response of individual frames needs to be evaluated. Particular attention is required for determining superstructure capacities and torsion effects in caps and outrigger bents. Interaction of mechanisms in the transverse and longitudinal direction needs to be considered.

LARGE EARTHQUAKE COUNTERMEASURES  
FOR BRIDGE SUBSTRUCTURES  
ON THE TOMEI EXPRESSWAY

Toshikazu Tsubouchi (I)  
Kenji Ohashi (II)  
Kazushige Arakawa (II)

SUMMARY

Forecasts have been made for many year warning of the possibility of a major earthquake, similar in scale to the Great Kanto Earthquake, occurring in Japan. This, the predictions indicate, will be the Tokai Earthquake believed to arise at the southern edge of a geographic region equivalent to the center of the Japanese isles. In other words, the tremor is predicted to have its center in Shizuoka prefecture. In readiness for the anticipated earthquake, countermeasures--social and economic ones--are being planned and executed.

The Japan Highway Public Corporation joins these efforts with the investigation and implementation of countermeasures directed against the possible Tokai Earthquake and its disastrous effects on the Tomei Expressway passing through the risk area. While some of the details of these planned countermeasures have already been reported, this paper focuses on the methods for assessing earthquake resistance. This paper follows an earlier publication on the subject and its aim is therefore to present some actual examples of retrofit measures.

INTRODUCTION

The Tomei Expressway has served as a vital lifeline in Japan's traffic system since it was opened to the public in 1969. Linking the country's major conurbations on its stretch from Tokyo through Yokohama to Nagoya, it fulfils a most essential role in social and economic terms, especially with the present accelerated growth of motorization. To ensure the functional availability of this major road, further efforts are and will be desirable to intensify road maintenance and management.

The Tomei Expressway passes through the Tokai region and the southern fringe of Shizuoka prefecture will be the epicenter of an earthquake, assumed to be of magnitude 8. This region has therefore been designated as falling within the Tokai Earthquake retrofit zone under the Special Measures for Major Earthquakes laid down by national government. Similarly, the Tomei Expressway has been designated a Post-Tremor Emergency Transport Road.

Approximately 220km, or roughly 70% of the total length of the Tomei Expressway lie within the region subject to intensified countermeasures against the risks of an earthquake disaster. This stretch of the Expressway has a total of 254 bridges. The designation of the Expressway as a post-seismic Emergency Transportation Route gave rise to the need to take suitable measures to retrofit the bridges concerned. Since the damage caused to the bridges will have a major effect on the restoration

- 
- (I) Manager, Second Maintenance Section, Tokyo First Operation Bureau,  
Japan Highway Public Corporation  
(II) Engineer, Second Maintenance Section, Tokyo First Operation Bureau,  
Japan Highway Public Corporation



work after the earthquake, the decision was taken to implement countermeasures specifically aimed at these bridges.

The most important anti-seismic measure for a bridge is the prevention of its superstructure from falling. The countermeasures have therefore concentrated on the fortification of the bridges' substructures to provide greater safety for the superstructure. To assess the resistance of bridges' substructures to earthquakes and to conduct retrofit techniques on the basis of unified principles, a Retrofit Measures Investigating Group was appointed to define the Specifications for the Investigation of Seismic Retrofit Measures (Ref. 1). In addition to the preventive measures to protect the general superstructures and constructions (devices for preventing superstructures from falling and length between the end of the girder and the edge of the superstructure, etc.) the preventive measures to safeguard against bridge collapse also concentrate on the substructures.

This paper introduces the above guideline specifications and describes some examples of how retrofit techniques are implemented on the basis of these specifications.

## ASSESSMENT

### Procedure for Assessing Earthquake Resistance

The anti-seismic assessment procedure for bridge is summed up in Fig. 1.

Resistance to earthquake is assessed by estimating the liquefaction behavior of the surrounding soil base, the safety of the bridge pier and foundation, and the safety of the abutment and backfill.

These investigations have been carried out on the basis of, and in accordance with, the Specifications for the Investigation of Seismic Retrofit Measures (Ref. 1), and this paper gives an outline of the assessment method. For fuller details, reference is made to the existing report (Ref. 2) which has already been published.

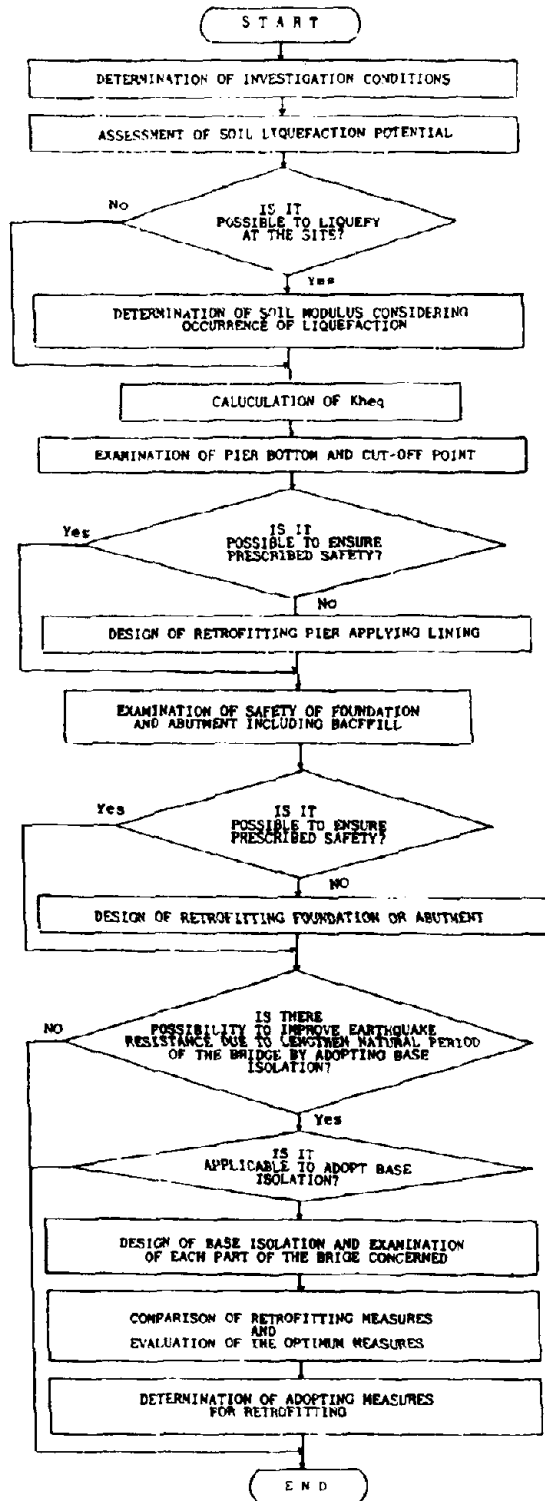


Fig.1 Flow Chart Showing for Procedure of Seismic Retrofitting for Bridges

Determining The Magnitude of Seismic Movement in The Affected Area

The size of the geographic fault associated with the anticipated Tokai Earthquake and the location of this fault are as shown in Fig. 2. The magnitude of the earthquake is assumed to be 8.0.

The intensity of the earthquake considered likely to occur in the Tokai Area, that is, the Tokai Earthquake, is evaluated in terms of the design elastic seismic coefficient. The elastic seismic coefficient is calculated from the earthquake's magnitude, the distance from the epicentral area of the tremor to the bridge location, the ground classification, the natural period of the particular substructure concerned, and the damping factor.

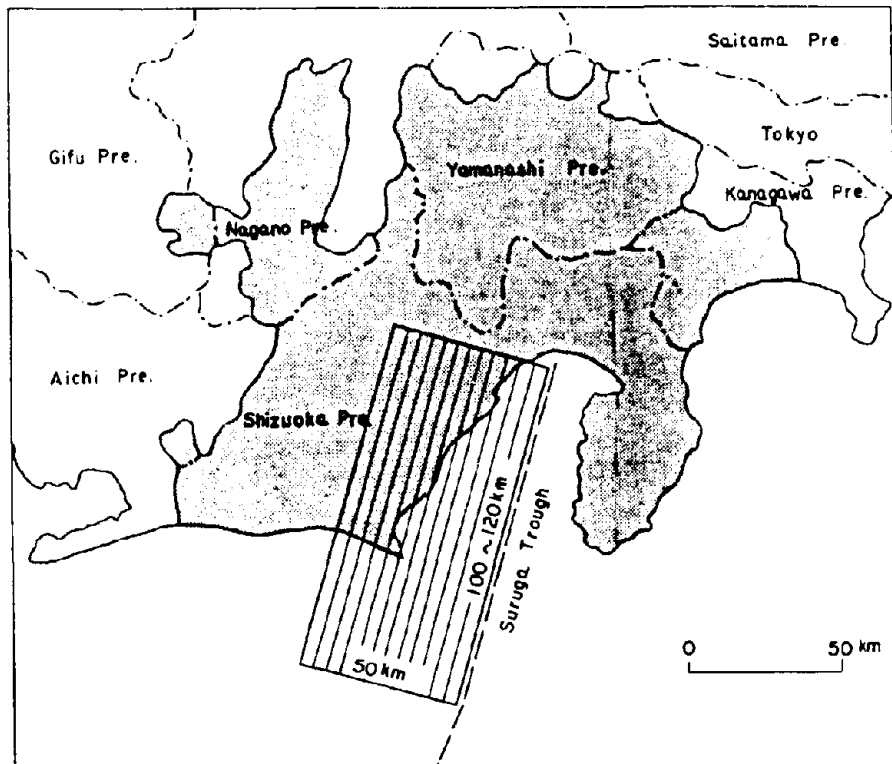


Fig. 2 Fault Model for Earthquake Anticipated in the Tokai Region and Geographic Zone Designated for Intensive Fortification Measures

## Assessment of Liquefaction Potential

The assessment of the liquefaction behavior of the soil surrounding the bridge location involves the following procedure which is schematically shown in the flow chart Fig. 3.

- a) Presence of a layer required for the assessment of soil liquefaction behavior
- b) Simple estimation of liquefaction potential from the resistance factor (I)
- c) Assessment allowing for irregularities in the soil's shear stress (II)
- d) Detailed assessment by dynamic analysis (III) if the earthquake is considered to have a major effect on the structures.

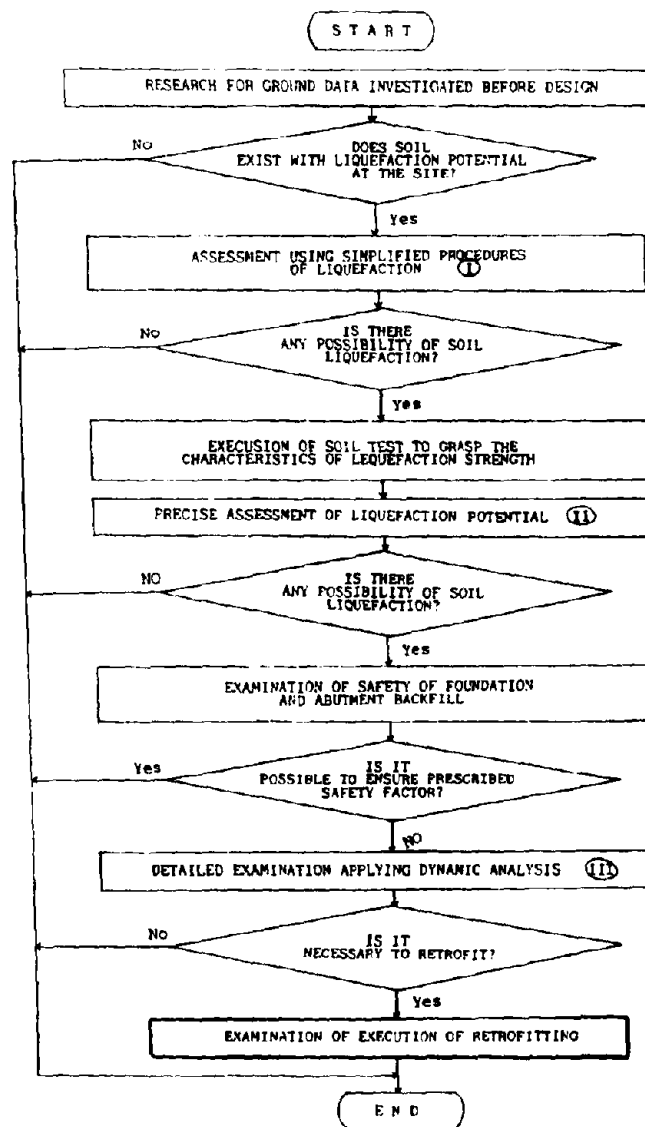


Fig. 3 Procedure for Examining Foundation Retrofitting by Considering Soil Liquefaction

## Assessment of Bridge Piers

The seismic resistance of the bridge piers constructed from steel-reinforced concrete is verified for the cut-off points of the main reinforcing bars and the bottom of the pier. The examination procedure for the bottom varies according to the failure pattern, that is, according as to whether flexural or shear failure precedes. If flexural failure precedes, the ductility of the pier structure is examined. If failure occurs in the shear mode, the shear capacity is examined.

Thus, the cut-off points are examined on the basis of either their flexural capacity or their shear capacity. Fig. 4 shows the examination procedure for a column-type or wall-type pier.

If the pier is a frame structure, it is modelled with a framework structure to examine the cross-section by an analysis procedure which takes the non-linear behavior into account.

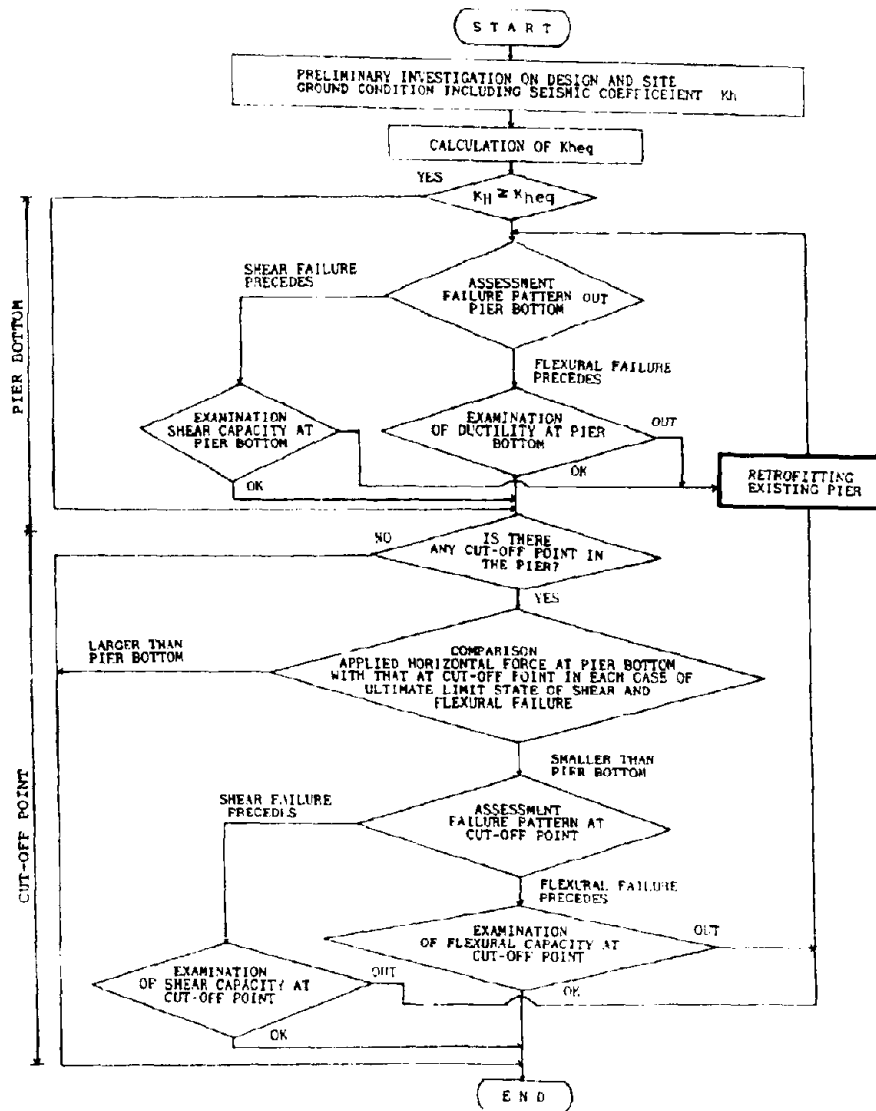


Fig. 4 Procedure for Evaluating Vulnerability of RC Piers

### Assessment of Foundations

There are essentially three different types of foundation in use; spread foundations, pile foundations, and caisson foundations.

For spread foundations, the perpendicular ground reaction is examined in terms of the ultimate perpendicular bearing capacity and the horizontal load in terms of the ultimate horizontal bearing capacity. The overturning movement is examined in terms of the moment of resistance with respect to the moment of overturn at the end face of the foundation.

For pile foundations, both the perpendicular and the horizontal loads are supported by the pile alone so that the reaction at the pile head is examined in terms of the ultimate bearing capacity. The sectional forces acting on the pile are examined in terms of the capacity of the pile. The displacement of the pile foundation is examined in terms of the degree to which it is possible to safeguard seismic resistance for the bridge as a whole.

For caisson foundations, the perpendicular ground reaction is determined in terms of the ultimate perpendicular bearing capacity and the horizontal load in terms of the ultimate horizontal bearing capacity. The moment of overturn is examined on the basis of the ultimate moment of resistance, consisting of the ultimate perpendicular and ultimate horizontal bearing capacity. The displacement of caisson foundations is examined in terms of the degree to which it is possible to safeguard seismic resistance for the bridge as a whole.

### Abutments and Backfills

The seismic resistance of the abutments is determined by examining the capacity in the ultimate condition of sectional failure.

Backfill assessment is carried out by the circular sliding method. Initially, the safety factor is determined by assuming that there is no abutment. If this factor has a value of 1.0 or less, the abutment piles are considered as being landslide-suppressing piles and the safety factor is then investigated on this basis.

Fig. 5 shows the procedure for examining the seismic resistance of the abutments and backfills.

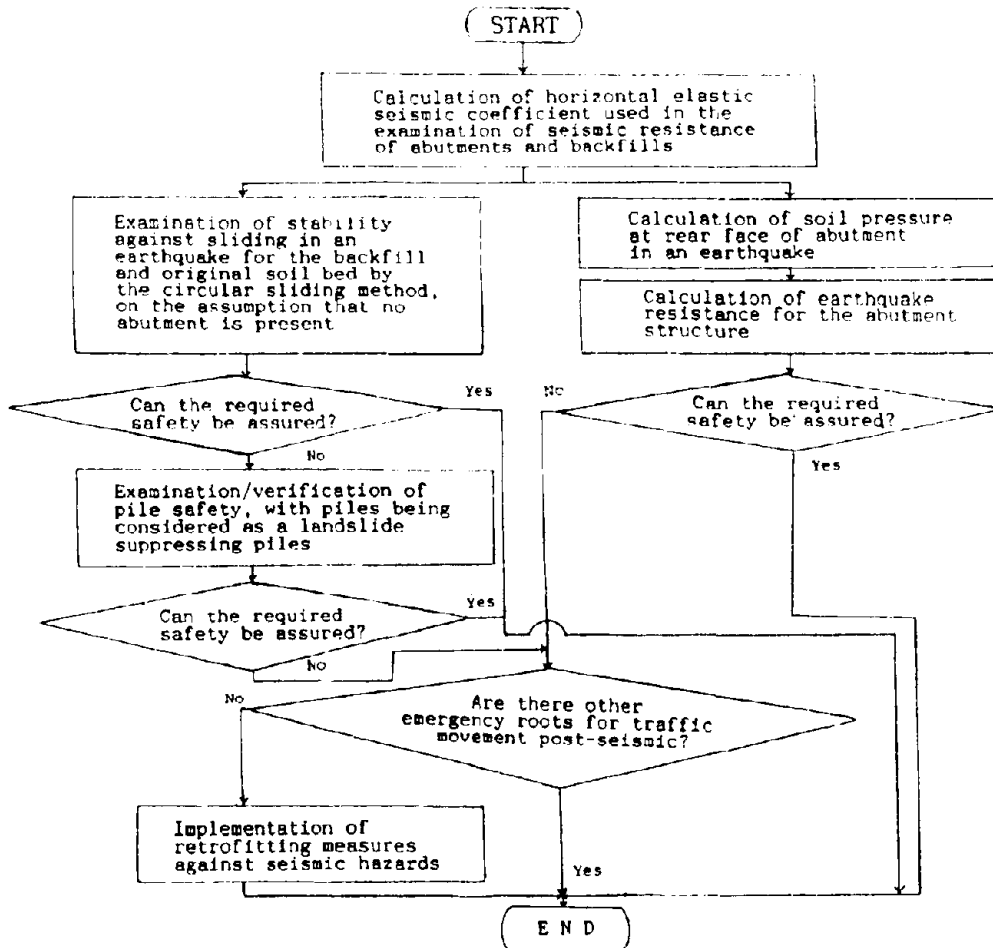


Fig. 5 Procedure for Examining the Seismic Resistance of Abutments and Backfills

## RETROFITTING MEASURES AND SUITABLE EXAMPLES

### Structures and Methods for Retrofitting

The above methods are used to study the seismic capacity of the bridges in the area assumed to be in the disaster zone of the anticipated Tokai Earthquake. If these assessment procedures demonstrate that seismic resistance cannot be assured, suitable countermeasures must be taken.

Table 1 sums up the countermeasures employed for the bridges on the Tomei Expressway. When it has been concluded that the soil surrounding the bridges is liable to liquefaction, this is reflected in the examination of the structures. For the foundation structures such as the piles, seismic resistance is examined by reducing the soil factors such as the

modulus of deformation. The procedure used for determining the slide safety factor of circular sliding on the backfill takes the rise in pore water pressure in the liquefied stratum into account.

Table - 1 Countermeasures Applied to Bridges

Target Structure	Countermeasure	Bridges Mainly Affected
Pier	RC lining	Torisaka Viaduct Sugegaya Viaduct
	RC shear wall	Nagasaki Viaduct Nishiokazu Viaduct
Foundation	Pile increase	Osakagawa Bridge Kuno Viaduct
Backfill	Coffering with steel pipe piles	Nagamachi Bridge Enoo Bridge
	Counterweight fill construction	Nagasaki Viaduct

These typical countermeasures are explained below in closer detail.

Example 1 : RC Lining

The provision of an RC lining is one of the retrofitting methods available for pillar-type or wall-type piers. There are various precedents in which retrofitting has been attempted with an RC lining, and to explain the method let us here introduce the RC lining retrofitted on the Torisaka Viaduct.

The Torisaka Viaduct is a bridge construction with a total bridge length of 218m. Its substructure consists of 12 piers and 2 abutments. Its superstructure consists of continuous 5+4+4 span RC hollow slab-bridge sections. Fig. 6 is a general view of the viaduct bridge. The piers are of double-pillar construction and the pile foundation consists of 508mm diameter steel-pipe piles.

The seismic resistance of the pier structure is investigated as shown in Fig. 4. The converted elastic seismic coefficient (Kheq) used for examining the seismic resistance is determined from factors such as the nature of the soil and the natural period of the substructure. The values are presented in Table 2. These values for the elastic seismic coefficient were used to check the ductility of the base sections of the typical piers. The results are shown in Table 3 and demonstrate that the base sections of the piers are safe. The seismic resistance of the cut-off points were investigated by comparing the acting moment of bending (M) and the bending capacity (Mu) applicable when the ultimate load acts on



the cut-off points. Table 4 gives the results. In the axial direction of the bridge P7, M becomes greater than  $\mu_u$ . For the movable piers P1, P5, and P9, M is smaller than  $\mu_u$  so that their safety is assured. In view of these results, the decision was taken to effect retrofitting work on piers P2, P3, P4, P6, P7, P11, and P12, with the reinforcement design aimed at the fixed piers similar in design to pier P7.

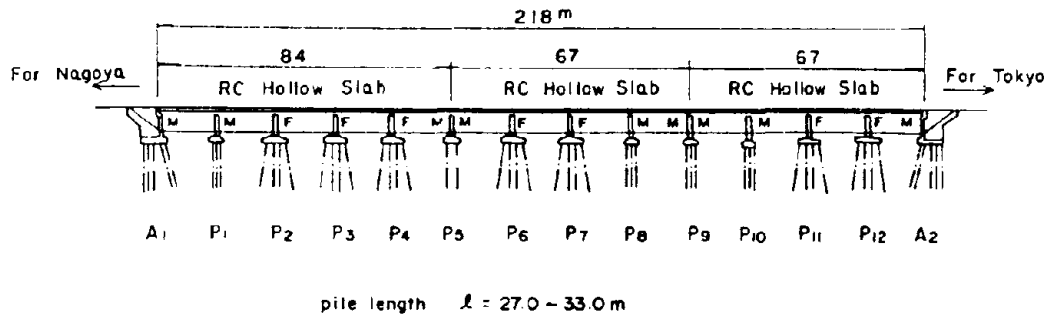


Fig. 6 General Schematic View of the Torisaka Viaduct Bridge

Table 2 - Converted Elastic Seismic Coefficient (Kheq)

		P1	P2	P3	P4	P5
A1 }	Bridge axis	0.51	0.87	0.87	0.87	0.51
	P5 Perpendicular	0.66	0.66	0.66	0.66	0.66
		P5	P6	P7	P8	P9
P5 }	Bridge axis	0.51	1.07	1.07	0.52	0.53
	P9 Perpendicular	0.66	0.66	0.66	0.66	0.66

Table 3 - Determination of the Ductility Factor ( $\mu$ ) for the Pier Base Sections

		$\delta y$ (cm)	$\delta u$ (cm)	$\mu_a = \delta u / \delta y$	$\delta o$ (cm)	$\mu = \delta o / \delta y$	$\mu_a > \mu$
P1	Bridge axis	4.25	32.2	6.0	3.25	0.76	OK
	Perpendicular	3.46	44.8	6.0	1.40	0.46	OK
P5	Bridge axis	4.21	35.1	6.0	2.90	0.69	OK
	Perpendicular	3.38	54.6	6.0	5.80	1.72	OK
P7	Bridge axis	4.76	23.4	4.9	15.89	3.34	OK
	Perpendicular	3.41	52.7	6.0	6.73	1.97	OK
P9	Bridge axis	4.71	39.8	6.0	4.24	0.90	OK
	Perpendicular	2.25	68.0	6.0	7.62	3.39	OK

$\delta y$  : Displacement when steel reinforcing bar yields (cm)  
 $\delta u$  : Ultimate displacement (cm)  
 $\mu_a$  : Allowable ductility factor  
 $\delta o$  : Actual horizontal displacement after allowing for the ductility of the pier base sections (cm)  
 $\mu$  : Ductility factor

Table 4 - Examination of Flexural Capacity for the Cut-off Points

		Po(tf)	h(m)	M(tfm)	Mu(tfm)	M < Mu
P1	Bridge axis	32.8	4.73	155.1	223.0	OK
	Perpendicular	30.2	5.82	175.8	354.3	OK
P5	Bridge axis	18.4	4.93	90.7	172.1	OK
	Perpendicular	60.1	6.01	361.2	373.4	OK
P7	Bridge axis	133.2	5.03	670.0	338.7	OUT
	Perpendicular	62.1	6.03	374.2	481.8	OK
P9	Bridge axis	39.7	4.64	184.2	284.7	OK
	Perpendicular	91.6	6.90	632.0	786.5	OK

$P_o$  : Converted horizontal force (tf)  
 $h$  : Height from position at which  $P_o$  acts to the cut-off location (m)  
 $M$  : Action moment at cut-off location (tfm)  
 $M_u$  : Ultimate bending moment (tfm)

The purpose of retrofitting the main steel-reinforced concrete cut-off points is to ensure that they are not damaged before damage occurs at the base sections. The retrofitting work consists of a steel-reinforced concrete lining applied around the pillar cross-section so that the flexural capacity ( $M_u$ ) after the retrofit will be greater than the acting flexural moment ( $M$ ). This means that the condition  $M_u > M$  is met. The 150mm thick concrete lining around the pillar has upright D22 steel inserts. The space between the concrete lining and the old concrete forms the joint and has been prepared with chipping 20mm of the thickness of the surface of the old concrete. Fig. 7 shows an example of the RC lining retrofit work.

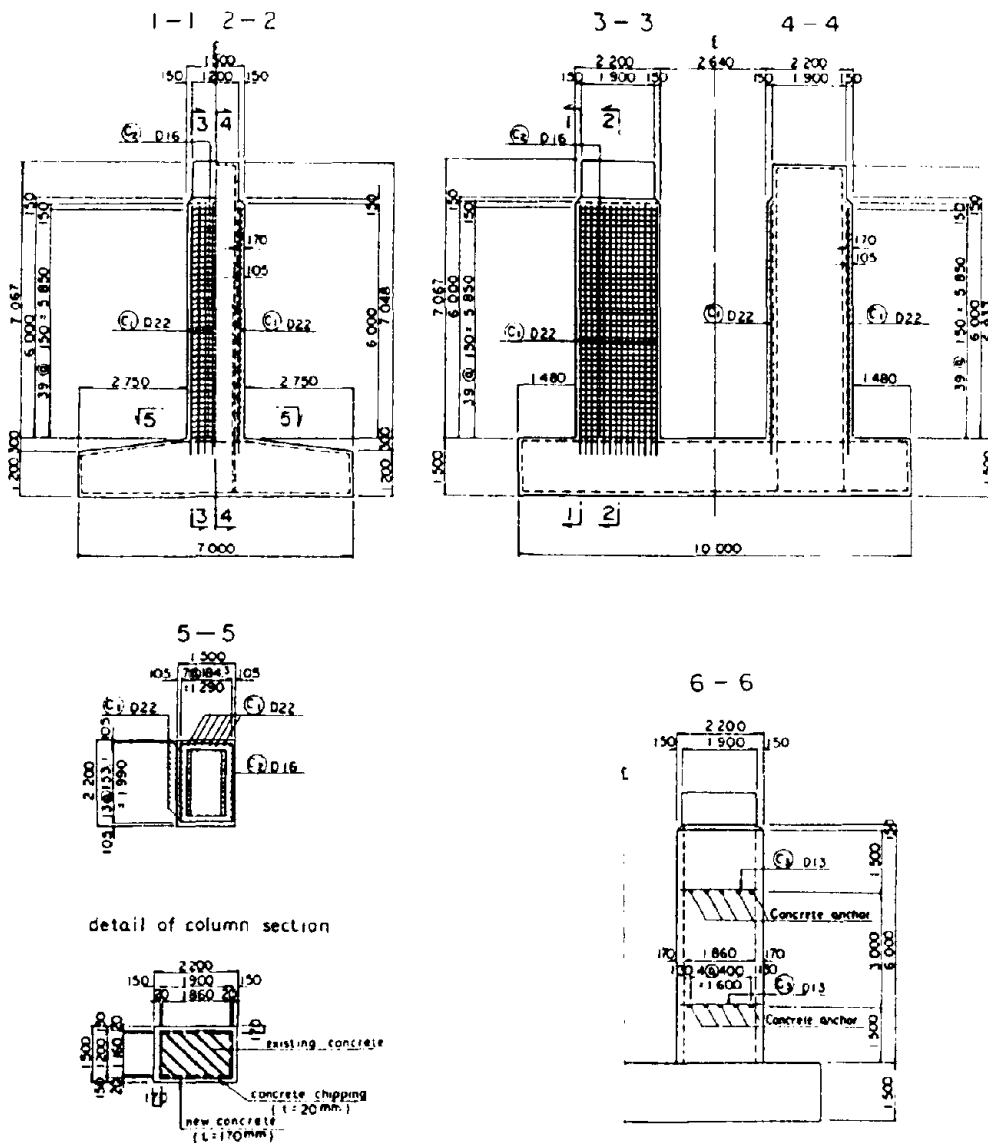


Fig. 7 Example of Seismic Retrofit Using an RC Lining

### Example 2 : RC Shear Wall

The Nishiokazu Viaduct (Ref. 4) has frame-construction piers which were retrofitted to render them earthquake-proof by erecting a steel-reinforced concrete (RC) shear wall designed to enhance their seismic resistance through the construction of a wall between the pillars.

The superstructure of the Nishiokazu Viaduct consists of a continuous five-span RC hollow slab and simple PC post-tensioning T beams. Its substructure consists of two abutments and five piers over a total bridge length of 101m. The piers are constructed so that P1 - P4 are double-pillars while P5 is a frame structure. The pile foundation consists of the 508mm diameter steel-piles. A schematic general view of the viaduct bridge is presented in Fig. 8.

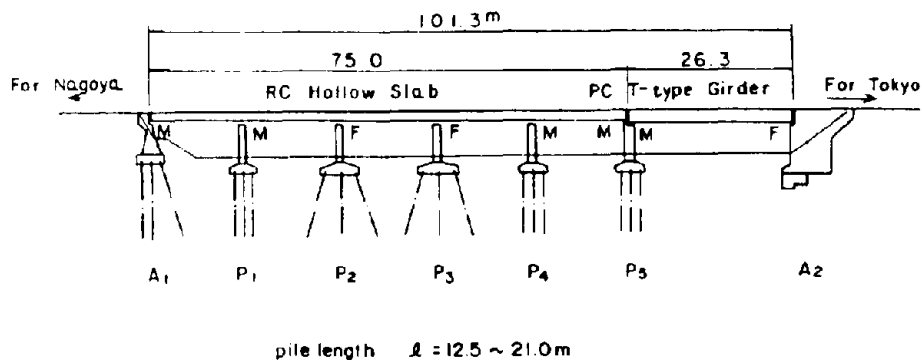
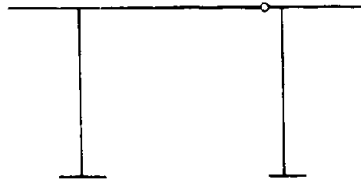


Fig. 8 Schematic General View of the Nishiokazu Viaduct Bridge

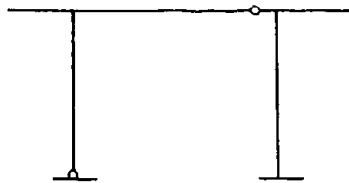
The seismic capacity of piers P1 - P5 in the axial direction of the bridge was investigated by the procedure shown in Fig. 4. Seismic capacity of pier P5 in the direction perpendicular to the bridge axis was studied by means of a non-linear analysis using a framework model since this pier is a frame construction. The seismic capacity for P5 in the direction perpendicular to the bridge axis is explained below.

The converted seismic coefficient ( $K_{heq}$ ) of pier P5 is 0.88 in the axial direction and 0.79 in the direction perpendicular to the axial direction. The investigation results, obtained by entering the above converted seismic coefficient as the input data to verify the seismic resistance, indicated that there was no need for retrofitting in the axial direction but that it was necessary to retrofit the structure in the perpendicular direction. The framework model for the perpendicular direction is a planar model made from beam and pillars as the members and the pillar bottoms for anchorage. Planar analysis was performed by applying the dead load reaction force at the top, the deadweight of the pier structures, and the horizontal seismic forces equivalent to the seismic intensity. The results of this analysis are collated in Fig. 9. A plastic hinge was found to form at the beam and the roots of the pillars on both sides, when the elastic seismic coefficient ( $k_h$ ) became the converted elastic seismic coefficient  $K_{heq} = 0.79$ .

(1) Beam failure for  $K_h = 0.58$



(2) Pillar root failure for  $K_h = 0.73$



(3) Failure of both pillar roots for  $K_h = 0.79$  (ultimate load)

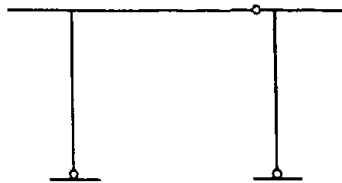


Fig. 9 Formation of Plastic Hinge and Corresponding Elastic Seismic Coefficient for P5 in the Direction Perpendicular to the Bridge Axis

When the beam and pillars are retrofitted separately, it is considered difficult to retrofit the beam section. For this reason a seismic shear wall was used with a simultaneous retrofit for the beam and pillars. fig. 10 is a schematic view of the seismic shear wall whose shape was determined by comparative shear capacity evaluation. In the examination, the shear capacity ( $Q_u$ ) has to be greater than the acting shear force ( $S$ ). The shear capacity is the sum total of the pillars' shear capacity and the shear capacity of the seismic shear wall. The acting shear force ( $S$ ) is multiplied the dead load of the superstructure and the substructure deadweight by the seismic coefficient. The results were as follows.

$$Q_u = 627 \text{ tf} > S = 448 \text{ tf}$$

To bind the seismic shear wall to the substructure, a 20mm thick chipping layer was applied and the 19mm dia. anchor rods were inserted into the structure to achieve an integral structure. Since it is difficult to cast concrete at the bottom of the beam, non-contracting mortar was injected instead.

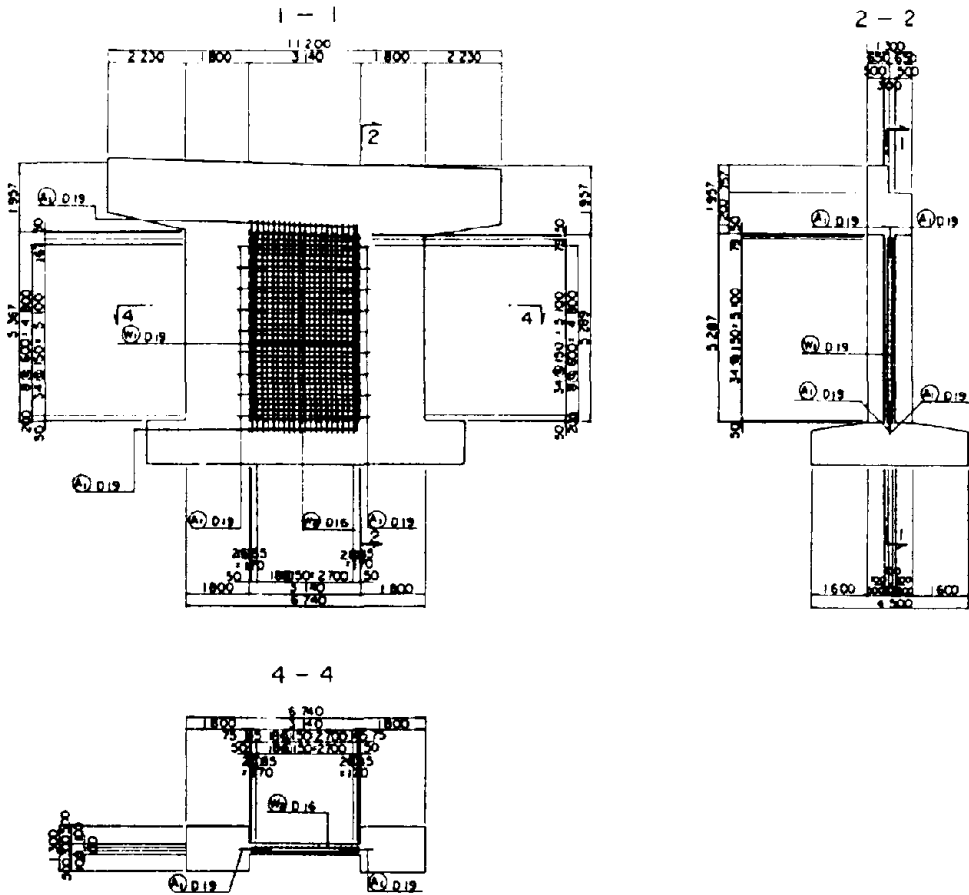


Fig. 10 Retrofit Example Using a Seismic Shear Wall

Example 3 : Pile Increase

Retrofitting measures on the Kuno Viaduct (Ref. 5) took the form of pile increase at the foundation of abutment A1.

The superstructure of the Kuno Viaduct consists of continuous 2+3+3 steel span non-composite plate girders. Its substructure consists of two abutments and seven piers, with a total bridge length of 240m. The abutments are an inverted T-shaped construction and the piers have a 609mm dia. steel-pipe pile foundation. Fig. 11 shows a schematic general view of the bridge as a whole.

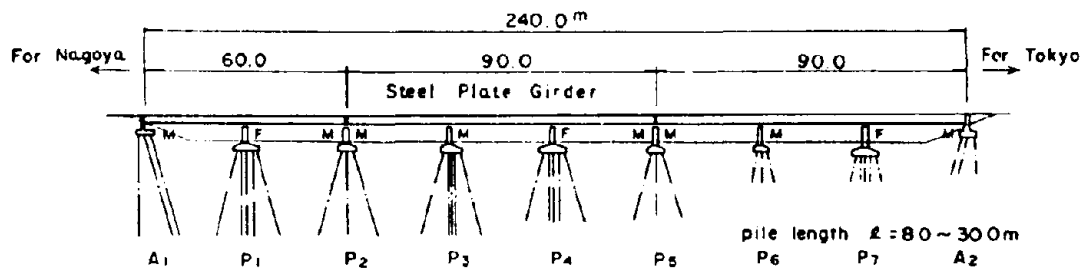


Fig. 11 Schematic General view of the Kuno Viaduct

The seismic resistance of the foundation of abutment A1 was examined by calculating its stability by the displacement method and by performing a dynamic analysis using the finite element method. The elastic seismic coefficient was taken as  $k_h = 0.37$ . The results of the stability calculation are gathered in Table 5. While the axial force is smaller than the ultimate bearing capacity, the stress for the steel-pipe was 6,100 kg.f./sq. cm, with the stress at the yield point being  $\sigma_y = 2,400$  kg.f./sq. cm.

Table 5 - Results of Stability Calculation

		Unit	Calculated Value	Allowable Bearing Capacity x Safety Factor = Ultimate Bearing Capacity
Axial force	PN	tf/each	200	$130 * 2 = 260$
Horizontal force	PH	tf/each	36	$9 * 2 = 18$
Pile head moment	Mt	tf/each	-146	-
Maximum underground moment	Mm	tf/each	-149	-
Horizontal displacement of ground surface in design	$\delta$	mm	83	-
Stress for pile	$\sigma_s$	kgf/cm <sup>2</sup>	6,100	Stress at yield point $\sigma_{sy} = 2,400$

Seismic response analysis was carried out for the A1 abutment and the soil surrounding it. For the response analysis, the dynamic analysis program FLUSH - a program using the finite element method - was employed. The seismic movements entered as the input data were the seismic waves for the Hachinohe port (superior for long-term components) and the Kaihoku bridge (superior for short-term components), the maximum acceleration entered was 370 gal. The results of the response analysis show that the stress for the pile structure is 8,000 kg.f./sq.cm.

Lateral motion of abutment A1 was confirmed from the inspection results. Investigation by calculating the lateral motion led to the conclusion that such motion is possible. For this reason, the decision was taken to retrofit the abutment A1 foundation to ensure that a major earthquake can be accommodated. This includes measures to meet the lateral movements of abutment A1 in the ordinary condition.

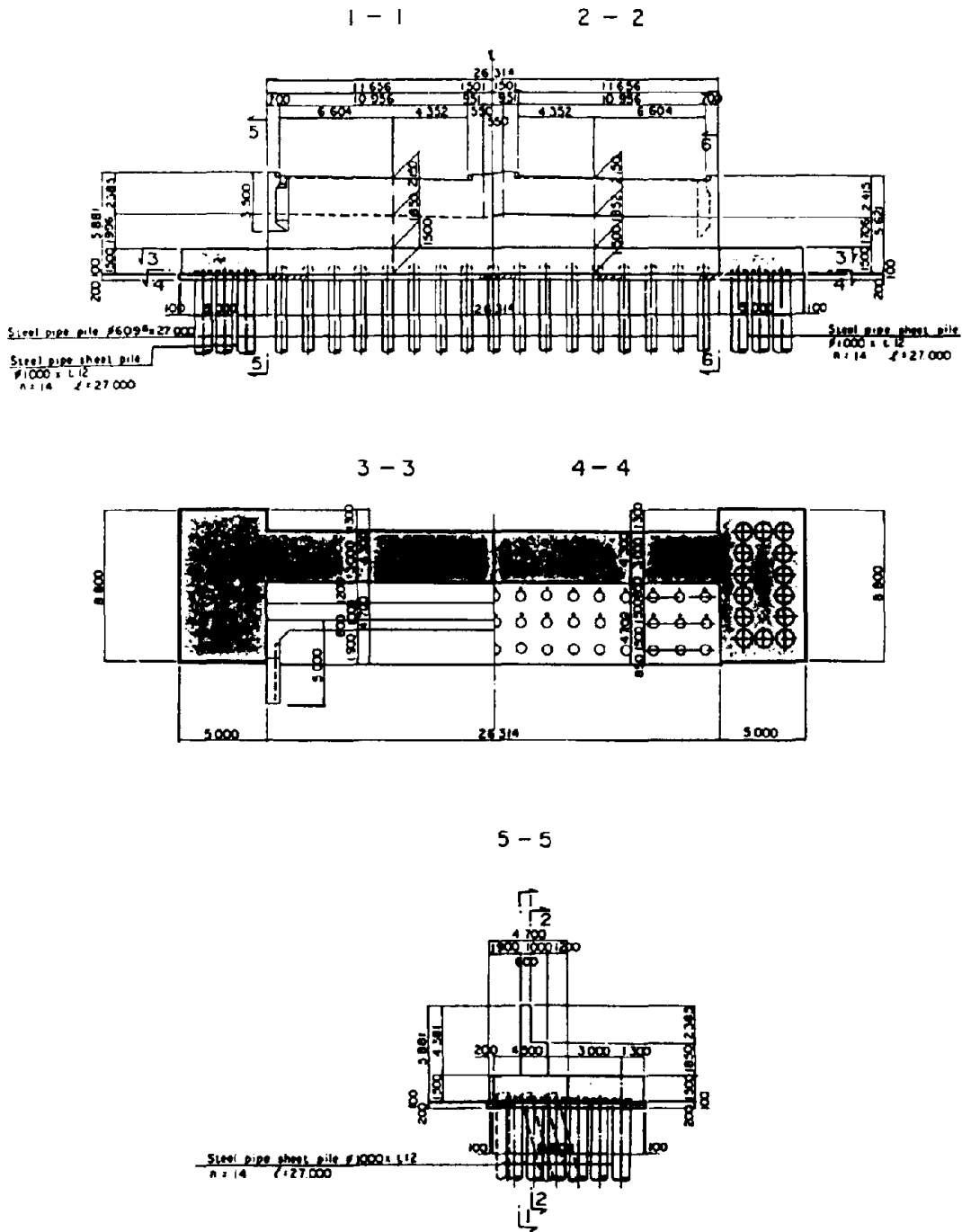


Fig. 12 Example Seismic Retrofit Using Piles Increase



The retrofit of the foundation was implemented by way of pile increase. Fig. 12 outlines the pile increase method in which steel-pipe sheet piles foundations were laid at both sides of the abutment. The steel-pipe/sheet piles on either side were joined with concrete beams positioned in front of the abutment so that it will share the horizontal force of the abutment. The abutment foundations, including the pile increase, were examined by performing dynamic analysis. The analysis results indicate that the abutment's stress of the 609mm dia. steel-pipe pile is 2,300 kg.f/sq.cm. The new and old concrete were rendered integral, using chipping and anchor steel bars.

#### Example 4 : Coffering by Execution of Steel-Pipe Piles

Coffering is designed to stabilize the backfill soil by using the steel sheet piles or steel-pipe piles. An example of coffering can be found at the Enoo Bridge (REF. 6).

The superstructure of the Enoo Bridge consists of continuous three-span non-composite plate girders. Its substructure consists of two abutments and two piers, with a total bridge length of 115m. The A1 abutment and the piers have the 609mm dia. steel-pipe piles foundation. The A2 abutment has a spread foundation. Fig. 13 shows a schematic general view of the bridge as a whole.

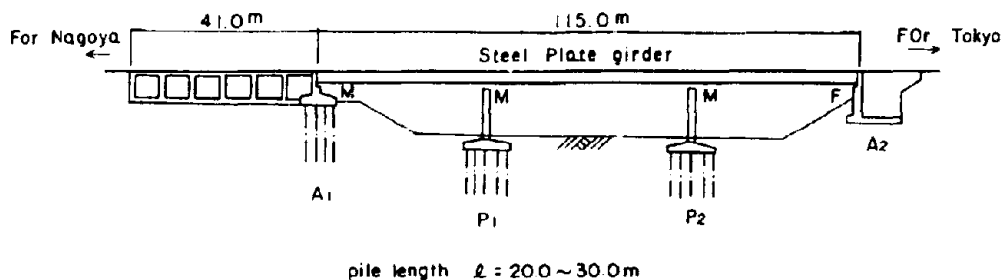


Fig. 13 Schematic General view of the Enoo Bridge

The seismic resistance of the backfill was examined, using the procedure shown in Fig. 5. The elastic seismic coefficient for examining the seismic resistance was taken as  $kh = 0.21$ . In the examination, attention was primarily given to the transverse direction of the road by concentrating on the backfill at the side of abutment A1. The safety factor for circular sliding of the backfill soil is as shown in Fig. 14, with a numerical value under 1.0, the minimum value for the safety factor being 0.8. An elasticity analysis using the finite element method was performed on the soil fill in the transverse direction of the road. The results show that the horizontal displacement of the soil fill shoulder is 130cm. This led to the decision to carry out a seismic retrofit to stabilize the soil fill at abutment A1.

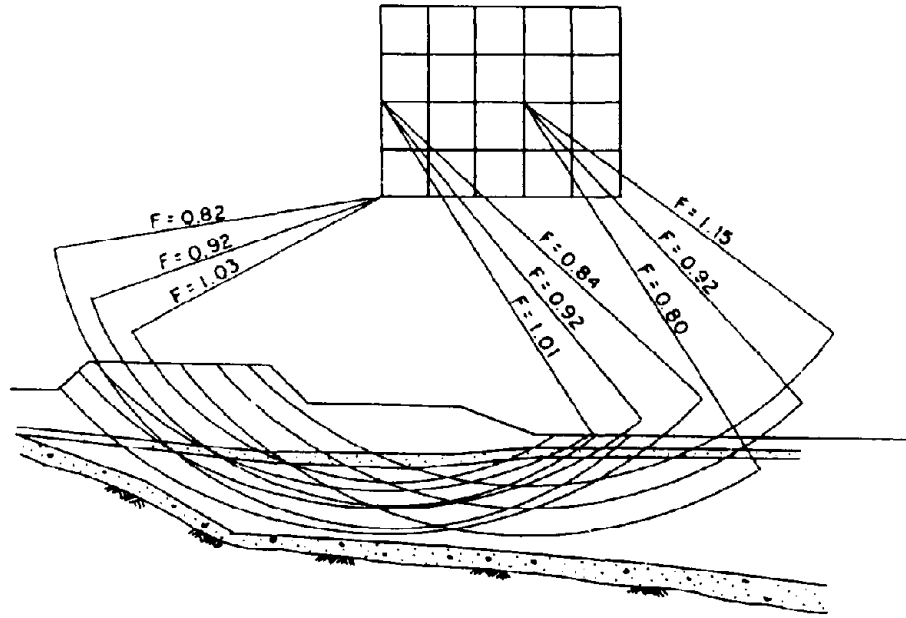


Fig. 14 Circular Slide Safety Factor

The soil backfill was carried out with a view to achieving a structure offering a circular slide safety factor of 1.0 or better than 1.0. The tight-fit steel-pipe piles were driven in near the outer end of the soil fill. The pile heads were covered with concrete. The circular slide safety factor after allowing for the steel-pipe piles were 1.3. Analysis using the finite element method was carried out and the results indicate that the horizontal displacement of the soil fill shoulder is 41cm, thus clearly demonstrating the improvement achieved by retrofitting.

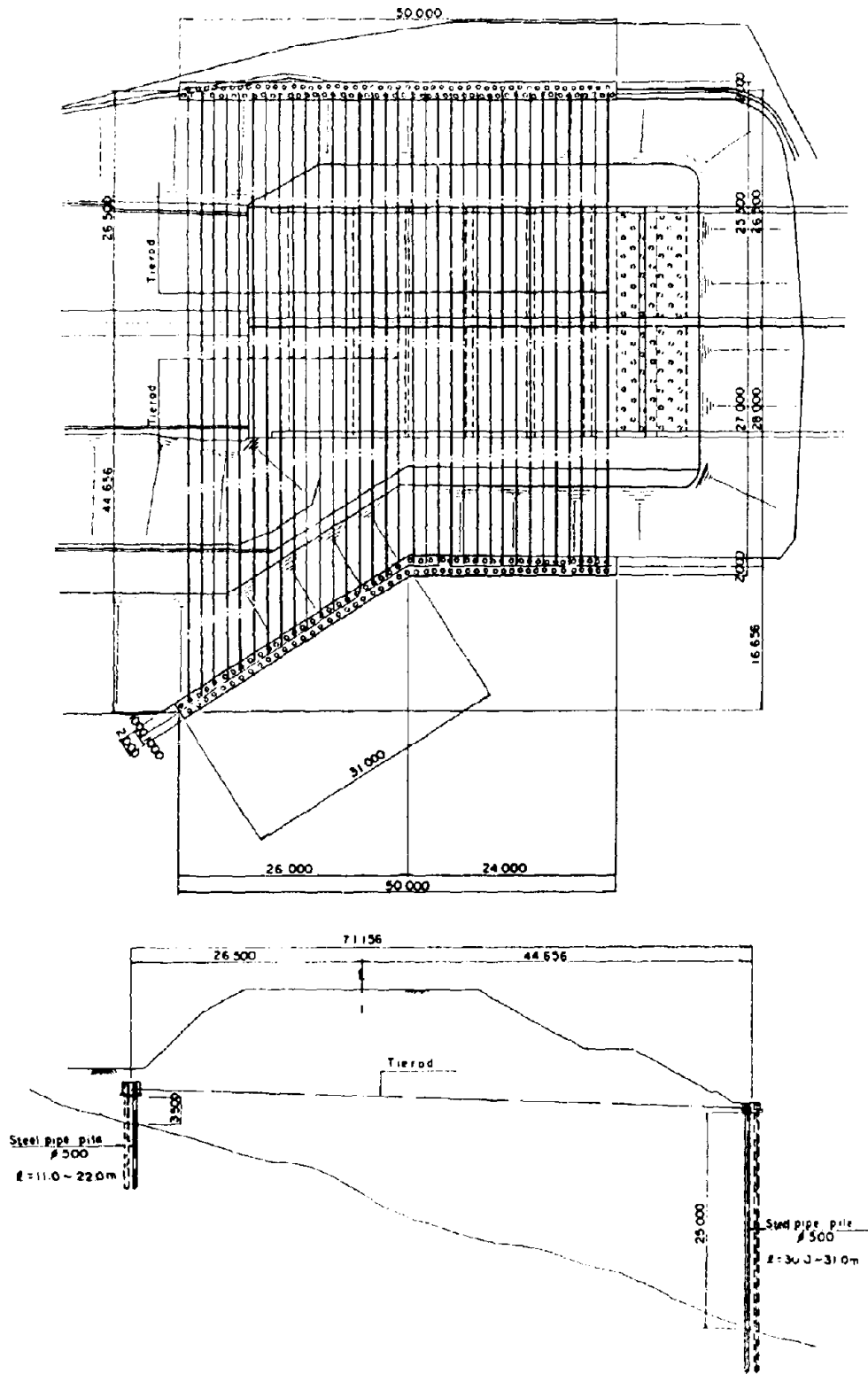


Fig. 15 Example of Seismic Retrofitting by Coffering

### Example 5 : Counterweight Fill

Retrofitting measures were carried out on the back fill of the Nagasaki Viaduct (Ref. 7) in the form of a counterweight fill.

The superstructure of the Nagasaki Viaduct consists of a continuous eightfold simple PC pretension T beam arrangement. Its substructure is comprised of two abutments and seven piers over a total bridge length of 100m. The pile foundations have 400mm diameter steel-reinforced (RC) concrete piles. The abutments are of frame construction with a top bedplate. There are three rows of pillars in the perpendicular direction. The backfill forms a footing overspill. A schematic general view of the viaduct bridge is presented in Fig. 16.

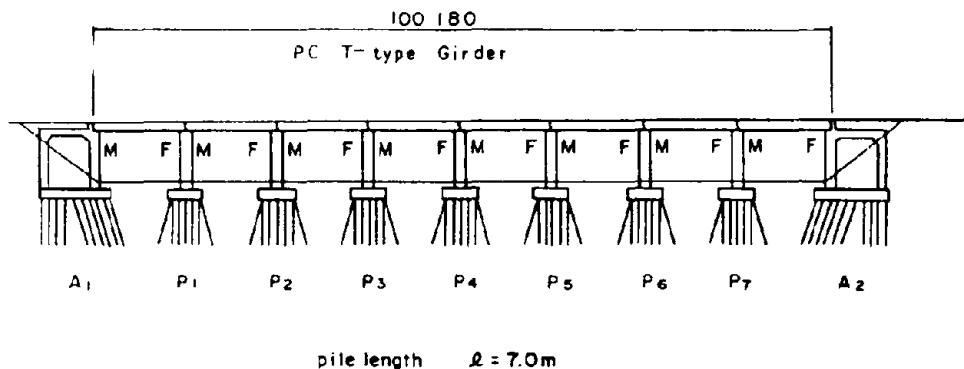
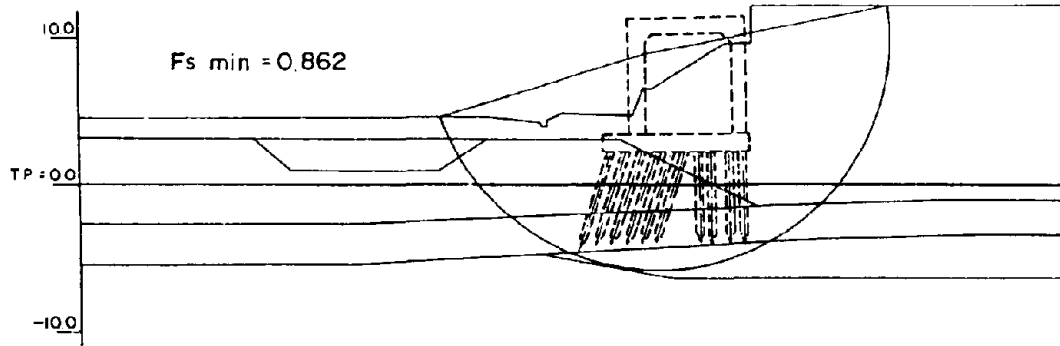


Fig. 16 Schematic General View of the Nagasaki Viaduct

The seismic resistance of the backfill was examined, using the procedure shown in fig. 5. The elastic seismic coefficient for examining the seismic resistance was taken as  $kh = 0.23$ . Examination was conducted on the backfill at the side of abutment A2 by using the circular sliding method for the direction of the road. The slide safety factor, allowing only for the elastic seismic coefficient, was 1.35. There is a sand stratum underneath the bearing stratum of abutment A2, and the examination results concerning the liquefaction behavior of this formation revealed a distinct possibility of liquefaction. The effects of liquefaction of this stratum formation were assessed in terms of the rise in pore water pressure, in other words, in terms of the reduction in effective stress, and the slide safety factor was found to be 0.86, as shown in Fig. 17 (a). Since the slide passes through the front end of the piles, it is considered possible for the bridge to be liable to the risk of overturning.

Retrofitting of the backfill was performed with a view to achieving a circular slide safety factor in the 1.0. For this purpose, the counterweight fill method was employed by making a low fill in front of the backfill to increase its resistance. Fig. 18 gives a schematic general view of the counterweight fill.

(a) No measures



(b) Construction of a Counterweight Fill

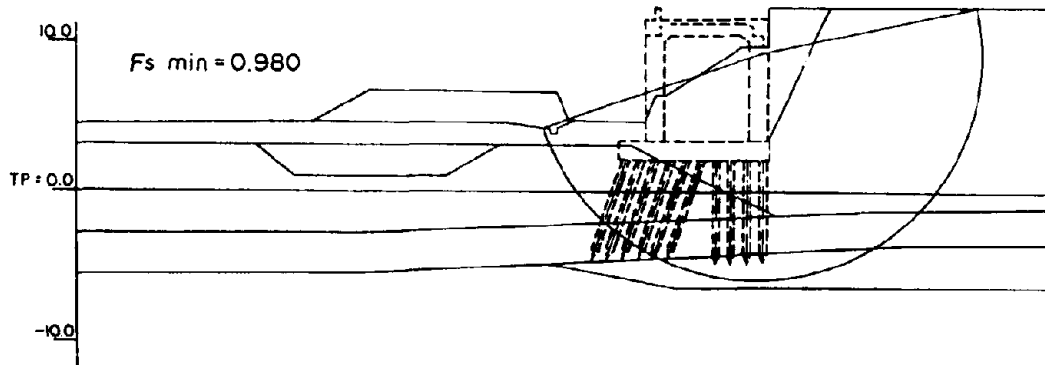


Fig. 17 Circular Slide Safety Factor

As shown in Fig. 17 (b), the slide safety factor allowing for the counterweight fill was approximately 1.0, with a value of 0.98 resulting, when the rise in pore water pressure is taken into consideration. The reason why no counterweight fill was made in front of the abutment is because the area in front of the abutment is used as a road. The height of the counterweight is roughly 3m.

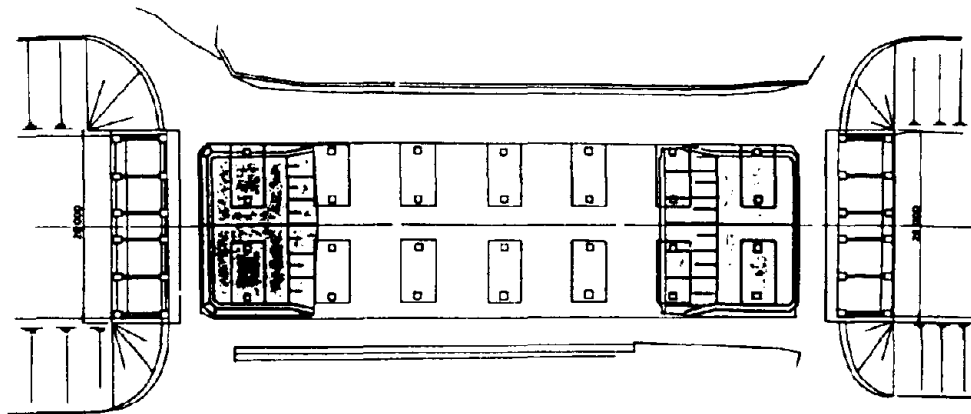
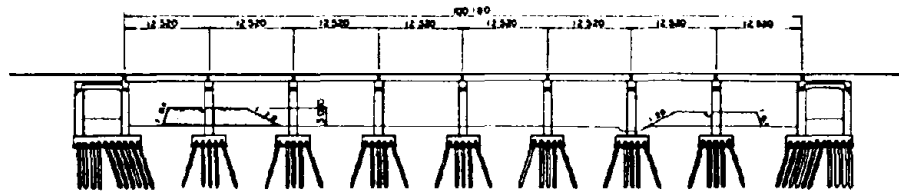


Fig. 18 Example of Seismic Retrofit Work Using a counterweight Fill

## Main Materials and Costs

Table 6 presents the main materials used and the costs involved in the construction work undertaken to implement the above retrofit measures.

Table 6 Main Materials and Costs

Counter-measures	Name of Bridge	Main Materials					Costs (million yen)	Remarks
		Concrete (m <sup>3</sup> )	Steel Reinforcing Bars (tf)	Steel-Pipe Piles (tf)	Tie-Rods (tf)	Soil Fill Volume (m <sup>3</sup> )		
RC Lining	Torisaka Viaduct	196	34.7	-	-	-	45	For 7 piers
RC Shear Wall	Nisiokazu Viaduct	10	2.1	-	-	-	3	For 2 piers
Piles Increase	Kuno Viaduct	248	27.0	220.8	-	-	92	For 1 pier
Coffering	Enoo Bridge	-	-	803.5	22.6	-	549	In 1 location
Counter-weight Fill	Nagasaki Viaduct	-	-	-	-	1515	-	In 2 location

## CONCLUSION

The Japan Highway Public Corporation has established a record of ten seismic retrofit construction projects on the bridges located on the Tomei expressway. This paper presents five of the most typical examples of these retrofit measures.

Further seismic retrofit measures are planned. These seismic measures are established, however, on a variety of assumptions on which the calculations are based. These hypotheses include the anticipated scale of the earthquake, the location of the seismic center, the structure in the location concerned or its topography and geological formation. In view of this, it is recognized that there are limits to the way in which the problems can be handled by seismic retrofit measures alone. In this

context, it is therefore felt essential to collect data on restoration work, conduct disaster prevention exercises, study precedents of past disasters, and establish post-seismic inspection procedures. All of these efforts should accompany and complement the seismic retrofit measures to ensure early road restoration in case of disaster.

#### ACKNOWLEDGMENTS

This project was examined and discussed by the Committee for Investigating Seismic Retrofitting Countermeasures for the Tomei Expressway Bridges. This Committee was set up by the Japan Highway Public Corporation and is chaired by Professor Shoji Ikeda of Yokohama National University. The authors would like to sincerely thank the chairman and all members of the Committee for their valuable guidance throughout the course of this work.

#### REFERENCES

1. Japan Highway Public Corporation: Guidelines for the Examination of Large-Scale Earthquake Retrofit Measures for Bridge Substructures (Draft) May, 1988.
2. Okawa, S., Maeda, Y., Kawashima, K. and Saeki, M.: Large Earthquake countermeasures for Tomei Expressway Bridges, 4th Joint U.S. - Japan Workshop on Bridge Engineering Performance, Strengthening, and Innovation, May 11 and 12, 1988. San Diego, California, U.S.A.
3. Japan Highway Public Corporation: Investigation and Designing of Seismic Retrofitting for the Substructure of the Torisaka Viaduct on the Tomei Expressway. Dec., 1988
4. Japan Highway Public Corporation: Investigation and Designing of Seismic Retrofitting for the Substructure of the Nishiokazu Viaduct on the Tomei Expressway. Oct., 1988
5. Japan Highway Public Corporation: Investigation and Designing of Seismic Retrofitting for the Substructure of the Kuno Viaduct on the Tomei Expressway. May, 1986
6. Japan Highway Public Corporation: Designing of Seismic Measures for the Substructure of the Enoo Bridge on the Tomei Expressway. May, 1984
7. Japan Highway Public Corporation: Investigation and Designing of Seismic Retrofitting for the Substructure of the Nagasaki Viaduct on the Tomei Expressway. May, 1986



## **S e s s i o n   4**

### **I n s p e c t i o n   a n d   S t r e n g t h e n i n g   M e t h o d s f o r   R e i n f o r c e d   C o n c r e t e   B r i d g e   P i e r s**

- 1) Seismic Inspection and Seismic Strengthening of Reinforced Concrete Bridge Piers with Termination of Main Reinforcement at Mid-Height  
(K.Kawashima, S.Unjoh and H.Iida)
- 2) Seismic Strengthening of Reinforced Concrete Bridge Piers on Metropolitan Expressway  
(T.Akimoto, H.Nakajima and F.Kogure)
- 3) Seismic Strengthening Method for Reinforced Concrete Bridge Piers on Hanshin Expressway  
(Y.Matsuura, I.Nakamura and H.Sekimoto)

**SEISMIC INSPECTION AND SEISMIC STRENGTHENING OF REINFORCED CONCRETE  
BRIDGE PIERS WITH TERMINATION OF MAIN REINFORCEMENT AT MID-HEIGHT**

K. Kawashima ( I )

S. Unjoh( II )

H. Iida( III )

Presenting Author : S. Unjoh

**SUMMARY**

This paper presents an experimental study on seismic inspection and seismic strengthening methods for reinforced concrete bridge piers which have termination of the main reinforcement, without enough anchorage lengths, at mid-height. The effect of the anchorage length of the main reinforcement was studied through the tests of 15 reinforced concrete pier specimens. The effect of the length and thickness of a steel jacket, and the use of injected material between the existing concrete and the steel jacket was also studied for developing a strengthening method.

**INTRODUCTION**

During recent earthquakes including the Miyagi-ken-oki Earthquake of 1978 and the Urakawa-oki Earthquake of 1982,<sup>1),2)</sup> reinforced concrete piers of highway bridges which have termination of main reinforcement at mid-height and short anchorage lengths have suffered serious damage. Photos 1 and 2 show the damage to reinforced concrete piers at this zone. Because the bending moment developed in the pier subjected to a lateral force P decreases as the height from the base increases, the amount of main reinforcement is generally decreased by terminating a number of bars at mid-height as shown in Fig.1. For short piers constructed prior to 1980, half of the reinforcement was terminated at approximately mid-height of the pier because in the design specifications, it was stipulated that the reinforcement can be terminated at the point 20 times of a diameter of the reinforcement higher than the point where the stress of reinforcement decreases to 50% of the allowable stress, therefore, only this length was generally provided. Since the damage to reinforced concrete piers at the anchorage zone results in a brittle shear failure,<sup>3)-6)</sup> such damage should be prevented.

Through the past experiences of damage to piers, the design specifications for highway bridges were revised in 1980,<sup>7)</sup> in which, anchorage length was increased from 20 times the diameter of the reinforcement to effective width of the pier plus 20 times of the diameter of the reinforcement. The allowable stress of concrete for shear in the anchorage zone also reduced by 33%.

---

( I ) Head, Earthquake Engineering Division, Earthquake Disaster  
Prevention Department, Public Works Research Institute,  
Ministry of Construction, Tsukuba Science City, 305, Japan

( II ) Research Engineer, ditto

( III ) Assistant Research Engineer, ditto

Because a large number of piers were designed according to the specifications issued prior to 1980, inspection and strengthening are required for piers with this short anchorage length.

The Ministry of Construction made seismic inspections of highway bridges throughout the country in 1971, 1976, 1979 and 1986. In the latest inspection, approximately 40 thousand bridges were inspected, and about 11 thousand bridges were found to require seismic strengthening. Although most of these bridges require installation of devices for preventing falling-off of the superstructure, some bridges detected require strengthening measures because of the short anchorage length of the main reinforcement in the pier.

There are several possible ways to strengthen such reinforced concrete piers. One method may be to place new reinforced concrete section around the existing section to support the lateral load. However, in this method, the increase of the mass of the pier tends to require an increase of the load resistance of the foundation. To avoid this situation, the pier may be strengthened by means of a steel jacket wrapped around the existing pier and construction will be simpler than adding new reinforced concrete.

In order to develop a seismic inspection method and seismic strengthening method for reinforced concrete bridge piers which have high vulnerability to develop serious damage at the mid-height where the main reinforcement is terminated during earthquakes, a series of dynamic loading tests were conducted at the Public Works Research Institute, partially in cooperation with the Metropolitan Expressway Public Corporation and the Hanshin Expressway Public Corporation.

This paper presents some of the preliminary results of the studies of effect of the anchorage length of the main reinforcement and length of the steel jacket required to prevent failure at the termination points.

## TEST SPECIMENS AND EXPERIMENTAL SET-UP

### Test Specimens

#### **a) Test specimens for evaluating vulnerability**

In order to evaluate the failure mode of the reinforced concrete piers with an inadequate anchorage length of the main reinforcement, 7 specimens with square sections of 50cm × 50cm were constructed as shown in Table 1. The scale of the specimens is assumed to be about 1/5 of a prototype pier.

Among the 7 specimens, Specimens 1, 2, 3 and 4, which have a shear span ratio of 5.4, were constructed with different anchorage lengths of main reinforcement as shown in Fig.2. Other characteristics are the same among the four specimens. Forty deformed reinforcing bars (yield strength is 3,000 kgf/cm<sup>2</sup>) with a diameter of 13mm were placed as main reinforcement so that main reinforcement ratio was 2.03% at the base. Round reinforcing bars (yield strength is 2,400 kgf/cm<sup>2</sup>) with a diameter of 9mm were placed every 25cm as tie reinforcement. The tie reinforcement ratio was 0.1%.

In Specimen 1, all reinforcement is continuous from the base to the top without termination at mid-height. In Specimen 2, the main reinforcement is terminated at the point where the stress induced in the reinforcement becomes one half of the allowable stress. Therefore, no anchorage length was provided in specimen 2. On the other hand, Specimens 3 and 4 were constructed with anchorage lengths of D/2 and D, respectively, in which D represents the width (= 50cm) of the pier.

Specimens 10, 11 and 12 had a shear span ratio of 9.9. Although reinforced concrete piers with such proportions are rarely adopted, the test was made to study the mode of failure under the condition that the bending moment will be more predominant than shear force in design. The layout of the main and tie reinforcement were the same as Specimens 1, 2, 3 and 4. Anchorage lengths were 0, D/2 and D for Specimens 10, 11 and 12, respectively, as shown in Fig.3.

#### **b) Test specimens for verifying strengthening method**

To study the effect of the steel jacket, 8 specimens were tested as shown in Table 2. Specimens from 13 to 17 had a square section of 50cm × 50cm, and a shear span ratio of 5.6 as shown in Fig.4. Forty six deformed reinforcing bars (yield strength is 3,000 kgf/cm<sup>2</sup>), each with a diameter of 10mm were placed as main reinforcement. The main reinforcement ratio was 1.31% at the base. Round reinforcing bars (yield strength is 2,400 kgf/cm<sup>2</sup>) with a diameter of 6mm were placed every 25cm as tie reinforcement. The tie reinforcement ratio was 0.05%. The effectiveness of a 1mm thick steel jacket with the length of 1D was studied in Specimens 13 and 14. The steel jacket was placed centrally about the termination point so that it covered the region of D/2 above and below this point. Two types of material were injected between the steel jacket and the surface of existing concrete piers to investigate their behaviour. They were nonshrinking concrete mortar (Specimen 13) and epoxy resin (Specimen 14). Because the length of a steel jacket of 1D was not enough to prevent the failure at the termination point, it was elongated to 1.5D for Specimen 15 (concrete mortar) and Specimen 16 (epoxy resin) as will be described later. The steel jacket was placed over the region D above and D/2 below the termination point, respectively. To study effect of the thickness of steel jacketing, a 0.6mm thick steel jacket was used on Specimen 17, in which the epoxy resin was adopted for injection.

Specimens 18, 19 and 20 had wall type construction with section dimensions of 40cm × 160cm as shown in Fig.5. Sixty four deformed reinforcing bars (yield strength is 3,000 kgf/cm<sup>2</sup>) with a diameter of 10mm were placed as the main reinforcement. The main reinforcement ratio was 0.76% at the base. Round reinforcing bars (yield strength is 2,400 kgf/cm<sup>2</sup>) with a diameter of 6mm were placed every 20cm. The tie reinforcement ratio is 0.08%. No strengthening was performed on Specimen 18 which had no anchorage length of the main reinforcement. Specimens 19 and 20 were strengthened by steel jackets with lengths of 1.5D and 2D, respectively, in which D represents the width of the shorter side of the section. Concrete mortar was injected into both specimens.

#### **Loading Conditions**

All specimens were laterally loaded at the top and were subjected to axial loading as shown in Fig.6. An electro-hydraulic dynamic actuator and static jack were used for the loading.

The specimens were subjected to a reversed cyclic lateral loading history under displacement control as shown in Fig.7.<sup>11, 12)</sup> The load was incrementally increased in about 10 steps up to the yielding of the main reinforcement at the base. The displacement developed at the pier crest, where the main reinforcement yielded at the base is defined hereafter as the yield displacement  $\delta_o$ , and it is used as a reference value to specify the

loading displacement applied to the specimens.

Extensive electric instrumentation was used to measure and record the basic deformation parameters such as the strain in the main and tie reinforcement as well as the displacement and acceleration at the loading point.

## **VULNERABILITY OF REINFORCED CONCRETE PIERS WITH INADEQUATE ANCHORAGE LENGTH**

### **Effect of Anchoring Length**

#### **a) Specimen with shear span ratio of 5.4**

**Fig.8** shows the effect of the anchorage length in the tests of Specimens 1, 2, 3 and 4, which had square cross sections of 50cm × 50cm and a shear span ratio of 5.4.

**Fig.8(a)** shows the failure mode of the specimens. In Specimen 1, in which main reinforcement was continuous from the bottom to the top without termination, flexural cracks were firstly developed at the base. As the loading increased, the cracks progressed and spalling-off of the cover concrete developed. The specimen finally failed in flexure at the base.

In Specimen 2, which had zero anchorage length, flexural cracks were firstly developed at the termination point. The flexural cracks progressed and the specimen finally failed in shear at the termination point.

In Specimen 3, which had an anchorage length of  $D/2$ , flexural cracks were developed at both the termination point and at the base of the pier. As the loading increased, the cracks at the base progressed significantly, and the specimen finally failed in flexure at the base.

In Specimen 4, which had an anchorage length of  $D$ , the failure mode was almost same with that of Specimen 1. The anchorage length of  $D$  was considered to be sufficient to prevent failure at the termination point.

Based on the test results of Specimens 1, 2, 3 and 4, the position where the cracks occurred was seen to give a indication of the position where failure would eventually occur.

**Fig.8(b)** compares the strain induced in the main reinforcement of the specimens. It should be noted that the accuracy of strain measurement over about  $3,000 \mu$  was poor due to the limited capability and damage of strain gauges.

Larger strains were developed at the base in Specimens 1 and 4 while a strain as large as that at the base was developed at the termination point in Specimens 2 and 3 and the strain at the termination point was larger in Specimen 2 than in Specimen 3. This corresponds to the difference of the failure mode observed in these specimens.

**Fig.8(c)** shows the envelope of load-displacement hysteresis loops and equivalent hysteresis damping ratio. It is obvious that the lateral load resistance of Specimen 2, which failed at the termination point, is considerably smaller than that of other specimens. The equivalent damping ratio did not seem to be affected directly by the failure mode.

#### **b) Specimens with shear span ratio of 9.9**

**Fig.9** shows the effect of the anchorage length on Specimens 10, 11 and 12, which had the same square cross section (50cm × 50cm) and a shear span ratio of 9.9.

**Fig.9(a)** shows the failure mode of the specimens. In Specimen 10, in which no anchorage length was provided, flexural cracks were firstly developed at the termination point. As the loading increased, the cracks progressed and spalling-off of the cover concrete developed. Although rupture of the main reinforcement did not occur, the load resistance of the pier suddenly decreased in the first cycle to  $5\delta_u$  in plus direction, therefore testing was terminated to protect the loading equipment. The specimen finally failed in shear.

In Specimen 11, which had an anchorage length of  $D/2$ , flexural cracks were developed at the termination point as well as at the base as shown in **Fig.10**. Slightly greater shear cracks were also initiated at the termination point during the cycles to  $2\delta_u$ . However, significant flexural cracks and spalling-off of the cover concrete developed after the cycles to  $3\delta_u$  and the specimen finally failed at the base. Tensile rupture of five reinforcing bars occurred at the base during the  $6\delta_u$  loading.

In Specimen 12, which had an anchorage length of  $D$ , the flexural cracks were developed at the base and a few cracks were observed at the termination point. The specimen finally failed in flexure at the base.

**Fig.9(b)** compares the strain induced in the main reinforcement of these specimens. The strain at the termination point and at the base reached the yield strain ( $1,800 \mu$ ) during the  $1\delta_u$  loading in all specimens. As the loading displacement increased, the strain substantially increased at these two points. In Specimen 12, which failed in flexure at the base, the strain at the termination point almost reached the yielding strain even during the  $1\delta_u$  loading. Although the difference in the strain distributions of the specimens was small up to the  $4\delta_u$  loading cycles it is thought that the difference in the strains of the specimens would increase after this value.

**Fig.9(c)** shows the envelope of the load-displacement hysteresis loops and the equivalent hysteresis damping ratio. Noticeable differences in the envelope are not observed up to the  $4\delta_u$  loading where a sudden decrease of the load occurred in the specimen 10. This corresponded to the failure at the termination point as was described above. Because the failure occurred on the first loading to  $+5\delta_u$ , the effect of failure was not observed in the equivalent damping ratio.

## SEISMIC STRENGTHENING BY MEANS OF A STEEL JACKET

### Reinforced Concrete Pier with Square Section

**Fig.11** shows the effect of the steel jacket strengthening method on Specimens 13, 14, 15, 16 and 17. The length of the steel jacket was the main interest in these tests.

**Fig.11(a)** shows the failure mode of the specimens. In Specimens 13 (mortar injection) and Specimen 14 (epoxy resin), which were strengthened with 1D long steel jackets, flexural cracks were developed at the base. As the loading increased, the cracks progressed, and the specimens finally failed in flexure at the base. **Fig.11(b)(1) and (2)** compare the strain induced in the main reinforcement in Specimens 13 and 14. Although the strain in the region covered by the steel jacket was small, the strain at the upper end of the steel jacket reached the yielding strain during the  $1\delta_u$  loading cycles. It became greater than the yielding strain with increasing loading displacement. **Fig.12** compares the deformation, in the vertical direction,

induced in the steel jacket. The strain was only about  $100\mu$  (Specimen 13) ~  $200\mu$  (Specimen 14) even during  $3\delta_0$  loading. As will be discussed later, the strain induced in Specimen 14 was slightly larger than that induced in Specimen 13. (This shows the difference of contact between the steel jacket and the concrete surface). After the  $7\delta_0$  loading cycles, the steel jacket was taken out to inspect the damage at the termination point. Although a single moderate crack was developed as shown in **Photo 3** and **4**, progress of the failure at the termination point was prevented by the steel jacket. Only minor cracking occurred at the upper end of the jacket. Based on the test results, it was considered that the length of 1D was insufficient to prevent failure at the termination point.

Specimen 15 (mortar injection) and Specimen 16 (epoxy resin) were strengthened by a 1.5D long steel jacket and were then tested.

In Specimen 15, flexural cracks were developed at the base. However, as the loading increased, shear cracks were developed at the lower end of the steel jacket and the specimen finally failed in shear at this zone as shown in **Fig.11(a)(3)**. The concrete mortar between the concrete surface and the steel jacket was crushed and the steel jacket deformed as shown in **Photo 5**. **Fig.11(b)(3)** shows the strain induced in main reinforcement. During the  $3\delta_0$  loading cycles, it exceeded the yield strain. The strain was slightly larger at the lower end of the jacket. The tie reinforcement yielded during the  $3\delta_0$  loading cycles and the concrete mortar was crushed and outward buckling of steel jacket occurred. **Fig.13(1)** shows the deformation, in the vertical direction, induced in the steel jacket. The strain takes the maximum value at the center of the jacket. The strain was about  $1200\mu$ , which is much larger than that induced in Specimen 13 which had a jacket length of 1D. It means that the steel jacket with length of 1.5D worked much effectively than the steel jacket with length of 1D. It should be noted that effect of the outward buckling of the steel jacket which was described above cannot be clearly seen in **Fig.13** because it shows the strain of steel jacket in vertical direction.

On the other hand, in Specimen 16, flexural cracks were developed at the base, where the specimen finally failed in flexure as shown in **Photo 6**. This clearly showed the difference of the injection material between the concrete surface and the steel jacket. Epoxy resin was better than the concrete mortar in this test because separation of the steel jacket from the concrete surface did not occur developed in the epoxy injected specimen. However, the effectiveness of such injected materials has to be evaluated from other viewpoints such as durability for long-term use. As shown in **Fig.11(b)(4)**, the strain induced in the main reinforcement was slightly smaller than that in Specimen 15. Deformation of the steel jacket in the vertical direction is almost the same as that of Specimen 15 as shown in **Fig.13(2)**.

In Specimen 17, in which a thinner steel plate ( $t=0.6\text{mm}$ ) was used. The failure mode was almost the same as that developed in Specimen 15 ( $t=1\text{mm}$ ). The crushing of the steel occurred at the lower end of the jacket, and the bond effect of epoxy resin were cut off during  $4\delta_0$  loading cycles. The deformation of the jacket were of the same order as that developed in Specimen 15. The strain induced in the main reinforcement and strain of the steel jacket in vertical direction were larger than those of Specimen 16 as shown in **Fig.11(b)(5)** and **Fig.13(3)**. This clearly shows the effect of the different thicknesses of the steel jacket.

## Reinforced Concrete Piers with Wall Type Section

Fig.14 shows the effect of the steel jacket strengthening method on Specimens 18, 19 and 20.

Fig.14(a) shows the failure mode of the specimens. In Specimen 18, which was not strengthened by the steel jacket, flexural cracks were developed both at the termination point and at the base. As the loading increased, the cracks significantly progressed at the termination point until the specimen finally failed at this zone.

In Specimen 19, which was strengthened by a 1.5D long steel jacket, cracks progressed at the base where the specimen finally failed in flexure. When the steel jacket was removed from the concrete pier after the  $7\delta_o$  loading cycles, a horizontal crack was found at the termination point.

In Specimen 20 which was strengthened by a 2D long steel jacket, the failure mode was almost identical with that of Specimen 19. However, no crack was observed at the termination point when the jacket was removed after the  $7\delta_o$  loading cycles.

Fig.14(b) compares the strain induced in the main reinforcement of Specimens 19 and 20. Although, the strain induced in the main reinforcement at the strengthened region was less than  $100\mu$  up to  $3\delta_o$  loading in Specimen 19, the strain suddenly increased and exceeded the yielding strain at the termination point during the  $4\delta_o$  loading cycles. On the other hand, the strain induced in the main reinforcement at the strengthened zone was small even during large displacements in Specimen 20. Therefore, 2D may be required as a length of the steel jacket in order for the termination point to have no effect. Fig.15 compares the strain induced in the steel jacket, in the vertical direction, it is very small, and takes a value of only  $200\mu$  even during the cycles to  $3\delta_o$  and yielding of the reinforcement was not developed in Specimens 19 and 20.

Fig.14(c) shows the envelope of the load-displacement hysteresis loops and the equivalent damping ratio. The load resistance of Specimen 18 suddenly decreased during the  $5\delta_o$  loading cycles. The load resistance of Specimens 19 and 20 increased by about 10% than that of Specimen 18 when the steel jacket was used. The difference in the load resistance of Specimens 19 and 20 was insignificant. The equivalent damping ratio of Specimen 20 during the  $5\delta_o$  and  $6\delta_o$  loading cycles was smaller than that of Specimen 21 because the number of main reinforcing bars ruptured at the base was greater than Specimen 20.

## EVALUATION OF VULNERABILITY

Based on the tests described above, it may be important to estimate the strength of reinforced concrete piers at the termination point in relation to the strength at the base. If the strength at the termination point is smaller than that at the base, shear failure, which results in extensive damage in a brittle manner, is likely to occur.

To evaluate the strength of piers, the load resistance is defined as shown in Fig.16 in terms of the bending moment as

$$S = S^T/S^E \quad (1)$$

$$S^T = M_o^T/M^T \quad (2)$$

$$S^E = M_o^E/M^E \quad (3)$$



where

- S : failure mode factor
- $S^T$  and  $S^B$  : a factor representing the strength at the termination point and at base, respectively
- $M^T$  and  $M^B$  : bending moment developed at the termination point and base, respectively when the pier is subjected to a lateral force at top
- $M_v^T$  and  $M_v^B$  : yielding bending moment at termination point and at base, respectively.

In Eqs.(2) and (3), the yielding bending moment is defined as the bending moment at which the reinforcement begins to yield.  $S^T$  and  $S^B$  defined in Eqs.(2) and (3) determine the likelihood of yielding at the termination point and base, respectively. If  $M_o^T$  is defined to be the bending moment developed at the termination point when  $M_v^T$  equals to  $M_v^B$ , Eq.(1) can be written as

$$S = M_v^T/M_o^T \quad (4)$$

Fig.17 shows how the failure mode factor varies along pier in the Specimens 1 and 3. Specimen 1 failed at the termination point while the specimen 3 failed at the base. The failure mode factor S at the termination point takes 0.92 and 1.1 in Specimen 1 and Specimen 3, respectively. Although the difference is not necessarily so large, it may be said that the failure mode factor may be used to identify the failure mode.

Fig.18 shows the failure mode factors at the termination point for all specimens which have termination of main reinforcement at mid-height. Failure is likely to be developed at the termination point when the failure mode factor is less than 1.1 although there are some scatters. On the other hand, flexural failure at the base tends to be developed when the failure mode factor is larger than or equal to 1.1.

Fig.19 shows the distribution of the failure mode factor for Specimen 13 which was strengthened by the steel jacket. For computing the failure mode factor by Eq.(1), it was assumed that no separation is developed between the concrete surface and the steel jacket, and that the steel jacket behaves as main reinforcement. The increase of concrete strength and ductility by increasing the confining pressure by means of the steel jacket was disregarded in the calculations.

Fig.20 shows the failure mode factor for all specimens strengthened. The minimum value of the failure mode factors at the upper end and lower end of the steel jacket as well as at the termination point is presented in Fig.20. All specimens strengthened failed at the base although two specimens (Specimens 15 and 17) suffered outward deformation of the steel jacket and shear failure occurred at the lower end of the jacketed zone. If such failure can be regarded as minor, it may be said failure at the termination zone was prevented when the failure mode factor was larger than 1.1. However, because the number of data is inadequate, this needs further study. Special attention should be paid to study the difference of injection material.

#### CONCLUDING REMARKS

For the evaluating seismic vulnerability of reinforced concrete bridge piers which have termination of main reinforcement and inadequate anchorage

length and for evaluating effectiveness of repair by using steel jackets, a series of dynamic loading tests were made on specimens with square and wall type sections. Based on the test results presented herein, the following conclusions are made:

- 1) For preventing shear failure at the termination point, the anchorage length should be longer than  $1D$ , where  $D$  is the width of the cross section.
- 2) Whether shear failure at the termination point is developed or not may be evaluated by the failure mode factor  $S$  defined by Eq. (1). If the failure mode factor  $S$  is smaller than 1.1, shear failure is likely to be developed at the termination point. When the failure mode factor  $S$  is larger than or equal to 1.1, flexural failure at the base tends to be developed.
- 3) Steel jackets can be used to strengthen piers vulnerable to shear failure at the termination point. The minimum length of the steel jacket may be from 1.5 to 2.0 times the pier width  $D$ .
- 4) Epoxy resin seems better than concrete mortar as an injection material, because separation of steel jacket from concrete surface is more restricted. However effectiveness of the epoxy resin should be examined from other aspects including durability for long-term use. Use of steel bars to anchor the steel jacket as well as the concrete mortar may be an alternative approach to be studied.
- 5) For evaluating the effectiveness of steel jackets, the failure mode factor  $S$  by Eq.(1) may be used. Although further study is required, it may be tentatively said that failure at the termination point is prevented if the failure mode factor is larger than 1.1.

#### REFERENCES

- 1) Public Works Research Institute, "Report on the Disaster Caused by the Miyagi-ken-oki Earthquake of 1978," Vol.159, March 1983 (In Japanese)
- 2) Narita, N., Murakami, M. and Asanuma, H., "Report of the Investigation on Earthquake Damage to Sizuna Bridge," 15th Joint Meeting, U.S.-Japan Panel on Wind and Seismic Effects, U.J.N.R., Tsukuba, Japan, 1983
- 3) Yamamoto, T., Ishibashi, T., Ohtsubo, M. and Kobayashi, S., "Experimental Study on Seismic Capacity of Bridge Piers with Termination of Longitudinal Reinforcement," Proc. of JSCE, Vol.348/V-1, Aug., 1984
- 4) Iwasaki, T., Kawashima, K., Hagiwara, R., Hasegawa, K., Koyama, T. and Yoshida, T., "Experimental Investigation on Hysteretic Behaviour of Reinforced Concrete Bridge Pier Columns," 17th Joint Meeting, U.S.-Japan Panel on Wind and Seismic Effects, U.J.N.R., Tsukuba, Japan, May, 1985
- 5) Ozaka, Y., Suzuki, M. and Kobayashi, S., "Investigation on the Effect of Termination of Longitudinal Reinforcement on Shear Strength of RC Beam," Proc. of JSCE, Vol.366/V-4, Feb., 1986
- 6) Ozaka, Y., Suzuki, M., Miyamoto, M. and Kobayashi, S., "Evaluation of Shear Strength of RC Beam with Termination of Longitudinal Reinforcement," Proc. of JSCE, Vol.378/V-1, Feb., 1987
- 7) Japan Road Association, "Specifications for Highway Bridges in Japan", May, 1980
- 8) Kawashima, K. and Unjoh, S., "An Inspection Method of Seismic Vulnerability of Existing Highway Bridges," Proc. of JSCE, No.416/I-13, April 1990
- 9) Japan Road Association, "Manual for Seismic Countermeasure Methods for Roads against Earthquakes," March 1988

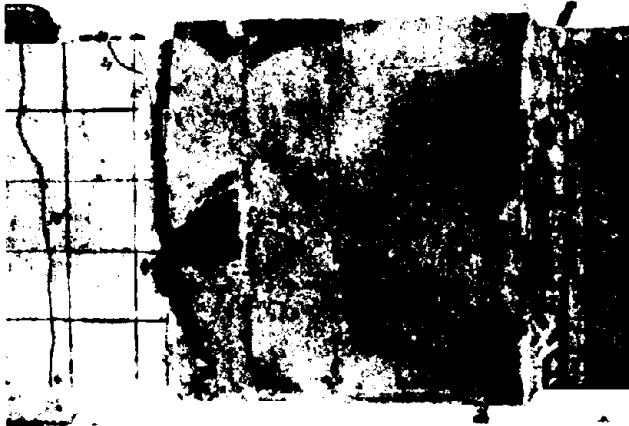
- 10) Kawashima, K., Unjoh, S. and Iida, H, "Seismic Inspection and Strengthening Methods for Reinforced Concrete Piers with Termination of Main Reinforcement at Mid-height," Technical Note of PWRI, Public Works Research Institute, Nov. 1990
- 11) Kawashima, K. and Koyama, Y., "Effect of Number of Loading Cycles on Dynamic Characteristics of Reinforced Concrete Bridge Pier Column," Proc. of JSCE, No.392/I-9, Apr. 1988
- 12) Kawashima, K. and Koyama, T., "Effects of Cyclic Loading Hysteresis on Dynamic Behavior of Reinforced Concrete Bridge Piers," Proc. of JSCE, No.398/I-10, Oct. 1988



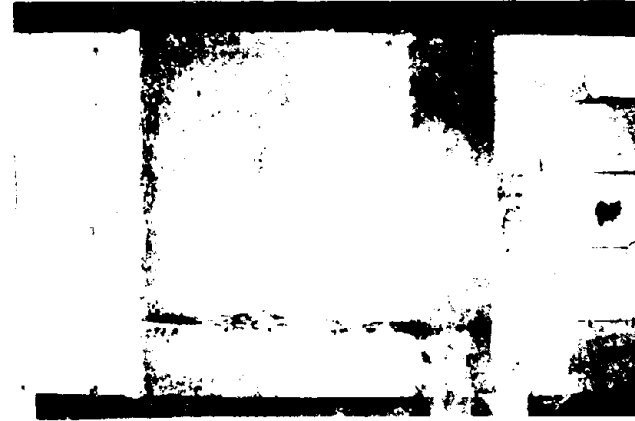
**Photo 1 Pier Damage of the Sendai Bridge during  
the Miyagi ken-oki Earthquake of 1978**



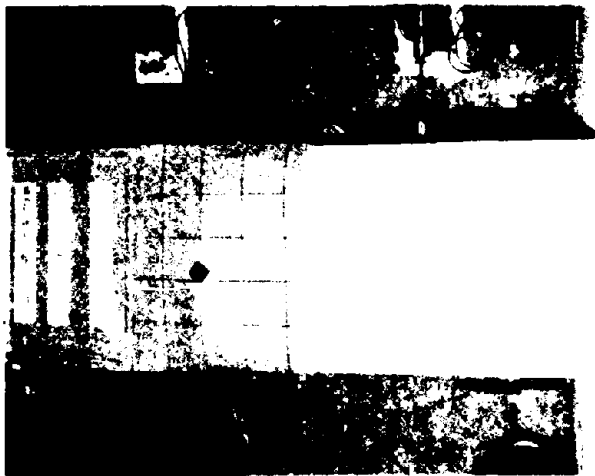
**Photo 2 Pier Damage of the Sizunai Bridge during  
the Urakawa-oki Earthquake of 1982**



**Photo 3 Crack along the Termination Point of Specimen 13 Strengthened by a 1D Long Steel Jacket with Concrete Mortar**



**Photo 4 Crack along the Termination Point of Specimen 14 Strengthened by a 1D Long Steel Jacket with Epoxy Resin**



**Photo 5 Deformed Steel Jacket and Crushing of the Injected Concrete Mortar in Specimen 15**



**Photo 6 Effect of a Steel Jacket for Strengthening Reinforced Concrete Square Pier with Shear Span Ratio of 5.6 (Specimen 16)**

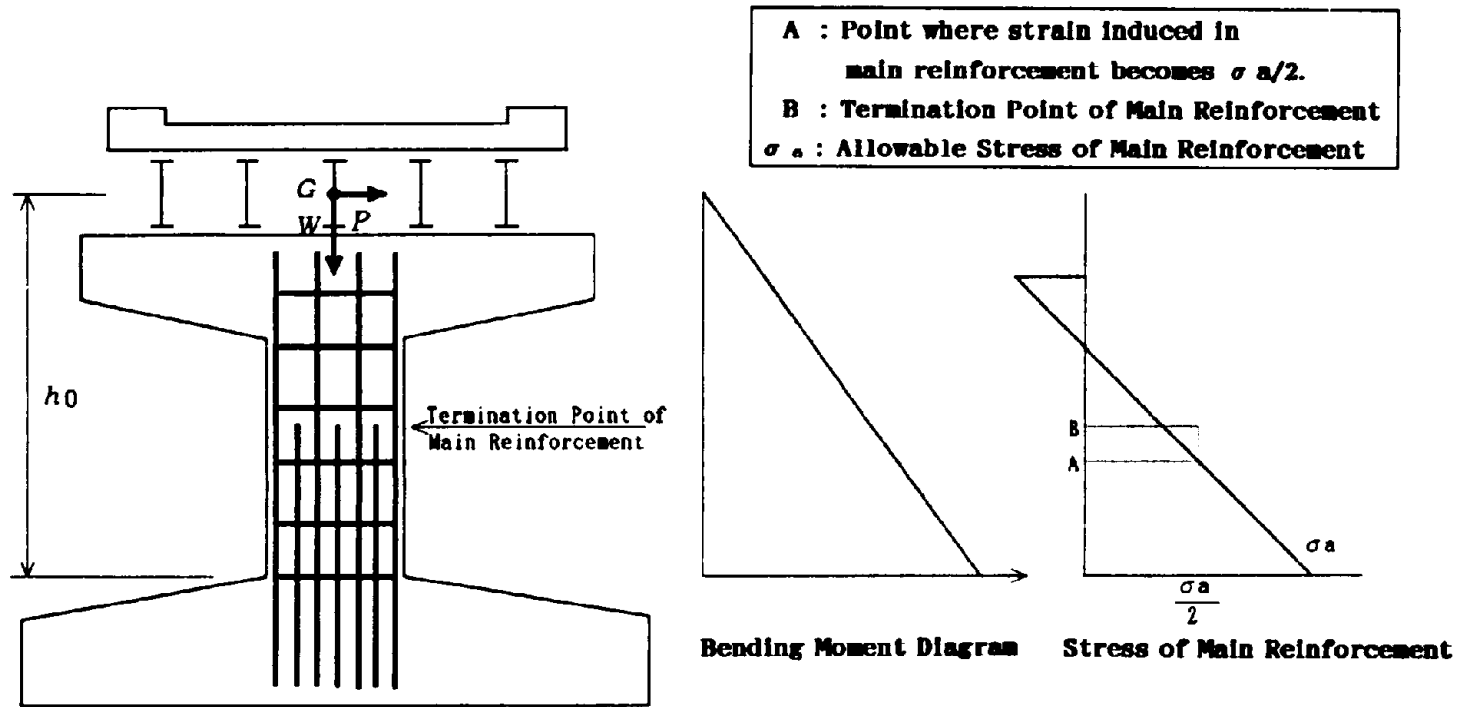
Table 1 Test Specimens for Evaluating Vulnerability

Specimen No.	S - 1	S - 2	S - 3	S - 4	S - 10	S - 11	S - 12	
Cross Section [cm]	50 × 50							
Covering Depth of Concrete [cm]	3.5							
Effective Height [cm]	250			460				
Shear-Span Ratio	5.4			9.9				
Longitudinal Reinforcing Bar (Deformed Bar)	Material and Diameter [mm]	SD30, D13						
	Termination Point of Main Reinforcement from Base [cm]	Without Termination	110	135	160	180	205	230
	Ratio of Reinforcement [%] (after Termination [%])	2.03 (1.02)						
	Yield Strength [kgf/cm <sup>2</sup> ]	3,144			3,525			
Hoop Tie	Material and Diameter [mm]	SR24. ϕ 9						
	Ratio of Reinforcement [%]	0.10						
	Yield Strength [kgf/cm <sup>2</sup> ]	2,776			2,910			
Concrete	Material	Portland Cement						
	Max Grain Size of Aggregate [mm]	10						
	Uni-Axial Strength [kgf/cm <sup>2</sup> ]	327	332	325	429	429	409	390
Lateral Force	Direction of Loading	1-direction						
	Velocity of Loading [cm/sec]	5			10			
	Number of Loading for Each Specific Displacement	10						
	Loading Displacement [cm]	1.3			4.25			
Axial Force	Axial Force [tf]	4.11			25			
	Axial Stress [kgf/cm <sup>2</sup> ]	1.64			10			

Table 2 Test Specimens for Verifying Strengthening Method

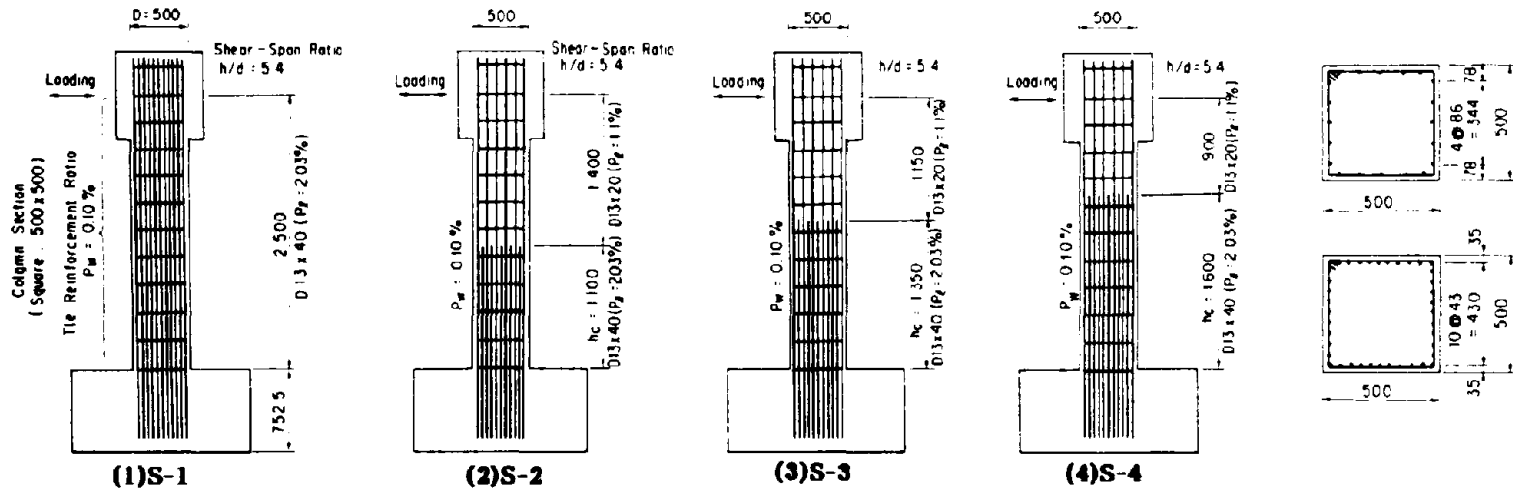
Specimen No.	S - 13	S - 14	S - 15	S - 16	S - 17	S - 18	S - 19	S - 20		
Cross Section [cm]	50 × 50					40 × 160				
Covering Depth of Concrete [cm]	3.5									
Effective Height [cm]	260									
Shear-Span Ratio	5.6					7.1				
Longitudinal Reinforcing Bar (Deformed Bar)	Material and Diameter [mm]	SD30, D10								
	Termination Point of Main Reinforcement from Base [cm]	90					80			
	Ratio of Reinforcement [%] (after Termination [%])	1.31 (0.63)					0.76 (0.38)			
	Yield Strength [kgf/cm <sup>2</sup> ]	3,640	4,173	3,640	4,173	3,740				
Hoop Tie	Material and Diameter [mm]	SR24, φ 6								
	Ratio of Reinforcement [%]	0.05					0.08			
	Yield Strength [kgf/cm <sup>2</sup> ]	2,501	4,423	2,501	4,423	3,637				
Concrete	Material	Portland Cement								
	Max Grain Size of Aggregate [mm]	10								
	Uni-Axial Strength [kgf/cm <sup>2</sup> ]	412	447	480	363	447	360	336	426	
Lateral Force	Direction of Loading	1-direction								
	Velocity of Loading [cm/sec]	5								
	Number of Loading for Each Specific Displacement	10								
	Loading Displacement [cm]	1.5					1.7			
Axial Force	Axial Force [tf]	28.8					64			
	Axial Stress [kgf/cm <sup>2</sup> ]	11.52					10			
Steel Jacket	Material (Width [cm], Thickness [mm])	SPCC (1D, 1)	SPCC (1D, 1)	SPCC (1.5D, 1)	SPCC (1.5D, 1)	SPCC (1.5D, 0.6)	-	SPCC (1.5D, 1)	SPCC (2D, 1)	
	Injection Material and Thickness [mm]	Concrete Mortar 20	Epoxy Resin 3	Concrete Mortar 20	Epoxy Resin 3	Epoxy Resin 3	-	Concrete Mortar 20	Concrete Mortar 20	

Note) SPCC represents "Cold Rolled Steel Sheet".

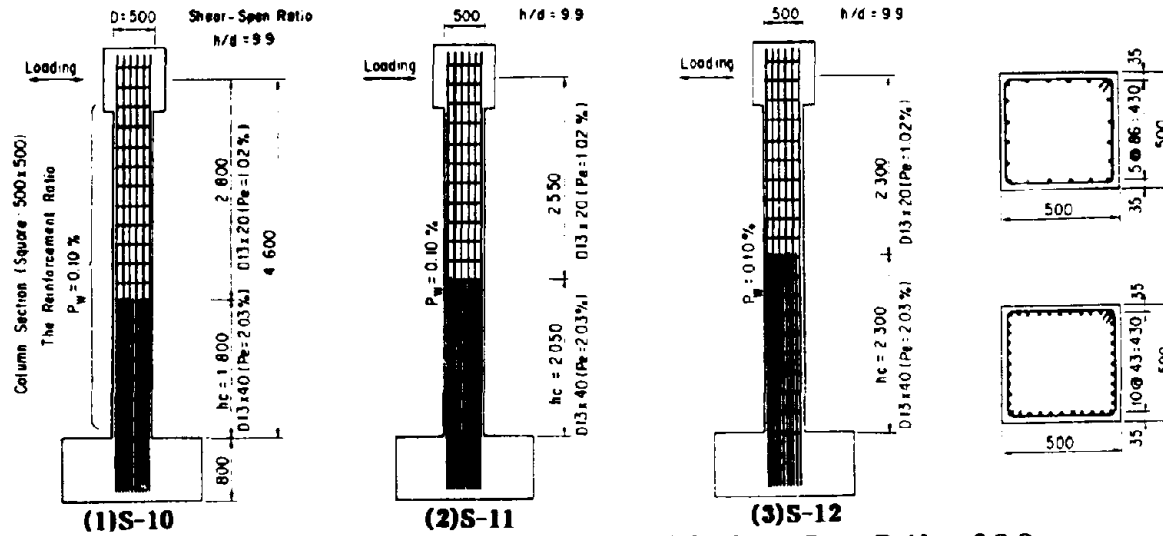


**Fig.1 Termination of Main Reinforcement at Mid-Height**

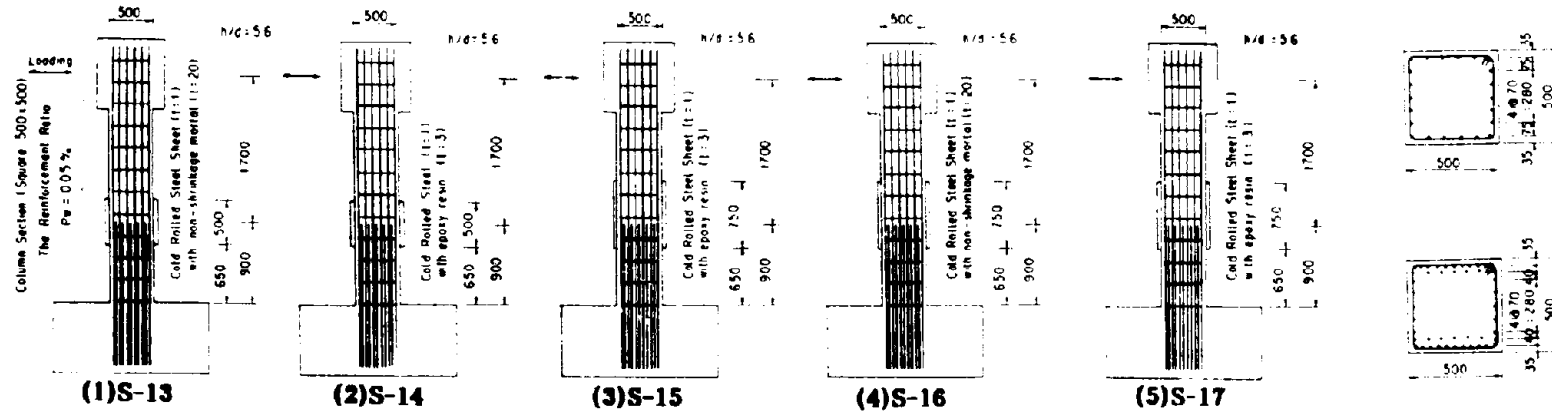




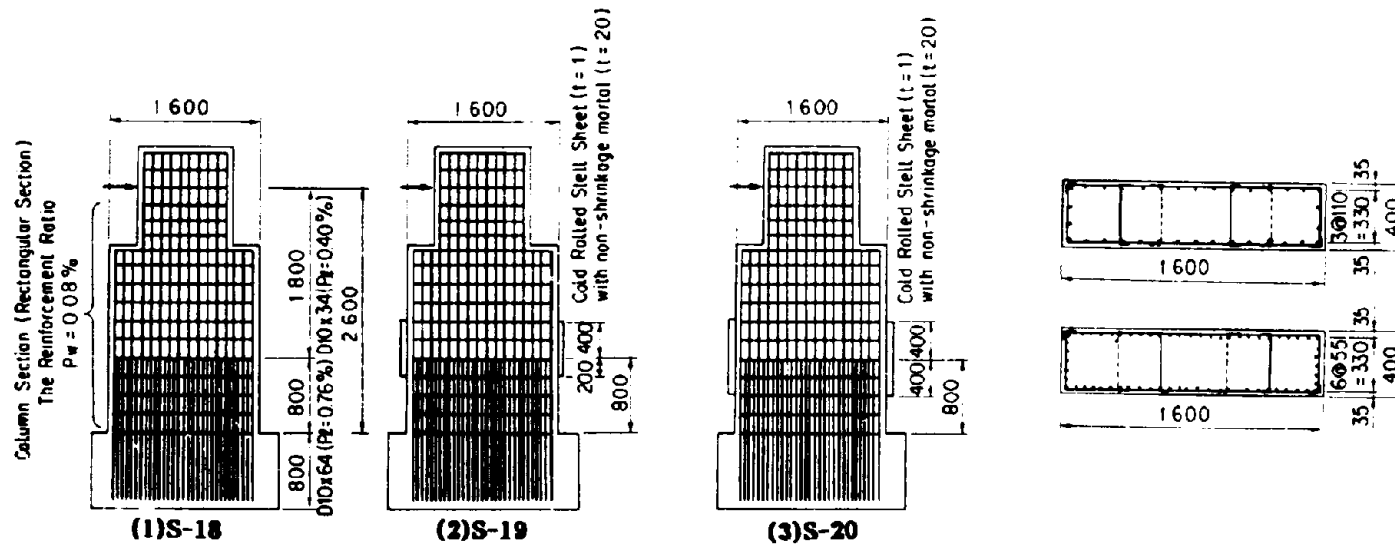
**Fig. 2 Reinforced Concrete Pier Specimens with Shear Span Ratio of 5.4 to study Effect of Anchorage Length of Main Reinforcement**



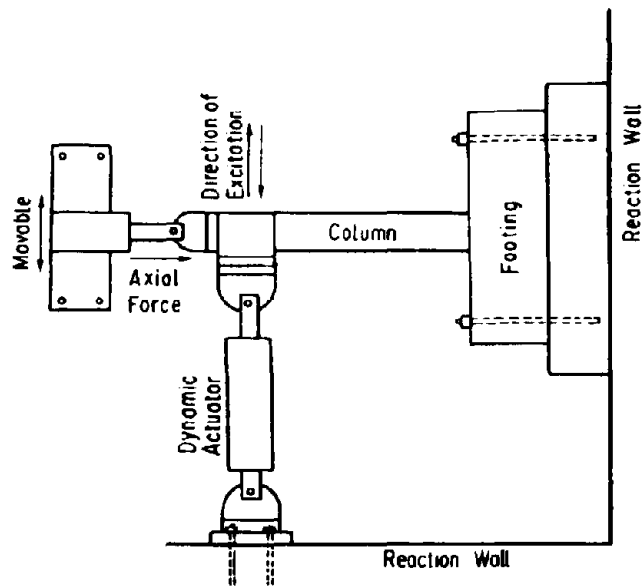
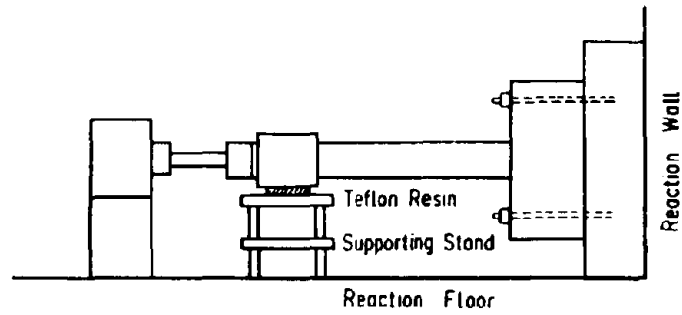
**Fig. 3 Reinforced Concrete Pier Specimens with Shear Span Ratio of 9.9 to study Effects of Anchorage Length of Main Reinforcement**



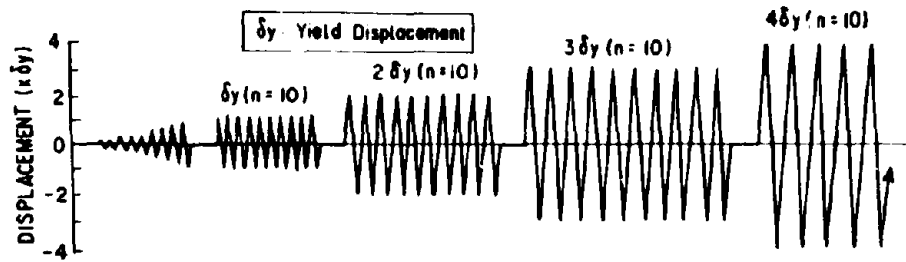
**Fig.4 Reinforced Concrete Square Pier Specimens with Shear Span Ratio of 5.6 to study Strengthening Method by Means of A Steel Jacket**



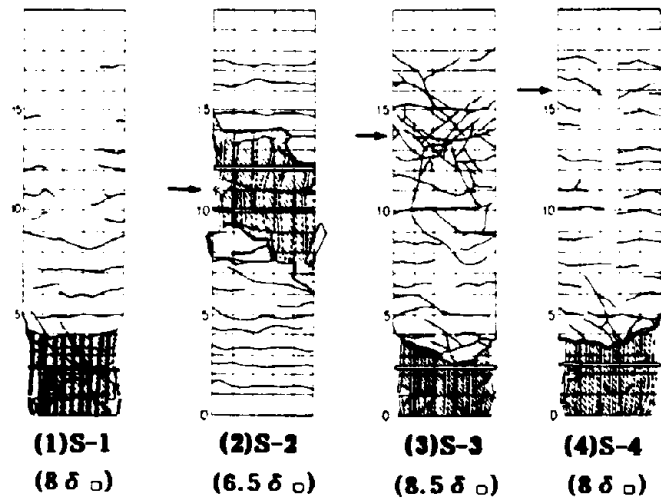
**Fig.5 Reinforced Concrete Wall Type Pier Specimens with Shear Span Ratio of 7.1 to study Strengthening Method by Means of A Steel Jacket**



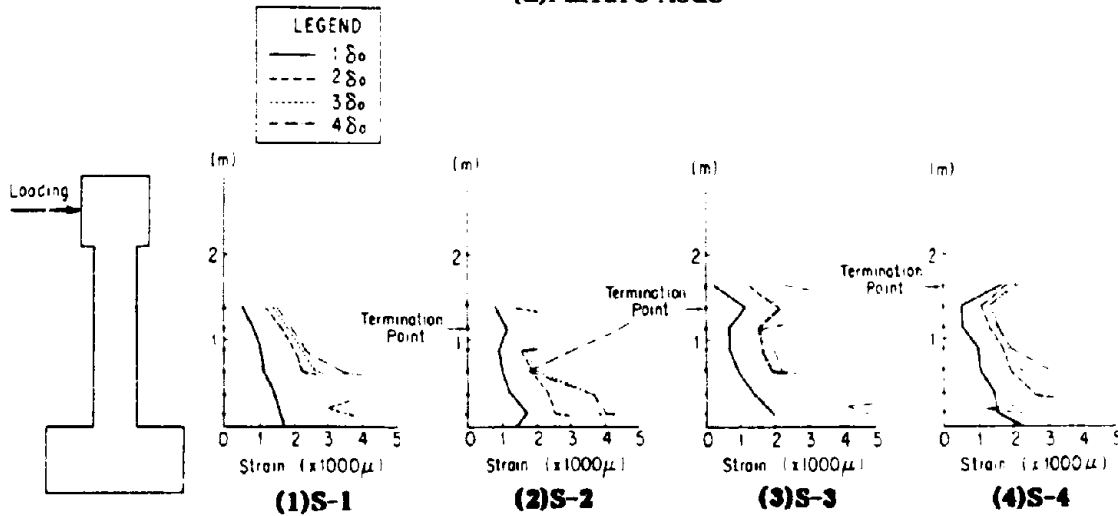
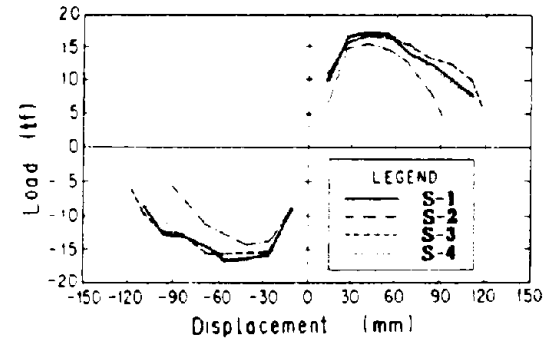
**Fig.6 Experimental Set-up**



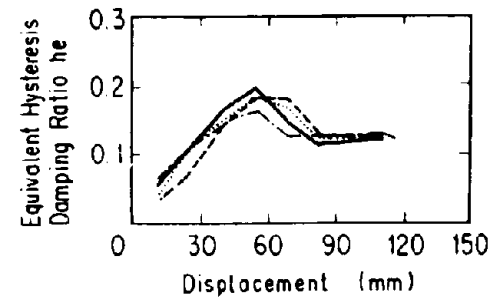
**Fig.7 Step-wise Increasing Symmetric Loading Displacement**



(a) Failure Mode

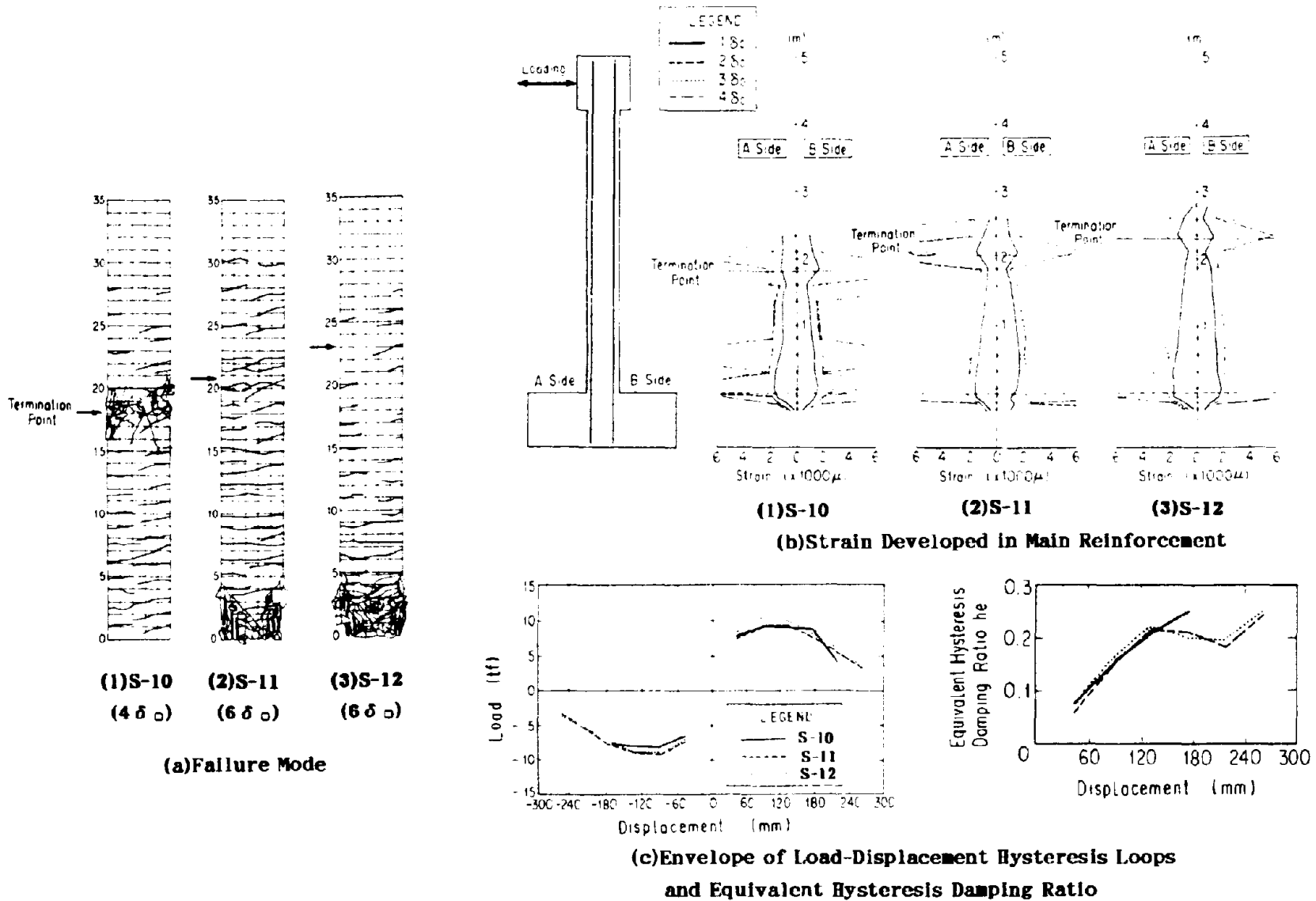


(b) Strain Developed in Main Reinforcement

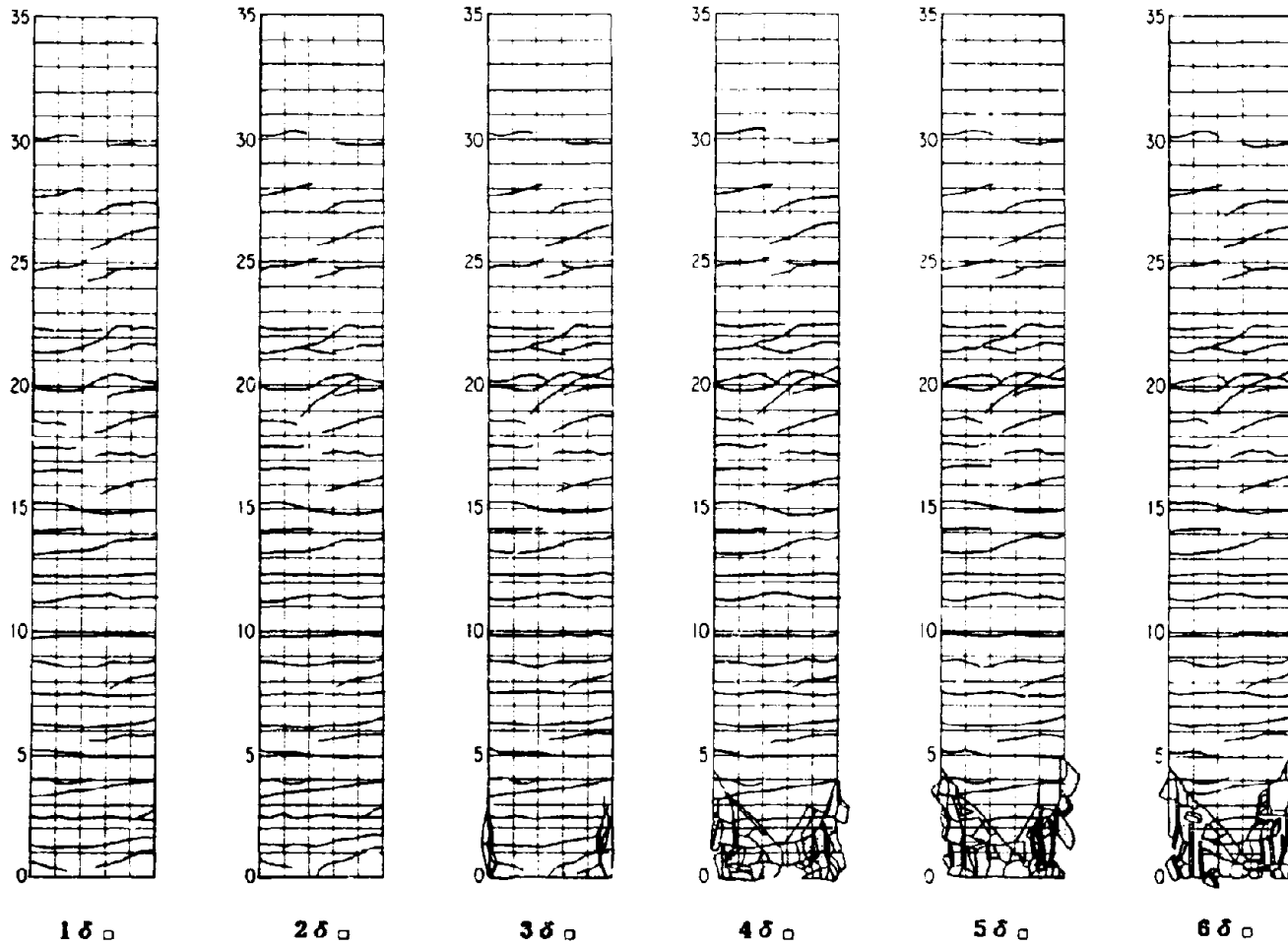


(c) Envelope of Load-Displacement Hysteresis Loops and Equivalent Hysteresis Damping Ratio

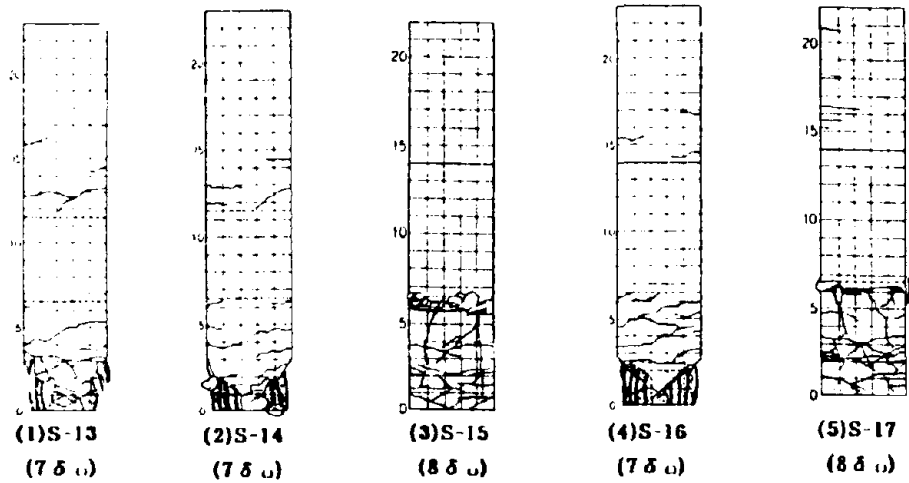
**Fig.8 Effect of Anchorage Length for Specimens with Shear Span Ratio of 5.4 (Specimens 1 to 4)**



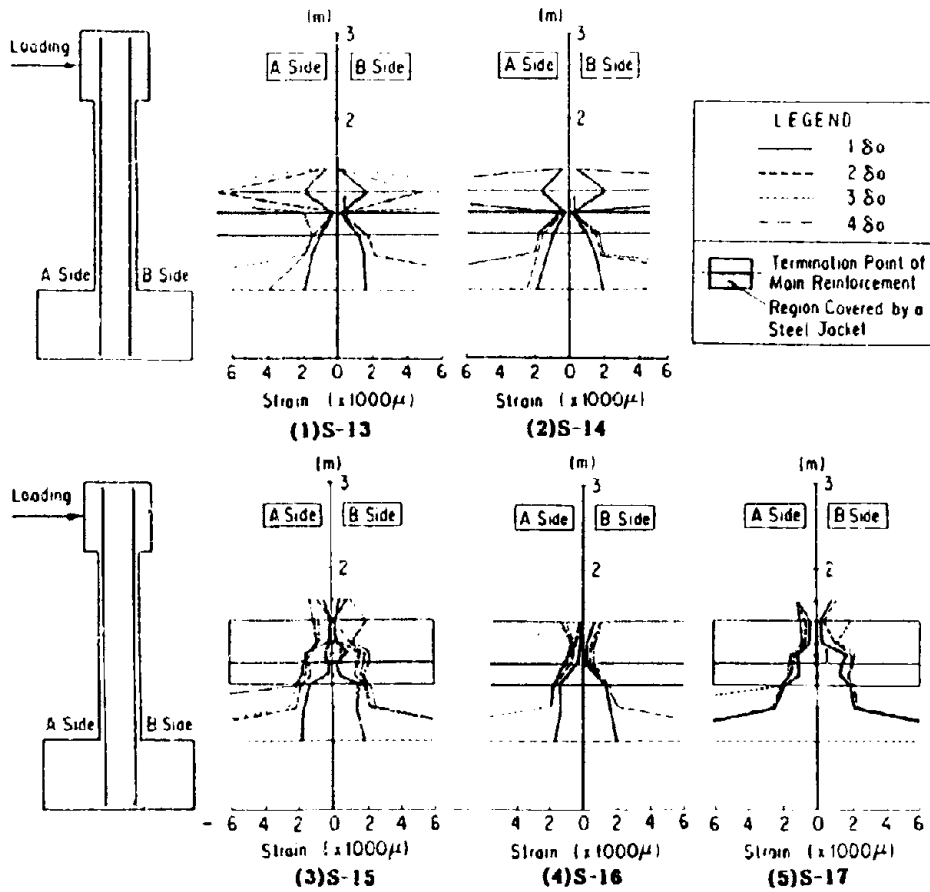
**Fig.9 Effect of Anchorage Length for Square Specimens with Shear Span Ratio of 9.9 (Specimens 10, 11 and 12)**



**Fig.10 Effect of Anchorage Length of Main Reinforcement in Terms of Progress of Failure Mode for Specimens with Shear Span Ratio of 9.9 (Specimen 11)**

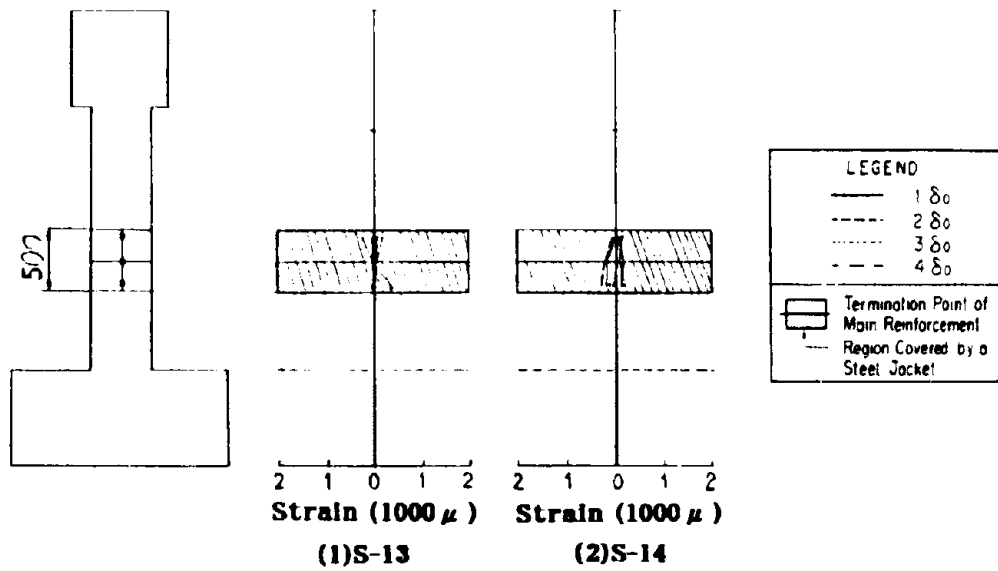


(a) Failure Mode

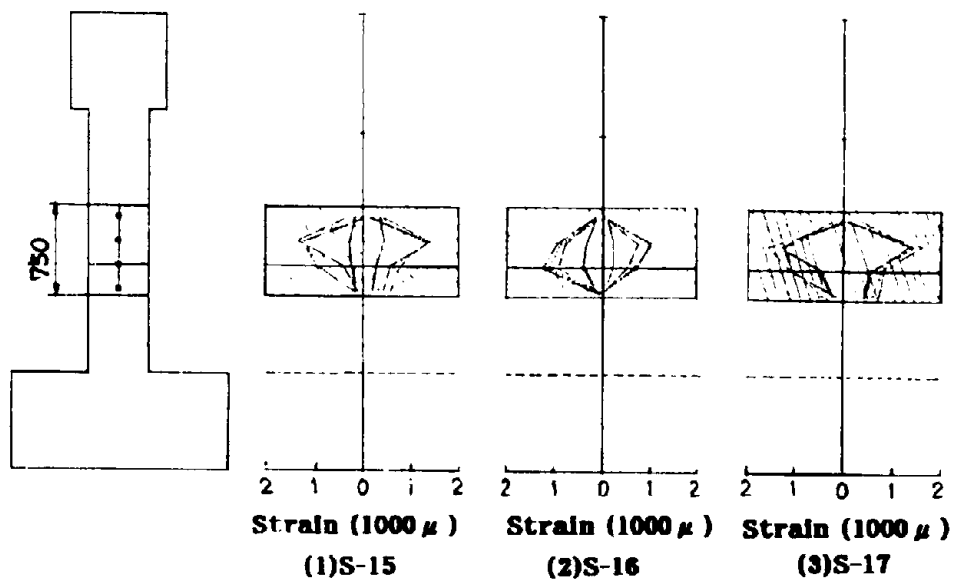


(b) Strain Developed in Main Reinforcement

Fig.11 Effect of Strengthening Method by A Steel Jacket for Square Specimens with Shear Span Ratio of 5.6 (Specimens 13 to 17)

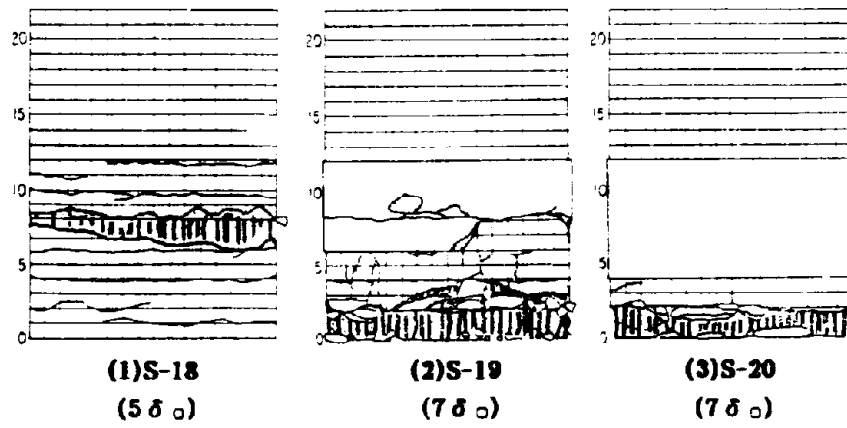


**Fig. 12 Strain Induced in the 1D Long Steel Jacket, in Vertical Direction, in Specimen 13 (Mortar Injection) and Specimen 14 (Epoxy Injection)**

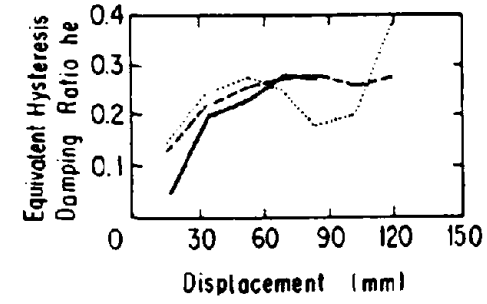
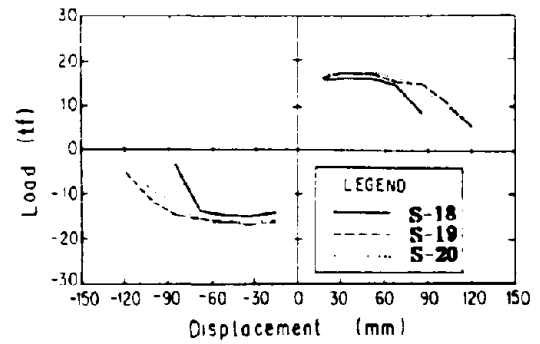


**Fig. 13 Strain Induced in the 1.5D Long Steel Jacket, in Vertical Direction, in Specimen 15 (Mortar Injection), Specimen 16 (Epoxy Injection) and Specimen 17 (Epoxy Injection,  $t=0.6\text{mm}$ )**

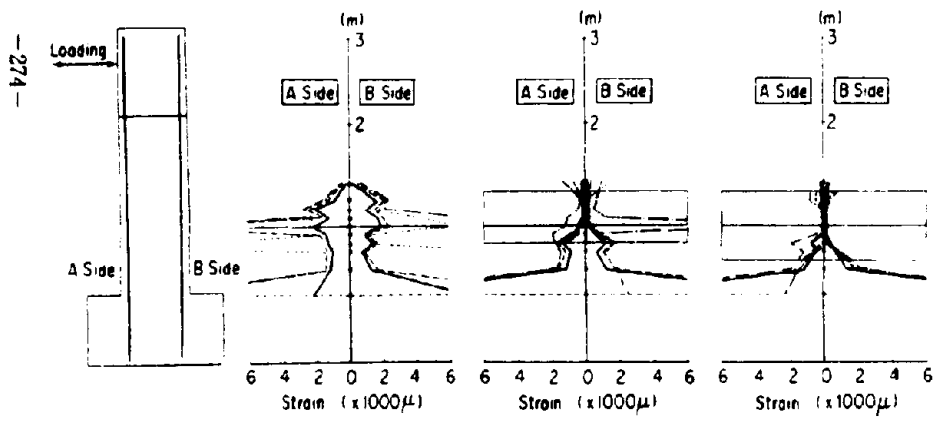




(a) Failure Mode

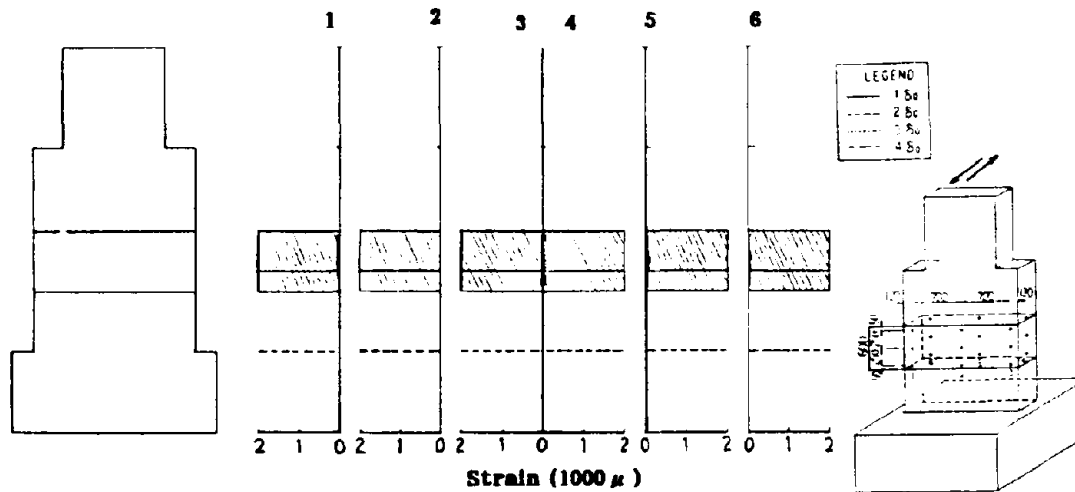


(c) Envelope of Load-Displacement Hysteresis Loops and Equivalent Hysteresis Damping Ratio

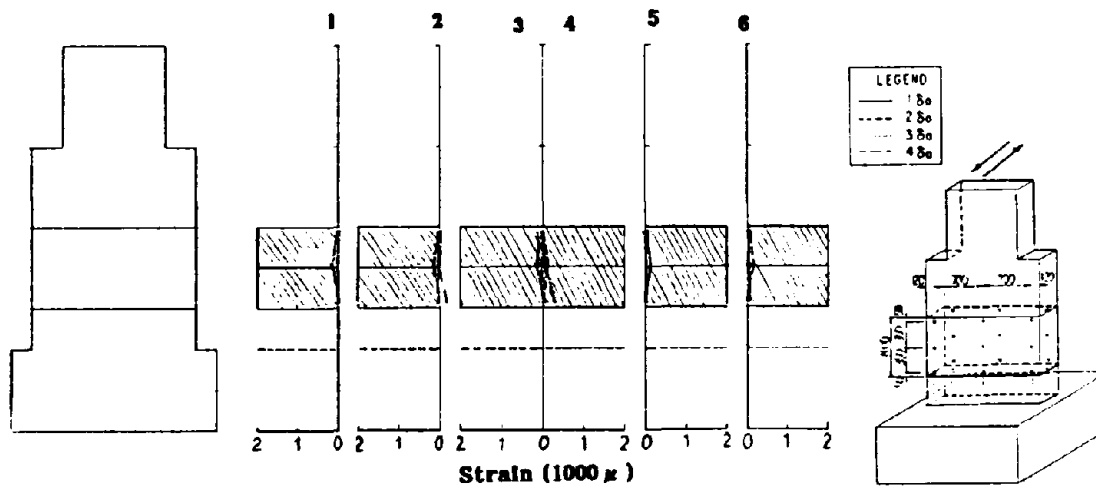


(b) Strain Developed in Main Reinforcement

Fig.14 Effect of Strengthening Method by a Steel Jacket for Wall Type Specimens with Shear Span Ratio of 7.1 (Specimens 18, 19 and 20)

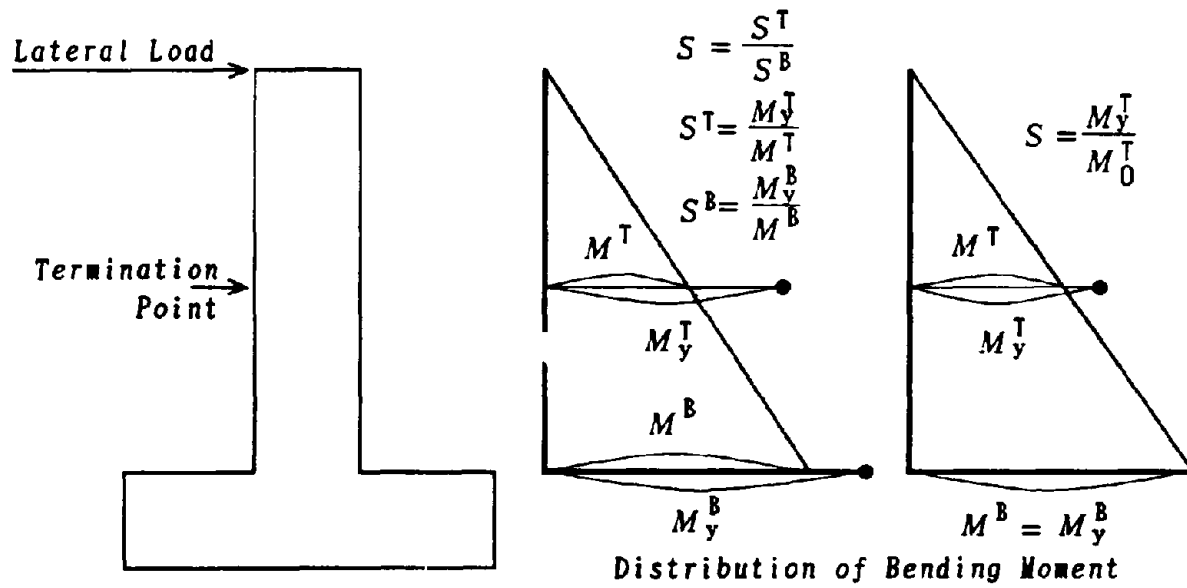


(1) Specimen 19 strengthened by 1.5D Long Steel Jacket and Mortar Injection

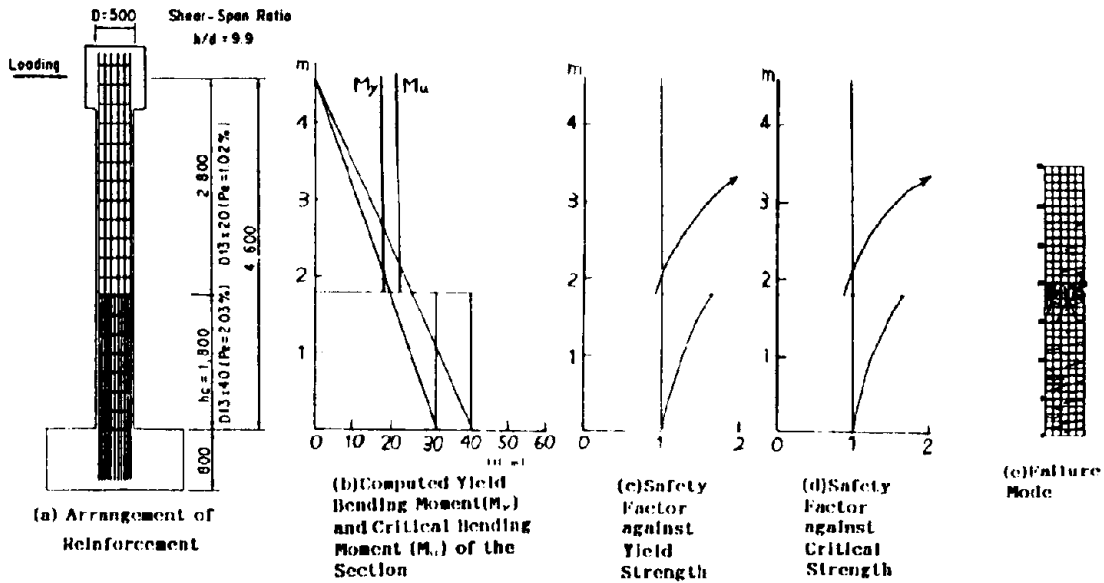


(2) Specimen 20 strengthened by 2D Long Steel Jacket and Mortar Injection

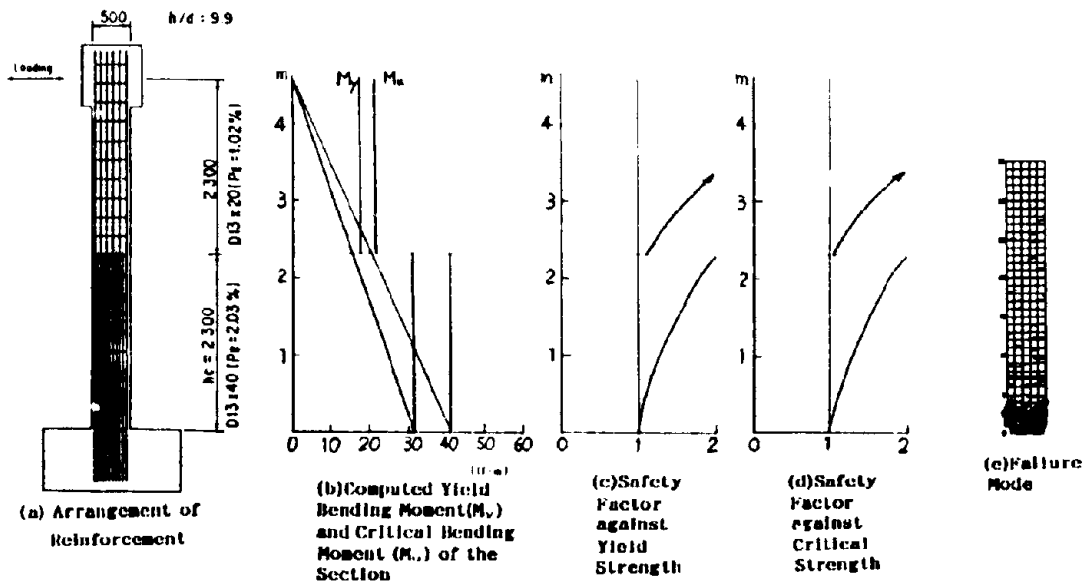
Fig.15 Strain induced in the Steel Jacket in Vertical Direction



**Fig.16 Definition of Failure Mode Factor to Evaluate Vulnerability of Reinforced Concrete Piers with Termination of Main Reinforcement**



(1) Specimen 1



(2) Specimen 3

Fig.17 Evaluation of Failure Mode Factors for Specimens 1 and 3

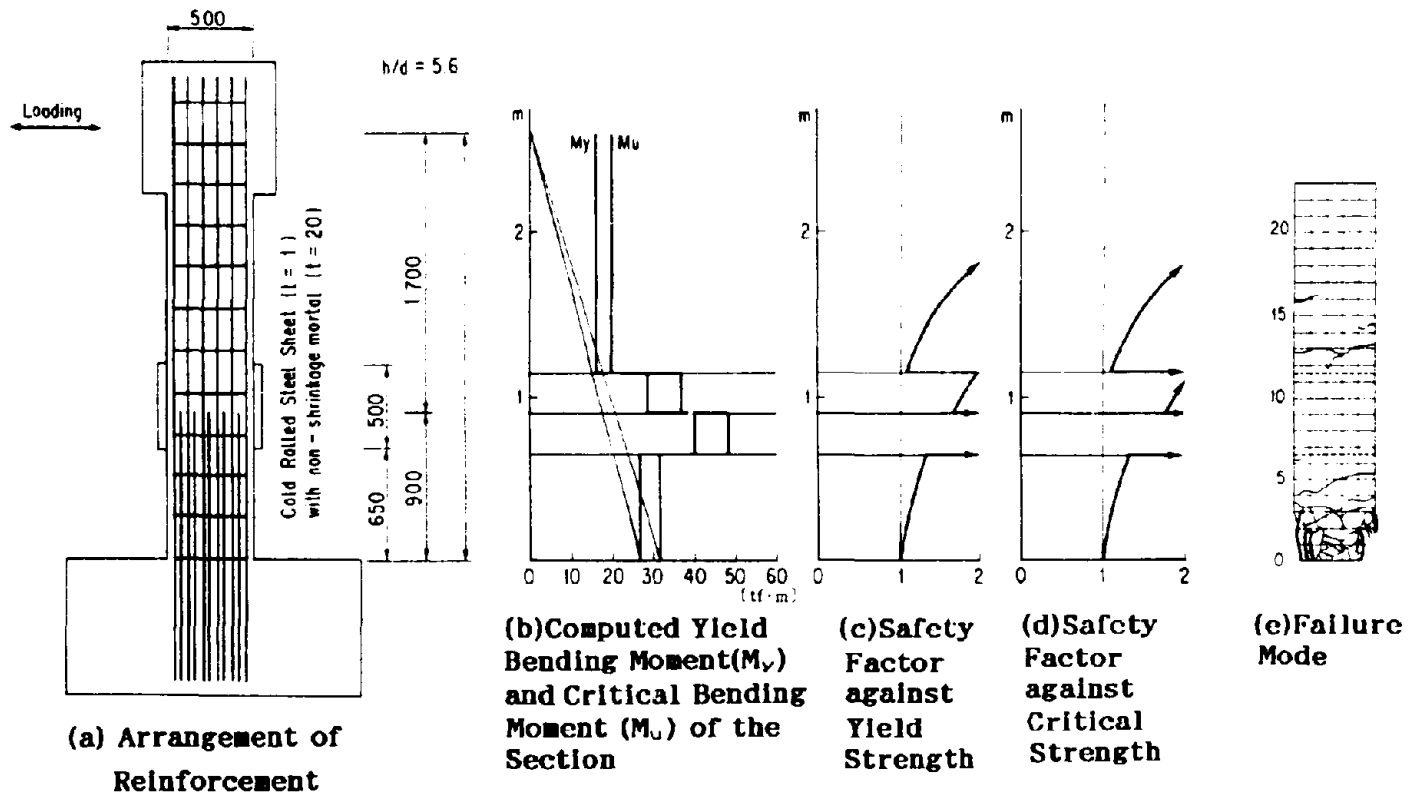
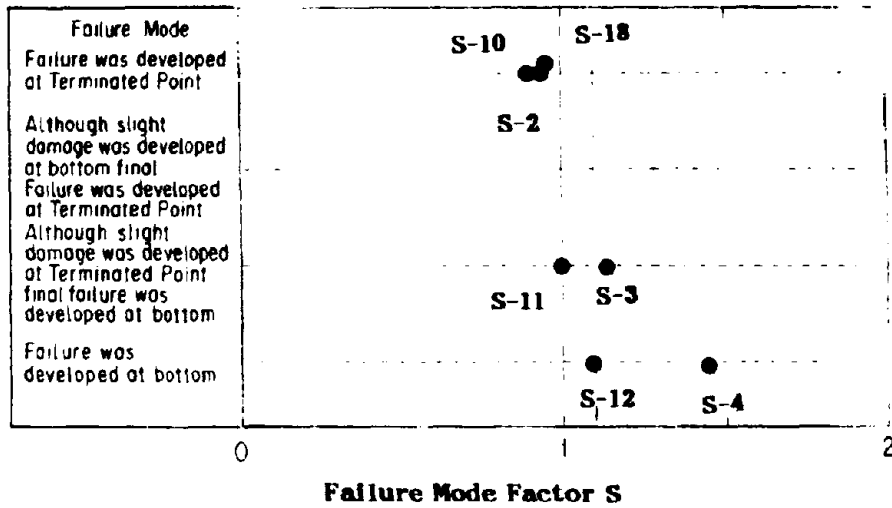
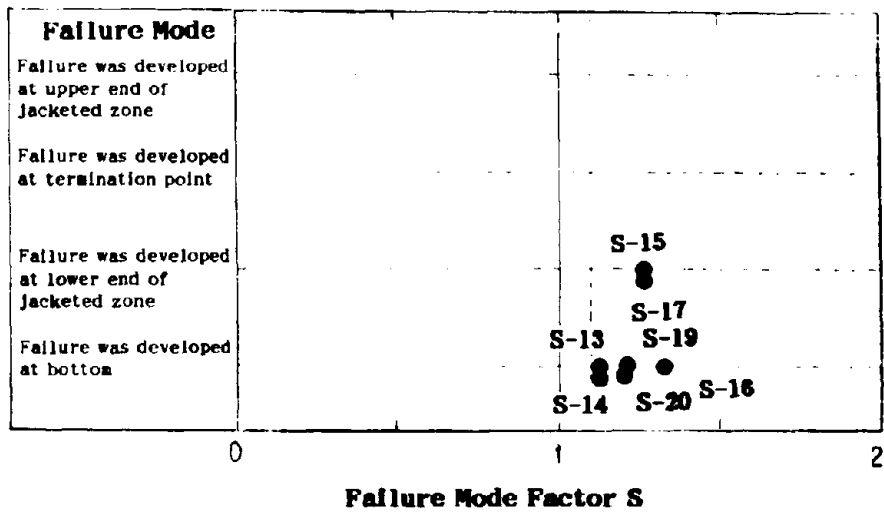


Fig.19 Evaluation of Failure Mode Factors for Specimen 13



**Fig.18 Evaluation of Failure Mode In Terms of Failure Mode Factor**



**Fig.20 Evaluation of Failure Mode In Terms of Failure Mode Factor for Specimens Strengthened by a Steel Jacket**

**SEISMIC STRENGTHENING OF REINFORCED CONCRETE PIERS  
ON METROPOLITAN EXPRESSWAY**

Taisuke Akimoto (I)  
Hiraku Nakajima (II)  
Fukashi Kogure (III)  
Presenting Author: Fukashi Kogure

**SUMMARY**

This paper presents a method of inspecting, designing, and strengthening the reinforced concrete (R/C) bridge piers which are judged to have inadequate strength against earthquake. On the Metropolitan Expressway Route No. 6, 36 R/C bridge piers were selected for strengthening. 9 piers were already jacketed with steel plate and epoxy resin based on the result of experiments. The thickness of the plate was determined to be 6 mm, assuming the plate would function completely together with reinforcement during earthquake. Aesthetic consideration was given to the design of anchors, color, and range of jacketing plate.

**INTRODUCTION**

In Japan, two big earthquakes (Miyagi-ken-oki earthquake in 1978 and Urakawa-oki earthquake in 1983) damaged many structures such as bridges and so on. As a result, in April 1986, Ministry of Construction ordered the following three types of inspection based on the notice titled "Regarding the Inspection of Existing Facilities for Seismic Safety". They are; (1) The First Level Inspection Concerning Superstructures, (2) The Second Level Inspection Concerning Soil Conditions, and (3) The Third Level Inspection Concerning Bridge Piers. The third level inspection is to check the safety of existing bridge piers in case of earthquake. The necessity of the third level inspection comes from a possibility that existing R/C bridge piers might lead to ductile shear failure due to the reduction in shear resistance caused by bending failure. Thus, the lack of the development length of main reinforcement tends to cause shear failure at mid-height of R/C bridge pier where part of main reinforcement is terminated. The failure is expected to take place when designed using the previous design code.

In 1980, "Specifications for Highway Bridges (Substructures)" was revised and the following articles concerning the above were changed. (1) The allowable shear stress of concrete was reduced (Article 3.2.2). (2) The position where part of main reinforcement was terminated at mid-height of R/C bridge pier was located at the effective height of member higher than before (Article 4.2.8).

- 
- (I) Head, Design & Research Division, Engineering Department, The Metropolitan Expressway Public Corporation, Tokyo 100, Japan
  - (II) Head, Maintenance Engineering Division, Maintenance & Facilities Department, The Metropolitan Expressway Public Corporation, Tokyo 100, Japan
  - (III) Senior Engineer, Design Division, Tokyo Maintenance Department, The Metropolitan Expressway Public Corporation, Tokyo 106, Japan

Consequently, The Metropolitan Expressway Public Corporation decided to check the safety of existing R/C bridge piers in case of earthquake. First, in 1986, the third level inspection was carried out concerning the existing R/C bridge piers and rough selection was made of the existing R/C bridge piers which met the following design conditions; (1) The fourth type soil condition, (The Metropolitan Expressway Route No. 6, 7, and 9 shown in Fig. 1), (2) Independent pier with round or rectangular cross section, (3)  $2 < h/D < 6$ , where  $h/D$ : Shear span ratio,  $h$ : Height of bridge pier column, and  $D$ : Diameter of bridge pier column, and (4)  $(\tau) > 36 \text{ (t/m}^2\text{)}$  or  $S_f < 1.2$ , where  $(\tau)$ : Applied shear stress at mid-height of R/C bridge pier where part of main reinforcement is terminated ( $\text{t/m}^2$ ) and  $S_f$ : Safety factor to yield strength at mid-height of R/C bridge pier where part of main reinforcement is terminated.

### EXPERIMENTS ON STRENGTHENING METHODS

The result of the third level inspection for checking the strength of the R/C bridge piers indicated that 36 bridge piers did not have enough strength. It became necessary to develop strengthening method and to strengthen the bridge piers immediately. Consequently, in 1987, Public Works Research Institute of Ministry of Construction, The Metropolitan Expressway Public Corporation, and The Hanshin Expressway Public Corporation performed model experiments as joint research to establish a guideline for seismic judgment. They were also aimed at affirming the effect of strengthening with steel jacketing. The experiments were divided into three parts and performed by each organization as follows; (1) Public Works Research Institute of Ministry of Construction performed the experiment on seismic judgment of R/C bridge piers at mid-height where part of main reinforcement is terminated, (2) The Metropolitan Expressway Public Corporation on the effect of strengthening R/C hollow bridge pier with round cross section, and (3) The Hanshin Expressway Public Corporation on the effect of strengthening R/C bridge pier with rectangular cross section.

The Metropolitan Expressway Public Corporation performed the experiment on the effect of strengthening R/C hollow bridge piers with round cross section using four types of specimens. In the experiment, steel jacketing method was adopted for strengthening, and dynamic loading tests were carried out using four different specimens. Attention was paid to the effect of the steel jacketing width and the grouting between steel jacketing and R/C bridge pier. The four specimens used in the experiment were as follows; (1) The specimen without strengthening, (2) The specimen with steel jacketing width of  $1.0D$  and with epoxy resin grouting, (3) The specimen with steel jacketing width of  $1.5D$  and with epoxy resin grouting, and (4) The specimen with steel jacketing width of  $1.5D$  and without epoxy resin grouting, where  $D$ : Diameter of R/C bridge pier. The steel plate was jacketed  $0.5D$  downwards, and  $0.5D$  or  $1.0D$  upwards from at mid-height of R/C bridge pier where part of main reinforcement was terminated.

The result of the experiments was summarized as follows; (1) Only when jacketed with the steel width of  $1.5D$  with epoxy resin grouting, the specimen showed bending failure at the bottom of the pier, and showed no indication of failure at mid-height. (2) When jacketed with the steel width of  $1.5D$  without epoxy resin grouting, the specimen showed failure at mid-height after the buckling of steel jacketing plate, and (3) The steel jacketing method could increase the ultimate strength of R/C bridge piers by approximately 30%. In addition, The Hanshin Expressway Public Corporation performed the same type of experiment using specimens with rectangular cross section and obtained almost the same results.





Fig. 1 Metropolitan Expressway Network

## THE THIRD LEVEL SEISMIC INSPECTION

In 1988, The Metropolitan Expressway Public Corporation performed the detailed third level inspection again concerning 156 R/C bridge piers on the Metropolitan Expressway Route No. 6 using the design drawings and documents. Consequently, 36 R/C bridge piers were selected for strengthening, which consist of 16 round solid piers, 9 round hollow piers, and 11 rectangular solid piers. The detailed design of strengthening was made. Fig. 2 shows the procedures for the third level inspection. Table 1 shows the selected R/C bridge piers for strengthening.

### Design Conditions

The design conditions and checking method for each item are; (1) Horizontal seismic design forces are  $k_h=0.26$  for bridge pier shorter than 15.0m and  $k_h=(h/15) \times 0.26=1.25 \times 0.26=0.33$  for bridge piers higher than 15.0m, (2) Specified concrete compressive strength is 270kg/cm<sup>2</sup> or 300kg/cm<sup>2</sup>, (3) Yield strength and Modules of Elasticity of reinforcing bar are 3,000kg/cm<sup>2</sup> and  $2.1 \times 10^6$ kg/cm<sup>2</sup>, respectively.

### Check for Yielding Safety Factor

The yielding safety factor at mid-height of R/C bridge pier where part of main reinforcement was terminated was checked based on the following equation;  $S_f=MR_n/M_c$  1.2 where  $MR_n$ : Yield bending moment at mid-height of R/C bridge pier where part of main reinforcement is terminated and  $M_c$ : applied bending moment at mid-height of R/C bridge pier where part of main reinforcement is terminated.

The yield bending moment  $MR_n$  was calculated assuming that the strain of reinforcing bar ( $\epsilon_s$ ) is  $\epsilon_s/E_s$  and four forces (Applied axial force  $N$  and induced compression and tension forces at the R/C cross section) are balanced (Fig. 3). The stresses of concrete and reinforcing bar are obtained from the relationship between stress and strain (Fig. 4). Fig. 5 shows the relationship between the amount of reinforcement and yield moment for a R/C bridge pier with a round cross section with the diameter of 3.0m when an axial force of 900 ton is applied.

### Checking for Average Shear Stress

The average shear stress at mid-height of R/C bridge pier where part of main reinforcement was terminated was checked using the following equation;  $(\tau)_{av}=S_c/A_c < (\tau)'_{al}$ , where  $S_c$ : applied shear force at mid-height of R/C bridge pier where part of main reinforcement is terminated (kg), and  $A_c$ : Cross sectional area at mid-height of R/C bridge pier where part of main reinforcement is terminated (cm<sup>2</sup>).

In addition, the allowable shear stress of concrete  $(\tau)'_{al}$  is calculated using the following equation;  $(\tau)'_{al}=(\alpha)(\tau)_{al}$ , where  $(\alpha)$  is a multiplier due to axial compression force and obtained from the following equation;  $(\alpha)=1+M_o/2M < 2.0$ , where  $M$ : Applied bending moment at mid-height of R/C bridge pier where part of main reinforcement is terminated and  $M_o$ : the bending moment which makes stress at the extreme tension fiber equal to 0.0 together with axial force, obtained from the following equation;  $M_o=N/A_c I_c/y$ , where  $N$ : Axial compressive force at mid-height of R/C bridge pier where part of main reinforcement is terminated (kg),  $A_c$ : Cross sectional area at mid-height of R/C bridge pier where part of main reinforcement is terminated (cm<sup>2</sup>),  $I_c$ : Moment of inertia about centroid

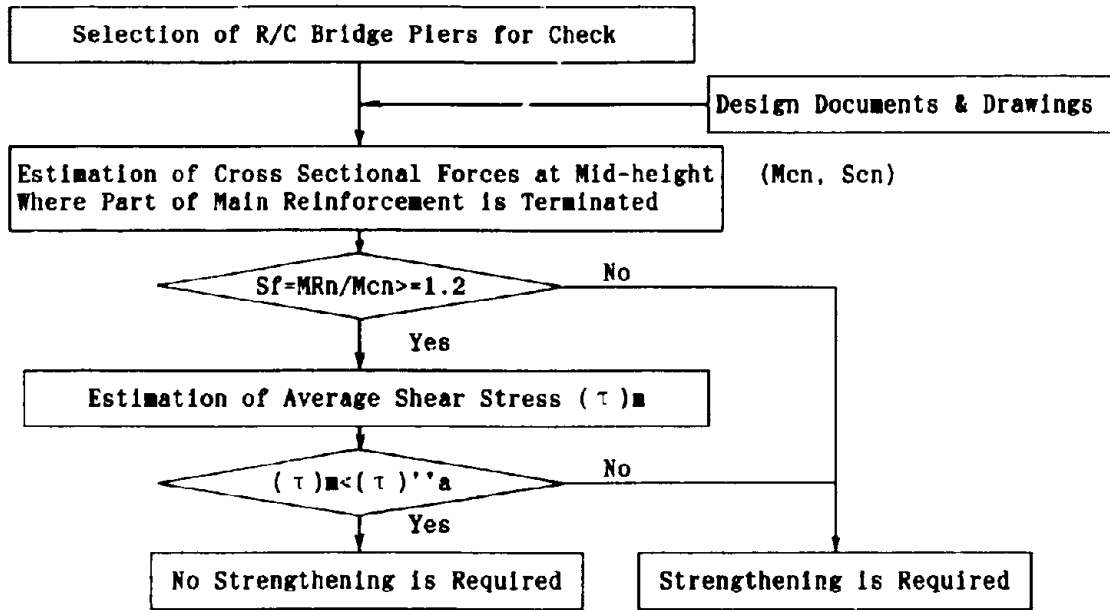


Fig. 2 The 3rd Level Inspection Flowchart

## (On the Metropolitan Expressway Route No. 6)

No.	Pier No.	Pier Type (1)	H(Column) (m)	D (m)	H/D	Original		Strengthened(2)	
						Sf	$\tau$	Sf	$\tau$
1	167	ROSC	14.023	3.0	4.7	1.17	OK	1.40	-
2	186	ROSC	11.366	3.2	3.6	1.00	OK	1.46	-
3	289	ROHC	7.685	3.0	2.6	OK	5.26	-	Stirup
4	290	ROHC	8.251	3.0	2.8	OK	5.76	-	Stirup
5	291	ROHC	10.363	2.5	4.1	OK	4.69	-	Stirup
6	292	ROHC	10.702	3.0	3.6	1.16	6.34	1.68	Stirup
7	293	ROHC	10.702	3.0	3.6	1.16	6.34	1.68	Stirup
8	294	ROHC	10.872	2.5	4.3	1.14	5.63	1.62	Stirup
9	295	ROHC	11.381	2.5	4.6	OK	5.33	-	Stirup
10	296	ROHC	11.381	2.5	4.6	OK	5.33	-	Stirup
11	297	ROHC	11.381	2.5	4.6	OK	5.33	-	Stirup
12	298	ROHC	9.951	3.0	3.3	OK	4.92	-	Stirup
13	300	ROSC	10.100	3.0	3.4	OK	4.50	-	Stirup
14	301	ROSC	10.100	3.0	3.4	OK	4.50	-	Stirup
15	302	ROSC	10.100	3.0	3.4	OK	4.50	-	Stirup
16	303	ROSC	12.500	3.0	4.2	OK	4.55	-	Stirup
17	304	ROSC	10.800	3.0	3.6	OK	4.55	-	Stirup
18	305	ROSC	13.500	3.0	4.5	1.00	OK	1.42	-
19	306	ROSC	12.800	3.0	4.3	1.08	OK	1.40	-
20	307	ROSC	12.400	3.0	4.1	1.10	OK	1.45	-
21	308	ROSC	11.500	3.0	3.8	1.12	OK	1.62	-
22	311	ROSC	10.300	3.5	2.9	1.10	OK	1.46	-
23	312	ROSC	10.100	3.0	3.4	1.16	OK	1.50	-
24	313	ROSC	9.600	3.0	3.2	1.10	OK	1.45	-
25	315	ROSC	9.600	3.0	3.2	1.08	4.57	1.38	Stirup
26	426-3	RESC	6.890	1.3x1.3	5.3	1.14	OK	1.85	-
27	426-4	RESC	5.460	1.3x1.3	4.2	1.19	OK	1.92	-
28	465	RESC	9.620	2.6x2.6	3.7	1.18	OK	1.68	-
29	496	RESC	5.042	3.0x2.5	2.0	1.04	OK	1.45	-
30	497	RESC	10.401	3.0x2.2	4.7	0.97	OK	1.27	-
31	503	RESC	9.248	3.0x2.2	4.2	0.88	OK	1.29	-
32	505	RESC	9.831	3.0x2.2	4.5	0.88	OK	1.29	-
33	509	RESC	7.517	2.0x2.0	3.8	0.81	OK	1.75	-
34	514	RESC	9.100	2.0x2.0	4.6	0.96	OK	1.75	-
35	515	RESC	10.289	3.0x2.2	4.7	1.07	OK	1.38	-
36	516	RESC	7.860	2.5x2.5	3.1	0.97	OK	1.82	-

- (1) ROSC: Round Solid Column  
ROHC: Round Hollow Column  
RESC: Rectangular Solid Column

- (2) In case strengthened with 4.5mm thick plate

Table 1 Selected R/C Bridge Piers

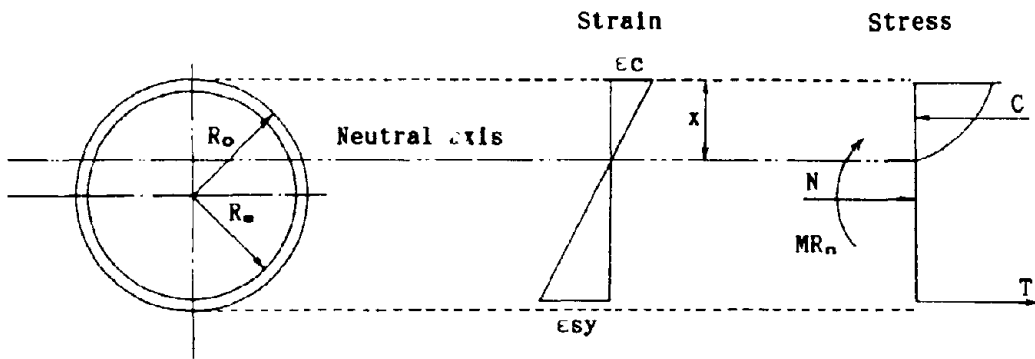
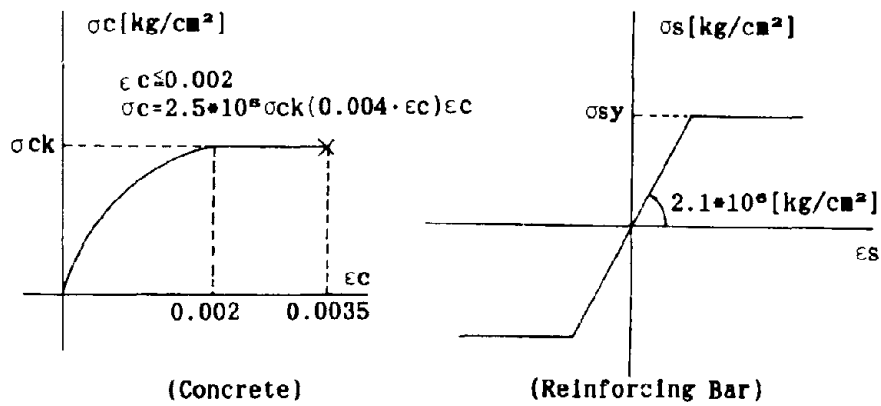


Fig. 3 Balance of Forces in Yielding



Note: The relationship between stress and strain in concrete can be assumed as in Fig. 3 when the column is provided hoop.

Fig. 4 Relationship between Stress and Strain

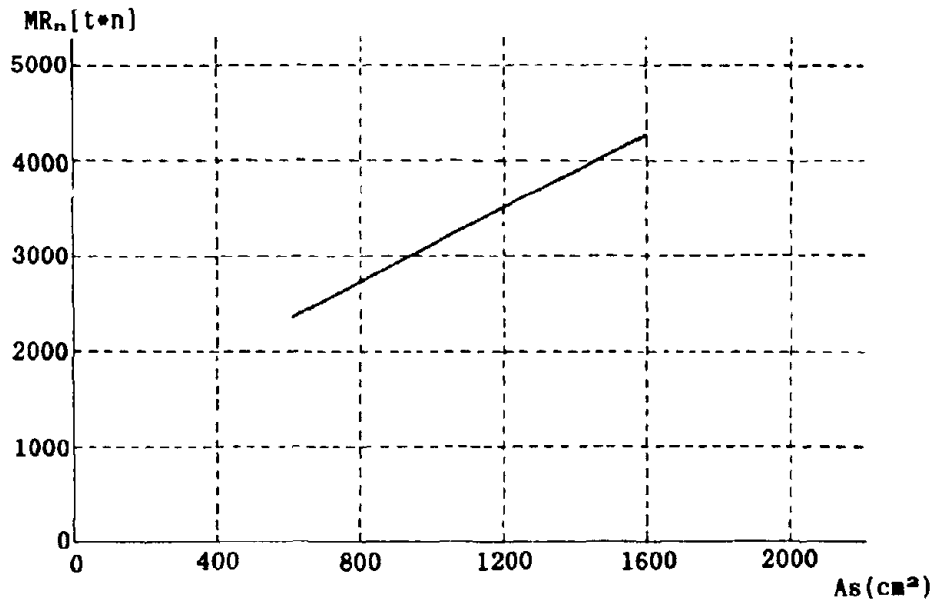


Fig. 5 Relationship between Amount of Reinforcement and Yield Moment

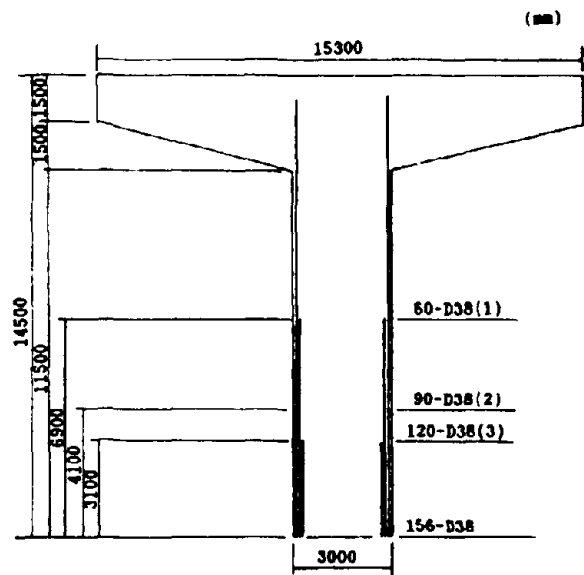


Fig. 6 Positions where Part of Main Reinforcement is Terminated

( $\text{cm}^4$ ), and  $y$ : Distance between centroid and tension fiber (cm).

The Inspector indicated that 36 bridge piers were needed to strengthen among 156 on Metropolitan Expressway Route No. 6 (16 round piers, 9 round hollow piers, and 11 rectangular piers as shown in Table 1). Fig. 6 shows where part of main reinforcement is terminated at mid-height in one of the typical R/C bridge pier. Table 2 and 3 show the result of safety check and cross sectional properties, respectively.

#### STRENGTHENING DESIGN

Strengthening design was made for the R/C bridge piers which were judged to be necessary to strengthen according to the seismic third level inspection. The steel jacketing method with epoxy resin was adopted for strengthening based on the result of the experiments of 1987.

##### Design for Seismic Load (After Completion)

When completed, the steel jacket is considered to function completely together with R/C bridge pier. Therefore, the thickness of the steel plate was designed for bending moment and horizontal force due to earthquake, assuming the steel plate resists the seismic loads in the same way as reinforcement. As a result, the thickness of 4.5mm was calculated to be enough. The steel plate of 6mm was, however, adopted to avoid deformation during fabrication, shipping, and grouting. The procedures for the design of thickness are; (1) In case yield safety factor  $S_f < 1.2$ , the steel plate is transformed to reinforcement and the thickness is determined to make  $S_f$  more than 1.2 at mid-height of R/C bridge pier where part of main reinforcement is terminated, (2) In case an average shear stress  $(\tau) > (\tau)'_a$ , the steel plate is transformed to reinforcement and the thickness is determined treating it as stirrup. Thus, one half of the load is carried by concrete, while the other half carried by reinforcement. The required amount of reinforcement as stirrup is obtained from "Specifications for Highway Bridges: (Substructures) 4.2.7".

##### Design for Grouting Pressure of Resin (During Construction)

Since the height of jacketing plate reaches several meters, the steel plate is subjected to bending moment and tension force due to grouting pressure during resin grouting. Consequently, excessive stress and deformation are expected in the steel plate. The steel plate is anchored with anchor bolts with adequate intervals to reduce excessive stress and deformation.

The anchor bolts pitch is designed for the stresses in the steel plate, the deformation, and the pull-out force of the anchor bolts due to the internal pressure, assuming the resin grouting pressure shows hydraulic pressure distribution. FEM was used for analyzing the deformation and stresses. It turned out to be enough to reinforce the steel plate of round R/C bridge pier with anchor bolts with a 100cm interval. As for the steel plate of rectangular bridge pier, the deformation was calculated to be excessive. Therefore, the anchor pitch was determined to be 50cm to avoid excessive deformation.

The range of strengthening bridge pier was determined to be from the ground level to just below the beam to reduce the anxiety of the public as well as to improve appearance, although the experiment indicated 1.5D (0.5D downwards and 1.0D upwards) was enough at mid-height of R/C bridge pier

Section	Cross-sectional forces		Yield safety factor	Average sheare stress
1	M (tm)	2185.8	Sf = 1.17 < 1.2 out	$\tau_m = 275900/70686$ = 3.90 < $\tau_a=4.50\text{kg/cm}^2$ O.K.
	N (t)	836.3		
	S (t)	275.9		
2	M (tm)	2981.3	Sf = 1.12 < 1.2 out	$\tau_m = 292300/70686$ = 4.14 < $\tau_a=4.43\text{kg/cm}^2$ O.K.
	N (t)	885.8		
	S (t)	292.3		
3	M (tm)	3129.6	Sf = 1.30 > 1.2 O.K.	$\tau_m = 298100/70686$ = 4.22 < $\tau_a=4.42\text{kg/cm}^2$ O.K.
	N (t)	903.4		
	S (t)	298.1		

Average sheare stress  $\tau_m = S/A_c$

$$A_c = \pi * 3.0 * 3.0 / 4 * 10000 = 70686 \text{cm}^2$$

Table 2 Result of Check for Safety Factor

Section 2 of Mukojima 308 Bridge Pier			
Outer Radius of Section	Ro	cm	150.00
Distance to Reinforcing Bar	Rs	cm	136.70
Sectional Area of 1 Reinforcing Bar	As	cm <sup>2</sup>	11.40
Number of Reinforcing Bars	Ns		90
Specified Concrete Compressive Strength	( $\sigma$ )ck	kg/cm <sup>2</sup>	270.0
Yield Stress of Reinforcement	( $\sigma$ )sy	kg/cm <sup>2</sup>	3000.0
Modulus of Elasticity of Reinforcement	Es	kg/cm <sup>2</sup>	2100000.0
Applied Bending Moment	Mcn	tm	2981.3
Applied Axial Force	N	t	885.80
Distance to Neutral Axis	x	cm	102.502
Yield Moment	MRn	tm	3341.09
Yield Safety Factor	Sf		1.121

Table 3 Sectional Properties



where part of main reinforcement is terminated.

The strengthening method is summarized as follows; (1) Strengthening method: Steel jacketing method with epoxy resin grouted between steel plate and concrete, (2) Strengthening range: From the ground level to just below the beam, (3) Steel plate: Thickness  $t=6\text{mm}$ , and material SS41, (4) Thickness of resin grouting:  $t=3\text{mm}$ , (5) Anchor pitch:  $100\text{cm}$  for a round column and  $50\text{cm}$  for a rectangular column, and (6) Anchor bolts: M16 concrete bolt with countersunk and chipped head for aesthetic appearance. Fig. 7 shows how to strengthen an R/C bridge pier.

#### FIELD WORKS OF STRENGTHENING R/C BRIDGE PIER

In 1989, 9 R/C bridge piers were jacketed with steel plate in Mukojima area on Metropolitan Expressway Route No. 6. Fig. 8 shows the field works procedures for strengthening R/C bridge pier at the construction site. Fig. 9 and 10 show the R/C bridge pier before and after strengthening, respectively.

#### Surveying

After setting up work platform (Fig. 11), the detailed surveying of R/C bridge piers, including obstacles such as drainpipe and inspection ladder, was carried out using survey equipments. The design for fabrication was made based on the result of surveying.

#### Fabrication

The steel jacketing plate was fabricated according to the design (Fig. 12). The procedures were; (1) Cutting and drilling, (2) Bending, (3) Sand blasting and primary painting, and (4) Two coats of painting. SS41 steel was used.

#### Concrete Coating

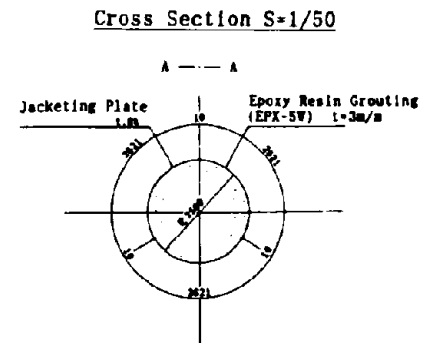
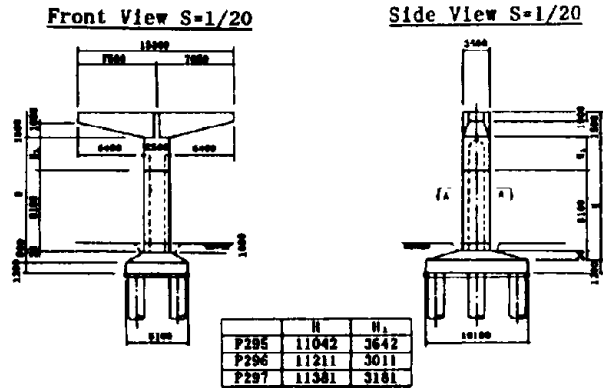
The surface of R/C bridge pier was cleaned with wire brush, sander, or thinner (Fig. 13). The obstacles were moved or removed if necessary. The concrete surface without steel jacketing was coated with four coats of resin.

#### Steel Jacketing

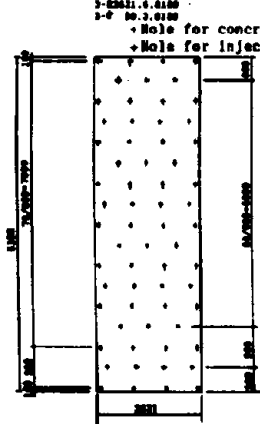
Temporary angles were anchored to the R/C bridge pier to support the steel jacketing plates at the required position. The jacketing plates were transported to the construction site, and lifted to the designated position by 5 ton crane (Fig. 14). The plate was placed on the angle, temporarily anchored, and wired. The erection was performed very carefully to avoid the deformation of the steel plate. The pier was drilled, and concrete anchor bolts were set into the drilled holes. The bolts with countersunk and chipped head were fixed to the anchor bolts with torque wrench.

The steel jacketing plate was carefully welded to one another from the bottom to the top of the welding line while controlling welding temperature (Fig. 15). The defects found in the welding parts were repaired and finished.

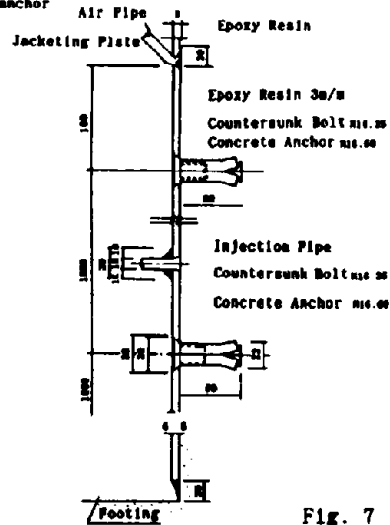
a. Round Cross Section



**Steel Plate S=1/50**



**Fixing of Steel Plate S=1/2**



**Welding S=1/2**

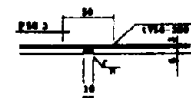


Fig. 7 The Strengthening of RC Bridge Pier

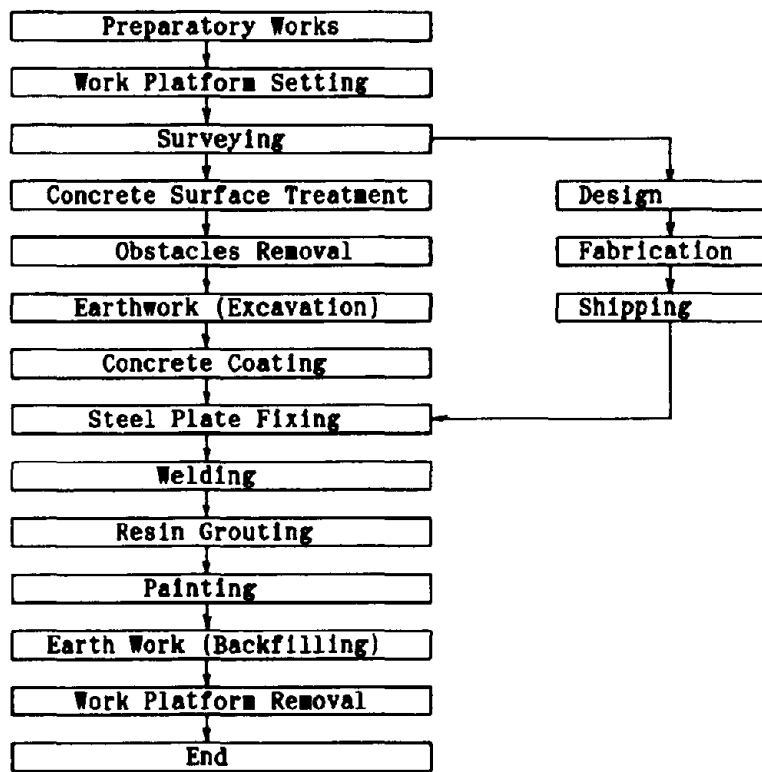


Fig. 8 Field Works of R/C Pier Strengthening

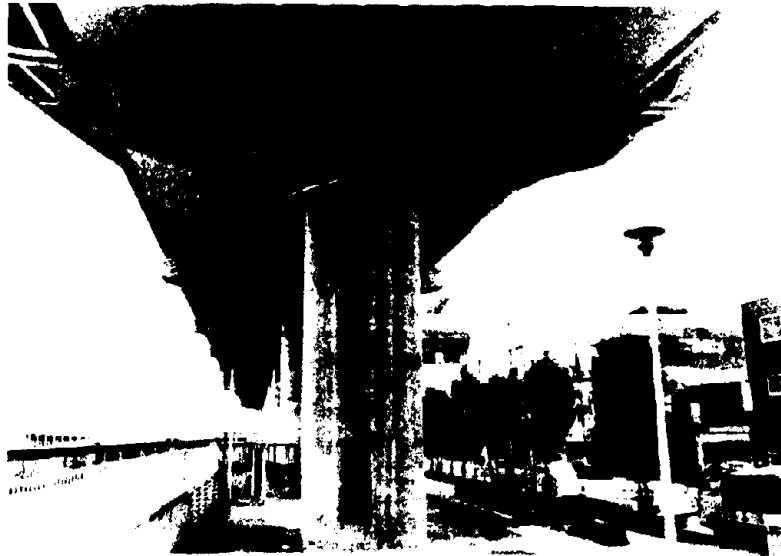


Fig. 9 Before Strengthening



Fig. 10 After Strengthening

### Epoxy Resin Grouting

Injection and air pipes were installed, and all the gaps in the jacketing plate were sealed with epoxy resin by hand. Epoxy resin was grouted through the injection pipe from the bottom to the top with manual pump (Fig. 16). In general, 3.0m of grouting was performed at the time, and the procedure was repeated depending on the required height. When epoxy resin hardened, the injection and air pipes were removed and finished.

### Painting of Steel Jacketing

For the aesthetic reason, the steel jacketing plate was painted in the same color as the concrete coating after cleaning the surface at the construction site. The in-situ painting consists of five coats at joint parts and two coats at the rest, respectively.

## CONCLUSIONS

It was almost for the first time for the Metropolitan Expressway Public Corporation that R/C bridge piers were strengthened with steel jacketing.

In the design, the following points were taken into accounts; (1) Anchor bolts with countersunk and chipped head were used for the appearance after completion, (2) To avoid giving an impression to the public that R/C piers are strengthened as well as to improve the aesthetic appearance, the surface of R/C bridge pier without steel jacketing plate was coated in the same color as the steel plate, (3) Although the steel jacketing plate of 4.5mm was enough from the design point of view, 6mm thick plate was used to avoid deformation during fabrication, transporting, and grouting as well as to use anchor bolts with countersunk and chipped head.

In the erection, the following points should be paid attention; (1) Before the fabrication of steel jacketing plate the dimensions of R/C bridge piers should be measured as accurately as possible, (2) To put anchor bolts with countersunk and chipped head exactly into place, the drilling of holes in the steel plate for anchor bolts should be performed as carefully as possible, and (3) In grouting resin, the height of grouting should be controlled, and the deformation of steel plate be checked especially in a rectangular R/C bridge pier.

As mentioned the above, the basic design for strengthening R/C bridge piers on Metropolitan Expressway Route No. 6 was already finished in 1988. 9 R/C bridge piers among them were jacketed in 1989, and 6 are now being strengthened. The rest of them are scheduled to strengthen soon. Since there are still some unknown factors especially in the erection, it will be necessary to improve the design method as well as to establish erection techniques through the strengthening experience.

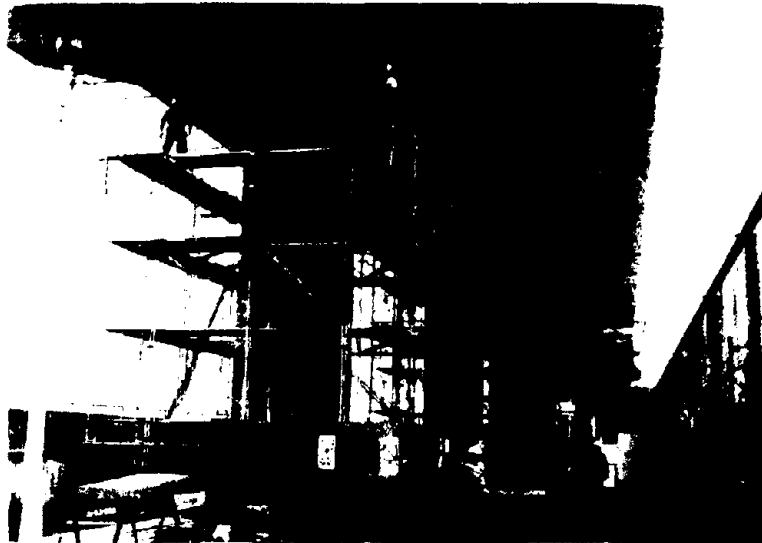


Fig. 11 Work Platform



Fig. 12 Steel Plate Fabrication



Fig. 13 Concrete Surface Treatment

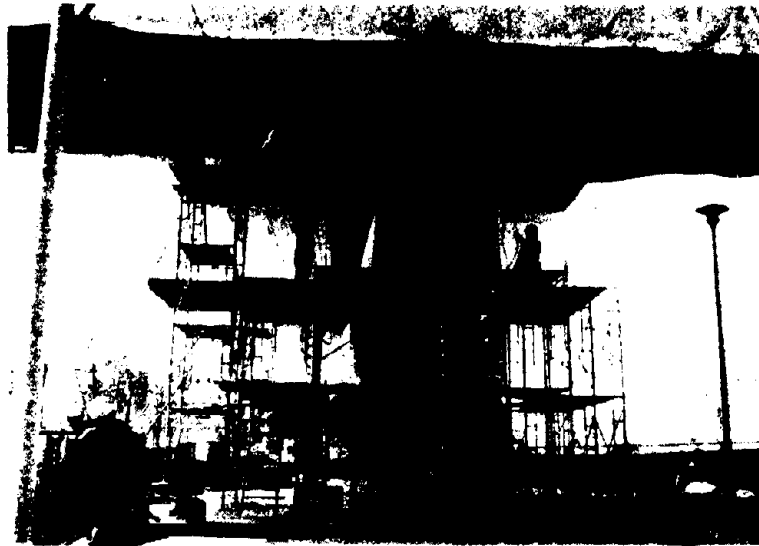


Fig. 14 Erection

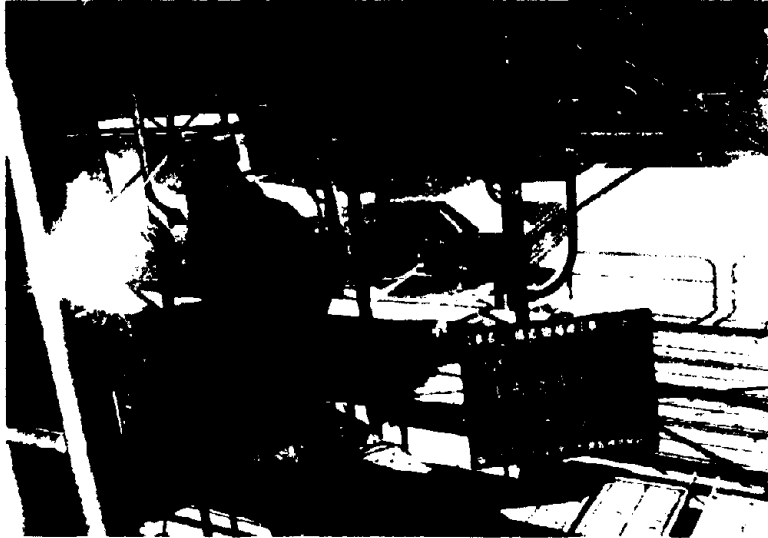


Fig. 15 Welding



Fig. 16 Grouting



### References

- 1) The Metropolitan Expressway Public Corporation, "Experiment on Strengthening Method of R/C Bridge Piers", March 1988.
- 2) The Metropolitan Expressway Public Corporation, "Structural Design 63-21", March 1989.
- 3) Hiroo Tominaga, "Strengthening Design of R/C Bridge Piers", Maintenance Technical Report 1989, pp. 4 - 7, The Metropolitan Expressway Public Corporation, March 1990.

SEISMIC STRENGTHENING METHOD FOR REINFORCED CONCRETE BRIDGE PIERS  
ON HANSHIN EXPRESSWAY

Yasuo MATSUURA ( I )

Ippei NAKAMURA ( II )

Hiroshi SEKIMOTO ( III )

Presenting Author : Ippei NAKAMURA

SUMMARY

This paper presents a series of investigations from inspection to field works of reinforced concrete piers for the strengthening against an earthquake.

When the anchorage length of main reinforcement of the reinforced concrete piers is insufficient, shear failure tends to cause at mid-height of reinforced concrete piers where part of main reinforcement is terminated.

As a result of investigation, steel jacketing method is effective for seismic strengthening. Namely, it is a strengthening method which bind a steel plate around a RC pier at its termination section of main reinforcements. The thickness of the steel plate is 6mm and the steel plate is jacketed 0.5D (where, D: the side length of a square section) below and 1.0D above the termination section of the main reinforcements and with epoxy resin grouting between steel plate and reinforced concrete pier.

INTRODUCTION

In the Off-Miyagi Prefecture Earthquake in 1978 and the Off-Uraga Earthquake in 1982, both in Japan, reinforced concrete piers among bridge members suffered from severe damages near the section of termination of the main reinforcements.

It seems that the damages near the termination section of the main reinforcements were due to brittle shear failure caused by a decrease in an effective sectional area for shear accompanied by flexural cracks of concrete, when the anchoring length of the reinforcements was not sufficient.

- 
- ( I ) Chief of Second Maintenance Section, Osaka Management Division, Hanshin Expressway Public Corporation, Osaka 541, Japan
  - ( II ) Assistant Chief Engineer, Maintenance Engineering Section, Maintenance and Facility Design Division, Hanshin Expressway Public Corporation, Osaka 541, Japan
  - ( III ) Civil Engineer, Maintenance Engineering Section, Maintenance and Facility Design Division, Hanshin Expressway Public Corporation, Osaka 541, Japan

Therefore, in the Japanese Highway Bridge Specifications revised in 1980, it is included that the allowable shearing stress of concrete was lowered, and the section of termination of the main reinforcements is to be extended by a length equal to an effective depth of a section of a member, beyond a point where the reinforcements are not required in the strength calculation.

On the other hand, existing bridges constructed before 1980 took an inspection in 1986 about the load-carrying capacity against an earthquake. As a result, the piers of which the load-carrying capacity was not sufficiently secured were urged to prepare for an earthquake. About 50 piers among the bridge piers of the present Hanshin Expressway were required to be strengthened against an earthquake.

Hanshin Expressway Public Corporation, the Public Works Research Institute of the Ministry of Construction and Metropolitan Public Corporation carried out a joint research on the method of seismic strengthening. As a result, it was recommended as an effective strengthening method to apply a binding up with a steel plate around a pier. The width and thickness of the steel plate and a filler material required to fill a gap between the pier body and the steel plate were proposed for the strengthening design.

The Corporation, in order to study on the applicability of the proposed method to actual piers, carried out test works for existing piers and examined the various design and works problems.

This paper presents an outline of a series of investigations from inspection to field works of reinforced concrete piers for the strengthening against an earthquake.

## 1. 1986 Inspection of Existing Highway Bridges against Earthquake

### 1-1 Outline of inspection

This inspection followed an official memorandum about "the Inspection of Public Facilities for Safety Against Earthquake"(No.6 Document of "Street" Division, City Bureau and No.5 Document of "Disaster Prevention" Division, Road Bureau, both of the Ministry of Construction, both issued on the 4th of April, 1986). Through this inspection, the earthquake proofing of existing bridges was evaluated, based on damages experienced at the Off-Uraga Earthquake in 1982, the Middle of Japan Sea Earthquake in 1983 and the West of Nagano Prefecture Earthquake in 1984.

Locations and items for the inspection were classified by three stages of inspection.

The first inspections are basic inspections of factors affecting greatly earthquake damages, and consist of surveys of deformation of super-structures, sub-structures and supports of all of the existing bridges, surveys of apparatuses to prevent the super-structures from falling down and surveys of earthquake proofing of the sub-structures.

The second inspections cover the ones of ground liquefaction of bridges and of the earthquake proofing of the sub-structures by simple calculations of strength of pier bodies and bearing capacity of foundation piles, both for the bridges which were evaluated to need further inspections.

The third inspections are carried out about the strength at the section of termination of the main reinforcements of reinforced concrete piers with a rectangular or circular section of the highway bridges which are supported by a reinforced concrete single column and designed before 1980. The inspection items are shown in Table-1.

The conditions requiring a strengthening work after the third inspections are as follows:

- ①  $2 < \text{shear span ratio } h/D < 6$ ,
- ② subsurface ground belongs to the 4th Group,
- ③ safety factor for yield strength at the section of termination  $< 1.2$  or shearing stress at the section of termination  $\geq 36tf/m^2$ .

Table-1 Items for 1986 Earthquake Proof Inspection of Highway Bridges

Third Inspection	Sub-structures	Strength at Section of Termination of Main Reinforcements of RC Bridge Piers	Shear Span Ratio (h/D) :
			$h/D \leq 2, h/D \geq 6, 2 < h/D < 6$
			Ground Conditions Classification: 1st, 2nd, 3rd and 4th Group
			Factor of Safety for Yield Strength at Termination Section of Main Reinforcements: larger than 1.2 or smaller than 1.2
			Shearing Stress $< 36tf/m^2$ or $\geq 36tf/m^2$

where, h = the distance from upper end of a footing to lower end of

a beam  
D = the side length of a square section, or the side length in  
direction perpendicular to bridge longitudinal direction of  
a rectangular section with long sides and short sides

## 1-2 Inspection results

The results of the 1st and the 2nd inspection works for the aseismic design of bridges along the existing routs showed there was no questionable member or element observed.

The following records were obtained about the strength of 5275 RC bridge piers designed before 1980 at the termination section of main reinforcements which were examined by the 3rd inspection. In 115 piers, the shear span ratio  $h/D$  was between 2 and 6, and the subsurface ground belonged to the 4th Group. In 51 piers, the safety for yield strength at their termination section of main reinforcements or the shearing stress was questionable.

## 2. Design of A Seismic Strengthening Works

### 2-1 Verification test for a seismic strengthening

A test was carried out jointly with the Public Works Research Institute of the Ministry of Construction and the Metropolitan Expressway Public Corporation, aiming at verifying the strengthening effect of binding a steel plate around a RC pier at its termination section of main reinforcements.

The reason why the steel plate strengthening was applied to existing concrete piers can be explained as follows. If reinforced concrete were cast around the existing RC piers, the strengthening work would have become larger in scale; noise and vibration would have occurred due to chipping works for joining new concrete to old concrete; the intringement to construction gauge due to an increase of pier section; and an excessive increase of the pier weight would have been produced.

#### 2-1-1 Model column specimens for test

Test columns for the experiment modeled piers with a square section which were judged to need reinforcement at a termination section of main reinforcements, as a result of the earthquake proof inspection of highway bridges carried out in 1986.

The size and shape of the test columns are given in Fig.1. The test column for a pier with a square section is provided with a section of 50cm×50 cm, a shear span ratio of 5.3 and a loaded height of 2.6m, all on a scale of 1/6. Further, an amount of rebars provided the test columns observes the same ratio of rebars as in the actual piers.

Four test cases were chosen by the width of steel jacket for binding, by whether filler material is provided between pier body and the steel jacket or not, and by the type of the filler material if it is used. The test columns were classified as follows:

- Test Column No. 1 : square section, no reinforcement by steel plate,
- Test Column No. 2 : square section, binding width of 1.0 D where D is a length of sides of a column section, and with non-shrinkage mortar injected,
- Test Column No. 3 : square section, binding width of 1.0 D, and with epoxy resin injected,
- Test Column No. 4 : square section, binding width of 1.5 D, and with epoxy resin injected,

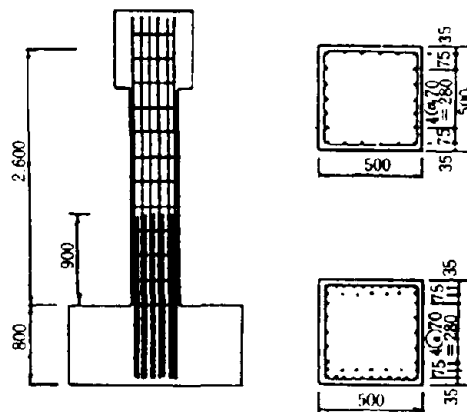


Fig. 1 Shape and Size of Square Section Test Columns

The steel plate for binding is of SPCC (= cold-rolled steel) of 1mm in thickness. For the test specimens of Nos. 2 and 3, a range of 0.5 D above and below a section of termination of main reinforcements, and for the test specimen of No. 4, a range of 1.0 D above and of 0.5 D below the termination section, were binded with steel plates. The thickness of the filler material was 20mm for non-shrinkage mortar and 3mm for epoxy resin.

#### 2-1-2 Test method

In the test, a test specimen was horizontally set, and an axial force of 28.8 tf for a square section was applied to the specimen by a loading device of axial force. The axial force was selected assuming a pier reaction from the superstructure. Then, keeping the axial force loaded, a dynamic load was further applied.

At the dynamic test, alternate dynamic loads were given by an actuator under displacement control in terms of positive and negative displacements. This forced displacements, which were integer multiples of the yielding strain  $\delta_y$  of the pier column (15mm for a square section), were applied to the top of the test column with 10 waves of the sine wave.

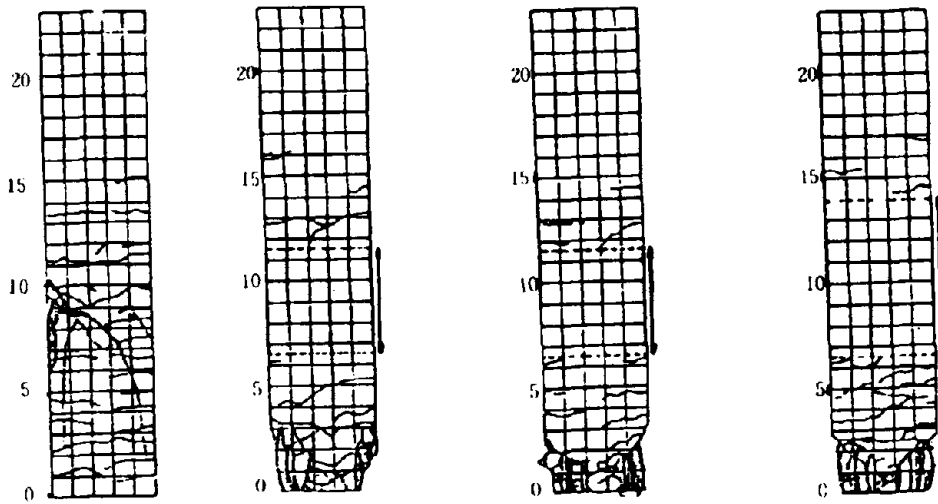
The yielding here was chosen at a point where the strain  $\epsilon_s$  took suddenly a large amount against an increase of the force P, in which P is an applied force at the top of the test column and  $\epsilon_s$  is a strain of reinforcements on the tension side at the extreme fiber of the column base.

Further, before the strain  $\epsilon_s$  reached the yielding, a load was statically applied with a gradual increase at about 10 steps of positive and negative alternate loading under load control.

#### 2-1-3 Test results

##### (1) Fracture modes

Fig. 2 shows fracture modes of the test columns after the loading tests ended.



(1) Test Specimen 1 (2) Test Specimen 2 (3) Test Specimen 3 (4) Test Specimen 4  
 (after static test) ( after 78 y loading )

Fig. 2 Drawings of Fracture of Test Columns

In the Test Columns of No. 1 without steel plate reinforcement, diagonal cracks occurred from a section of termination of the main reinforcements and failed at this section accompanied by shear failure.

In Nos. 2 and 3 Test Columns which were binded by a steel plate with 1.0 D width, the failure section moved to the column base.

In No. 4 for which the binding width was 1.5 D, the failure occurred at the base of the columns.

(2) Relationship between load and displacement

The relationships between load and displacement are given in Fig. 3. All of the Test Columns which were strengthened showed an increase of the ultimate strength by about 30 % in the maximum, compared with the No. 1 Test Specimen without the reinforcement of steel plate.



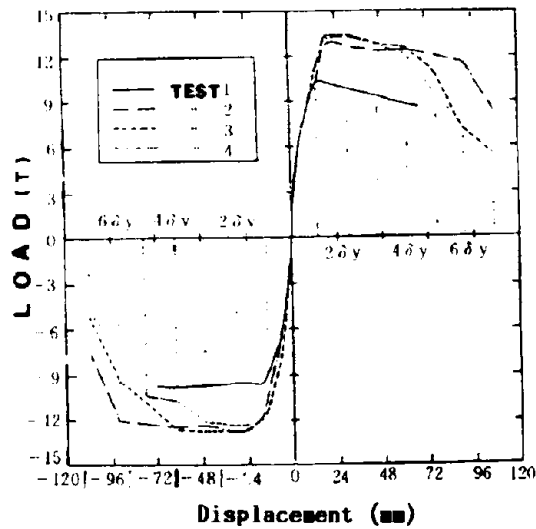
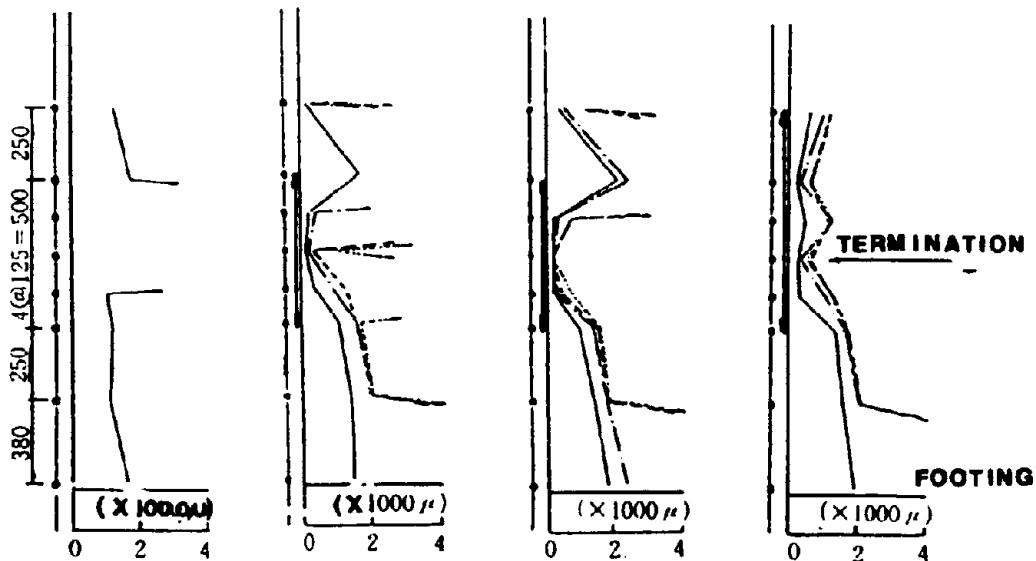


Fig. 3 Relationship between Load and Displacement

(3) Strain distribution of axial reinforcements

The distribution of strains in axial rebars of the Test Columns is shown in Fig. 4. Since No. 1 Test Column without the reinforcement by a steel plate had failed at the static test, the dynamic test of No. 1 Column was not carried out.



(1) Test Specimen 1 (2) Test Specimen 2 (3) Test Specimen 3 (4) Test Specimen 4  
(Static Test)

Fig. 4 Strain Distribution of Axial Reinforcements

In Nos. 2 and 3 Test Columns with a square section which were binded by a steel plate over the width of 1.0 D, strains of rebars near the middle of the steel plate were small, but reached the yielding under the 1.0 $\delta$ y displacement loading. The examination of the effect of injection of non-shrinkage mortar and epoxy resin showed that restraint by the latter was more effective than by the former.

In No. 4 Test Column with a rectangular section which was binded by a steel plate over the width of 1.5 D, the column reinforcements of the portion binded by the steel plate did not reach the yielding until 4 $\delta$ y loading.

#### (4) Summary - strengthening method and strengthening range -

The test results showed that the reinforcement for a RC bridge pier applied to No. 4 was at least required in terms of the strengthening method and range against an earthquake.

Namely, the steel plate jacketing method at the section of termination of main reinforcements proved to be effective against an earthquake by strengthening over the width of about 1.5 D consisting of 1.0 D above and 0.5 D below the termination section. Also, it was required to inject non-shrinkage mortar or epoxy resin between pier body and steel plate.

Metropolitan Expressway Public Corporation carried out the same type of experiment using specimens with circular cross section and obtained almost the same results.

#### 2-2 Evaluation equation of a seismic strengthening works

Since basic methods and ranges of the strengthening against an earthquake were verified by the experiment for confirmation of the effect of the reinforcement, furthermore, the design of the strengthening was examined and an evaluation equation for strengthening standard was proposed. Information for the examination was obtained from the results carried out at the Public Works Research Institute of the Ministry of Construction and Metropolitan Expressway Public Corporation in addition to the test results reported above.

Three parameters were selected for an evaluation equation:

- ①  $S_{fn}$  = safety against yielding at checking section (termination section)
- ②  $\tau_n$  = mean shearing stress at checking section (termination section)
- ③  $S_{mn}$  = ratio of  $S_{fn}$  to yielding at the base of column.

Since a column failed at the section of termination at the tests for even shear span ratio  $h/D \geq 6.0$ , it was excluded from the parameter. Table-3 shows evaluation equations.

Table-3 Evaluation Equation of Standard Reinforcement against Earthquake

①	3	$S_{fn} < 1.2$	②	2	$\tau_n > 4.2 \text{ kgf/cm}^2$	③	3	$S_{mn} < 1.2$
	1	$S_{fn} \geq 1.2$		1	$\tau_n \leq 4.2 \text{ kgf/cm}^2$		2	$1.2 \leq S_{mn} < 1.4$
Evaluation Equation $P = ① * ② * ③$							1	$S_{mn} \geq 1.4$
c								

It was proposed to determine the strengthening range and steel plate thickness for a seismic strengthening by the equation in Table-3

$$P_c = S_{fn} \cdot \tau_n \cdot S_{mn} \leq 2$$

In general, steel plate thickness of 4.5mm was calculated to be suitable. The steel plate of 6mm was, however, adopted to avoid deformation during fabrication, shipping, and grouting.

$S_{fn}$  took the number of 3, since the safety factor less than 1.2 was considered in the same way as in the 1986 inspection for earthquake proofing of highway bridges.

Since some test columns did not show the failure even when the shearing stress  $\tau_n$  was over the allowable value,  $\tau_n$  was classified by the allowable shearing stress with the upper limit of 2.0.

The failure at the section of termination might be brittle due to small toughness, and therefore the safety of the section was increased relatively. Since  $S_{mn}$  was less than 1.2 for the test columns which failed at the section of termination or at the section of termination and of the base, 3.0 was proposed for  $S_{mn}$ .

Further, since the reserved horizontal ultimate strength even for the safety factor larger than 1.2 was different from the strength for the safety factor larger than 1.4, 2.0 was proposed to  $S_{mn}$  for the factor smaller than 1.4.

### 3 Anti-Earthquake Strengthening Works

#### 3-1 Procedure of a seismic strengthening works

Fig. 5 shows the general drawing of strengthening works for earthquake proofing, and the operation steps are as follows:

Preparation works  $\Rightarrow$  falseworks erection  $\Rightarrow$  under treatment works  $\Rightarrow$  measurement works  $\Rightarrow$  temporary anchoring  $\Rightarrow$  seat installation works  $\Rightarrow$  finishing of shop drawing  $\Rightarrow$  fabricating and straightening of steel plate  $\Rightarrow$  carrying in of steel plate  $\Rightarrow$  installation of steel plate  $\Rightarrow$  anchoring works  $\Rightarrow$  field welding  $\Rightarrow$  sealing works  $\Rightarrow$  injection works  $\Rightarrow$  finishing works  $\Rightarrow$  painting  $\Rightarrow$  false works removal  $\Rightarrow$  clearing away.

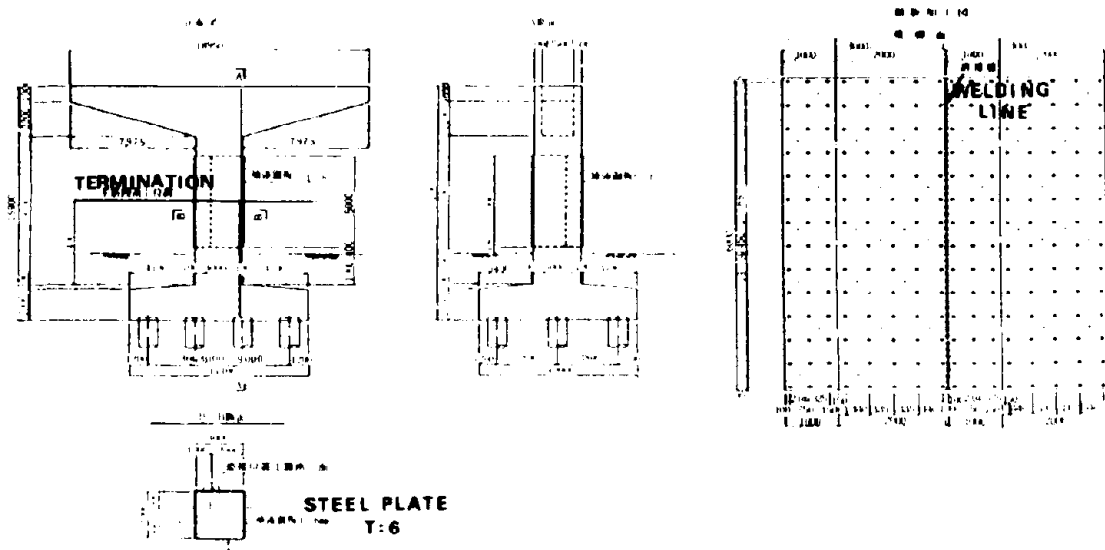


Fig. 5 General Drawing of A Seismic Reinforcement Works

### 3-2 Test works at site of a seismic strengthening

To study on the applicability of a seismic strengthening works to site conditions, test works were carried out for the pier No.P-461 at the Airport Line of the Hanshin Expressway. The following items were examined:

- ① flatness of surface of existing pier columns which is important at the time of installation of a steel plate or of injection of a filler material,
- ② operation of installation of a long steel plate,
- ③ interval of anchor bolts and anchoring conditions,
- ④ field welding works of reinforcing steel plate and its heat effect,
- ⑤ installation works of reinforcing steel plate,
- ⑥ properties of filler material,
- ⑦ injection conditions of filler material, etc.

For the comparison of epoxy resin with non-shrinkage mortar as a filler material, the properties of filler materials, conditions of injection of the filler materials and the selection of the filler material, are reported in this paper.

#### 3-2-1 Properties of filler materials

The basic properties of epoxy resin and non-shrinkage mortar were verified in advance by indoor tests ( model injection test, physical and chemical properties test ). As a non-shrinkage mortar group, in addition to

non-shrinkage mortar, cement grout material, self-leveling floor bed material, polymer cement material were tested. The performance required for the filler material was as follows:

- ① easy operation and usefulness for injection into a small gap,
- ② the approximately same compressive strength (  $\sigma_{ck}=270 \text{ kgf/cm}^2$  ) as that of pier concrete,
- ③ no breeding during injection of a filler material,
- ④ no volume change during hardening of concrete.

Since the injection of epoxy resin was experienced at steel plate bonding works for slab repairing, there was no problem for the injection into a 4 mm width gap.

The indoor test revealed that about 10 mm gap was required for the group of non-shrinkage mortar. For this thickness for injection, all of the materials showed nearly satisfactory results about usefulness, strength and hardening conditions as the filler material.

The maximum compressive force to which the reinforcing steel plate was subjected during the injection, was a pressure near the injection point at the lowest end of the steel plate, and it was nearly equal to side pressure due to hydrostatic pressure produced by the difference of elevation of the injection material.

### 3-2-2 State of injection of filler material

The examination of injection operation of epoxy resin or non-shrinkage mortar was carried out by a test works on the assumption that a reinforcing steel plate of 6 mm in height was installed around an existing pier. The height of 6 mm was chosen, because the installation of a steel plate slightly larger than a range necessary for the reinforcement was considered from the point of scenery.

A supporting interval of anchor bolts for the installation of the steel plate was determined from pressure acting on the plate during the injection works. Since a divided injection of 3 mm in height was planned from the amount of pressure, the pressure for epoxy resin was chosen to be  $0.3 + 0.1 \text{ kgf/m}^2$  and the pressure for non-shrinkage mortar to be  $0.6 + 0.1 \text{ kgf/m}^2$ .

The supporting interval of anchor bolts was decided by an analysis of a bending problem of a plate supported by lines of columns with an equal interval, so that the deflection of the steel plate could be maintained below 3 mm.

Thus, for epoxy resin, the support by one hole-in-anchor per 50 cm X 50 cm was necessary, and for non-shrinkage mortar a combined support of staging members ( [ - 300 X 90 X 9 X 13 and [ - 200 X 90 X 8 X 13.5 ) and hole-in-anchors was needed.

In a test injection, the measurement of deflection and stress of an installed steel plate and of injection pressure of a filler material was carried out.

The deflection of the steel plate was measured by a displacement meter of dial gauge type, the stress by strain meters affixed to the steel plate and the injection pressure by a pressure meter of dial gauge type.

Fig. 6 shows the measurement records of the deflections of the installed steel plate at the time of injection of the epoxy resin. The maximum deflection was 2.89. The maximum deflection of the plate during the injection of non-shrinkage mortar was 2.87 mm which was below the allowable value of 3.0 mm.

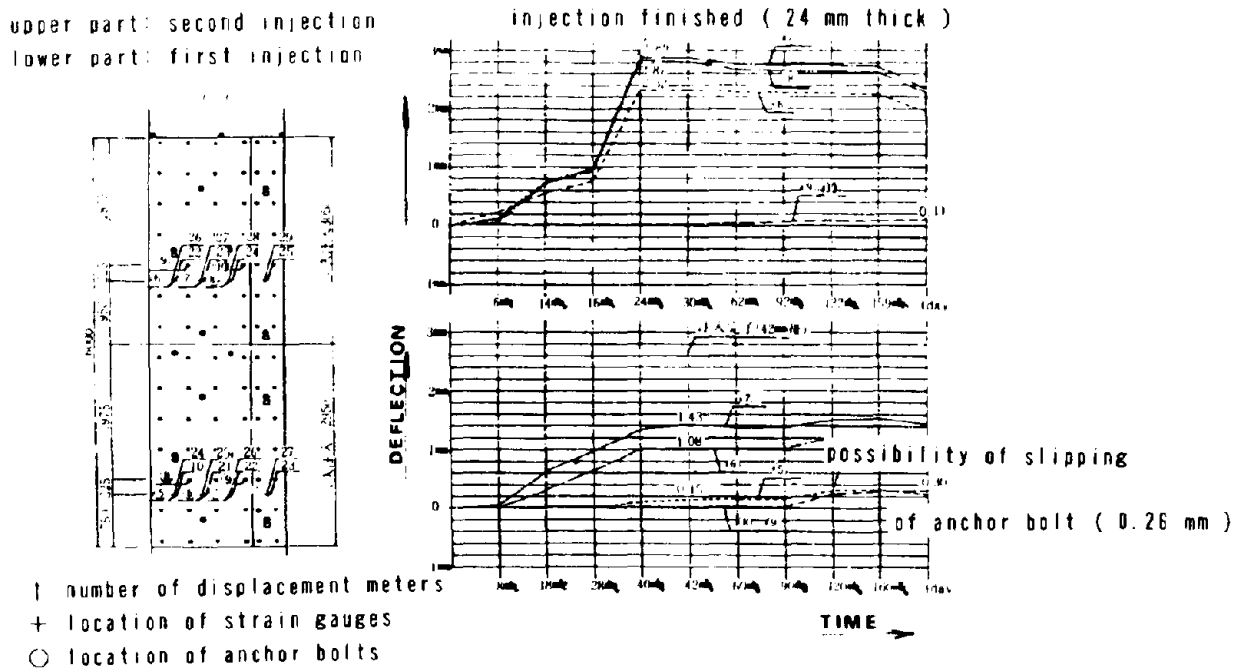
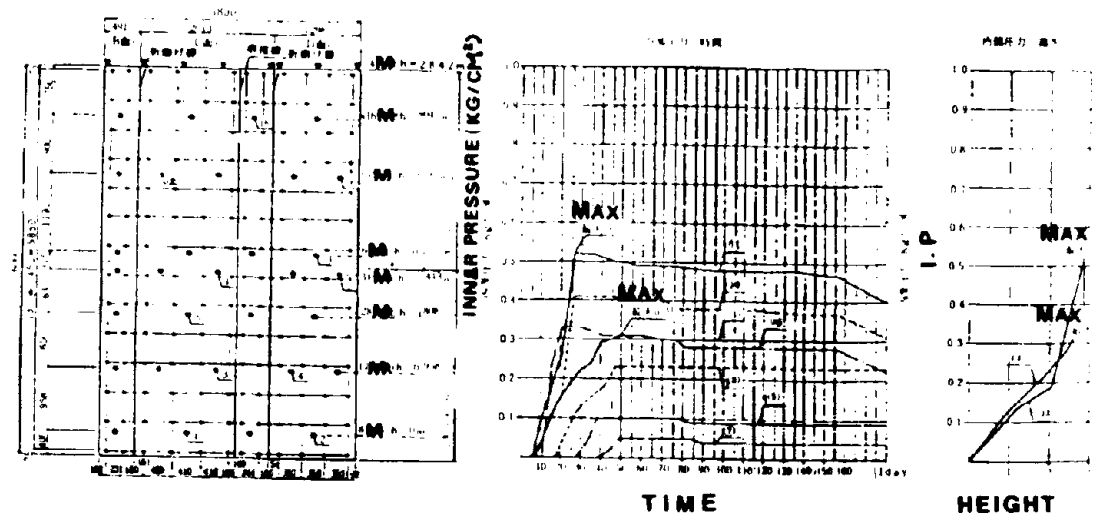


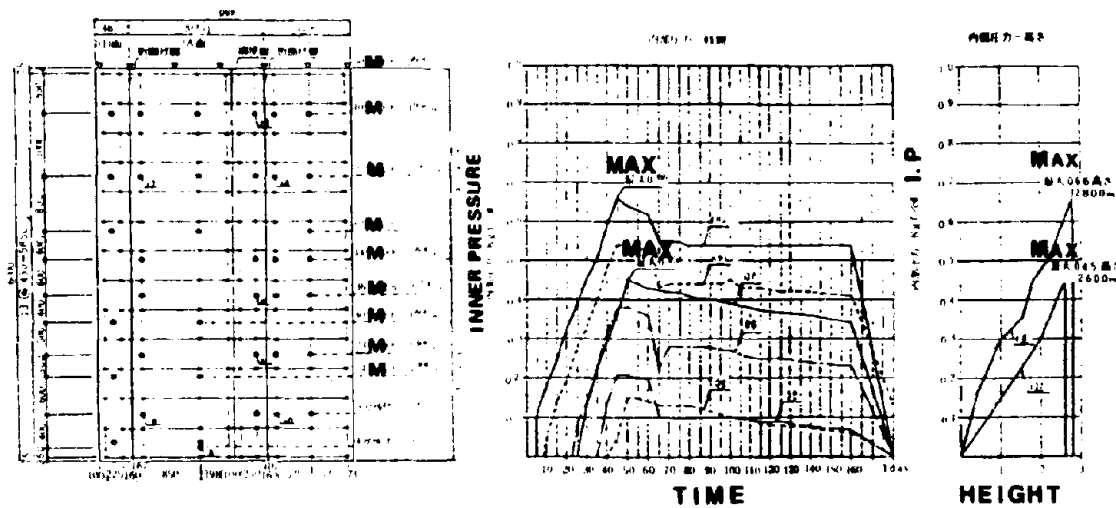
Fig. 6 Record of Measured Deflections of Installed Steel Plate

The stress on the installed steel plate during the injection was about 550 kgf/cm<sup>2</sup> for the epoxy resin and about 750kgf/cm<sup>2</sup> for the non-shrinkage

mortar, both in the maximum. The recorded injection pressures of the filler materials were given in Fig. 7.



( a ) epoxy resin



( b ) non-shrinkage mortar

Fig. 7 Measurement Record of Injection Pressure of Filler Materials

For the epoxy resin, the injection pressure was increased up to the maximum of  $0.54 \text{ kgf/cm}^2$  to finish the injection for a certain test column, but



in other cases, a pressure equal to a hydrostatic pressure due to the difference of elevation of the filler was measured as in the indoor test.

### 3-2-3 Selection of filler material

By the field test works stated above, it was verified that the installation method of a steel plate and the injection method which were important during the injection works, were appropriate.

For the selection of such a filler material as non-shrinkage mortar or epoxy resin,

- (1) how the difference of thickness necessary for injection ( 4 mm for epoxy resin and 10 mm for non-shrinkage mortar ) affects the site conditions and scenery, and
- (2) how the difference of supporting method of an installed steel plate ( only bolting for epoxy resin, but combined bolting and staging for non-shrinkage mortar ) affects the site conditions, working conditions and scenery, were investigated. Finally, the epoxy resin was selected.

### 3-3 Anchor Bolt

Countersunk head bolt adopted by reason of a fine sight. Fig.8 shows the anchor bolt which used in the field works. In general, it is said that this kind of bolt is weak against the pull out force. Then improvement of the fix anchor and the the pull out force tests of improved bolt with epoxy resin between bolt and the drilled hole were carried out . As a result, this anchor bolt could increase the ultimate the pull out strength and decrease the deformation.

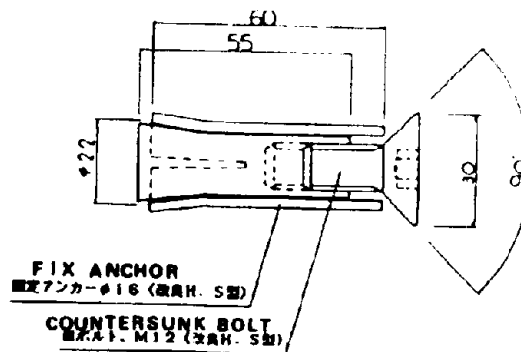


Fig.8 Improved Anchor Bolt

### 3-4 Field Welding

The steel jacketing plates welded on condition that the route gap is 2 mm. While welding, the temperature of the steel jacketing plate was about 1,000°C at the welding point, 100°C at a distance of 5cm from the welding point and below 50°C at a distance of 5cm from the welding point. Maximum inner stress by the conduction of heat was 304kg/cm<sup>2</sup> and decreased to 88kg/cm<sup>2</sup> . As above, though the heat by welding was rather high at welding point, the velocity of spreading was fast and there was no problem about the welding.

## Conclusion

The Hanshin Expressway Public Corporation started works for a seismic strengthening from last year, based on the investigation results discussed above. Since the works are maintenance and repair works, there might be much restriction at the site and other various problems, too, but it can be said that the basic application of proposed strengthening methods was confirmed.

A fundamental idea for anti-earthquake design has made progress and expanded with newer experience of earthquake damages. In future, the need for similar a seismic strengthening as proposed here will be pointed out further for existing structures. In the maintenance and management of continuously elevated bridges such as seen in the Hanshin Expressway, structural behavior of the bridges and features of seismic motion, topography, and ground have to be grasped. At the same time, it will be required that a series of structures has to be provided with the same degree of earthquake proofing.

## References:

- 1) Ministry of Construction, "Inspection of Public Facilities for Safety against Earthquake, " No.6 Document of Street Div. of City Bureau, and No.5 Document of Disaster Prevention Section of Road Bureau, April 17, 1986.
- 2) Hanshin Expressway Public Corporation, "3rd Service Report on Study of Earthquake Proofing of Existing Structures, " March 1987.
- 3) Public Works Research Institute, Ministry of Construction, "Survey and study on Technique for Durability Estimation and Improvement of Existing Bridges (■), " Research Material No. 2682, Dec. 1988.
- 4) Hanshin Expressway Public Corporation, "Report of Experiment on Ultimate Strength of Reinforced Concrete Piers at Step-Down Section of Main Reinforcements, " March 1988.
- 5) Hanshin Expressway Public Corporation, "Study on Reinforcing Method of RC Piers at Step-Down Section of Main Reinforcements, " October 1988.

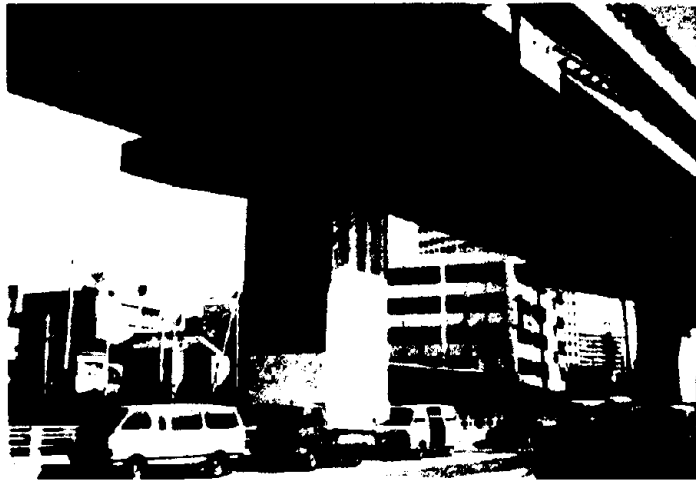


PHOTO-1 BEFORE WORKS



PHOTO-2 INSTALLATION OF STEEL PLATE

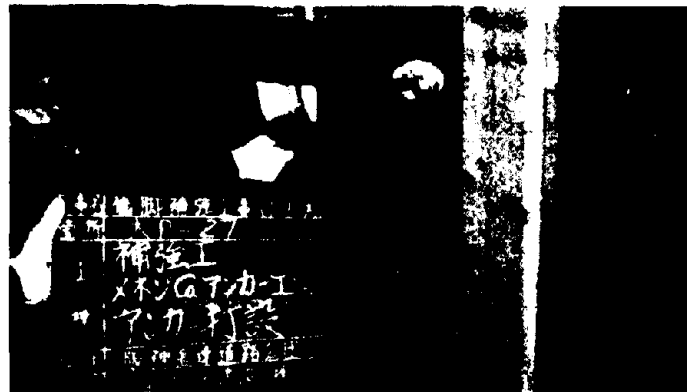


PHOTO-3 ANCHORING WORKS



PHOTO-4 FIELD WELDING



PHOTO-5 INJECTION WORKS



PHOTO-6 AFTER WORKS

# **S e s s i o n 5**

## **R e s e a r c h o n S e i s m i c R e t r o f i t t i n g a n d S t r e n g t h e n i n g o f R e i n f o r c e d C o n c r e t e B r i d g e P i e r s**

- 1) Retrofit of Bridges Columns for Enhanced Seismic Performance  
(Y.H.Chai, M.J.N.Priestley and F.Selble)
- 2) Study on Ductility Estimation of Fiber Mixed RC Members  
(S.Kobayashi, H.Kawano, K.Morihama and H.Watanabe)
- 3) Effect of Carbon Fiber Reinforcement as a Strengthening Measure  
for Reinforced Concrete Bridge Piers  
(T.Matsuda, T.Sato, H.Fujiwara and N.Higashida)

*Reproduced from  
best available copy*

## RETROFIT OF BRIDGE COLUMNS FOR ENHANCED SEISMIC PERFORMANCE

Y.H. Chai<sup>1</sup>  
M.J.N. Priestley<sup>2</sup>  
F. Seible<sup>2</sup>  
Presenting Author: Y.H. Chai

### SUMMARY

Collapse or severe damage of a number of California bridges in recent moderate earthquakes has emphasized the need to develop effective retrofit measures to enhance the flexural strength and ductility, and shear strength, of bridge columns designed before the current seismic design provisions. This paper reports on the status and preliminary results of an extensive research program currently in progress at the University of California, San Diego to investigate various retrofit methods for deficient bridge columns. Results from the first phase of testing indicates that steel jacketing provides an effective means of enhancing the flexural performance of tall circular columns. Similar enhancement of performance was observed for rectangular columns encased with elliptical shape jacket. The second phase of research focuses on shear strength enhancement of short columns. Initial results indicates that, by extending the cylindrical steel jacket over the full height of short columns, brittle shear failure can be avoided and the column encouraged to exhibit ductile behavior.

### INTRODUCTION

The 1971 San Fernando Earthquake [1], the 1987 Whittier Earthquake [2], and the 1989 Loma Prieta Earthquake [3] all provided painful reminders of the potential hazard that exist in many of the older bridge structures in the United States. Considerable progress has made by Caltrans in implementing retrofit measures to upgrade the seismic resistance of these bridges in California [4]. Deficiencies inherent in the columns of the older bridges are inadequate flexural strength and ductility, undependable flexural capacity, inadequate shear strength, insufficient joint and footing strength. These problems have been discussed in detail elsewhere [5].

The current approach for seismic design of bridge columns relies on proper confinement of the potential plastic hinge regions by closely-spaced transverse hoops or spirals. Such provision allows the ultimate compressive strain to increase from a value of about 0.005 in unconfined concrete to a value of 0.03 or higher in confined concrete. The increase in ultimate compressive strain significantly enhances the ductility capacity of the concrete section. Research results [6] have shown that well confined columns can develop stable hysteresis loops during inelastic cycling to displacement ductility factor exceeding six.

The same effective confinement can be provided to existing substandard circular columns by encasing the potential plastic hinge regions with a site-welded cylindrical steel

<sup>1</sup>Graduate Research Assistant, University of California, San Diego, U.S.A.

<sup>2</sup>Professors of Structural Engineering, University of California, San Diego, U.S.A.

sleeve or jacket. The jacket is introduced slightly oversize for ease of construction. The gap between the jacket and column is subsequently filled with cement-based grout. The use of a close-fitted steel jacket to a rectangular column, however, would not be effective in enhancing the flexural behavior, since the level of confinement available depends on the curvature of the jacket. The out-of-plane flexibility of the rectangular jacket cannot provide effective confinement to the column except at the jacket corners. Stiffeners are required on the jacket to increase the radial resistance to the expansion of cover concrete which occurs at large column lateral displacement. However, by encasing the rectangular column with an elliptical jacket, continuous confinement can be achieved in both directions of the column. A suggested alternative to a stiffened rectangular jacket is to assemble structural steel channels into an integral enclosure using bolted connections which can be tightened to induced active confinement to the column. The gap between the channel section and column would be filled with concrete.

The failure to provide adequate transverse steel, as with the pre-1971 design, may lead to brittle shear failure in short columns, with limited displacement ductilities. Inelastic cyclic response of these columns is characterized by poor energy dissipation, rapid strength, stiffness and physical degradation. The use of steel jacket would, in addition to provide confinement, enhance the shear strength of the column. A satisfactory shear retrofit would be to increase the shear strength of the column to a level above the flexural strength to avoid brittle shear failure, and the column after retrofit can exhibit ductile flexural response. For circular columns, a cylindrical jacket is appropriate, while for rectangular columns, an elliptical jacket is desirable.

Regardless of flexural or shear retrofit, the jacket is terminated slightly short of the adjoining member to ensure that only confinement is provided to the column concrete, rather than an increase in the size of the critical section which may increase the moment capacity and overload the footing.

In order to verify the effectiveness of the retrofit techniques for enhancing the seismic performance of bridge columns, a test program was initiated at the University of California, San Diego, in 1988. The program is still continuing and involves testing of large-scale circular and rectangular columns in 'as-built' and retrofit conditions for both flexural and shear response. Columns are constructed at 0.4 geometric scale of the prototype, using materials and design details appropriate for columns designed in the mid 1960's.

## FLEXURAL COLUMN TESTS

### Flexural Column Details

The flexural program includes testing of 6 circular columns of 24 inches in diameter and 6 rectangular columns of 28.75 inches by 19.25 inches in cross-section. The test columns are constructed with a footing so that foundation influence on the column behavior can be included. The column height is 144 inches from the top of footing to the center of horizontal load. An axial load of 400 kips is applied to the test column using two 2 inch high strength bars before imposing lateral displacements. Each bar is stressed with a center-hole jack which reacts against the test floor. The bar forces are transferred to the column by a cross-beam mounted on top of the column loadstub. Fig. 1 shows the test configuration for a circular flexural column.

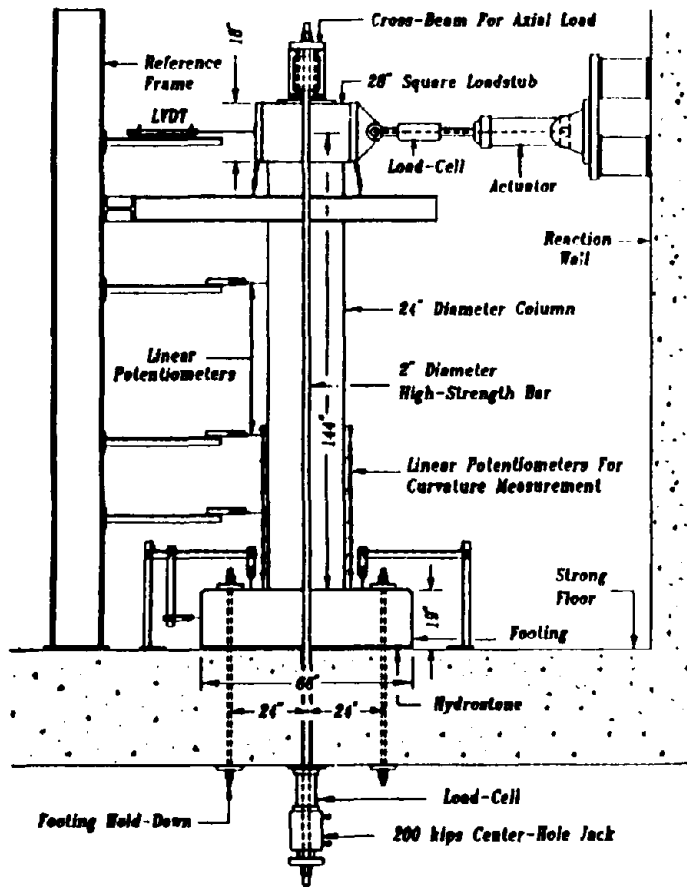


Figure 1: Flexural Test Setup

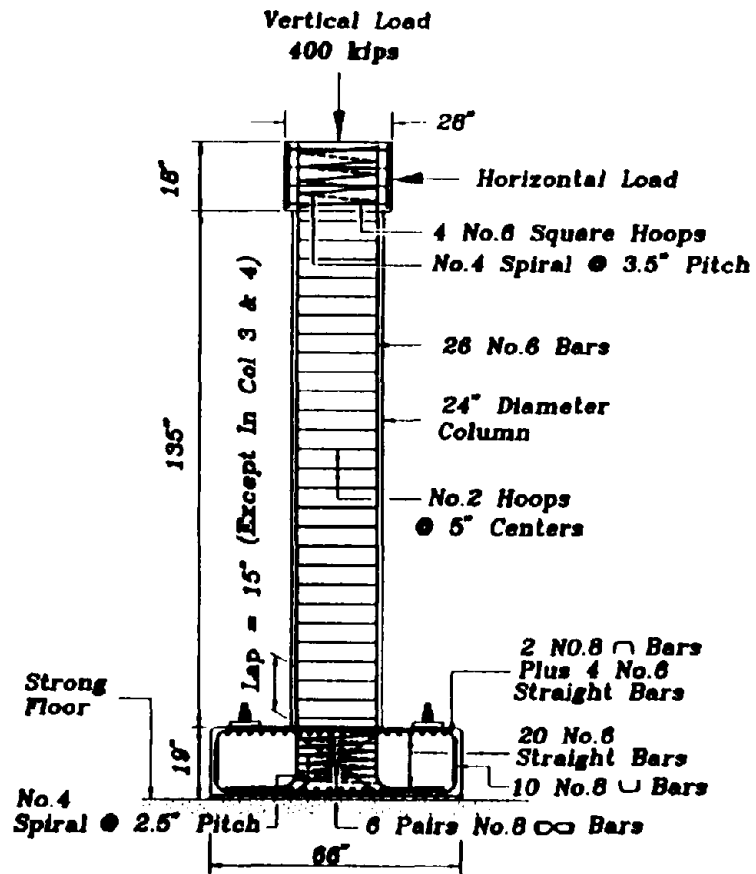


Figure 2: Typical Reinforcement Details for Circular Flexural Columns



A target concrete compressive strength of  $f'_c = 5000$  psi at 28 days is used in all test columns to represent a 67 % overstrength when compared to the typical 1960's design strength of 3000 psi. The overstrength is to reflect both the conservative concrete mix design and batching practices of the 1960's and the strength gain that has occurred in more than twenty years of natural aging. Grade 40 reinforcement is used in all flexural columns. Longitudinal reinforcement for circular columns consists of 26 #6 deformed bars, uniformly distributed around the column. A concrete cover of 0.8 inch was provided for the longitudinal reinforcement. Yield strength for the #6 bar averages 45.7 ksi. Transverse reinforcement is provided by #2 circular hoops at 5 inches uniform spacing. Fig. 2 shows a typical reinforcement detail for a circular flexural column. For the rectangular columns, the longitudinal reinforcement consists of 32 #6 bars distributed into single layer, as shown in Fig. 5(a). Transverse steel for the rectangular column was similar to that of circular column i.e. #2 perimeter hoops at uniform spacing of 5 inches. It should be noted that both the circular and rectangular columns are designed to contain the same longitudinal steel area ratio i.e. 2.53%.

Circular columns 1, 2, 5 and 6, and all of rectangular columns were constructed with a lap-splice of 20 times the longitudinal bar diameter in the potential plastic hinge region. Such practice was common in the moment-resisting footing of the 1960's. Circular column 3 and 4 were reinforced with continuous longitudinal bars anchored by 90 degree hooks in the footing. Cylindrical jackets for circular columns were fabricated from 3/16 inch thick A36 hot rolled steel ( $f_y = 36$  ksi). Fig. 3 shows the cross-section of a retrofitted circular column. A 1/4 inch gap is provided between the jacket and column, and subsequently pressure filled with a cement-based grout which contains a small dose of water-reducing, expansive additive. Compressive strength of 2 inch diameter grout cylinders varied between 2000 and 2500 psi at age of 14 days.

Fig. 4 illustrates the confining action of the steel jacket. Under the combined effect of axial compression and flexure, the compression zone attempts to dilate as the flexural strength of the member is approached. The dilation is restrained by the radial stiffness of the jacket; placing the jacket in circumferential tension and the concrete in radial compression. The lateral pressure exerted by the jacket increases both the compressive strength and ductility of the concrete.

To ensure that the jacket does not bear against the footing when in compression, a nominal gap of 1 inch is provided between the toe of the jacket and the footing. The length of cylindrical jacket was chosen to be 48 inches to ensure that the moment demand immediately above the jacket do not exceed 75% of the original flexural capacity.

Design variations between columns are given in Table 1 and 2. The first pair of circular columns were constructed with a 1960's footing using only straight reinforcement (two orthogonal layers of 24 #6 bars each) in the bottom region of the footing. The footing was supporting on 1 inch high by 8 inch diameter blocks simulating pile support. A strong footing details was used in the remaining columns, including rectangular columns, when footing shear failure was noted in the second column after retrofitted with a steel jacket. Reinforcement for the strong footing were redesigned to include top and bottom layers of #8 bars bent at both ends, 6 pairs of #8 diagonal bars placed close to the column/footing joint and # 4 spiral at 2.5 inches pitch within the joint, as shown in Fig. 2. Instead of using simulated rigid pile-blocks, the footing were uniformly supported on a thin layer of hydrostone and clamped against the test floor.

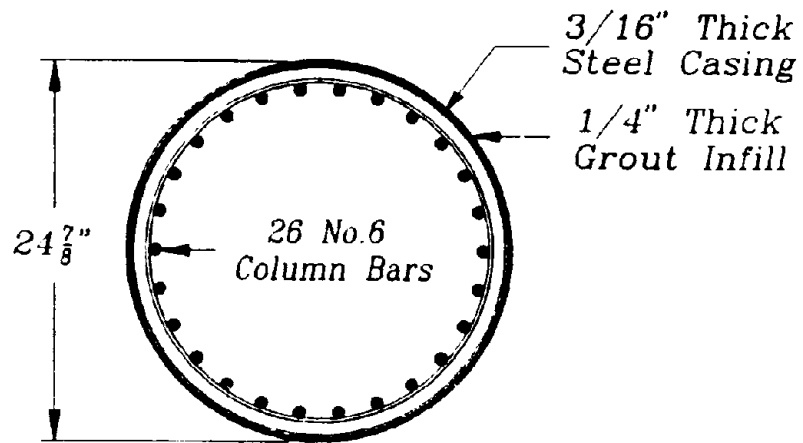


Figure 3: Cross-section of Retrofitted Circular Column

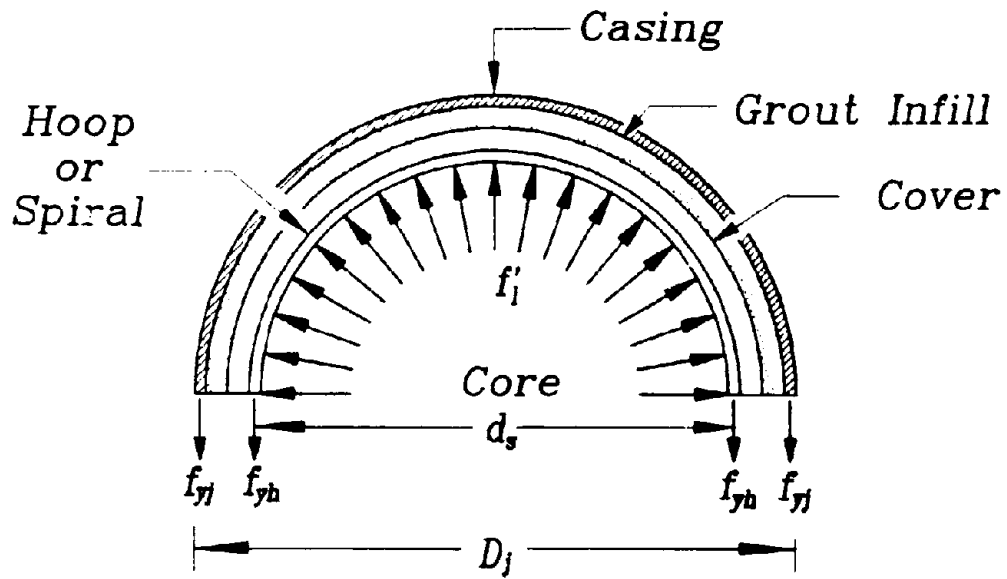


Figure 4: Confining Action of Steel Jacket

Table 1: Test Matrix for Circular Flexural Columns

Test Units	Column & Footing Details		Remarks
1	20 $d_b$ Lap For Long. Bars Without Steel Jacket	Weak Footing	Reference
2	20 $d_b$ Lap For Long. Bars With Steel Jacket	Weak Footing	Full Retrofit
3	Continuous Column Bars Without Steel Jacket	Strong Footing	Reference
4	Continuous Column Bars With Steel Jacket	Strong Footing	Full Retrofit
5	20 $d_b$ Lap For Long. Bars 1/4" Styrofoam Wrap and Jacket	Strong Footing	Partial Retrofit
6	20 $d_b$ Lap For Long. Bars With Steel Jacket	Strong Footing	Full Retrofit
1-R	20 $d_b$ Lap For Long. Bars Repaired By Steel Jacket	Weak Footing 300 kips Prestress	Full Retrofit

Table 2: Test Matrix for Rectangular Flexural Columns

Test Units	Retrofit Details	Load Directions	Status
1	'As-Built' (Reference)	Strong Axis	Completed
2	Elliptical Jacket	Strong Axis	Completed
3	'Built-up' Channels	Strong Axis	Completed
4	Stiffened Rectangular Jacket	Strong Axis	Completed
5	'As-Built' (Reference)	Weak Axis	Completed
6	Elliptical Jacket	Weak Axis	Pending

A partial retrofit approach was undertaken in circular column 5 to investigate the possibility of containing the column base without attempting to improve the flexural strength or ductility. This could be adopted in design where the lateral strength of a column would not be needed to ensure satisfactory response of the bridge as a whole and where full retrofit might place excessive moment demand on the footing. To this end, a thin sheet of styrofoam (1/4 in thick) was added between the column and grout infill to allow a controlled dilation of the cover concrete at large lateral displacement. Complete loss of cover concrete was prohibited by the presence of the jacket.

The flexural program also investigated the possible use of steel jacket for post-earthquake repair of columns. Circular column 1 was repaired with a steel jacket of the same dimensions after initial test (indicated as 1-R in Table 1), and retested using the same load history. Loose cover concrete around the splice region of the main reinforcement was removed before installing the jacket. The weak footing was strengthened by external prestressing to a total of 300 kips at mid-height of the footing and in the direction of the lateral load. Instead of being supported on simulated pile blocks, the repaired column was placed in uniform bearing as with the strong footing setup.

Two directions of lateral loading were considered for the rectangular flexural column

i.e. in the strong and weak axis directions. Five rectangular columns have been tested to date; the first four columns were loaded in the strong direction, and the fifth column in the weak direction. Cross-sectional details of the 'as-built' column and the retrofit devices for other three columns are shown in Fig. 5. The elliptical jacket for rectangular column 2 has an outside dimensions of 38.25 inches and 29.25 inches in the two principal directions. Note that the dimensions shown in Fig. 5(b) are for the centerline of the jacket. The jacket was fabricated from 3/16 inch A36 hot-rolled steel, similar to that for circular column. Column 4 used a rectangular jacket with a grid of stiffening fins as retrofit. Both the elliptical and stiffened jackets were 48 inches tall. Column 3 used a bolted system of steel channels with transverse braces to confine the concrete in the potential plastic hinge region. The bolts were tightened to induce active pressure on the column concrete. Height of this retrofit device was 28.8 inches.

### Load-Deflection Response of Circular Flexural Columns

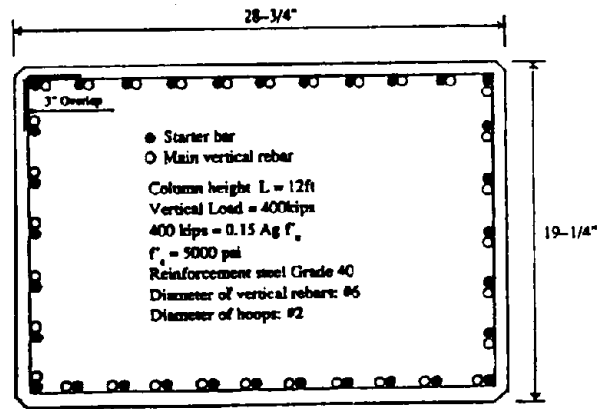
Plots of lateral force versus displacement of circular columns with lapped starter bars are shown in Fig. 6. In these diagrams,  $V_y$  represents the lateral force corresponding to first yield of the extreme tension reinforcement,  $V_i$  is the lateral force corresponding to the theoretical ideal flexural capacity of the unconfined column section, and  $V_p$  is equivalent to  $V_i$  but including the effect of confinement provided by the steel jacket for retrofitted columns and was assessed at an extreme tension steel strain of 0.005.

Fig. 6(a) shows that the hysteresis loops of the 'as-built' column 1 degrade rapidly after the first cycle to  $\mu = 1.5$ . A maximum lateral load of 49 kips was noted during the push cycle to  $\mu = 1.5$  and was 97% of the theoretical ideal capacity  $V_i$ . The strength envelope is seen to degrade asymptotically after  $\mu = 1.5$  to the moment resisted purely by the axial load which corresponds to a shear force of 19 kips.

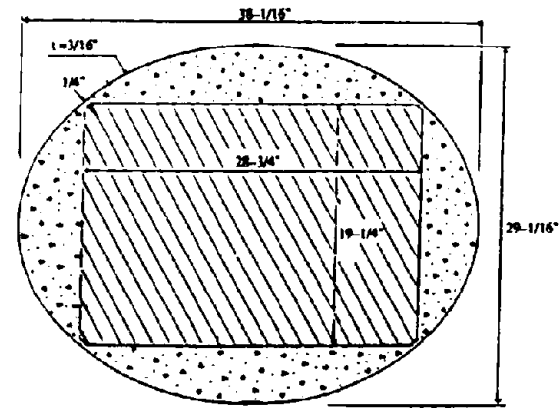
The hysteresis loops of column 2 are stable up to  $\mu = 3$  after which rapid degradation occurred (see Fig. 6(b)), due to footing joint shear failure. Vertical load carrying capacity of the column was affected. Column 2 just attained its plastic lateral force,  $V_p$ , prior to failure. Note that column 2 showed a 19% increase in lateral stiffness after retrofit. The lateral stiffness of the column is defined as  $V_i$  or  $V_p$  divided by the corresponding experimental yield displacement. It should be noted that, although part of the stiffness increase results from the steel jacket, early bond failure in the longitudinal reinforcement of column 1 has contributed to a smaller estimation of lateral stiffness for that column.

The response of column 6 after retrofit with a steel jacket and a strengthened footing, shows remarkably stable hysteresis loops up to  $\mu = 7$  which corresponds to a drift ratio (displacement divided by height) of 5.3% (see Fig. 6(c)). The column exhibits the high energy absorption and small degradation of peak lateral force upon recycling to a given ductility level. Peak lateral forces at  $\mu \geq 3$  exceed  $V_p$  as a result of strain-hardening of the longitudinal reinforcement. Low cycle fatigue fracture of longitudinal reinforcement which occurred during the first cycle to  $\mu = 8$ , is accompanied by comparatively rapid strength degradation, although good energy absorption capacity is maintained.

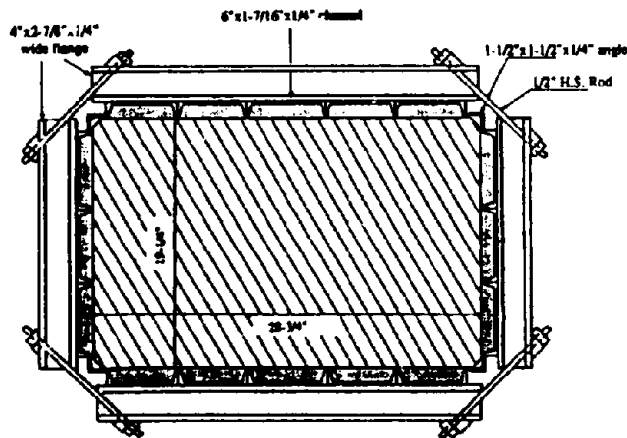
Column 5, with a partial retrofit detail, performed as expected i.e. with a bond failure at the lap-splice at  $\mu = 1.5$ . The soft styrofoam wrap acted as cushion to allow dilation of cover concrete and relative slip between the main reinforcement and starter bars to occur. It was however possible to displace the column to drift ratios exceeding 5% without affecting vertical load carrying capacity. Without complete loss of cover concrete,



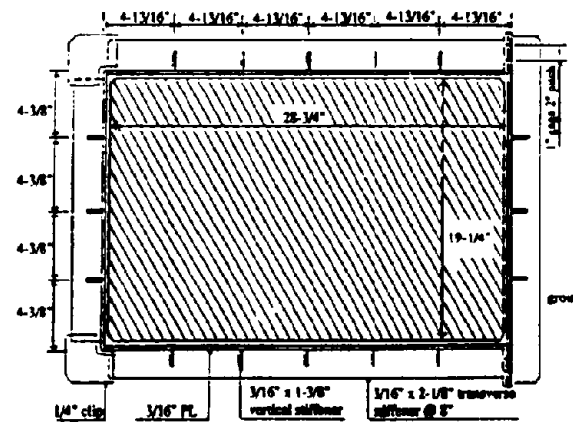
(a) Column 1 - 'As-Built'



(b) Column 2 - Elliptical Retrofit



(c) Column 3 - 'Built-up' Steel Channels



(d) Column 4 - Stiffened Rectangular Jacket

Figure 5: Rectangular Flexural Column Sections

strength degradation was less rapid than column 1.

Lateral force displacement hysteresis loops for columns 3 and 4 which used continuous reinforcement are shown in Fig. 7. Column 3 was tested 'as-built' and showed much improved performance over column 1. Spalling of the cover concrete was initiated at  $\mu = 3$ , but the response remained stable up to  $\mu = 4$ . Final failure did not occur until  $\mu = 5$ , when compression buckling of the longitudinal reinforcement destroyed the integrity of the concrete compression zone causing rapid strength degradation. The hysteretic loops however show good energy dissipation.

The retrofitted column 4 behaved essentially the same as column 6 with stable response up to high ductility levels (see Fig. 7(b)). Failure again resulted from low-cycle fatigue of longitudinal reinforcement. Failure occurred after two cycles to a maximum displacement of 8.7 inches, corresponding to  $\mu = 8$  or a drift ratio of  $\Delta/L = 6\%$ .

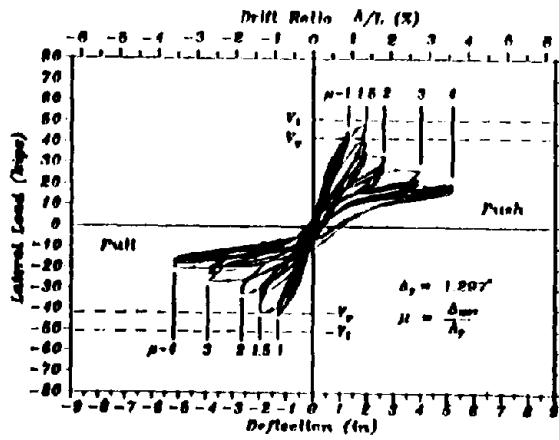
Hysteresis loops for column 1 after repaired with a steel jacket are shown in Fig. 8. The behavior is not as good as column 6, but is greatly improved over the initial performance indicated in Fig. 6(a). The theoretical moment capacity was exceeded at  $\mu = 3$ , and degraded comparatively slowly at larger displacements. The degradation of lateral load was caused by relative sliding between the main reinforcement and starter bars. At  $\mu = 6$ , corresponding to a drift ratio in excess of 5%, the lateral strength is still more than 70% of theoretical ultimate. Note, however, that the energy absorption capacity, as represented by the area within the loops, is less than 50% of that for the retrofitted (as distinct from repaired) column.

Fig. 9(a) and (b) show the load-deflection envelopes for all six columns. It can be seen that a substantial improvement in column performance was achieved using steel jacket.

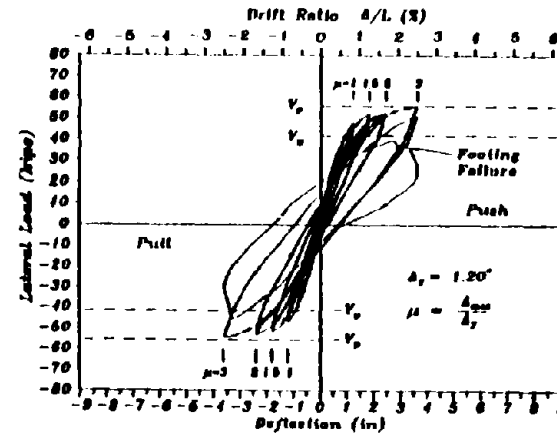
### Load-Deflection Response of Rectangular Flexural Columns

Hysteretic responses of the rectangular columns in the strong axis direction are shown in Fig. 10(a)-(d). The notations on these plots are  $V_y$  for lateral load at first yield of the extreme tension steel, and  $V_u$  for the ideal capacity calculated using the ACI equivalent stress block. The response of 'as-built' rectangular column is very similar to that of circular column i.e. with a bond failure at the lap-splices of the main reinforcement. Even though testing of the 'as-built' rectangular column in the weak direction has been completed, the plot of the hysteretic response is not available at the time of writing this paper, and therefore will not be discussed. The ideal capacity of the column in the strong direction is estimated to be 78 kips, but could not be reached by the column. Bond failure occurred prior to reaching  $\mu = 1.5$ , and subsequent response was characterized by rapid degradation with very narrow energy loops.

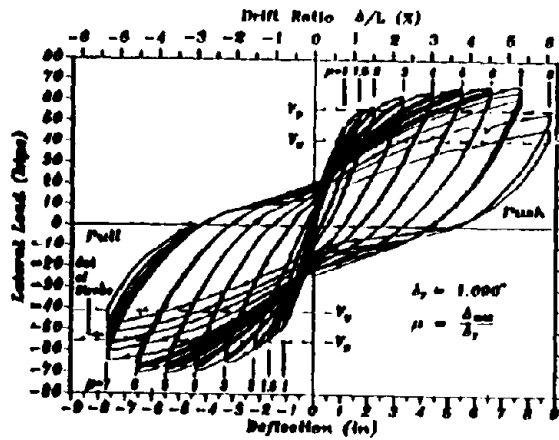
With an elliptical jacket, the column showed a substantial improvement in the load-deflection response. The ideal capacity of the original column was exceeded at  $\mu = 1.5$ . Significant increase in lateral load was subsequently noted. The maximum load recorded was 106 kips, which was the same in both push and pull directions. Unlike the circular columns with cylindrical jackets which failed by low-cycle fatigue fracture, the final failure of rectangular column was caused by bond failure at the lap-splice of the main reinforcement. Strength degradation due to relative sliding between main reinforcement and starter bars was minor and was not significant until after  $\mu = 7$ . The presence of the elliptical jacket restrained the spalling of cover concrete, and therefore allowed a more gradual degradation of strength. Hysteretic loops showed a rather impressive dissipation of energy by the column.



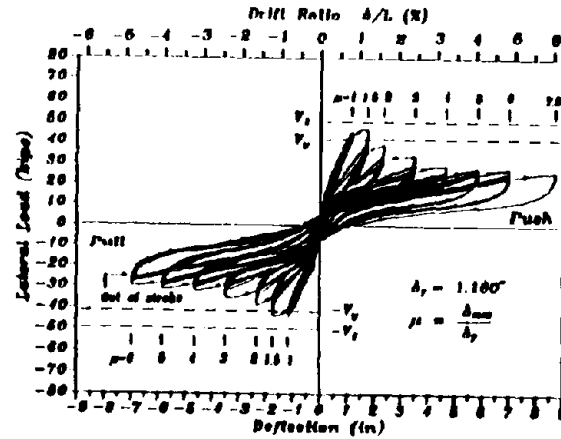
(a) Column 1 - 'As-Built' Weak Footing



(b) Column 2 - Retrofit Weak Footing



(c) Column 3 - Retrofit Strong Footing



(d) Column 5 - Partial Retrofit Strong Footing

Figure 6: Hysteretic Response of Circular Flexural Columns With Lapped Starter Bars

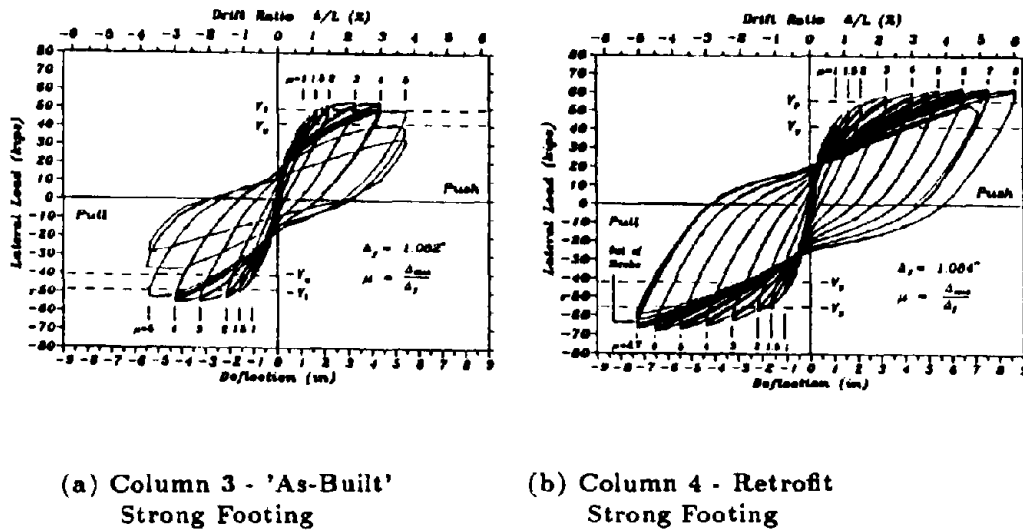


Figure 7: Hysteretic Response of Circular Flexural Columns with Continuous Reinforcement

The hysteretic response of column 3 which uses a bolted system of retrofit using 'built-up' steel channels (see Fig. 5(c)) is shown in Fig. 10(c). Stable response was observed up to  $\mu = 6$ , after which bond failure at the lap-splices was again the cause for strength degradation. Ideal capacity of the original column was exceeded at  $\mu = 1.5$ . Maximum load recorded was 97 kips in the push cycle at  $\mu = 4$ , and was only 9% lower than that observed for column with an elliptical jacket. Even though the response is satisfactory, the maximum drift ratio of 2.7% is significantly less than with the elliptical jacket.

Column 4 with a stiffened rectangular jacket indicated an earlier and more rapid degradation of strength when compared to the previous two methods of retrofit (see Fig. 10(d)). Even though there was no difficulty in attaining the ideal capacity of the original column, the enhancement in displacement ductility was rather small. The dependable drift ratio was about 1.9 %. A peak load of 92 kips was observed during the first push cycle to  $\mu = 4$ , but rapid reduction in stiffness and load soon followed in subsequent cycles to the same displacement.

Fig. 11 shows the load-deflection envelopes for the rectangular columns loaded in the strong axis direction. In this diagram, 'San Francisco 1' refers to retrofit using 'built-up' steel channels and 'San Francisco 2' refers to retrofit by stiffened rectangular jacket. It can be seen that the elliptical jacket provided the optimal method of retrofit for rectangular columns.



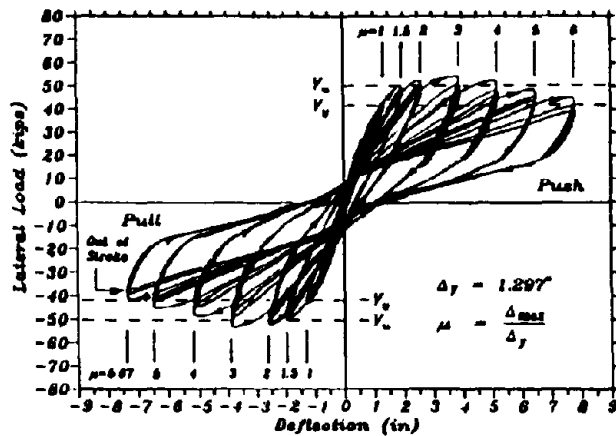
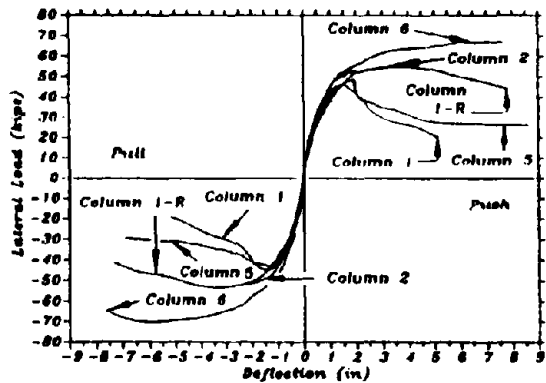
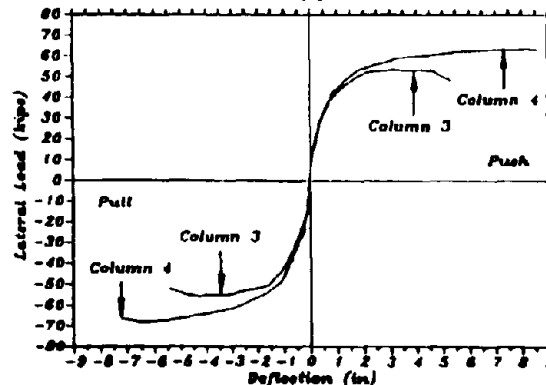


Figure 8: Hysteretic Response of Circular Flexural Column 1 After Repair

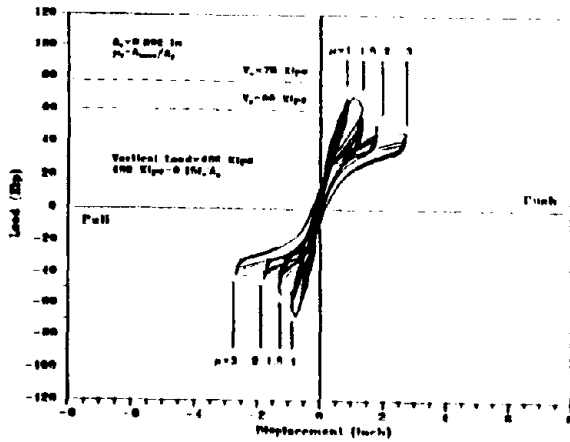


(a) Columns With Lapped Starter Bars

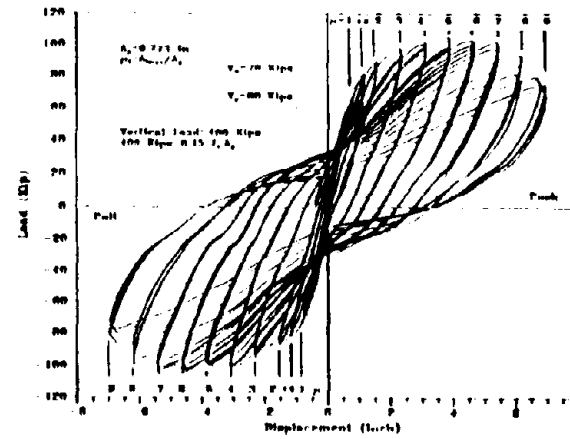


(b) Columns With Continuous Reinforcement

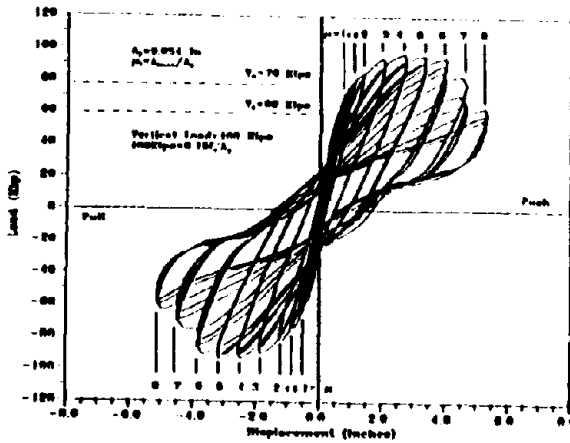
Figure 9: Load-Deflection Envelopes For Circular Flexural Columns



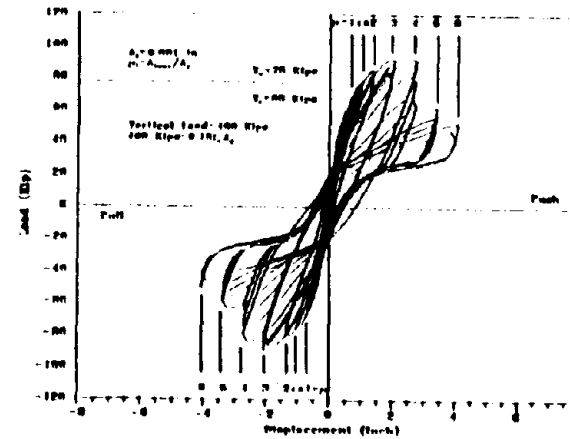
(a) Column 1 - 'As-Built'



(b) Column 2 - Elliptical Retrofit



(c) Column 3 - 'Built-up' Steel Channels



(d) Column 4 - Stiffened Rectangular Jacket

Figure 10: Hysteretic Response of Rectangular Flexural Columns

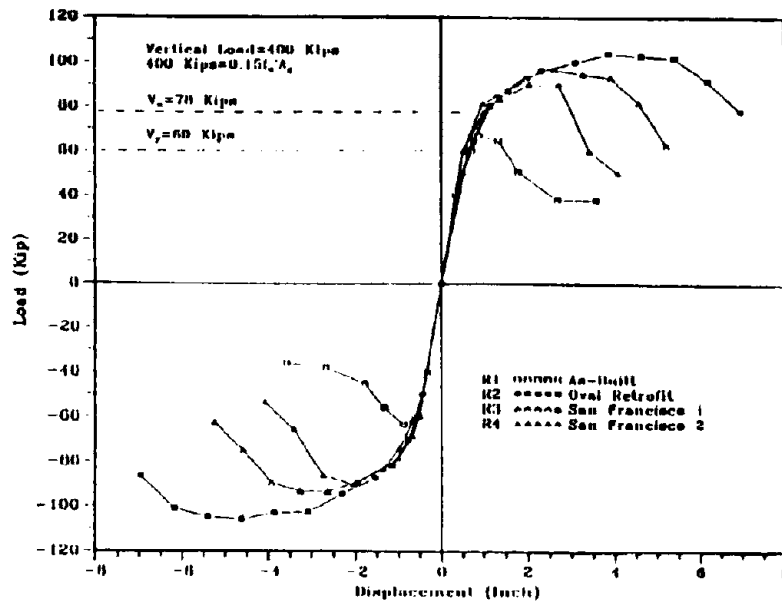


Figure 11: Load-Deflection Envelopes for Rectangular Flexural Columns

## SHEAR COLUMN TESTS

### Shear Column Details

The shear retrofit program involves testing of 6 circular columns of the same diameter as that of the flexural columns and 6 rectangular columns of a smaller cross-section (24 inches x 16 inches), when compared to its flexural counterpart. The aspect ratios for the column as defined by,  $M/(VD)$ , are 2 and 1.5, where  $M$  and  $V$  denote the moment and shear force, respectively, and  $D$  represents the diameter of circular column or depth of rectangular section. In addition to the difference in aspect ratios, the following parameters are varied between columns: (i) longitudinal steel ratio, (ii) axial load level, (iii) yield strength of longitudinal reinforcement. These variations are summarized in Table 3 and 4. Only circular columns C1 and C2, and 'as-built' rectangular column R1 have been tested to date.

A different test setup is used for the shear columns. The lateral load mechanism consists of displacing the column in double-curvature with the point of inflection occurring at mid-height of the column. A stiff loading arm connects the top of the column to a horizontal double-acting actuator located at mid column height. Loadstub rotation is minimized by a load-balancing system which is designed to compensate for the weight of the loading arm. The axial load is applied to the column using the same high-strength flexible rods, as for flexural columns. The shear test setup is shown in Fig. 12.

Continuous longitudinal reinforcement are used in all shear columns i.e. without lap-splice in the potential plastic hinge regions. Fig. 13 shows the reinforcement details for a circular shear column. Longitudinal and transverse steel for the first two pairs of circular columns are the same as that of circular flexural column. Steel area will be increased to

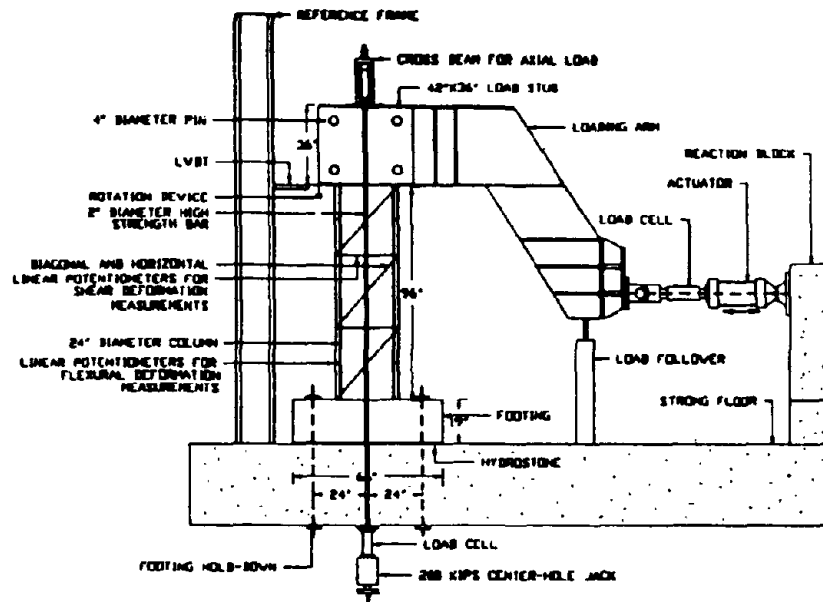


Figure 12: Shear Test Setup

Table 3: Test Matrix for Circular Shear Columns

Test Unit	Longitudinal Steel	Axial Load	M/VD	Retrofit
C1	Grade 40	133 kips	2	No Jacket 'As-Built'
C2	Steel Area = 2.5 %	133 kips	2	Cylindrical Jacket (3/16")
C3	Grade 40	400 kips	2	No Jacket 'As-Built'
C4	Steel Area = 2.5 %	400 kips	2	Cylindrical Jacket (3/16")
C5	Grade 60	400 kips	1.5	No Jacket 'As-Built'
C6	Steel Area = 4 %	400 kips	1.5	Cylindrical Jacket (3/16")

4% for the third pair of columns and Grade 60 steel will be used. Main reinforcement for the first two pairs of rectangular columns consisted of 22 # 6 bars uniformly distributed around the column. A similar increase of steel area to 4% shall be made for the third pair of rectangular columns.

Retrofit of circular columns involves encasing to almost the full height of the column with a 3/16 inch thick cylindrical jacket. A vertical gap of 1 inch is provided between the jacket cutoff and the adjoining footing or loadstub. The same 1/4 inch grout gap is used between the jacket and column. Elliptical jackets of 28 inches by 24 inches outside dimensions in the two principal axes will be used for retrofit of rectangular columns.

#### Load-Deflection Response of Circular Shear Columns

Lateral load-deflection hysteresis loops for the initial 'as-built' circular column are shown in Fig. 15 (a). The lateral forces corresponding to the theoretical ultimate flexural strength of the column,  $V_p$ , and at first yield of extreme tension reinforcement,  $V_y$ , calculated

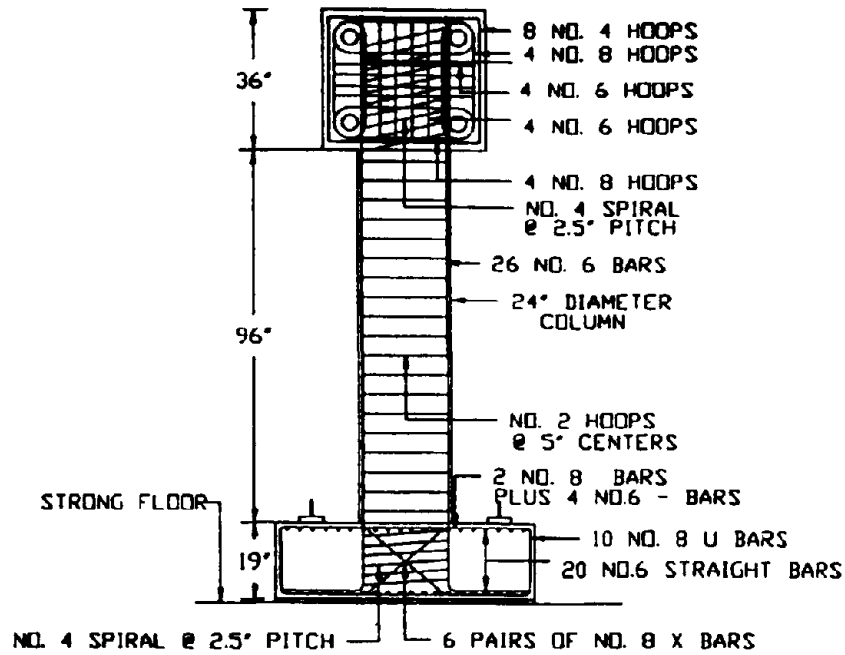


Figure 13: Reinforcement Details for Circular Shear Column

Table 4: Test Matrix for Rectangular Shear Columns

Test Unit	Longitudinal Steel	Axial Load	M/VD	Retrofit
R1	Grade 40	114 kips	2	No Jacket 'As-Built'
R2	Steel Area = 2.5 %	114 kips	2	Elliptical Jacket (3/16")
R3	Grade 60	114 kips	2	No Jacket 'As-Built'
R4	Steel Area = 2.5 %	114 kips	2	Elliptical Jacket (3/16")
R5	Grade 60	400 kips	1.5	No Jacket 'As-Built'
R6	Steel Area = 4 %	400 kips	1.5	Elliptical Jacket (3/16")

using the Mander model for confined concrete [7], are shown by dashed lines in these figures. In addition, the theoretical shear capacity predicted by the ACI [8] is included as linked line.

The 'as-built' circular shear column exhibits relatively stable response up to displacement ductility factor  $\mu = 2$ . Flexural cracks were deeply inclined indicating the strong influence of shear. Web shear cracks appeared at  $\mu = 1$  near middle portion of the column, independent of flexural cracks which tended to concentrate near the column ends. The crack pattern was remarkably symmetrical about mid-height of the column. Although the theoretical flexural capacity ( $V_p = 119.4$  kips) was reached at  $\mu = 1.5$ , the column failed in a brittle manner during first push cycle to  $\mu = 3$ . The maximum load attained was 129 kips which is considerably higher than the ACI shear strength prediction of 71 kips. Final failure involved a major diagonal crack initiated from crushing of concrete in the compression zone in the upper region of the column. The final crack pattern is shown in Fig. 14(a).

The hysteretic response of circular shear column after retrofit shows an impressive

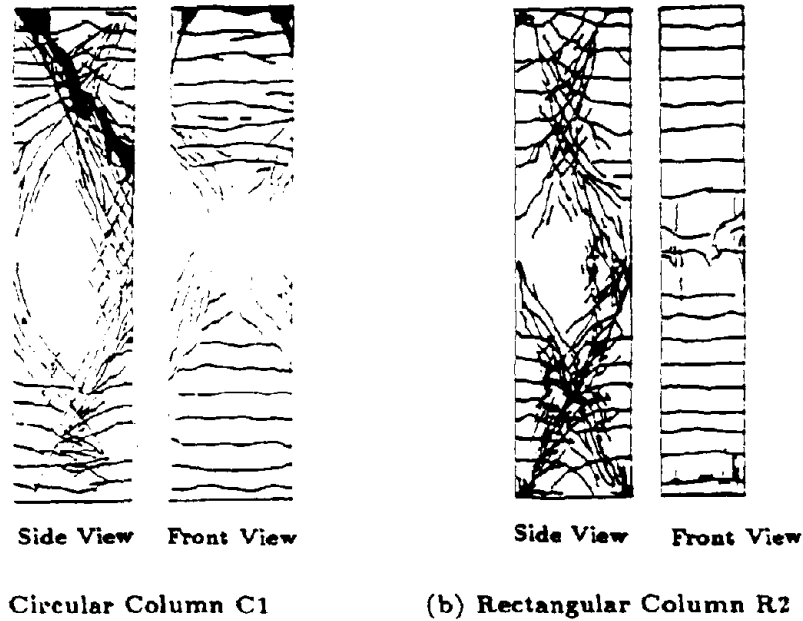
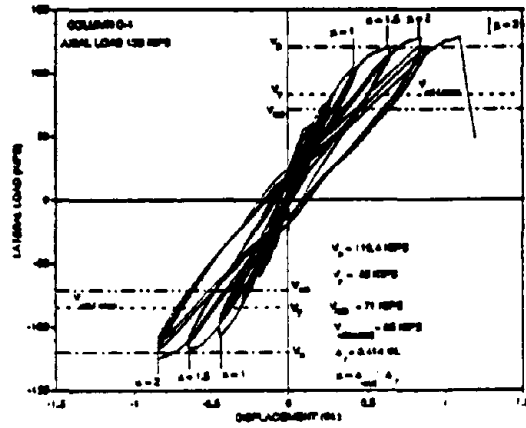


Figure 14: Crack Patterns for 'As-Built' Shear Columns

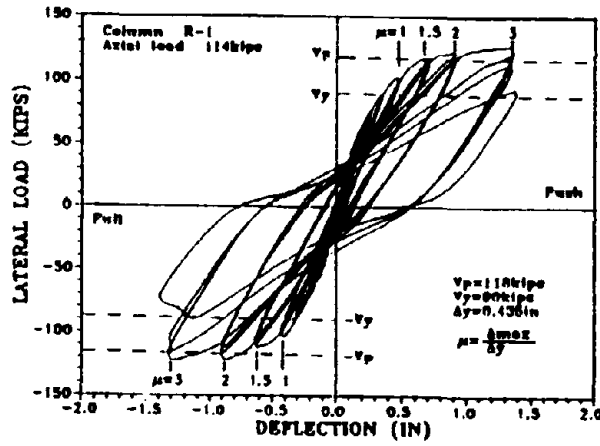
increase in displacement ductility and energy absorption (see Fig. 15(c)). Displacement to ductility factor  $\mu = 10$  or drift ratio of 4.37% was possible without serious strength or stiffness degradation. In addition to spalling of column cover concrete within the 1 inch gap, minor shallow splitting was observed on top of the footing. The theoretical flexural strength,  $V_p$ , calculated using yield strength of the main steel, was 127 kips. This load was first exceeded at  $\mu = 2$ , about the same ductility level when strain-hardening was noted to occur in circular flexural column. The maximum lateral load recorded was 162 kips, occurring at peak displacement in the first push cycle to  $\mu = 10$ . Test was discontinued after three cycles to  $\mu = 10$ , as displacement is limited by the travel range of the vertical load follower. Note that the experimental displacement for retrofitted column is larger than the yield displacement for the 'as-built' column. The increase is due to the extrapolation of displacement to theoretical ultimate flexural capacity which is higher in the case of retrofitted column.

#### Load-Deflection Response of 'As-Built' Rectangular Shear Column

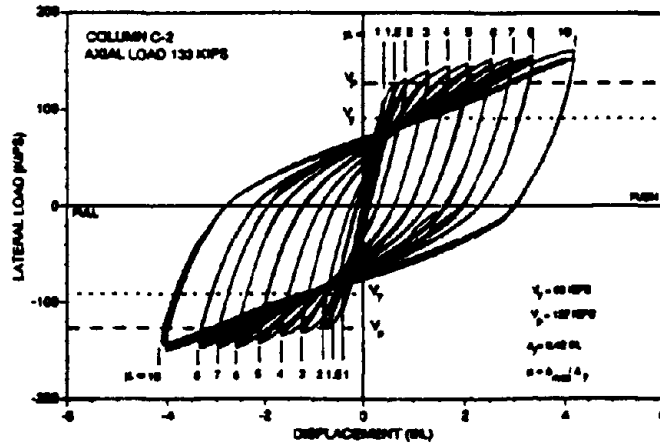
The lateral load-deflection hysteretic response for rectangular column R1 loaded in the strong axis direction is shown in Fig. 15(b). Although the theoretical ultimate flexural capacity of  $V_p = 118$  kips was achieved at displacement ductility factor  $\mu = 1.5$ , the degradation of lateral load was significant during the three cycles to  $\mu = 3$ . Considerable spread of bond cracks and inclined shear cracks had developed by this stage and had affected the lateral strength of the column. Final failure occurred at  $\mu = 3$  when concrete crushed in the bottom compression zone and a major diagonal crack propagated through the lower



(a) 'As-Built' Circular Column



(b) 'As-Built' Rectangular Column - Strong Direction



(c) Retrofitted Circular Column

Figure 15: Hysteretic Responses of Shear Columns

region of the column, destroying the vertical load carrying capacity of the column. The final crack pattern for 'as-built' rectangular column is shown in Fig. 14(b).

## CONCLUSIONS

Cylindrical steel jacketing of the potential plastic hinge region has been shown to enhance the flexural strength and ductility of tall circular columns. A dependable drift ratio exceeding 5% is available. For circular columns with small aspect ratio, brittle shear failure can be avoided by encasing over the full height of the column with cylindrical steel jacket. A stable and ductile plastic hinging can be developed in the column, providing drift ratio of at least 4%. Elliptically shaped steel jacket appeared to be best suited for providing confinement to column concrete in the potential plastic hinge region of tall rectangular column. Although the test program is incomplete, elliptical steel jacketing is considered the best option for shear retrofit of squat rectangular column.

## ACKNOWLEDGMENT

The research described in this paper has been funded by the California Department of Transportation and the Federal Highway Administration. The helpful comments of Guy Mancarti and James Gates are gratefully acknowledged. Contributions to the paper by Z. L. Sun, R. Verma and Y. Xiao are also appreciated. The comments and conclusions made in this paper are solely those of the authors and do not necessarily reflect the views of CalTrans or the FHA.



## References

- [1] G.G. Fung, R.J. Lobeau, E.D. Klein, J. Belvedere, and A.F. Goldschmidt. *Field Investigation of Bridge Damage in the San Fernando Earthquake*. Technical Report, Bridge Department, Division of Highways California Department of Transportation, Sacramento, California, 1971.
- [2] M.J.N. Priestley. Damage of the I-5/I-605 Separator in the Whittier Earthquake of October 1987. *Earthquake Spectra*, 4(2):389-405, 1988.
- [3] H.S. Lew, editor. *Performance of Structures During the Loma Prieta Earthquake of October 17, 1989*. Gaithersburg, MD 20899, 1990. NIST Special Publication 778.
- [4] R. Zelinski. California highway bridge retrofit strategy and details. In *Second Workshop on Bridge Engineering Research in Progress*, National Science Foundation and Civil Engineering Department, University of Nevada, Reno, October 29-30 1990.
- [5] M.J.N. Priestley, F. Seible, Y.H. Chai, and Z.L. Sun. Steel jacketing of bridge columns for enhanced flexural performance. In *Second Workshop on Bridge Engineering Research in Progress*, National Science Foundation and Civil Engineering Department, University of Nevada, Reno, October 29-30 1990.
- [6] M.J.N. Priestley and R. Park. Strength and ductility of concrete bridge columns under seismic loading. *ACI Struct. Jour.*, 84(1):61-76, Jan/Feb 1987.
- [7] J.B. Mander, M.J.N. Priestley, and R. Park. Observed stress-strain behavior of confined concrete. *Jour. Struct. Div., ASCE*, 114(8):1827-1849, Aug. 1988.
- [8] *Building Code Requirements For Reinforced Concrete (ACI 318-83 Revised 1986)*. American Concrete Institute, Detroit, Michigan, 1987.

## STUDY ON DUCTILITY ESTIMATION OF FIBER MIXED RC MEMBERS

S. Kobayashi (I)  
K. Kawano (II)  
K. Morihama (III)  
H. Watanabe (III)

### SUMMARY

We are currently carrying out the study to improve the ductility of reinforced concrete members by mixing the fiber in concrete from 1989. In this study the bending test of fiber mixed reinforced concrete beams by reversal static loading has been done. From the test results obtained so far, it is shown that the ductility of fiber mixed reinforced concrete beams is larger than that of normal reinforced concrete beams. And it is shown that the ductility factor of fiber mixed reinforced concrete beams can be calculated if the tensile strength and ultimate compressive strain are known.

### 1. INTRODUCTION

Japanese Earthquake Resistant Design Specification for Road Bridges has been revised this year. It requires to design bridges not to collapse in 1.0G horizontal ground acceleration. Bridge piers which can't bear such a strong inertial force theoretically are required to have enough ductility to absorb the dynamic energy. It is mentioned that the inertial force acting to the concrete members can be reduced according to the following formula in the specification;

$$P' = \frac{P}{\sqrt{2\mu - 1}} \quad (\text{eq. 1})$$

where, P : restoring force of the elastic member  
P' : restoring force of the elasto-plastic member  
 $\mu$  : ductility factor (Fig.1.1)

Thus, it is very important to ensure enough ductility for the concrete members resistable against a strong ground acceleration without losing their strength. But as concrete is brittle material, some concrete structures can not possess requested ductility.

The purpose of our study is to develop reinforced concrete members ductile enough to survive a very strong earthquake. There are some methods to improve the ductility of reinforced concrete members. To reduce amount of tensile reinforcement is the most simple method to improve the ductility, but since the strength of member reduces, it is not an appropriate method.

In this study, we tried to improve the ductility of reinforced concrete members by mixing fiber into the concrete. As fiber mixed concrete can transfer tensile stress after tension crack occurs in concrete, the shear strength and, thus, the ductility of fiber mixed reinforced concrete members will be greater than that of normal reinforced concrete. But it is very complicated to estimate the ductility of members which fail by shear and bending together. Thus we discuss the ductility of reinforced concrete members which fail by bending alone in this paper.

### 2. CHARACTERISTICS OF FIBER REINFORCED CONCRETE

- 
- (I) Director, Geology and Chemistry Department, Public Works Research Institute(PWRI), Ministry of Construction, Tukuba, Japan  
(II) Head, Concrete Division, Geology and Chemistry Department, PWRI.  
(III) Research Engineer ,ditto

### Generals

The most common method used in Japan to calculate the ultimate strength and ductility of reinforced concrete members was proposed by Ohta(1980)<sup>1)</sup>. This method is now adopted in the specification for highway bridge in Japan after some modifications. If we can use this method to calculate ultimate strength and ductility of fiber mixed reinforced concrete members, it is very convenient to design concrete members.

But it seems that we can't use this method directly, because fiber mixed concrete has the following properties ;

- (1) Compressive ductility is larger than that of plain concrete.
- (2) Tensile strength is not zero after tension crack occur.

We have to take account of these properties to estimate the ultimate strength and the ductility of fiber mixed reinforced concrete members. Especially, the values of compressive ductility (ultimate compressive strain) affect calculated ultimate curvature of cross section, and the values of tensile strength of concrete affect the location of neutral axis and resistable bending moment of cross section of reinforced concrete members in the design.

In this chapter we discuss the compressive ductility and tensile strength of fiber mixed concrete.

### Mix Proportion of Fiber mixed concrete

We used three types of fibers(Photo.1), of which mechanical properties are shown in Table 2.1. The volume percentage of fiber content in concrete was varied from 0% to 2%. Water cement ratio of concrete was fixed at 50%, 60%, and 70%. Unit water content is so determined that the slump of concrete which contains 1% of fiber became about 8cm. Thus the concrete which contains more than 1% of fiber had less slump. The maximum size of aggregate was 10mm.

### Compressive Toughness Test of Fiber Mixed Concrete

We carried out the compressive toughness test of fiber mixed concrete. The size of cylinder specimens was  $\phi 10\text{cm} \times 20\text{cm}$ . The compressive strain of specimens was measured with a compresso meter. Teflon sheets were attached at the both ends of the concrete cylinder to eliminate the friction between the specimens and the loading plates. If we don't remove this friction, the toughness would be measured larger than the actual value<sup>2)</sup>.

The test results of compressive strength of fiber mixed concrete is shown in Table 2.3. The difference of compressive strength from plain concrete was very little.

The compressive toughness coefficient is usually defined as the average compressive strength from 0% compressive strain to 0.75% compressive strain<sup>3)</sup>. But according to this method, the value of compressive toughness coefficient is affected not only by the compressive ductility of concrete, but also by the compressive strength of concrete. The compressive toughness coefficient of brittle high strength concrete may be bigger than that of ductile low strength concrete. Therefore, we used the other index to express the compressive ductility of fiber mixed concrete.

We compared the compressive strain of fiber mixed concrete at the point where the compressive stress is 85% of compressive strength of concrete( $E_{0.85}$ )(Fig.2.1). The result of  $E_{0.85}$  of fiber mixed concrete is shown in Fig.2.2.

The reinforcing effect with the fibers to concrete became more clear in the case of low strength concrete than the high strength concrete. In other words, large amount of fiber is needed to make the high strength concrete ductile. This tendency is the same in any kind of the fiber used in this test.

### Flexural Strength Test of Fiber Mixed Concrete

It is very important to estimate the tensile strength of fiber mixed concrete. Many types of testing method<sup>4)</sup> are proposed to measure the tensile strength of fiber mixed concrete. But measuring the tensile strength of fiber mixed concrete directly is so difficult that we carried out the flexural test in this study and tried to calculate the approximate value of tensile strength from the flexural strength. The specimen was  $10\text{cm} \times 10\text{cm} \times 40\text{cm}$  prism. With the assumption of the stress distribution in the cross section of concrete prism as shown in Fig.2.3, the bending moment in the mid-span of concrete prism would be expressed as follows.

$$M = 0.408x^2 \cdot b \cdot f_c' + 0.5 \cdot (d-x)^2 \cdot b \cdot f_t \quad (\text{eq. 2})$$

where,

- M : bending moment in the mid-span (kgf·cm)
- d : height of the cross section of specimen (cm)
- b : width of the cross section of specimen (cm)
- x : distance from extreme compression fiber to neutral axis (cm)
- f<sub>c</sub>' : compressive strength of fiber mixed concrete obtained from the test (kgf/cm<sup>2</sup>)
- f<sub>t</sub> : approximated tensile strength of fiber mixed concrete when the width of tension crack equals to 2·l mm. (kgf/cm<sup>2</sup>)

While bending the concrete specimens, the tension crack occurs in the mid-span. And the plastic hinge is formed. The deformation of the specimen is modeled as Fig.2.4 with the assumption that only one crack is formed. The width of tension crack may be represented as follows.

$$w = (d-x) \cdot \theta \quad (\text{eq. 3.1})$$

$$\theta = \delta' \cdot l / (l \cdot (L-1)) \quad (\text{eq. 3.2})$$

$$\delta' = 2 \cdot l \cdot \delta / L \quad (\text{eq. 3.3})$$

where,

- w : crack width (cm)
- δ : displacement measured by the transducer at the center of the specimen (cm)
- δ' : displacement at the crack point of the specimen (mm)

The approximate tensile strength of fiber mixed concrete calculated from these equations is shown in Fig.2.5, according to the procedure described in Table.2.5. The tensile strength increases as the fiber content increases. But the rate of the increase became smaller as the fiber content increases.

### 3. LOADING TEST OF FIBER MIXED REINFORCED CONCRETE MEMBERS

#### Test specimens

As shown in Fig.3.1, all of the specimens were reinforced concrete beams with the same cross section and the same amount of reinforcement which were designed to lend the failure in flexure. The ratio of shear span length to effective depth of the beam was 3.5 for all specimens. The mix proportion of the specimens are shown in Table.3.1.

#### Loading program

The static loading test was carried out for all specimens by the displacement control. The specimen 1 to 3 were loaded monotonically, and other specimens were loaded cyclically. The program of cyclic loading is shown Fig 3.2.

#### Test results

Hysteretic behavior of fiber mixed reinforced concrete beams are shown in Fig.3.3, and failure patterns of specimens are described in Table.3.2. Fiber mixed reinforced concrete beams which were loaded monotonically had large ductility. In this test, all of the specimens had enough amount of web reinforcement, and so the shear failure of the beams did not occur in the case of the monotonic loading test.

The ductility of fiber mixed reinforced concrete beams was larger than that of normal reinforced concrete beam in the cyclically loading test.

But compared to the beams loaded monotonically, the ductility of the beams loaded cyclically was small. The failure occurred in tensile reinforcing bar or failure of concrete in compression and consequent buckling of compressive reinforcing bar.

#### Analysis of Ductility of Fiber Mixed Reinforced Concrete Beams

We calculated the ductility factor and the ultimate strength of fiber mixed

reinforced concrete beams according to Ohta's method. The assumptions in the calculation were as follows;

- (1) The ultimate compressive strain of fiber mixed concrete is equal to  $\epsilon_{0.85}$  which is obtained from the compressive strength test of concrete.
- (2) The tensile strength of fiber mixed concrete is  $f_t$  which is calculated from the flexural test.
- (3) The stress distribution in cross section of the beams is assumed to be described as Fig 3.4.

We calculated the displacement ( $\delta$ ) at the center of the beam. The ductility factor  $\mu$  is defined as the following form.

$$\mu = \frac{\delta_u}{\delta_y} \quad (\text{eq. 4})$$

where  $\delta_y$ : the displacement at the center of the beam when the tensile reinforcing bar yield

$\delta_u$ : the displacement at the center of the beam when the strain of concrete reaches to ultimate compressive strain.

Measured and calculated ductility factor is shown in Table.3.3. We also calculated the ductility factor of the beams with the assumption that the ultimate compressive strain of fiber mixed concrete is equal to 0.33%. The results of calculation are shown in Table.3.4. The calculated ductility factors correspond well to the measured ductility factors when we use the  $\epsilon_{0.85}$  as ultimate compressive strain of concrete, while it is not the case when we used 0.33%, where we underestimated the ductility factor of fiber mixed reinforced concrete beams. Since the tensile stress of fiber mixed concrete is not zero after tensile crack has occurred in the concrete, the ratio of tensile reinforcement of the beam appear to be increased apparently by mixing fiber in concrete, and the distance from extreme compression fiber to neutral axis of the cross section of the beams becomes longer. Thus, if we use the 0.33%, the calculated curvature of the cross section of the beam in the ultimate state becomes smaller as the tensile strength of fiber mixed concrete becomes higher. Therefore the increase of ultimate compressive strain of the concrete by mixing fiber into concrete must be taken into account to calculate the ultimate deformation of the fiber mixed reinforced concrete beams.

Calculated and measured ultimate load and yield load are shown in Table.3.5. The calculated load is smaller than the measured load. The reasons of this are thought to be as follows;

- (1) We neglect the effect of strain hardening of reinforcing steel.
- (2) The tensile strength of fiber mixed concrete is higher than that used in the calculation.
- (3) The ultimate compressive strength used in the calculation is 85% of the compressive strength obtained by the test.

But the difference between the calculated value and the measured value is small and the calculated value is on the safe side, that makes no problem practically.

#### 4. CONCLUSION

The following conclusions are obtained from this study;

- (1) The compressive ductility of fiber mixed concrete becomes larger as fiber content in concrete increases.
- (2) It is possible to estimate the approximate value of tensile strength after the tensile crack occur in the fiber mixed concrete.
- (3) The ductility factor of fiber mixed reinforced concrete beams can be calculated by means of Ohta's method. But the ultimate compressive strain and the tensile strength of fiber mixed concrete have to be determined by the test.

(4) Even if fiber is mixed in the concrete, the buckling of compressive reinforcement in beams under bending load can't be prevented.

#### REFERENCE

- 1) Ohta, M: "A Study on Earthquake Resistant Design for Reinforced Concrete Bridge Piers of Single-Column Type.", Report of PWRI, No.153-3, 1980.(in Japanese)
- 2) Uomoto, T. and Nishimura, T.: "Compressive Toughness Test Method of Steel Fiber Reinforced Concrete.", Review of 37th General Meeting -technical session-, The Cement Association of Japan, 1983.
- 3) Recommendation for Design and Construction of Steel Fiber Reinforced Concrete Structures (tentative), Concrete Library, Japan Society of Civil Engineering, 1983.
- 4) Cho, R. Kobayashi, K and Nishimura, T: "Testing Method for Tensile Strength of Steel Fiber Reinforced Concrete(I), -Tension Test of Axially Reinforced Specimen-", Monthly Journal of Institute of Industrial Science, Vol.31.1, University of Tokyo, 1979.

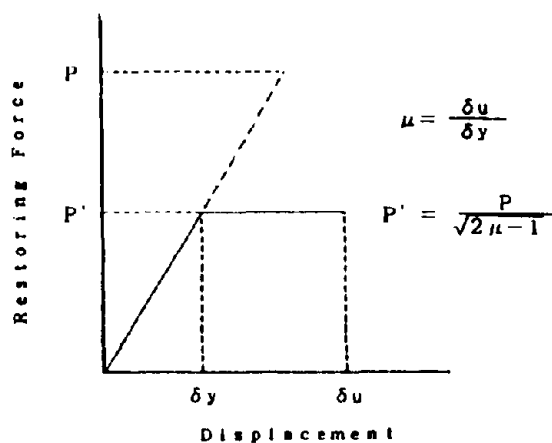
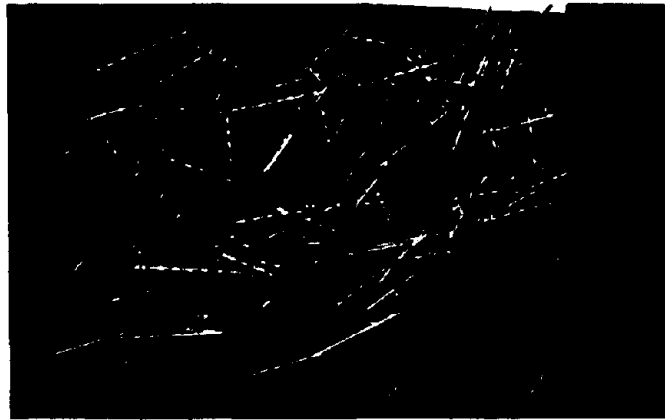


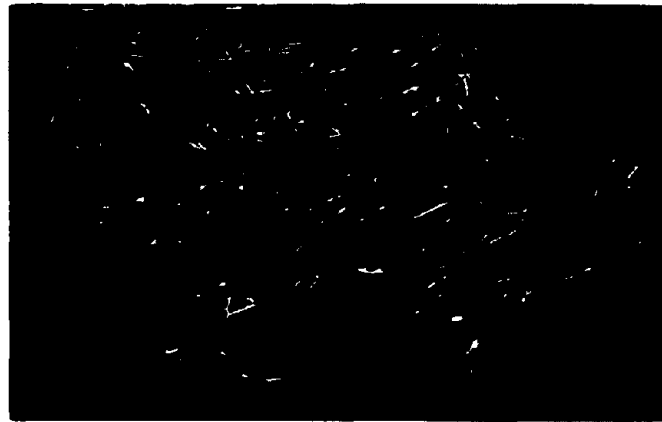
Fig.1.1 Reduction of restoring force of elasto-plastic members

Table.2.1 Specification and mechanical properties of fibers

Fiber	Steel fiber a	Steel fiber b	Aramid fiber
Cross section(mm)	φ 0.6	□ 0.5	φ 0.4
Length(mm)	30	30	30
Aspect ratio	50	60	75
Specific gravity	7.85	7.85	1.38
Tensile strength (kgf/mm <sup>2</sup> )	120.8	77.3	300.0
Young's modulus (kgf/mm <sup>2</sup> )	21000	21000	7000



Steel fiber a



Steel fiber b



Aramid fiber

Photo.1 Fibers used in this study

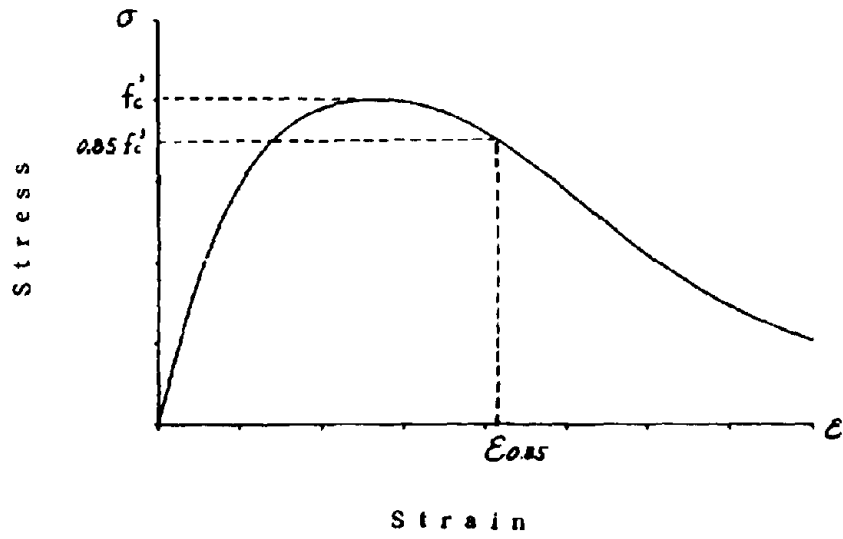


Fig.2.1 Definition of  $\epsilon_{0.95}$  of fiber mixed concrete

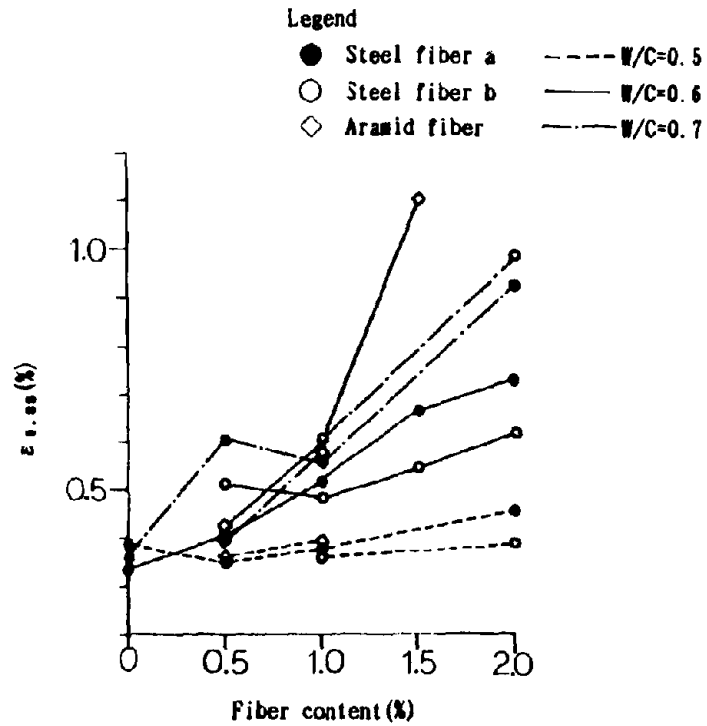


Fig.2.2 Ultimate compressive strain( $\epsilon_{0.95}$ ) of fiber mixed concrete



Table 2.2 Mix proportions of fiber mixed concrete

Fiber	Water cement ratio (%)	Fiber. percent by volume (%)	s/a (%)	water (kg/m <sup>3</sup> )	cement (kg/m <sup>3</sup> )	sand (kg/m <sup>3</sup> )	gravel (kg/m <sup>3</sup> )	measured	
							10mm~5mm	slump (cm)	Air content (%)
Steel fiber a	50	0	65	220	440	1023	559	9.0	5.0
		1.0		220	440	1006	550	8.0	5.2
		2.0		220	440	989	541	5.0	5.3
	60	0	65	220	367	1063	580	11.0	5.3
		0.5		220	367	1054	576	12.0	5.0
		1.0		220	367	1045	572	7.5	5.5
		1.5		220	367	1037	567	6.5	4.1
		2.0		220	367	1028	562	4.9	4.3
		0		220	314	1091	596	12.9	5.5
	70	1.0	65	220	314	1074	587	7.5	5.4
		2.0		220	314	1057	578	3.9	4.7
		1.0		220	440	1006	550	9.4	5.0
Steel fiber b	50	2.0	65	220	440	989	541	8.0	5.0
		1.0		220	367	1045	571.5	11.3	4.6
	60	2.0	65	220	367	1028	562	6.3	4.6
		1.0		220	314	1074	567	6.5	4.8
	70	2.0	65	220	314	1057	578	7.7	4.7
		0.5		240	480	959	524	12.7	4.1
Aramid fiber	50	1.0	65	240	480	950	520	7.6	4.2
		0.5		240	400	1002	548	10.3	4.0
	60	1.0	65	240	400	994	543	15.6	4.1
		0.5		240	363	1022	559	15.5	4.1
	70	1.0	65	240	363	1013	554	10.5	4.1

Table 2.3 Results of compressive strength of fiber reinforced concrete specimens

(kgf/cm<sup>2</sup>)

kind of fiber	water cement ratio (%)	fiber content (%)				
		0	0.5	1.0	1.5	2.0
steel fiber a	50	485	-	498	-	538
	60	372	323	381	351	430
	70	276	-	282	-	347
steel fiber b	50	-	-	487	-	515
	60	-	-	388	-	404
	70	-	-	343	-	315
aramid fiber	50	-	507	453	-	-
	60	-	365	357	-	-
	70	-	348	305	-	-

Table 2.4 Procedure of calculating tensile strength of fibre mixed concrete

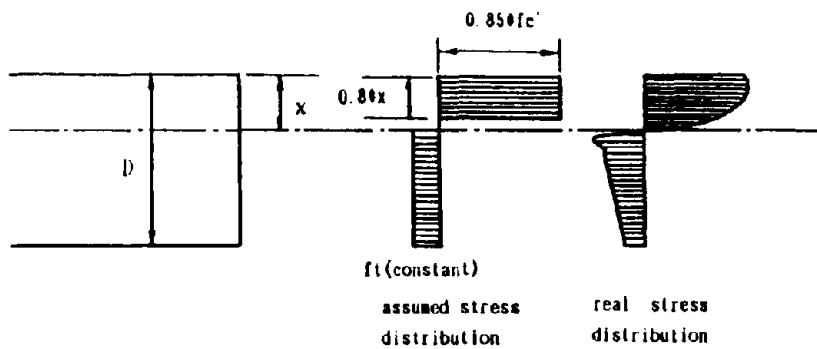
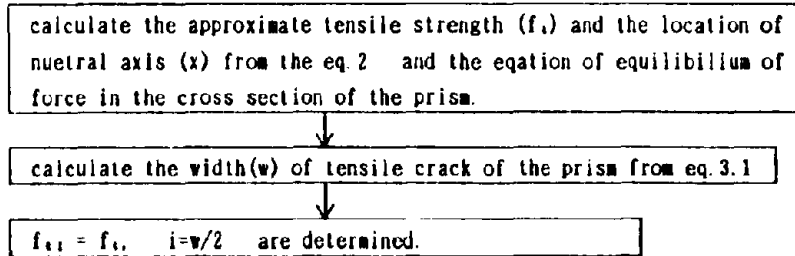


Fig. 2.3 Stress distribution of the cross section of fiber mixed concrete specimens in the flexural test

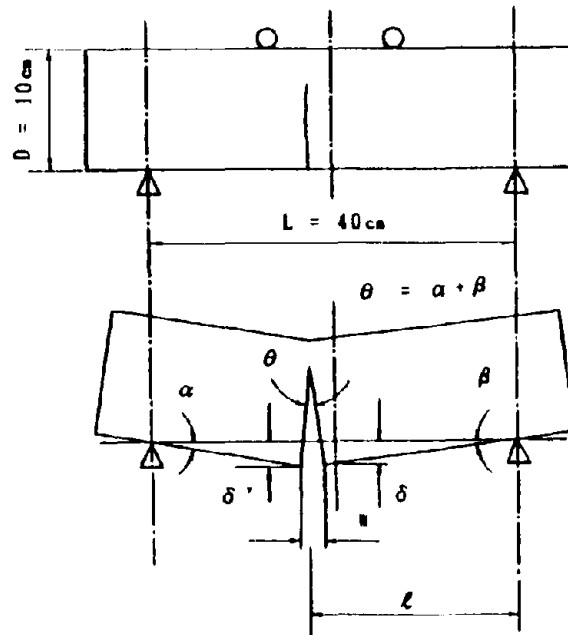


Fig. 2.4 Deformation model of fiber mixed concrete specimens in bending

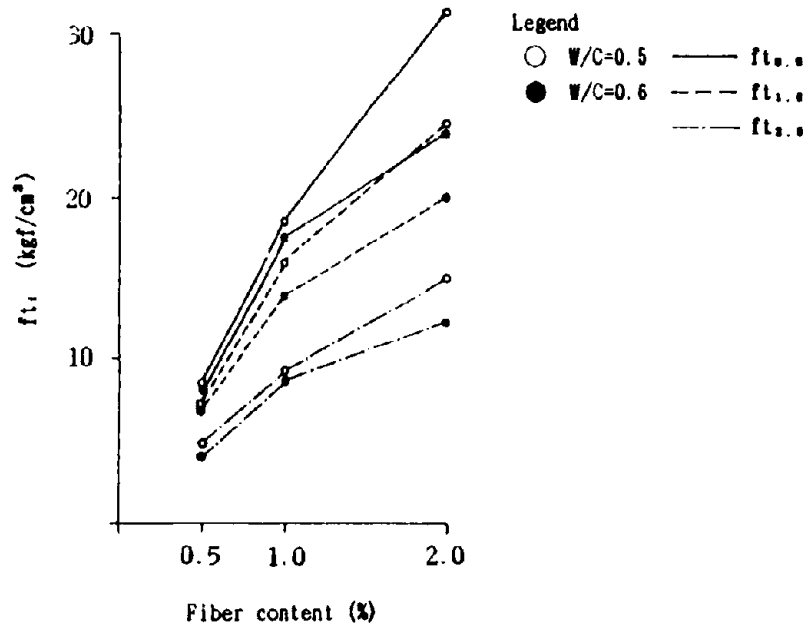


Fig. 2.5 Approximate tensile strength of fiber mixed concrete

Table 3.1 Mix proportions of fiber mixed reinforced concrete beams

(kg/m<sup>3</sup>)

Beam no.	Water	Cement	Sand	Gravel	Fiber	Kind of fiber
1 & 4	220	367	1063	580	0	no fiber
2 & 7	220	367	1028	562	157	steel fiber A
3 & 8	240	400	994	543	14	aramid fiber
5	220	367	1045	572	78.5	steel fiber A
6	220	367	1037	566	117.8	steel fiber A
9	220	367	1028	562	157	steel fiber B

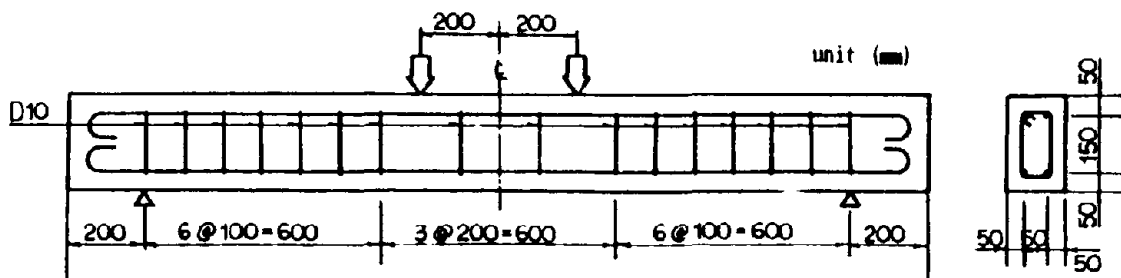


Fig. 3.1 Dimension of beam specimens

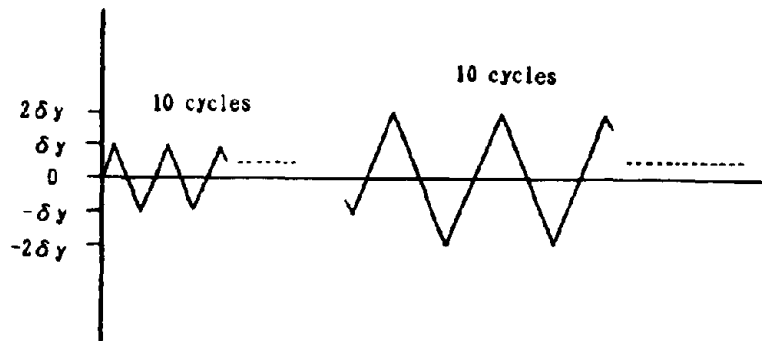


Fig. 3.2 Cyclic loading program

Table 3.2 Failure pattern of fiber mixed reinforced concrete beams

Beam no.	Fiber used in the specimen	Fiber, percent by volume	Failure pattern of the beam
1	no fiber	0.0	Compression failure of concrete occurred in the compression zone.
2	steel fiber a	2.0	No failure occurred within the displacement amplitude $20\delta y$ .
3	aramid fiber	1.0	No failure occurred within the displacement amplitude $20\delta y$ .
4	no fiber	0.0	Buckling of compression steel occurred at the 9th cycle of $4\delta y$ .
5	steel fiber a	1.0	Failure of tension steel occurred at the 9th cycle of $6\delta y$ .
6	steel fiber a	1.5	Buckling of compression steel occurred at the 1st cycle of $6\delta y$ .
7	steel fiber a	2.0	Failure of tension steel occurred at the 1st cycle of $7\delta y$ .
8	aramid fiber	1.0	Failure of tension steel occurred at the 2nd cycle of $7\delta y$ .
9	steel fiber b	2.0	Buckling of compression steel occurred at the 1st cycle of $6\delta y$ .

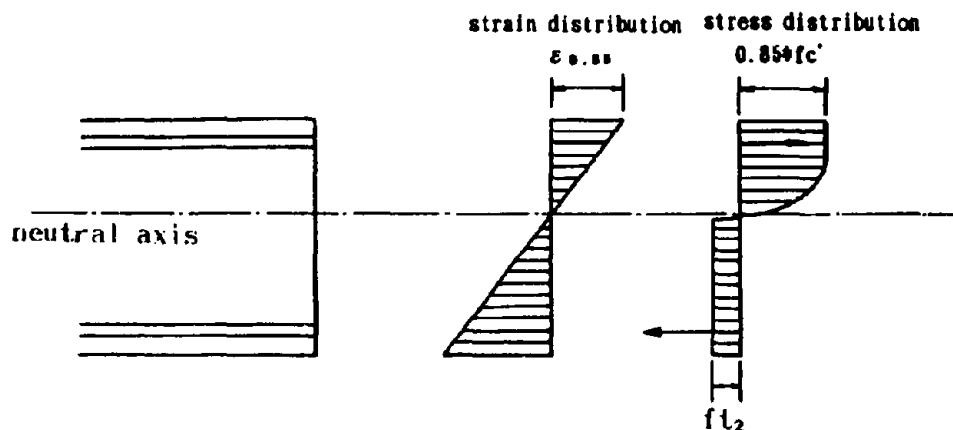


Fig. 3.4 Assumed stress distribution in the cross section of fiber mixed reinforced concrete beam (ultimate state)

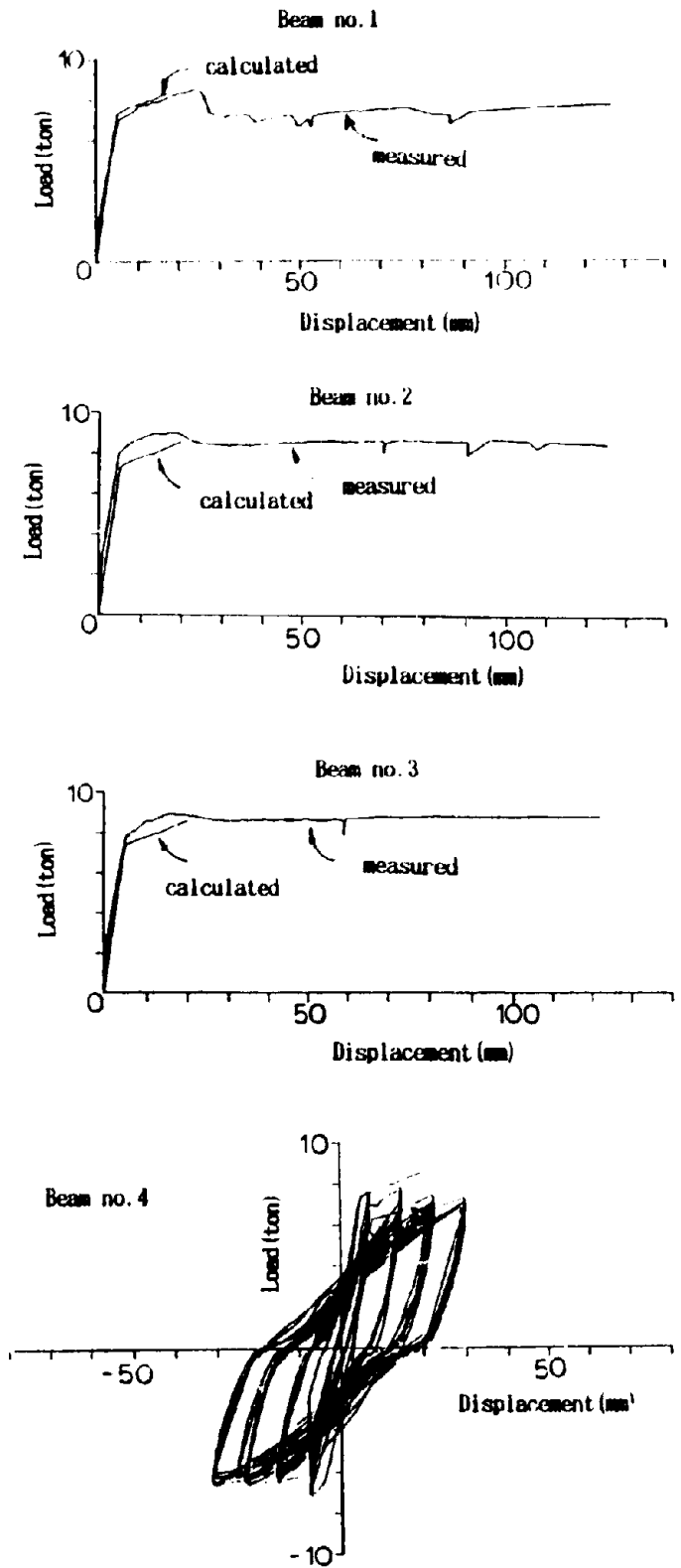


Fig. 3.3 Load-Displacement curves of beams

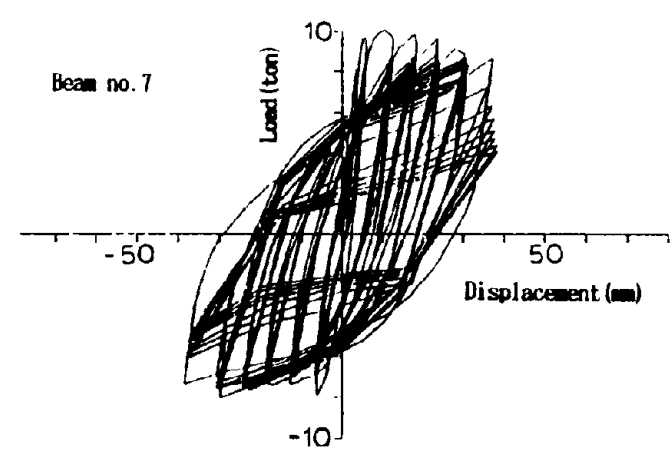
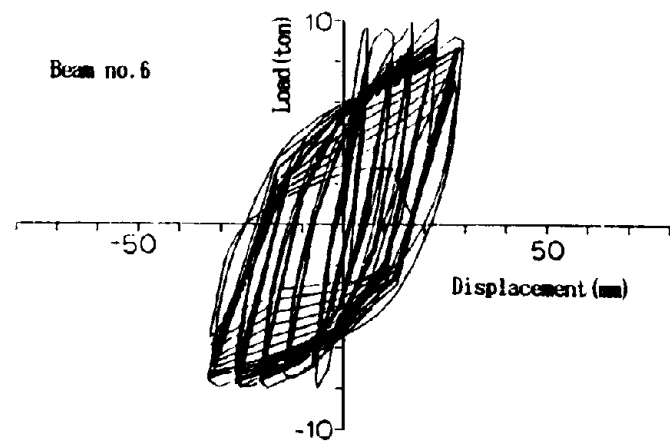
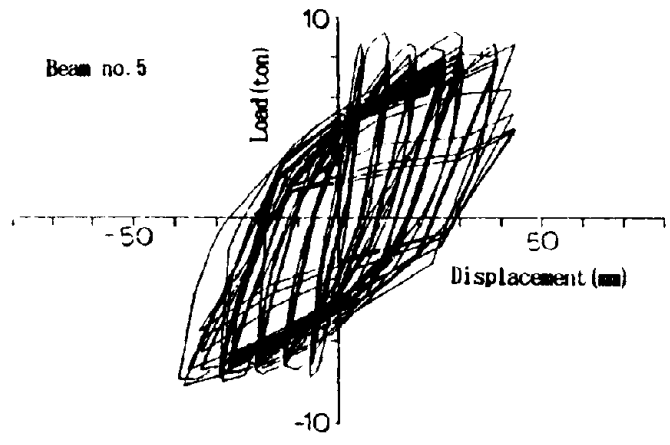


Fig. 3.3 Load-Displacement curves of beams

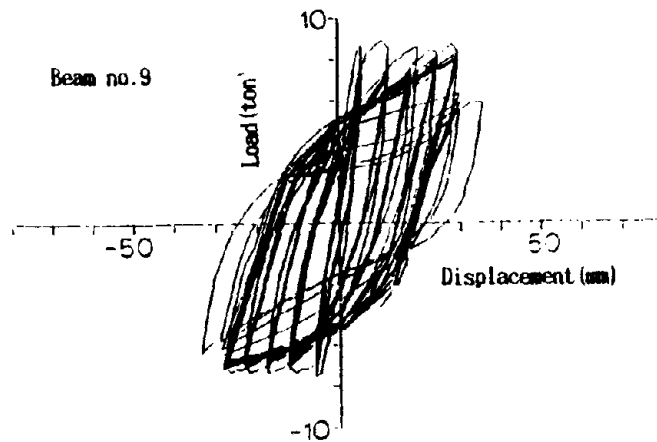
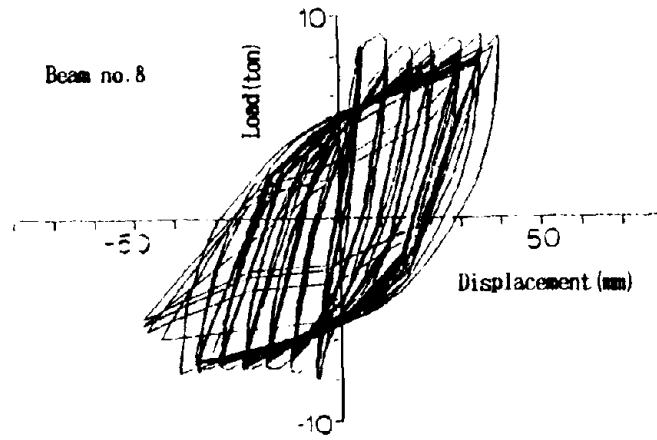


Fig. 3.3 Load-Displacement curves of beams

Table 3.3 Tensile strength and ultimate compressive strain of fiber mixed concrete

Beam no.	Tensile strength (kgf/cm <sup>2</sup> )	Ultimate compressive strain ( $\times 10^{-3}$ )
4	0.0	3300
5	8.68	5200
6	10.48	6700
7	12.28	7300
8	12.20	5800
9	13.02	5700

Table 3.4 Calculated and measured ductility factors

(The values of ultimate compressive strain adopted in the calculation are shown in Table 3.3)

Beam no.	Ductility Factor (calculated)	Ductility factor (measured)
4	3.02	3
5	4.29	5
6	5.47	5
7	5.93	6
8	4.66	6
9	4.63	5

Table 3.5 Calculated and measured ductility factors

(The values of ultimate compressive strain adopted in the calculation are assumed to be 0.33%)

Beam no.	Ductility Factor (calculated)	Ductility factor (measured)
4	3.02	3
5	2.83	5
6	2.81	5
7	2.78	6
8	2.78	6
9	2.77	6

Table 3.6a Measured and calculated yield strength loads and ultimate strength loads

(The values of ultimate compressive strain adopted in the calculation are shown in table 3.3)

Beam no.	Yield strength load(ton)		Ultimate strength load(ton)	
	Measured	Calculated	Measured	Calculated
4	3.84	3.77	3.93	4.02
5	4.34	4.00	4.63	4.25
6	4.50	4.04	5.03	4.42
7	4.52	4.08	5.06	4.52
8	4.31	4.08	4.58	4.35
9	4.36	4.10	4.44	4.36

Table 3.6b Measured and calculated yield strength loads and ultimate strength loads

(The values of ultimate compressive strain adopted in the calculation are assumed to be 0.33%)

Beam no.	Yield strength load(ton)		Ultimate strength load(ton)	
	Measured	Calculated	Measured	Calculated
4	3.84	3.77	3.93	4.02
5	4.34	4.00	4.63	4.22
6	4.50	4.04	5.03	4.26
7	4.52	4.08	5.06	4.32
8	4.31	4.08	4.58	4.32
9	4.36	4.10	4.44	4.34



EFFECT OF CARBON FIBER REINFORCEMENT AS A STRENGTHENING MEASURE  
FOR REINFORCED CONCRETE BRIDGE PIERS

Tetsuo Matsuda (I)  
Takashi Sato (II)  
Hiroshi Fujiwara (III)  
Norimasa Higashida (IV)  
Presenting Author: Norimasa Higashida

Summary

A new method of strengthening reinforced concrete bridge piers in seismic regions is described. In this method, rather than using reinforced concrete or steel tubes, carbon fiber is wrapped around the section. This paper presents the fundamental mechanical properties of the carbon fibers and the design concept of them applied to existing piers. The seismic resistance of the bridge piers with carbon fibers was evaluated through the experimental investigation using scaled models.

Introduction

Generally, longitudinal reinforcing steel in the existing reinforced concrete piers is curtailed from the viewpoint of efficient bar arrangement. It has been pointed out that under an extremely severe earthquake loading, large amounts of damages may occur in piers above this rapid change in reinforcement.

Recently, the regions of steel curtailment has been improved by encasing the piers with reinforced concrete and/or with steel tubes. Instead of the above materials, the authors have adopted the carbon fibers, which were applied to columns in experiments and chimneys on site as reported by Katsumata and Kobatake<sup>1) 2)</sup>, and they demonstrated their validity. This improved method utilizes the excellent properties of carbon fibers such as high strength, high modulus of elasticity and lightness. Therefore the method results in the following advantages; (1) very slight increase in weight and the shape-dimension (2) small change of rigidity (3) easy construction and high durability.

This paper describes the fundamental mechanical properties<sup>3)</sup> of carbon fibers related with the earthquake-resistant reinforcement of piers and the possibility of using carbon fibers<sup>4)</sup> for the improvement of the earthquake resistance of the piers. Further, the paper demonstrates the experimental results with a scaled model test, <sup>5) 6)</sup> which was conducted to verify the validity of the method using carbon fibers for bridge piers.

- 
- (I) Manager, Structural Engineering Division  
Laboratory of Japan Highway Public Corporation (JHPC)  
(II) Deputy Manager, Structural Engineering Division (JHPC)  
(III) Deputy Manager, Structural Engineering Division (JHPC)  
(IV) Engineer, Structural Engineering Division (JHPC)

## Carbon fiber (derived from reference<sup>3)</sup>)

### Outline

Ordinary users of carbon fibers have been (1) aircraft manufacturers and (2) sporting goods manufacturers. Since the use of carbon fibers in these areas is not large enough to satisfy the carbon fibers manufacturers, the building construction and/or civil engineering field is assumed a large potential consumer.

Carbon fibers are still very expensive (approximately 100 times that of steel per unit weight) and it seems very unlikely the price will drastically fall by using the current production technique. In repair work, however, the cost of the material is only a small percentage of the total cost since the amount of material is very small and labor for the work is considerably large. The percentage of the labor cost and/or preparatory work is much larger than material cost. Carbon fiber is applicable to repair work from this point of view. Moreover, in usual repair work, concentration is paid to; (1) the improvement of structural performance, (2) retaining the functions demanded by the structure. Cost is a secondary matter in any repair work.

Apart from repair work at this moment carbon fibers are being introduced to newly built structures. The cost of carbon fibers prevents it from being used for newly built structures though the remarkable performance of carbon fibers has been recognized among some engineers. Research investigation on carbon fibers began in Japan and it shows special promise, for example;

- (1) offshore and/or onshore structures of high durability with carbon fibers, and
- (2) prestressing tendons using high strength and modulus carbon fibers.

### Products

Carbon fibers are composed of more than 90% carbon. In the fiber, groups of carbon atoms are continuously connected in the direction of the fiber. Carbon fibers can be classified into many grades depending upon mechanical properties and into two types of fiber length. In this paper, only HP (high performance) grade and continuous type carbon fiber is discussed; where the HP grade is a continuous type with a tensile strength of 300kgf/mm<sup>2</sup> and a Young's modulus of approximately 24 tf/mm<sup>2</sup>. Fiber length is not limited and may be greater than 2 km.

The smallest unit of this type of carbon fiber is called a "monofilament" (see Fig. 1), which is a very fine fiber. A practical unit is called a "strand" and consists of 1000 to 12000 monofilaments. Strands are usually impregnated with epoxy resin as described later. Other practical product of carbon fibers is UD tape in which strands are stretched in one direction, like a cloth.

Generally, we use the UD tape impregnated with resin to strengthen structures and also the strands impregnated with resin for transverse reinforcement (see Fig. 2).

### Stress-strain relationship and impregnation with resin

The properties of HP grade carbon fiber compared with those of steel are shown in Fig. 3. Tensile strength, Young's modulus, weight density, and durability are strong points for structural material, but elongation is so small. From an ideal stress-strain relationship of these two materials, it is seen that a carbon fiber has neither marked yield plateau nor hysteretic energy dissipation, which are highly expected for steel. The following attention should be paid when using carbon fibers.

- 1) Use of carbon fibers is limited to the part where the significant strength is required.
- 2) Carbon fibers subjected to concentrated stress may easily rupture since stress redistribution is not expected due to its brittle behaviour. Some techniques to reduce stress concentration should be employed.
- 3) Carbon fibers are vulnerable to sharp edges, like a knife cut, and hence some protection on the concrete surface is necessary.

One measure to reduce the stress concentration is to impregnate the carbon fiber strands or UD tape with resin. Non-impregnated carbon fiber strands are very weak but impregnated carbon fiber strands are as strong as monofilaments (see Fig. 4). We can estimate the strength of the impregnated strand as the sum strength of the monofilaments. Also, the area of the strands is assumed to be equal to the net area of carbon fiber excluding the area of epoxy resin. The area of UD tape is defined in the same manner as the impregnated strands.

### Curing of resin

The retrofit technique utilizes carbon fiber strands and tapes which provide excellent flexibility and easy handling before the impregnating resin is hardened. While carbon fibers are being impregnated with resin, carbon fiber strands or tapes are glued or wound on the concrete surfaces. Then the curing of resin on the concrete surface is started. Trying to impregnate the carbon fiber strands after gluing or winding has been found unreliable.

In ordinary airplane or sporting goods factories using carbon fibers, impregnating resin is cured at high temperatures over 100°C for more than 2 hours. In the retrofit work for existing concrete structures, however, such curing cannot be adopted at all. Therefore, the resin cured for 14 to 4 days (7 days at 20°C) under ordinary temperatures of 10 to 40°C has been developed. LTC (low temperature curing) type resin was used in this experiment.

### Strength of carbon fiber (strands) on beveled corners

When a square (rectangular) column is retrofitted by transversely winding, carbon fibers at corners may easily rupture. Therefore some pretreatments, such as rounding the concrete corners, are necessary. In order to investigate the influence of the radius R on the tensile strength of carbon fiber strands, the following tensile test was carried out.

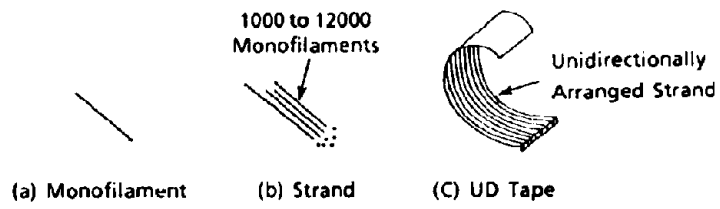


Fig 1 Carbon Fiber Products

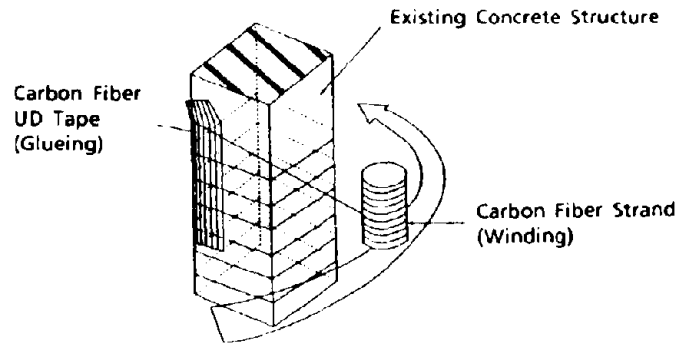


Fig 2 Retrofit Method with Carbon Fibers

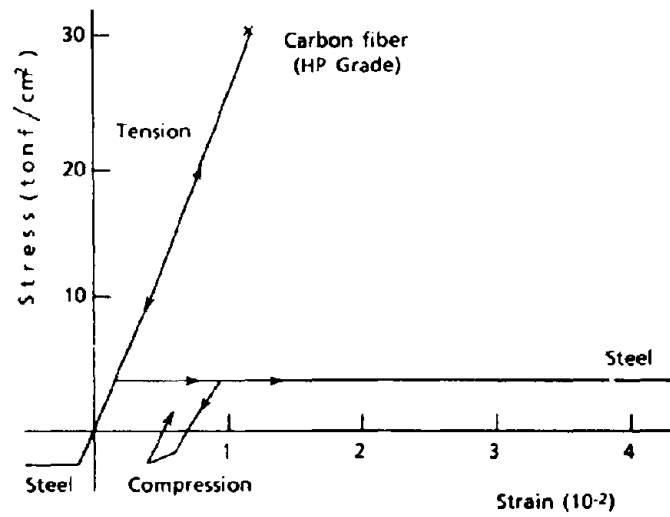


Fig.3 Stress Strain Relationship

Each test specimen, as shown in Fig. 5, consists of two end connections and two carbon fiber strands impregnated with epoxy resin in the same way as ordinary construction. The test parameters are of the same dimension and shape as the end connections.

- 1) circle pulley connection: varying the radius  $R$  ( $R = 1, 2, 3$  and  $5$  cm), and
- 2) octagonal pulley connection whose angles are sharp: corresponding to  $R = 0$

An ordinary tensile test of carbon fiber strands was also conducted by employing straight ( $R = \infty$ ) carbon fiber strands. The strength corresponding to the radius  $R = 0, 1, 2, 3, 5$  cm and  $\infty$  were therefore found.

The relationship between the radius  $R$  and tensile strength  $\sigma_{CF}$  is shown in Fig.6. The smaller radius, the lower strength; the scatter of the test results was great. On the other hand, the strength of the test specimens, with  $R = 3$  and  $5$  cm were approximately 5% less than that of ordinary specimens ( $R = \infty$ ); the scatter was also small. From these test results it is concluded that the decrease in the tensile strength of carbon fibers on corners can be ignored if the radius of the corner is 3 cm or greater.

#### Earthquake-resistant retrofitting method<sup>4)</sup>

##### Ductility oriented retrofitting

It is convenient to explain the behaviour of a structure during an earthquake by using an energy rather than a dynamic force. In order to improve the performance of structures subject to earthquakes, the increase in strength (strength oriented type retrofitting) or deformation capacity (ductility oriented retrofitting) is considered. This is done to improve the energy absorption (Fig. 7). The comparison of the strength oriented type method with the ductility oriented type method is shown in Table 1. In the case of the strength type, accessories (such as signal guide sign) are easily damaged as the response acceleration increase. Additionally the increase of weight may have effects upon the foundation. On the other hand for the ductility oriented type, the large displacement of the pier may be a problem, however, the rigidity does not increase and the increase in weight is small. Therefore, it is a feasible design option.

##### Retrofitting method

###### (1) Outline

The retrofitting methods with carbon fibers, for existing RC members, are classified into the following two types: (a) "flexural strengthening" improved shear strength by the increasing the main reinforcement by longitudinally glueing carbon fiber UD tape on the concrete surface (b) "ductility improvement" by glueing UD tape transversely (or spirally winding carbon fiber strands onto the column surface). The combination of (a) and (b) is also possible. As shown in Fig. 8, the ductility oriented type method introduced by Kobatake-Katsumata is that the pier is reinforced in order that the base becomes vulnerable because of the increase in the

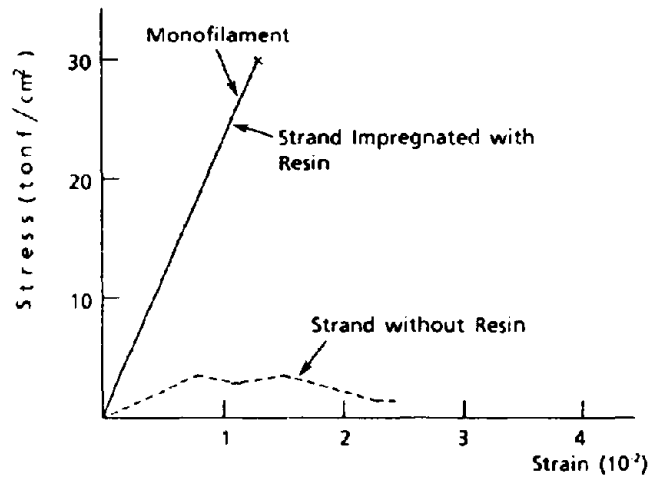


Fig.4 Impregnation Effect

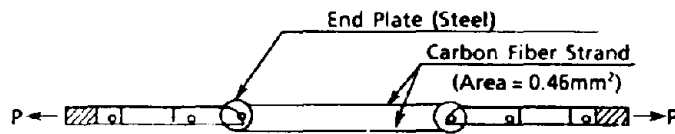


Fig 5 Test Piece for Tensile Test

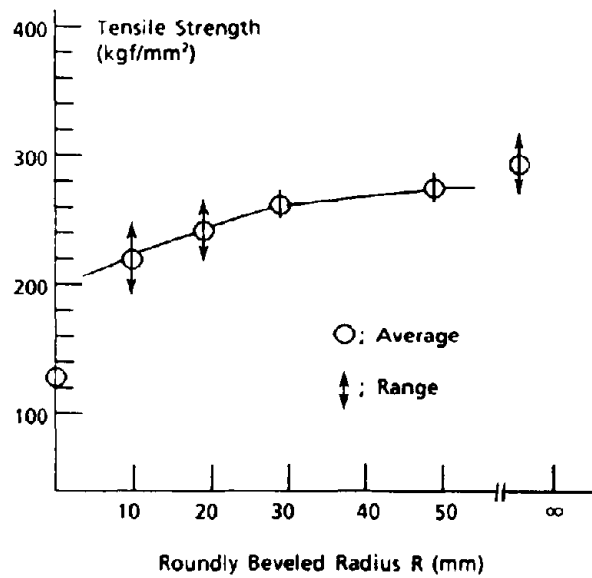


Fig 5 Influence of Beveleing on Tensile Strength

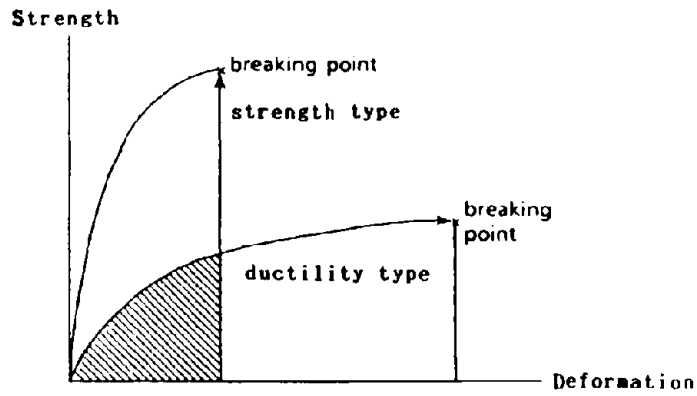


Fig.7 Strength type and ductility type

Table-1 Comparison of retrofitting method

retrofitting method	increase of weight	response deformation (response acceleration)	remarks
strength oriented type (RC encasing)	large	small (large)	difficult maintenance for accessory
ductility oriented type (retrofitting with carbon fiber)	small	large (small)	slightly large deformation

yield strength at the top and bottom of the reinforcing termination point by methods (a) and (b). Further, in the case of the small shear strength of the base, the main reinforcement at the base yields in flexure in order to improve a plastic deformation capacity (ductility performance)(method (b)). In this retrofitting method with carbon fibers, only the deformation capacity (ductility performance) can be improved considerably without increase of the induced seismic force. The retrofitting methods of (a) and (b) are described below.

## (2) Flexural strength improvement

It has already been pointed out that under an extremely severe earthquake loading, some existing piers may be damaged at the curtailment position (Fig. 9 (a)). Therefore, the curtailment points are strengthened in order to increase the lateral load resistance of the whole pier. Existing piers are improved by longitudinally glueing carbon fiber UD tape with epoxy resin on to the concrete surface. This means that increasing main reinforcement provides sufficient flexural strength. In the case of flexural strengthening, UD tape relieves the stress of the main reinforcements at termination points. This is a kind of lap joint and the carbon fibers transmit the stress through the cover of the concrete. Therefore, the complete anchoring and bonding of the carbon fibers are very important.

The flexural strength after the pasting of the UD tape can be obtained with standard bending analyses assuming plane section theory.

## (3) Ductility Improvement

In this case UD tapes are glued in an upward direction by hooping (or, strands are winded spirally). This means that the increase of hoop compression improves the shear strength by confining the concrete. In the existing piers, there are many cases where not only is the bending strength insufficient, the ductility is also small because of the small amount of hoops and shear strength. In addition to the above flexural strengthening, the ductility is improved by providing the increase of shear strength which leads to the flexural failure at the pier bottom (Fig. 9 (b)).

## Load test<sup>(a)(b)</sup>

### Outline of the experiment

#### (1) Specimen

The list of specimens is shown in Table 2. The scale of the specimen was one-third of the actual size of bridge piers (section of 1.2m x 1.8m and the height of about 8m) of the Tomei Expressway. The longitudinal reinforcement and the hoops were D16, D10 (SD30) and  $\phi$  6mm (SR30) with 200mm spacing respectively. The dimensions and bar arrangements in the specimen and the load test configuration are shown in Fig. 10 and Fig. 11 respectively. The properties of the materials used are shown in Table 3. The experimental parameters are presence, classification and area of the retrofitting of the termination of reinforcement and the quantity of shear reinforcement at the base. Further, as for shear reinforcement, both



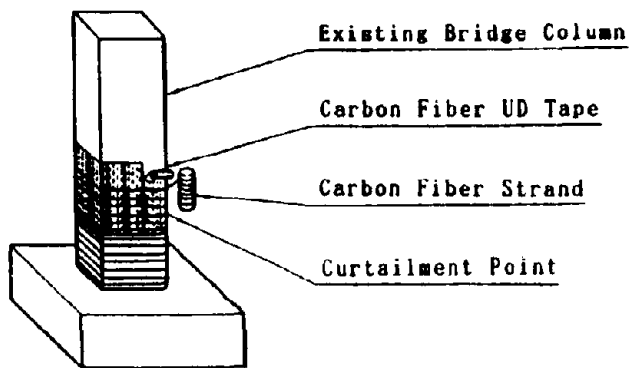


Fig-8 Retrofit Method Bridge Pier

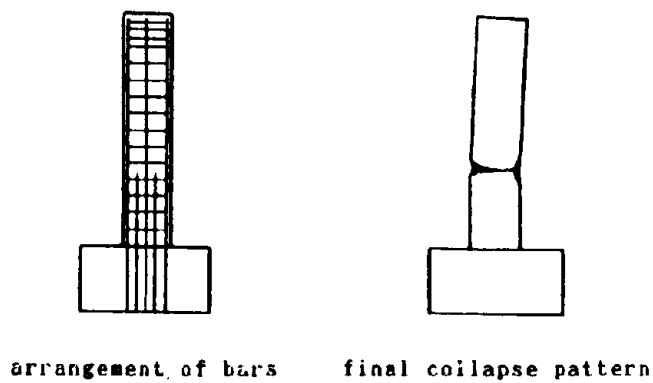


Fig-9(a) Collapse of the curtailment point of existing piers

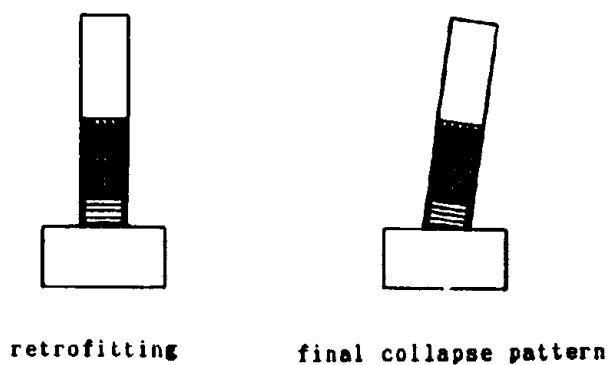


Fig-9(b) Collapse after the retrofitting with carbon fiber

**Reproduced from  
best available copy**

Table 2 List of specimens

Classification of specimens	Curtailment point	Strengthening method	Length of reinforcement
No. 1	Included	non-reinforcement	Basic specimen
No. 2	Included	Reinforcement with steel plate	Reinforced length of upper-40cm and lower-20cm of the curtailment point (t=2.3mm, SS41)
No. 3	Included	Reinforcement with carbon fibers	(Longitudinally) reinforced length of each 45cm of upper & lower of the curtailment point with two layer UD tapes  (Transversely) reinforced length of each 45cm of upper & lower of the curtailment point with two layer UD tapes
No. 4	Included	Reinforcement with carbon fibers	(Longitudinally) reinforced length of upper-30cm and lower-25cm of the curtailment point with two layer UD tapes  (Transversely) reinforced length from upper-30cm of the curtailment point to the top of the footing with strands (strand: 2.5mm spacing)
No. 5	Not Included	Reinforcement with carbon fibers	(Transversely) reinforced length of upper-60cm from the top of the footing with two layer UD tapes
No. 6	Included	Reinforcement with carbon fibers	(Transversely) reinforced length of upper-60cm from the top of the footing with strands (strand: 5.0mm spacing)

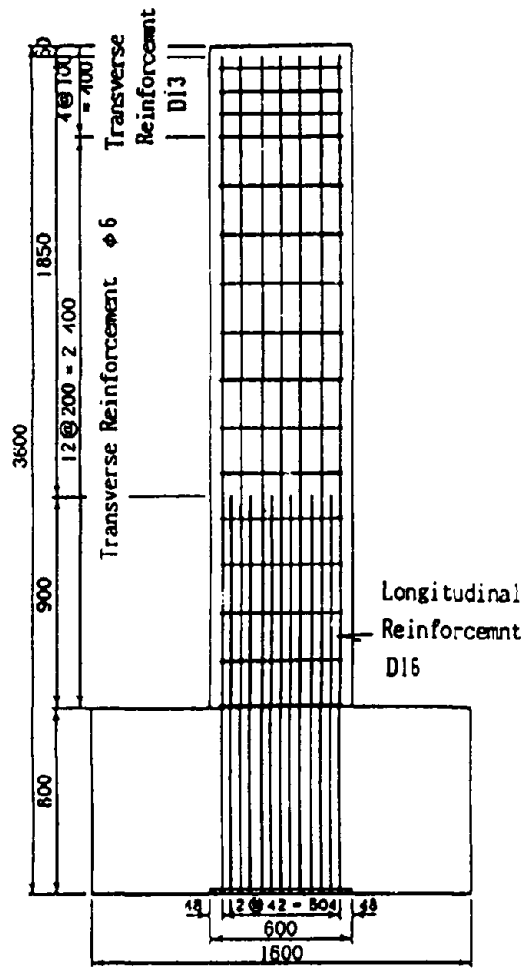


Fig. 10 Specimen of Bridge Pier

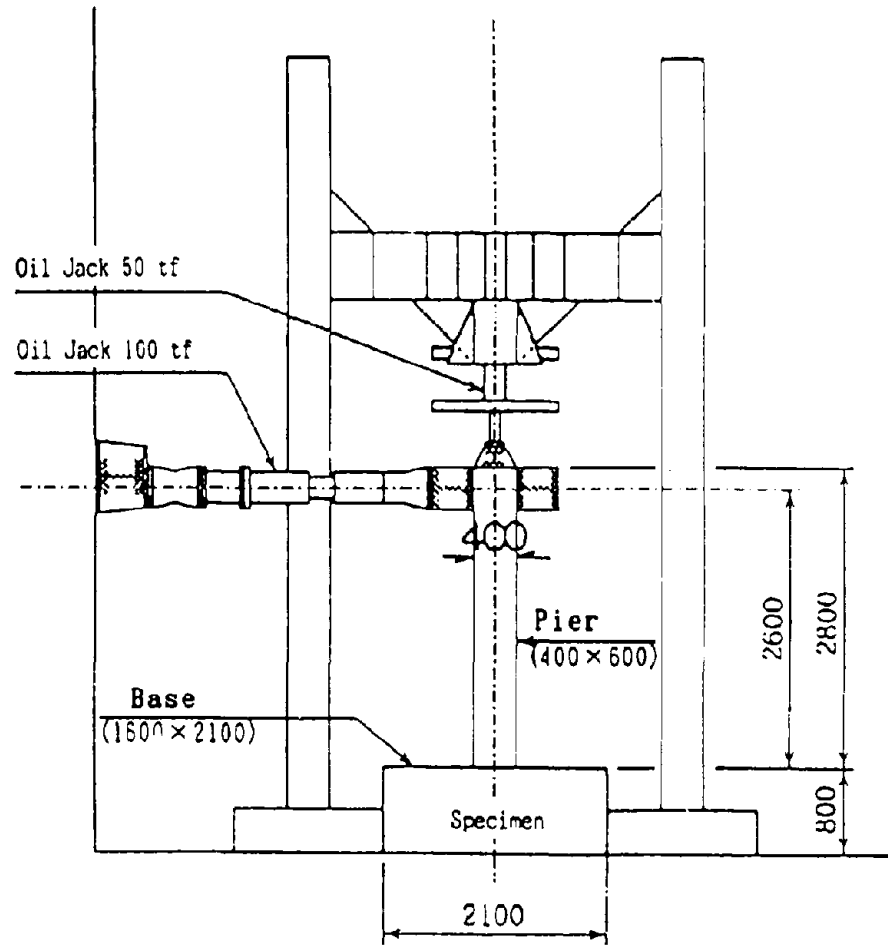


Fig. 11 Loading Apparatus

pasting and winding methods of application were compared.

Specimen No. 1 was a typical existing pier model with termination of the main reinforcement. The position of the termination was 90cm above the base and half of the longitudinal reinforcement was curtailed there.

Specimen No. 2 was encased with a steel plate sheath ( $t=2.3\text{mm}$ , SS41). The length was 1.5D (600mm). It was placed 1D (pier width in bridge axis direction: 400mm) above to 0.5D (200mm) below the termination points. These plates were connected with epoxy resin and bolts.

Specimen No. 3 was reinforced with two UD tape layers ( $175\text{g}/\text{m}^2$  per layer; total:  $350\text{g}/\text{m}^2$ ) in both longitudinal and transverse directions. The layers were glued with an epoxy adhesive agent and had the total length of 900mm which was about 1-D (450mm including additional length of 50mm) at both the upper and lower sides of the termination points.

Specimen No. 4 was reinforced with two UD tape layers in the longitudinal direction ( $175\text{g}/\text{m}^2$  per layer; total:  $350\text{g}/\text{m}^2$ ). They were glued with an epoxy adhesive agent in the total length of 550mm (300mm above and 250mm below the termination point respectively). The bottom 1200mm of the pier was provided transversely with strands (2.5mm spacing). The longitudinal reinforcing length of specimen No. 4 was smaller than that of No. 3, but the length of transverse reinforcing was over the bottom 650mm of the pier.

Specimen No. 5 had two layers of transverse UD tapes ( $175\text{g}/\text{m}^2$  per one layer, total:  $350\text{g}/\text{m}^2$ ), which were glued with epoxy resin onto the specimen. The reinforcement was not curtailed in this specimen and UD tapes extended to 600mm from the base.

Specimen No. 6 without the termination point was reinforced by strands (pitch: 5.0mm) in the area of bottom 600mm of the pier. The reinforcement quantity was one half of that of No. 5.

The difference in the repair techniques and the reinforcing effect was confirmed by specimens No. 1 to No. 3. Next, the length, quantity and method of the retrofitting with carbon fibers at the curtailment point were investigated by specimens No. 1, No. 3 and No. 4. Further, the length, quantity and method of the retrofitting with carbon fibers at the base were evaluated by specimens No. 5 and No. 6. Since quantitative data is necessary for the shear design of the base, reinforcing quantity at the base in specimen No. 5 was reduced to one half of that of No. 6.

## (2) Loading

The load was applied to the pier with the base fixed to the reaction floor. The loading hysteresis was decided depending upon the measured strain of the main reinforcement. After several loadings with the predetermined tensile stress of the reinforcement, a repeated loading regime was performed with displacement amplitude of integral multiple of the yielding displacement- $\delta y$  of the reinforcing bars ( $\delta y, 2\delta y, \dots$ ).

The details of the loading hysteresis are shown in Fig. 12. In the 1st cycle, a crack initiation load was given. At the 2nd or 3rd cycles, a

Table 3 List of the material strength

Reinforcing bars. (kg/cm <sup>2</sup> ) Yield strength (tensile strength)	D16	3770 (5480)
	D10	3760 (5350)
	ø6	3370 (4430)
Compressive strength of concrete (kgf/cm <sup>2</sup> )	Footing part	362
	Pier part	296
Carbon fiber* (kgf/cm <sup>2</sup> ) (Tensile strength)	UD tape	28000
	Strand	29100

\* Evaluated with the actual sectional area

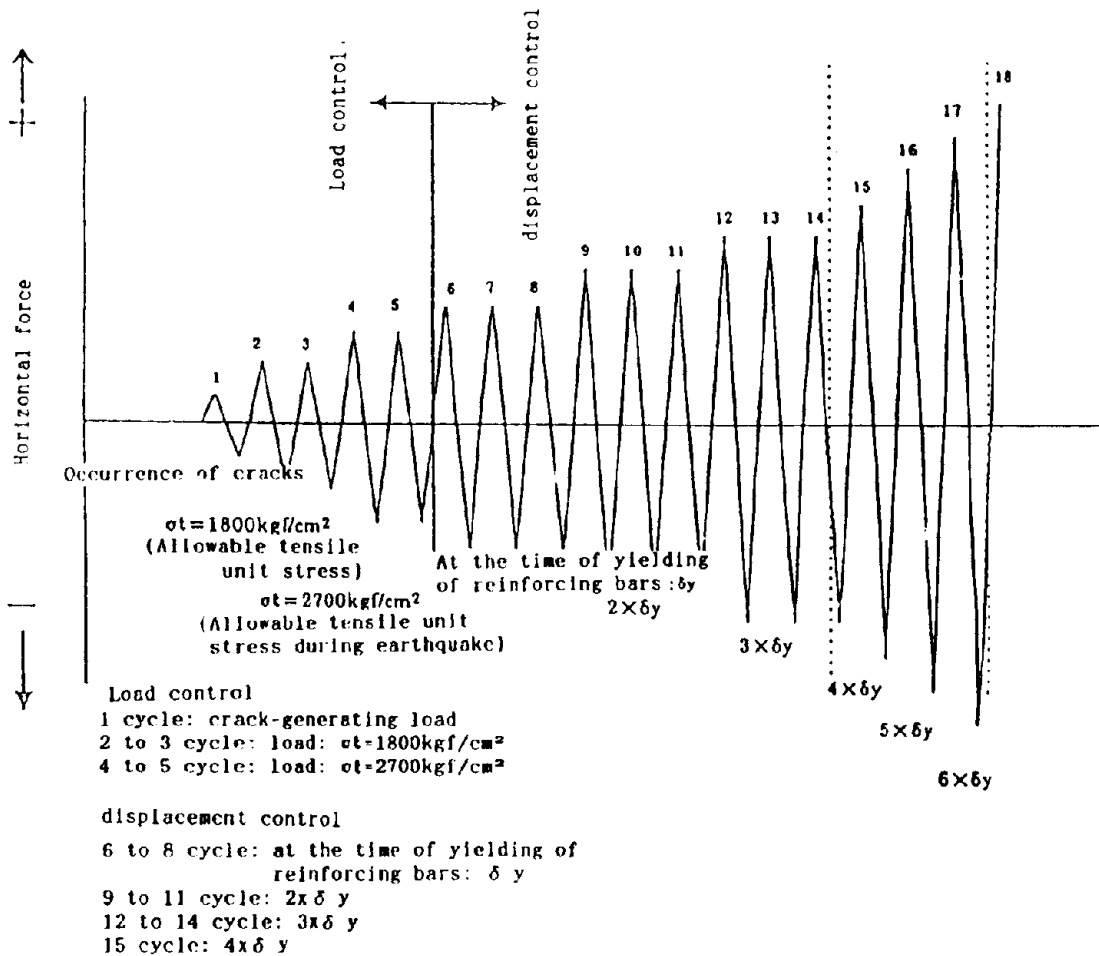


Fig. 12 Loading pattern

load corresponding to the allowable steel tensile stress ( $\sigma_s = 1800\text{kgf/cm}^2$ ) was applied. At the 4th or 5th cycles, a load corresponding to the steel tensile stress ( $\sigma_s = 2700\text{kgf/cm}^2$ ) during earthquake was applied. Cycles 6 to 8 were carried out to a reinforcement yield stress of  $\delta y$ . In addition the following loads were given respectively:  $2\delta y$  at cycles 9 to 11,  $3\delta y$  at cycles 12 to 14,  $4\delta y$  at cycle 15,  $5\delta y$  at cycle 16, and  $6\delta y$  at cycle 17. Up to cycle 5, the testing was load controlled, then the displacement control was introduced. The constant axial compression of 14.4 ton was applied in any case.

#### Experimental results

##### (1) Loading condition

The list of experimental results is shown in Table 4. Both the load-deformation relationships and cracks at the end of the experiment are shown in Fig. 13.

##### . Non-strengthened specimen (Specimen No. 1):

At  $2\delta y$  the main reinforcement above the termination point yielded, and the cracks propagated there. At  $3\delta y$ , the concrete was expanded in the horizontal direction due to buckling of the compression reinforcement above the termination point during the first cycle to this displacement, then the sustained load decreased. At the termination point, the spalling of the cover concrete and buckling of the compression main reinforcement was observed.

##### . Specimen with steel plate (Specimen No. 2):

Flexural cracks grew just below the reinforced section during the repeated loading to  $2\delta y$  and the steel plate yielded, and the sustained load decreased.

##### . Reinforced specimen with curtailment (Specimen No. 3):

Flexural-shear cracks occurred below the reinforced section during loading to  $4\delta y$ , and a part of the UD tape was damaged with the growth of the cracks. The sustained load also decreased.

##### . Reinforced specimen with curtailment (Specimen No. 4):

Since the strengthened region was reduced, the main reinforcement yielded just above the strengthened area, and the main reinforcement of the base yielded simultaneously. When the load increased up to  $4\delta y$ , the bond of the UD tape with the concrete failed and the sustained load decreased. Further, with an increase of the load, large flexural cracks occurred on the lower end of the strengthened region of the UD tape, and the expansion of the concrete around the cracks initiated at the last cycle to  $6\delta y$ . However, at the deformation up to  $7\delta y$ , the reduction of the sustained load was rather small. The carbon fibers failed only at the part of the strands.

Table 4 Experimental results

Classification of specimen	Cracking load (tf)		Yielding load (tf)		Maximum load (tf)	
	Load (tf)	Displacement (mm)	Load (tf)	Displacement (mm)	Load (tf)	Displacement (mm)
No. 1	2.8	2.1	10.4	20.6	11.5	61.7
No. 2	3.0	2.1	12.0	24.4	13.2	53.4
No. 3	2.5	1.9	12.4	26.0	13.9	55.3
No. 4	2.5	1.9	12.7	27.3	13.7	53.7
No. 5	2.3	1.8	11.9	22.0	15.5	244.2
No. 6	2.5	1.9	13.2	28.3	13.9	52.1

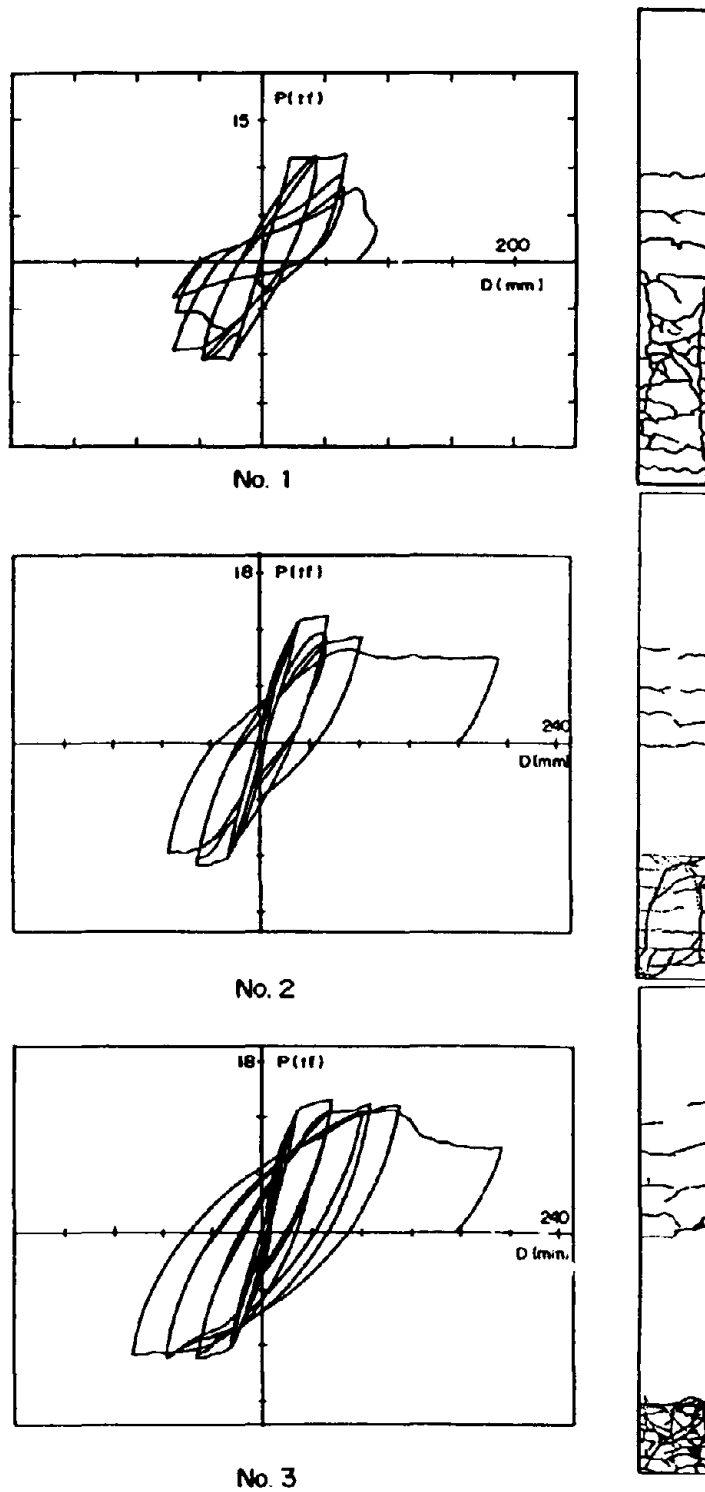


Fig.13(a) Load-deformation relationship and cracks at the end of the experiment



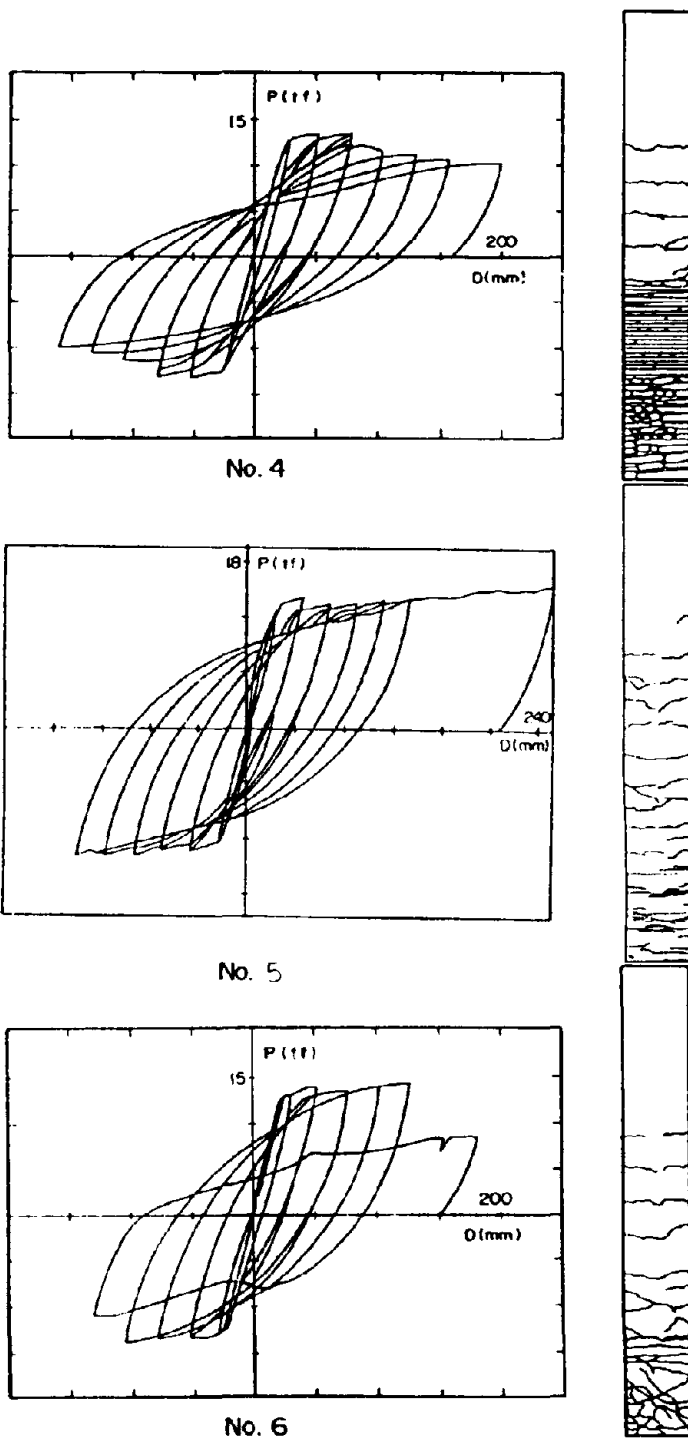


Fig.13(b) Load-deformation relationship and cracks at the end of the experiment

. Specimen with reinforced base (Specimen No. 5):

Specimen No. 5 sustained the load up to  $11\delta$  y (the maximum capacity of the loading apparatus). Though the concrete of the base of the piers was subject to local damage, the concrete covered with the UD tape did not fail.

. Specimen with reinforced base (Specimen No. 6):

The main reinforcement yielded at the base, and the cover concrete began to swell due to the buckling of the compression reinforcement of the base at the descent load cycle to  $5\delta$  y. The behaviour was different from that of specimen No. 6 where the carbon fiber strands of the swelled part failed, and simultaneously the sustained load decreased. With further loading, most of the carbon fiber strands in the distance of  $D$  from the base failed.

(2) Curvature ratio

Specimen No. 1 had the maximum curvature ratio at the base during the loading of  $1\delta$  y, while the curvature at the termination point was maximum after the loading of  $2\delta$  y.

In specimen No. 2 the curvature of the reinforced area was minimum up to the load of  $2\delta$  y. However, later the curvature just below the reinforced area was maximum at the load of  $3\delta$  y.

In specimen No. 3, it was found that the curvature changed on the lower side of the reinforced area after  $2\delta$  y. After  $4\delta$  y, this behaviour became remarkable, and then failure was observed.

When specimen No. 4 is compared with specimen No. 1, it is found that the curvature of specimen No. 4 is smaller than that of specimen No. 1 probably because the termination point of specimen No. 4 was reinforced. However, just below (300 to 500mm high) the reinforced area with UD tape, the curvature of specimen No. 4 was larger than that of No. 1 specimen. The curvature of specimen No. 4 at the base was larger than that of specimen No. 1. And, the curvature at the area higher than 139cm was almost zero. This means that a rigid behavior was predominant.

Specimen No. 5 showed the maximum curvature around the base.

Specimen No. 6 showed a fairly large curvature at the base. In the final cycle, curvature increased rapidly in between the height of 500 and 700mm, probably because the failure of carbon fibers lost the confining pressure and then the curvature increased. Except for the final load cycle, the curvature decreased with an increase in the height. And, at the area with a height of 700mm, the curvature was almost zero. This means that a rigid behavior was predominant.

### Concluding remarks

Through the experiments on the scaled models for piers with or without carbon fibers, the following conclusions can be drawn.

- 1) Due to the application of the UD tape in the vertical direction for the reinforcement at the termination point, the flexural strength increased, and the failure of the piers was moved from the position of termination of reinforcement to the base.
- 2) Since the concrete and the main reinforcement are confined by applying UD tape transversely (or winding of carbon fiber strands) at the reinforcement of the bases, a sufficient ductility may be obtained.
- 3) The general evaluation on the experimental results shows that the carbon fibers for existing RC piers with a small change in rigidity provides the effective earthquake resistance.
- 4) There are only minor differences between the winding method with carbon fiber strands and the pasting method transversely with carbon fiber UD tape as the shear reinforcement in the transverse direction.
- 5) Experiments are continuing to evaluate the effect of carbon fibers in the repair of RC piers quantitatively.

### References

- 1) H. KATSUMATA, Y. KOBATAKE, etc. [A STUDY ON THE STRENGTHENING WITH CARBON FIBER FOR EARTHQUAKE-RESISTANT CAPACITY OF EXISTING REINFORCED CONCRETE COLUMNS]  
Workshop on Repair and Retrofit of Existing Structures, U.S.-Japan Panel on Wind and Seismic Effects, UJNR, Tsukuba, Ibaraki, Japan, May 8-9, 1987.
- 2) H. KATSUMATA, Y. KOBATAKE, etc. [A STUDY ON STRENGTHENING WITH CARBON FIBER FOR EARTHQUAKE-RESISTANT CAPACITY OF EXISTING REINFORCED CONCRETE COLUMNS]  
Proceedings of the Ninth World Conference on Earthquake Engineering, August 2-9, 1988, Tokyo-Kyoto, Japan (Vol. VII)
- 3) H. KATSUMATA, K. KIMURA, etc. [APPLICATIONS OF RETROFIT METHOD WITH CARBON FIBER FOR EXISTING REINFORCED CONCRETE STRUCTURES]  
THE 22nd JOINT UJNR PANEL MEETING, on Repair and Retrofit of Existing Structures, U.S.-Japan Workshop, Gaithersburg, MD., May 12-14, 1990.
- 4) Y. KOBATAKE, H. KATSUMATA, etc. [ANTISEISMIC RETROFITTING WITH CARBON FIBER FOR EXISTING RC PIERS] (part-1: Reinforcing method)  
45th annual lecture meeting of the Japan Society of Civil Engineers.
- 5) TAKUWA, HIGASHIDA, etc. [RETROFITTING EFFECTS OF EXISTING RC COLUMNS]  
45th annual lecture meeting of the Japan Society of Civil Engineers.
- 6) ISHIDA, OKAJIMA, etc. [ANTISEISMIC RETROFITTING WITH CARBON FIBER FOR EXISTING RC PIERS] (part-2: load test)  
45th annual lecture meeting of the Japan Society of Civil Engineers.

# **S e s s i o n 6**

## **R e s e a r c h o n S e i s m i c R e t r o f i t t i n g a n d S t r e n g t h e n i n g**

- 1) Failure Criteria of Original and Repaired RC Members with Hybrid Experiments  
(H.Iemura, K.Izuno and Y.Yamada)
- 2) Formulation of Ductility of R/C Members and Influence of Ductility on Response of Behavior in R/C Frame Structures  
(H.Mutsuyoshi and A.Machida)
- 3) Repair and Retrofit of Steel Piers  
(G.A.Macrae, K.Kawashima and K.Hasegawa)

## FAILURE CRITERIA OF ORIGINAL AND REPAIRED RC MEMBERS WITH HYBRID EXPERIMENTS

H. Iemura (I)  
K. Izuno (II)  
Y. Yamada (III)

### SUMMARY

Using experimental simulation of the inelastic restoring force properties by HYLSEER (Hybrid Loading System of Earthquake Response), seismic behavior and failure criteria of original and repaired reinforced concrete (RC) members are investigated. This paper presents effect of different repair techniques on the stiffness - deteriorating process and energy - absorbing capacity. Results show that the stiffness deterioration of the repaired specimens resembled that of the unrepaired originals when suitable repair methods were used. Energy - absorbing capabilities also were regained for adequately repaired specimens. Seismic risk of unrepaired specimens with minor cracks was also evaluated using the damage index.

### INTRODUCTION

Some structures that were rendered nonfunctional by earthquakes could be reused after repair and/or strengthening of the damaged parts. The use of epoxy resin in repairing RC members has been found to be applicable and effective (Ref. 1). The important thing to determine is how such repaired structures will respond during future earthquakes. Current analytical models cannot account for the additional material inhomogeneity introduced by repair materials to the already complex RC section. Hybrid experiments provide a very effective, powerful techniques with which to investigate the earthquake responses of such complicated materials as RC members and soils (Refs. 2, 3, 4, 5).

A description of HYLSEER (Hybrid Loading System of Earthquake Response) used to analyze repaired RC members under varying bending loads and constant axial force, and an analysis of the stiffness deterioration process for these members during earthquakes are given. A comparison of the energy - absorbing capability of the original and repaired members also is made.

### HYBRID LOADING SYSTEM OF EARTHQUAKE RESPONSE (HYLSEER)

#### Test Pieces

Eleven specimens were used, all having the dimensions  $100 \times 150 \times 1900$  mm (Fig. 1) and a distance between supports of 1500 mm. Two specimens were doubly reinforced by deformed bars D16 (steel ratio  $p = 3.1\%$ ), whereas the rest were doubly reinforced by D10 bars ( $p = 1.1\%$ ). Concrete was confined by providing stirrups (6 mm in diameter) every 70 mm. Mechanical properties of the concrete and reinforcing bars are shown

- 
- (I) Associate Professor, Dept. of Civil Engineering, Kyoto University, Japan  
(II) Research Associate, Dept. of Civil Engineering, Kyoto University, Japan  
(III) Professor, Dept. of Civil Engineering, Kyoto University, Japan

in Tables 1 and 2.

### HYLSER System

A hybrid loading system of earthquake response, called HYLSEER (Fig. 2), was used to test specimens modeled as a single - degree - of - freedom system (Fig. 3). A microcomputer was used to solve the equation of motion in order to obtain the deformation at the next time step.

$$m\ddot{x}(t) + c\dot{x}(t) + F(x(t)) = -m\ddot{z}(t) \quad (1)$$

in which,  $m$  is the mass;  $x(t)$  the relative displacement at time  $t$ ,  $c$  the damping constant,  $F(x(t))$  the hysteretic restoring force at time  $t$ ,  $\ddot{z}$  the ground acceleration; and a dot ( $\dot{\phantom{x}}$ ) indicates the time derivative.

Dividing Eq. (1) by  $m$  leads to

$$\ddot{x}(t) + \frac{c}{m}\dot{x}(t) + \frac{F(x(t))}{m} = -\ddot{z}(t) \quad (2)$$

Considering the initial condition, the third term of Eq. (2) becomes

$$\frac{F(x(0))}{m} = \omega^2 \quad (3)$$

in which,  $\omega$  is the initial natural angular frequency.  $\omega$  is calculated from

$$\omega = \frac{2\pi}{T} \quad (4)$$

in which,  $T$  is the initial natural period of the modeled structure (Fig. 3). Using Eqs.(3) and (4), corresponding mass used in the experiments for a given structure is determined from

$$m = \frac{F(x(0))}{\omega^2} = \frac{F(x(0))}{4\pi^2} T^2 \quad (5)$$

In addition, the second term of Eq.(2) can be calculated with known relation of

$$\frac{c}{m} = 2h\omega \quad (6)$$

in which,  $h$  is the damping ratio. We assumed  $T=0.5$  sec and  $h=0.02$  for all cases.

Both the linear acceleration and central differential methods were used for the step - by - step integration. In solving Eq. (1),  $F(x(t))$  could be estimated directly from the on - line experiment. The actuator controls the midspan of the specimen using the computed displacement  $x(t)$  sent through a DA (digital to analog) converter. In return, the computer gets the measured restoring force  $F(x(t))$  from the actuator received through an AD (analog to digital) converter. The flowchart for this on - line procedure is given in Fig. 4.

The axial force - generating mechanism, in which a constant axial force is sustained by high - pressure oil built up by pressurizing air is shown in Fig. 5. The three values of the axial load used ( $N = 4.0$  tonf [39 kN], 2.0 tonf [20 kN] and 2.7 tonf [27 kN]) reflect values for real bridge piers based on Ref. 6.

The NS - components of the El Centro record (1940 Imperial Valley earthquake, U.S.A.) and the Hachinohe record (1968 Tokachi - Oki earthquake, Japan) were the input earthquake excitations used. 30 seconds of these records were used. They were set to have the maximum values in the range of 100 to 300 gal

(cm/sec<sup>2</sup>). During the experiment the specimens were pseudo-dynamically tested over a period about 80 times longer in order to observe detail of the response. The schedule of loadings for the entire experiment is shown in Table 3.

## REPAIRING

Three repair methods were used as follows.

### Type I: The Epoxy Resin Grouting Method

Most of the test pieces were repaired by this method. First, mixed epoxy resin and sand were put on the heavily damaged parts, then, setting pipes were attached to the cracks, and sealed with epoxy bond. After that, epoxy resin was grouted into the cracks using the BICS (Balloon Injector for Concrete Structures, Ref. 7) at a low pressure of about 3 kgf/cm<sup>2</sup> (0.3 MN/m<sup>2</sup>). The BICS is diagrammed in Fig. 6.

### Type II: The Reinforcing Bar Welding Method

Two specimens, in which the reinforcing bars had buckled, were repaired by this method. First the axial force was unloaded, and the concrete around the damaged bars removed. The same type of steel as in the damaged bars (two times the length of the buckled segment) was welded to the reinforcing bar, after which the segment was repaired with a mixture of epoxy resin and sand. Epoxy resin was grouted into the cracks by the BICS device used for Type I repair.

### Type III: The Steel Plate Covering Method

Three specimens were repaired by this method. The damaged segment (Fig. 7 - a) was filled with mixture of epoxy resin and sand (Fig. 7 - b), after which steel plates were bonded to the damaged part with epoxy resin (Fig. 7 - c). Epoxy resin then was grouted into the cracks by the technique used for Type I.

The steel plates used were the same length as the damaged segment of concrete for specimen 5, but twice the length of the damaged segment for specimens 1 and 10. The thickness of the steel plate used was computed as having the same moment of inertia as the original reinforcing bars; that is, the moment of inertia of the specimen was restored to the original value by the steel plates used, assuming that the damaged reinforcing bars were totally incapacitated.

This method is much easier to use than the Type II method in that no unloading of the axial force nor removal of the concrete around the damaged part is necessary. Nevertheless, careful attention must be paid to how the steel plates are bonded to the damaged segment.

## EXPERIMENTAL RESULTS

### Original Specimens

- Data for the original specimens were taken from a previous study (Ref. 8), for which the main results were:
- (1) a high axial force resulted in a higher yielding level and lower ductility of the specimens.
  - (2) the stiffness of the specimens with higher reinforcement ratios (specimens 10 and 11) was 50% more than that of the others, but the yielding loads were 100% more.
  - (3) when a high axial force was acting, a specimen failed with just one large plastic deformation.

### Type I Repair (The Epoxy Resin Grouting Method)

The hysteresis loops shown in Fig. 8 are for three similar specimens subjected to different input levels of

acceleration. Note that the original maximum values for the restoring force were reached even after repair. In tests without axial force (Ref. 8), damage took place not to the repaired segment but adjacent to it. In tests made under axial force, cracking and crushing of the concrete appeared midspan in the test pieces. This is because damage to the reinforcing bars at the center was severe.

For a maximum acceleration of 300 gal (Fig. 8 - c), the maximum restoring force was almost the same as before repairs were made; but, reduced ductility caused early crushing of the repaired specimen. For specimens in which the reinforcing bars are badly buckled, repair by this method does not restore the original high strength under dynamic loads; therefore, Type I repair should be used with caution.

The center of each hysteretic cycle for the repaired specimens drifts much more than originals. Though the repaired specimens behave stable for a low input motion, they show a big displacement response for a strong impulsive input. As the repaired specimen consists of concrete, steel and randomly varied epoxy resin, complex material caused this unstable response.

#### Cross Sectional Views of the Type I Repaired Specimen

The damaged specimen 8 after the loading test was cut into several pieces using a diamond cutter to see the cross sections precisely. Figure 9 shows the places at which the specimen was cut, and Fig. 10 shows the cross sectional views of the specimen. The solid lines are cracks of the first loading test filled with epoxy resin, the dotted lines are new cracks of the second loading test, and the shadowed areas are epoxy mortar used to repair the broken unconfirmed segment. The loading direction was vertical in this figure. The following things were observed:

- (1) Epoxy resin was filled even in the cracks of 0.1 mm wide. Accordingly, it was verified that repair work has been successfully done.
- (2) The cracks of the second loading test were much less than those of the first loading test. And they did not appear in the same region of the first loading, nor the unconfined concrete did not fall as before. These were caused by the higher tensile strength of the repaired specimen with the grouted epoxy resin.
- (3) The cracks of the second loading were totally wider than those of the first loading. As the cracks were less than before, deformation might be concentrated to those cracks.

#### Type II Repair (The Reinforcing Bar Welding Method)

The hysteretic loops before and after repair of specimens are shown in Fig. 11. After repair, the specimen was stronger in one direction than in the other. This was because the two repaired reinforcing bars were located on one side of the specimen.

#### Second Loading without Repair

In a previous study (Ref. 8), we found that specimens with minor cracks could be adequately repaired with epoxy resin. In the study reported here, strong acceleration also was applied to unrepaired specimens to obtain heavily damaged specimens and to observe the destruction process. All the test pieces were damaged at their midspans. Two of them (specimens 1 and 5) collapsed, but the specimen with the high reinforcement ratio (specimen 10) was not completely crushed. After the first large deformation, however, the specimen simply folded and never again straightened.

Large deformations were present after only a few cycles (Figs. 12 - b, 13 - b). This means that all the specimens were severely damaged after the first loading tests. As the yielding accelerations of the reinforcing bars were estimated to be 90-120 gal (Ref. 8), these bars might already have yielded after the first loading tests.



### Type III Repair (The Steel Plate Covering Method)

A comparison of Fig. 12 - a and c, and of Fig. 13 - a and c, shows an increase in the restoring - force capacities of the repaired specimens. Two causes can be cited: In calculating the thickness of the steel plate, the old reinforcing bars were assumed to be totally ineffective; whereas, in reality, these may have retained some resistances. Also, as the location of the plastic hinge moved from the center to the edge of the steel plate, a larger force was needed to bend the specimens.

After the third loading, strong accelerations again was applied to the repaired specimens (Type III), without any further repair, to observe their behavior in an extreme state. The hysteretic loops shown in Figs. 12 - d and 13 - d, specimen 5 whose steel plate was as long as its damaged part, was severely mangled, the concrete being crushed at the edge of the steel plate under compression. In contrast, the other specimens, whose steel plates were twice the length of their damaged parts, did not suffer great damage. The steel plates came away from these specimens at midlength, and many cracks developed in the concrete in the vicinity of their midspans. The hysteretic loops for these specimens also were stable; accordingly, the length of the steel plate to be used in repairs must be carefully considered. In addition, further study is needed to determine the adequate thickness of the steel plates.

## STIFFNESS DETERIORATION PROCESS

### Suitable Index for Stiffness Deterioration

There are many definitions of equivalent stiffness. For example, the slope between the origin and the point of maximum restoring force is the well known definition for the equivalent stiffness. But this equivalent stiffness underestimates the stiffness when the center of the hysteresis loops goes away from the origin (Ref. 5). For this reason, we looked for other definitions of stiffness to obtain a parameter for describing the stiffness deteriorating process. We considered two definitions as shown graphically in Fig. 14.

The "equivalent stiffness",  $K_{EQ}$ , is defined as the slope between the midpoint of two zero points of restoring forces and the point of maximum restoring force in a half cycle. Taking into account the half cycle of the hysteresis loop, from time  $t_1$  to  $t_2$ ,  $K_{EQ}$  can be written

$$K_{EQ} = \frac{F(x(t_2))}{x(t_2) - \frac{x(t_1) + x(t_1)}{2}} \quad (7)$$

in which,  $t_1$  is the time when the loop crosses the x - axis,  $F(x(t_1))=0$ ,  $t_2$  the time when the restoring force has its maximum value; and  $t_3$  the time when the restoring force again is zero,  $F(x(t_3))=0$ . In contrast, the "unloading stiffness",  $K_U$ , is defined as the slope between the starting and end points of the unloading process.

$$K_U = \frac{F(x(t_2))}{x(t_2) - x(t_3)} \quad (8)$$

in which,  $t_2$  is the time when unloading begins. These two stiffnesses were compared for all the tested specimens in order to obtain an adequate description of the stiffness deterioration process.

The stiffness deterioration process for specimen 6 in terms of the two defined stiffnesses is shown in Fig. 15. At about 2 seconds, both stiffnesses begin to deteriorate, after which the equivalent stiffness,  $K_{EQ}$ , increases somewhat, whereas the unloading stiffness,  $K_U$ , remains almost constant. A similar comparison (Fig. 16) was made for specimen 5, on which a second loading was imposed without repairing the damage sustained during the initial loading. About 2 seconds into the second loading test (32 seconds after initiation of the test), the specimen collapsed. Interestingly, at the start of the 2nd loading,  $K_{EQ}$  regained its initial undeteriorated

stiffness value. Also  $K_{i0}$  became exceedingly small when deformation was large, resulting in an abrupt drop in the computed  $K_{i0}$  value. For these two reasons, the stiffness deterioration process cannot be properly described by equivalent stiffness ( $K_{i0}$ ).

Although the unloading stiffness ( $K_i$ ) also varied, its trend was as expected for a degrading system. The  $K_i$  stiffness therefore is considered an adequate index of the stiffness deterioration process.

#### Stiffness Deterioration Process in Repaired Specimens

Three time histories of the  $K_i$  unloading stiffness are shown in Fig. 17.  $K_i$  began to decrease (initially markedly) when the specimen was undergoing severe deformation. This was about 2 seconds after the beginning of loading when the El Centro record was the input used (Fig. 17 - b, c), and after about 8 seconds for the Hachinohe record (Fig. 17 - a).  $K_i$  took almost constant value after the maximum response of the specimen. Both processes would have been similar if the input earthquake motions had been the same. In general, we conclude that the characteristics of the input earthquake are the dominant factors in stiffness deterioration; the characteristics of the specimens have little effect on it.

The final deterioration ratios shown in Table 4 are defined as the ratio of the  $K_i$  unloading stiffness at the end of the test to the  $K_i$  at the beginning; smaller values represent greater deterioration. For all the specimens, except No. 1, the deterioration ratios of the repaired specimens are larger than those of the unrepaired specimens.

The initial stiffnesses of the specimens repaired by the epoxy resin grouting method (Type I) are about 80% those of the unrepaired originals. For the originals, the deterioration ratio is proportional to the strength of the input acceleration; whereas, there is no correlation for the repaired specimens (see Figs. 15 - a, 17 - b and Table 4). Possibly, the difference in the amount of epoxy resin used in relation to the degree of damage may have produced the variations in the characteristics of the repaired test pieces.

The deterioration ratios of specimens repaired by the reinforcing bar welding method (Type II) and the steel plate covering method (Type III) are larger than the original ratios, particularly for Type II specimens which are much larger (Fig. 17 - c and Table 4). During the experiment, we observed that deformations of repaired specimens were smaller than those of the unrepaired originals. The initial stiffnesses of specimens repaired by the Types II and III methods are about 100 to 110% those of the unrepaired specimens.

### ENERGY DISSIPATION

Energy - absorbing capabilities should be taken account when investigating damage to specimens. Energy partitioning is calculated from the following equation derived from the equation of motion, Eq.(1):

$$m \int_0^t \ddot{x} \dot{x} dt + c \int_0^t \dot{x}^2 dt + \int_{x_0}^{x_t} F(x) dx = -m \int_0^t \dot{x} \ddot{x} dt \quad (9)$$

The first term on the left side of Eq.(9) represents the kinetic energy,  $W_k$ , of a specimen at time  $t$ , the second the absorbed viscous damping energy,  $W_v$ , and the third the absorbed hysteretic energy,  $W_h$ . The right side of Eq.(9) represents the energy imported,  $E$ , by earthquake motion. The absorbed hysteretic energy,  $W_h$ , is a major factor in the structural damage produced by cyclic loadings. It is calculated as being the area enclosed by the hysteresis loops. Each term of Eq.(9) per a half cycle of the hysteresis loop is calculated step by step for all the tested specimens.

The difference between the hysteretic energy dissipation of the original specimens and that of the repaired specimens can be estimated. First, the ratios of  $W_h$  and  $W_k$  during earthquake response are compared.

There is little difference between the energy participation of the original specimens and that of the repaired material, except when the input acceleration is not strong (Fig. 18 - a). The ratio of the damping energy,  $W_d$ , for the repaired specimen is considerably larger and the participation of the hysteretic energy,  $W_h$ , less than that of the original. This is because the elastic range of the RC members was wider after repair. When the input is low, specimens behave like elastic members.

As the input earthquake becomes stronger, the difference between the energy participation ratio of the repaired members and that of the originals decreases, (Fig. 18 - b and c) For instance, there is no difference when the input acceleration was the El Centro record with maximum values set at 200 and 250 gal. This means that the same maximum deformation is to be expected from the same degree of earthquake motion even after repair.

The ratio of the hysteretic energy ( $W_{hr}$ ) dissipated during one experiment to the total input energy ( $E_i$ ) is plotted in Fig. 19. The broken line shows  $W_{hr} = E_i$ . The solid line is derived from the least square fit of a straight line:

$$W_{hr} = a E_i - b \quad (10)$$

in which,  $a = 0.68$ ,  $b = 3.4$ . The ratio of  $W_{hr}$  to  $E_i$  is derived from Eq.(10) when  $W_{hr}, E_i > 0$ :

$$\frac{W_{hr}}{E_i} = \begin{cases} 0 & (0 < E_i \leq 5) \\ a - \frac{b}{E_i} & (E_i > 5) \end{cases} \quad (11)$$

The total absorbed hysteretic energy is in proportion to the total input energy. For a low input excitation of  $E_i \leq 5 \text{ tonf}\cdot\text{cm}$  ( $0.5 \text{ kN}\cdot\text{m}$ ), the total  $E_i$  input energy changes to  $W_d$  and  $W_k$ ; i.e.,  $W_{hr} = 0$ . As the input earthquake becomes stronger, the contribution of  $W_h$  increases, and for a large input excitation, the ratio of  $W_{hr}$  to  $E_i$  is almost constant. Let  $E_i$  in Eq.(11) be infinity, then the ratio of  $W_{hr}$  to  $E_i$  becomes  $a = 0.68$ .

Fig. 19 shows that the ratio of  $W_{hr}$  to  $E_i$  is not affected by any difference in the specimens or the input acceleration, except for a low range of  $E_i$ , as discussed before (Fig. 18). Because a constant damping ratio of  $h = 0.02$  was assumed for all cases, no effect of the damping ratio need be considered.

#### SEISMIC RISK OF UNREPAIRED DAMAGED MEMBERS

The damaged members could be left unrepaired after an earthquake if damage is not so serious. The response, however, for the next earthquake is quite different compared with a new specimen. This section discusses effect of the unrepaired damage to the future seismic response using the damage index. Park, Ang and Wen (Ref. 9) proposed the damage index as a following equation to measure seismic damage of RC structures.

$$D = \frac{\delta_w}{\delta_u} + \frac{\beta}{Q_y \delta_u} \int dE \quad (12)$$

in which,  $D$  is the damage index;  $\delta_w$  the maximum displacement response;  $\delta_u$  the ultimate deformation capacity;  $Q_y$  the yield capacity;  $dE$  the dissipated energy increment;  $\beta$  a constant for the strength deterioration per cycle.  $\beta$  was set to 0.25 according to Ref. 9. The damage index takes values between 0 and 1, where 1 expresses collapse. The first term of Eq. (12) represents damage suffered by the maximum deflection, and the second term represents damage due to the energy - absorbing procedure discussed in the previous section.

Fig. 20 shows the damage indices - time histories of the specimens. To see effect of unrepaired damage for the future response, specimens 1 and 7 were compared in Fig. 20 - a, an input acceleration for the second loading of specimen 1 and for the first loading of specimen 7 were the same. For the same reason, Fig. 20 - b compares specimens 2 and 6. The damage indices,  $D$ , became larger than 1 in all cases of Fig. 20; it signifies

collapse of the specimens which corresponds to the experimental results.

$D$  of specimen 6 became 1 at 13 seconds from the beginning of the experiment (a broken line in Fig. 20-b), and it increased little to the last value of 1.1.  $D$  of specimen 2, to the contrary, took 1 at only 2 seconds from the beginning of the second loading test, which is shown in a solid line of Fig. 20-b. For specimens 1 and 7 shown in Fig. 20-a, their damage indices reached 1 simultaneously, but they behave quite different after that.  $D$  of specimen 1 increased rapidly and the specimen collapsed while  $D$  of specimen 7 stays 1.7. The damage index,  $D$ , showed effect of unrepaired damage to the future seismic behavior numerically.

The values of the first term and the second term of Eq. (12) are also plotted in Fig. 20. The first term increases when the input acceleration becomes large; at 2 second for El Centro record and at 10 second for Hachinohe record. After that, it keeps the same value during a response. The second term keeps on increasing throughout a response. As the input earthquake motions were strong and short, the effect of the first term to  $D$  was high, which shows damage resulting from the large deflection was major.

## CONCLUSIONS

The stiffness-deteriorating and energy-absorbing processes of repaired RC members were studied. The main results are as follows.

1. Specimens repaired by the epoxy resin grouting method showed similar dynamic behavior if their reinforcing bars had not buckled.
2. Specimens repaired by the reinforcing bar welding method showed asymmetric hysteresis loops when only one side had been repaired.
3. Specimens repaired by the steel plate covering method could bear more load than the unrepaired originals when the thickness of the steel plates had been selected as having the same moment of inertia as the original reinforcing bars.
4. Stiffness deterioration can be estimated from the unloading stiffness,  $K_{l-}$ .
5. The characteristics of the input accelerogram, not those of the specimens, are the major factors operating in stiffness deterioration.
6. Stiffness deterioration in repaired specimens depends on the method of repair. The process in a specimen repaired by the epoxy resin grouting method is similar to that of the unrepaired original; whereas, the stiffness of specimens repaired by the reinforcing bar welding and steel plate covering methods deteriorated only 50% in comparison to values for unrepaired specimens.
7. The ratios of the initial stiffnesses of the repaired specimens to those of the unrepaired originals were about 80% for the epoxy resin grouting method and about 100-110% for the reinforcing bar welding and steel plate covering methods.
8. The ratio of the hysteretic energy dissipated during one loading to the total input energy was an almost constant 70% when the constant damping ratio was used and the input earthquake was strong enough to produce inelastic deformation.
9. The damage index-time histories verified that the seismic risk of unrepaired specimens with minor cracks were much higher than new specimens.

## ACKNOWLEDGMENTS

We thank Mr. Y. Mizumoto of the Hanshin Highway Public Corporation for his encouragement and aid. We also are grateful to Mr. M. Shigeyoshi, Mr. K. Domon and Mr. K. Aoki of Sho-Bond Co., Ltd. for their

help with our experiments. In addition, thanks are owed to Mr. S. Nakanishi, Mr. T. Shikata, Mr. O. Ohmoto, Mr. K. Hama, Mr. H. Geshi and Mr. W. Tanzo for their cooperation with us on the experiments and the numerical calculations.

#### REFERENCES

- 1) Yamamoto, Y. and Imai, H. : A case study on repair effect of an earthquake - damaged R/C structure repaired by injecting epoxy resin, The 30th Symposium on Structural Engineering, pp. 153-161, 1984 (in Japanese).
- 2) Iemura, H. : Development and future prospect of hybrid experiments, Proc. of JSCE, No.356/I- 3, pp. 1-10 , 1985 (in Japanese).
- 3) Hakuno, M. and Shidawara, M. : Dynamic failure tests of a member by an earthquake type external force, Proc. of the 3rd Japan Earthquake Engineering Symposium, pp. 675-682, 1970.
- 4) Wight, J.K., editor : Earthquake Effects on Reinforced Concrete Structures, U.S. - Japan Research, ACI, SP-84, 1985.
- 5) Yamada, Y. and Iemura, H. : Inelastic aseismic design of reinforced concrete structures, 12th Congress of International Association for Bridge and Structural Engineering, Vancouver, BC, Canada, pp. 1198-1199, 1984.
- 6) Hanshin Highway Public Corporation : Deformation of RC bridge piers during earthquake motion, Research Data for the Technical Committee of Seismic Design, No. 8 - 3, 1981 (in Japanese).
- 7) Sho - Bond Construction Co., Ltd. : The BICS technique, Sho - Bond Catalog, 1981 (in Japanese).
- 8) Iemura, H. : Hybrid experiments on earthquake failure criteria of reinforced concrete structures, Proc. of the 8th World Conference on Earthquake Engineering, U.S.A., Vol. VI, pp. 103-110, 1984.
- 9) Park, Y. J., Ang, A. H - S. and Wen, Y. K. : Mechanistic seismic damage model for reinforced concrete, Journal of Structural Engineering, ASCE, Vol. 111, No. 4, pp. 722-739, 1985.

Table 1 Strength of concrete.

Compression	300 kgf/cm <sup>2</sup>	(29 MN/m <sup>2</sup> )
Tension	30 kgf/cm <sup>2</sup>	(2.9 MN/m <sup>2</sup> )
Young's Modulus	1.4 × 10 <sup>4</sup> kgf/cm <sup>2</sup>	(14 GN/m <sup>2</sup> )

Table 2 Mechanical properties of the reinforcing bars.

	D10	D16
Nominal Diameter	0.953 cm	1.590 cm
Section Area	0.713 cm <sup>2</sup>	1.986 cm <sup>2</sup>
Yield Stress	3800 kgf/cm <sup>2</sup> (373 MN/m <sup>2</sup> )	
Young's Modulus	2.1 × 10 <sup>4</sup> kgf/cm <sup>2</sup> (205 GN/m <sup>2</sup> )	

Table 3 Sequences of loading. Type I: epoxy resin grouting method; Type II: reinforcing bar welding method; Type III: steel plate covering method; E, El Centro NS (1940 Imperial Valley Earthquake, U.S.A.); H, Hachinohe NS (1968 Tokachi - oki Earthquake, Japan); digits 100-300, the maximum acceleration in gal=cm/sec<sup>2</sup>.

No.	steel ratio $\rho$	axial force N	initial loading	second loading	loading after repair			ultimate loading
					Type I	Type II	Type III	
1	1.1%	4.0 t	100 H	→ 250 E			→ 100 H	→ 250 E
2			150 H	→ 200 E	→ 150 H			
3			250 H	→ 250 H				
4			300 H	→ 300 H				
5			150 E	→ 300 E			→ 150 E	→ 300 E
6			200 E	→ 200 E				
7			250 E	→ 250 E				
8			300 E	→ 300 E				
9			2.0 t	150 E	→ 300 E	→ 150 E		
10	3.1%	2.7 t	150 E	→ 250 E			→ 150 E	→ 300 E
11			300 E	→ 300 E				

Table 4 Deterioration ratio of stiffness. Type I: epoxy resin grouting method; Type II: reinforcing bar welding method; Type III: steel plate covering method.

No.	steel ratio $\rho$	axial force N	initial loading	second loading	loading after repair			ultimate loading
					Type I	Type II	Type III	
1	1.1%	4.0 t	0.73	→ 0.54			→ 0.67	→ 0.50
2			0.58	→ 0.48	→ 0.83			
3			0.46	→ 0.55				
4			0.46	→ 0.58				
5			0.56	→ 0.31			→ 0.59	→ 0.59
6			0.46	→ 0.48				
7			0.40	→ 0.68				
8			0.35	→ 0.40				
9			2.0 t	0.46	→ 0.32	→ 0.85		
10	3.1%	2.7 t	0.80	→ 0.50			→ 0.85	→ 0.36
11			0.30	→ 0.59				

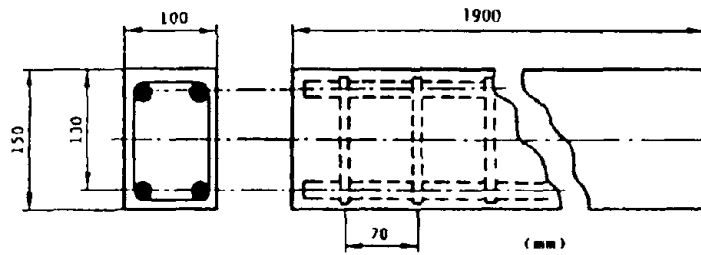
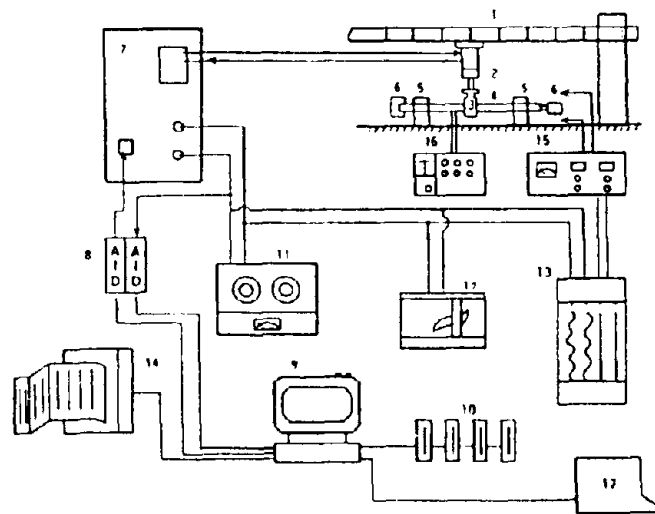


Fig. 1 Specimen dimensions.



- |                       |  |
|-----------------------|--|
| 1. Frame              | 10. Floppy Disk                        |
| 2. Actuator           | 11. Data Recorder                      |
| 3. Loading Frame      | 12. X-Y Recorder                       |
| 4. Test Piece         | 13. Pen Recorder                       |
| 5. Simple Support     | 14. Line Printer                       |
| 6. Axial Force System | 15. Dynamic Strain Gage                |
| 7. Central Controller | 16. Strain Gage (Static)               |
| 8. AD-DA Converter    | 17. Kyoto Univ. Data Processing Center |
| 9. Microcomputer      |  |

Fig. 2 HYLSEER (Hybrid Loading System of Earthquake Response) diagram.

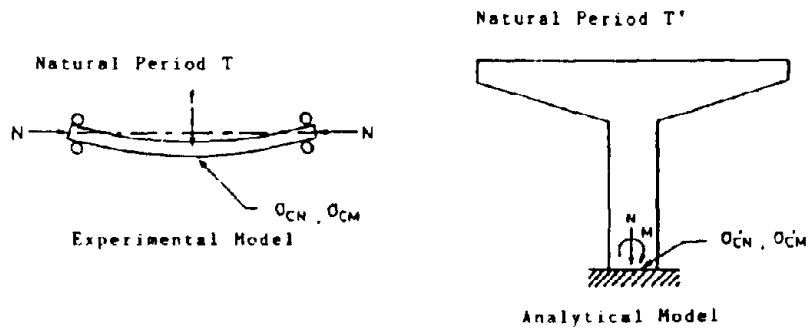


Fig. 3 Bridge pier and its experimental model.

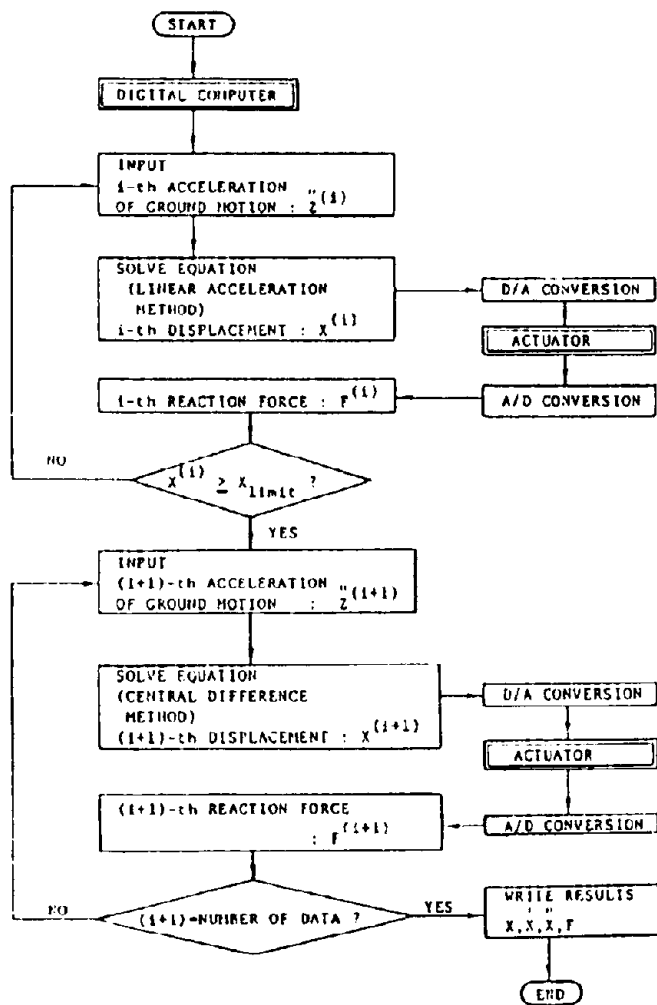
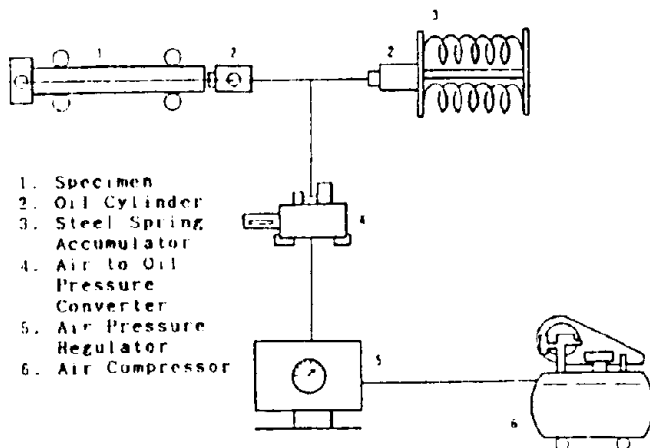


Fig. 4 HYLSEK flow chart.



1. Specimen
2. Oil Cylinder
3. Steel Spring Accumulator
4. Air to Oil Pressure Converter
5. Air Pressure Regulator
6. Air Compressor

Fig. 5 Mechanism for generating axial force.



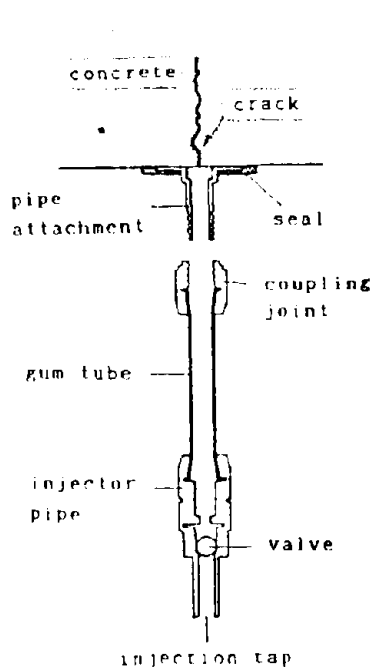


Fig. 6 BICS (Balloon Injector for Concrete Structures, Ref. 7)

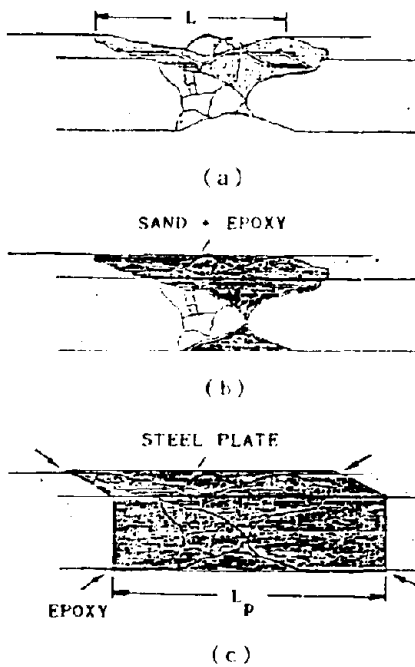


Fig. 7 Steel plate covering method: (a) Damaged segment. ( $L$ : length of damaged segment) (b) Fill with sand and epoxy resin mixture. (c) Cap with a steel plate and bond with epoxy resin. ( $L_p$ : length of the steel plate)  $L_p=L$  for specimen 5.  $L_p=2L$  for specimens 1 and 10.

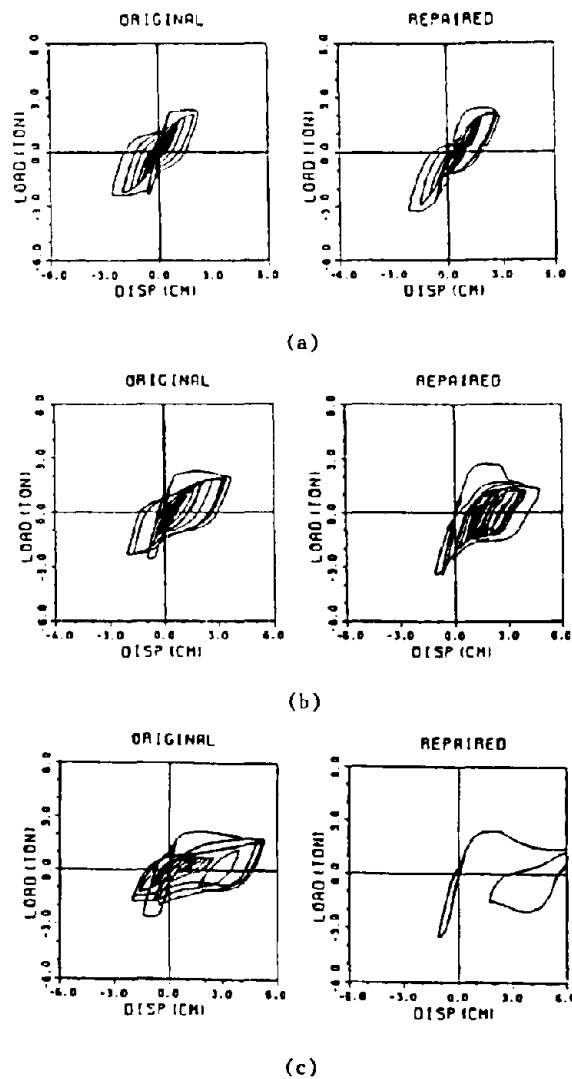


Fig. 8 Hysteresis loops for the original and repaired specimens. (Repaired by the epoxy resin grouting method; Type I)  
 (a) Specimen 6 (El Centro, 200 gal)  
 (b) Specimen 7 (El Centro, 250 gal)  
 (c) Specimen 8 (El Centro, 300 gal)

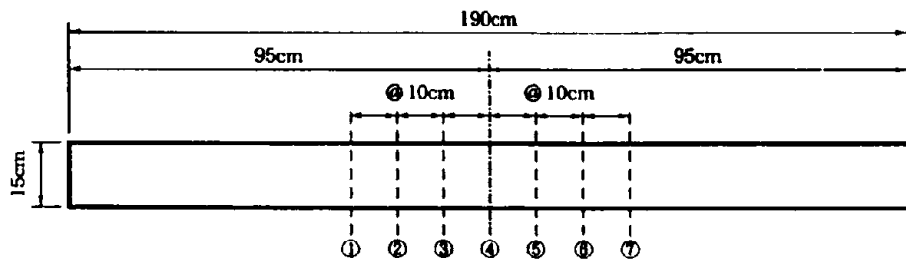


Fig. 9 Section numbers at which the specimen was cut.



Fig. 10 Cross sectional views of the specimen.

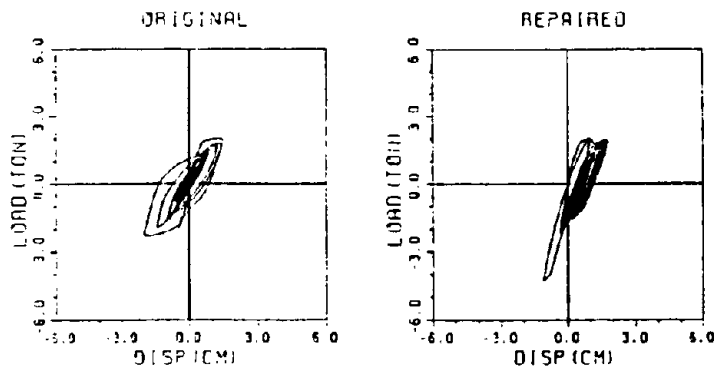


Fig. 11 Hysteresis loops for the original and repaired specimen 9.  
(Repaired by the reinforcing bar welding method; Type II)

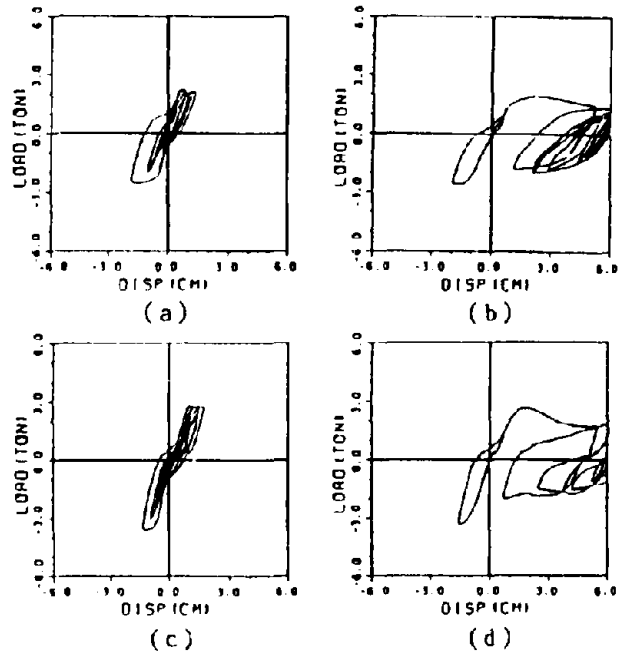


Fig. 12 Hysteresis loops for the original and repaired specimen 5. (Repaired by the steel plate covering method; Type III) (a) Initial loading (max. 150gal). (b) Second loading without repair (max. 300gal). (c) Loading after repair (max. 150gal). (d) Ultimate loading (max. 300gal).

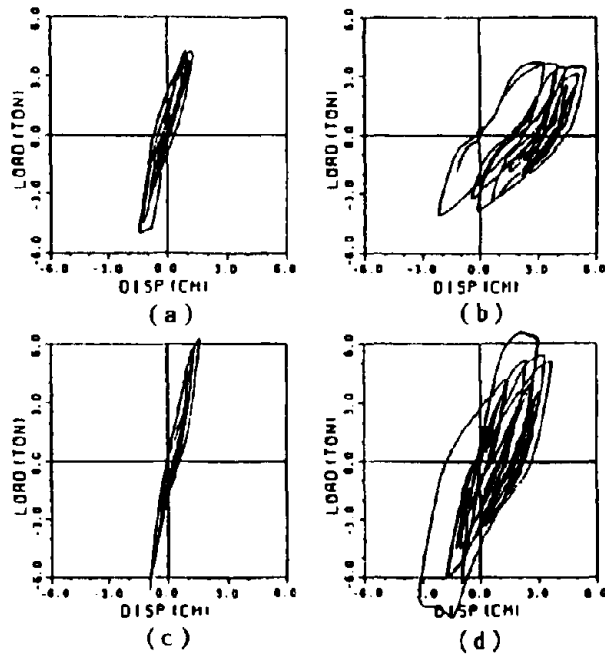


Fig. 13 Hysteresis loops for the original and repaired specimen 10. (Repaired by the steel plate covering method; Type III) (a) Initial loading (max. 150gal). (b) Second loading without repair (max. 250gal). (c) Loading after repair (max. 150gal). (d) Ultimate loading (max. 300gal).

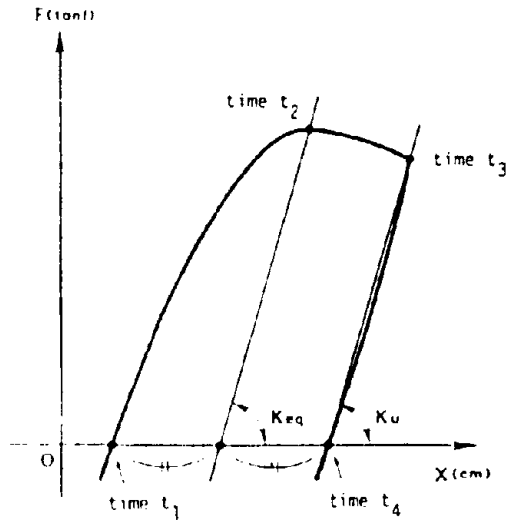


Fig 14 The unloading stiffness,  $K_u$ , and the equivalent stiffness,  $K_{eq}$ . The hysteretic loop crosses the x - axis at time  $t_1$  and has its maximum value at time  $t_2$ . The unloading process begins at time  $t_2$ . The restoring force again becomes zero at time  $t_4$ .

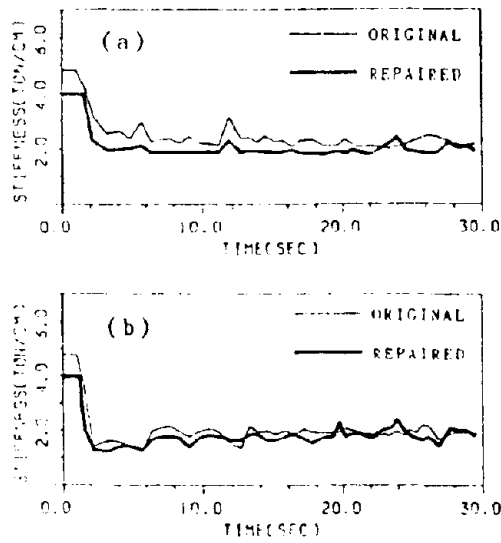


Fig. 15 Stiffness - time histories of the original and repaired specimen 6. (a)  $K_u$  (b)  $K_{eq}$  (El Centro, 200 gal. Repaired by the epoxy resin grouting method; Type I)

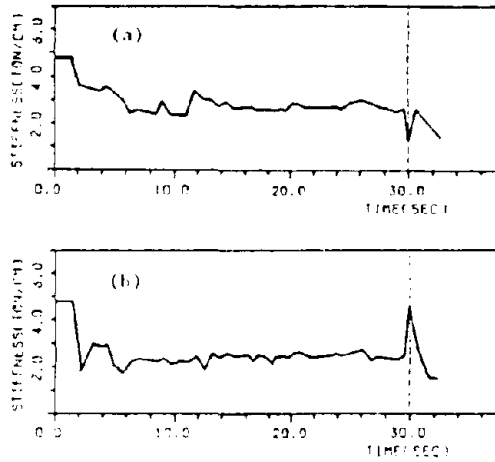


Fig 16 Stiffness - time histories of specimen 5. (a)  $K_u$  (b)  $K_{eq}$  (Initial loading, 0-30 sec: El Centro, 150 gal. Second loading, 30-32 sec: El Centro, 300 gal).

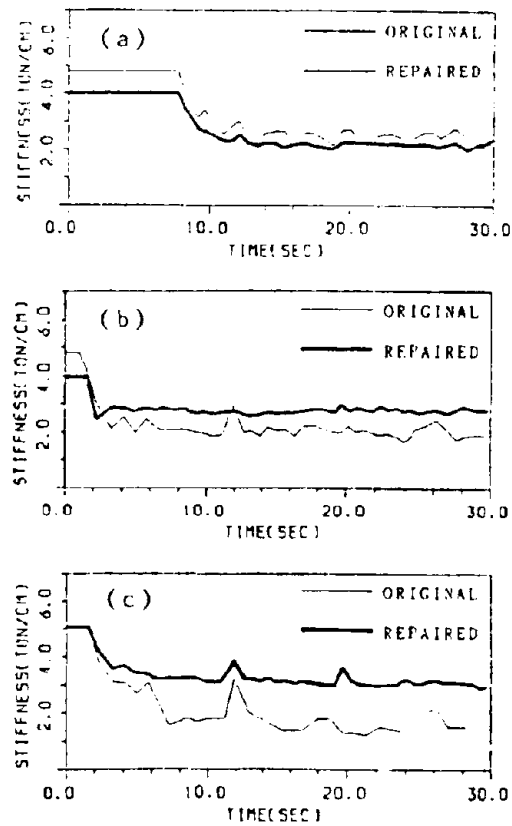
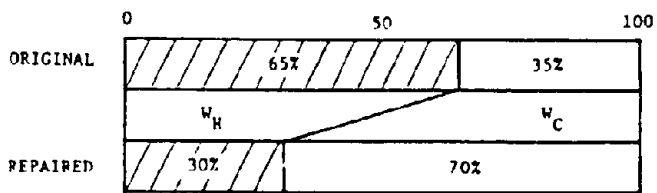
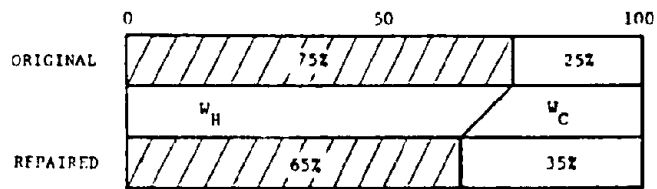


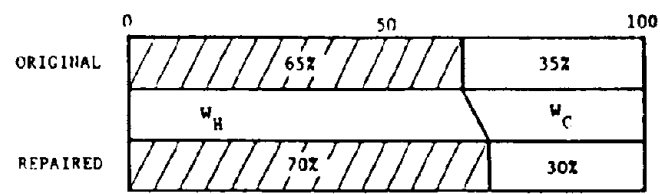
Fig. 17 Examples of stiffness - time histories: (a) Specimen 4 (Hachinohe, 300 gal. Type I) (b) Specimen 7 (El Centro, 250 gal. Type I) (c) Specimen 11 (El Centro, 300 gal. Type II)



(a)



(b)



(c)

Fig. 18 Energy participation ratios ( $W_H$ : hysteric energy.  $W_C$ : damping energy).

(a) Specimen 2 (Hachinohe, 150 gal).

(b) Specimen 4 (Hachinohe, 300 gal).

(c) Specimen 7 (El Centro, 250 gal).

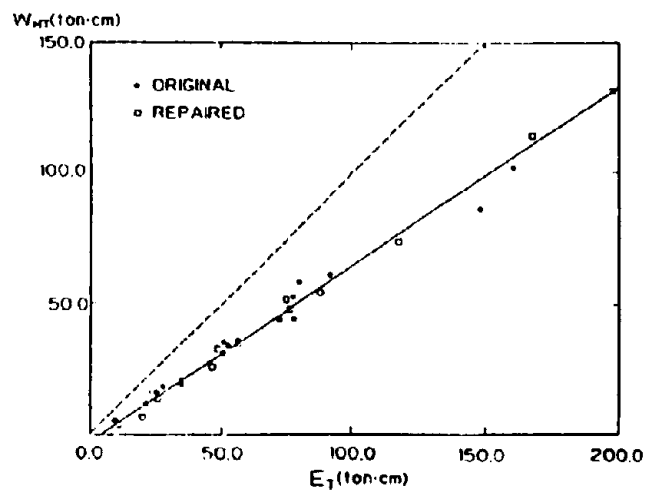
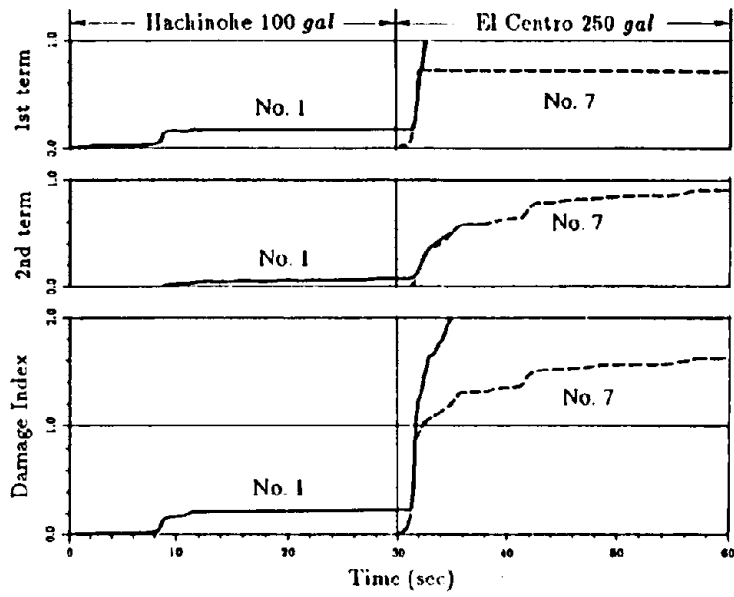
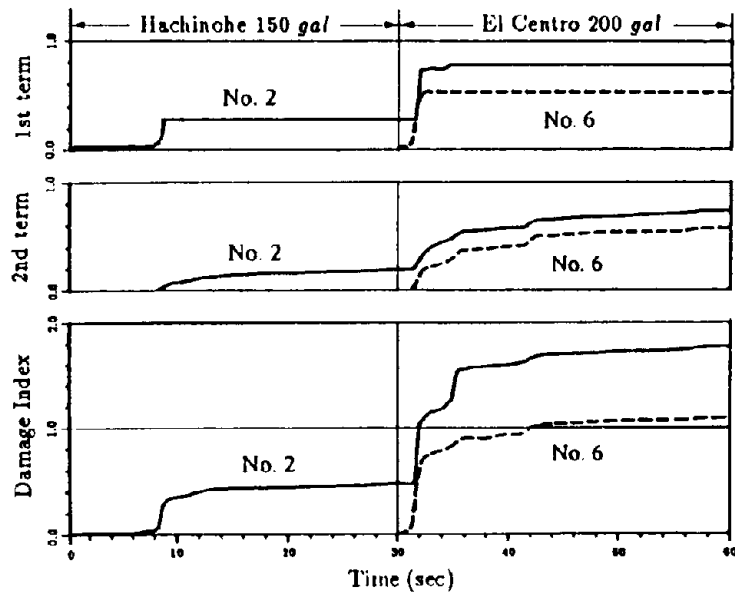


Fig. 19 Relation of the hysteric energy,  $W_H$ , to the total energy,  $E_T$ .



(a)



(b)

Fig. 20 Damage index - time histories. (a) Specimens 1 and 7. (b) Specimens 2 and 6.

**FORMULATION OF DUCTILITY OF R/C MEMBERS AND INFLUENCE OF  
DUCTILITY ON RESPONSE BEHAVIOUR IN R/C FRAME STRUCTURES**

**Hiroshi Mutsuyoshi and Atsuhiko Machida**

Department of Construction Engineering, Saitama University,  
Shimo-okubo, Urawa, Japan

**ABSTRACT**

In order to establish a reliable equation to evaluate ductility of R/C members, reversed cyclic loading tests were carried out using 33 specimens whose sectional characteristics are similar to ordinary R/C single column piers used in Japan. Based on the test results, the effects of various variables on ductility were investigated one by one. The results were summarized as a series of equations to estimate ductility quantitatively in the form of a ductility factor. It was confirmed that the ductility of the R/C members derived from the proposed equation resulted in a satisfactory agreement with the test results obtained by other researchers.

Moreover, in order to investigate the influence of ductility of members on inelastic response behaviour in R/C frame structures subjected to earthquake motion, shaking table tests and pseudodynamic tests were carried out using small scale two-story one-bay R/C bridge piers. It was observed from the tests that the inelastic behaviour of R/C frame structures depends strongly on the capacity of ductility for each member. To calculate accurately the response behaviour of R/C frame structures up to collapse, a new restoring force-displacement model which can represent ductility of each member was proposed.

**INTRODUCTION**

The concept of ductility is adopted in recent seismic design codes for R/C buildings and bridge structures. It is well known that the design seismic forces are generally much less than the elastic response force induced by a major earthquake. However, due to lack of information on ductility evaluation, it has hardly been clarified how ductile a designed R/C structure can become during a major earthquake. This is because no reliable method to evaluate the ductility of R/C members has yet been established. There are some failure mechanisms at ultimate state in R/C columns and beams. A flexural failure mode is a typical one, but it may have no problems from the point of ductility because flexural failure generally shows a ductile behaviour up to failure. On the other hand, a R/C member under reversed cyclic loading sometimes loses its load carrying capacity,

finally showing the characteristics of a shear failure after the yielding of longitudinal reinforcement. Such a failure mode is very complicated and cannot be analyzed easily. The first objective in this paper is to establish a reliable equation to evaluate the ductility of such R/C members quantitatively as described above.

The influence of ductility on the overall response behaviour of a single column type structure can be well understood. However, the effect of ductility for each member on the entire response behaviour of a R/C frame structure has hardly been clarified. Generally, a statically indeterminate structure such as a R/C rigid-frame structure will not collapse even if one of the members of the structure fails completely. However, the inelastic response behaviour of the structure may be influenced by the failure of such a member. The second objective is to clarify experimentally and analytically the influence of ductility in members on the inelastic response behaviour of R/C frame structures subjected to strong ground motion.

#### OUTLINE OF EXPERIMENT FOR DUCTILITY

The reversed cyclic loading tests were carried out using cantilever type specimens as shown in Fig. 1. The variables in the tests were tensile reinforcement ratio ( $p_t = 0.59-1.66\%$ ), web reinforcement ratio ( $p_w = 0-0.24\%$ ), compressive strength of concrete ( $f_c' = 128-565 \text{ kg/cm}^2$ ), shear span ratio ( $a/d = 2.5-6$ ), axial compressive stress ( $\sigma_0 = 0-30 \text{ kg/cm}^2$ ) and the number of repetitions of loading at a certain displacement amplitude ( $n = 1-30$  cycle). Table 1 and Table 2 show the experimental variables and the mechanical properties of the reinforcing bars respectively.

The load was applied to the top of the specimen monotonically until the yield load, which was calculated based on the elastic theory. The measured displacement at the yield load was defined as the yield displacement ( $\delta_y$ ). However, when the measured strain for the main reinforcement at the bottom of the column reaches the yield strain before the yield load, the displacement at the yield strain is defined as the yield displacement. After the yield displacement, the displacement of the integral multiples of the yield displacement was applied cyclically by controlling the displacement of the specimen.

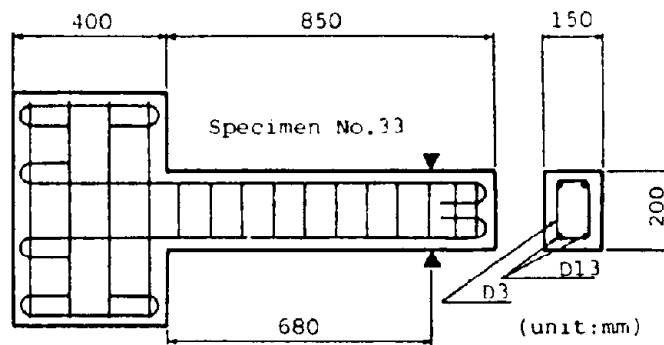


Fig. 1 Dimensions of test specimens

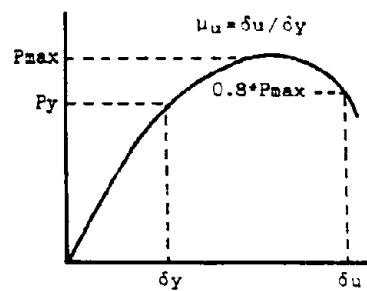


Fig. 2 Definition of Ductility factor



**FORMULATION OF EFFECT OF VARIOUS FACTORS ON DUCTILITY OF R/C**

Table 1  
Test variables

Ductility factor ( $\mu_u$ ), that is, the ratio of ultimate displacement ( $\delta_u$ ) to yield displacement ( $\delta_y$ ), was adopted as a quantitative index of ductility for R/C members. The yield displacement was defined as described above, and the ultimate displacement was defined as the limit displacement when the load carrying capacity decreases to 80% of the measured maximum strength (see Fig.2).

To formulate ductility quantitatively, one attempt was tried at first to express the effects of various factors on ductility inclusively based on the strength ratio. That is, the ratio of shear strength to flexural strength of R/C members. However, the results indicated that the inclusive expression was immoderate because the effects of various factors on ductility were slightly different from those on shear strength [1]. Therefore, it was concluded that the effect of various variables must be investigated one by one. In formulating, the relations between the measured ductility factor and each variable were investigated using the test results. In this case, each relation was obtained by changing only a single variable while the other ones were kept constant. The equation was derived so that the best fit for the plots could be obtained. To estimate the influence of the experimental variables on ductility factor, standardized ductility factor ( $\mu_t$ ), which is the ratio of the measured ductility factor to the ductility factor obtained in a certain variable, was used. Thirty three test results were used for the formulation.

No.	pt	pw	a/d	$\sigma_0$	fc'	n	$\mu_u$	
1	1.06	0.12	4.00	0	203	10	5.5	
2					279		4.7	
3	0.59	0.12	4.00	0	406	10	IV 7.1	
4					357			7.1
5					1.66			338
6	1.06	0.00	4.00	0	413	10	3.6	
7		0.08			400		4.9	
8		0.23			318		7.5	
9	1.06	0.12	3.00	0	309	10	3.8	
10			5.00		389		6.5	
11			6.00		363		IV 4.3	
12	1.06	0.12	4.00	10	294	10	4.0	
13				20	301		3.4	
14	0.89	0.12	3.00	0	330	10	6.5	
15	1.66		5.00	0	376		4.2	
16	1.06		3.00	10	307		3.5	
17	0.99	0.12	4.00	10	330	10	4.5	
18	0.99	0.12	4.00	0	308	10	5.6	
19				5	298		5.8	
20				20	321		4.3	
21				30	326		4.2	
22	0.99	0.12	4.00	10	335	10	—	
23					254		4.0	
24	0.99	0.12	4.00	10	565	10	4.3	
25					140		5.1	
26	0.99	0.12	4.00	10	327	1	6.0	
27					323	3	4.9	
28					319	30	4.3	
29	0.99	0.12	2.50	10	337	10	4.3	
30			5.50		348		4.6	
31	0.99	0.24	4.00	10	128	10	5.4	
32		0.12			128		4.4	
33		0.06			128		3.5	

Note: pt=tensile reinforcement ratio (%), pw=web reinforcement ratio (%), a/d=shear span ratio,  $\sigma_0$ =axial compressive stress, fc'=compressive strength of concrete (kg/cm<sup>2</sup>), n=number of repetitions of loads,  $\mu_u$ =measured ductility factor

Figure 3 shows the effect of the tensile reinforcement ratio on the standardized ductility factor. The following equation which can express the influence of only main reinforcements on ductility factor was derived

Table 2  
Mechanical properties of reinforcing bars

Type	Yield Stress (kg/cm <sup>2</sup> )	Yield Strain (μ)	Ultimate Stress (kg/cm <sup>2</sup> )	Area of Reinforcement (cm <sup>2</sup> )
SD30,D10	3650	2440	5380	0.7133
SD30,D13	A	3960	2480	1.267
	B	3800	2330	
	C	3840	2100	
SD30,D16	3580	2090	5910	1.986
SD30,D3	A	2740	2030	0.06905
	B	2400	1650	0.07280
	C	2540	1750	

Note: Type A was used for specimens No.1~16.  
Type B was used for Specimens No.17~30.  
Type C was used for Specimens No.31~33.

from the test results.

$$\beta t = \mu_t - 1 = (p_t)^\alpha - 1 \dots\dots\dots(1)$$

$$\alpha = (-0.146 / (a/d - 2.93) - 0.978) \dots\dots(2) \quad (a/d \geq 3.0)$$

where,  $\mu_t$ : standardized ductility factor,  $p_t$ : tensile reinforcement ratio(%),  
 $\beta t = 0$  when  $p_t = 1\%$ ;  $a$  is a function depending on  $p_w$  and  $a/d$ .

The other equations were derived in almost the same manner as above for all the variables adopted in the tests. Figure 4 shows the relation between the web reinforcement ratio and  $\mu_t$ . It is clear that the relation

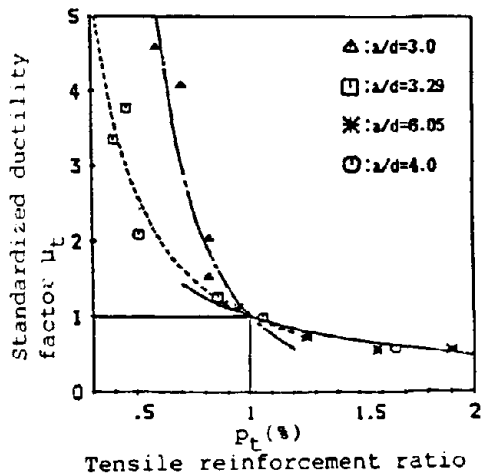


Fig.3 Standardized ductility factor and tensile reinforcement ratio

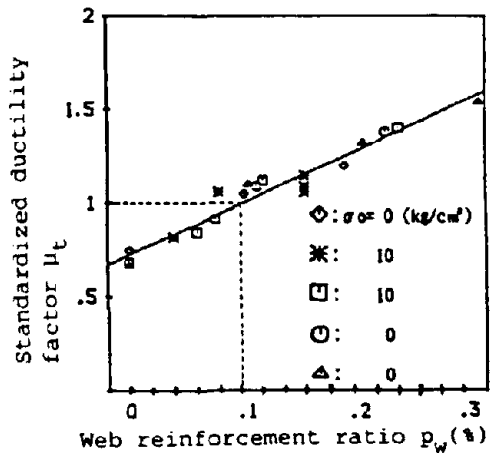


Fig.4 Standardized ductility factor and web reinforcement ratio

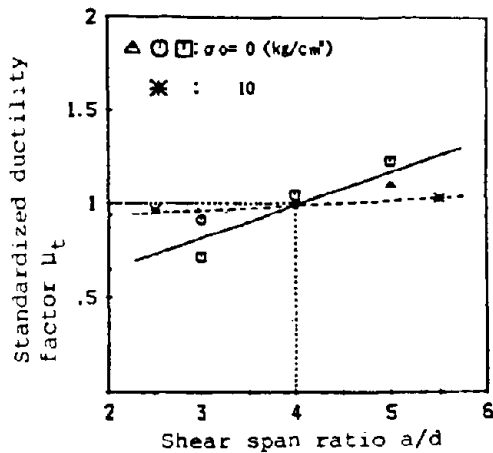


Fig.5 Standardized ductility factor and shear span ratio

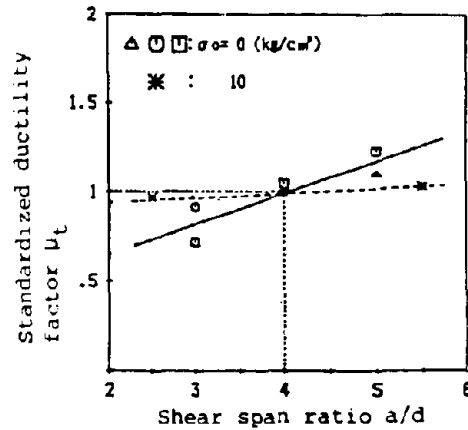


Fig.6 Standardized ductility factor and compressive strength of concrete

between them is almost linear. The following equation can be given.

$$\beta_w = \mu_t - 1 = 2.70 (p_w - 0.1) \dots\dots(3)$$

where,  $p_w$ : web reinforcement ratio (%)

Figure 5 shows the relation between shear span ratio ( $a/d$ ) and  $\mu_t$ . The following equation was derived.

$$\beta_a = \mu_t - 1 = \begin{cases} (-0.0153\sigma_0 + 0.175)(a/d - 4.0) \dots\dots(4) \\ \quad \text{(where, } \sigma_0 \leq 11. \text{ kg/cm}^2) \\ 0 \dots\dots(5) \\ \quad \text{(where, } \sigma_0 > 11. \text{ kg/cm}^2) \end{cases}$$

Figure 6 shows the influence of compressive strength of concrete ( $f_c'$ ) on  $\mu_t$ . The result indicates that  $f_c'$  has less effect on the ductility factor when the web reinforcement is arranged. Therefore, the derived equation is alternative as shown in the following equation.

$$\beta_c = \mu_t - 1 = \begin{cases} 0.00170(f_c' - 300) & (p_w = 0\%) \dots\dots(6) \\ 0 & (p_w \neq 0\%) \dots\dots(7) \end{cases}$$

$f_c'$ : compressive strength of concrete ( $\text{kg/cm}^2$ )

Figure 7 shows the relation between axial compressive stress and  $\mu_t$ . The equation is given as follows.

$$\beta_N = \mu_t - 1 = 2.18 (\sigma_0 + 10)^{-0.260} - 1 \dots\dots(8)$$

$\sigma_0$ : axial compressive stress ( $\text{kg/cm}^2$ )

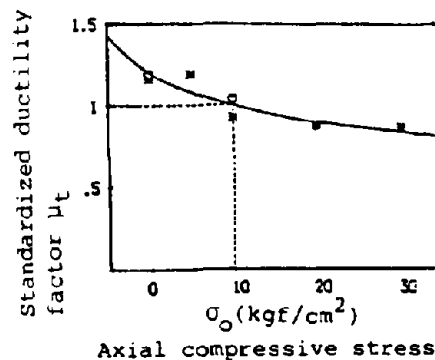


Fig.7 Standardized ductility factor and axial compressive stress

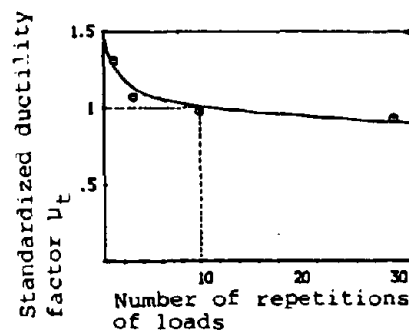


Fig.8 Standardized ductility factor and number of load repetitions

Figure 8 shows the influence of the number of load repetitions in a certain displacement amplitude on  $\mu_t$ . The equation is shown as follows.

$$\beta_n = \mu_t - 1 = 1.26 (n)^{-0.0990} - 1 \dots\dots(9)$$

n: number of load repetitions

#### PROPOSAL OF EQUATION TO ESTIMATE DUCTILITY

The following equation to evaluate ductility factor quantitatively was proposed in the form of summation of the effects of various variables on ductility factor.

$$\mu_u = \beta_0 (1 + \beta_t + \beta_w + \beta_c + \beta_n + \beta_a + \beta_n) \dots\dots(10)$$

where  $\mu_u$ =ductility factor ( $\delta_u/\delta_y$ )

The proposed equation can express only the main effect of each variable on ductility. The interactions among the variables are included in each  $\beta$ . The coefficient  $\beta_0$  in the equation was introduced to express the influence of effective depth  $d$ , that is size effect, which was not taken into account.  $\beta_0$  was obtained by the regression analysis from many test results. It was recognized that the relation between  $\beta_0$  and  $1/d$  was almost linear.

$$\beta_0 = 28.4/d + 2.03 \dots\dots(11)$$

where  $d$ : effective depth

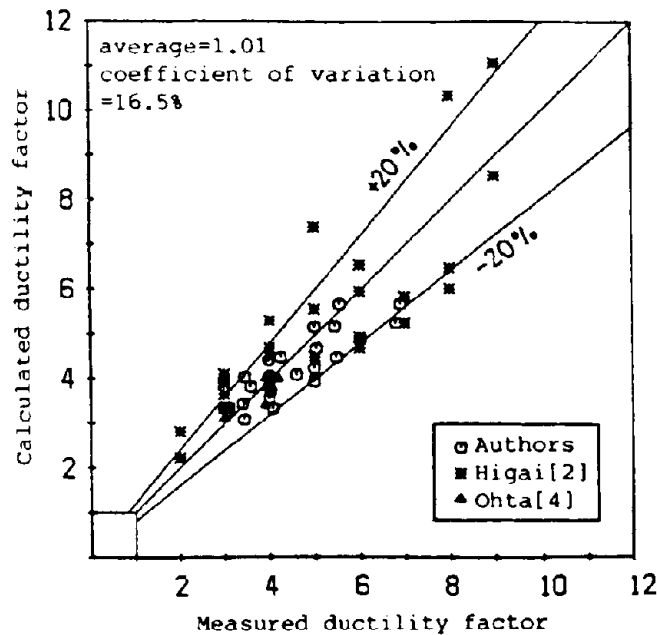


Fig.9 Comparison of calculated ductility factor with experimental ductility factor

Reproduced from  
best available copy

### EVALUATION OF PROPOSED EQUATION

The precision of the proposed equation was investigated using many test data including other researchers' [2], [3], [4], [5], which were not used in the formulation. Figure 9 shows the relation between the calculated ductility factors from the proposed equation and the measured ones. It is recognized that the calculated values agree generally well with the experimental ones. The average of the ratios of the experimental values to the calculated ones for all data is 1.01 and the coefficient of variation is 16.5%. These values also indicate that the proposed equation can give satisfactory results.

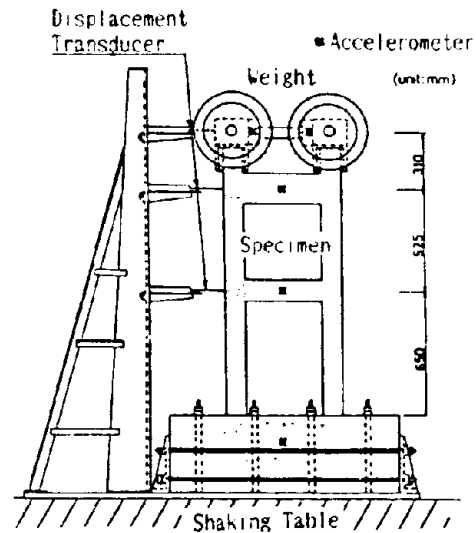


Fig.10 Test setup for simulated earthquake test

### OUTLINE OF EXPERIMENT FOR R/C FRAME STRUCTURES

In order to investigate the influence of ductility of members on inelastic response behaviour of R/C frame structures subjected to earthquake motion, shaking table tests and pseudodynamic tests were carried out. The test structures are two-story one-bay R/C frames which are similar to typical bridge piers used for the elevated railways of the Shinkansen in Japan. A general view of the test setup is shown in Fig.10. The test structures were designed assuming that the following failure modes would occur; 1)flexural failure at the bottom of the first-level column(structures RD-1 and RP-1), 2)flexural failure in the first-level beam(RD-3), 3)shear failure after yielding of the main reinforcement in the first-level beam(RD-4 and RP-4). To produce the above failure modes, the tensile reinforcement ratio and the web reinforcement ratio in the first-level beam were changed, as shown in Table 3. In every test, a weight of 963 kgf, which produces an axial stress of 9.6 kgf/cm<sup>2</sup> in the columns, was installed at the top of each second-column. Three structures, RD-1, RD-3 and RD-4, were tested under simulated earthquakes, and two structures, RP-1 and RP-4, were tested pseudodynamically.

Table 3 Details of test structures

#### Common Members

Member Name	Tensile Reinforcement Ratio (%)	Web Reinforcement Ratio (%)	Relative Stiffness Ratio (#)
First-Level Column	0.75(06X2)	0.29(03)	1.00
Second-Level Column			1.24
Second-Level Beam	0.76(06X2)		4.35

#### First-Level Beam

Specimen Name	Tensile Reinforcement Ratio (%)	Web Reinforcement Ratio (%)	Relative Stiffness Ratio (#)
RD-1	0.85(06X2)	0.29(03)	1.24
RP-1			
RD-3	0.43(03X5)	0.058(02)	1.21
RD-4	0.73(03X9)	0.0	1.26
RP-4			

Note (#): The stiffness of the first-level column is the standard value (1.0).

Reproduced from  
best available copy

In the simulated earthquake tests, the first 10 seconds of EL CENTRO-NS earthquake was repeated three times continuously. To excite the test structure into an inelastic range, the original time scale was compressed by a factor of 2 while the maximum base acceleration was amplified to 0.8G.

**RESPONSE ANALYSIS BASED ON ORDINARY RESTORING FORCE MODEL**

In order to obtain analytically the response behaviour of the structures, member-by-member analysis based on one component model [10,9] was carried out. Takeda's model [7] and Takeda's slip model [8] were used for columns and beams as a restoring force model respectively. It was proved that the used model is available for frame structures on the condition that all members fail in a ductile manner [9]. Figure 11 shows the measured and calculated time histories for RD-4 whose first-level beam failed in shear. The period of the calculated responses is clearly shorter than that of the measured ones after shear failure occurred (1.0 sec) in the first-level beam. This result indicates that the overall response behaviour of the structure can not be simulated accurately using the ordinary restoring force model after shear failure occurred in some members and then the load carrying capacity of the member decreased suddenly. In a statically indeterminate structure such as a R/C rigid-frame structure, the inelastic response behaviour of the structure depends on ductility of the members even if the structure does not collapse. Therefore, the restoring force model which can effectively represent ductility for all members is required to calculate precisely overall response behaviour.

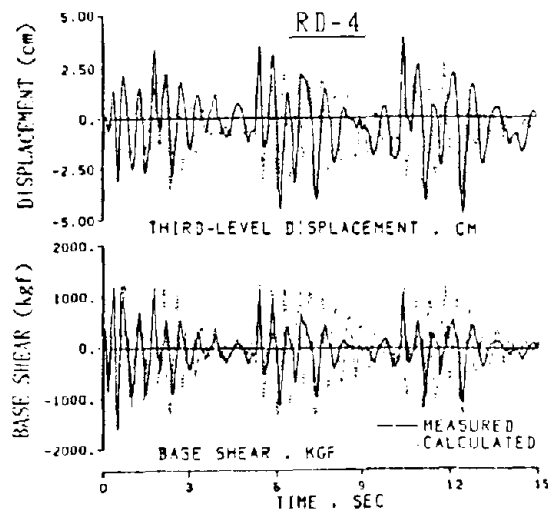


Fig.11 Time histories of top displacement and base shear obtained from test and analysis

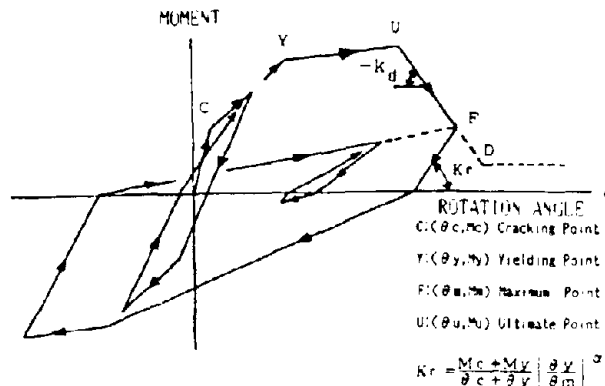


Fig.12 Proposed restoring force model

**RESPONSE ANALYSIS BASED ON DUCTILITY OF MEMBERS**

In order to resolve the above problem, the new restoring force model which can express the ductility for all members was proposed. Figure 12 indicates the new restoring force model, in which the decrease in load carrying

Reproduced from  
best available copy

capacity after reaching the maximum strength was taken into consideration. The ultimate deformation (point U in Fig.12) at which the load carrying capacity begins to decrease was determined from the proposed equation(10) for ductility previously. The slope after the point U was defined by Equation(12) derived from numerous test results. The hysteresis rule of the proposed model was the same as used in that of the ordinary model.

Using the proposed restoring force model, response analyses were carried out for all the test structures. Figure 13 shows the time histories of the top displacement obtained from the tests and analyses for structure RP-4 whose first-level beam failed in shear after the yielding of the longitudinal reinforcement. The response values and the periods of excitation obtained from the analysis agree well with those from the tests after shear failure occurred in the first-level beam(after 1.0 sec). That is, the inelastic response behaviour can be calculated accurately by using the proposed restoring force model even if the load carrying capacity of some members decreased suddenly due to the occurrence of shear failure.

Figure 14 shows the measured and calculated base shear-displacement curves. The calculated ones were obtained from both the ordinary model and the proposed one. The inelastic behaviour cannot be represented accurately by the ordi

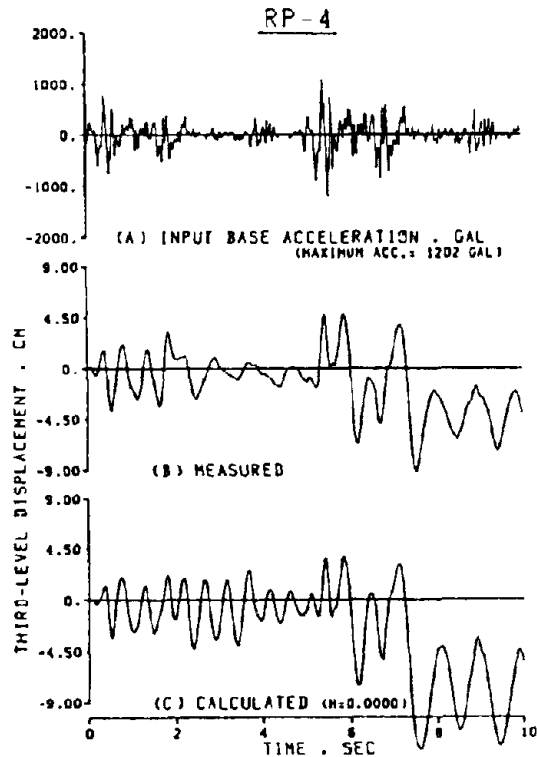


Fig.13 Time histories of top displacement obtained from test and analysis using proposed model

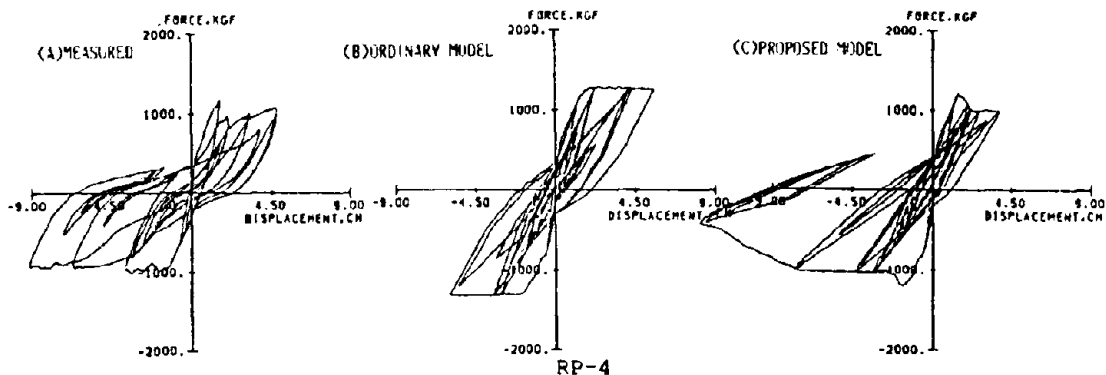


Fig.14 Base shear-displacement curves obtained from tests and analysis

**Reproduced from  
best available copy**

nary model after the load carrying capacity of one member decreased due to the occurrence of shear failure. However, the overall behaviour of the structure can be obtained up to failure by the newly proposed model with satisfactory accuracy. Moreover, the proposed model can be a powerful method to predict the extent of damage of each member as well as that of a structure.

### CONCLUSION

In order to establish a reliable equation to evaluate the ductility of R/C members, reversed cyclic loading tests were carried out. Based on the test results, the effects of various variables on ductility were investigated one by one. The results were summarized as a series of equations so as to estimate ductility quantitatively in the form of a ductility factor. It was confirmed that the ductility of R/C members derived from the proposed equation resulted in satisfactory agreement with the test results obtained by other researchers. Moreover, the influence of ductility of members on inelastic response behaviour in R/C frame structures subjected to earthquake motion was investigated. It was observed from the tests that the inelastic behaviour of R/C frame structures depends strongly on the ductility capacity of each member. To calculate accurately the response behaviour of R/C frame structures up to collapse, a new restoring force-displacement model which can represent ductility of each member was proposed. Using the proposed restoring force model, the inelastic response behaviour of R/C frame structures could be calculated with satisfactory accuracy even if some members failed completely.

### REFERENCES

1. Toyoda, K., Mutsuyoshi, H. and Machida, A., Experimental Study on Evaluation of Ultimate Deflection of Reinforced Concrete Members. Transactions of JCI, Vol.7, 1985.
2. Higai, T., Rizkalla, S., Ben-Omran, H. and Saaday, F., Shear Failure of Reinforced Concrete Members Subjected to Large Deflection Reversals. Proceedings of Sixth Annual JCI Meeting, 1984 (in Japanese).
3. Ishibashi, T., Aoki, K. and Yoshino, S., Ductility Factor of Reinforced Concrete Members. Data of Structural Design, No.79, 1984 (in Japanese).
4. Ohta, M., Study on Seismic Resistant Design of Reinforced Concrete Piers of Single Column Type, Report of Public Works Research Institute, Ministry of Construction, Japanese Government, No.153, 1980(in Japanese).
5. Earthquake Disaster Prevention Branch, Experimental Study on Dynamic Load Carrying Capacity of R/C Piers (1), Research Material at Public Works Research Institute, Ministry of Construction, Japanese Government, No.153, 1980(in Japanese).
6. Giberson, M.F., Two Nonlinear Beams with Definitions of Ductility. Proc. of ASCE, Vol.95, No.ST2, 1969.
7. Takeda, T., Nielsen, N.N. and Sozen, M.A., Reinforced Concrete Response to Simulated Earthquakes. Proc. of ASCE, Vol.96, No.ST12, 1970.12.
8. Eto, H. and Takeda, T., Inelastic Response Analysis of R/C Frame Structures. Annual Meeting of Japan Architectural Association, 1977.
9. Machida, A., Mutsuyoshi, H. and Tsuruta, K., Inelastic Response of Reinforced Concrete Frame Structures Subjected to Earthquake Motion. Concrete Library of JSCE No.10. Dec. 1987.



# REPAIR AND RETROFIT OF STEEL PIERS

Gregory A. MACRAE<sup>1</sup>  
Kazuhiko KAWASHIMA<sup>2</sup>  
Kinji HASEGAWA<sup>3</sup>

Presenting Author: Gregory A. MacRae

## ABSTRACT

Two types of external steel plates were welded onto the outside of rectangular hollow steel bridge pier specimens in order to repair them after they had been subjected to moderate and large amounts of earthquake-type action. The strength and ductility capacity of the repaired specimens was found to be better than that of the original specimens when further deformation was imposed. Retrofit of piers by adding concrete increased the strength of the piers by up to 34% but brittle fracture sometimes decreased the ductility capacity. A method of increasing the deformation capacity without increasing the strength was proposed.

## INTRODUCTION

Steel bridge piers have been used over the past 30 years for the construction of bridges on the national road transportation network in Japan. The construction cost of these piers is generally more than that of reinforced concrete piers but the section size is significantly smaller making them ideal for use in city locations where land prices are high and where there are restrictions on construction space. Damage has not been observed in this sort of pier to date during a real earthquake and tests to understand their strength, ductility capacity and reparability have only recently been performed.

It is anticipated that steel piers supporting existing bridges may yield in a major earthquake because inertia forces of more than three times the design load resistance level are expected to be developed. These piers are expected to behave in one of two ways:

- 1) Piers may successfully resist the earthquake by deforming inelastically. However, if there is a major loss of strength or a large amount of deformation then effective repair methods will be required so that the pier resistance will be sufficient during future major earthquakes, or
- 2) Piers may suffer severe damage and be unrepairable. Retrofit is therefore required before the earthquake occurs in order to ensure satisfactory behaviour.

The tests described here were carried out to find effective methods for repair and retrofit of steel piers [1] and the results were included in the Manual of Seismically Damaged Civil Engineering Structures [2].

A typical steel pier of the sort used in Japan is shown in Figure 1. It consists of four plates welded together into a box shape and other plates are welded internally to provide longitudinal and lateral stiffness. Design of this pier type is carried out according to the "Specifications for Highway Bridges" issued by the Ministry of Construction [3]. Two types of buckling which are checked during the design are:

- a) overall buckling of one side, and
- b) local buckling of the panel between the longitudinal stiffeners (local panel buckling).

These deformation modes are shown in Figure 2(a) and (b) respectively. An indication of which of these modes of buckling is likely to occur first is also available [4].

The method of retrofit which should be used on a pier depends on the type of buckling deformation and failure mechanism which is likely to occur. Tests on twenty two piers have been conducted at PWRI in order to understand their strength and deformation capacity [5]. Points of interest from these tests related to the mode of failure of piers and which may affect the retrofit or repair procedure are:

- 1) The height of the major buckle was midway between the base and the first lateral stiffener in the piers which failed by overall buckling of one side.

<sup>1</sup> Researcher, Earthquake Engineering Division, Public Works Research Institute, Tsukuba, Japan

<sup>2</sup> Head, Earthquake Engineering Division, Public Works Research Institute, Tsukuba, Japan

<sup>3</sup> Senior Research Engineer, Earthquake Engineering Division, PWRI, Tsukuba, Japan

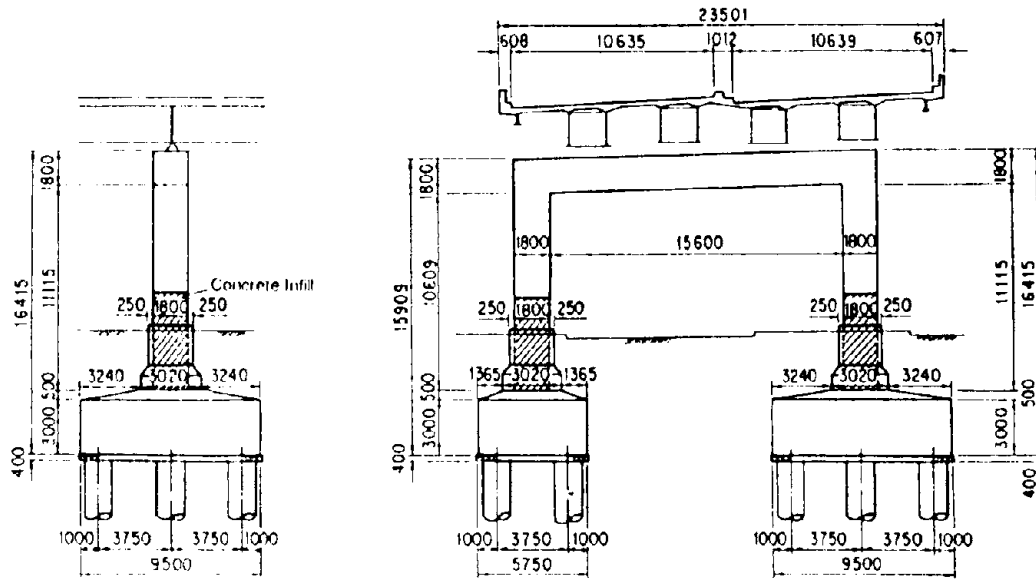


Figure 1. Elevation of a Typical Pier

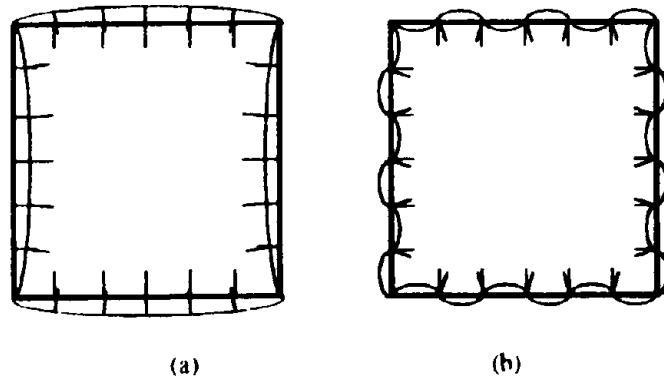


Figure 2. Modes of Buckling

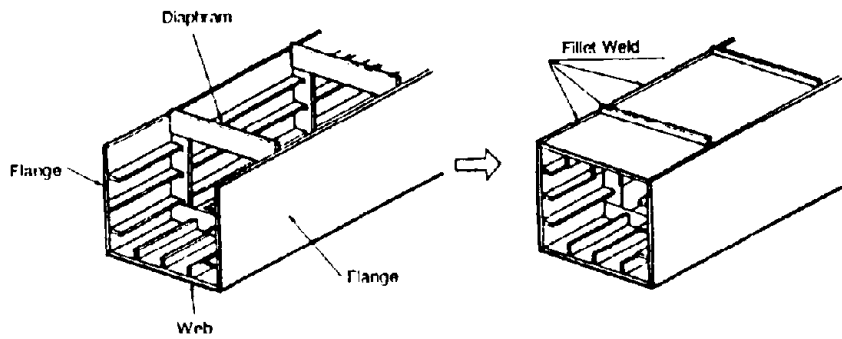


Figure 3. Construction Drawing

- 2) Piers which failed by local panel buckling sustained either a very localized buckle or no buckle at all and failed by fracture of the steel near or in the weld at the base.
- 3) Some piers with concrete infill over the bottom third of their height were also tested. The added concrete may be considered as a method of pier retrofit. The results of these tests are discussed later in this paper.
- 4) Piers tested on the shaking table underwent very little yield reversal and the displacement at the top increased only in one direction. Large residual displacements were observed at the top of the piers after the tests were completed which indicated that full repair may be difficult to perform.

## REPAIR OF STEEL PIERS

### Test Specimens

Real piers are generally large enough that a person may enter and weld from the inside but the pier specimens used in these tests were too small for this construction technique to be used. The pier was therefore constructed in stages as shown in Figure 3. Weld was applied to the inside of the specimen before the final web-plate was welded into place from the outside. The diaphragms extended outside the section on one side to facilitate the welding of the final web plate to the specimen. The longitudinal stiffeners on the inside of the final web plate were discontinuous at the diaphragm positions and at the base.

Four piers of the type shown in Figure 4 were tested in the test configuration shown in Figure 5. The effectiveness of repair with "strengthening plates" or "contact plates" as shown in Figure 6 was investigated. These methods are discussed in detail later in the paper. The third panel from the top was constructed from a weaker steel (SM50Y steel) than the other panels (SM58 steel). This region was made weak so that the inelastic action would occur there and so that repair could be carried out easily. Damage in actual piers would be expected to occur in the base section and foundation concrete may need to be dug out in order to retrofit. The section sizes are given in Table 1 and the calculated yield strengths, yield displacements and plastic strength of each specimen are given in Table 2. Displacement-controlled cyclic applied lateral loading was applied to multiples of the yield displacement,  $d_y$ , where  $d_y$  was calculated as the displacement at the loading point when the compression flange at the base of the middle section (SM50Y steel) yielded.

Table 1: Specimen Sizes (mm)

Region	Steel	Flange Size $b_f \times t_f$	Web Size $b_w \times t_w$	Rib Size $b_r \times t_r$
Central Region	(SM50Y Steel)	600 x 7.1	600 x 6.4	50 x 6.4
		600 x 8.2	600 x 7.3	50 x 6.3
		600 x 7.1	600 x 6.4	50 x 6.4
Base Region	(SM58 Steel)	600 x 7.1	600 x 6.4	50 x 6.4
		600 x 8.2	600 x 7.3	50 x 6.3
		600 x 7.1	600 x 6.4	50 x 6.4

The diagram shows a rectangular cross-section of a steel pier. It is divided into three horizontal regions. The top region is labeled 'Central Region' and the bottom region is labeled 'Base Region'. Dimensions are indicated:  $b_f$  (flange width),  $b_w$  (web width), and  $b_r$  (rib width) for each region. Thicknesses are indicated:  $t_f$  (flange thickness),  $t_w$  (web thickness), and  $t_r$  (rib thickness). An arrow labeled 'Loading Face' points to the top edge of the central region.

Table 2: Predicted Yield Force,  $P_y$ , Yield Displacement,  $d_y$ , and Plastic Force,  $P_p$ .

Specimen Number	Repair Method	$P_y$ (tf)	$d_y$ (mm)	$P_p$ (tf)	
Original Pier	1, 2, 3, 4	47	2.8	62	
Repaired Pier	2R	Strengthening Plate	125	3.6	139
	3R	Strengthening Plate	125	3.4	140
	4R	Contact Plate	76	3.6	76

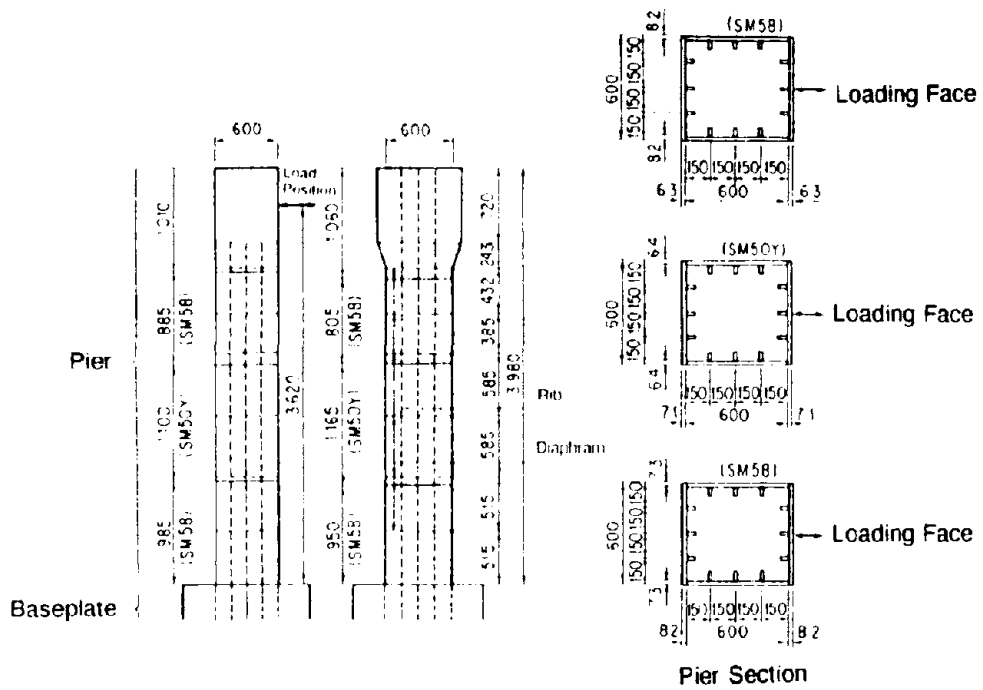


Figure 4. Piers Tested

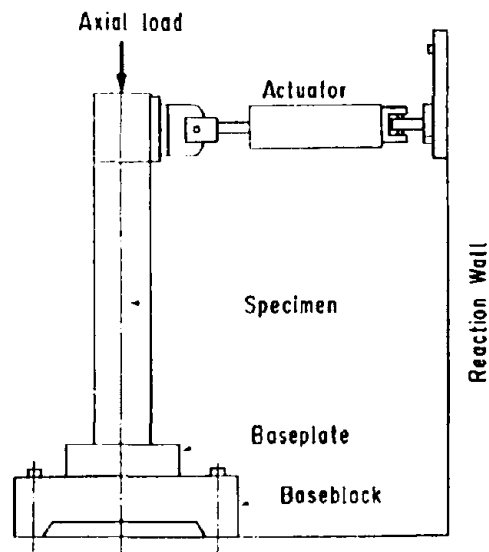


Figure 5. Test Set-up

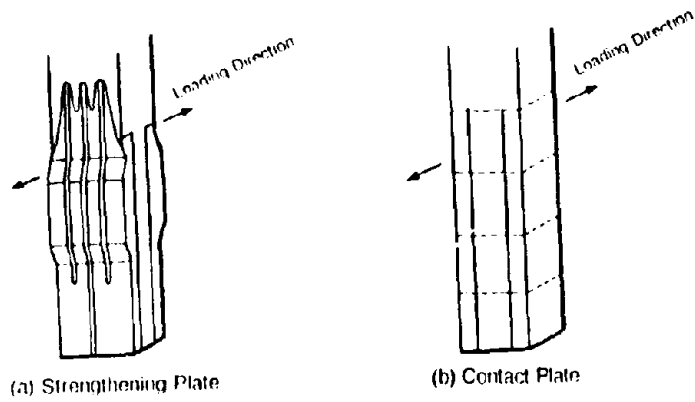


Figure 6. Repair Methods

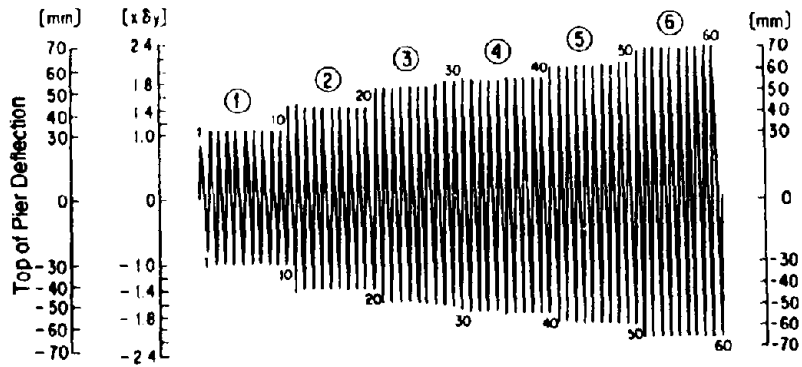


Figure 7. Loading Regime of Specimen 1

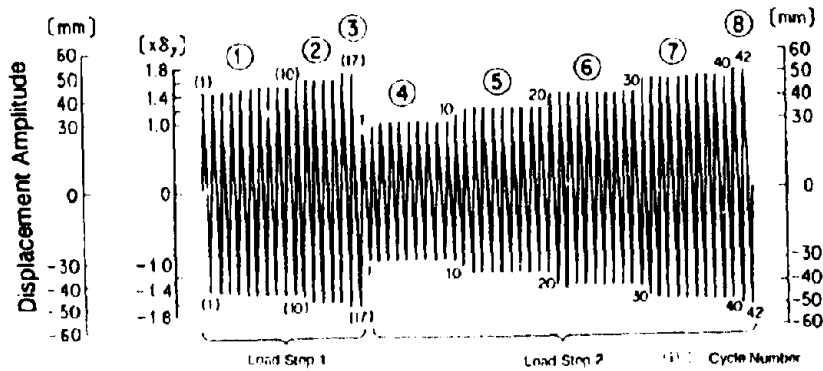


Figure 8. Loading Regime of Specimen 2

## Purpose and Procedure for Each Test

### Test 1 (Specimen 1)

Specimen 1 was tested in order to obtain the maximum load resistance, the load-displacement hysteresis relationship and the amount of buckling deformation of an unrepaired specimen at each displacement ductility step. This specimen was treated as a standard for the testing of the later specimens. It was tested quasi-statically (2.4mm/sec) with 10 cycles of repeated cyclic loading to the same displacement amplitude using displacement-controlled applied loading. The displacements used were  $1.0d_y$ ,  $1.4d_y$ ,  $1.6d_y$ ,  $1.8d_y$ , etc. increasing in steps of  $0.2d_y$  until the ultimate condition as shown in Figure 7.

### Test 2 (Specimen 2)

This test was conducted in two stages as shown in the loading regime of Figure 8. The aim of the first stage was to damage the pier. The loading regime was then reapplied in the second stage so that the influence of the smaller, gradually increasing cyclic displacements could be observed. This was done to give an indication of the behaviour of a pier under reapplied load such as may occur during aftershocks.

Firstly, ten cycles of loading were carried out to the displacement at which 10mm buckling deformation was observed to occur in Specimen 1. As the buckling deformation was still smaller than 10mm after this applied loading, 10 more cycles were applied at each displacement step, which was increased by  $0.1d_y$ , until this deformation was attained as shown in load steps 1 to 3 of Figure 8. Thereafter, in order to investigate the behaviour when the load was reapplied, 10 cycles of repeated cyclic loading were carried out with amplitudes increasing from  $d_y$  with a step of  $0.2d_y$  until the flange deformation increased to 15mm as shown in load steps 4 to 8 of Figure 8.

### Test 3 (Specimen 2R)

The reparability of Specimen 2 with **strengthening plates** was checked with the applied lateral load method of Test 1 after it had been damaged in Test 2.

### Test 4 (Specimen 3)

The specimen was to be damaged to the maximum predicted deformation for which repair with **strengthening plates** could be performed (20mm). Ten cycles of loading were carried out to the displacement at which 20mm buckling deformation was observed to occur in Specimen 1. As the buckling deformation was still smaller than this value after this applied loading, 10 more cycles were applied to each displacement step, which was increased by  $0.1d_y$ , until this deformation was attained.

### Test 5 (Specimen 3R)

Specimen 3 was retested after it had been repaired with **strengthening plates** using the applied lateral load method of Test 1.

### Test 6 (Specimen 4)

Specimen 4 was damaged to the maximum predicted deformation for which repair with **contact plates** could be carried out (5mm). Ten cycles of loading were applied to the displacement at which this buckling deformation was observed to occur in Specimen 1. As the buckling deformation was still smaller than 5mm after this applied loading, 10 more cycles were applied to each displacement step, which was increased by  $0.1d_y$ , until this deformation was attained.

### Test 7 (Specimen 4R)

Specimen 4 was retested with the applied lateral load method of Test 1 after it had been repaired with **contact plates**.

## Repair Method

### i) Repair by Strengthening Plates

The strengthening plate method of repair was used when the buckling was large and the lateral resistance of the pier was negligible. This was carried out by attaching stiffening plates, with a strength equivalent to the strength of the original plates, to the pier. A set of stiffening plates were placed on the middle section of the piers (SM50Y steel) as shown in Figure 9. The non-bracketed values in this figure were the measured sizes from Specimen 2R and the bracketed values were from Specimen 3R. The stiffening plate was placed 20mm from the pier face so that repair could be made if buckling out from the face of the pier occurred. The repair process, as shown in Figure 10, was carried out in the following stages:

- 1) A plate was welded flush against the web.
- 2) A spacer was welded at the diaphragm position, and
- 3) The strengthening plate was welded into position.

### ii) Repair by Contact Plates

The contact plate method was used when the deformation sustained by the pier was small and when significant residual strength of the flange was expected. A contact plate of breadth 140mm (one-quarter of the pier breadth) and thickness 6mm was attached as shown in Figure 11. The contact plates were sized and the connected to the pier according to "Part II Steel Bridges" of the "Specifications for Highway Bridges" [3]. The limits for the thickness of the plate,  $t_1$ , to be attached on the outside are :

$$1.5 t_2 \geq t_1 \geq b_2/24 \quad (1)$$

where  $t_2$  is the inside flange thickness and  $b_2$  is the outside attached flange thickness. A plate thickness of 6mm was used which was satisfactory as  $t_2$  was 7.3mm (over the SM50Y middle portion),  $b_2$  was 140mm and Equation (1) became

$$11\text{mm} \geq t_1 \geq 5.8\text{mm} \quad (2)$$

## Results

### Specimen 1

Approximately the same hysteresis loop shape was observed at each load-displacement cycle to the same displacement ductility and buckling was observed on at least two sides before the maximum load resistance of 60.9tf was attained as shown in Figure 12. This strength was greater than the theoretical yield load but less than the theoretical plastic load of 62tf given in Table 2 due to buckling. Panel buckling deformation increased and rapid stiffness and force deterioration was observed after the maximum force was reached. It may be seen that most of the inelastic deformation occurred over the weak panel as illustrated in Figure 13 as was desired. The mode of buckling was overall buckling of one side as shown in Figure 2a.

### Specimens 2R, 3R and 4R

The maximum strength of Specimen 2 was 62tf and the flange deformation was 15mm after it had been loaded with the regime shown in Figure 8. This strength was close to that obtained from Specimen 1 of 60.9tf. No strength degradation occurred even during the second stage of loading where 42 cycles were applied. The maximum strength after repair was 129tf as illustrated in the load-displacement hysteresis diagram of Figure 14. This test was stopped prematurely because the lateral loading ram malfunctioned. It is probable that a higher strength and deformation could have been attained with further cycles of loading because no strength degradation occurred. The deformation of these panels at the end of Test 3 was very small as shown in Figure 15.

The maximum strength of Specimen 3 was 60tf and the flange deformation was 20mm. No strength degradation occurred during these cycles as shown in Figure 16 and this strength was close to that obtained from Specimen 1 of 60.9tf. The repaired specimen, like the other specimens, was tested to

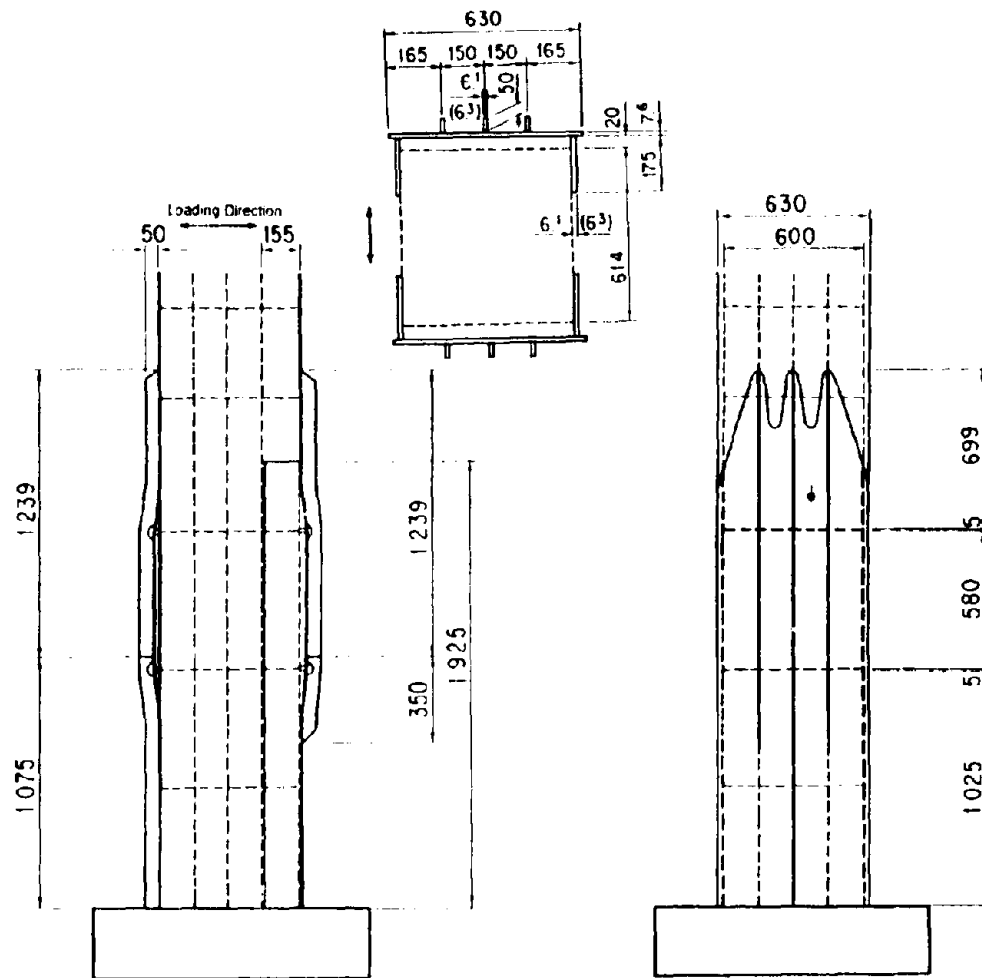


Figure 9. Strengthening Plate Repair Method

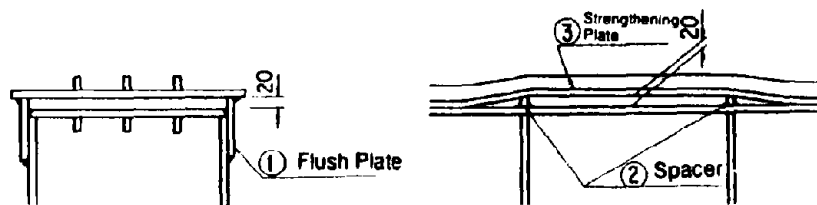


Figure 10. Order of Repair for the Strengthening Method



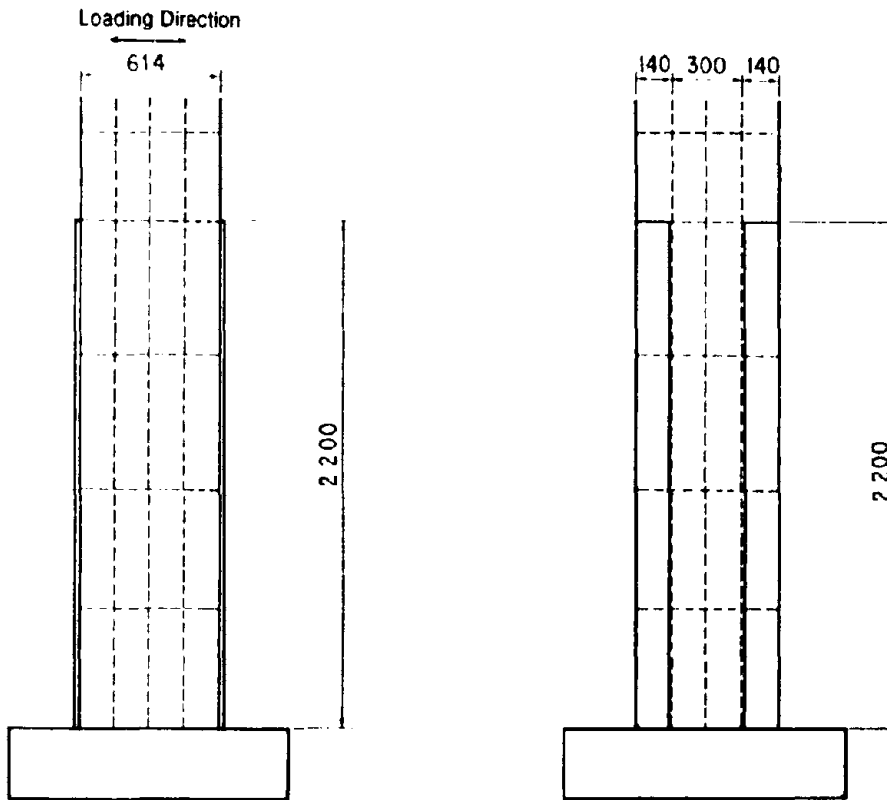


Figure 11. Contact Plate Repair Method

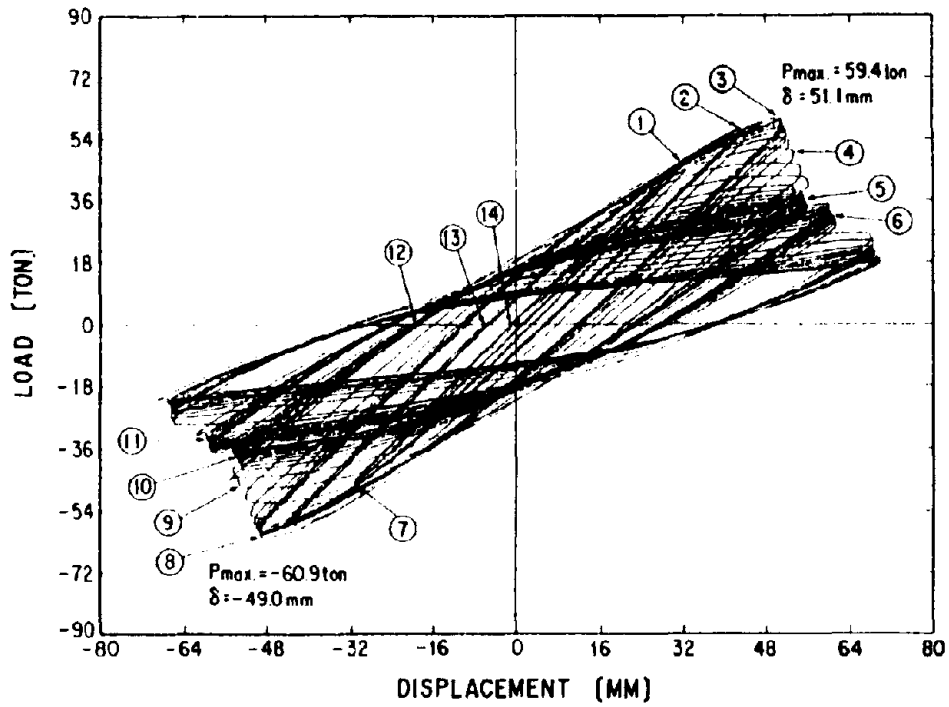


Figure 12. Hysteresis Loops of Specimen I

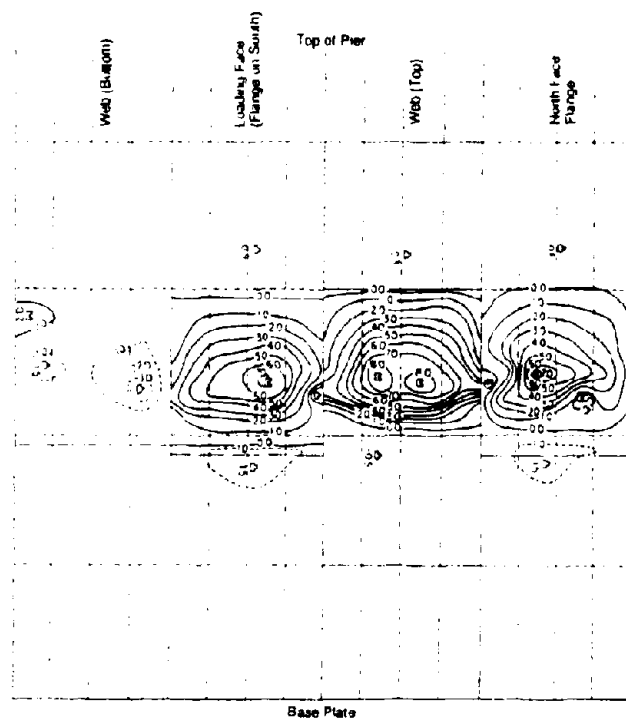


Figure 13. Deformation of Specimen 1

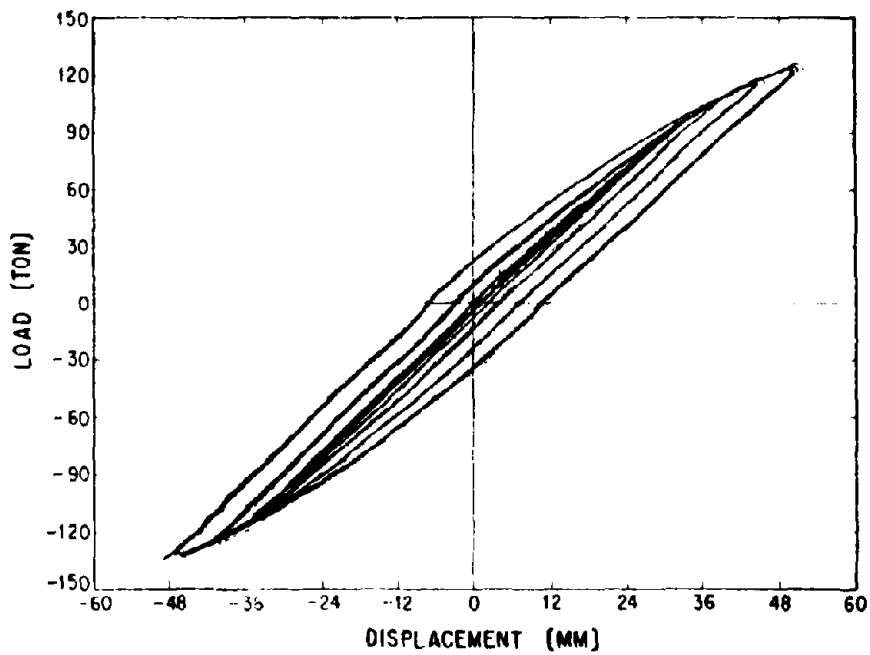


Figure 14. Hysteresis Loops of Specimen 2R

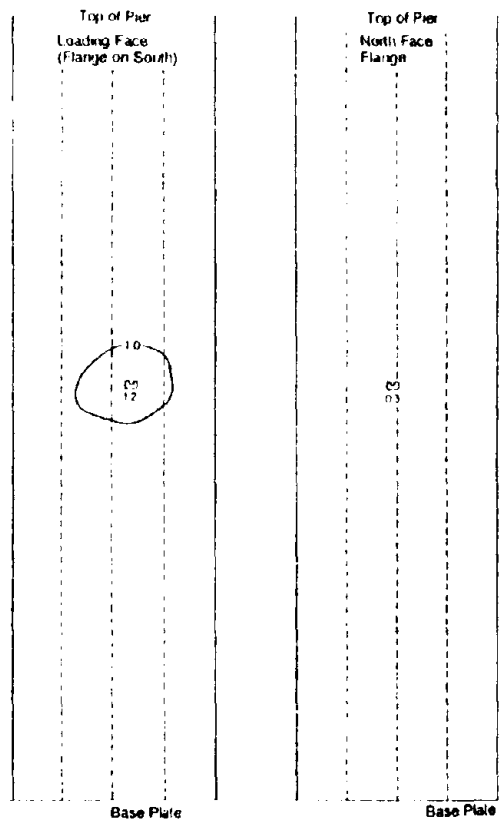


Figure 15. Specimen 2R Deformation

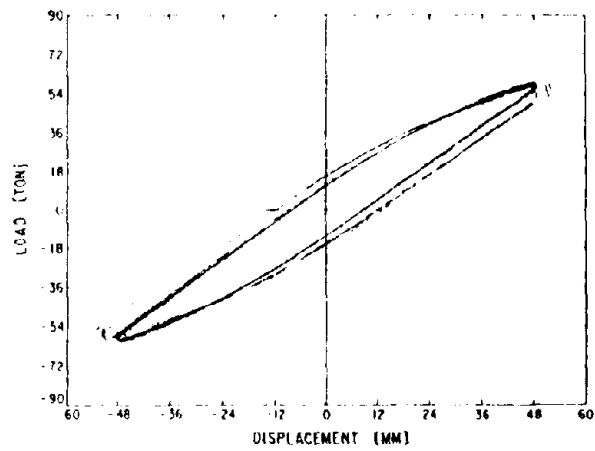


Figure 16. Specimen 3 Hysteresis Loops

the stage at which it could be shown that the behaviour, in terms of both strength and deformation capacity, was better than that of Specimen 1. Severe strength loss occurred after the maximum strength of 130tf was attained as shown in Figure 17 and buckling deformation of up to 6.5cm was observed as illustrated in Figure 18.

The remaining strength of Specimen 4 was 61tf and the flange deformation was 5mm. No strength degradation occurred during these cycles. The maximum strength after repair was 81tf, as shown in Figure 19, and buckling deformation of up to 50mm was observed as illustrated in Figure 20.

The fact that Specimen 2 sustained no strength degradation even during the second stage of loading in which 42 cycles were applied shows that the number of cycles of applied loading up to the displacement of  $1.8d_y$  and panel deformation of 15mm was not an important parameter to assess the behaviour of this pier. However, at larger displacements a significant decrease in strength with each load cycle occurred as a result of the accumulation of buckling deformation as was seen in the behaviour of Specimen 1 during the cycles to a displacement ductility of 2.2. It is shown in Figure 21 that the responses of Specimens 2R and 3R, which were repaired by the same method, were almost identical and that all the repair methods were effective in increasing the lateral load resistance and the deformation capacity of the specimens above that of the unrepaired specimen.

## RETROFIT OF PIERS WITH CONCRETE INFILL

### Piers Tested

Four piers were filled with concrete over the bottom part of their height as part of the testing program of 22 piers at PWRI [5]. Filling real piers with concrete is commonly carried out to reduce the damage which may occur as a result of a vehicle collision with the pier. Before the testing it was thought that the addition of concrete to the piers would increase the deformation capacity because buckling of the plate toward the centre of the section was inhibited.

#### a) Large Pier Testing (800mm x 800mm)

Two specimens which were filled with concrete over the bottom one-third of their height were tested and one further test was carried out on a regular hollow pier. The first concrete-filled specimen had regular "I"-shaped longitudinal stiffeners while the second had "T"-shaped ones as shown in Figure 22. It was considered that the "T"-shaped stiffener would be beneficial to increase the pier deformation capacity by reducing the possibility of buckling of the panel away from the pier face. Ten load cycles were applied to displacement ductilities of 1, 2, 3, and 4 ... etc. The ultimate displacement for calculating the displacement ductility was taken as the point when the backbone curve of the hysteresis loop became less than the calculated yield strength. The effect of the concrete infill was neglected in all calculations.

#### Large Pier Test Results

The backbone curves for the concrete-filled piers and the hollow pier are compared in Figure 23. The calculated maximum strengths divided by the yield strength were 1.69, 1.69 and 1.35 and the ductilities were 3.57, 3.57 and 3.99 for the concrete-filled specimens and the hollow specimen respectively. It may be seen that the specimen with the "T"-shaped stiffeners behaved in an almost identical manner to the regular specimen with "I"-shaped stiffeners because the mode of failure of both concrete-filled specimens was brittle fracture of the steel above the base weld rather than buckling failure as was observed in the hollow specimen. The "T"-shaped stiffener had no beneficial effect in concrete-filled specimens. It is thought that cracking of the concrete at the base of the piers occurred causing all inelastic deformation to be concentrated in the steel beside the weld as shown in Figure 24 [5]

#### b) Small piers (320mm x 320mm)

Two other smaller specimens, each one-third filled with concrete, were also tested. The first was tested by applied lateral loading (10 cycles to displacement ductilities of 1, 2, 3... etc. until failure) and the second was tested on the shaking table. Identically constructed hollow specimens were also tested in the same way. It was found in these tests that the fillet weld at the base of the concrete-filled specimens fractured and that the deformation capacity was the same as that of the hollow piers.

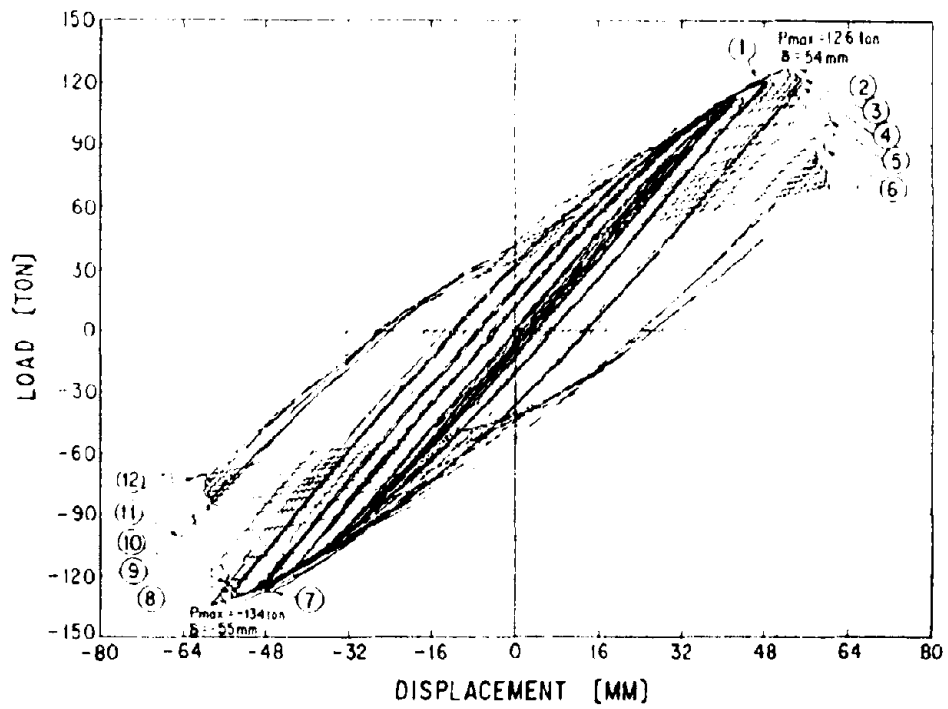


Figure 17. Specimen 3R Hysteresis Loops

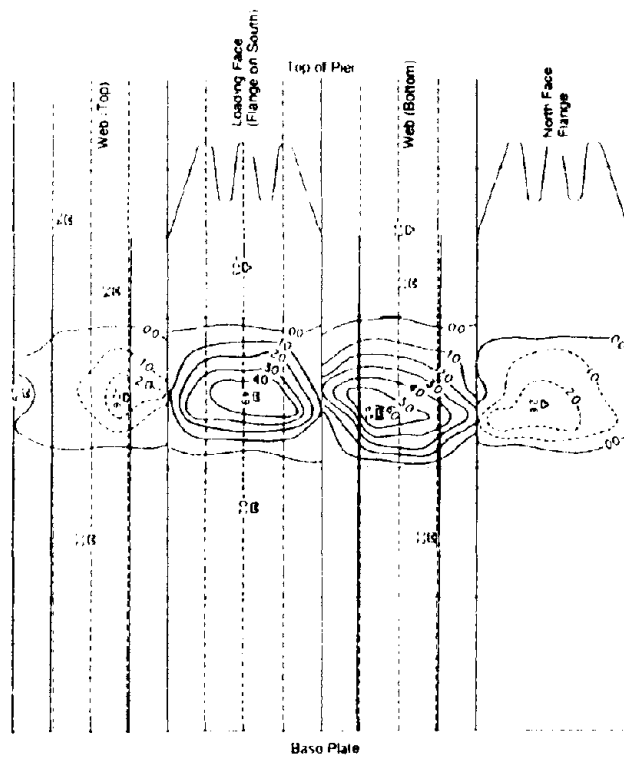


Figure 18. Specimen 3R Deformation

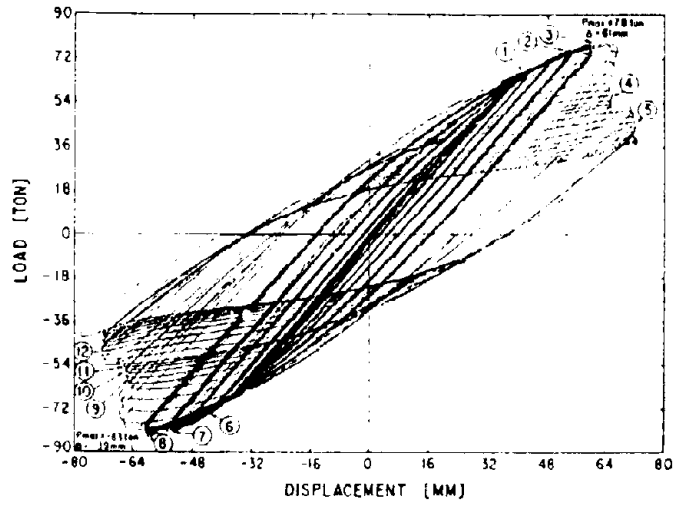


Figure 19. Hysteresis Loops of Specimen 4R

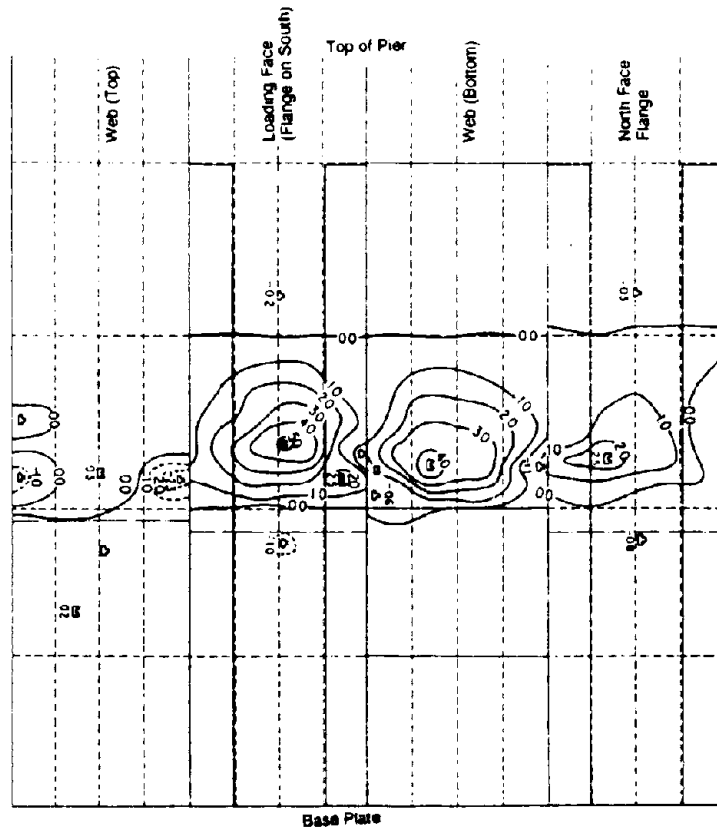


Figure 20. Deformation of Specimen 4R

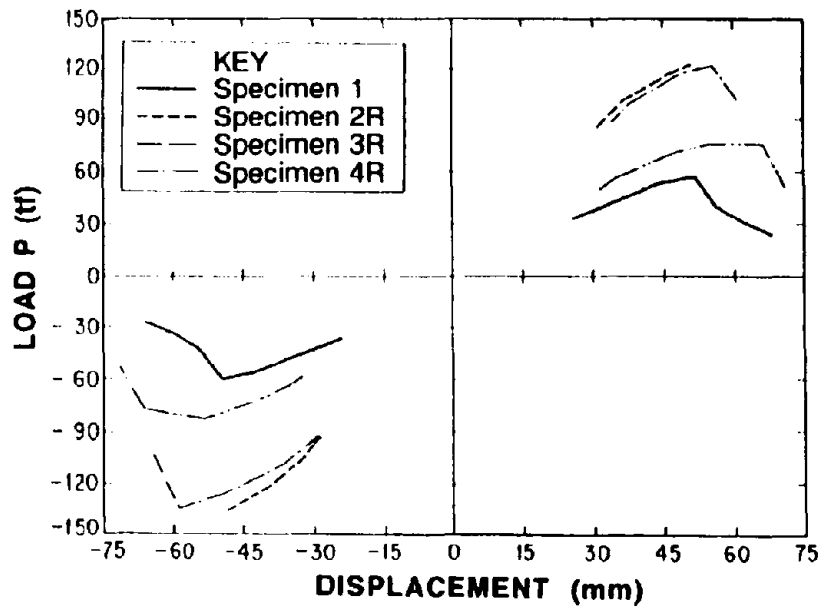


Figure 21. Retrofitted Specimens Backbone Curve Comparison

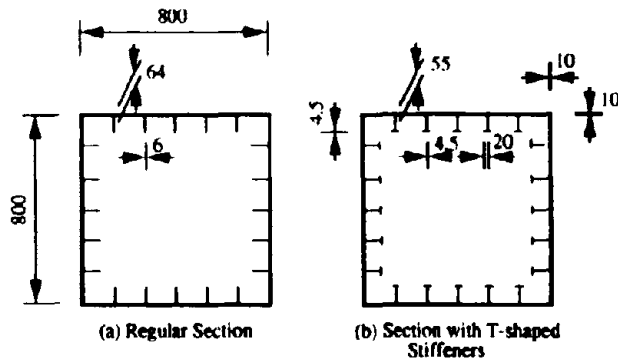


Figure 22. Concrete-filled Section Types

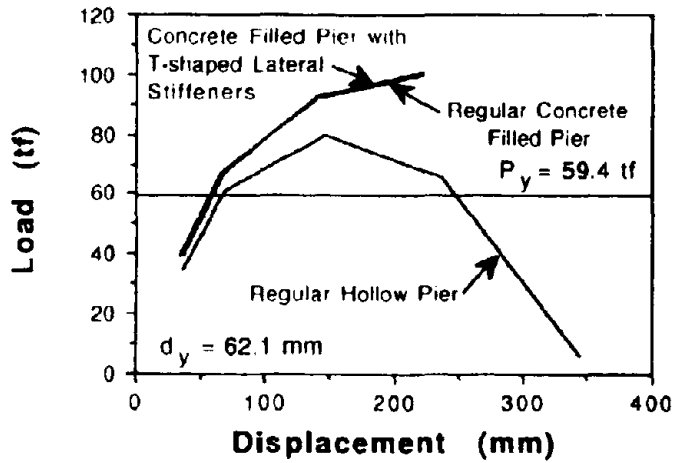


Figure 23. Backbone Curves of Empty and Concrete-Filled Piers

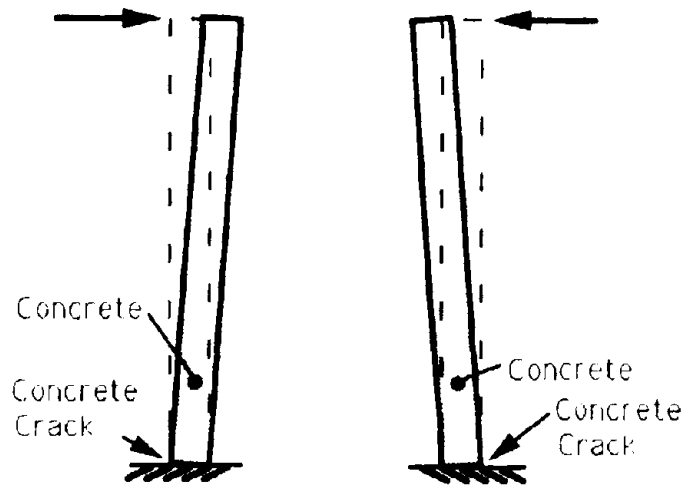


Figure 24. Concrete-Filled Pier Deformation

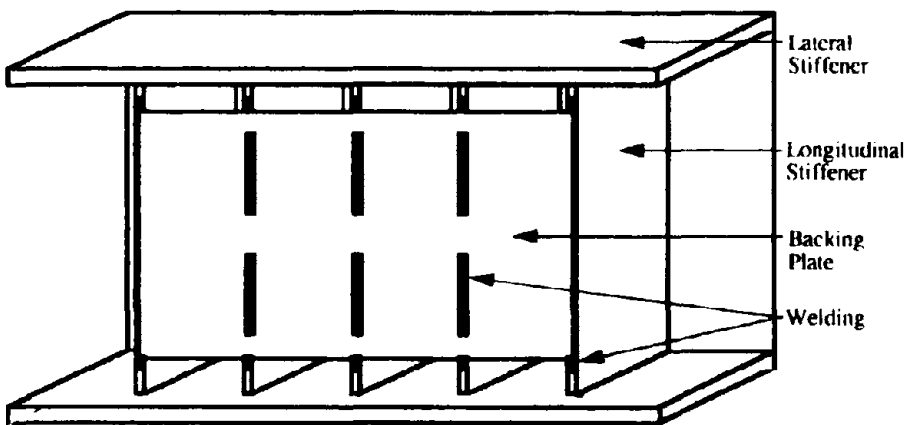


Figure 25. Retrofit by using an Internal Steel Plate



The strength of the specimens retrofitted by concrete infill was increased by between 17% and 34% and a sudden brittle failure occurred at the base of the specimens at the same or at a lower displacement than in the hollow piers. The overall seismic resistance of the specimens when evaluated by the equal energy methods was increased by the addition of concrete, however, the overall seismic resistance may decrease when the equal displacement methods are used.

### ALTERING DEFORMATION CAPACITY WITHOUT INCREASING STRENGTH

While it may be generally desirable to increase the strength as well as the deformation capacity of piers in order to provide greater earthquake resistance, there may be instances where the ductility capacity alone is desired to be increased. If the load resistance of the foundation is similar to that of the pier, an increase in the pier strength will result in a movement of the area of damage from the pier into the foundation. A method to increase the deformation capacity of the pier without increasing the strength may be required if inelastic foundation deformation is undesirable. The method proposed is to use a steel plate on the back of the longitudinal stiffeners as illustrated in Figure 25 in order to reduce the twisting of these stiffeners and to provide the centre of the side with a greater flexural strength to resist buckling. If the steel plate is only placed in the middle region of the panel then the overall strength of the pier should not increase significantly. It is thought that care may be required in the attachment of the plate to the pier in order to avoid concentration of strain in the pier below the plate. This method is expected to be most effective in piers which fail by overall buckling of one side because the buckle of these piers is concentrated in the centre where the stiffeners will be of most effect. The method may be of little or no use in piers which fail by weld fracture.

### CONCLUSIONS

The following conclusions may be made about the repair and retrofit methods of rectangular steel piers using steel plates and concrete infill which were investigated:

- 1) Repair using "strengthening plates" and "contact plates" increased the strength of the damaged piers and at least the same deformation capacity was obtained in the cases examined.
- 2) "T"-shaped longitudinal stiffeners were of no benefit because the mode of failure of concrete-filled piers was brittle fracture near the base weld rather than buckling.
- 3) Retrofit by filling piers with concrete may increase the strength but may even decrease the ductility capacity.
- 4) It may be possible to increase the deformation capacity without increasing the stiffness by using internal stiffening plates.

### ACKNOWLEDGEMENTS

The authors wish to express their thanks to the Metropolitan Expressway Public Corporation and the Hanshin Expressway Public Corporation for their support in conducting the research described herein.

### REFERENCES

1. Kawashima K., Hasegawa K., Koyama T. and Yoshida T., "Dynamic Loading Tests of Steel Bridge Piers for Developing Repair Methods", Technical Note of PWRI, Vol. 2498, Public Works Research Institute, 1988 (in Japanese).
2. Public Works Research Institute: Manual for Repair Methods for Civil Engineering Structures Damaged by Earthquakes, Technical Note of the Public Works Research Institute, Vol. 45, December 1986 (in Japanese). Translated version is published from the National Centre for Earthquake Engineering Research, University of New York, Buffalo, USA.
3. Japan Road Association, "Specifications for Highway Bridges", February 1990.
4. Subcommittee on Stability Design, "Guidelines for the Stability of Steel Structures", edited by Fukumoto Y., Committee on Steel Structures, Japan Society of Civil Engineers, 1987.
5. Kawashima K., MacRae G. A. and Hasegawa K., "The Strength and Ductility of Steel Piers", Technical Report of PWRI, Public Works Research Institute, Tsukuba, Japan (to be published).

# RESOLUTIONS

## RESOLUTIONS

1. Both Japanese and U.S. participants gained insights into the retrofit needs and technical solutions for bridge retrofit in the other countries as a result of the workshop. It is recommended that a further workshop be held in one to two years.
2. Considerable progress has been made in implementing retrofit techniques to restrain bridge spans from falling. As a consequence future research and implementations should be directed into more critical areas.
3. Both countries are actively involved in developing retrofit techniques for improving performance of bridge piers. The research being carried out has been complementary rather than duplicate, which emphasizes the value of the current information exchange. Japanese research is directed primarily to problems associated with premature termination of longitudinal reinforcement. U.S. research has been directed toward improving flexural ductility and shear strength of piers. Continuing cooperation and information exchange is recommended in this area.
4. Both sides recognize the importance and difficulty of effective retrofit of bridges on foundations of inadequate strength or stability. Increased efforts to develop and implement effective solutions is urged.

# APPENDICES

## A P P E N D I C E S

### WORKSHOP PROGRAM

#### Mon. Dec. 17

- 8:15 Leave Hotel Sunroute Tsukuba  
8:30 Leave Hotel Grand Shinonome  
8:45 - 9:20 Registraton
- 

#### **9:30 Opening Session**

(Chairman : K.Kawashima, M.J.N.Priestley)

Address by Dr.T.Iwasaki, Director-General, PWRI

Address by Dr.H.S.Lew, Chief of Structural Division, National  
Institute for Standards and Technology

---

9:50 Break

---

#### **10:30 Session 1 : History of Seismic Damage and Preparation of Seismic Design Codes**

(Chairman : G.A.Macrae)

- 10:30 1) Seismic Design, Seismic Strengthening and Repair of Highway  
Bridges in Japan  
(K.Kawashima)  
10:50 2) Bridge Substructures and Design Methods  
(M.Okahara, S.Takagi and S.Nakatani)  
11:10 3) Design Details of Reinforced Concrete Bridges in Japan  
(T.Akimoto)  
11:30 Discussions
- 

12:15 Lunch (At 1F, PWRI)

---

#### **13:30 Session 2 : Damage to San Francisco Bridges in the Loma Prieta Earthquake**

(Chairman : J.Gates)

- 13:30 1) An Overview of Damage to Bridges in the Loma Prieta  
Earthquake of October 1989  
(H.S.Lew)  
13:50 2) San Francisco Double Deckers - Observed Damage and a  
Possible Retrofit Solution  
(M.J.N.Priestley, F.Seible)

14:10 3) Full-scale Tests on the Cypress Viaduct  
(S.Mahin and J.Moehle)

14:30 Discussions

---

15:00 Break

---

**15:30 Session 3 : Assessment and Prioritization of Vulnerable Bridges**

(Chairman : H.S.Lew)

15:30 1) Assessment and Retrofit Research for Multi-level, Multi-column  
Bents  
(S.Mahin and J.Moehle)

15:50 2) Prioritizing Bridges for Seismic Retrofit  
(J.Gates and B.Maroney)

16:10 3) Damage and Performance Assessment of Existing Concrete Bridges  
Under Seismic Loads  
(F.Seible and M.J.N.Priestley)

16:30 4) Large Earthquake Countermeasures for Bridge Substructures on  
Tomei Expressway  
(T.Tsubouchi, K.Ohashi and K.Arakawa)

16:50 Discussions

---

17:35 Adjourn

17:45 Leave PWRI

18:00 Dinner at Steak House ASAKUMA

20:00 Arrive Hotel Grand Shinonome

---

**Tue. Dec. 18**

9:00 Leave Hotel Grand Shinonome

9:10 Leave Guest House of PWRI

-----  
**9:30 Session 4 : Inspection and Strengthening Methods for Reinforced  
Concrete Bridge Piers**

(Chairman : S.Mahin)

- 9:30 1) Seismic Inspection and Seismic Strengthening of Reinforced  
Concrete Bridge Piers with Termination of Main Reinforcement  
at Mid-Height  
(K.Kawashima, S.Unjoh and H.Iida)
- 9:50 2) Seismic Strengthening of Reinforced Concrete Bridge Piers on  
Metropolitan Expressway  
(T.Akimoto, H.Nakajima and F.Kogure)
- 10:10 3) Seismic Strengthening of Reinforced Concrete Bridge Piers on  
Hanshin Expressway  
(Y.Matsuura, I.Nakamura and H.Sekimoto)
- 10:30 Discussions

-----  
11:00 - 11:20 Visit Vibration Laboratory

11:20 - 11:40 Visit Earthquake Engineering Laboratory

11:40 - 12:00 Visit Structure Engineering Laboratory

-----  
12:00 - 12:30 Lunch (At 1F, PWRI)

-----  
12:30 - 13:25 **Special Session on Japanese Culture (At B1F)**

-----  
**13:30 Session 5 : Research on Seismic Retrofitting and Strengthening of  
Reinforced Concrete Bridge Piers**

(Chairman : H.Iemura)

- 13:30 1) Retrofit of Columns for Enhanced Seismic Performance  
(Y.H.Chai, M.J.N.Priestley and F.Seible)
- 13:50 2) Study on Ductility Estimation of Fiber Mixed RC Members  
(S.Kobayashi, H.Kawano, K.Morihamada and H.Watanabe)
- 14:10 3) Effect of Carbon Fiber Reinforcement as a Strengthening  
Measure for Reinforced Concrete Bridge Piers  
(T.Matsuda, T.Sato, H.Fujiwara and N.Higashida)
- 14:30 Discussions

---

15:00 Break

---

15:30 **Session 6 : Research on Seismic Retrofitting and Strengthening**  
(Chairman : F.Selble)

15:30 1) Earthquake Failure Criteria of Original and Repaired RC  
Members with Hybrid Experiments

(H.Iemura, K.Izuno and Y.Yamada)

15:50 2) Formulation of Ductility of Reinforced Concrete Members and  
Influence of Ductility on Response of Reinforced Concrete  
Frame Structures

(H.Mutsuyoshi and A.Machida)

16:10 3) Repair and Retrofit of Steel Piers

(G.A.MacRae, K.Kawashima and K.Hasegawa)

16:30 Discussions

---

17:00 **Closing Session : Adoption of Resolution**

(Chairman : N.J.M.Priestley, K. Kawashima)

---

17:30 Closure

17:45 Leave PWRI

---

18:15 **Reception at Hotel Grand Shinonome**

---



## ITINERARY OF STUDY-TOUR

---

### Wed. Dec. 19

- 9:15 Leave Tsukuba (Grand Hotel Shinonome) for Tokyo by PWRI Bus  
Visit **Tokyo Metropolitan Expressway** (TME Corporation) by TMEC Bus
- Strengthening of RC Piers
  - Yokohama Bay Bridge
  - Route 12 (Suspension Bridge under Construction)
- 16:00 Stay at Hotel Shinbashi Dalichi

---

### Thu. Dec. 20

- 9:00 Leave Hotel for Tokyo St.  
9:32 Take Super-Express Train (Kodama No.473) for Kakegawa in Sizuoka  
11:30 Arrive at Kakegawa St.  
Visit **Tomei Expressway** (Japan Highway Corporation) by JHC Bus
- Retrofit of RC Piers against Tokai Earthquake
- 16:21 Leave Hamamatu St. for Nagoya by Super-Express Train (Kodama No.441)  
17:27 Leave Nagoya St. for Okayama (Change Train to Hikari No.119)  
19:31 Arrive at Okayama St.  
19:50 Stay at the Guest House of Honshu-Shikoku Bridge Authority

---

### Fri. Dec. 21

- 8:30 Leave Hotel for the Honshu-Shikoku Bridge  
Visit **Seto-Ohashi** (Honshu-Shikoku Bridge Authority) by HSBA Bus  
13:03 Leave Okayama St. for Osaka by Super-Express Train (Hikari No.114)  
14:02 Arrive at Shin-Osaka St.  
Visit **Hanshin Expressway** (Hanshin Expressway Corporation) by HEC Bus
- Retrofit of RC Piers
- 17:00 Arrive at the Guest House of Hanshin Expressway Corporation

---

### Sat. Dec. 22

- Free (Visit Kobe or Kyoto : Japanese Culture)  
Leave Japan from Osaka International Airport
-

**PARTICIPANTS IN THE WORKSHOP**

**PARTICIPANTS FROM THE U.S. SIDE**

**Mr. Y. H. CHAI**  
Department of Applied Mechanics and  
Engineering Sciences,  
University of California, San Diego,  
La Jolla, California 92093, U.S.A.  
Fax : (916)534-6373

**Mr. James H. GATES**  
Division of Structures  
Department of Transportation  
State of California  
1801 30th Street,  
West Building, Room 504  
Sacramento, CA 95816  
Mail : P.O. Box 942374  
Sacramento, CA 94274-0001  
Tel : (916)445-1439  
Fax : (916)445-0574

**Dr. H. S. LEW**  
Chief of Structural Division  
Center for Building Technology  
National Institute for Standards and  
Technology  
U.S. Department of Commerce  
Gaithersburg, Maryland 20899, U.S.A.  
Tel : (301)975-6061  
Fax : (301)975-4032

**Dr. Stephen A. MAHIN**  
Professor  
Department of Civil Engineering  
Chairman, Structural Engineering  
Mechanics and Materials  
University of California, Berkeley  
Berkeley, CA94720, U.S.A.  
Tel : (415)642-4021  
Fax : (415)643-5264

**Dr. M. J. Nigel PRIESTLEY**  
Professor of Structural Engineering  
Department of Applied Mechanics and  
Engineering Sciences  
University of California, San Diego,  
B-010  
La Jolla, California 92093, U.S.A.  
Tel : (916)534-5951  
Fax : (916)534-6373

**Dr. Frieder SEIBLE**  
Associate Professor of Structural  
Engineering  
Department of Applied Mechanics and  
Engineering Sciences,  
University of California, San Diego,  
B-010  
La Jolla, California 92093, U.S.A.  
Tel : (916)534-4640  
Fax : (916)534-6373

**PARTICIPANTS FROM THE JAPAN SIDE**

**Mr. Taisuke AKIMOTO**  
Manager  
Design & Research Division  
Engineering Department  
Main Office of Metropolitan Expressway  
Public Corporation  
1-4-1, Kasumigaseki, Chiyoda-ku,  
Tokyo, 100, Japan  
Tel : 03-502-7311

**Mr. Tadashi ARAKAWA**  
Manager  
Construction Fourth Section  
Main Office of Japan Highway Public  
Corporation  
3-3-2, Kasumigaseki, Chiyoda-ku, Tokyo,  
100, Japan  
Tel : 03-506-0272

**Mr. Kazushige ARAKAWA**  
Engineer  
Second Maintenance Section  
Tokyo First Operation Bureau of Japan  
Highway Public Corporation  
1-1, Minamidaira-dai, Miyamae-ku,  
Kawasaki-shi, 213, Japan  
Tel : 044-877-4181

**Mr. Gerardo BERUMEN**  
Graduate Student  
Department of Civil Engineering  
Kyoto University  
Yoshida-hon-machi, Sakyo-ku,  
Kyoto-shi, 606, Japan  
Tel : 075-753-7531  
Fax : 075-761-0646

**Mr. Hiroshi FUJIWARA**

Deputy Manager  
Structural Engineering Division  
Laboratory of Japan Highway Public  
Corporation  
1-4-1, Tadao, Machida-shi, Tokyo, 194,  
Japan  
Tel : 0427-91-1621

**Mr. Hidenori HAYASHI**  
Manager  
Development Second Section  
Research and Development Department  
Hanshin Expressway Public Corporation  
Center  
4-5-7, Minami-moto-machi, Chuoh-ku,  
Osaka-shi, 541, Japan  
Tel : 06-282-0171  
Fax : 06-282-1060

**Mr. Norio HIGASHIDA**  
Engineer  
Structural Engineering Division  
Laboratory of Japan Highway Public  
Corporation  
1-4-1, Tadao, Machida-shi, Tokyo, 194,  
Japan  
Tel : 0427-91-1621

**Dr. Hirokazu IEMURA**  
Associate Professor  
Department of Civil Engineering  
Kyoto University  
Yoshida-hon-machi, Sakyo-ku,  
Kyoto-shi, 606, Japan  
Tel : 075-753-7531  
Fax : 075-761-0646

**Mr. Akira IGARASHI**

Department of Applied Mechanics and  
Engineering Sciences  
University of California, San Diego,  
La Jolla, California 92093, U.S.A.

**Mr. Hiroyuki IIDA**

Assistant Research Engineer  
Earthquake Engineering Division  
Public Works Research Institute  
Tsukuba Science City,  
Ibaraki-ken, 305, Japan  
Tel : 0298-64-2211  
Fax : 0298-64-2840

**Dr. Toshio IWASAKI**

Director-General  
Public Works Research Institute  
Tsukuba Science City,  
Ibaraki-ken, 305, Japan  
Tel : 0298-64-2211  
Fax : 0298-64-2840

**Mr. Kazuyuki IZUNO**

Research Associate  
Department of Civil Engineering  
Kyoto University  
Yoshida-hon-machi, Sakyo-ku,  
Kyoto-shi, 606, Japan  
Tel : 075-753-7531  
Fax : 075-761-0646

**Mr. Hirotaka KAWANO**

Head  
Concrete Division  
Public Works Research Institute  
Tsukuba Science City,  
Ibaraki-ken, 305, Japan  
Tel : 0298-64-2211  
Fax : 0298-64-2840

**Dr. Kazuhiko KAWASHIMA**

Head  
Earthquake Engineering Division  
Public Works Research Institute  
Tsukuba Science City,  
Ibaraki-ken, 305, Japan  
Tel : 0298-64-2211  
Fax : 0298-64-2840

**Mr. Shigetoshi KOBAYASHI**

Director  
Geology and Chemistry Department  
Public Works Research Institute  
Tsukuba Science City,  
Ibaraki-ken, 305, Japan  
Tel : 0298-64-2211  
Fax : 0298-64-2840

**Dr. Jyuro KODERA**

Chairman of Board  
Yachiyo Engineering Corporation  
1-10-21, Naka-Meguro,  
Meguro-ku, Tokyo-to, 135, Japan  
Tel : 03-715-1231

**Mr. Shin KOGURE**

Senior Engineer  
Design Division  
Tokyo Maintenance Bureau of  
Metropolitan Expressway Public  
Corporation  
1-1-3, Shintomi, Tyuoh-ku, Tokyo, 104,  
Japan  
Tel : 03-552-1441

**Dr. Gregory A. MACRAE**

Research Scholar  
Earthquake Engineering Division  
Public Works Research Institute  
Tsukuba Science City,

Ibaraki-ken, 305, Japan

Tel : 0298-64-2211

Fax : 0298-64-2840

**Mr. Tetsuo MATSUDA**

Manager

Structural Engineering Division  
Laboratory of Japan Highway Public  
Corporation

1-4-1, Tadao, Machida-shi, Tokyo, 194,  
Japan

Tel : 0427-91-1621

**Dr. Hiroshi MUTSUYOSHI**

Associate Professor

Department of Construction  
Engineering

Saitama University  
255, Shimo-ohkubo, Urawa-shi,  
Saitama-ken, 338, Japan

Tel : 0488-52-2111

**Mr. Hiroyuki NAGASHIMA**

Assistant Research Engineer  
Earthquake Engineering Division  
Public Works Research Institute  
Tsukuba Science City,  
Ibaraki-ken, 305, Japan

Tel : 0298-64-2211

Fax : 0298-64-2840

**Mr. Hiraku NAKAJIMA**

Manager

Maintenance Engineering Division  
Engineering Department  
Main Office of Metropolitan Expressway  
Public Corporation

1-4-1, Kasumigaseki, Chiyoda-ku,  
Tokyo, 100, Japan

Tel : 03-502-7311

**Mr. Ippel NAKAMURA**

Chief Engineer

Maintenance Engineering Section  
Maintenance and Facility Design  
Division

Main Office of Hanshin Expressway  
Public Corporation

4-1-3, Kyutarou-cho, Chuoh-ku,  
Osaka-shi, 541, Japan

Tel : 06-252-8121

**Mr. Yoneo OKA**

Chief Engineer

Concrete Division

Laboratory of Japan Highway Public  
Corporation

1-4-1, Tadao, Machida-shi, Tokyo, 194,  
Japan

Tel : 0427-91-1621

**Mr. Michio OKAHARA**

Head

Foundation Division  
Public Works Research Institute  
Tsukuba Science City,  
Ibaraki-ken, 305, Japan

Tel : 0298-64-2211

Fax : 0298-64-2840

**Mr. Kenji OHASHI**

Engineer

Second Maintenance Section  
Tokyo First Operation Bureau of Japan  
Highway Public Corporation  
1-1, Minamidaira-dai, Miyamae-ku,  
Kawasaki-shi, 213, Japan

Tel : 044-877-4181

**Mr. Kazuya OHSIMA**

**Investigator**  
**Design Engineering Section**  
**Main Office of Hanshin Expressway**  
**Public Corporation**  
4-1-3, Kyutarou-cho, Tyuoh-ku,  
Osaka-shi, 541, Japan  
Tel : 06-252-8121

**Mr. Hajime OHUCHI**  
**Chief Research Engineer**  
**Structural Engineering Dept. No.1**  
**Technical Research Institute**  
**Obayashi Corporation**  
4-640, Shlmokiyoto, Kiyose-shi  
Tokyo, 204, Japan  
Tel : 0424-91-1111  
Fax : 0424-92-1855

**Dr. Yasushi SASAKI**  
**Director**  
**Earthquake Disaster**  
**Prevention Department**  
**Public Works Research Institute**  
**Tsukuba Science City,**  
**Ibaraki-ken, 305, Japan**  
Tel : 0298-64-2211  
Fax : 0298-64-2840

**Mr. Takashi SATOH**  
**Dputy Manager**  
**Structural Engineering Division**  
**Laboratory of Japan Highway Public**  
**Corporation**  
1-4-1, Tadao, Machida-shi, Tokyo, 194,  
Japan  
Tel : 0427-91-1621

**Mr. Hideyuki SHIMIZU**  
**Assistant Research Engineer**  
**Earthquake Engineering Division**

**Public Works Research Institute**  
**Tsukuba Science City,**  
**Ibaraki-ken, 305, Japan**  
Tel : 0298-64-2211  
Fax : 0298-64-2840

**Mr. Shoji TAKAGI**  
**Senior Research Engineer**  
**Foundation Division**  
**Public Works Research Institute**  
**Tsukuba Science City,**  
**Ibaraki-ken, 305, Japan**  
Tel : 0298-64-2211  
Fax : 0298-64-2840

**Mr. Keiichi TAMURA**  
**Senior Research Engineer**  
**Ground Vibration Division**  
**Public Works Research Institute**  
**Tsukuba Science City,**  
**Ibaraki-ken, 305, Japan**  
Tel : 0298-64-2211  
Fax : 0298-64-2840

**Mr. Tohru TERAYAMA**  
**Engineer**  
**Design & Research Division**  
**Engineering Department**  
**Main Office of Metropolitan Expressway**  
**Public Corporation**  
1-4-1, Kasumigaseki, Chiyoda-ku,  
Tokyo, 100, Japan  
Tel : 03-502-7311

**Mr. Kenichi TOKITA**  
**Head**  
**Ground Vibration Division**  
**Public Works Research Institute**  
**Tsukuba Science City,**  
**Ibaraki-ken, 305, Japan**

Tel : 0298-64-2211  
Fax : 0298-64-2840

**Mr. Hiroshi TOMIOKA**  
Manager  
Bridge Engineering Section  
Main Office of Honshu-Shikoku Bridge  
Authority  
5-1-5, Toranomonn, Minato-ku, Tokyo,  
105, Japan  
Tel : 03-434-7281

**Mr. Toshikazu TSUBOUCHI**  
Manager  
Second Maintenance Section  
Tokyo First Operation Bureau of Japan  
Highway Public Corporation  
1-1, Minamidaira-dai, Miyamae-ku,  
Kawasaki-shi, 213, Japan  
Tel : 044-877-4181

**Mr. Shigeki UNJOH**  
Research Engineer  
Earthquake Engineering Division  
Public Works Research Institute  
Tsukuba Science City,  
Ibaraki-ken, 305, Japan  
Tel : 0298-64-2211  
Fax : 0298-64-2840

**Mr. Hiroshi WATANABE**  
Research Engineer  
Concrete Division  
Public Works Research Institute  
Tsukuba Science City,  
Ibaraki-ken, 305, Japan  
Tel : 0298-64-2211  
Fax : 0298-64-2840

**Mr. Kazuhiko YAMAGISHI**

Deputy Manager  
Design Engineering Third Section  
Main Office of Honshu-Shikoku Bridge  
Authority  
5-1-5, Toranomonn, Minato-ku, Tokyo,  
105, Japan  
Tel : 03-434-7281

